R&T

2002 Research and Technology




Glenn Research Center
at Lewis Field
Cleveland • Ohio
NASA/TM—2003-211990

About the cover (from left to right):

The flutter analysis code TURBO was used to calculate the observed flutter of this forward-swept experimental fan, which was designed to reduce noise (pp. 174–175).

This utility vehicle was tested with ultracapacitors instead of lead acid batteries. Ultracapacitors require no maintenance, have unlimited life, and can be charged in minutes rather than hours (p. 244).

NASA's Ultra-Efficient Engine Technology project is developing revolutionary turbine engine propulsion technologies that will enable the development of future vehicles over a wide range of flight speeds from subsonic to supersonic. The GE90 engine shown here incorporated technologies from previous NASA research; new technologies being developed under this project are expected to be incorporated into future engines like the GE90 (pp. 2–3).

The sample processing unit shown here is one of the two main pieces of flight hardware that were assembled and tested for the Coarsening in Solid-Liquid Mixtures-2 (CSLM–2) experiment—a materials science space flight experiment whose purpose is to investigate the kinetics of competitive particle growth within a liquid matrix (pp. 227–228).

Research & Technology 2002

National Aeronautics and Space Administration

Glenn Research Center
Cleveland, Ohio 44135-3191

NASA/TM—2003-211990

Trade names or manufacturers' names are used in this report for identification only. This usage does not constitute an official endorsement, either expressed or implied, by the National Aeronautics and Space Administration.

Available from

NASA Center for Aerospace Information
7121 Standard Drive
Hanover, MD 21076

National Technical Information Service
5285 Port Royal Road
Springfield, VA 22100

Available electronically at http://www.grc.nasa.gov/WWW/RT

Introduction

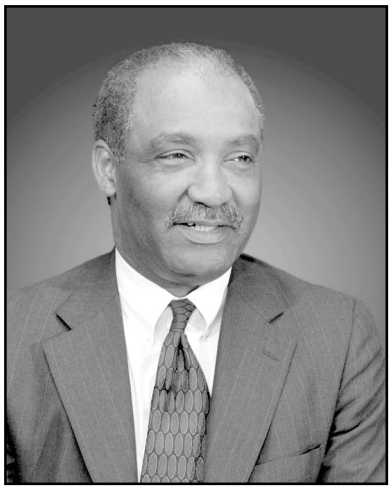

The NASA Glenn Research Center at Lewis Field, in partnership with U.S. industries, universities, and other Government institutions, is responsible for developing and transferring critical technologies that address national priorities in aeropropulsion and space applications. Our work is focused on research for new aeropropulsion technologies, aerospace power, microgravity science (fluids and combustion), electric propulsion, and communications technologies for aeronautics, space, and aerospace applications.

As NASA's premier center for aeropropulsion, aerospace power, and turbomachinery, our role is to conduct world-class research and to develop and transfer key technologies to U.S. industries. We contribute to economic growth and national security through safe, superior, and environmentally compatible U.S. civil and military aircraft propulsion systems. Our Aerospace Power Program supports all NASA Enterprises and major programs, including the International Space Station, Advanced Space Transportation, and new initiatives in human and robotic exploration.

Glenn Research Center leads NASA's research in the microgravity science disciplines of fluid physics, combustion science, and acceleration measurement. Almost every space shuttle science mission has had an experiment managed by NASA Glenn, and we have started to conduct a wide array of similar experiments on the International Space Station.

We are committed to enabling U.S.-based aerospace and nonaerospace industries to benefit directly from the technologies developed through our programs. Technology spinoffs from our efforts are found in all aspects of our daily lives, from solar cells to pagers. Our goal is to maximize the benefit of our activities to the Nation and to optimize the return on each taxpayer's investment.

The Glenn staff consists of over 3200 civil service employees and support service contractor personnel. Scientists and engineers comprise more than half of our workforce, with technical specialists, skilled workers, and an administrative staff supporting them. We aggressively strive for technical excellence through continuing education, increased diversity in our workforce, and continuous improvement in our management and business practices so that we can expand the boundaries of aeronautics, space, and aerospace technology.

Glenn Research Center is a unique facility located in northeast Ohio. Situated on 350 acres of land adjacent to the Cleveland Hopkins International Airport, Glenn comprises more than 140 buildings, including 24 major facilities and over 500 specialized research and test facilities. Additional facilities are located at Plum Brook Station, which is about 50 miles west of Cleveland. Plum Brook Station has four large, major world-class facilities for space research available for Government and industry programs.

Knowledge is the end product of our activities. The R&T reports help make this knowledge fully available to potential users—the aircraft engine industry, the space industry, the energy industry, the automotive industry, the aerospace industry, and others. It is organized so that a broad cross section of the community can readily use it. Each article begins with a short introductory paragraph that should prove valuable for the layperson. These articles summarize the progress made during the year in various technical areas and portray the technical and administrative support associated with Glenn's technology programs.

We hope that this information is useful to all. If additional information is desired, readers are encouraged to contact the researchers identified at the end of each article and to visit Glenn on the World Wide Web at http://www.grc.nasa.gov.

Donald J. Campbell
Director

NASA Glenn Research Center Senior Management

* Acting
** Interim Chief

CD–48534
February 24, 2003

NASA Glenn Research Center at Lewis Field*

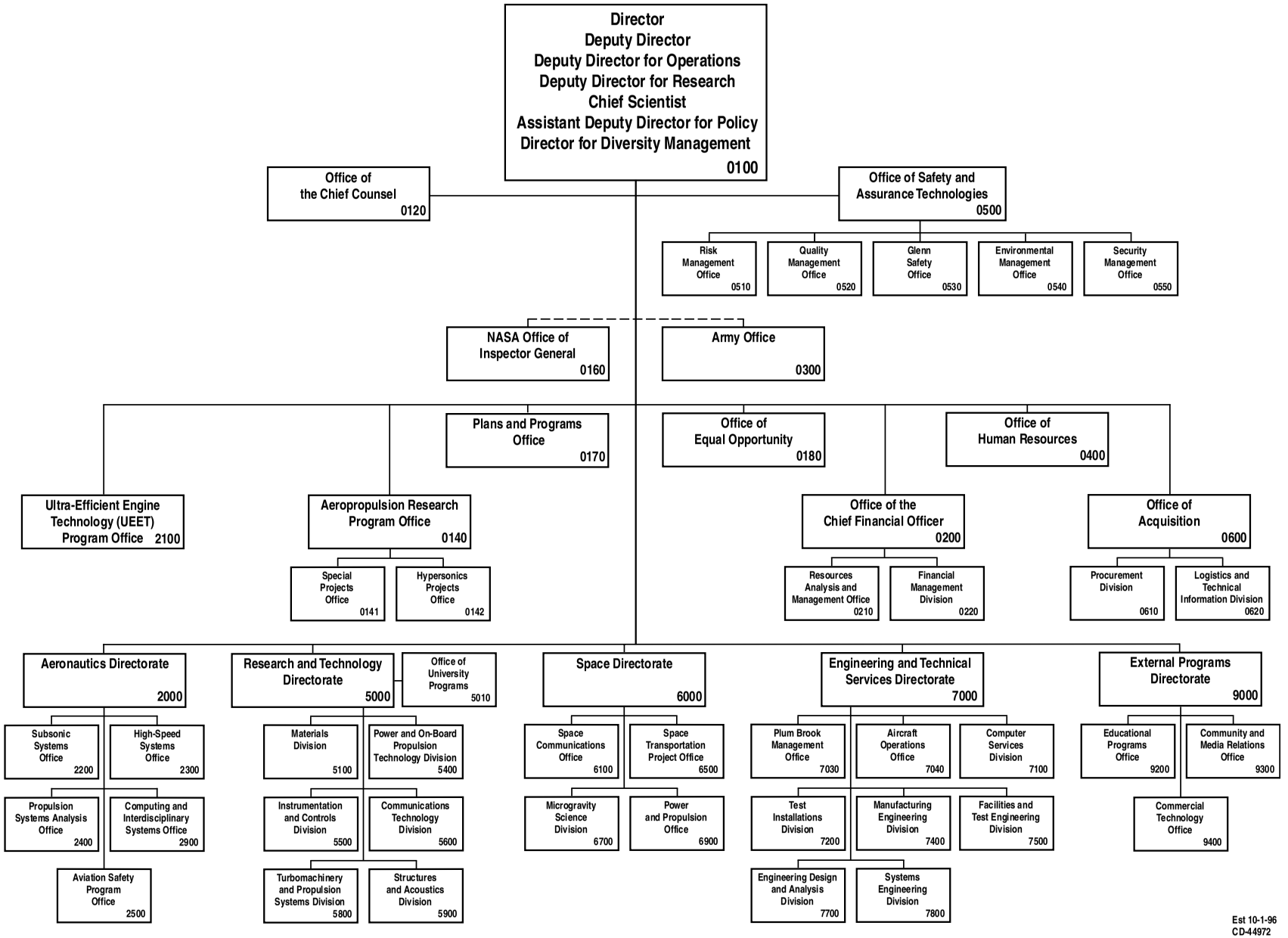

*This chart was being updated at the time of printing.

Contents

Aeronautics

Ultra-Efficient Engine Technology Program

Ultra-Efficient Engine Technology Project Continued to Contribute to Breakthrough Technologies 2

Air-Breathing Systems Analysis

Preliminary Results Obtained in Integrated Safety Analysis of NASA Aviation Safety Program Technologies 3
Computer Code for Gas Turbine Engine Weight and Disk Life Estimation Improved 4

Research and Technology

Materials

Universal Responses of Cyclic-Oxidation Models Studied 8
Alloy Design Workbench—Surface Modeling Package Developed 10
Ballistic Impact Response of Advanced Silicide Alloys Tested in the IHPTET Program 12
Versatile Turbine Disk Alloy Designed and Processed for Higher Temperature Applications 13
Superalloy Disk With Dual-Grain Structure Spin Tested 14
High-Temperature Oxidation-Resistant and Low Coefficient of Thermal Expansion NiAl-Base Bond Coat Developed for a Turbine Blade Application 15
Superior Ballistic Impact Resistance Achieved by the Co-Base Alloy Haynes 25 16
Alloy Design Data Generated for B2-Ordered Compounds 17
Superalloy Lattice Block Developed for Use in Lightweight, High-Temperature Structures 19
Processing Methods Established To Fabricate Porous Oxide Ceramic Spheres for Thermal Barrier Coating Applications 21
Creep Resistance of ZrO_2 Ceramic Improved by the Addition of a Small Amount of Er_2O_3 22
Oxidation of Carbon Fibers in a Cracked Ceramic Matrix Composite Modeled as a Function of Temperature . . 23
Cooled Ceramic Composite Panel Tested Successfully in Rocket Combustion Facility 25
Uncooled C/SiC Composite Chamber Tested Successfully in Rocket Combustion Lab 26
Ultra-High-Temperature Ceramics Evaluated for Aeropropulsion Use 27
Polymer/Silicate Nanocomposites Developed for Improved Strength and Thermal Stability 28
New Method Developed To Purify Single Wall Carbon Nanotubes for Aerospace Applications 29
High-Temperature Polymer Composites Studied for Space Propulsion Applications 31
Multiple Knudsen Cell Configuration Improved for Alloy Activity Studies 32
Studies Conducted of Sodium Carbonate Contaminant Found on the Wing Leading Edge and the Nose Cap of the Space Shuttle Orbiter 34
Advanced Environmental Barrier Coatings Developed for SiC/SiC Composite Vanes 36
Low Thermal Conductivity Thermal Barrier Coatings Developed 37
New Oxide Ceramic Developed for Superior High-Temperature Wear Resistance 39
NASA Glenn/AADC-Rolls Royce Collaborated to Measure Erosion Resistance on Coated Polymer Matrix Composites 40

Oxidation of Carbon Fibers in Water Vapor Studied 42
NiAl Coatings Investigated for Use in Reusable Launch Vehicles 43
Combustor and Vane Features and Components Tested in a Gas Turbine Environment 45

Power and On-Board Propulsion Technology

New Voltage and Current Thresholds Determined for Sustained Space Plasma Arcing 48
Systems Analysis Initiated for All-Electric Aircraft Propulsion 49
Polymer Energy Rechargeable System Battery Being Developed 50
High-Power Hall Thruster Technology Evaluated for Primary Propulsion Applications 52
Development Efforts Expanded in Ion Propulsion: Ion Thrusters Developed With Higher Power Levels 53
Pulsed Plasma Thruster (PPT) Technology: Earth Observing-1 PPT Operational and Advanced Components Being Developed 54
New Technique of High-Performance Torque Control Developed for Induction Machines 55
New Active Optical Technique Developed for Measuring Low-Earth-Orbit Atomic Oxygen Erosion of Polymers 56
Thermal Contributions to the Degradation of Ground-Laboratory- and Space-Irradiated Teflon Investigated . . . 58
Greener Method Developed for Intercalating Graphite Fibers With Bromine 59
Solar Selective Coatings Prepared From Thin-Film Molecular Mixtures and Evaluated 60
Power Electronics Being Developed for Deep Space Cryogenic Applications 61
Microelectromechanical System (MEMS) Device Being Developed for Active Cooling and Temperature Control 62
Three-Dimensional Magnetic Analysis Technique Developed for Evaluating Stirling Convertor Linear Alternators 63
Brayton Power Conversion Unit Tested—Provides a Path to Future High-Power Electric Propulsion Missions 64
Stirling Convertor Technologies Being Developed for a Stirling Radioisotope Generator 65
Mercury Conditions for the MESSENGER Mission Simulated in High-Solar-Radiation Vacuum Tests 67

Instrumentation and Controls

Advanced Packaging Technology Used in Fabricating a High-Temperature Silicon Carbide Pressure Sensor . . 68
Ceramic Packages Designed, Fabricated, and Assembled for SiC Microsystems 69
Thin-Film Air-Mass-Flow Sensor of Improved Design Developed 70
Microfabricated Gas Sensors Demonstrated in Fire and Emission Applications 72
Silicon Carbide Nanotube Synthesized 74
Improved Silicon Carbide Crystals Grown From Atomically Flat Surfaces 75
Multiwavelength Pyrometer Developed for Use at Elevated Temperatures in Aerospace Applications 76
Collaboration of the NASA Glenn Research Center and Rolls-Royce Developed Thin Film Multilayered Dielectrics for Harsh Environments 77
Fiber-Optic Bragg Gratings and Optical Holography Compared as Vibration Detectors 78
High-Temperature Sprayable Phosphor Coating Developed for Measuring Surface Temperatures 80
Optical Tweezers Array and Nimble Tweezers Probe Generated by Spatial-Light Modulator 81

Mobile Sensor Technologies Being Developed 83
Rayleigh Scattering Diagnostic Used to Measure Velocity and Density Fluctuation Spectra 84
Microelectromechanical Systems (MEMS) Broadband Light Source Developed 86
Digital Particle Image Velocimetry (DPIV) Used for Space-Time Correlations in Nozzle Flow 87
Compressor Performance Enhanced by Active Flow Control Over Stator Vanes 88
Active Control of High-Frequency Combustor Instability Demonstrated 90
Data-Mining Toolset Developed for Determining Turbine Engine Part Life Consumption 91
Performance Enhancement of Unsteady Ejectors Investigated Using a Pulsejet Driver 92

Communications Technology

Aerospace Communications Security Technologies Demonstrated 94
Multibeam Phased-Array Antennas Developed and Characterized 96
Fiber-Optic Network Architectures for Onboard Avionics Applications Investigated 98
Laser-Ablated $Ba_{0.50}Sr_{0.50}TiO_3/LaAlO_3$ Films Analyzed Statistically for Microwave Applications 100
Effects of a Scanning Reflectarray Antenna on Modulated Data Modeled 101
Quantum Sensing and Communications Being Developed for Nanotechnology 104
Space Networking Demonstrated for Distributed Human-Robotic Planetary Exploration 105

Turbomachinery and Propulsion Systems

Mechanisms of Rotating Instability in Axial Compressors Investigated 108
Two-Stage Axial Compressor Rig Designed To Develop and Validate Advanced Aerodynamic Technologies 109
Centrifugal Compressor Surge Controlled 111
Significance of Compressor Blade Row Interactions on Loss Production Investigated 112
Glenn-HT Code Validated for Complex Turbine Blade Cooling Passage 113
National Combustion Code Validated Against Lean Direct Injection Flow-Field Data 114
High-Pressure Gaseous Burner (HPGB) Facility Became Operational 116
Spontaneous Raman Scattering (SRS) System for Calibrating High-Pressure Flames Became Operational . . 118
Nanotechnology Investigated for Future Gelled and Metallized Gelled Fuels 120
Solid Hydrogen Particles and Flow Rates Analyzed for Atomic Fuels 122
Low NO_x, Lean Direct Wall Injection Combustor Concept Developed 123
Large-Eddy Simulation Code Developed for Propulsion Applications 124
Sound Sources Identified in High-Speed Jets by Correlating Flow Density Fluctuations With Far-Field Noise 125
Air-Breathing Launch Vehicle Technology Being Developed 127

Structures and Acoustics

High-Fidelity Micromechanics Model Enhanced for Multiphase Particulate Materials 129
Structural Anomalies Detected in Ceramic Matrix Composites Using Combined Nondestructive Evaluation and Finite Element Analysis (NDE and FEA) 130
Thermal Response of Cooled Silicon Nitride Plate Due to Thermal Conductivity Effects Analyzed 131

Methods Developed by the Tools for Engine Diagnostics Task to Monitor and Predict Rotor Damage in Real Time . . . 133
Hydrostatic Stress Effects Incorporated Into the Analysis of the High-Strain-Rate Deformation of Polymer Matrix Composites . . . 135
Delaminations Investigated With Ultrasonic Spectroscopy . . . 136
Fretting Fatigue of Gamma TiAl Studied . . . 137
Strength Differential Measured in Inconel 718: Effects of Hydrostatic Pressure Studied . . . 139
Flaw Detection for Composite Materials Improved by Advanced Thermal Image Reconstruction Techniques . . . 140
A Step Made Toward Designing Microelectromechanical System (MEMS) Structures With High Reliability . . . 141
High-Performance Acousto-Ultrasonic Scan System Being Developed . . . 144
Methodology Improved for Estimating Life-Prediction Parameters for the Design of Industrial Components . . . 145
Life-Prediction Parameters of Sapphire Determined for the Design of a Space Station Combustion Facility Window . . . 147
Time-Dependent Material Data Essential for the Durability Analysis of Composite Flywheels Provided by Compressive Experiments . . . 148
Particulate Titanium Matrix Composites Tested—Show Promise for Space Propulsion Applications . . . 149
Unsteady Flowfield in a High-Pressure Turbine Modeled by TURBO . . . 151
High-Frequency Testing of Composite Fan Vanes With Erosion-Resistant Coating Conducted . . . 152
Optimal Controller Tested for a Magnetically Suspended Five-Axis Dynamic Spin Rig . . . 154
Ultra-High-Power-Density Motor Being Developed for Future Aircraft . . . 156
Spin Testing for Durability Began on a Self-Tuning Impact Damper for Turbomachinery Blades . . . 157
Flywheels Upgraded for Systems Research . . . 159
Active Blade Vibration Control Being Developed and Tested . . . 160
Noninterference Systems Developed for Measuring and Monitoring Rotor Blade Vibrations . . . 162
New Tools Being Developed for Engine-Airframe Blade-Out Structural Simulations . . . 163
Experimental and Analytical Studies of Smart Morphing Structures Being Conducted . . . 164
Explicit Finite Element Techniques Used to Characterize Splashdown of the Space Shuttle Solid Rocket Booster Aft Skirt . . . 165
Analytical Failure Prediction Method Developed for Woven and Braided Composites . . . 166
Dynamic Spin Rig Upgraded With a Five-Axis-Controlled Three-Magnetic-Bearing Support System With Forward Excitation . . . 168
Neural Network and Regression Methods Demonstrated in the Design Optimization of a Subsonic Aircraft . . . 170
Magnetic Suspension Being Developed for Future Lube-Free Turbomachinery Application . . . 171
Probabilistic Aeroelastic Analysis Developed for Turbomachinery Components . . . 172
Fast-Running Aeroelastic Code Based on Unsteady Linearized Aerodynamic Solver Developed . . . 173
Forward-Swept Fan Flutter Calculated Using the TURBO Code . . . 174
Influence of Shock Wave on the Flutter Behavior of Fan Blades Investigated . . . 176
Fan Noise Source Diagnostic Test Completed and Documented . . . 177
Spiral-Bevel-Gear Damage Detected Using Decision Fusion Analysis . . . 179

Control Surface Seals Investigated for Re-Entry Vehicles . . . 181
Thermal Behavior of High-Speed Helical Gear Trains Investigated . . . 183
High-Speed, High-Temperature Finger Seal Test Evaluated . . . 185
Oil-Free Turbomachinery Research Enhanced by Thrust Bearing Test Capability . . . 187
Alloy Interface Interdiffusion Modeled . . . 189
Industry Needs Fulfilled by Patented NASA PS300 Solid Lubricant Technology . . . 191
Transition of PS300 Solid Lubricant Coating Technology to Field Aided by Demonstration on Key Substrate Alloys . . . 192
White Light Used to Enable Enhanced Surface Topography, Geometry, and Wear Characterization of Oil-Free Bearings . . . 194
In Situ, On-Demand Lubrication System Developed for Space Mechanisms . . . 195
Radial Clearance Found To Play a Key Role in the Performance of Compliant Foil Air Bearings . . . 197
Commercialization of NASA PS304 Solid Lubricant Coating Enhanced by Fundamental Powder Flow Research . . . 198
NASA PS304 Lubricant Tested in World's First Commercial Oil-Free Gas Turbine . . . 200

Space

Space Communications

Phased-Array System Characterized . . . 204

Microgravity Science

Field Effects of Buoyancy on a Premixed Turbulent Flame Studied by Particle Image Velocimetry . . . 206
Fan Beam Emission Tomography Demonstrated Successfully in the Reduced-Gravity Environment of Drop Towers . . . 208
Radiative Enhancement Effects on Flame Spread (REEFS) Project Studied "Green House" Effects on Fire Spread . . . 209
Interaction Between Flames and Electric Fields Studied . . . 210
Ocular Blood Flow Measured Noninvasively in Zero Gravity . . . 211
Contact Angle of Drops Measured on Nontransparent Surfaces and Capillary Flow Visualized . . . 213
Two-Fluid Interface Instability Being Studied . . . 215
Growth and Remodeling of Blood Vessels Studied In Vivo With Fractal Analysis . . . 216
Diffusivity Measured as a Function of Concentration . . . 219
Design Study Conducted of a Stirred and Perfused Specimen Chamber for Culturing Suspended Cells on the International Space Station . . . 221
Advanced Microgravity Acceleration Measurement Systems (AMAMS) Being Developed . . . 222
Physics of Colloids in Space (PCS): Microgravity Experiment Completed Operations on the International Space Station . . . 224
Coarsening Experiment Prepared for Flight . . . 227
New Technologies Being Developed for the Thermophoretic Sampling of Smoke Particulates in Microgravity . . . 228

Power and Propulsion

Multifunctional Inflatable Structure Being Developed for the PowerSphere Concept 230
International Space Station Solar Array Bifacial Electrical Performance Model Developed 231
International Space Station Power System Telemetry Compared With Analytically Derived Data for Shadowed Cases 233

Engineering and Technical Services

Facilities and Test Engineering

Microsystems Fabrication Laboratory—New Class 100 Cleanroom Completed and Certified 236
Static Frequency Converter System Installed and Tested 237
6-ft High-Power Electric Propulsion Test Port, EPL Tank 5 Installed 238
Research Combustion Lab Facility Capabilities and Throughput Enhanced by New Test Stands 239
Short Takeoff and Vertical Landing Capability Upgraded in NASA Glenn's 9- by 15-Foot Low-Speed Wind Tunnel 240

Engineering Design and Analysis

Liquid Propellant Manipulated Acoustically 242
Midinfrared Temperature Measurement Technique Developed 243
Hybrid Power Management (HPM) Program Resulted in Several New Applications 244
Modular Avionics Concept Developed for Microgravity Space Experiments—FEANICS 245
Hydrogen Fuel Capability Added to Combustor Flametube Rig 246
Light Microscopy Module Fan Disturbance Characterized Through Microgravity Emissions Laboratory Testing 247
Integrated Propulsion/Vehicle System Structurally Optimized 249

Commercial Technology

Space Act Agreement Maker (SAAM) With Electronic Routing System (E-Router) Developed 252

Appendixes

Definitions of NASA Headquarters Program Offices 253
Definitions of Programs and Projects 254
Index of Authors and Contacts 256

R&T 2002

Aeronautics

Ultra-Efficient Engine Technology Program

Ultra-Efficient Engine Technology Project Continued to Contribute to Breakthrough Technologies

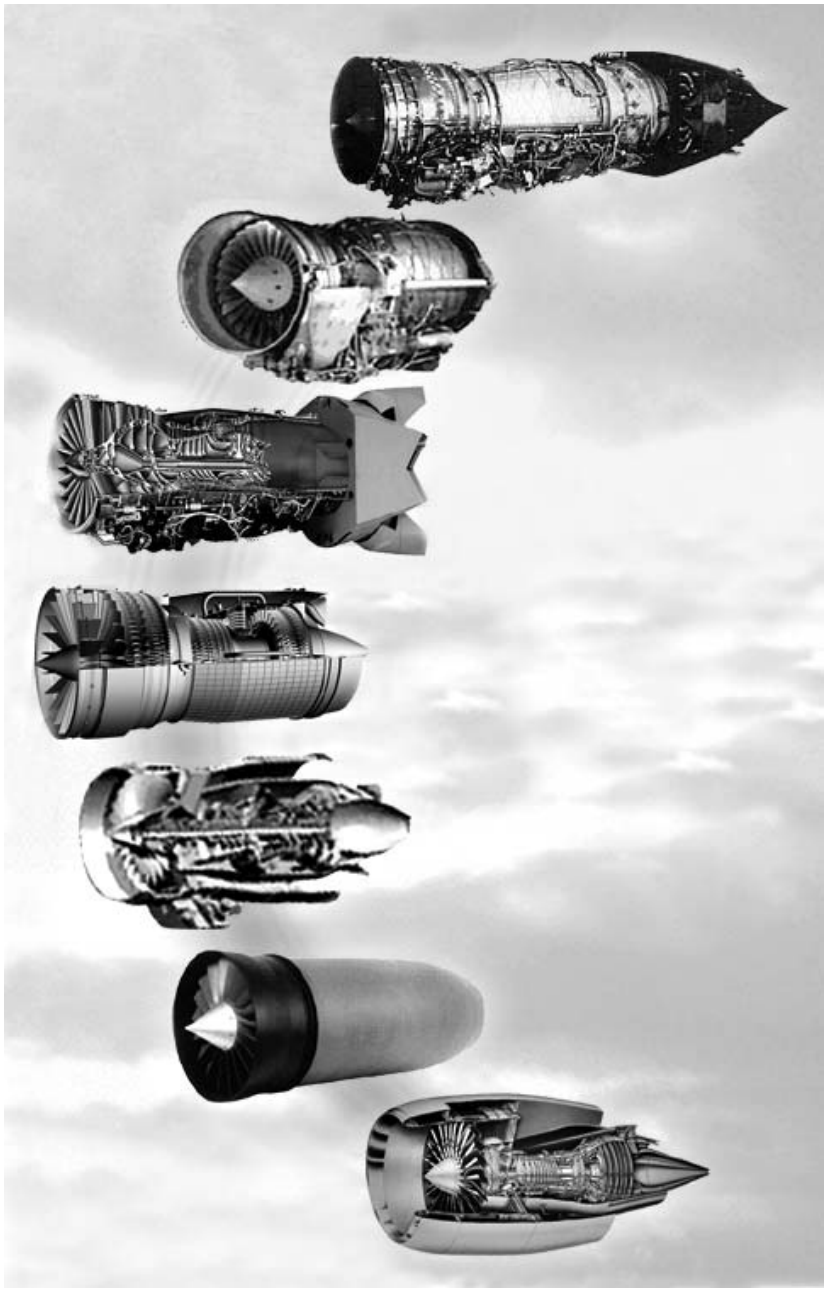

As NASA's turbine engine technology program, the vision of the Ultra-Efficient Engine Technology project is to develop and hand off revolutionary turbine engine propulsion technologies that will enable future generation vehicles over a wide range of flight speeds.

The International Civil Aviation Organization (ICAO), the U.S. Environmental Protection Agency (EPA), local environmental groups, and the public have become increasingly concerned over damage to local air quality from aircraft emissions and the impact of producing greenhouse gases. The NASA Glenn Research Center has been working to develop revolutionary technologies to minimize environmentally harmful engine emissions, such as nitrogen oxides, carbon dioxide, aerosols, and particulates.

Beginning in fiscal year 2000, Glenn began the 6-year, $300-million Ultra-Efficient Engine Technology (UEET) Program. In fiscal year 2003, the UEET Program became a project within the Vehicle Systems Program in NASA's Aerospace Technology Enterprise.

The two objectives of UEET are (1) to develop technologies to reduce nitrogen oxide (NO_x) emissions by 70 percent below 1996 ICAO regulations and (2) to decrease carbon dioxide emissions (CO_2) by dramatically increasing performance and efficiency. High-temperature engine materials, ultra-low-NO_x combustor designs, efficient, highly loaded turbomachinery, and propulsion-airframe integration analysis are technologies being developed at Glenn to meet these goals. Technology developed in the previous Advanced Subsonic Technology Program is being put into commercial production for large and regional aircraft to reduce NO_x emissions 50 percent below 1996 ICAO regulations for landing and takeoff cycles. UEET will take the technology to the next quantum leap—reducing emissions to 70 percent below the ICAO regulations level. In addition, NASA-developed research will significantly reduce carbon monoxide, unburned hydrocarbons, and corresponding cruise NO_x levels for the next generation of aircraft engines.

Technologies are being developed for subsonic and supersonic commercial engine applications. In addition, key technologies from the UEET Program are critical to advanced engine technology programs within the Department of Defense, which relies on NASA technology in this area.

Glenn's UEET research will be useful across the whole range of flight: subsonic, supersonic, and hypersonic. It will improve the subsonic transportation that the public depends on, contribute to supersonic commercial aircraft, improve military aircraft, and contribute to the design of a future hypersonic vehicle. These technologies are contributing to a better quality of life on Earth.

The overall UEET project includes research efforts at Glenn, the NASA Langley Research Center, and the NASA Ames Research Center, as well as at the five U.S. gas turbine manufacturers (GE Aircraft Engines, Pratt & Whitney, Allison Advanced Development Corporation/Rolls-Royce, Honeywell, and Williams International), two major airframe companies (the Boeing Company and Lockheed Martin), and a number of universities and small businesses.

Glenn contacts:
Dr. Robert J. Shaw, 216–977–7135, Robert.J.Shaw@nasa.gov, and
Lori A. Manthey, 216–433–2484, Lori.A.Manthey@nasa.gov

Author: Dr. Robert J. Shaw, UEET project manager

Headquarters program office: OAT

Programs/Projects:
Vehicle Systems, UEET

Air-Breathing Systems Analysis

Preliminary Results Obtained in Integrated Safety Analysis of NASA Aviation Safety Program Technologies

The goal of the NASA Aviation Safety Program (AvSP) is to develop and demonstrate technologies that contribute to a reduction in the aviation fatal accident rate by a factor of 5 by the year 2007 and by a factor of 10 by the year 2022. Integrated safety analysis of day-to-day operations and risks within those operations will provide an understanding of the Aviation Safety Program portfolio. Safety benefits analyses are currently being conducted. Preliminary results for the Synthetic Vision Systems (SVS) and Weather Accident Prevention (WxAP) projects of the AvSP have been completed by the Logistics Management Institute under a contract with the NASA Glenn Research Center. These analyses include both a reliability analysis and a computer simulation model.

PRELIMINARY RESULTS SHOWING SAFETY GAIN FROM SYNTHETIC VISION

Turn rate, °/s	Envelope distance, ft	Air traffic control only, $P_{accident}$	Synthetic vision and air traffic control, $P_{accident}$	Safety gain
1.4	17 500	9.50×10^{-1}	8.42×10^{-2}	11.3
1.4	20 000	5.10×10^{-1}	2.90×10^{-3}	175.8
3.0	10 000	8.90×10^{-1}	6.33×10^{-2}	14.1
3.0	12 500	5.10×10^{-1}	2.01×10^{-3}	253.2
5.3	7 500	7.90×10^{-1}	3.78×10^{-2}	20.9
5.3	10 000	4.20×10^{-1}	1.00×10^{-3}	420.0

The integrated safety analysis method comprises two principal components: a reliability model and a simulation model. In the reliability model, the results indicate how different technologies and systems will perform in normal, degraded, and failed modes of operation. In the simulation, an operational scenario is modeled.

The primary purpose of the SVS project is to improve safety by providing visual-flight-like situation awareness during instrument conditions. The current analyses are an estimate of the benefits of SVS in avoiding controlled flight into terrain. The scenario modeled has an aircraft flying directly toward a terrain feature. When the flight crew determines that the aircraft is headed toward an obstruction, the aircraft executes a level turn at speed. The simulation is ended when the aircraft completes the turn.

The preceding table shows preliminary results for SVS, where safety gain is defined as the baseline-case accident probability divided by the variant-case accident probability. Therefore, a safety gain of 420.0 means that the aircraft is 420 times safer with SVS than without SVS.

COMPARISON OF ENCOUNTER PROBABILITIES

Lead time, s	No WxAP	WxAP
30	0.210	0.216
60	.219	.212
90	.212	.214
120	.216	.215
180	.208	.191
240	.219	.030
300	.210	.031

ALTITUDE ESCAPE AND SLOWDOWN PROBABILITIES WITH WxAP TECHNOLOGY

Lead time, s	Altitude escape	Full slowdown
30	0.0	0.0
60	0.0	0.0
90	0.0	.169
120	0.0	.875
180	.055	1.0
240	.861	1.0
300	.852	1.0

AVERAGE WARNING TIME

Lead time, s	Warning time, s
30	24.2
60	59.5
90	99.4
120	146.1
180	242.1
240	340.9
300	438.0

The WxAP project was created to address the fact that approximately one-third of commercial aviation accidents are at least partially attributed to adverse weather. Timely and accurate information about weather could reduce accidents caused by weather.

The analyses are aimed at estimating the benefits of WxAP in detecting turbulence and either avoiding it altogether or mitigating its effect if it cannot be avoided. The scenario used to assess turbulence assumes that the aircraft is flying into an area in which there is a turbulence cell. For this scenario, the pilot must perform several actions, including reducing the speed of the aircraft, requesting an altitude change, and beginning to change altitude.

Safety metrics for turbulence are less obvious than those for terrain features, so several results are presented instead of a single-value safety gain. The three tables to the left show, respectively, encounter probability with and without the WxAP technology and for varying lead times, altitude escape and slowdown probabilities with the WxAP technology for varying lead times, and warning times achieved with the WxAP technology for varying lead times. Although these results are preliminary, it is clear that the AvSP technologies provide significant safety benefits.

Find out more about NASA's Aviation Safety Program:
http://avsp.larc.nasa.gov

Glenn contact:
Mary Reveley, 216–433–6511, Mary.S.Reveley@nasa.gov

Author: Mary S. Reveley

Headquarters program office: OAT

Programs/Projects: AvSP

Computer Code for Gas Turbine Engine Weight and Disk Life Estimation Improved

Engine weight is a key design parameter for any new aircraft engine. It affects aircraft range and is a key element in fuel burn. Weight is also considered to be an indicator of engine cost. Reliable engine-weight estimation at the conceptual design stage is critical to the development of new aircraft engines. It helps to identify the best engine concept from among several candidates.

Equally important, aircraft engines must meet safety demands. Fatigue loading of turbine components associated with continuous aircraft takeoff/cruise/landing cycles is a principal source of degradation in turbomachinery. A disk burst is potentially the most catastrophic failure possible in an engine, and thus disks are designed with overspeed capability and low-cycle-fatigue life as primary objectives. The requirement for higher turbine stage work without additional stages has resulted in increased turbine blade tip speeds and higher turbine inlet temperatures in advanced commercial aircraft engines. This trend has resulted in significant increases in turbine stage disk rim loading and a more severe thermal environment, thereby making it more difficult to design turbine disks for a specific life requirement meeting current goals. The current trend indicates that both turbine blade tip speeds and turbine inlet temperatures will continue to increase in advanced commercial engines as higher turbine

work levels are achieved. Advanced turbine disk concepts are required to ensure long life disks in commercial engines, without resulting in severe weight, performance, or cost penalties.

At the NASA Glenn Research Center, the Weight Analysis of Turbine Engines (WATE) computer code, originally developed by Boeing Aircraft, is being used to estimate the engine weight of various conceptual engine designs. The code was originally developed for NASA in 1979, but since then substantial improvements were made to the code to improve the weight calculations for most of the engine components. Recently, a series of efforts were performed at Glenn to enhance the capability of the WATE code. The major enhancements include the incorporation of improved weight-calculation routines for the compressor and turbine disks using the finite-difference technique. In addition, the stress distribution for various disk geometries was incorporated for a life-prediction module to calculate disk life. A material database, consisting of the material data of most of the commonly used aerospace materials was also incorporated into WATE. Collectively, these enhancements provide a more realistic and systematic way to calculate engine weight. The current effort paves the way for an integrated engine design tool, which would easily allow engine developers to perform design tradeoffs between engine weight, durability, and cost. To demonstrate the new capabilities, Glenn researchers used the improved WATE code to perform an engine weight/life tradeoff assessment on a 90 000-lb-thrust-class commercial turbofan engine.

Bibliography

Tong, Michael T.; Ghosn, Louis J.; and Halliwell, Ian; A Computer Code for Gas Turbine Engine Weight and Disk Life Estimation. ASME Paper GT–2002–30500, 2002.

Glenn contact:
Michael T. Tong, 216–433–6739, Michael.T.Tong@nasa.gov

Author: Michael.T. Tong

Headquarters program office: OAT

Programs/Projects:
Propulsion and Power, Propulsion Systems R&T, UEET

R&T 2002

Research and Technology

Materials

Universal Responses of Cyclic-Oxidation Models Studied

Oxidation is an important degradation process for materials operating in the high-temperature air or oxygen environments typical of jet turbine or rocket engines. Reaction of the combustion gases with the component material forms surface layer scales during these oxidative exposures. Typically, the instantaneous rate of reaction is inversely proportional to the existing scale thickness, giving rise to parabolic kinetics. However, more realistic applications entail periodic startup and shutdown. Some scale spallation may occur upon cooling, resulting in loss of the protective diffusion barrier provided by a fully intact scale. Upon reheating, the component will experience accelerated oxidation due to this spallation.

Cyclic-oxidation testing has, therefore, been a mainstay of characterization and performance ranking for high-temperature materials. Models simulate this process by calculating how a scale spalls upon cooling and regrows upon heating (refs. 1 to 3). Recently released NASA software (COSP for Windows) allows researchers to specify a uniform layer or discrete segments of spallation (ref. 4). Families of model curves exhibit consistent regularity and trends with input parameters, and characteristic features have been empirically described in terms of these parameters. Although much insight has been gained from experimental and model curves, no equation has been derived that can describe this behavior explicitly as functions of the key oxidation parameters.

A series summation equation has been developed to model a special case of parabolic scale growth and interfacial spallation of a constant area fraction, occurring only at the thickest portions (a deterministic interfacial cyclic-oxidation spalling model, or DICOSM, ref. 5). The input parameters are the parabolic growth rate constant k_p, spall area fraction F_A, oxide stoichiometry S_c, and cycle duration Δt. The output data include the net weight change, amount of oxygen and metal consumed, and amount of oxide spalled. This simplicity allows all output data and characteristic features to be represented by explicit algebraic functions (ref. 5). The net weight change can be described by the following relations, depending on whether the number of thermal-exposure cycles j is less than or greater than the number of segments n_o (case *A* or *B*), where n_o is defined as $1/F_A$:

$$\left(\frac{\Delta W}{A}\right)_{GSA,A} \cong F_A\sqrt{k_p \Delta t}\left\{\frac{1}{2}(2n_o - S_c)(j)^{1/2} + \frac{1}{3}(1-2S_c)(j)^{3/2}\right\} \qquad \text{(A)}$$

$$\left(\frac{\Delta W}{A}\right)_{GSA,B} \cong F_A\sqrt{k_p \Delta t}\left\{\left((1-S_c)\,j - \frac{1}{2}S_c\right)(n_o)^{1/2} + \frac{1}{3}(1+S_c)(n_o)^{3/2}\right\} \qquad \text{(B)}$$

Classic weight-change curves are produced with an initial maximum and final linear weight-loss rate, as shown in the top figure. The maximum in weight change varied directly with the parabolic rate constant and cycle duration and inversely with the spall fraction, all to the 1/2 power. The number of cycles to reach maximum and zero weight change, j_{max} *and* j_o, varied only with the inverse of the spall fraction, and the ratio of these is exactly 1:3.

It was found that all variations of model parameters for one oxide type (S_c) could be represented by a single relationship. Here weight change is normalized by the weight at maximum, $(\Delta W/A)_{max}$, and cycles are normalized by the number to achieve this maximum, j_{max}. The result is shown in the bottom figure, where the universal curve (dashed line for equation shown) is unique for all oxides up to the cycle number that represents n_o; then a new branch is followed for each oxide type. Nevertheless, all model responses for any combination of k_p, Δt, and F_A have been consolidated into a single curve, indicating the universality of the key characteristics of the model.

Although net weight change is informative regarding cyclic-oxidation behavior, the ultimate figure of merit for material performance is the amount of metal reacted or consumed by oxidation. Also obtained as a normal output of these models, it too was normalized by using the parameter $(S_c - 1)\sqrt{k_p \Delta t / F_A}$, and the cycle number was normalized by n_o. Again, there are two cases depending on whether j is less than or greater than n_o. In the final figure, the responses for all values of S_c, k_p, Δt, and F_A are described by these two relations and the lines are plotted. In the extremes, it is seen that the amount of metal consumed varies with the square root of the cycle number or is linear with the cycle number. These universal constructions provide a strong indication of the regularity of model cyclic-oxidation responses. Future work is planned to categorize actual cyclic-oxidation data according to these constructions and evaluate their universality of behavior.

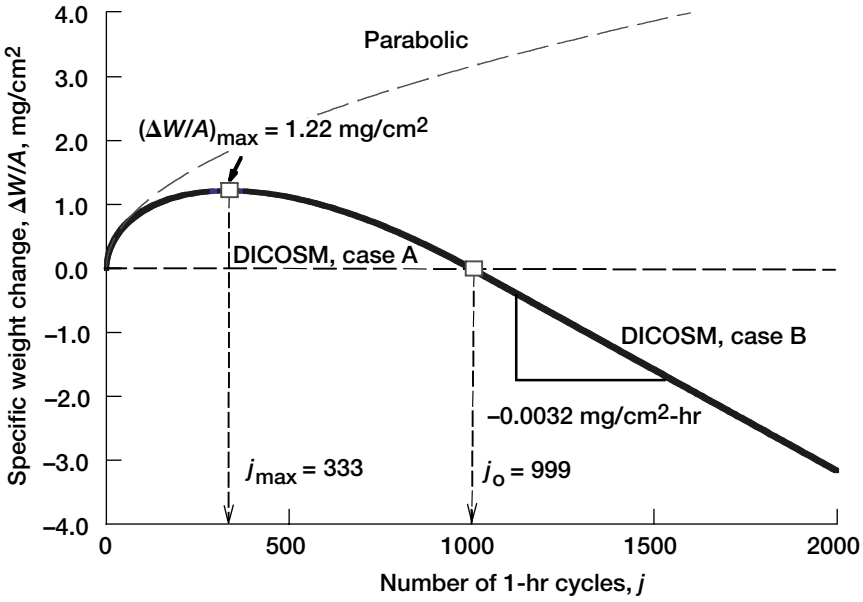

Typical DICOSM weight-change curve, showing maximum weight, time to cross zero, and linear final slope of weight loss. Oxide stoichiometry, S_c, 2.0; parabolic growth rate constant, k_p, 0.01; cycle duration, Δt, 1.0; and spall area fraction, F_A, 0.006.

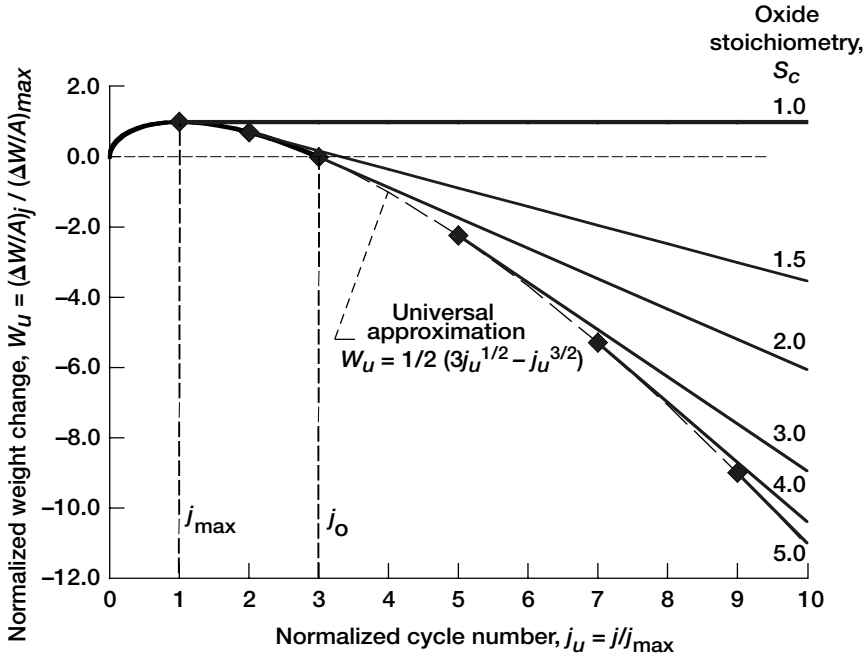

Dimensionless DICOSM weight-change curves, normalized for all parabolic growth rate constants k_p, cycle durations Δt, and spall area fractions F_A.

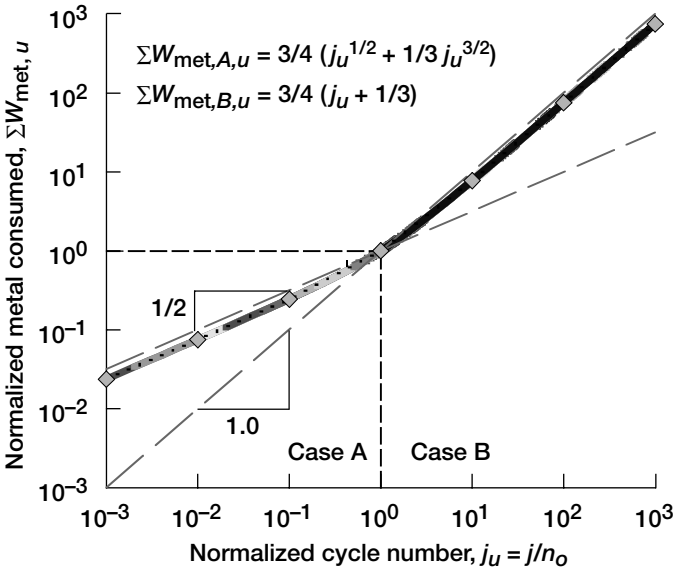

Dimensionless plot of metal consumed for DICOSMs, normalized for all oxide stoichiometry S_C, parabolic growth rate k_p, cycle durations Δt, and spall area fraction F_A, where $\sum W_{met,u} = \sum W_{met} \Big/ \left[(S_C - 1)\sqrt{k_p \Delta t / F_A} \right]$.

Find out more about this research: http://www.grc.nasa.gov/WWW/EDB/

References

1. Smialek, J.L.: Oxide Morphology and Spalling Model for NiAl. Metall. Trans.-A, vol. 9A, 1978, pp. 309–320.
2. Smialek, J.L., et al.: Cyclic Oxidation Testing and Modelling: A NASA Lewis Perspective. NASA/TM—2000-209769, 2000. http://gltrs.grc.nasa.gov/cgi-bin/GLTRS/browse.pl?2000/TM-2000-209769.html
3. Lowell, Carl E., et al.: COSP: A Computer Model of Cyclic Oxidation. Oxid. Met., vol. 36, nos. 1/2, 1991, pp. 81–112.
4. Smialek, James L.; and Auping, Judith V.: COSP for Windows: Strategies for Rapid Analyses of Cyclic Oxidation Behavior. NASA/TP—2002-211108, 2002. http://gltrs.grc.nasa.gov/cgi-bin/GLTRS/browse.pl?2002/TP-2002-211108.html
5. Smialek, J.L.: A Deterministic Interfacial Cyclic Oxidation Spalling Model. NASA/TM—2002-211906, Parts 1 and 2, 2002. http://gltrs.grc.nasa.gov/cgi-bin/GLTRS/browse.pl?2002/TM-2002-211906-PART1.html and http://gltrs.grc.nasa.gov/cgi-bin/GLTRS/browse.pl?2002/TM-2002-211906-PART2.html

Glenn contact:
Dr. James L. Smialek, 216–433–5500, James.L.Smialek@nasa.gov

Author: Dr. James L. Smialek

Headquarters program office: OAT

Programs/Projects:
Propulsion Systems R&T, UEET

Alloy Design Workbench—Surface Modeling Package Developed

NASA Glenn Research Center's Computational Materials Group has integrated a graphical user interface with in-house-developed surface modeling capabilities, with the goal of using computationally efficient atomistic simulations to aid the development of advanced aerospace materials, through the modeling of alloy surfaces, surface alloys, and segregation. The software is also ideal for modeling nanomaterials, since surface and interfacial effects can dominate material behavior and properties at this level. Through the combination of an accurate atomistic surface modeling methodology and an efficient computational engine, it is now possible to directly model these types of surface phenomenon and metallic nanostructures without a supercomputer.

Fulfilling a High Operating Temperature Propulsion Components (HOTPC) project level-I milestone, a graphical user interface was created for a suite of quantum approximate atomistic materials modeling Fortran programs developed at Glenn. The resulting "Alloy Design Workbench—Surface Modeling Package" (ADW–SMP) is the combination of proven quantum approximate Bozzolo-Ferrante-Smith (BFS) algorithms (refs. 1 and 2) with a productivity-enhancing graphical front end. Written in the portable, platform-independent Java programming language, the graphical user interface calls on extensively tested Fortran programs running in the background for the detailed computational tasks. Designed to run on desktop computers, the package has been deployed on PC, Mac, and SGI computer systems.

The graphical user interface integrates two modes of computational materials exploration. One mode uses Monte Carlo simulations to determine lowest energy equilibrium configurations. The second approach is an interactive

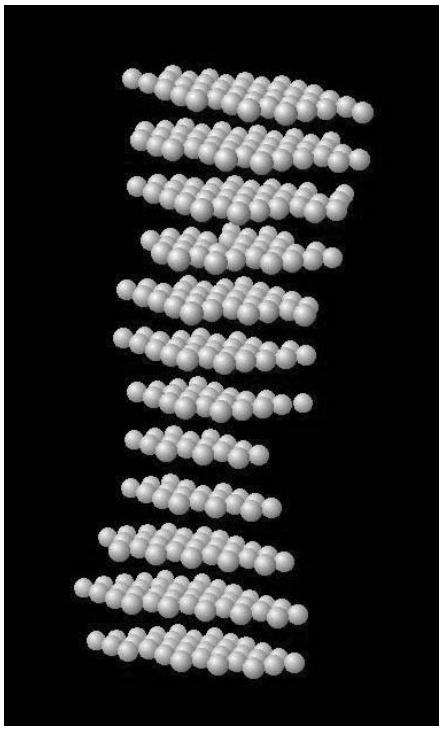

Display from the ADW–SMP of an annealed face-centered cubic [111] copper nanowire showing initial indications of local thinning.

"what if" comparison of atomic configuration energies, designed to provide real-time insight into the underlying drivers of alloying processes.

By using a Metropolis Monte Carlo algorithm for atomic exchanges, ADW–SMP can simulate an annealing run on an alloy, prompting the user for the number of temperature stages, the number of atomic exchanges per stage, and the temperature of each stage of the anneal. At each temperature, a Metropolis algorithm is used to determine if two unlike atoms in the alloy should be exchanged, considering whether the exchange lowers or raises the total energy of the material. Another option of particular importance for surfaces is a lattice position relaxation calculation, in which the coordinates of each atom can be optimized. Because they are located on the surface, atoms can rearrange to lower the total energy of the computational cell in a process called surface reconstruction, which can greatly affect subsequent surface interactions. The ADW–SMP program then gives the user a graphical representation of the results, as well as available statistical summaries such as the coordination of each type of atom in the computational cell, indicating the type and number of neighboring atoms at nearest- and next-nearest-neighbor distances.

In the second approach to alloy modeling implemented in ADW–SMP, the static energies of similar collections of atoms are computed and compared. This allows users to explore how arranging atoms in different configurations affects the total energy. The ability to perform atom-by-atom analysis of the energetics helps users to understand most surface processes in greater detail. For example, users can learn why, energetically, specific alloy components may segregate preferentially to a surface, either promoting or poisoning catalytic reactions, or determine why some otherwise immiscible metals will form surface alloys, mixing only in the presence of a surface.

The preceding figure depicts an example computational cell, showing the real-time, three-dimensional representation of the array of atoms as seen by a user. Shown is an annealed copper nanowire with local thinning becoming visible. Extensive atom display routines enable on-screen manipulation to better visualize and understand the atomic arrangements and their energetically favored configurations, under interactive pointer control. Incorporated editing capabilities allow users to graphically choose atoms to move or modify or to choose where to place additional alloying components.

With the ever-increasing computational power available to researchers on their own desktops, more sophisticated simulation tools become increasingly attractive. For materials scientists engaged in the creation of advanced alloys, the ADW–SMP software suite should become an interesting tool to potentially guide and instruct parallel experimental work. With immediate, on-screen feedback, researchers can design and launch alloy simulations to guide the much more expensive laboratory explorations of alloy properties, or use the simulations to aid in detailed interpretation of experimental results.

Find out more about this research:
http://www.icmsc.org

References

1. Bozzolo, G., et al.: An Introduction to the BFS Method and Its Use to Model Binary NiAl Alloys. J. Computer-Aided Mater. Design, vol. 6, no. 1, 1999, pp. 1–32.
2. Bozzolo, G., et al.: Surface Segregation in Multicomponent Systems: Modeling of Surface Alloys and Alloy Surfaces. Comput. Mater. Sci., vol. 15, no. 2, 1999, pp. 169–195.

Glenn contacts:
Dr. Phillip B. Abel, 216–433–6063, Phillip.B.Abel@nasa.gov; and
Dr. Ronald D. Noebe, 216–433–2093, Ronald.D.Noebe@nasa.gov

Ohio Aerospace Institute (OAI) contact:
Dr. Guillermo Bozzolo, 440–962–3103, Guillermo.H.Bozzolo@grc.nasa.gov

Authors: Dr. Phillip B. Abel, Dr. Ronald D. Noebe, Dr. Guillermo H. Bozzolo, Dr. Brian S. Good, and Elaine S. Daugherty

Headquarters program office: OAT

Programs/Projects:
Propulsion and Power, HOTPC

Ballistic Impact Response of Advanced Silicide Alloys Tested in the IHPTET Program

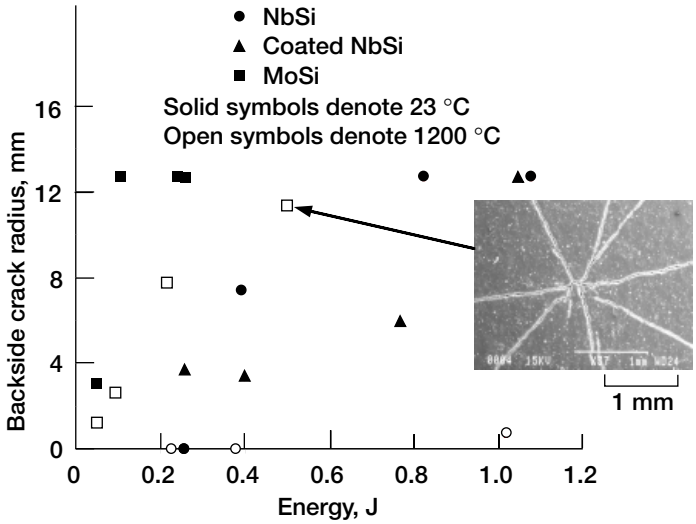

Backside crack radius for MoSiB- and NbSi-base materials at room temperature and 1200 °C.

Pratt & Whitney has been developing a molybdenum-base alloy and GE has been developing a niobium-base alloy under the Integrated High Performance Turbine Engine Technology's (IHPTET) Revolutionary Blade Material program, which is developing advanced materials to replace today's superalloys in the hot sections of turbine engines. The IHPTET program had a milestone to compare the status and potential of these materials by July 2002. As one of several criteria used in the evaluation, the NASA Glenn Research Center was asked by the Air Force to perform ballistic impact testing to simulate foreign object damage. The purpose of this work was to examine the ballistic impact response of the two candidate alloys as one of several critical properties needed for engine application.

Ballistic testing of NbSi and MoSiB, as well as of samples of NbSi that had been coated with an oxidation-resistant coating, was performed at room temperature and 1200 °C at a variety of impact energies. The backside crack radius, after impact testing, was measured and plotted as a function of impact energy. At 1200 °C, both silicide materials performed better than they did at room temperature. This is somewhat surprising, because previous research on other intermetallics, NiAl and TiAl, did not show strong temperature dependence. The improvement was quite dramatic for NbSi but more moderate for MoSiB. The plot illustrates that the niobium alloy was clearly more impact resistant than the molybdenum alloy at both room and elevated temperature.

On the basis of these preliminary results, the NbSi material probably has sufficient impact resistance to perform as a high-pressure turbine blade. Its room temperature behavior is adequate, and its high-temperature behavior is very good, far surpassing any other advanced intermetallic or ceramic tested in our labs. A more accurate assessment of NbSi would require more exact knowledge of the actual engine environment and a series of tests to examine thermal history effects and postimpact mechanical performance. However, the current MoSiB alloy is inadequate for rotating parts, even if the improved high-temperature data are taken into account, and the alloy would need further refinement to accommodate potential foreign or domestic impact damage.

Glenn contacts:
Susan Draper, 216–433–3257, Susan.L.Draper@nasa.gov; and
Dr. Michael Nathal, 216–433–9516, Michael.V.Nathal@nasa.gov

Authors: Susan L. Draper and Dr. Michael V. Nathal

Headquarters program office: OAT

Programs/Projects: HOTPC

Versatile Turbine Disk Alloy Designed and Processed for Higher Temperature Applications

Advanced turbine engine configurations using higher temperature combustor and airfoil concepts require compressor and turbine disks that can withstand temperatures higher than the 650 °C typical of current engines. This requires disk alloy and processing improvements. A versatile disk alloy was needed that could be given either fine grain heat treatments for high strength and fatigue and creep resistance up to 704 °C or given coarse grain heat treatments for high strength and creep and dwell crack-growth resistance at higher temperatures. This alloy could produce disks with uniform microstructures and properties, as well as with varied, optimized microstructures at disk bore and rim sections.

A series of experimental disk alloys were designed and processed to give subscale disks about 13 cm in diameter and 4 cm thick. These alloys had varying levels of key elements to affect mechanical properties and change the "solvus" solution heat-treatment temperature necessary to produce coarse grain microstructures. Disks were given coarse grain heat treatments followed by rapid oil quenching and slower fan air quenching. These heat treatments were intended to simulate the cooling paths of rapidly cooled full-scale disks at the outermost rim and interior bore locations, respectively. Preliminary quench tests of tensile specimens and coin-size minidisks had indicated that alloys having high solvus temperatures were more prone to cracking during rapid quenching from coarse grain heat treatments. These findings were confirmed in the subscale disks, where such alloys did form undesirable quench cracks.

Mechanical tests were performed on specimens from subscale disks given these coarse grain heat treatments, as well as on specimens given a fine grain heat treatment. Tensile, creep, and crack growth tests were performed at 704 °C and higher temperatures. A versatile alloy was identified that had a low solvus temperature for resistance to quench cracking as well as an optimal combination of high levels of strengthening refractory elements that produced balanced high mechanical properties for both fine grain and coarse grain microstructures. This low-solvus, high-refractory (LSHR) alloy has been scaled-up to produce prototype full-scale turbine disks typical of regional jet turbofan engines. Disks were successfully heat treated to give uniform coarse grain and uniform fine grain microstructures. Additional disks were given a NASA dual microstructure heat treatment (DMHT) that intentionally varied the solution heat-treatment temperatures between the disk rim and bore (ref. 1). The disk rim was heated to a high enough temperature to produce a coarse grain microstructure, while the bore was maintained at a lower temperature to produce a fine grain microstructure (see the figure). This DMHT can produce optimal high strength, fatigue, and creep resistance up to 704 °C in the cooler running disk bore, and high strength, creep resistance, and dwell crack growth resistance at higher temperatures for the hotter disk rim. Extensive mechanical testing is being initiated to compare the mechanical properties of the uniform and DMHT disks.

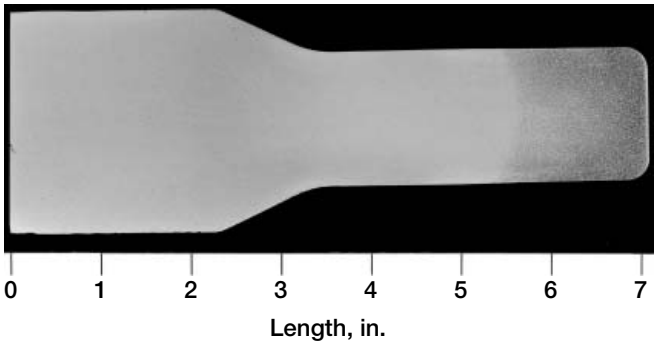

Dual microstructure produced by the DMHT process on a low-solvus, high-refractory alloy.

Find out more about the research of Glenn's Materials Division:
http://www.grc.nasa.gov/WWW/MDWeb/

Reference

1. Gayda, John; and Kantzos, Pete T.: Superalloy Disk With Dual-Grain Structure Spin Tested. Research & Technology 2002. NASA/TM—2003-211990, 2003, p. 14. http://www.grc.nasa.gov/WWW/RT2002/5000/5120gayda.html

Glenn contacts:
Tim Gabb, 216–433–3272, Timothy.P.Gabb@nasa.gov; and John Gayda, 216–433–3273, John.Gayda-1@nasa.gov

Authors: Dr. Timothy P. Gabb, Dr. John Gayda, Dr. Jack Telesman, Dr. Pete T. Kantzos, and Jason D. Miller

Headquarters program office: OAT

Programs/Projects:
HOTPC, AvSP, UEET

Superalloy Disk With Dual-Grain Structure Spin Tested

Advanced nickel-base disk alloys for future gas turbine engines will require greater temperature capability than current alloys, but they must also continue to deliver safe, reliable operation. An advanced, nickel-base disk alloy, designated Alloy 10, was selected for evaluation in NASA's Ultra Safe Propulsion Project. Early studies on small test specimens showed that heat treatments that produced a fine grain microstructure promoted high strength and long fatigue life in the bore of a disk, whereas heat treatments that produced a coarse grain microstructure promoted optimal creep and crack growth resistance in the rim of a disk. On the basis of these results, the optimal combination of performance and safety might be achieved by utilizing a heat-treatment technology that could produce a fine grain bore and coarse grain rim in a nickel-base disk.

Alloy 10 disks that were given a dual microstructure heat treatment (DMHT) were obtained from NASA's Ultra-Efficient Engine Technology (UEET) Program for preliminary evaluation. Data on small test specimens machined from a DMHT disk were encouraging. However, the benefit of the dual grain structure on the performance and reliability of the entire disk still needed to be demonstrated. For this reason, a high-temperature spin test of a DMHT disk was run at 20 000 rpm and 1500 °F at the Balancing Company of Dayton, Ohio, under the direction of NASA Glenn Research Center personnel. The results of that test showed that the DMHT disk exhibited significantly lower crack growth than a disk with a fine grain microstructure. In addition, the results of these tests could be accurately predicted using a two-dimensional, axisymmetric finite element analysis of the DMHT disk. Although the first spin test demonstrated a significant performance advantage associated with the DMHT technology, a second spin test on the DMHT disk was run to determine burst margin. The disk burst in the web at a very high speed, over 39 000 rpm, in line with the predicted location and speed. Furthermore, significant growth of the disk was observed before failure, in line with predictions, clearly demonstrating the reliability and safety of the DMHT technology.

DMHT disk before and after burst testing.

Although successful spin testing in Ultra Safe's Nickel Disk Program represents a significant milestone for DMHT technology, realistic engine operation will require repeated loading of a DMHT nickel disk. For this reason, a cyclic spin test study of DMHT nickel disk technology has been proposed to start in fiscal year 2003 under NASA's Aviation Safety Program. The goal of this program will be to determine the fatigue failure mechanism in DMHT nickel disks, thereby demonstrating the reliability and safety of DMHT technology under repetitive loading conditions encountered in realistic engine operation.

Glenn contact:
Dr. John Gayda, 216–433–3273,
John.Gayda-1@nasa.gov

Ohio Aerospace Institute (OAI) contact:
Dr. Pete Kantzos, 216–433–5202,
Pete.T.Kantzos@grc.nasa.gov

Authors:
Dr. John Gayda and Dr. Pete T. Kantzos

Headquarters program office: OAT

Programs/Projects:
Ultra Safe, UEET, AvSP

High-Temperature Oxidation-Resistant and Low Coefficient of Thermal Expansion NiAl-Base Bond Coat Developed for a Turbine Blade Application

Many critical gas turbine engine components are currently made from Ni-base superalloys that are coated with a thermal barrier coating (TBC). The TBC consists of a ZrO_2–based top coat and a bond coat that is used to enhance the bonding between the superalloy substrate and the top coat. MCrAlY alloys (CoCrAlY and NiCrAlY) are currently used as bond coats and are chosen for their very good oxidation resistance. TBC life is frequently limited by the oxidation resistance of the bond coat, along with a thermal expansion mismatch between the metallic bond coat and the ceramic top coat.

The aim of this investigation at the NASA Glenn Research Center was to develop a new longer life, higher temperature bond coat by improving both the oxidation resistance and the thermal expansion characteristics of the bond coat. Nickel aluminide (NiAl) has excellent high-temperature oxidation resistance and can sustain a protective Al_2O_3 scale to longer times and higher temperatures in comparison to MCrAlY alloys. Cryomilling of NiAl results in aluminum nitride (AlN) formation that reduces the coefficient of thermal expansion (CTE) of the alloy and enhances creep strength. Thus, additions of cryomilled NiAl-AlN to CoCrAlY were examined as a potential bond coat. In this work, the composite alloy was investigated as a standalone substrate to demonstrate its feasibility prior to actual use as a coating.

About 85 percent of prealloyed NiAl and 15 percent of standard commercial CoCrAlY alloys were mixed and cryomilled in an attritor with stainless steel balls used as grinding media. The milling was carried out in the presence of liquid nitrogen (ref. 1). The milled powder was consolidated by hot extrusion or by hot isostatic pressing. From the consolidated material, oxidation coupons, four-point bend, CTE, and tensile specimens were machined. The CTE measurements were made between room temperature and 1000 °C in an argon atmosphere. The figure on the left shows that the CTE of the NiAl-AlN-CoCrAlY composite bond coat is lower than that of the commercially used coating alloy 16–6.

To examine the potential of NiAl-AlN-CoCrAlY as a bond coat, we subjected two samples to cyclic furnace testing. The furnace cycle consisted of 45 min at 1163 °C (2125 °F) followed by 15 min of cooling out of the furnace. The current NASA baseline TBC is a NiCrAlY bond coat below the 7YSZ top coat.[1] The average TBC life for this baseline coating on René N5 is 188±19 cycles as shown in the figure on the right. NiAl-AlN-CoCrAlY specimens coated with the same 7YSZ top coat were still intact even after 1000 cycles.

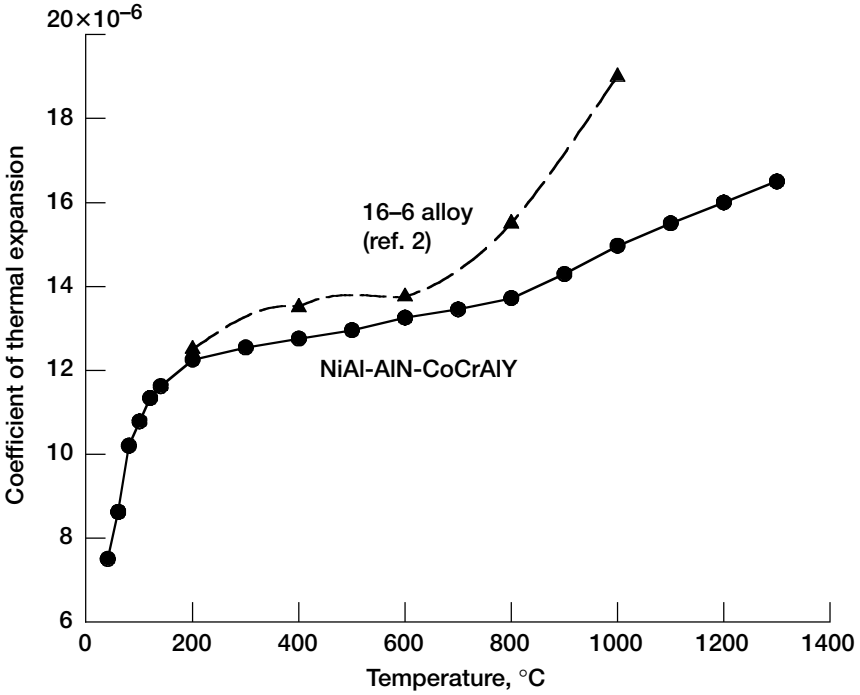

CTE of NiAl-AlN-CoCrAlY compared with that of a Ni-base bond coat (16–6 alloy).

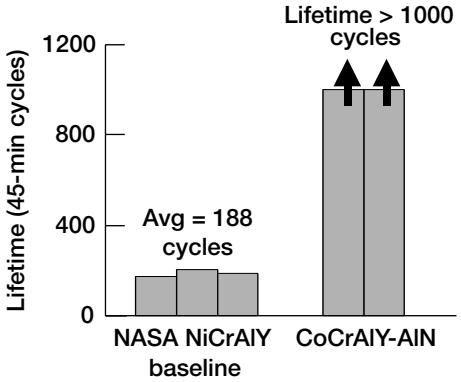

TBC lifetime of NiAl-AlN-CoCrAlY compared with that of the NASA NiCrAlY baseline alloy.

[1]Yttria-stabilized zirconia.

Therefore, the NiAl-AlN-CoCrAlY as a bulk substrate material, exhibits more than 5 times the life of the current state-of-the-art material. The next step is to evaluate this material as a coating on the same superalloy substrate.

Find out more about this research at the Materials Division Web site:
http://www.grc.nasa.gov/WWW/MDWeb/

References

1. Hebsur, Mohan G.: Oxidation Resistant and Low Coefficient of Thermal Expansion NiAl-CoCrAlY Alloy. U.S. Patent 6,454,992, Sept. 2002.
2. Brindley, W.J.: Thermal Barrier Coating Workshop. NASA CP–3312, Proceedings of the Thermal Barrier Coating Workshop, 1995.

Ohio Aerospace Institute (OAI) contact:
Dr. Mohan G. Hebsur, 216–433–3266, Mohan.G.Hebsur@grc.nasa.gov

Glenn contact:
Dr. Michael V. Nathal, 216–433–9516, Michael.V.Nathal@nasa.gov

Authors: Dr. Mohan G. Hebsur, Dr. James A. Nesbitt, and Charles A. Barrett

Headquarters program office: OAT

Program: HOTPC

Superior Ballistic Impact Resistance Achieved by the Co-Base Alloy Haynes 25

The fan case in a jet engine is required to contain a fan blade in the rare event of a blade loss during operation. Because of its function, the fan case is the largest structural component in high-bypass-ratio turbofan engines used in commercial aircraft. Therefore, the use of lighter and stronger materials would be advantageous in most engines and is practically a necessity in the latest generation of high-bypass engines.

Small panels, 7 in. wide by 7 in. long, of a number of metallic alloys were impact tested at room temperature with a 0.50-caliber blunt-nose titanium alloy projectile at the NASA Glenn Research Center (ref. 1). These metallic systems included several high-strength aluminum (Al) alloys, Al-based laminates, aluminum metal matrix composites (Al-MMCs), nickel-base superalloys (Inconel 718 and 625), several titanium (Ti) alloys in different heat-treated conditions, 304L stainless steel, a stainless-steel-based laminate, and a high-strength steel (Nitronic 60). It was determined that a simple Co-base alloy (Haynes 25) had the best impact resistance on an areal weight basis as shown in the following graph. Haynes 25 was at least 10 percent better than IMI 550, the best titanium alloy tested to date, and it was far superior to other metals, especially at higher impact velocities (greater than 1100 ft/sec).

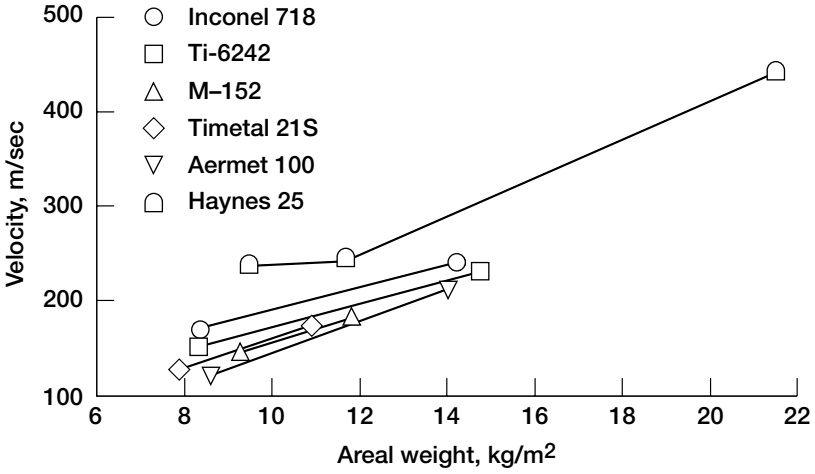

Ballistic limit versus areal weight for Haynes 25 and several other metallic systems at room temperature, showing the advantage achieved by Haynes 25, especially at higher velocities.

Because this material could be ideal for fan containment applications in supersonic aircraft as a replacement for titanium, impact tests were also conducted at 371 °C and compared with results from alloys tested at elevated temperature under previous programs (i.e., Inconel 718, Ti-6242, M–152, Timetal 21S, and Aeromet 100). The final graph clearly indicates that Haynes 25 is approximately 10 percent better than the Ti-6242 and approximately 20 percent better than Inconel 718, evaluated on the basis of velocity versus areal weight.

Although cobalt-base alloys are used in some high-temperature engine applications, to our knowledge they are not used in any containment systems. Advantages of cobalt over titanium include lower cost, easier processing, better high-temperature strength, and no fire hazard if tip rub occurs. Future plans include testing of lightweight sandwich panels with Haynes 25 as a core material in the form of a foam or lattice block structure and scaling up the current tests by using blade-simulating projectiles impacting large plates and half rings.

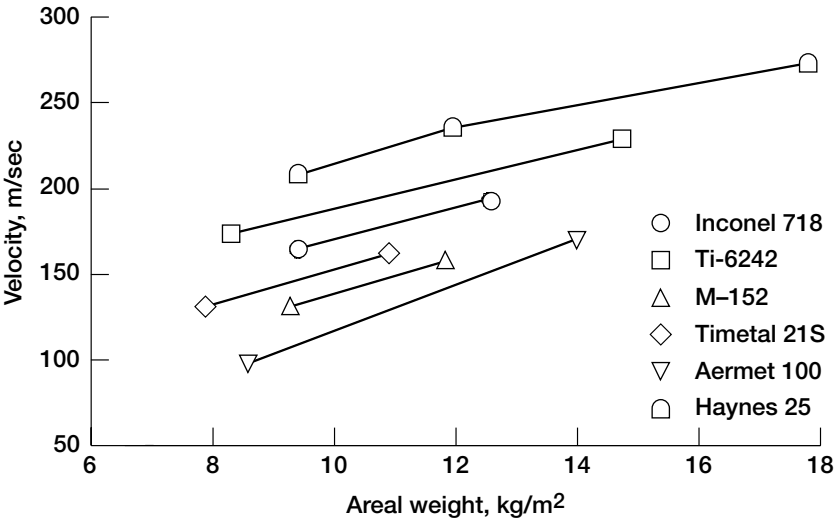

Ballistic limit versus areal weight for Haynes 25 and several other metallic systems at 371 °C, demonstrating the superior performance of Haynes 25 at elevated temperatures.

Find out more about this research: http://ballistics.grc.nasa.gov

Reference

1. Roberts, Gary D., et al.: Impact Testing of Composites for Aircraft Engine Fan Cases. NASA/TM—2001-210887, 2001. http://gltrs.grc.nasa.gov/cgi-bin/GLTRS/browse.pl?2001/TM-2001-210887.html

Ohio Aerospace Institute (OAI) contact:
Dr. Mohan Hebsur, 216–433–3266, Mohan.G.Hebsur@grc.nasa.gov

Glenn contact:
Dr. Ronald D. Noebe, 216–433–2093, Ronald.D.Noebe@nasa.gov

Authors: Dr. Mohan G. Hebsur, Dr. Ronald D. Noebe, and Duane M. Revilock

Headquarters program office: OAT

Programs/Projects:
Propulsion and Power, Ultra Safe

Alloy Design Data Generated for B2-Ordered Compounds

Developing alloys based on ordered compounds is significantly more complicated than developing designs based on disordered materials. In ordered compounds, the major constituent elements reside on particular sublattices (see the drawing). Therefore, the addition of a ternary element to a binary-ordered compound is complicated by the manner in which the ternary addition is made (at the expense of which binary component). When ternary additions are substituted for the wrong constituent, the physical and mechanical properties usually degrade. In some cases the resulting degradation in properties can be quite severe. For example, adding alloying additions to NiAl in the wrong combination (i.e., alloying additions that prefer the Al sublattice but are added at the expense of Ni) will severely embrittle the alloy to the point that it can literally fall apart during processing on cooling from the molten state (ref. 1). Consequently, alloying additions that strongly prefer one sublattice over another should always be added at the expense of that component during alloy development. Elements that have a very weak preference for a sublattice can usually be safely added at the expense of either element and will accommodate any deviation from stoichiometry by filling in for the deficient component. Unfortunately, this type of information is not known beforehand for most ordered systems.

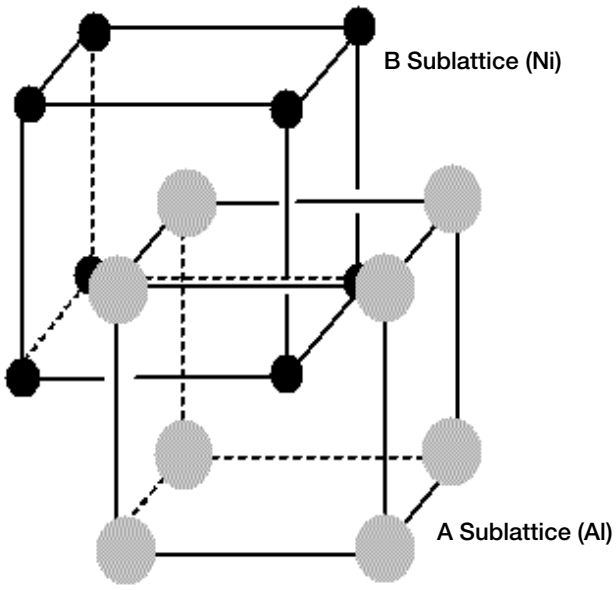

Structure of a B2 compound showing the two interpenetrating simple-cubic sublattices. In the case of stoichiometric NiAl, Ni atoms would occupy one sublattice and Al atoms the other.

SITE OCCUPANCY PREFERENCE FOR TERNARY ALLOYING ADDITIONS IN VARIOUS B2-ORDERED COMPOUNDS
[Italicized data represent the sum total of previously realized information prior to this study.]

A(B,X)	Preference for sites in the A sublattice				Preference for sites in the B sublattice			
(A,X)B	Strong	Medium	Weak	Very weak	Very weak	Weak	Medium	Strong
Ni(Al,X) **(Ni,X)Al**	Co Ru	Fe	SiCu	Cr Zr Hf	***Fe*** Ru Ta Mo W Nb V Ti	***Ta*** Cu ***Cr Mo Hf W Nb Zr***	***V***	Co ***Ti*** Si
Fe(Al,X) **(Fe,X)Al**	Ru Ni	Co	Ru ***Ni*** Zr Hf Si Cu	***Co*** Cr	W Mo V Ta Nb	Zr Si W Mo Cu Ti	***Cr*** Nb Ta Hf	***V Ti***
Co(Al,X) **(Co,X)Al**		Fe Ni	Zr Hf Cu Ru	Cr	Ni Zr Fe W Mo Ta V Nb Ti	W Hf Mo Cu Al Ta Ru Cr Nb	V	Si Ti
Co(Fe,X) **(Co,X)Fe**			Ni	Si Co Cu V Mo W Ta Ni Zr Si V Mo W Cu Ta	Ti Al Hf Ti Nb Al Hf Cr	Ru	Cr	
Co(Hf,X) **(Co,X)Hf**	Ni Fe Ru		V Cr Mo W	Nb Ta	Fe Ni Ru W Cu Si Zr Al Ti	Cr Mo V	Cu Ta Zr	Nb Si Ti Al
Co(Ti,X) **(Co,X)Ti**	Fe Ru	Al Ni	V Cr Cu Hf	Zr	W Si Mo Nb Ta	W Ni	Cu Cr Al Mo Zr Hf Ta	V Nb Si
Fe(Ti,X) **(Fe,X)Ti**	Ni Co Ru	Al	V Cr Hf Cu	Co Ru Zr	Ni Si Mo W Nb Ta	Al Cu Cr	Zr W Mo V Hf Ta Nb	Si
Ru(Al,X) **(Ru,X)Al**			Hf Ta Ti Nb Mo Ni Co Cu Zr Cr Fe	Mo Ta Fe Cr Si W V	Zr Nb Hf Ti V Cu	Co Ni W		Si
Ru(Si,X) **(Ru,X)Si**	Fe	V Ti Mo Ta Cr	Cu W Ni Co Zr Hf Nb	V Zr Hf Nb Ti Fe Cr Mo Ta Al		W Cu Ni Co	Al	
Ri(Hf,X) **(Ru,X)Hf**	Ni Fe Co		Ta V Cr Mo W	Ni Fe Co Nb	Cu Si Al Zr Ti	Cr Mo W Cu	V Nb Ta	Si Al Zr Ti
Ru(Ti,X) **(Ru,X)Ti**	Co Fe	Ni	V Cr Cu Hf Al	Co Zr Si	Fe Ni Cu Mo Nb W Ta	Cr	Hf Mo Al W Ta Nb V	Si Zr
Ru(Zr,X) **(Ru,X)Zr**	Ni	Ta Cr	Cu Fe Si W V Mo Nb	Ni Ti Co Al Hf	Cr	Co Cu Fe Mo V W Nb	Ta Si	Hf Ti Al
Ru(Ti,X) **(Ru,X)Ti**	Co Fe	Ni	V Cr Cu Hf Al	Co Zr	Fe Ni Cu Si Mo W Nb Ta	Cr	Hf Mo Al W Ta Nb V	Si Zr

Therefore, a computational survey study, using a recently developed quantum approximate method, was undertaken at the NASA Glenn Research Center to determine the preferred site occupancy of ternary alloying additions to 12 different B2-ordered compounds including NiAl, FeAl, CoAl, CoFe, CoHf, CoTi, FeTi, RuAl, RuSi, RuHf, RuTi, and RuZr. Some of these compounds are potential high-temperature structural alloys; others are used in thin-film magnetic and other electronic applications. The results are summarized in the preceding table. The italicized elements represent the previous sum total alloying information known and verify the computational method used to establish the table. Details of the computational procedures used to determine the preferred site occupancy can be found in reference 2. As further substantiation of the validity of the technique, and its extension to even more complicated systems, it was applied to two simultaneous alloying additions in an ordered alloy (ref. 3).

The information in this table can be used to guide future alloy design programs involving any of these systems. Significant savings in time, money, and effort should result because the focus will be on the most energetically stable compositions. In addition, the methodology can handle other alloys and types of ordered structures.

Find out more about this research:

International Computational Material Science Consortium: http://www.icmsc.org/

Ronald D. Noebe: http://www.grc.nasa.gov/WWW/MDWeb/People/20NRD.html

References

1. Noebe, R.D.; Bowman, R.R.; and Nathal, M.V.: Physical and Mechanical Properties of the B2 Compound NiAl. International Materials Reviews, vol. 38, no. 4, 1993, pp. 193–232.
2. Bozzolo, Guillermo H.; Noebe, Ronald D.; and Amador, Carlos: Site Occupancy of Ternary Additions to B2 Alloys. Intermetallics, vol. 10, no. 2, 2002, pp. 149–159.
3. Bozzolo, Guillermo, et al.: Atomistic Modeling of Quaternary Alloys: Ti and Cu in NiAl. Metallurgical and Materials Transactions B, vol. 33B, issue 2, 2002, pp. 265–284.

Glenn contact:
Dr. Ronald D. Noebe, 216–433–2093, Ronald.D.Noebe@nasa.gov

Ohio Aerospace Institute (OAI) contact:
Dr. Guillermo Bozzolo, 440–962–3103 or 216–433–5824, Guillermo.H.Bozzolo@grc.nasa.gov

Authors: Dr. Ronald D. Noebe, Dr. Guillermo H. Bozzolo, and Dr. Phillip B. Abel

Headquarters program office: OAT

Programs/Projects:
Propulsion and Power, HOTPC

Superalloy Lattice Block Developed for Use in Lightweight, High-Temperature Structures

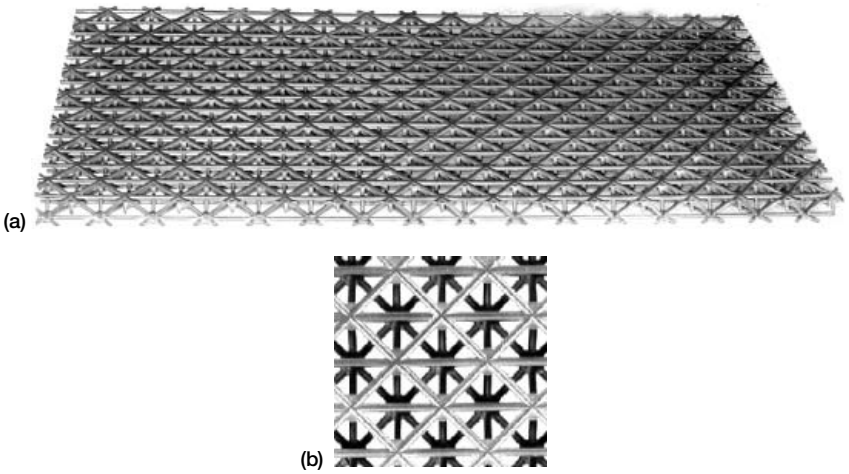

IN 718 superalloy open cell lattice block panel formed by small-diameter, straight ligaments in a triangulated trusslike geometry. Top: Overview. Bottom: Magnified view.

Successful development of advanced gas turbine engines for aircraft will require lightweight, high-temperature components. Currently titanium-aluminum- (TiAl) based alloys are envisioned for such applications because of their lower density (~4 g/cm^3) in comparison to superalloys (~8.5 g/cm^3), which have been utilized for hot turbine engine parts for over 50 years. However, a recently developed concept (lattice block) by JAMCORP, Inc., of Willmington, Massachusetts, would allow lightweight, high-temperature structures to be directly fabricated from superalloys and, thus, take advantage of their well-known, characterized properties.

In its simplest state, lattice block is composed of thin ligaments arranged in a three-dimensional triangulated trusslike configuration that forms a structurally rigid panel as illustrated in the preceding figure. This panel, which was produced by investment casting, contains about 2250 ligaments, 1.6 mm in diameter, which form a 130- by 290- by 11-mm-thick netlike structure that weighs 85-percent less than a similar size solid plate. Because lattice block can be fabricated by casting, correctly sized hardware is produced with little or no machining; thus very low cost manufacturing is possible.

Together, the NASA Glenn Research Center and JAMCORP have extended their lattice block methodology for lower melting materials, such as Al alloys, to demonstrate that investment casting of superalloy lattice block is possible. This effort required advances in lattice block pattern design and assembly, higher temperature mold materials and mold fabrication technology, and foundry practice suitable for superalloys (ref. 1). Lattice block panels have been cast from two different Ni-base superalloys: IN 718, which is the most commonly utilized superalloy and retains its strength up to 650 ºC; and MAR M247, which possesses excellent mechanical properties to at least 1100 ºC. In addition to the open-cell lattice block geometry illustrated in the figure, same-sized lattice block panels containing a thin (~1-mm-thick) solid face on one side have also been cast from both superalloys.

Initial tensile, compression, bend, and fatigue tests of samples machined from IN 718 open-cell lattice block (see the figure) have been completed and are described in reference 2. This work indicated that the trusslike structure can redistribute the applied load, which provides the redundancy leading to graceful failure. The test data, when combined with finite element analysis of the ligament structure, indicate that the ligaments could support stresses consistent with the strength of IN 718.

The elevated-temperature mechanical properties of the open cell and face-sheeted superalloy lattice block panels are currently being examined, and the microstructure is being characterized in terms of casting defects. In addition, a small study (ref. 3) is being undertaken with GE Aircraft Engines to determine the suitability of superalloy lattice block for engine components.

References

1. Hebsur, M.G.: Processing of IN–718 Lattice Block Castings. Processing and Properties of Lightweight Cellular Metals and Structures, Third Global Symposium on Materials Processing and Manufacturing (NASA/CR—2002-211332), Amit K. Ghosh, T.H. Sanders, and T.D. Claar, eds., TMS, Warrendale, PA, 2002, pp. 85–96. http://gltrs.grc.nasa.gov/cgi-bin/GLTRS/browse.pl?2002/CR-2002-211332.html
2. Krause, D.L., et al.: Mechanical Testing of IN718 Lattice Block Structures. Processing and Properties of Lightweight Cellular Metals and Structures, Third Global Symposium on Materials Processing and Manufacturing (NASA/TM—2002-211325), Amit K. Ghosh, T.H. Sanders, and T.D. Claar, eds., TMS, Warrendale, PA, 2002, pp. 233–242. http://gltrs.grc.nasa.gov/cgi-bin/GLTRS/browse.pl?2002/TM-2002-211325.html
3. Ott, E.: GEAE—NASA RASER Task Order 14, Superalloy Lattice Block, NAS3–01135, July 12, 2002.

Glenn contact:
Dr. J. Daniel Whittenberger,
216–433–3196,
John.D.Whittenberger@nasa.gov

Authors: Dr. Mohan G. Hebsur, Dr. J. Daniel Whittenberger, and David L. Krause

Headquarters program office: OAT

Programs/Projects: UEET

Processing Methods Established To Fabricate Porous Oxide Ceramic Spheres for Thermal Barrier Coating Applications

As gas turbine technology advances, the demand for efficient engines and emission reduction requires a further increase in operating temperatures, but combustion temperatures are currently limited by the temperature capability of the engine components. The existing thermal barrier coating (TBC) technology does not provide sufficient thermal load reduction at a 3000 ^{O}F (1649 ^{O}C) operating condition. Advancement in thermal barrier coating technology is needed to meet this aggressive goal.

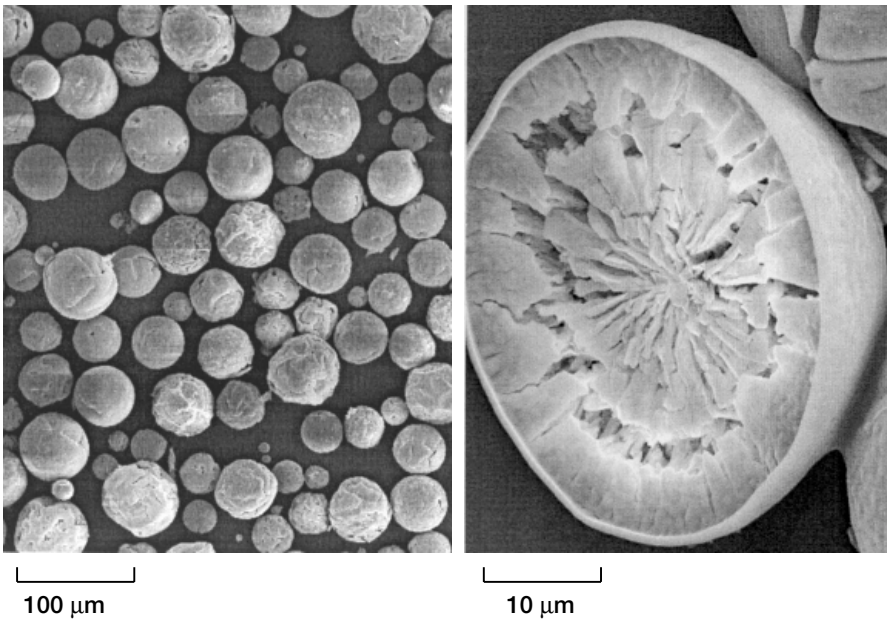

Porous zirconia ceramic spheres with pore channels produced by a cation exchange reaction.

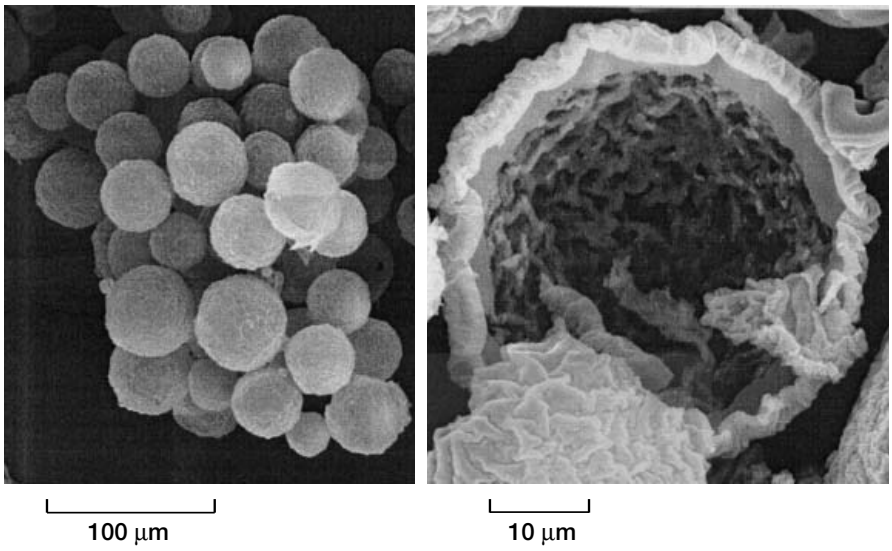

Hollow spheres derived by surface templating a strong acid cation exchange resin.

One concept for improving thermal barrier coating effectiveness is to design coating systems that incorporate a layer that reflects or scatters photon radiation. This can be achieved by using porous structures. The refractive index mismatch between the solid and pore, the pore size, and the pore density can be engineered to efficiently scatter photon radiation. Under NASA's Ultra-Efficient Engine Technology (UEET) Program, processing methods to fabricate porous ceramic spheres suitable for scattering photon radiation at elevated temperatures have been established.

A straightforward templating process was developed at the NASA Glenn Research Center that requires no special processing equipment. The template was used to define particle shape, particle size, and pore size. Spherical organic cation exchange resins were used as a structure-directing template. The cation exchange resins have dual template capabilities that can produce different pore architectures. This process can be used to fabricate both metal oxide and metal carbide spheres.

This templating process was used first to fabricate porous zirconia spheres with pore channels. An aqueous solution of a metal salt was used to perform the cation exchange reaction:

$$(ZrO)^{+2} + 2Cl^{-1} + 2(R - SO_3)^{-}H^{+} \leftrightarrow 2\ R - SO_3)^{-}\ (ZrO)^{+2} + 2\ HCl$$

In this reaction, the hydrogen ion is exchanged with the $(ZrO)^{+2}$ ion. Pyrolyzing the resin beads in an oxidative environment produces metal oxide spheres.

The templating process also was modified to produce hollow spheres. Fabricating hollow spheres allows

researchers to explicitly control the size and shape of a pore. A chemical reaction at the resin surface was used to coat the resin particle. Cation exchange resins can retain up to 50 wt% water, which can be utilized to initiate and feed a chemical reaction with metal alkoxides ($M(OR)_n$):

$$Zr(OC_3H_7)_4 + H_2O \leftrightarrow ZrO_2 + 4(C_3H_7OH)$$

The process strategy was an emulsion approach analogous to water in oil. The resin beads were mixed with a nonpolar liquid and surfactant. (Water is immiscible in the nonpolar liquid.) Diluted metal alkoxide solution was prepared by mixing the metal alkoxide with the nonpolar liquid and slowly adding this mixture to the resin bead solution. The chemical reaction deposited a coating on the resin bead surfaces. Pyrolyzing the resin beads in an oxidative environment produced hollow metal oxide spheres. Coating systems are currently being developed using porous and hollow spheres fabricated by the templating process.

Find out more about this research:

Glenn's Ceramics Branch:
http://www.grc.nasa.gov/WWW/Ceramics/homepage.htm

Glenn's Environmental Durability Branch:
http://www.grc.nasa.gov/WWW/EDB/

Glenn contact:
Dr. Fred Dynys, 216–433–2404, Frederick.W.Dynys@nasa.gov

Author: Dr. Frederick W. Dynys

Headquarters program office: OAT

Programs/Projects: UEET

Creep Resistance of ZrO_2 Ceramic Improved by the Addition of a Small Amount of Er_2O_3

Zirconia (ZrO_2) has great technological importance in structural, electrical, and chemical applications. It is the crucial component for state-of-the-art thermal barrier coatings and an enabling component as a solid electrolyte for solid-oxide fuel cell systems. Pure ZrO_2 is of limited use for industrial applications because of the phase transformations that occur. Upon the addition of "stabilizers," cubic (c-ZrO_2) and tetragonal (t-ZrO_2) forms can be preserved. It is the stabilized and partially stabilized forms of zirconia that function as thermal barrier coatings, solid electrolytes, and oxygen sensors and that have numerous applications in the electrochemical industry. The cubic form of ZrO_2 is typically stabilized through Y_2O_3 additions. However, Y_2O_3-stabilized zirconia is susceptible to deformation at high temperatures (>900 °C) because of the large number of slip systems and the high oxygen diffusion rates, which result in high creep rates at high temperatures. Successful use of ZrO_2 at high temperatures requires that new dopant additives be found that will retain or enhance the desirable properties of cubic ZrO_2 and yet produce a material with lower creep rates.

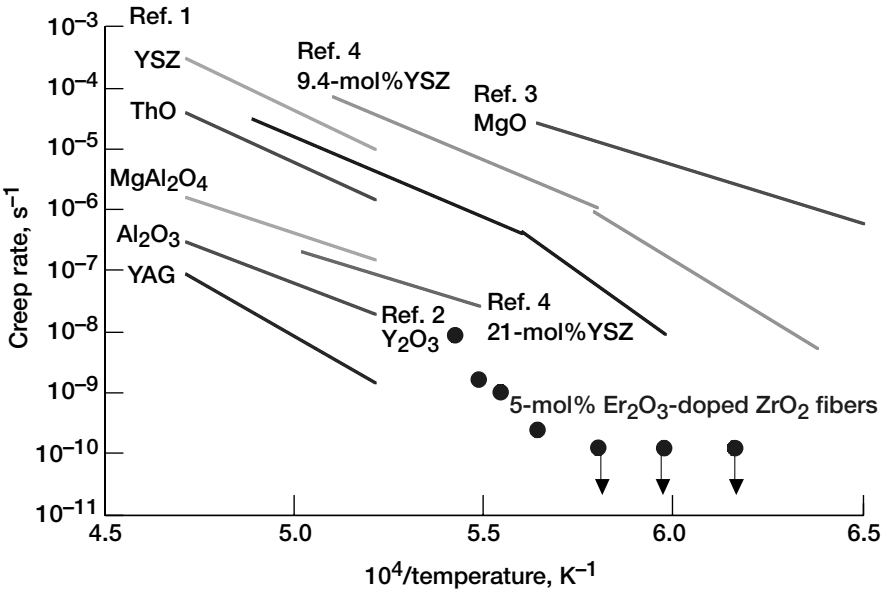

Comparison of creep data of high-temperature oxides. Low creep values for Er_2O_3-doped ZrO_2 obtained in this study are shown as filled circles.

At the NASA Glenn Research Center, erbium oxide (Er_2O_3) was identified as a promising dopant for improving the creep resistance of ZrO_2. The selection of Er_2O_3 was based on the strong interactions of point defects and dislocations. Single crystals of 5 mol% Er_2O_3-doped ZrO_2 rods (4 mm in diameter) and monofilaments (200 to 300 μm in diameter and 30 cm long) were grown using the laser-heated float zone technique, and their creep behavior was measured as a function of temperature. The addition of 5 mol% Er_2O_3 to single-crystal ZrO_2 improved its creep resistance at high temperatures by 2 to 3 orders of magnitude over state-of-the-art Y_2O_3-doped

crystals. Detailed microstructural characterization of ZrO_2-Er_2O_3 single crystals has identified new mechanisms for improving the creep resistance of this class of materials. Adding Er_2O_3 to ZrO_2 results in a microstructure of stable and metastable tetragonal precipitates that with thermal treatment evolve to a tweed structure of nanosize tetragonal lamellae. The superior high-temperature creep resistance of Er_2O_3-doped ZrO_2 is attributed to nanoscale precipitation hardening.

Doping with Er_2O_3 will significantly increase the upper-use temperature limit of ZrO_2. Potential applications include using Er_2O_3-doped ZrO_2 as a high-temperature fiber for structural applications and adding Er_2O_3 to reduce the sintering rates of ZrO_2 thermal barrier coatings. This work was conducted at Dpto. de Física de la Materia Condensada, Universidad de Sevilla, Spain, and at NASA Glenn.

Find out more about this research:
http://www.grc.nasa.gov/WWW/Ceramics/homepage.htm

References

1. Corman, G.S.: High-Temperature Creep of Some Single Crystals Oxides. Ceram. Eng. Sci. Proc., vol. 12, nos. 9–10, 1991, pp. 1745–1766.
2. Garboriaud, Par R.J.: Fluage Haute Temperature du Sesquioxyde d'yttrium: Y_2O_3. Philos. Mag. A, vol. 44, no. 3, 1981, pp. 561–587.
3. Clauer, A.H.; and Wilcox, B.A.: High Temperature Tensile Creep of Magnesium Oxide Single Crystals. J. Am. Ceram. Soc., vol. 59, nos. 3 to 4, 1976, pp. 89–96.
4. Martinez-Fernandez, J., et al.: High Temperature Precipitation Hardening in Y_2O_3 (Y–PSZ) Partially-Stabilized ZrO_2 (Y–PSZ) Single Crystals—III. Effect of Solute Composition and Orientation on the Hardening. Acta. Metall. Mater., vol. 43, no. 6, 1995, pp. 2469–2484.

Glenn contact: Dr. Serene Farmer, 216–433–3289, Serene.C.Farmer@nasa.gov

Case Western Reserve University contacts:
Dr. Ali Sayir, 216–433–3289, Ali.Sayir@grc.nasa.gov; and
Dr. Julian Martinez-Fernandez, martinez@us.es

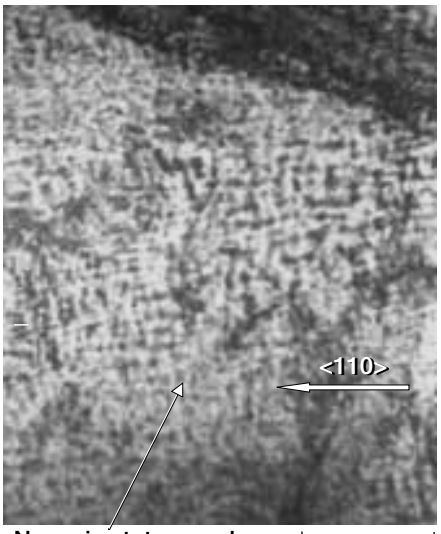

Nanosized precipitates in the microstructure are responsible for the improved creep resistance of ZrO_2. Nanosize tetragonal precipitates are visible (dark contrast) within the cubic matrix (light contrast) in the transmission electron micrograph.

Authors: Dr. Julian Martinez-Fernandez (lead researcher), Dr. Ali Sayir, and Dr. Serene C. Farmer

Headquarters program office: OAT

Programs/Projects: HOTPC

Oxidation of Carbon Fibers in a Cracked Ceramic Matrix Composite Modeled as a Function of Temperature

Carbon-fiber-reinforced ceramic matrix composites (CMCs) offer great potential for use in advanced space transportation applications. The composite system is currently being considered for many components such as nozzles, cooled panels, bladed disks, and leading edges. However, the susceptibility of carbon fiber to oxidation can inhibit its use in certain reusable and long-term applications. To better determine the potential applications for these materials, researchers need a greater understanding of the oxidation kinetics and the resultant material degradation. To address this issue, NASA, U.S. Army, and Case Western Reserve University researchers at the NASA Glenn Research Center developed a finite-difference oxidation model as part of the CMC Life Prediction Methods Program. The oxidation model simulates the oxidation of the reinforcing carbon fibers within a ceramic matrix composite material containing as-fabricated microcracks. The physics-based oxidation model uses theoretically and experimentally determined variables as input for the model.

The model simulates the ingress of oxygen through microcracks into a two-dimensional plane within the composite material. Model input includes temperature, oxygen concentration, the reaction rate constant, the diffusion coefficient, and the crack opening width as a function of the mechanical and thermal loads. The model is run in an iterative process for a two-dimensional grid system in which oxygen diffuses through the porous and cracked regions of the material and reacts with carbon in short time steps.

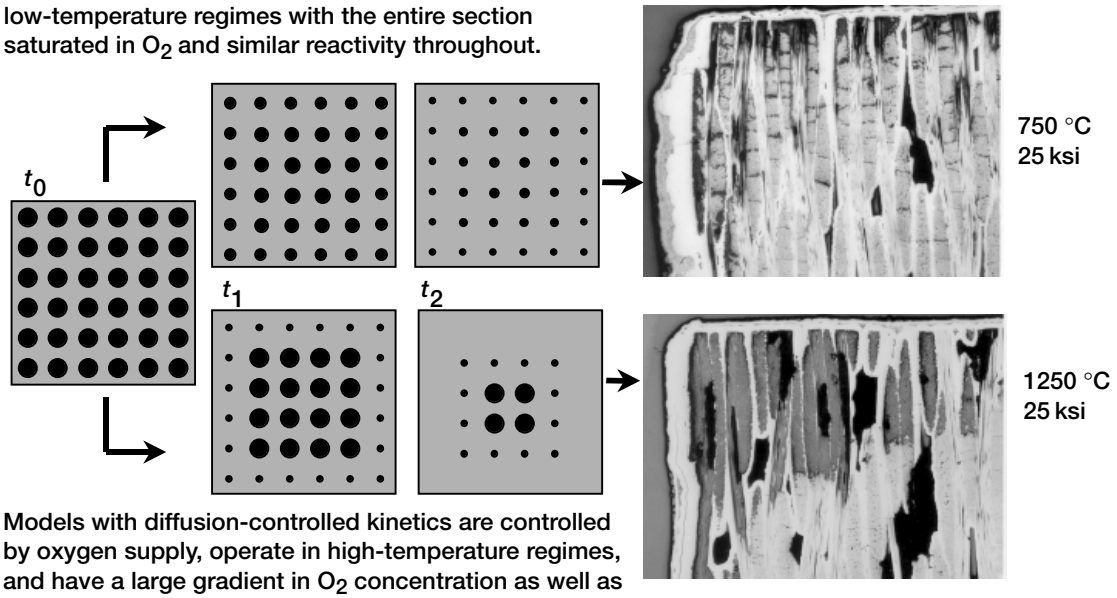

Oxidation model for carbon fibers in a CMC as a function of temperature.

The model allows the local oxygen concentrations and carbon volumes from the edge to the interior of the composite to be determined over time. Oxidation damage predicted by the model was compared with that observed from microstructural analysis of experimentally tested composite material to validate the model for two temperatures of interest.

When the model is run for low-temperature conditions, the kinetics are reaction controlled. Carbon and oxygen reactions occur relatively slowly. Therefore, oxygen can bypass the carbon near the outer edge and diffuse into the interior so that it saturates the entire composite at relatively high concentrations. The kinetics are limited by the reaction rate between carbon and oxygen. This results in an interior that has high local concentrations of oxygen and a similar amount of consumed carbon throughout the cross section.

When the model is run for high-temperature conditions, the kinetics are diffusion controlled. Carbon and oxygen reactions occur very quickly. The carbon consumes oxygen as soon as it is supplied. The kinetics are limited by the relatively slow rate at which oxygen is supplied in comparison to the relatively fast rate at which carbon and oxygen reactions occur. This results in a sharp gradient in oxygen concentration from the edge where it is supplied to the nearest source of carbon, which is where the oxygen is quickly consumed. A moving reaction front is seen in which the outlaying carbon is consumed before the next inner layer of carbon begins to react.

The model allows for the oxidation of reinforcing carbon fibers within a CMC to be studied with input parameters that relate to application conditions (environment, temperature, and stress). With correlation to failure models, the oxidation model can be used to determine strength reduction and/or failure of CMCs due to oxidation of the reinforcing carbon fibers.

Find out more about this research:
http://www.grc.nasa.gov/WWW/MDWeb/

U.S. Army Vehicle Technology Directorate at Glenn contact:
Michael C. Halbig, 216–433–2651, Michael.C.Halbig@grc.nasa.gov

Authors: Michael C. Halbig, Dr. James D. Cawley, and Dr. Andrew J. Eckel

Headquarters program office: OAT

Programs/Projects: Gen 3

Cooled Ceramic Composite Panel Tested Successfully in Rocket Combustion Facility

Regeneratively cooled ceramic matrix composite (CMC) structures are being considered for use along the walls of the hot-flow paths of rocket-based or turbine-based combined-cycle propulsion systems. They offer the combined benefits of substantial weight savings, higher operating temperatures, and reduced coolant requirements in comparison to components designed with traditional metals. These cooled structures, which use the fuel as the coolant, require materials that can survive aggressive thermal, mechanical, acoustic, and aerodynamic loads while acting as heat exchangers, which can improve the efficiency of the engine.

A team effort between the NASA Glenn Research Center, the NASA Marshall Space Flight Center, and various industrial partners has led to the design, development, and fabrication of several types of regeneratively cooled panels. The concepts for these panels range from ultra-lightweight designs that rely only on CMC tubes for coolant containment to more maintainable designs that incorporate metal coolant containment tubes to allow for the rapid assembly or disassembly of the heat exchanger. One of the cooled panels based on an all-CMC design was successfully tested in the rocket combustion facility at Glenn. Testing of the remaining four panels is underway.

The all-CMC cooled panel, developed by Rockwell Science Center, consists of a woven coolant channel design that increases heat exchanger efficiency by employing thin CMC walls to maximize heat transfer and by eliminating metal coolant tubes, which can lead to increased thermal contact resistance at the tube-to-CMC interface. The CMC material used in this design consists of carbon-fiber-reinforced silicon carbide. Thin wall tubes were fabricated by a combination of fiber-preforming and polymer-impregnated pyrolysis techniques. The cooling channels were formed during the weaving process. This process results in an array of integrally woven tubes with greater structural integrity

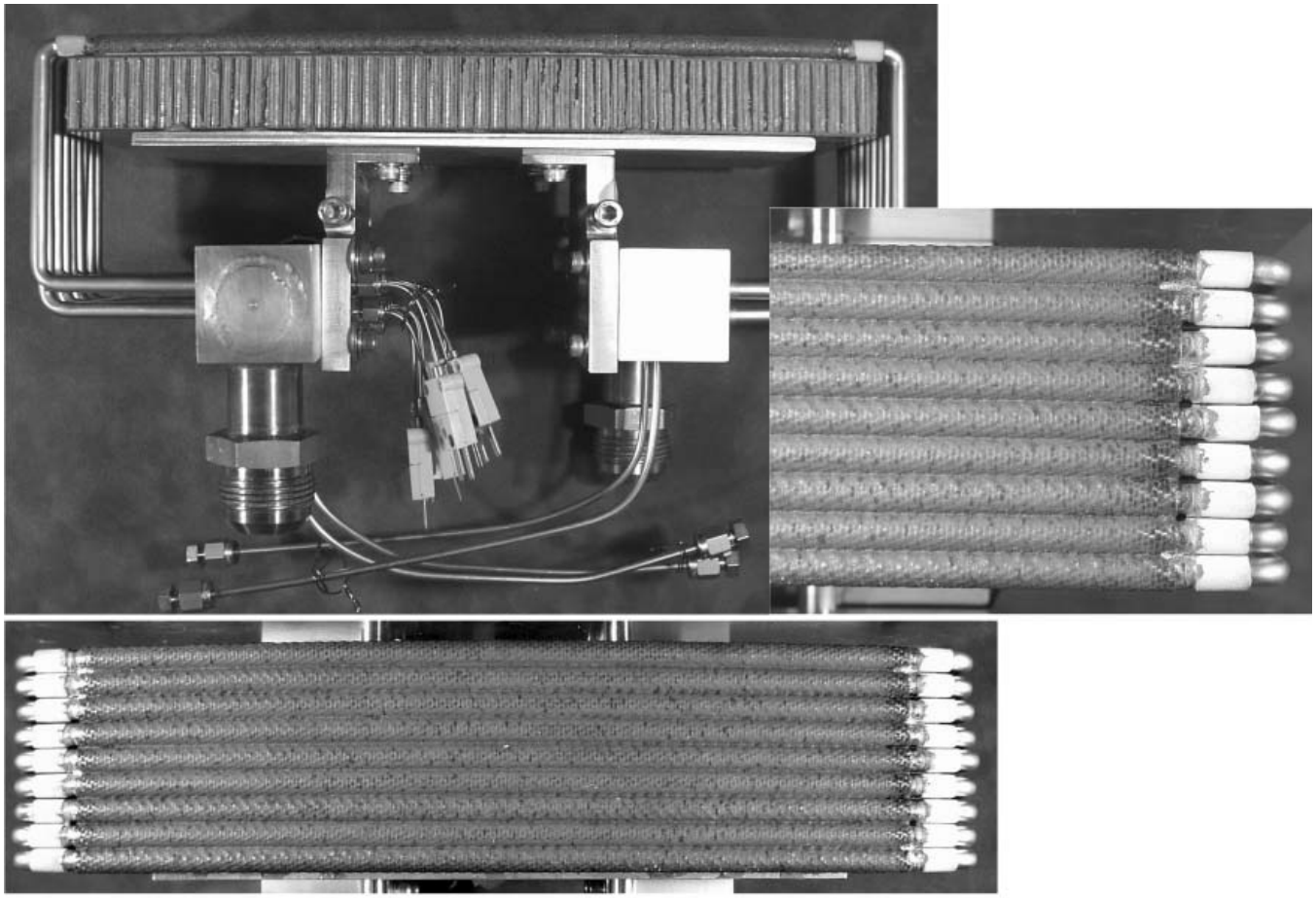

Cooled CMC panel with woven coolant channels before test firing.

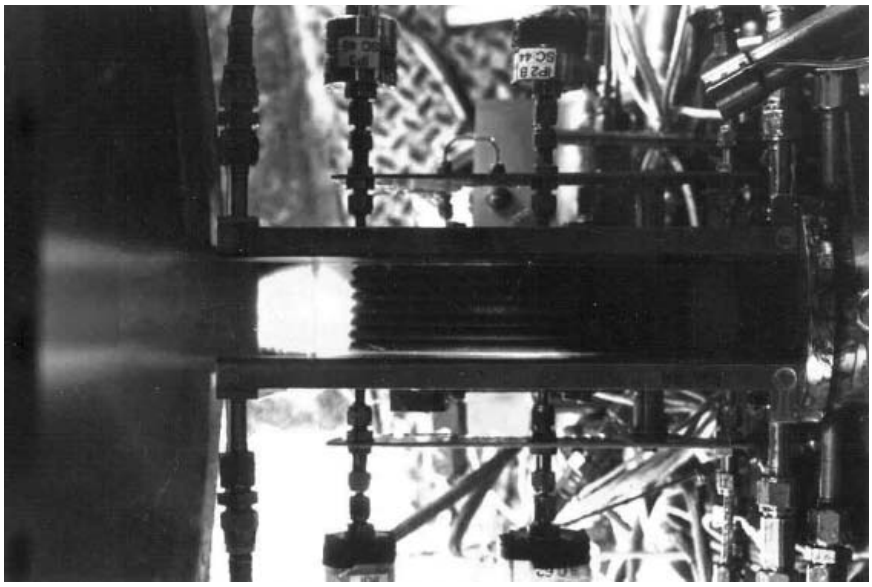

Woven CMC coolant channel design being tested in rocket engine with gaseous hydrogen and oxygen.

at the tube-to-tube connections. Metal tubes brazed at either end of the CMC panel serve as a coolant delivery system. The 2.5- by 10-in. cooled CMC panels were tested under rocket combustion conditions with gaseous hydrogen and gaseous oxygen as the propellants. A rectangular nozzle was designed for the engine to simulate two-dimensional flow over the panels. For these subscale ground-based tests, water was used as the coolant. The cooled CMC structure survived the test without any coolant leakage and without any visible structural damage. Testing of this panel is continuing with increasingly aggressive engine conditions, longer duration runs, and increased cycles.

Find out more about this research:
http://www.grc.nasa.gov/WWW/Ceramics/homepage.htm

Glenn contact:
Martha H. Jaskowiak, 216–433–5515, Martha.H.Jaskowiak@nasa.gov

Author: Martha H. Jaskowiak

Headquarters program office: OAT

Programs/Projects: Gen 3, Hypersonics Investment Area

Uncooled C/SiC Composite Chamber Tested Successfully in Rocket Combustion Lab

In a joint effort between the NASA Glenn Research Center, the NASA Marshall Space Flight Center, Material Research and Design, Inc., Boeing Rocketdyne, and GE Powers Systems Composites, an uncooled carbon-fiber-reinforced silicon carbide (C/SiC) ceramic matrix composite (CMC) was developed and successfully tested in Glenn's Rocket Combustion Lab. CMCs offer the potential for substantial weight saving over traditional metallic parts. When uncooled, an additional savings in weight can be achieved because the complex structures associated with the cooling system can be reduced. Several designs were considered, including a double-walled, braided CMC chamber exhibiting permeability at –12 to –13 log Darcy's constant.

On the basis of gas-permeability considerations, the double-walled, braided design was selected for hot fire testing. This design consists of two C/SiC melt-infiltration composite cylinders in coaxial formation joined to a metal injector and nozzle component. The braided

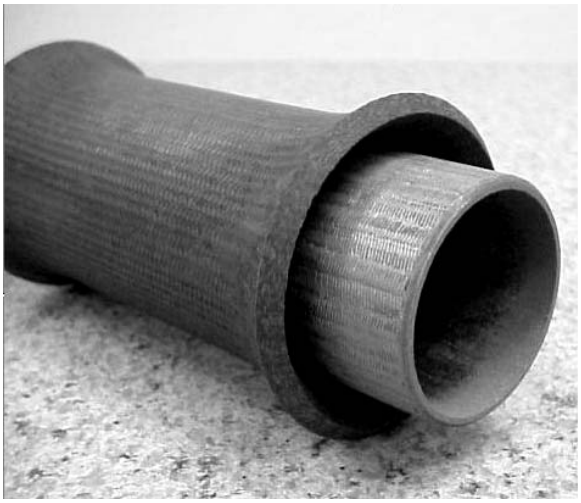

Uncooled C/SiC melt-infiltration composite cylinders.

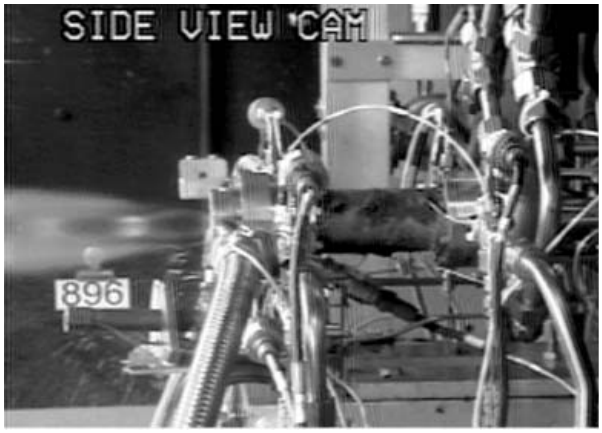

Uncooled C/SiC melt-infiltration composite being hot-fire tested.

architectures of the inner and outer cylinder, respectively, were configured to address the design needs for hoop and axial load integrity. The cylinders were fabricated by GE Powers Systems Composites, formerly known as Honeywell Advanced Composites, Inc.

The CMC combustion chamber was hot-fire tested in Glenn's rocket combustion laboratory. The objective of this test was to assess the CMC combustion chamber's performance under rocket firing conditions. Of particular interest were the hot gas permeability through the composite walls and the structural integrity of the chamber. Testing was conducted in a gaseous O_2/H_2 environment. The test matrix included an oxygen-to-hydrogen ratio of 1.5 for 14 runs with chamber pressures ranging from 100 to 1000 psi. Steady-state internal wall temperatures of the inner cylinder were in excess of 2600 °F, with the outer cylinder's outer wall temperatures averaging 1000 °F for successful 10-sec runs.

The tests demonstrated that the hot gases could be contained inside the CMC combustion chamber without permeating through the CMC walls. The tests also demonstrated the structural integrity of the CMC combustion chamber under rocket firing conditions.

Find out more about this research:

Glenn's Ceramics Branch:
http://www.grc.nasa.gov/WWW/Ceramics/homepage.htm

Space Transportation at Glenn:
http://stpo.grc.nasa.gov/home.htm

Glenn contact:
Dr. Jerry Lang, 216–433–6675, Jerry.Lang-1@nasa.gov

Author: Dr. Jerry Lang

Headquarters program office: OAT

Programs/Projects: STPO

Ultra-High-Temperature Ceramics Evaluated for Aeropropulsion Use

Ultra-high-temperature ceramics (UHTC) are a group of materials consisting of zirconium diboride (ZrB_2) or hafnium diboride (HfB_2) plus silicon carbide (SiC), and in some instances, carbon (C). They offer a combination of properties that make them candidates for airframe leading edges on sharp-bodied reentry vehicles. These UHTCs perform well in the environment for such applications (i.e., air at low pressures). The purpose of this study at the NASA Glenn Research Center was to examine three of these materials under conditions more representative of a propulsion environment: that is, higher oxygen partial pressure and total pressure. Relatively long, multiple-exposure cycles were emphasized. We completed an in-house study of ZrB_2 plus 20 vol% SiC (abbreviated as ZS), ZrB_2 plus 14 vol% SiC and 30 vol% C (ZSC), and SCS-9a SiC fiber-reinforced ZrB_2 plus 20 vol% SiC (ZSS). HfB_2-based compositions were not included in the study because of their high cost.

The capability of UHTC for propulsion applications must be compared with that of mature, available, and commercially used ceramics such as silicon nitride (e.g., AS–800) to put things in proper perspective. In terms of mechanical properties, UHTCs fall short in terms of strength and fracture toughness. At about 1300 °C, the creep resistance of ZS appears to be superior to the creep resistance reported for AS–800. However, the stress rupture life for Si_3N_4 under stress and temperature conditions similar to those used in this study is measured in hundreds of hours. Because of oxidation, ZS could not achieve such lives.

In terms of oxidation resistance, acceptable amounts of material recession in 1 hour to thousands of hours, depending on the specific propulsion application, are on the order of 100 to 300 μm. This converts to an acceptable range of parabolic recession rate constants k_p" of

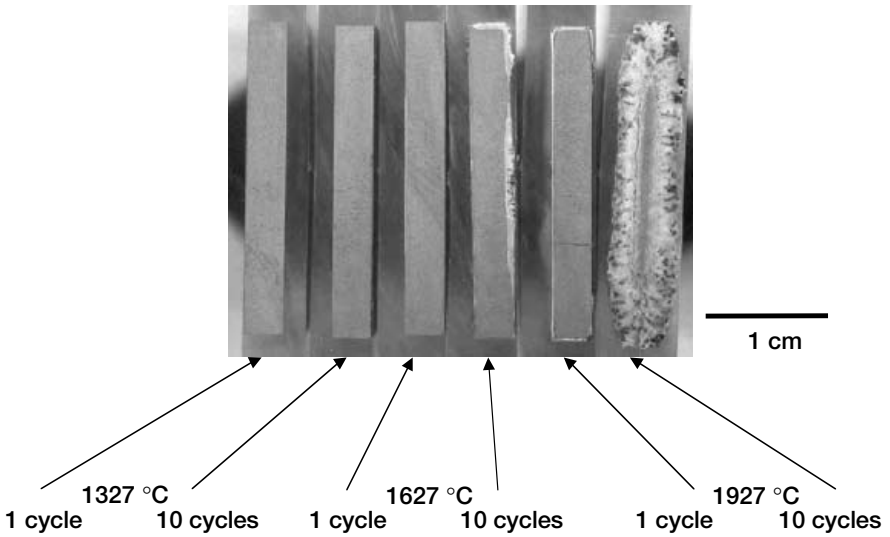

Cross sections of ZrB_2-SiC oxidized in air for 10-min cycles show rapid attack.

approximately less than or equal to 10^{-1} to 10^{-2} mm^2/hr for a 1-hr application. For a 100-hr application, an acceptable range of k_p" would be less than or equal to those values divided by 100. For the more oxidation resistant ZS material, measured parabolic recession rate constants were $4.7+10^{-3}$ mm^2/hr at 1327 °C, $7.8+10^{-2}$ mm^2/hr at 1627 °C, and 1.3 mm^2/hr at 1927 °C. Thus, recession rate constants for ZS are acceptable at 1327 °C for a 1-hr application, but here silicon nitride is a superior material. At 1627 °C, ZS oxidation is marginal for a 1-hr application, but dimensional growth would be an issue. In a 100-hr application, ZS cannot be considered at any temperature.

Our cursory examination of thermal shock, both from a theoretical and experimental viewpoint, indicated that the ZS and ZSC UHTCs are inferior to AS–800 silicon nitride. On the basis of this limited study, UHTCs are not ready to be considered as aeropropulsion materials for any applications longer than a few minutes. Current materials suffer from aggressive oxidation and moisture attack (Quynhgiao Nguyen, NASA Glenn, and Raymond C. Robinson, QSS Group, Inc., Cleveland, OH, 2002, private communication), and they are susceptible to thermal shock. For long-term propulsion applications, major improvements in environmental durability are needed. Work is in progress to improve the oxidation resistance of UHTC materials.

Find out more about this research:

Glenn's Ceramics Branch:
http://www.grc.nasa.gov/WWW/Ceramics/homepage.htm

Glenn's Environmental Durability Branch:
http://www.grc.nasa.gov/WWW/EDB/

Bibliography
Levine, Stanley, R., et al.: Evaluation of Ultra-High Temperature Ceramics for Aeropropulsion Use. J. Eur. Ceram. Soc., vol. 22, 2002, pp. 2757–2767.

Glenn contact:
Dr. Stanley R. Levine, 216–433–3276, Stanley.R.Levine@nasa.gov

Cleveland State University contact:
Dr. Elizabeth J. Opila, 216–433–8904, Elizabeth.J.Opila@grc.nasa.gov

Authors: Dr. Stanley R. Levine, Dr. Elizabeth J. Opila, Michael C. Halbig, James D. Kiser, Dr. Mrityunjay Singh, and Dr. Jonathan A. Salem

Headquarters program office: OAT

Programs/Projects:
Propulsion Systems R&T, UEET, STR

Polymer/Silicate Nanocomposites Developed for Improved Strength and Thermal Stability

Over the past decade, polymer-silicate nanocomposites have been attracting considerable attention as a method of enhancing polymer properties. The nanometer dimensions of the dispersed silicate reinforcement can greatly improve the mechanical, thermal, and gas barrier properties of a polymer matrix.

In a study at the NASA Glenn Research Center, the dispersion of small amounts (< 5 wt%) of an organically modified layered silicate (OLS) into the polymer matrix of a carbon-fiber-reinforced composite has improved the thermal stability of the composite. The enhanced barrier properties of the polymer-clay hybrid are believed to slow the diffusion of oxygen into the bulk polymer, thereby slowing oxidative degradation of the polymer. Electron-backscattering images show cracking of a nanocomposite matrix composite in comparison to a neat resin matrix composite. The images show that dispersion of an OLS into the matrix resin reduces polymer oxidation during aging and reduces the amount of cracking in the matrix significantly.

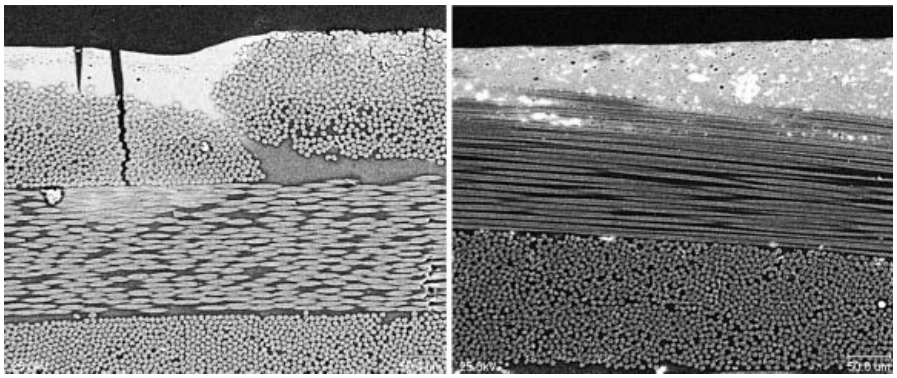

Electron backscatter images. Left: Neat resin (BAX) matrix composite. Right: Nanocomposite (BAX-2 wt% OLS) matrix composite.

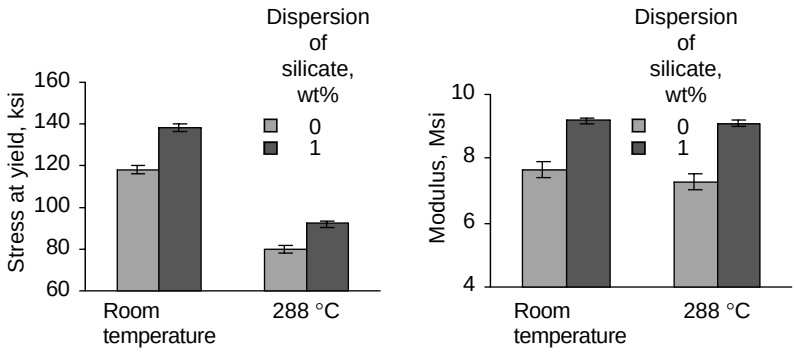

Improvements in strength and modulus with the addition of OLS.

Improvements in composite flexural strength, flexural modulus, and interlaminar shear strength were also obtained with the addition of OLS. An increase of up to 15 percent in these mechanical properties was observed in composites tested at room temperature and 288 °C. The best properties were seen with low silicate levels, 1 to 3 wt%, because of the better dispersion of the silicate in the polymer matrix.

Glenn contact:
Sandi Campbell, 216–433–8489,
Sandi.G.Campbell@nasa.gov

Author: Sandi G. Campbell

Headquarters program office: OAT

Programs/Projects:
Propulsion Systems R&T, ZCET

New Method Developed To Purify Single Wall Carbon Nanotubes for Aerospace Applications

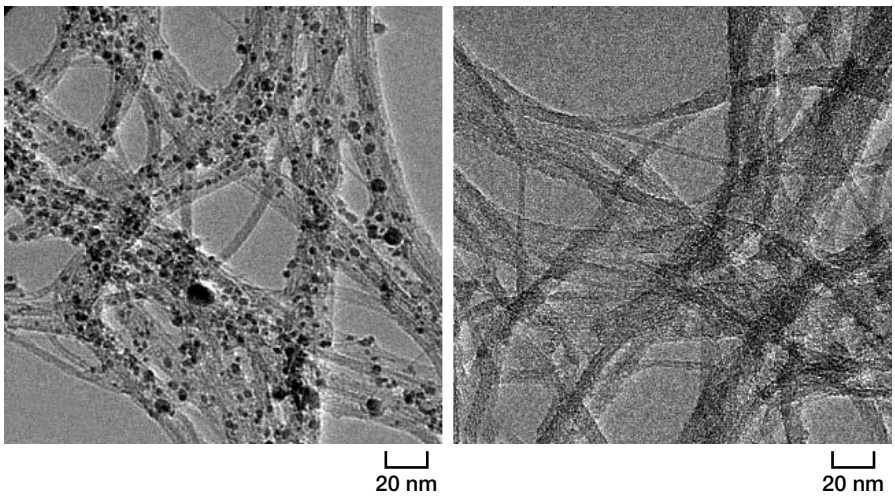

Transmission electron micrographs of carbon nanotubes. Left: Crude. Right: Purified. Note the absence of iron catalyst particles (black spots) in the purified tubes.

Single wall carbon nanotubes have attracted considerable attention because of their remarkable mechanical properties and electrical and thermal conductivities. Use of these materials as primary or secondary reinforcements in polymers or ceramics could lead to new materials with significantly enhanced mechanical strength and electrical and thermal conductivity. Use of carbon-nanotube-reinforced materials in aerospace components will enable substantial reductions in component weight and improvements in durability and safety. Potential applications for single wall carbon nanotubes include lightweight components for vehicle structures and propulsion systems, fuel cell

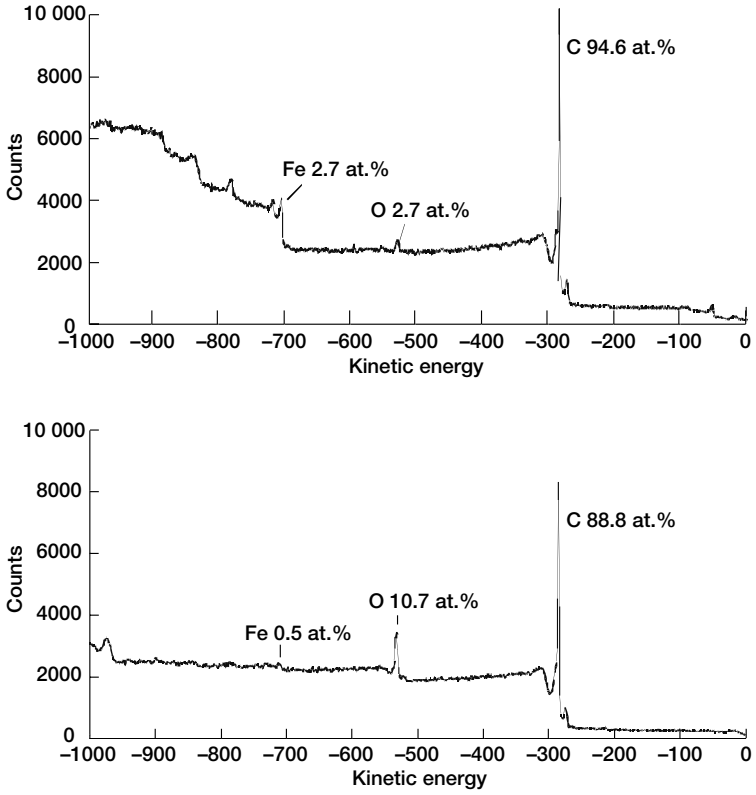

X-ray photoelectron spectra of carbon nanotubes. Top: Crude. Bottom: Purified. Note the decrease in iron content in the purified tubes and the increased oxygen content due to the formation of carboxylic acid groups on the nanotube surface.

components (bipolar plates and electrodes) and battery electrodes, and ultralightweight materials for use in solar sails.

A major barrier to the successful use of carbon nanotubes in these components is the need for methods to economically produce pure carbon nanotubes in large enough quantities to not only evaluate their suitability for certain applications but also produce actual components. Most carbon nanotube synthesis methods, including the HiPCO (high-pressure carbon monoxide) method developed by Smalley and others (ref. 1), employ metal catalysts that remain trapped in the final product. These catalyst impurities can affect nanotube properties and accelerate their decomposition. The development of techniques to remove most, if not all, of these impurities is essential to their successful use in practical applications.

A new method has been developed at the NASA Glenn Research Center to purify gram-scale quantities of single wall carbon nanotubes. This method, a modification of a gas-phase purification technique previously reported by Smalley and others (ref. 2), uses a combination of high-temperature oxidations and repeated extractions with nitric and hydrochloric acid. This improved procedure significantly reduces the amount of impurities (catalyst and nonnanotube forms of carbon) within the nanotubes, increasing their stability significantly. The onset of decomposition of the purified nanotubes (determined by thermal gravimetric analysis in air) is more than 300 °C higher than that of the crude nanotubes. Transmission electron microscopy analysis of nanotubes purified by this method reveals near complete removal of iron catalyst particles (see the preceding photomicrographs). Analysis of the nanotubes using inductively coupled plasma spectroscopy revealed that the iron content of the nanotubes was reduced from 22.7 wt% in the crude nanotubes to less than 0.02 wt%. X-ray photoelectron spectroscopy (see the graphs) revealed a decrease in iron content after purification as well as an increase in oxygen content due to the formation of carboxylic acid groups on the surface of the nanotubes. Nanotubes purified by this improved method can be readily dispersed in common organic solvents, in particular N,N dimethylformamide, using prolonged ultrasonic treatment. These dispersions can then be used to incorporate single wall carbon nanotubes into polymer films.

This work is a collaboration between Glenn and the NASA Center for High Performance Polymers and Composites at Clark Atlanta University.

Find out more about research by Glenn's Polymers Branch:
http://www.grc.nasa.gov/WWW/MDWeb/5150/Polymers.html

References

1. Nikolev, Pavel, et al.: Gas-Phase Catalytic Growth of Single-Walled Carbon Nanotubes From Carbon Monoxide. Chem. Phys. Lett., vol. 313, nos. 1–2, 1999, pp. 91–97.
2. Chiang, I.W., et al.: Purification and Characterization of Single-Wall Carbon Nanotubes (SWNTs) Obtained From the Gas-Phase Decomposition of CO (HiPco Process). J. Phys. Chem. B., vol. 105, no. 35, 2001, pp. 8297–8301.

Glenn contact:
Dr. Michael A. Meador, 216–433–9518, Michael.A.Meador@nasa.gov

Clark Atlanta University contact:
Marisabel Lebron, 216–433–2292, Marisabel.Lebron@grc.nasa,gov

Authors: Marisabel Lebron and Dr. Michael A. Meador

Headquarters program office: OAT

Programs/Projects:
Propulsion and Power, RAC

High-Temperature Polymer Composites Studied for Space Propulsion Applications

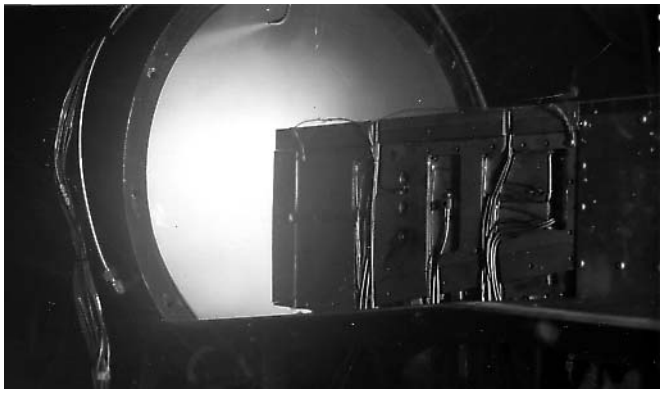

Combustion chamber on a rocket-based combined-cycle demonstrator.

Polyimide composites are being used in lightweight support structures designed to preserve the flow geometry within thin shell combustion chambers of future space launch propulsion systems. The flexible shell chamber is a rectangular metallic tube (as shown in the photograph). Principles of lightweight design and innovative manufacturing techniques have yielded an asymmetric sandwich structure that can sustain the applied thermal, acoustic, and pressure loads. The Boeing-Rocketdyne-designed thin-wall inner shell contains cooling channels that transport heat and maintain component temperature. Titanium honeycomb is bonded to the metal inner shell, and the outer surface is faced with a thin carbon fiber polyimide skin. Whereas the continuous carbon fiber enables a laminated skin of high specific stiffness, the polyimide matrix resin ensures that the rigidity and durability is maintained at high temperatures. As a supporting engine flow path structure, strong flexural rigidity is required since deflections and distortions due to operation loading are held to strict limits. Significant weight savings (~30 wt%) over the all-metal support structure are expected.

The prototype structure is the result of ongoing collaboration between the Boeing Company and the NASA Glenn Research Center seeking to introduce polyimide composites to the harsh environmental loads familiar to space launch propulsion systems. Thermal, physical, and mechanical properties of the composites and sandwich structures were studied over a range of hygrothermal states. A variety of graphite fiber architectures (unidirectional, woven fabrics, triaxially braided, and stitch patterns) were examined to optimize the component design. Several in-service exposure simulation tests—such as isothermal biaxial loading, plate flexure, thermal mechanical fatigue, rapid heating hygrothermal cycling, and combinations of these experiments—will verify the durability of high-temperature polymer matrix composites in reusable space vehicle propulsion structures.

Design tradeoff analyses were carried out using relevant closed-form solutions and approximations for high-temperature polymer composites in sandwich beams and panels. Analyses confirm that significant thermal stresses exist when materials whose coefficients of thermal expansion (CTEs) differ by a factor of 10 are combined (such as a polymer composite and titanium and steel structures). A full-scale combustion chamber support structure will be hot-fire tested on the basis of the composite sandwich structure's stress analysis, performance, and durability data.

Find out more about the research of Glenn's Polymers Branch:
http://www.grc.nasa.gov/WWW/MDWeb/5150/Polymers.html

Glenn contact:
Dr. James K. Sutter, 216–433–3226, James.K.Sutter@nasa.gov

Ohio Aerospace Institute (OAI) contacts:
E. Eugene Shin, 216–433–2544, Euy-sik.E.Shin@grc.nasa.gov; and Dr. John C. Thesken, 216–433–3012, John.C.Thesken@grc.nasa.gov

Authors: Dr. John C. Thesken, E. Eugene Shin, Jeffery Fink, and Dr. James K. Sutter

Headquarters program office: OAT

Programs/Projects:
Propulsion and Power, HOTPC

Multiple Knudsen Cell Configuration Improved for Alloy Activity Studies

Knudsen effusion mass spectrometry (KEMS) allows the simultaneous determination of the identity and pressure of vapor species in equilibrium with a condensed phase as a function of temperature (ref. 1). This information can be used to determine the thermodynamic properties of materials. The partial pressure of species *j* in the cell is related to the measured intensity of the ion *k* formed from *j*, I_{jk}^{+}, and the absolute temperature *T,* where S_{jk} is the sensitivity factor.

$$p_j = \frac{I_{jk}^{+} T}{S_{jk}} \qquad (1)$$

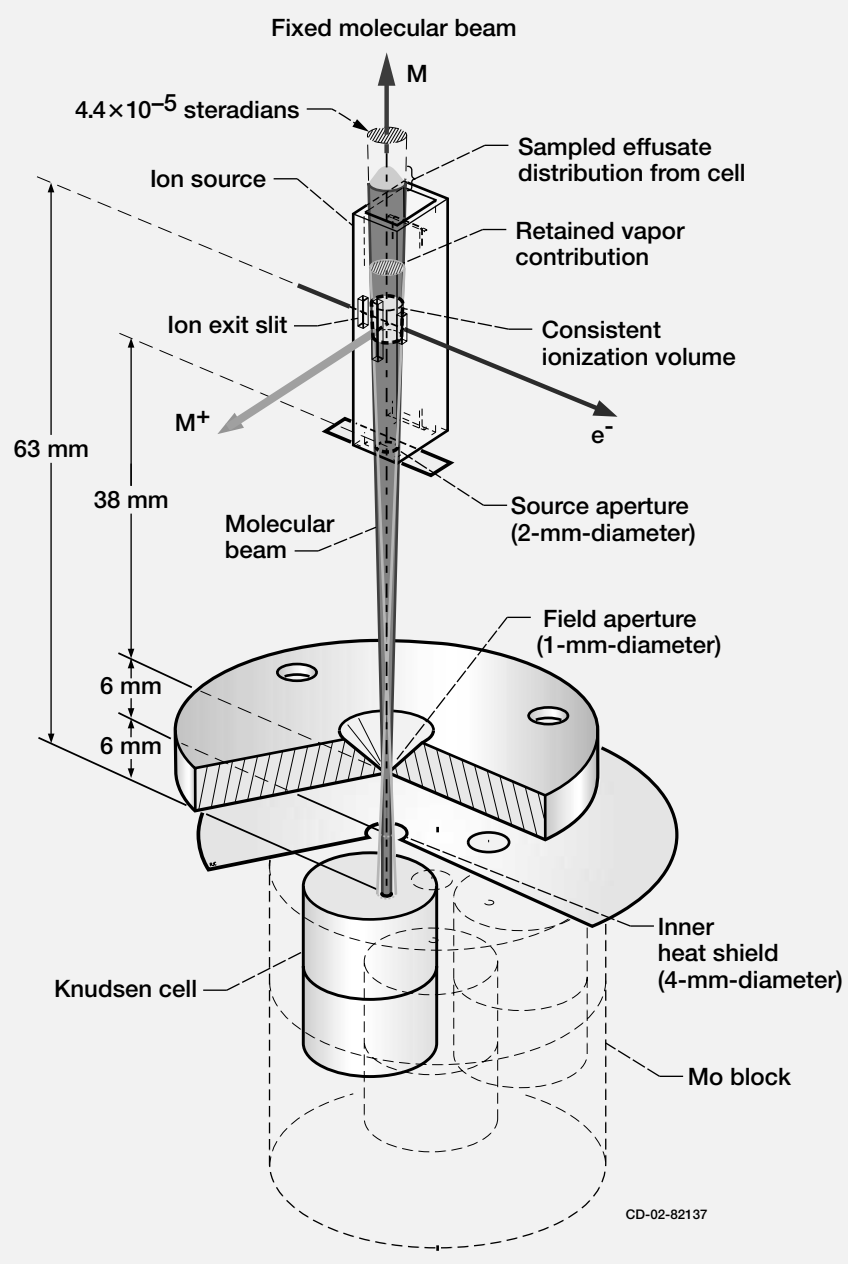

Schematic of the fixed field and source apertures that attenuate a fixed molecular beam. The effusate is sampled by accurately aligning each cell with the fixed apertures.

Measurement of absolute pressures requires the determination of S_{jk}, which is a difficult problem in KEMS. The inclusion of multiple effusion cells in the isothermal zone of a furnace allows direct comparison of the partial pressure of species in equilibrium with various condensed samples and can remove the need to determine S_{jk}. This provides a method to directly determine the thermodynamic activity of solution components at elevated temperatures (refs. 2 to 4), where *A* and *R* represent measurements from the alloy and reference, respectively.

$$a_j = \frac{P_j(A)}{P_j(R)} = \frac{I_{jk}^{+}(A) \cdot T}{I_{jk}^{+}(R) \cdot T} \cdot \frac{S_{jk}(R)}{S_{jk}(A)} = \frac{I_{jk}^{+}(A)}{I_{jk}^{+}(R)} \qquad (2)$$

Despite its theoretical simplicity, it is based on S_{jk} remaining constant, which introduces a range of challenging experimental conditions. All these issues have been resolved in a comprehensive redesign of the multiple-cell configuration of KEMS at the NASA Glenn Research Center that now allows accurate activity measurements to be made in a range of important metallic and ceramic systems. The following is a brief summary of the major changes.

Two fixed apertures—field and source apertures—were added between the effusion cell and the ion source (shown on the left). These apertures define a fixed molecular beam and maintain a constant ionization volume, while an

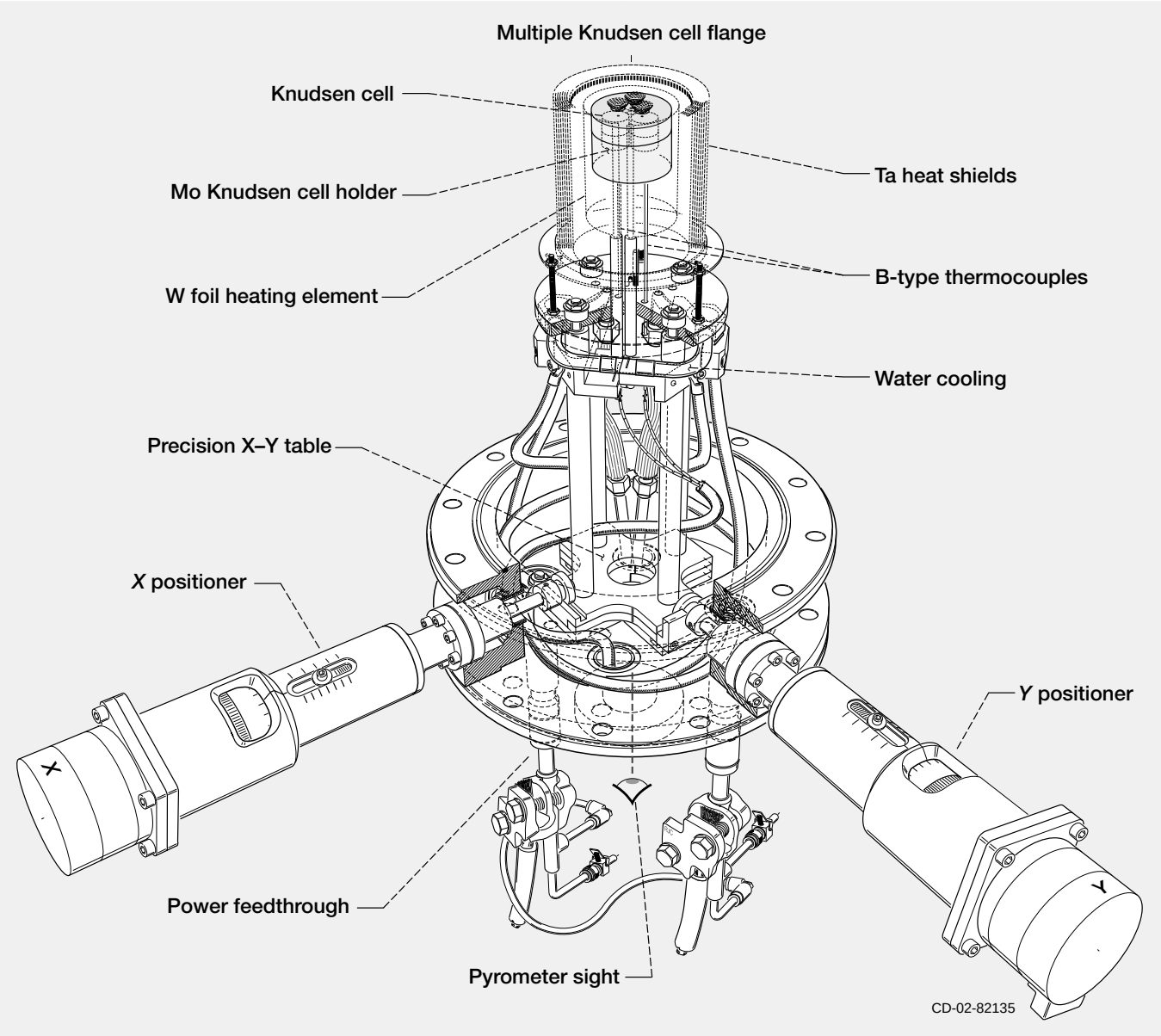

Effusion cell furnace and the X–Y table that is used to accurately position the effusion cells.

accurate positioning mechanism (automated X–Y table, shown here) ensures that the same portion of the effusate distribution is sampled from all cells (refs. 5 to 9). The relative difference in effusate distribution, due to variation in orifice shape, is measured by loading a reference material into all cells and comparing the ion intensities (refs. 7 to 9). With these changes, the factors affecting the measured ion intensity of species effusing from a cell are limited to the composition and temperature of the condensed sample.

This technique relies on the ability to sample the effusate from all cells at one temperature and, therefore, a furnace that can maintain a constant temperature with time and cell position and has an isothermal zone large enough to contain all effusion cells. A resistance furnace was constructed by placing three effusion cells, with radial symmetry (ref. 10) in a molybdenum block at the center, surrounded by a cylindrical tungsten sheet-heating element (25-μm-thick) and a seven-layer tantalum heat-shield pack. A sheet-heating element provides the most uniform radiation heat transfer, while conduction in the molybdenum block further reduces any thermal gradients. The required temperature stability was achieved after separating the water-cooling circuit from the electrical power circuit. The temperature of each effusion cell is measured independently with B-type thermocouples and a single-color, disappearing filament optical pyrometer.

These changes have created a world-class facility for the study of the thermodynamics of metallic and ceramic systems. This type of fundamental information is required to understand the behavior of materials used at high temperatures. Current studies are focused on Ti- and Ni-based alloys.

Acknowledgments
The X–Y table was designed by Ben Ebihara and fabricated by W. Wazniac. A computer program developed by Dr. Judith Auping controls all aspects of the KEMS operation: data acquisition, furnace control, mass analysis, ion counting, and movement of the X–Y table. We also thank Dr. C. Chatillon of LPTCM, ENSEEG, Grenoble, France.

Find out more about this research:
http://www.grc.nasa.gov/WWW/EDB/Facilities/mass.htm

References

1. Inghram, Mark G.; and Drowart, Jean: Mass Spectrometry Applied to High Temperature Chemistry. Proceedings of an International Symposium on High Temperature Technology, McGraw-Hill, New York, NY, 1959, pp. 219–240.
2. Bucheler, A.; and Stauffer, J.J.: Thermodynamics; Proceedings. Proceedings of the Symposium on Thermodynamics with Emphasis on Nuclear Materials and Atomic Transport in Solids, IAEA, Vienna, 1966, p. 271.
3. Pattoret, A.; Smoes, S.; and Drowart, J.: Thermodynamics; Proceedings. Proceedings of the Symposium on Thermodynamics with Emphasis on Nuclear Materials and Atomic Transport in Solids, IAEA, Vienna, 1966, p. 377.
4. Morland, P.; Chatillon, C.; and Rocabois P.: High-Temperature Mass Spectrometry Using the Knudsen Effusion Cell I—Optimization of Sampling Constraints on the Molecular Beam. High Temp. Mater. Sci., vol. 37, no. 3, 1997, pp. 167–187.
5. Whitman, Charles I.: On the Measurement of Vapor Pressures by Effusion. J. Chem. Phys., vol. 20, no. 1, 1952, pp. 161–164.
6. Motzfeldt, Ketil: The Thermal Decomposition of Sodium Carbonate by the Effusion Method. J. Phys. Chem., vol. LIX, 1955, pp. 139–147.
7. Wang, K.C.; and Wahlbeck, P.G.: Effusion. I. Angular Number Distributions of Gaseous CsCl from a Near-Ideal Orifice into Vacuum. J. Chem. Phys., vol. 47, no. 11, 1967, pp. 4799–4809.
8. Wahlbeck, P.G.; and Phipps, T.E.: Effusion II. Angular Number Distributions of Gaseous Cadmium from a Right-Circular Cylindrical Orifice into Vacuum. J. Chem. Phys., vol. 49, no. 4, 1968, pp. 1603–1608.
9. Grimley, Robert T.; Wagner, L.C.; and Castle, Peter M.: Angular Distributions of Molecular Species Effusing from Near-Ideal Orifices. J. Phys. Chem., vol. 79, no. 4, 1975, pp. 302–308.
10. Chatillon, C., et al.: High-Temperature Mass Spectrometry With the Knudsen Cell: II. Technical Constraints in the Multiple-Cell Method for Activity Determinations. High Temp. High Pressures, vol. 34, no. 2, 2002, pp. 213–233.

Case Western Reserve University contact:
Evan Copland, 216–433–3738,
Evan.H.Copland@grc.nasa.gov

Glenn contact:
Dr. Nathan Jacobson, 216–433–5498,
Nathan.S.Jacobson@nasa.gov

Authors: Evan H. Copland and
Dr. Nathan S. Jacobson

Headquarters program office: OAT

Programs/Projects: HOTPC, UEET

Studies Conducted of Sodium Carbonate Contaminant Found on the Wing Leading Edge and the Nose Cap of the Space Shuttle Orbiter

In early 2001, three of the space shuttle orbiters were found to have a sodium carbonate contaminant on the wing leading edge and nose cap. These parts are made of a reinforced carbon/carbon material protected by silicon carbide (SiC) and a glass coating. The glass coating is known as Type A and is primarily sodium silicate with particles of SiC. NASA Glenn Research Center's Environmental Durability Branch was asked to determine the chemistry of this deposit formation and assess any possible detrimental effects.

A thorough literature review revealed that sodium silicate and sodium carbonate are often found together. At high temperatures, sodium silicate (written in general terms as $Na_2O \cdot n(SiO_2)$) is made from sodium carbonate (Na_2CO_3) and silica (SiO_2) from the following reaction:

$$Na_2CO_3 + nSiO_2 = Na_2O \cdot n(SiO_2) + CO_2$$

At low temperatures, the reverse reaction is favorable. Previous studies of the corrosion of glass show that carbon dioxide in the presence of water does form sodium carbonate on sodium silicate glass (ref. 1). It is quite likely that a similar scenario exists for the orbiter wing leading edge. All three orbiters that formed sodium carbonate were exposed to rain.

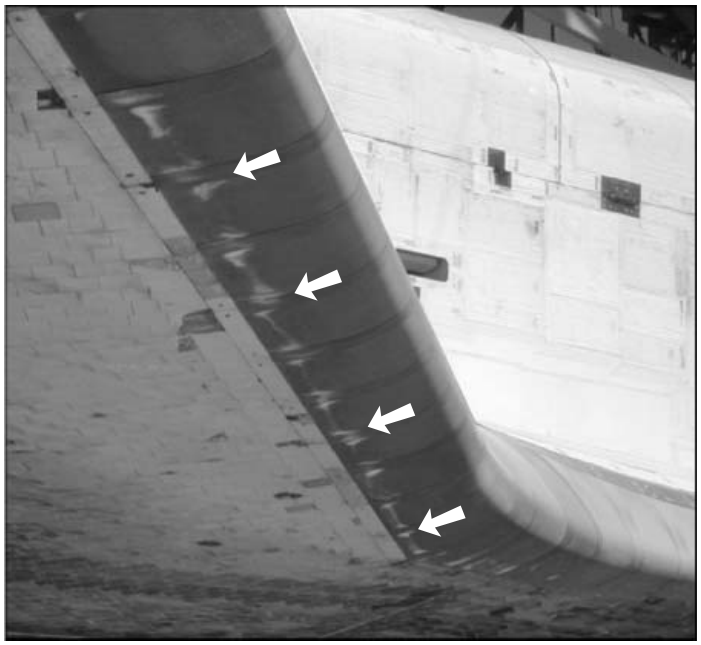

Carbonate deposit (see white arrows) found under wing leading edge. Photograph courtesy of Michael Gordon, NASA Kennedy Space Center.

This formation of sodium carbonate was duplicated in the laboratory. The Type A glass, which coats the wing leading edge and nose cap, was made in a freestanding form and exposed to water in two separate experiments. In one set of experiments, the coating was placed in a petri dish filled with water. As the water evaporated, sodium carbonate formed. In another case, water was slowly dripped on the coating and sodium carbonate formed. The sodium carbonate was detected by chemical analysis and, in some cases, x-ray diffraction showed a hydrated sodium carbonate.

The next step was to examine possible detrimental effects of this sodium carbonate. There are three likely scenarios for the sodium carbonate deposit: (1) it may be removed with a simple rinse, (2) it may remain and flow back into the Type A glass after heating during reentry, or (3) it may remain and flow onto unprotected SiC and/or other parts after heating during reentry. The effect of case 1 is to remove the Na_2O constituent from the Type A glass, thus decreasing its effectiveness as a sealant. Even so, overall, it is probably the best approach and was used by the NASA Kennedy Space Center when the deposits were first observed. The effect of case 2 is minimal and would actually restore the the Type A glass to its composition before carbonate formation. However, the problem with allowing the carbonate to remain leads to the third scenario, the deposit flowing onto other parts. A series of tests were conducted on unprotected SiC, and minimal effects were found in the short-term, but other ceramic and metal parts could be damaged by the molten sodium carbonate and would require close monitoring.

Reference

1. Darby, G.; Clark, D.; and Simmons, J.: FT–IRRS Analysis of Surface Reactions in Alkali Silicate Glasses. Ceram. Trns., vol. 101, 2000, pp. 141–151.

Glenn contact:
Dr. Nathan S. Jacobson, 216–433–5498, Nathan.S.Jacobson@nasa.gov

Kennedy contact:
Jaime Palou, 321–867–2906, Jaime.J.Palou@nasa.gov

Authors: Dr. Nathan S. Jacobson and Jaime J. Palou

Headquarters program office:
Funded by NASA Johnson Space Center

Programs/Projects: Space shuttles

Advanced Environmental Barrier Coatings Developed for SiC/SiC Composite Vanes

Ceramic components exhibit superior high-temperature strength and durability over conventional component materials in use today, signifying the potential to revolutionize gas turbine engine component technology. Silicon-carbide fiber-reinforced silicon carbide ceramic matrix composites (SiC/SiC CMCs) are prime candidates for the ceramic hot-section components of next-generation gas turbine engines. A key barrier to the realization of SiC/SiC CMC hot-section components is the environmental degradation of SiC/SiC CMCs in combustion environments. This is in the form of surface recession due to the volatilization of silica scale by water vapor. An external environmental barrier coating (EBC) is a logical approach to achieve protection and long-term durability.

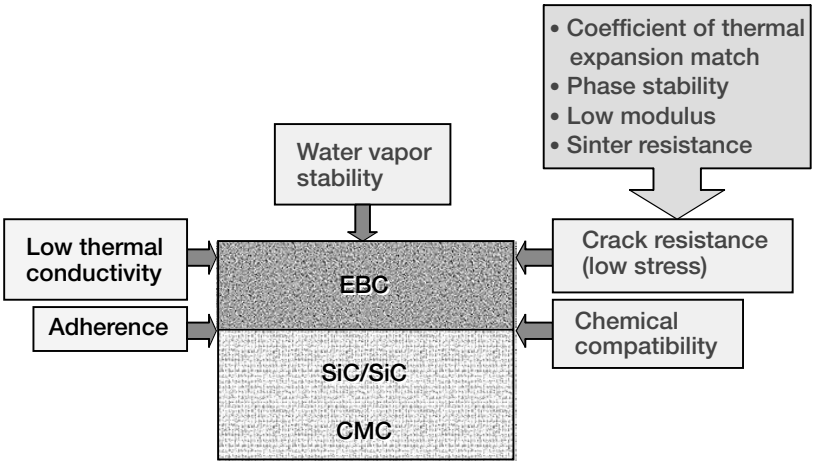

Key EBC requirements.

At the NASA Glenn Research Center, research was undertaken in the Ultra-Efficient Engine Technology (UEET) Program to develop advanced, multilayer environmental barrier coatings (EBCs), having a temperature capability of 2700 °F (1482 °C) at the EBC surface and 2400 °F (1316 °C) at the EBC/CMC interface. The preceding figure indicates the key requirements for a successful EBC. These include water vapor stability, chemical stability between the multiple layers of the EBC and at the EBC/CMC interface, low thermal expansion and phase stability for minimizing the stresses, and environmental durability in combustion environments. It is also desirable for an EBC to have a low thermal conductivity to maximize its thermal insulation potential.

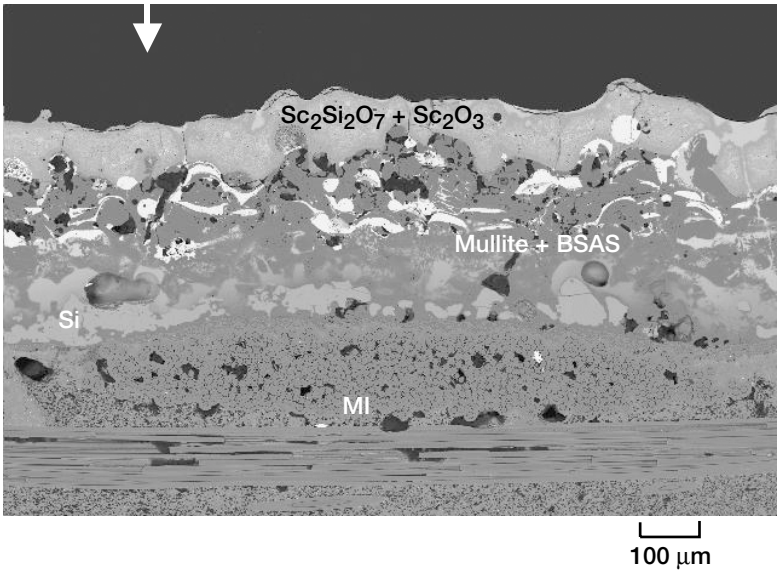

Cross section of Si/mullite+BSAS/$Sc_2Si_2O_7$+Sc_2O_3 EBC-coated SiC/SiC CMC after 300 hr at 1400 °C with 1-hr cycles in a simulated combustion environment (90 vol% H_2O-balance O_2) .

Two very promising EBC systems have evolved from this work: silicon/mullite+BSAS/rare earth silicates and silicon/mullite+BSAS/hafnia-based oxides (U.S. patent pending). Mullite is an alumina-silica system, of the form $3Al_2O_3$-$2SiO_2$, and BSAS is a barium-strontium-alumina-silicate system, of the form BaO-SrO-Al_2O_3-$2SiO_2$. The photomicrographs show cross sections of melt infiltrated (MI) SiC/SiC CMCs coated with silicon mullite+BSAS/scandium silicate+scandia EBC and silicon/mullite+BSAS/hafnia+mullite EBC, respectively, after 300 hr at 1400 °C with 1-hr cycles in a simulated combustion environment (90 vol% H_2O-balance O_2). Both coating systems show excellent performance with minimal oxidation, cracking, and chemical reactions.

The new EBCs meet or exceed the UEET Program goal. The coatings are stable in water vapor (no material

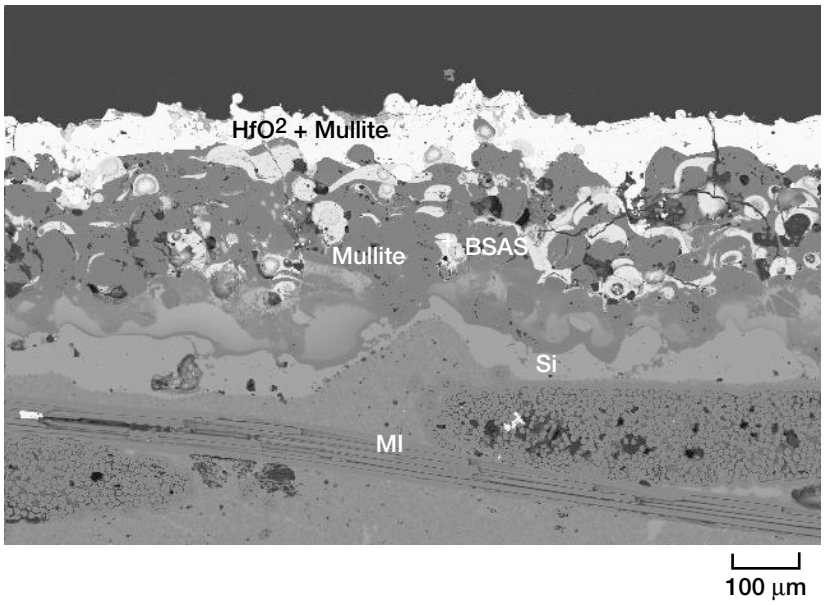

Cross section of Si/mullite+BSAS/HfO_2+mullite EBC-coated SiC/SiC CMC after 300 hr at 1400 °C with 1-hr cycles in a simulated combustion environment (90 vol% H_2O-balance O_2).

recession) at 1500 °C, are chemically stable (no detrimental interfacial chemical reactions) at temperatures up to 1400 °C, and have demonstrated environmental durability in a simulated combustion environment at temperatures from 1316 to 1400 °C. The new EBC top layers possess thermal conductivity as much as a factor of 2 lower than that of zirconia-8 wt% yttria—the current state-of-the-art thermal barrier coating—making them excellent thermal barrier coatings as well. The new EBCs will be optimized, scaled-up, and applied on SiC/SiC vanes. The performance of the coated CMC components will be evaluated in Glenn's high-pressure, high-velocity combustion burner rig during the upcoming year.

Find out more about the research of Glenn's Environmental Durability Branch:
http://www.grc.nasa.gov/WWW/EDB

Cleveland State University contact:
Dr. Kang N. Lee, 216–433–5634, Kang.N.Lee@grc.nasa.gov

Glenn contact:
Dennis S. Fox, 216–433–3295, Dennis.S.Fox@nasa.gov

Authors: Dr. Kang N. Lee, Dennis S. Fox, Dr. Jeffrey I. Eldridge, Dr. Dongming Zhu, Dr. Narottam P. Bansal, and Dr. Robert A. Miller

Headquarters program office: OAT

Programs/Projects: UEET

Low Thermal Conductivity Thermal Barrier Coatings Developed

Thermal barrier coatings (TBCs) are used extensively in modern gas turbine engines to thermally insulate air-cooled metallic components from the hot gases in the engine. These coatings typically consist of a zirconia-yttria ceramic that has been applied by either plasma spraying or physical vapor deposition. Future engines will rely even more heavily on TBCs and will require materials that have even higher temperature capability with improved insulation (i.e., lower thermal conductivity even after many hours at high temperature). This report discusses new TBCs that have been developed with these future requirements in mind. The Ultra-Efficient Engine Technology Program at the NASA Glenn Research Center is funding this effort, which has been conducted primarily at Glenn with contractor support (GE and Howmet) for physical vapor deposition.

As stated, the new TBC not only had to be more insulating but the insulation had to persist even after many hours of exposure—that is, the new TBC had to have both lower conductivity and improved sintering resistance. A new type of test rig was developed for this task. This new test approach used a laser to deliver a known high heat flux in an essentially uniform pattern to the surface of the coating, thereby establishing a realistic thermal gradient across its thickness. This gradient was determined from surface and backside pyrometry; and since the heat flux and coating thickness are known, this permitted continuous monitoring of thermal conductivity. Thus, this laser rig allowed very efficient screening of candidate low-conductivity, sinter-resistant TBCs.

The coating-design approach selected for these new low-conductivity TBCs was to identify oxide dopants that had the potential to promote the formation of relatively large and stable groupings

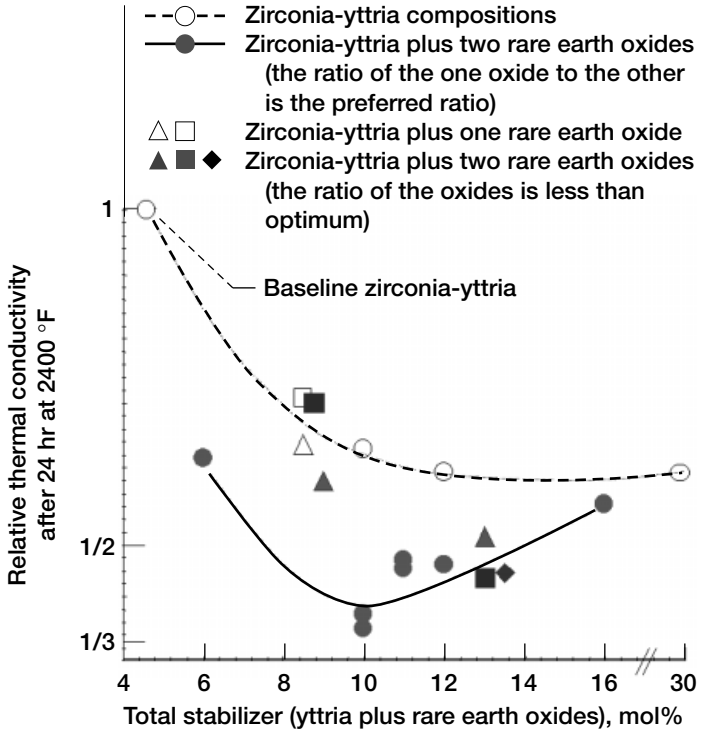

Thermal conductivity, k, after 20 hr of exposure in the laser rig test. The plot shows an approximately 40-percent reduction in the thermal conductivity of the preferred compositions, which are represented by the solid circles.

of defects known as defect clusters. This approach was used because it was felt that such clusters would reduce conductivity while enhancing stability. The approach proved to be successful: low-conductivity TBCs having improved sintering resistance were developed. The figure illustrates the improvement achieved for plasma-sprayed TBCs. In this graph, the mean thermal conductivity of the TBC after 20 hr of exposure in the laser rig at high temperature is plotted versus the mole percent of the oxides that were added to the zirconia. The graph shows an expected result: higher levels of stabilizer lead to lower conductivity even in the binary zirconia-yttria system. The graph also appears to indicate that the conductivity of ternary oxide systems may also more-or-less follow the curve for the binaries.

However, the greatest improvement was observed with certain, somewhat more complex systems—especially those points, indicated by the solid circles, that had been selected according to a certain "recipe." For this particular set of data, the conductivity of the new material after 20 hr at a high surface temperature was about 40 percent of the zirconia-yttria baseline. Furthermore, higher temperatures and longer times have actually increased the relative reduction further.

Thus, these new low-conductivity coatings have successfully met the initial programmatic milestones, and although more work is required, they have demonstrated their potential to improve performance significantly in the demanding applications envisioned for future advanced gas turbine engines.

Bibliography

Zhu, Dongming; and Miller, Robert A.: Thermal Conductivity and Sintering Behavior of Advanced Thermal Barrier Coatings. NASA/TM—2002-211481, 2002. http://gltrs.grc.nasa.gov/cgi-bin/GLTRS/browse.pl?2002/TM-2002-211481.html

Glenn contact:
Dr. Robert A. Miller, 216–433–3298, Robert.A.Miller@nasa.gov

U.S. Army, Vehicle Technology Directorate at Glenn contact:
Dr. Dongming Zhu, 216–433–5422, Dongming.Zhu@grc.nasa.gov

Authors: Dr. Robert A. Miller and Dr. Dongming Zhu

Headquarters program office: OAT

Programs/Projects: UEET

New Oxide Ceramic Developed for Superior High-Temperature Wear Resistance

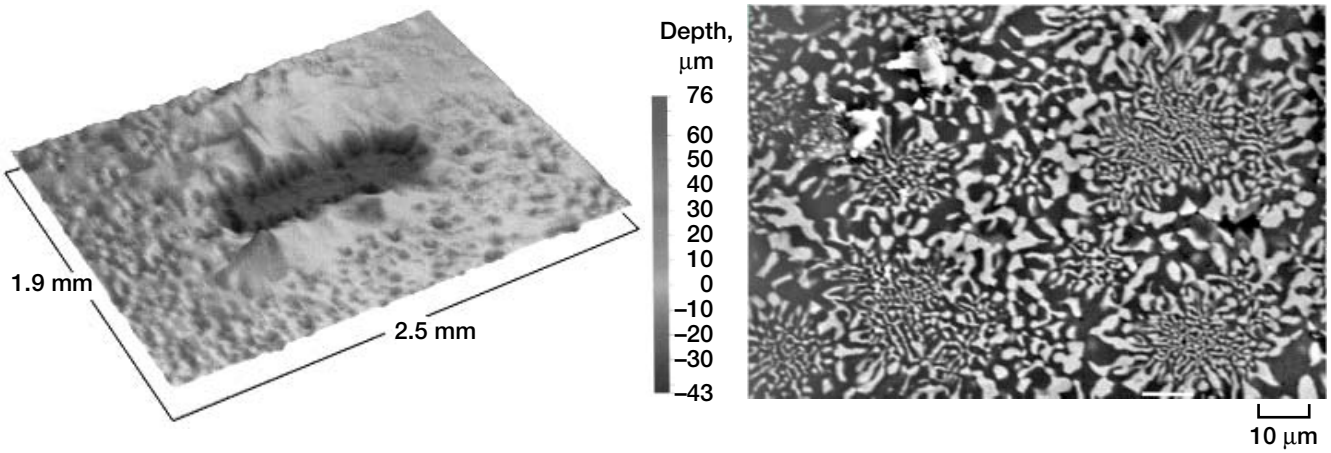

Wear track of new oxide ceramic material on B_4C. Left: Three-dimensional interactive display of B_4C showing track. Right: Photomicrograph of new oxide ceramic.

Ceramics, for the most part, do not have inherently good tribological properties. For example friction coefficients in excess of 0.7 have been reported for silicon nitride sliding on silicon nitride or on bearing steel (ref. 1). High friction is always accompanied by considerable wear. Despite their inherently poor tribological properties, the high strength and high toughness of silicon nitride (Si_3N_4) ceramics has led to their successful use in tribological applications (refs. 1 to 4). The upper temperature limit for the application of Si_3N_4 as wear-resistant material is limited by reaction with the tribological environment (ref. 3). Silicon nitride is known to produce a thin silicon dioxide film with easy shear capability that results in low friction and low wear in a moist environment (ref. 5). At elevated temperatures, the removal of the reaction product that acts as lubricant causes the friction coefficient to increase and, consequently, the wear performance to become poor. New materials are sought that will have wear resistance superior to that of Si_3N_4 at elevated temperatures and in harsh environments.

A new class of oxide ceramic materials has been developed with potential for excellent high-temperature wear resistance. The new material consists of a multicomponent oxide with a two-phase microstructure, in which the wear resistance of the mixed oxide is significantly higher than that of the individual constituents. This is attributed to the strong constraining effects provided by the interlocking microstructures at different length scales, to the large aspect ratio of the phases, to the strong interphase bonding, and to the residual stresses. Fretting wear tests were conducted by rubbing the new ceramic material against boron carbide (B_4C). The new ceramic material produced a wear track groove on B_4C, suggesting significantly higher wear resistance for the oxide ceramic. The new material did not suffer from any microstructural degradation after the wear test. The wear rate of the new ceramic material at 600 °C was determined to be on the order of 10^{-10} mm^3/N-m, which is 3 to 5 orders of magnitude lower than that for the current state-of-the-art wear-resistant materials (Si_3N_4 and B_4C). The friction coefficient of the new ceramic materials is on the order of 0.4, which is significantly lower than that of silicon nitride.

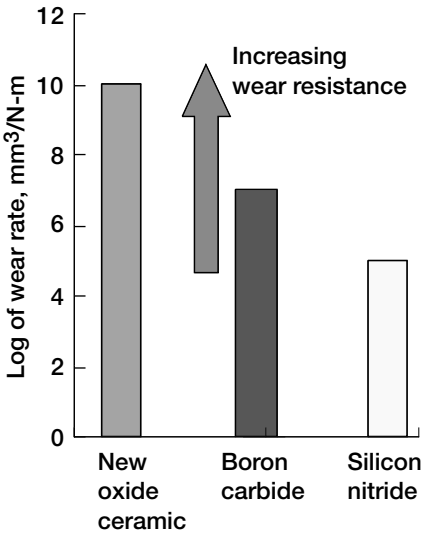

Comparison of wear resistance at 600 °C for various materials.

This new class of oxide materials has shown considerable potential for applications requiring high wear resistance at high temperatures and in harsh environments. New understanding of the wear behavior of ceramic materials is emerging as a result of the surprisingly high wear resistance of two-phase oxide ceramics. There is excellent potential for further improvements in the wear

resistance of oxide ceramics through optimizing the microstructure and altering the crystallographic properties of specific oxide materials as a second phase to reduce the coefficient of friction at elevated temperatures.

Find out more about this research:
http://www.grc.nasa.gov/WWW/Ceramics/homepage.htm

References

1. Buckley, Donald H.; and Miyoshi, Kazuhisa: Fundamental Tribological Properties of Ceramics. Ceram. Eng. Sci. Proc. (Am. Cer. Soc. Bul.), vol. 6, 1985, pp. 919–939.
2. Miyoshi, Kazuhisa.: Aerospace Mechanisms and Tribology Technology: Case Studies. Solid Lubrication Fundamentals and Applications, ch. 7, Marcel Deckker, New York, NY, 2001, pp. 293–332.
3. Sliney, H.E., et al.: Tribology of Selected Ceramics at Temperatures to 900 °C. Ceram. Eng. Sci. Proc., vol. 7, 1986, pp. 1039–1051.
4. Ishigaki, Hiroyuki; and Miyoshi, Kazuhisa: Tribological Properties of Ceramics. Proceedings of the 6th International Conference on Production Engineering, Osaka, Japan, 1987, pp. 661–666.
5. Miyoshi, Kazuhisa: Properties of Contaminated Surfaces: Adhesion, Friction, and Wear. Solid Lubrication Fundamentals and Applications, ch. 4, Marcel Dekker, New York, NY, 2001, pp. 145–219.

Glenn contacts:
Dr. Kazuhisa Miyoshi, 216–433–6078, Kazuhisa.Miyoshi-1@nasa.gov; and Dr. Serene Farmer, 216–433–3289, Serene.C.Farmer@nasa.gov

Case Western Reserve University contact: Dr. Ali Sayir, 216–433–3289, Ali.Sayir@grc.nasa.gov

Authors: Dr. Ali Sayir, Dr. Kazuhisa Miyoshi, and Dr. Serene C. Farmer

Headquarters program office: OAT

Programs/Projects: HOTPC

NASA Glenn/AADC-Rolls Royce Collaborated to Measure Erosion Resistance on Coated Polymer Matrix Composites

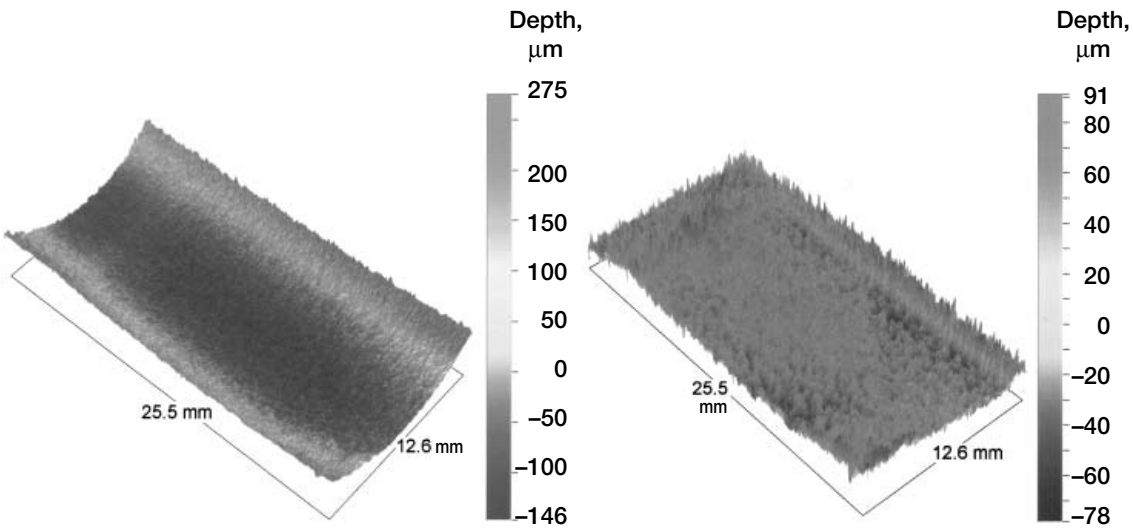

Three-dimensional optical interferometry images of the eroded wear scar of a coated PMC sample obtained after an erosion test. The eroded surface appears as a large scar containing abrasive particles in the direction of the airstream. The erosion test was conducted with Arizona Road Dust particles at an impingement angle of 20° and a velocity of 229 m/s. Left: From measurement. Right: Removed cylindrical shape. This figure is shown in color in the online version of this article (http://www.grc.nasa.gov/WWW/RT2002/5000/5160miyoshi2.html).

Polymer matrix composites (PMCs) are increasingly used in aerospace and automotive applications because of their light weight and high strength-to-weight ratio relative to metals. However, a major drawback of PMCs is poor abrasion resistance, which restricts their use, especially at high temperatures. Simply applying a hard coating on PMCs to improve abrasion and erosion resistance is not effective since coating durability is short lived (ref. 1). Generally, PMCs have higher coefficients of thermal expansion than metallic or ceramic coatings have, and coating adhesion suffers because of poor interfacial adhesion strength.

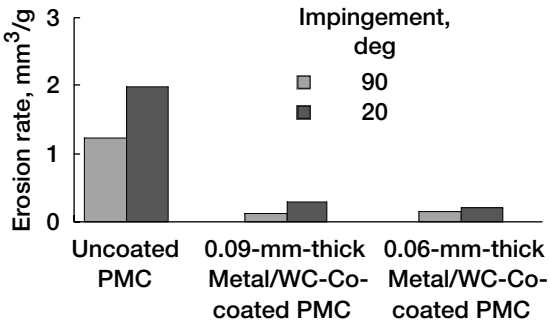

Erosion rate of uncoated and coated PMC samples measured by scanning optical interferometry. Erosion tests were conducted at a velocity of 229 m/s with Arizona Road Dust particles at impingement angles of 20º and 90º. Coated PMCs had lower erosion rates by a factor of ~10.

One technique commonly used to improve coating adhesion or durability is the use of bond coats that are interleaved between a coating and a substrate with vastly different coefficients of thermal expansion. An example of this remedy is the use of bondcoats for ceramic thermal barrier coatings on metallic turbine components (ref. 2). Prior collaborative research between the NASA Glenn Research Center and the Allison Advanced Development Company (AADC) demonstrated that bond coats sandwiched between PMCs and high-quality plasma-sprayed, erosion-resistant coatings substantially improved the erosion resistance of PMCs (ref. 3). One unresolved problem in this earlier collaboration was that there was no easy, accurate way to measure the coating erosion wear scar. Coating wear was determined by both profilometry and optical microscopy. Both techniques are time consuming. Wear measurement by optical microscopy requires sample destruction and does not provide a comprehensive measure of the entire wear volume.

An even more subtle, yet critical, problem is that these erosion coatings contain two or more materials with different densities. Therefore, simply measuring specimen mass loss before and after erosion will not provide an accurate gauge for coating and/or substrate volume loss. By using a noncontact technique called scanning optical interferometry, which was recently developed at Glenn, researchers can accurately determine the wear performance of erosion-coated PMCs while preserving the sample. An example of this interferometry technique is shown in the figure on the preceding page for an erosion-coated inlet guide vane from a Rolls Royce AE3007 regional gas turbine jet engine. Erosion was conducted with coated and uncoated PMC vanes, with the abrasive material moving at a velocity of 229 m/s at impingement angles of 20º and 90º. The coatings for PMCs remarkably reduced the erosion volume loss by a factor of approximately 10 (see the bar chart to the left). Currently, several erosion coatings for PMCs are being compared and down-selected for engine testing at Rolls Royce.

Find out more about the research of Glenn's Polymers Branch:
http://www.grc.nasa.gov/WWW/MDWeb/5150/Polymers.html

References

1. Harding, David R., et al.: Oxidation Protective Barrier Coatings for High-Temperature Polymer Matrix Composites. J. Mater. Res., vol. 9, no. 6, 1994, pp. 1583–1595.
2. Miller, R.A.: Current Status of Thermal Barrier Coatings—An Overview. Surf. Coatings Technol., vol. 30, no. 1, 1987, pp. 1–11.
3. Naik, Subhash K., et al.: Erosion Coatings for High Temperature Polymer Composites. Proceedings of the 44th International SAMPE Symposium and Exhibition, vol. 44, book 1, SAMPE, 1999, pp. 68–81.

Glenn contacts:
Dr. Kazuhisa Miyoshi, 216–433–6078, Kazuhisa.Miyoshi-1@nasa.gov; and
Dr. James K. Sutter, 216–433–3226, James.K.Sutter@nasa.gov

Authors: Dr. Kazuhisa Miyoshi, Dr. James K. Sutter, Richard Mondry, Kong Ma, Dick Horan, Dr. Subhash Naik, and Randall Cupp

Headquarters program office: OAT

Programs/Projects:
Propulsion and Power, HOTPC

Oxidation of Carbon Fibers in Water Vapor Studied

T–300 carbon fibers (BP Amoco Chemicals, Greenville, SC) are a common reinforcement for silicon carbide composite materials, and carbon-fiber-reinforced silicon carbide composites (C/SiC) are proposed for use in space propulsion applications. It has been shown that the time to failure for C/SiC in stressed oxidation tests is directly correlated with the fiber oxidation rate (ref. 1). To date, most of the testing of these fibers and composites has been conducted in oxygen or air environments; however, many components for space propulsion, such as turbopumps, combustors, and thrusters, are expected to operate in hydrogen and water vapor (H_2/H_2O) environments with very low oxygen contents. The oxidation rate of carbon fibers in conditions representative of space propulsion environments is, therefore, critical for predicting component lifetimes for real applications. This report describes experimental results that demonstrate that, under some conditions, lower oxidation rates of carbon fibers are observed in water vapor and H_2/H_2O environments than are found in oxygen or air. At the NASA Glenn Research Center, the weight loss of the fibers was studied as a function of water pressure, temperature, and gas velocity. The rate of carbon fiber oxidation was determined, and the reaction mechanism was identified.

At temperatures of 1100 °C and above, the fiber oxidation rate is controlled by the transport of oxidant in the gas phase to the fiber surface. The oxidation rate depends on the gas velocity, is directly proportional to the oxidant partial pressure, and is nearly independent of temperature. The oxidation rate in this regime is the same in oxygen and water vapor for the same amount of oxidant. At temperatures below 1100 °C, the fiber oxidation rate is controlled by the chemical reaction of the oxidant with the fiber surface. The fiber oxidation rate in this regime is independent of the gas velocity, has a complex fractional dependence on the oxidant partial pressure, and is strongly dependent on the oxidation temperature. In this regime, the oxidation rate varies strongly with the oxidant species. Oxidation in water vapor is much slower than oxidation in oxygen for the same amount of oxidant. Oxidation rates in H_2/H_2O mixtures are slower still. A comparison of fiber oxidation rates in different environments in the chemical-reaction-controlled regime is shown in the graph. The temperature at which the regime change occurs depends on the gas velocity. Higher gas velocities drive the transition temperature higher.

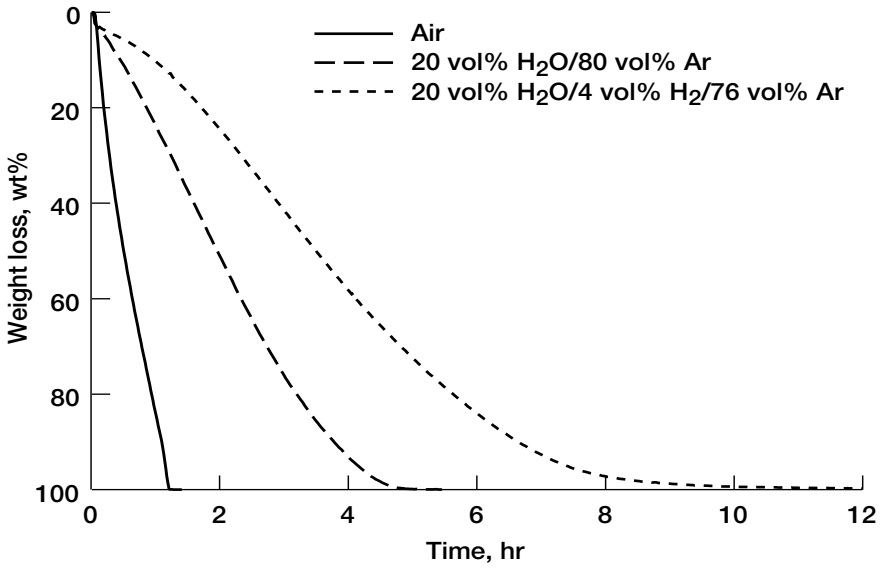

Comparison of the oxidation rate of T–300 carbon fibers in different gas environments. All exposures were conducted at 900 °C with a gas velocity of 4.4 cm/sec.

The conclusion of this study is that C/SiC composites used in high-gas-velocity H_2/H_2O environments in the chemical-reaction-controlled regime will have lifetimes much longer than those that would be expected on the basis of testing in air or oxygen. These relatively low-temperature, high-gas-velocity H_2/H_2O environments may be ideal conditions for the application of these materials. Future work will examine in more detail the oxidation rates of carbon fibers in high-hydrogen-content environments.

Find out more about the research of Glenn's Environmental Durability Branch:
http://www.grc.nasa.gov/WWW/EDB/

Reference

1. Verrilli, M.J., et al.: Effect of Environment on Stress-Rupture Behavior of a Carbon Fiber-Reinforced Silicon Carbide (C/SiC) Ceramic Matrix Composite. In preparation for J. Amer. Ceram. Soc.

Cleveland State University contact:
Dr. Elizabeth J. Opila, 216–433–8904, Elizabeth.J.Opila@grc.nasa.gov

Glenn contact:
Michael J. Verrilli, 216–433–3337, Michael.J.Verrilli@nasa.gov

Author: Dr. Elizabeth J. Opila

Headquarters program office: OAT

Programs/Projects: STPO, Gen 3

NiAl Coatings Investigated for Use in Reusable Launch Vehicles

As part of its major investment in the area of advanced space transportation, NASA is developing new technologies for use in the second- and third-generation designs of reusable launch vehicles. Among the prototype rocket engines being considered for these launch vehicles are those designed to use liquid hydrogen as the fuel and liquid oxygen as the oxidizer. Advanced copper alloys, such as copper-chromium-niobium (Cu-8(at.%)Cr-4(at.%)Nb, also referred to as GRCop-84), which was invented at the NASA Glenn Research Center, are being considered for use as liner materials in the combustion chambers and nozzle ramps of these engines. However, previous experience has shown that, in rocket engines using liquid hydrogen and liquid oxygen, copper alloys are subject to a process called blanching, where the material undergoes environmental attack under the action of the combustion gases. In addition, the copper alloy liners undergo thermomechanical fatigue, which often results in an initially square cooling channel deforming into a dog-house shape. Clearly, there is an urgent need to develop new coatings to protect copper liners from environmental attack inside rocket chambers and to lower the temperature of the liners to reduce the probability of deformation and failure by thermomechanical fatigue.

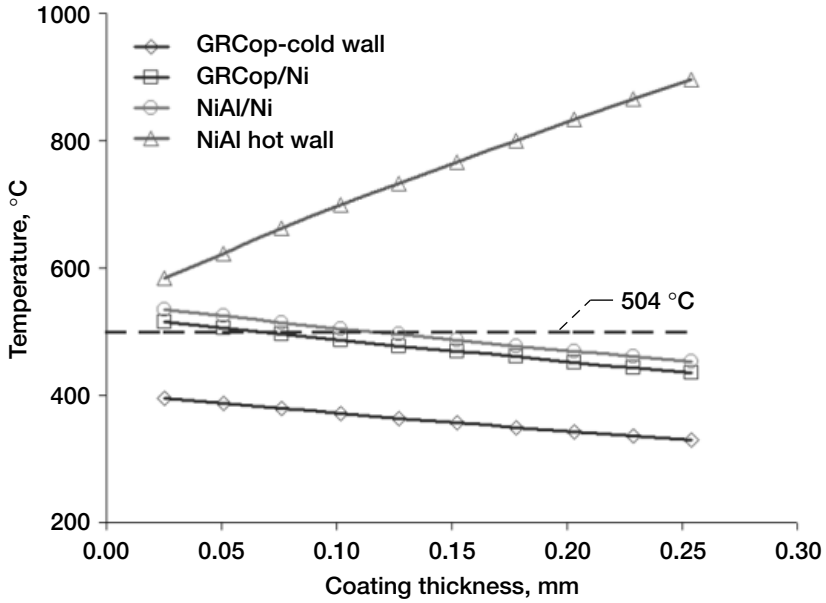

Effect of NiAl coating thickness on the expected temperature distribution of the GRCop-84 substrate in a rocket engine. Temperature of the hot gas, 3277 °C; coolant temperature, –176 °C; convective heat transfer coefficient of the hot gas, 12 363 W/m^2/K; convective heat transfer coefficient of the coolant, 58 283 W/m^2/K.

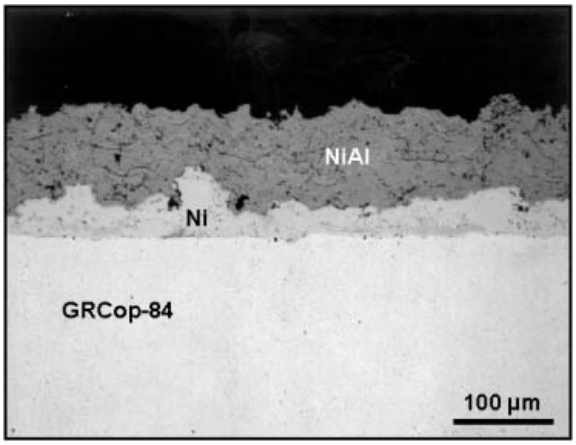

As-sprayed NiAl/Ni/GRCop-84.

Glenn is actively developing and characterizing several advanced protective coatings for GRCop-84 liners and nozzle ramps for reusable launch vehicle applications. Nickel aluminide (NiAl), which has been extensively investigated at Glenn for aircraft engine applications, was chosen as a coating in this study because of its mechanical and oxidation properties. It is well established that NiAl possesses excellent oxidation properties, has a lower density than GRCop-84, and a higher thermal conductivity than NiCrAlY. These desirable characteristics make it a logical choice as a candidate for study. Thermal modeling also suggests that NiAl can remain effective under the high-heat-flux conditions characteristic of a rocket engine combustion chamber (see the graph). These calculations indicate that the applied coating thickness should exceed 0.1 mm to ensure that the substrate temperature stays below 500 °C.

The photomicrograph to the left shows the cross section of a GRCop-84 substrate coated with a NiAl outer coating and a Ni bond coat by the

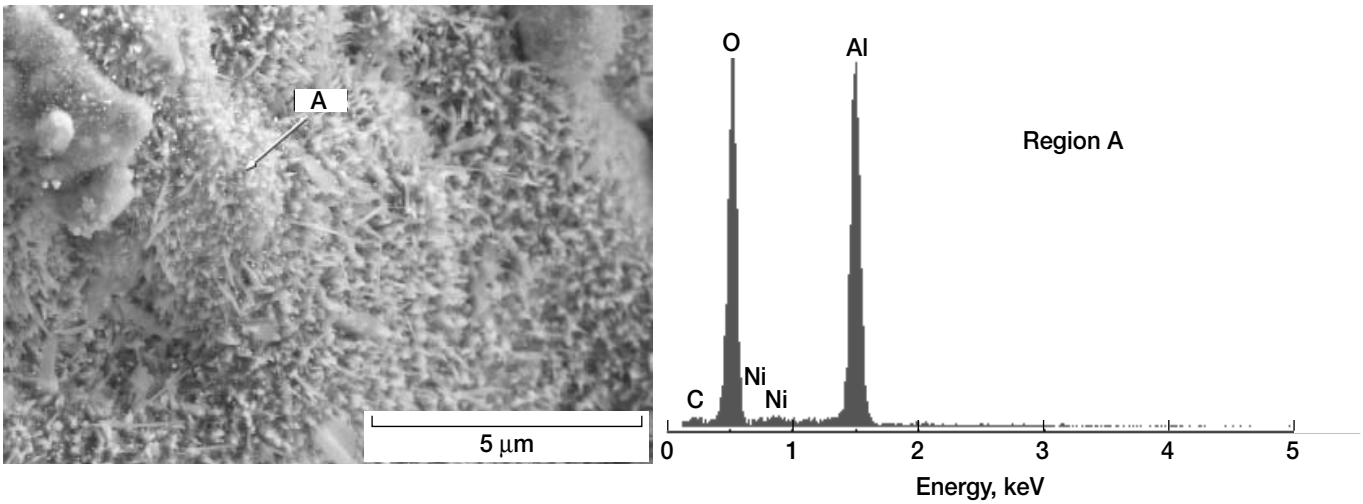

Microstructure and chemical analysis of the NiAl coating after annealing in pure hydrogen at 900 °C for 50 hr.

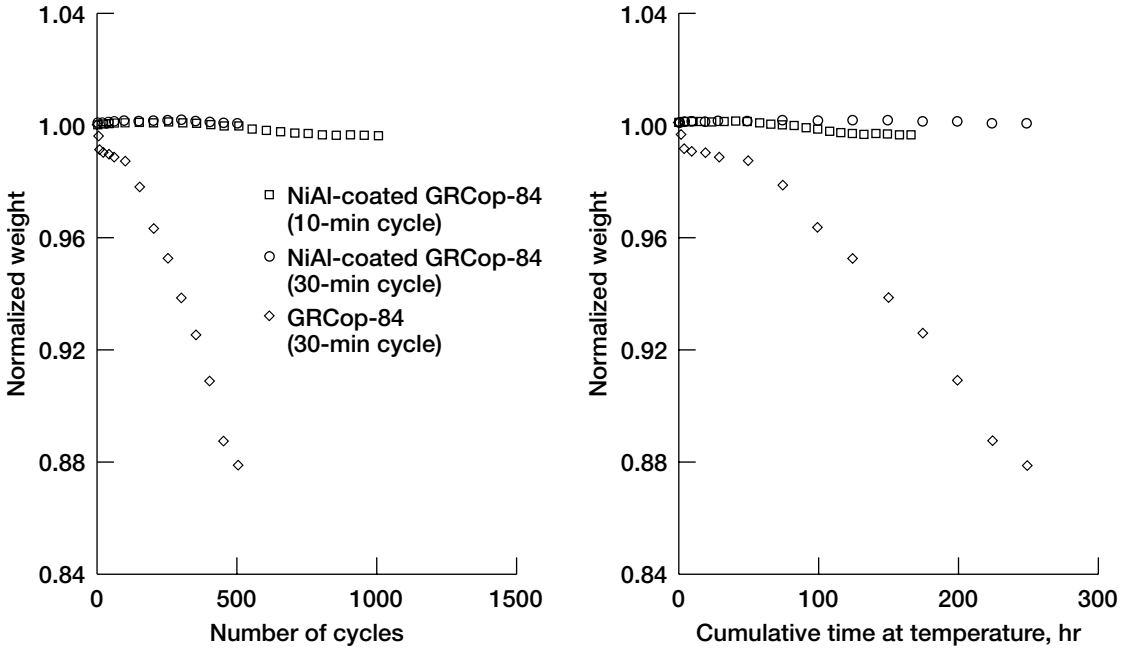

Thermal cycling behavior of coated and uncoated GRCop-84 at 600 °C.

low-pressure plasma-spraying process. The stability of the coating in hydrogen was tested by exposing coated specimens to flowing gas at 900 °C for various times up to 50 hr. Microstructural and chemical analysis of the coated surfaces revealed that the coating did not form nickel hydride and that only a stable protective alumina layer was observed (see the figure at the top of this page). The effectiveness of the coating in protecting the substrate in an oxidizing environment was tested by thermally cycling disk specimens, coated on both faces, in air at 600 °C. Each cycle consisted of exposing the specimen to temperature for either 10 or 30 min followed by cooling to ambient temperature in 5 min. Periodic weight change and microstructural observations were made during the course of the tests and compared with similar observations of uncoated substrates. The graphs confirm that the NiAl coating can protect the substrate from the oxidation effects of air as evidenced by the negligible change in weight for a proposed 30-min third-generation mission cycle (500 cycles, i.e., 250 hr) and for a planned 10-min second-generation mission cycle (100 cycles, i.e., 16.7 hr) before engine overhaul. In fact, the NiAl-coated substrate exceeded the proposed 100 mission cycles by a factor of 10. In contrast, the uncoated material lost about 13 percent of

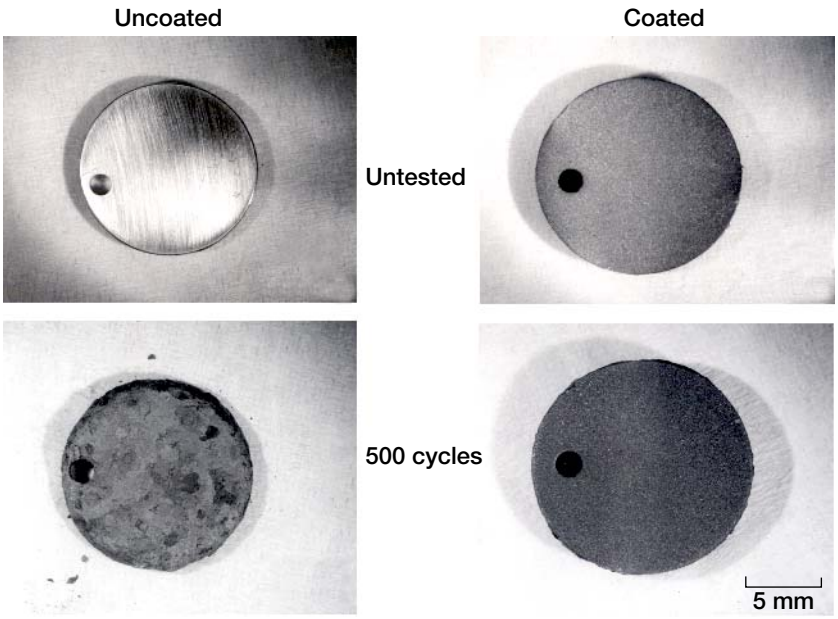

Macrographs of coated and uncoated GRCop-84 thermally cycled at 600 °C.

its original weight after 500 cycles. Microstructural observations of the surfaces of the coated and uncoated specimens before and after 500 cycles revealed that uncoated GRCop-84 oxidized and spalled profusely during the course of the test, thereby resulting in a significant weight loss (see the photographs to the left). In comparison, the surfaces of the coated substrate were crack free and intact. Further studies are underway to optimize the plasma spraying conditions and demonstrate the stability of the coatings in a high-heat-flux environment.

Find out more about this research:
http://www.grc.nasa.gov/WWW/EDB/

Glenn contact:
Dr. Sai V. Raj, 216–433–8195,
Sai.V.Raj@nasa.gov

Authors: Dr. Sai V. Raj, Dr. Louis J. Ghosn, and Charles A. Barrett

Headquarters program office: OAT

Programs/Projects: Gen 3

Combustor and Vane Features and Components Tested in a Gas Turbine Environment

The use of ceramic matrix composites (CMCs) as combustor liners and turbine vanes provides the potential of improving next-generation turbine engine performance, through lower emissions and higher cycle efficiency, relative to today's use of superalloy hot-section components. For example, the introduction of film-cooling air in metal combustor liners has led to higher levels of nitrogen oxide (NO_x) emissions from the combustion process. An environmental barrier coated (EBC) silicon-carbide-fiber-reinforced silicon carbide matrix (SiC/SiC) composite is a new material system that can operate at higher temperatures, significantly reducing the film-cooling requirements and enabling lower NO_x production.

Evaluating components and subcomponents fabricated from these advanced CMCs under gas turbine conditions is paramount to demonstrating that the material system can perform as required in the complex thermal

EBC coupon test module with four specimens.

stress and environmentally aggressive engine environment. To date, only limited testing has been conducted on CMC combustor and turbine concepts and subelements of this type throughout the industry. As part of the Ultra-Efficient Engine Technology (UEET) Program, the High Pressure Burner Rig (HPBR) at the NASA Glenn Research Center was selected to demonstrate coupon, subcomponent feature, and component testing because it can economically provide the temperatures, pressures, velocities, and combustion gas compositions that closely simulate the engine environments. The results have proven the HPBR to be a highly versatile test rig amenable to multiple test specimen configurations essential to coupon and component testing. Typical conditions include 6 to 8 atm of pressure (10 vol% water vapor), 50 to 100 ft/sec gas velocities, and 2400 to 2550 °F material temperatures.

Testing of subcomponent features for combustor liners began on lean transition liners that had been developed for testing in a fuel-rich quick-quench fuel-lean combustor sector rig at Glenn. Only limited exposure time was available because of operational and cost issues. In the current effort, the geometry of these liners, their CMC attachments, and the HPBR configuration were adapted to accommodate continued testing. A water-cooled test module that slipped into existing flanges allowed for separate gas and backside cooling paths and provided access ports for obtaining both surface and substrate temperatures using both optical and fiber-optic measurement techniques. The baseline cycle adopted was a 30-min transient with 15 min of dwell time at a gas temperature of approximately 2700 °F and surface temperatures between 1800 and 2400 °F, depending on cooling flows. To date, the original set of six lean transition liners and numerous attachments have been exposed to over 180 hr (280 cycles). Tests such as these are successfully demonstrating the feasibility of using CMCs integrated with metallic parts in a combustor application.

A second feature test for the combustor application incorporates a unique SiC/SiC combustor liner, designed and fabricated to replace the original metal component in the HPBR. This EBC-coated CMC liner, equipped with an integral attachment flange, will be installed in the test rig and run parallel to other ongoing testing for over 1000 hr of exposure. This test will provide valuable long-term durability data on recession and microstructural damage for a stressed, actively cooled CMC component in a high-water-vapor combustion gas environment.

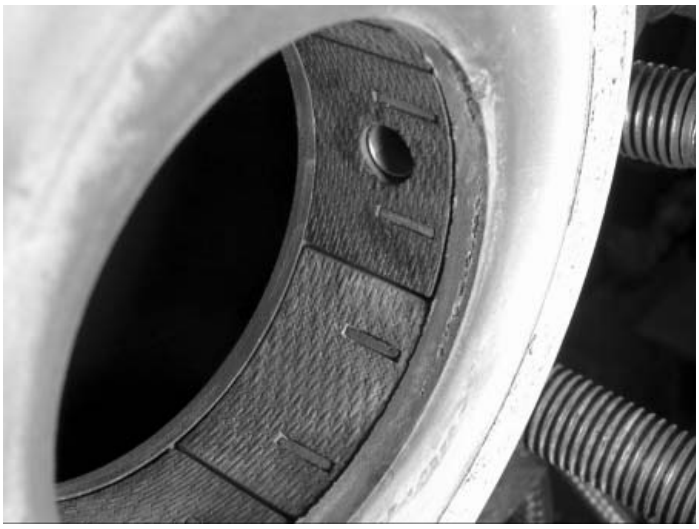

CMC lean transition liners mounted in the HPBR.

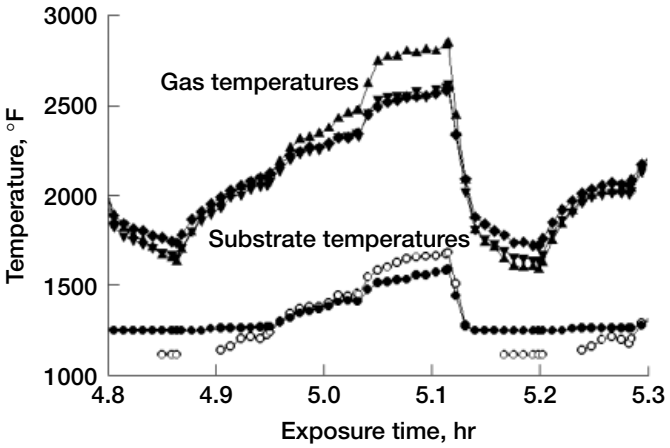

Cycle and material temperature for lean transition liners tested in the HPBR.

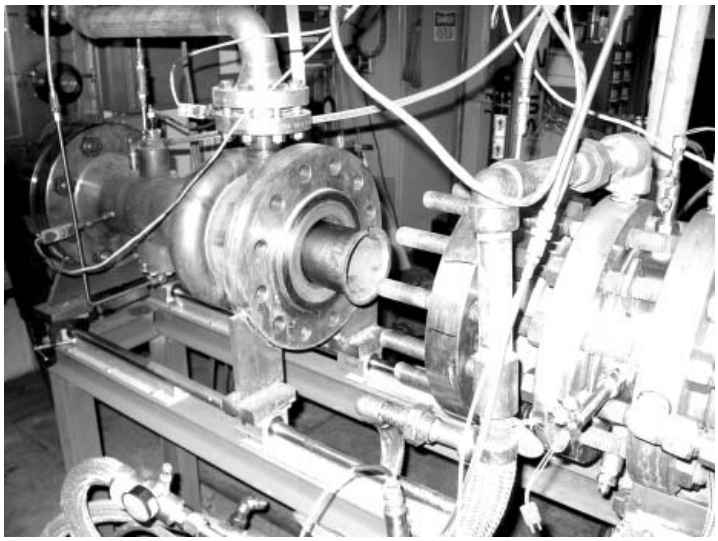

SiC/SiC CMC combustor liners installed in the HPBR.

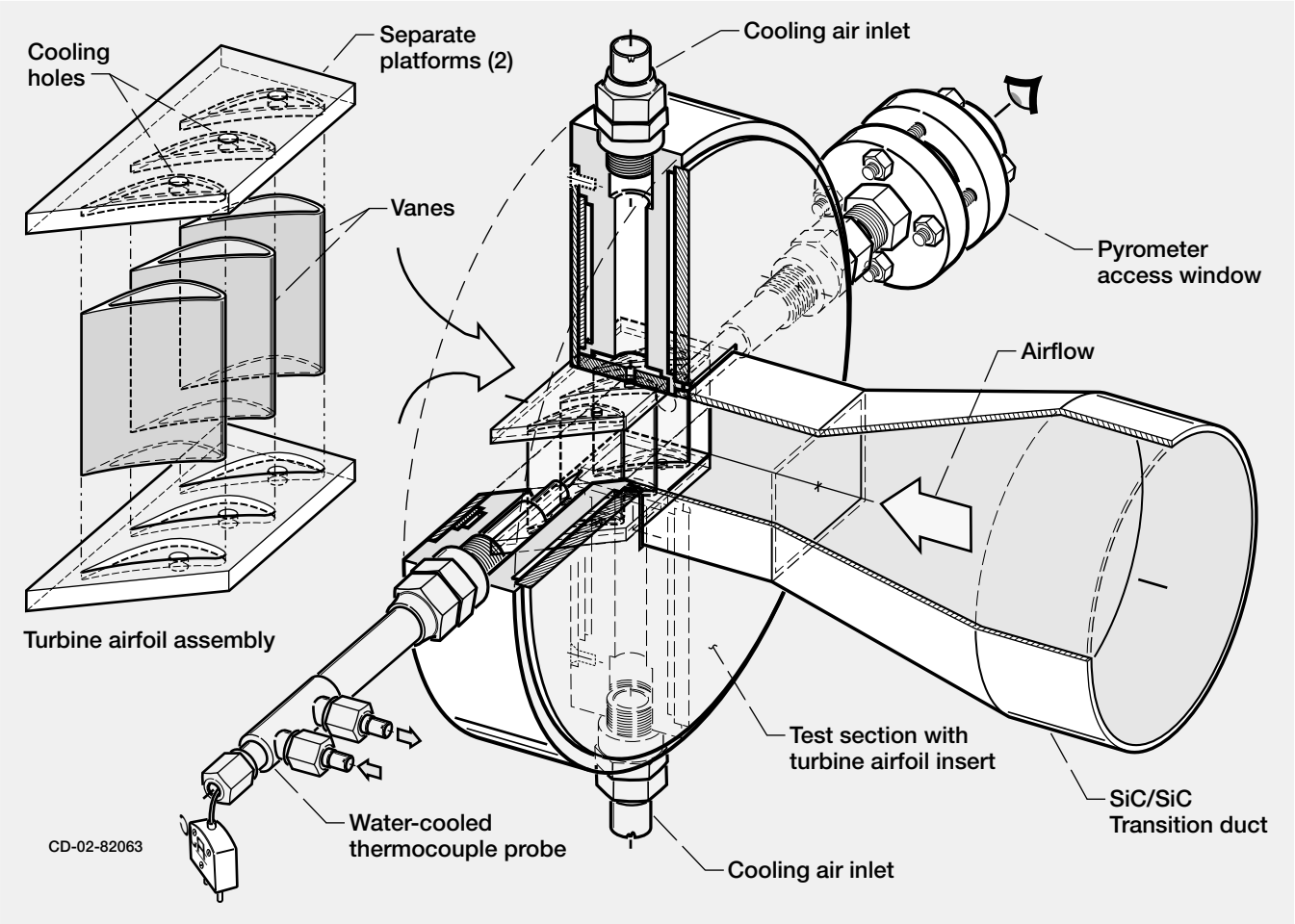

HPBR turbine test configuration.

A test to expose SiC/SiC CMC airfoils in a configuration similar to a stationary inlet guide vane will be used to demonstrate the technology readiness of fabricating a generic EBC-coated, melt-infiltrated, SiC/SiC airfoil as well as meeting the mechanical capability and environmental durability requirements imposed by the combustion gas environment. The test module requires three vanes (with separate metal platforms) to provide the proper boundary conditions for both the "pressure" and "suction" side of the center airfoil. The configuration employs a SiC/SiC transition duct to accelerate the incoming flows, provides internal cooling to the airfoils, and has designs to monitor the resulting temperatures and pressures. Typical gas conditions in the test section will include 6 to 8 atm, 300 ft/sec, and 2650 °F.

Testing and evaluation of advanced materials for turbine engines require studies to address the scaleup issues inherent in coupon-level studies in the application engine or at least in testing situations as close to simulating the actual application environment as is possible. The combustion environment provided by the HPBR as well as the versatility in test fixturing and design make it a valuable test rig for evaluating new materials for gas turbine engines.

Find out more about the research of Glenn's Environmental Durability Branch:
http://www.grc.nasa.gov/WWW/EDB

QSS Group, Inc., contact:
R. Craig Robinson, 216–433–5547,
Raymond.C.Robinson@grc.nasa.gov

Glenn contacts:
Michael J. Verrilli, 216–433–3337,
Michael.J.Verrilli@nasa.gov; and
Dr. Anthony M. Calomino,
216–433–3311,
Anthony.M.Calomino@nasa.gov

Authors: R. Craig Robinson and Michael J.Verrilli

Headquarters program office: OAT

Programs/Projects: UEET, HOTPC

Power and On-Board Propulsion Technology

New Voltage and Current Thresholds Determined for Sustained Space Plasma Arcing

Sustained arc on the Terra satellite test article in ground tests at Glenn.

It has been known for many years, based partly on NASA Glenn Research Center testing, that high-voltage solar arrays arc into the space plasma environment. Solar arrays are composed of solar cells in series with each other (a string), and the strings may be connected in parallel to produce the entire solar array power. Arcs on solar arrays can damage or destroy solar cells, and in the extreme case of sustained arcing, entire solar array strings, in a flash. In the case of sustained arcing (discovered at Glenn and applied to the design and construction of solar arrays on Space Systems/Loral (SS/Loral, Palo Alto, CA) satellites, Deep-Space 1, and Terra), an arc on one solar array string can couple to an adjacent string and continue to be powered by the solar array output until a permanent electrical short is produced. In other words, sustained arcs produced by arcs into the plasma (so-called trigger arcs) may turn into disastrous sustained arcs by involving other array strings.

Previous work at Glenn has shown that for each solar array design there is a voltage threshold for the trigger arc, and voltage and current thresholds for the sustained arcs. Trigger arc thresholds vary from about –100 to about –250 V, depending on solar array design parameters, such as the thickness of the solar cell coverglasses and the amount of coverglass overhang beyond the cell edges. Sustained arc voltage thresholds can be less than the trigger arc thresholds. For instance, if two adjacent solar array strings have a difference in cell voltage of 60 V but either is operating at –250 V, a trigger arc can occur that will evolve into a sustained arc between strings. Among the techniques used to prevent sustained arc discharges are lowering the voltage between adjacent strings and lowering the current that can get to the trigger-arc site. If either or both of these values are less than the thresholds, a sustained arc cannot get started. Previously, the lowest sustained arc voltage threshold was determined to be about 55 V. The work described here showed that sustained arcs can occur at voltages as low as 40 V and currents as low as 1 amp.

Several small solar array samples were tested in a simulated plasma in a vacuum-plasma chamber in the Plasma Interactions Facility at Glenn. The plasma was produced by a Penning type source, using xenon gas. The array panels were 3 by 12 solar cells, and the cells were 4 by 6 silicon cells on a Kapton (Dupont) substrate. Adjacent strings were separated by 0.8 mm. The strings were biased from –400 to –450 V, and the voltage difference between the strings was increased until the arcs produced became sustained arcs. The lowest sustained arc thresholds were obtained for solar cells for which the coverglass thickness was 300 μm (6 mils) and the coverglasses did not overhang the cell edges. For thinner (150 μm) coverglasses with no overhang, the thresholds found were 60 V and 2 amp. Coverglasses that were 150 μm thick with a 250-μm (10-mil) overhang had thresholds of 80 V and 1.6 amp. These new sustained arcing thresholds will allow array designers to prevent sustained arcing that could damage or destroy their satellite arrays in the harsh space environment.

Glenn contacts: Joel T. Galofaro, 216–433–2294, Joel.T.Galofaro@nasa.gov; and Dr. Dale C. Ferguson, 216–433–2298, Dale.C.Ferguson@nasa.gov

Ohio Aerospace Institute (OAI) contact:
Boris V. Vayner, 216–433–8058, Boris.V.Vayner@grc.nasa.gov

Authors: Dr. Dale C. Ferguson, Joel T. Galofaro, and Boris V. Vayner

Headquarters program office: OAT

Programs/Projects: Space Solar Power

Systems Analysis Initiated for All-Electric Aircraft Propulsion

A multidisciplinary effort is underway at the NASA Glenn Research Center to develop concepts for revolutionary, nontraditional fuel cell power and propulsion systems for aircraft applications. There is a growing interest in the use of fuel cells as a power source for electric propulsion as well as an auxiliary power unit to substantially reduce or eliminate environmentally harmful emissions.

A systems analysis effort was initiated to assess potential concepts in an effort to identify those configurations with the highest payoff potential. Among the technologies under consideration are advanced proton exchange membrane (PEM) and solid oxide fuel cells, alternative fuels and fuel processing, and fuel storage. Prior to this effort, the majority of fuel cell analysis done at Glenn was done for space applications. Because of this, a new suite of models was developed. These models include the hydrogen-air PEM fuel cell; internal reforming solid oxide fuel cell; balance-of-plant components (compressor, humidifier, separator, and heat exchangers); compressed gas, cryogenic, and liquid fuel storage tanks; and gas turbine/generator models for hybrid system applications. Initial mass, volume, and performance estimates of a variety of PEM systems operating on hydrogen and reformate have been completed for a baseline general aviation aircraft. Solid oxide/turbine hybrid systems are being analyzed.

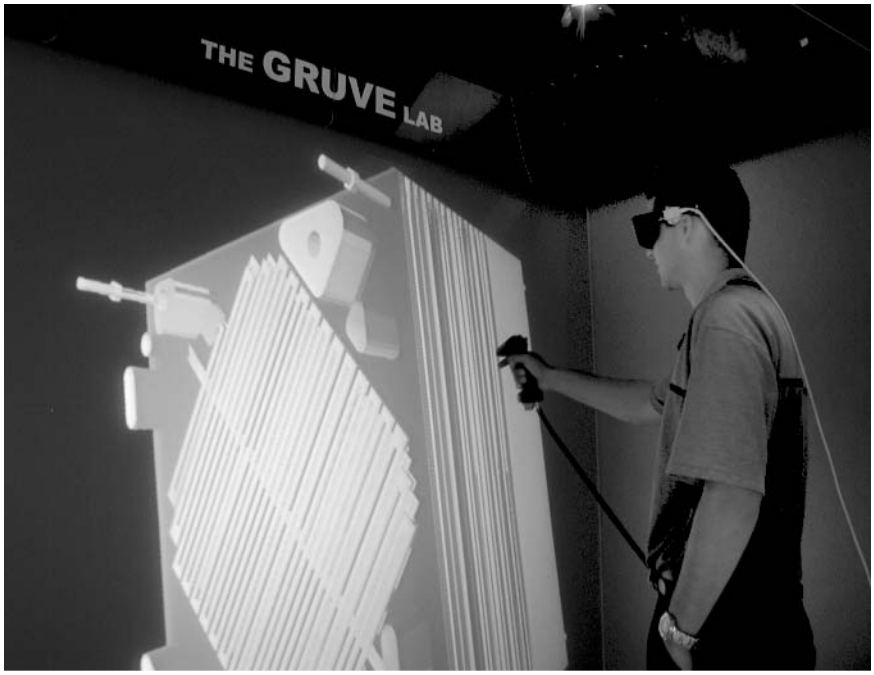

Fuel cell visualization model in GRUVE lab.

In conjunction with the analysis efforts, a joint effort has been initiated with Glenn's Computer Services Division to integrate fuel cell stack and component models with the visualization environment that supports the GRUVE lab, Glenn's virtual reality facility. The objective of this work is to provide an environment to assist engineers in the integration of fuel cell propulsion systems into aircraft and provide a better understanding of the interaction between system components and the resulting effect on the overall design and performance of the aircraft. Initially, three-dimensional computer-aided design (CAD) models of representative PEM fuel cell stack and components were developed and integrated into the virtual reality environment along with an Excel-based model used to calculate fuel cell electrical performance on the basis of cell dimensions (see the figure). CAD models of a representative general aviation aircraft were also developed and added to the environment. With the use of special headgear, users will be able to virtually manipulate the fuel cell's physical characteristics and its placement within the aircraft while receiving information on the resultant fuel cell output power and performance. As the systems analysis effort

progresses, we will add more component models to the GRUVE environment to help us more fully understand the effect of various system configurations on the aircraft.

Find out more about this research:

Polymer Energy Rechargeable System:
http://www.grc.nasa.gov/WWW/Electrochemistry/doc/pers.html

GRUVE lab: http://gruve.grc.nasa.gov

Glenn contacts:
Lisa L. Kohout, 216–433–8004,
Lisa.L.Kohout@nasa.gov; and
Dr. Jay G. Horowitz, 216–433–5194,
Jay.G.Horowitz@nasa.gov

Author: Lisa L. Kohout

Headquarters program office: OAT

Programs/Projects:
Propulsion and Power, RAC

Polymer Energy Rechargeable System Battery Being Developed

In fiscal year 2000, NASA established a program to develop the next generation, lithium-based, polymer electrolyte batteries for aerospace applications. The goal of this program, known as Polymer Energy Rechargeable Systems (PERS), is to develop a space-qualified, advanced battery system embodying polymer electrolyte and lithium-based electrode technologies and to establish world-class domestic manufacturing capabilities for advanced batteries with improved performance characteristics that address NASA's future aerospace battery requirements.

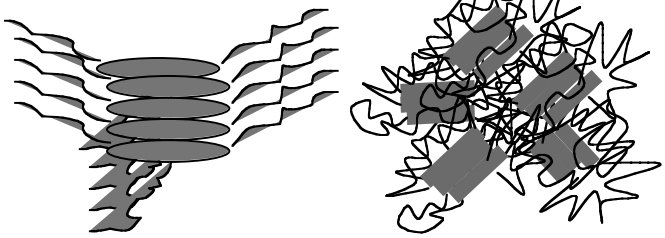

Discotic liquid crystals

Rod-coil polymers

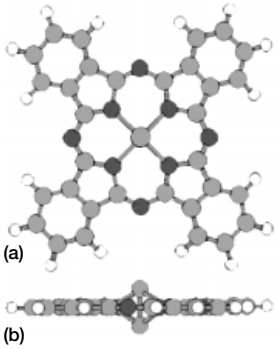

Lithium-ion conducting channel dilithium phthalocyanine (Li_2Pc) (a) Top view. (b) Side view.

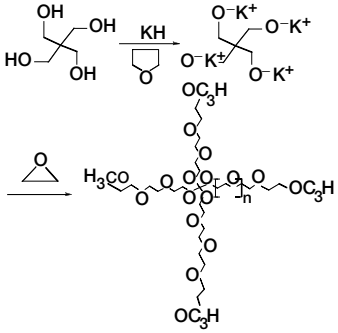

Novel star polyethlylene oxide structures

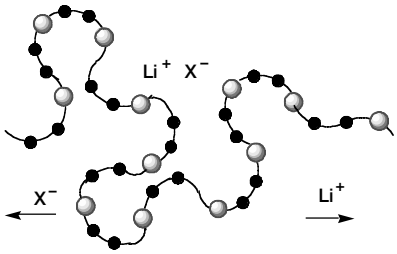

Polyethylene oxide + lithium salt (Li^+X^-)

● Carbon atom
○ Oxygen atom

Composite polyethlylene oxide materials

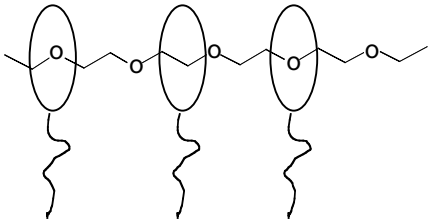

Homopolyrotaxanes

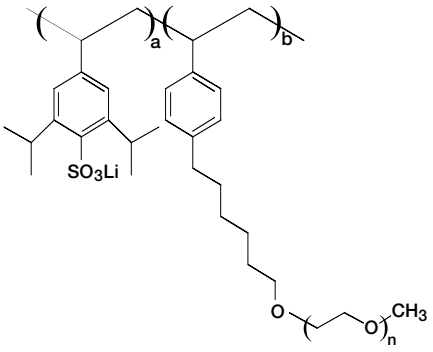

Diblock copolymers

Representative solid polymer electrolyte concepts under investigation for PERS batteries.

This advanced lithium-based battery chemistry is of interest for the following reasons:

(1) It has a high cell voltage: 3.6 V compared with 1.3 V for conventional alkaline chemistries. Consequently, the battery can achieve a desired system voltage with fewer cells and, hence, reduced system complexity and lower manufacturing and assembly costs.

(2) It has a high specific energy and energy density: 25 percent of the mass and/or volume of conventional alkaline cells. The improvements in specific energy (watt-hours per kilogram) and energy density (watt-hours per liter) realized by this battery system can enhance any mission that uses rechargeable batteries for energy storage and can enable missions that have critical weight and/or volume margins. Lighter weight systems also contribute to lower launch costs.

(3) It incorporates environmentally safe materials and has safe battery operation. Because there are no free liquids in the battery, polymer electrolyte systems are inherently safe systems. The polymer electrolyte enables a flexible, conformable battery that does not generate internal pressure during operation.

(4) It offers improved coulombic and energy efficiencies comparable to those of conventional systems and exhibits low self-discharge rates that contribute to more efficient operations.

(5) It operates over a wide range of temperatures centered on the ambient temperature. This flexibility simplifies thermal system design and expands the envelope of operational parameters under which the battery can be used.

A NASA Research Announcement was released in fiscal year 2000 to solicit efforts to address the development of the polymer electrolytes, cathodes, and anodes for PERS batteries. Development of a polymer with room-temperature conductivity in the range of 10^{-3} S/cm has been identified as the enabling technology breakthrough required for this battery system. There are currently seven contracts and seven grants in place that address various aspects of component-level development required for the PERS batteries. The current contractors are the Lawrence Berkley National Laboratory, Max Power, Inc., Naval Air Warfare Center Weapons Division, Physical Sciences Inc., Yardney Technical Products, Inc., Eagle Picher Technologies, LLC (Joplin, MO), and Lithium Power Technologies, Inc. Grantees include Northwestern University, the University of Utah, Indiana University, the University of Minnesota, Texas Engineering Experiment Station, and the University of Akron. In addition to these contracts and grants, research and development activities have been supported at the Jet Propulsion Laboratory, the Air Force Research Laboratory, and the NASA Glenn Research Center.

A component-screening facility has been established at NASA Glenn, and procedures have been developed to evaluate the materials developed via the supported research and development efforts. This includes the construction of a state-of-the-art dry room facility that will be used to conduct research relating to lithium batteries, and the installation of analytical equipment that will be used for component characterization and analysis. Recently, researchers reported room-temperature conductivities in the range of 10^{-4} S/cm for the polymer electrolytes under development. This represents an increase of nearly 2 orders of magnitude over conductivities exhibited by the state-of-the-art polymer electrolyte at room temperature. The progress to date has been encouraging, and several concepts offer the promise of meeting the program goals.

Find out more about this research:
http://www.grc.nasa.gov/WWW/Electrochemistry/doc/pers.html

Glenn contact:
Michelle A. Manzo, 216–433–5261, Michelle.A.Manzo@nasa.gov

Author: Michelle A. Manzo

Headquarters program office: OAT

Programs/Projects:
Space Science, ESE, HEDS, aeronautics, commercial satellites

High-Power Hall Thruster Technology Evaluated for Primary Propulsion Applications

High-power electric propulsion systems have been shown to be enabling for a number of NASA concepts, including piloted missions to Mars and Earth-orbiting solar electric power generation for terrestrial use (refs. 1 and 2). These types of missions require moderate transfer times and sizable thrust levels, resulting in an optimized propulsion system with greater specific impulse than conventional chemical systems and greater thrust than ion thruster systems. Hall thruster technology will offer a favorable combination of performance, reliability, and lifetime for such applications if input power can be scaled by more than an order of magnitude from the kilowatt level of the current state-of-the-art systems. As a result, the NASA Glenn Research Center conducted strategic technology research and development into high-power Hall thruster technology.

Glenn researcher Robert Jankovsky compares the NASA–457M Hall thruster, the largest ever built and tested, with a kilowatt-class Hall thruster.

During program year 2002, an in-house fabricated thruster, designated the NASA–457M, was experimentally evaluated at input powers up to 72 kW. These tests demonstrated the efficacy of scaling Hall thrusters to high power suitable for a range of future missions. Thrust up to nearly 3 N was measured. Discharge specific impulses ranged from 1750 to 3250 sec, with discharge efficiencies between 46 and 65 percent. This thruster is the highest power, highest thrust Hall thruster ever tested.

References

1. Gefert, Leon P.; Hack, Kurt J.; Kerslake, Thomas W.: Options for the Human Exploration of Mars Using Solar Electric Propulsion. Proceedings of the Conferences on Applications of Thermophysics in Microgravity and on Next Generation Launch Systems and the 16th Symposium on Space Nuclear Power and Propulsion, AIP Conference Proceedings No. 458, 1999, pp. 1275–1280.
2. Oleson, S.: Advanced Propulsion for Space Solar Power Satellites. AIAA Paper 99–2872, 1999.

Glenn contact:
David T. Jacobson, 216–433–3691, David.T.Jacobson@nasa.gov

Authors: David H. Manzella, Robert S. Jankovsky, and Richard R. Hofer

Headquarters program office:
OSF, OAT

Programs/Projects:
ESE, Space Science, HEDS

Development Efforts Expanded in Ion Propulsion: Ion Thrusters Developed With Higher Power Levels

The NASA Glenn Research Center was the major contributor of 2-kW-class ion thruster technology to the Deep Space 1 mission, which was successfully completed in early 2002. Recently, NASA's Office of Space Science awarded approximately $21 million to Glenn to develop higher power xenon ion propulsion systems for large flagship missions such as outer planet explorers and sample return missions. The project, referred to as NASA's Evolutionary Xenon Thruster (NEXT), is a logical follow-on to the ion propulsion system demonstrated on Deep Space 1. The propulsion system power level for NEXT is expected to be as high as 25 kW, incorporating multiple ion thrusters, each capable of being throttled over a 1- to 6-kW power range. To date, engineering model thrusters have been developed, and performance and plume diagnostics are now being documented. The project team—Glenn, the Jet Propulsion Laboratory, General Dynamics, Boeing Electron Dynamic Devices, the Applied Physics Laboratory, the University of Michigan, and Colorado State University—is in the process of developing hardware for a ground demonstration of the NEXT propulsion system, which comprises a xenon feed system, controllers, multiple thrusters, and power processors. The development program also will include life assessments by tests and analyses, single-string tests of ion thrusters and power systems, and finally, multistring thruster system tests in calendar year 2005.

NEXT project 40-cm ion thruster.

In addition, NASA's Office of Space Science selected Glenn to lead the development of a 25-kW xenon thruster to enable NASA to conduct future missions to the outer planets of Jupiter and beyond, under the High Power Electric Propulsion (HiPEP) program. The development of a 100-kW-class ion propulsion system and power conversion systems are critical components to enable future nuclear-electric propulsion systems. In fiscal year 2003, a team composed of Glenn, the Boeing Company, General Dynamics, the Applied Physics Laboratory, the Naval Research Laboratory, the University of Wisconsin, the University of Michigan, and Colorado State University will perform a 6-month study that will result in the designs of two 25-kW ion thrusters, a propellant feed system, and power processing architectures. The following 2 years may involve hardware development, wear tests, single-string tests of the thruster-power circuits and the xenon feed system, and subsystem service life analyses.

The 2-kW-class ion propulsion technology developed for the Deep Space 1 mission will be used for NASA's discovery mission Dawn, which involves maneuvering a spacecraft to survey the asteroids Ceres and Vesta. The 6-kW-class ion thruster subsystem technology under NEXT is scheduled to be flight ready by calendar year 2006. The less mature 25-kW ion thruster system under HiPEP is expected to be ready for a flight advanced development program in calendar year 2006.

Find out more about this research:

Ion propulsion research at Glenn:
http://www.grc.nasa.gov/WWW/Ion/

Glenn chosen to lead development of NEXT ion engine:
http://www.grc.nasa.gov/WWW/PAO/pressrel/2002/02-046.html

NASA selects team to lead development of advanced technology for future in-space propulsion applications:
ftp://ftp.hq.nasa.gov/pub/pao/pressrel/2002/02-167.txt

Glenn contact:
Michael J. Patterson, 216–977–7481, Michael.J.Patterson@nasa.gov

Authors: Michael J. Patterson, Vincent K. Rawlin, and James S. Sovey

Headquarters program office: OSS

Programs/Projects: Deep Space 1, NSTAR, NEXT, HiPEP

Special recognition:
Aviation Week & Technology 42nd Annual Aerospace Laurels (1999), Turning Goals into Reality Award (2001), Discover Magazine's Award for Technological Innovation (1999), R&D 100 Award (2001)

Pulsed Plasma Thruster (PPT) Technology: Earth Observing-1 PPT Operational and Advanced Components Being Developed

In 2002 the pulsed plasma thruster (PPT) mounted on the Earth Observing-1 spacecraft was operated successfully in orbit. The two-axis thruster system is fully incorporated in the attitude determination and control system and is being used to automatically counteract disturbances in the pitch axis of the spacecraft. The first tests conducted in space demonstrated the full range of PPT operation, followed by calibration of control torques from the PPT in the attitude control system. Then the spacecraft was placed in PPT control mode. To date, it has operated for about 30 hr. The PPT successfully controlled pitch momentum during wheel de-spin, solar array acceleration and deceleration during array rewind, and environmental torques in nominal operating conditions. Images collected with the Advanced Landsat Imager during PPT operation have demonstrated that there was no degradation in

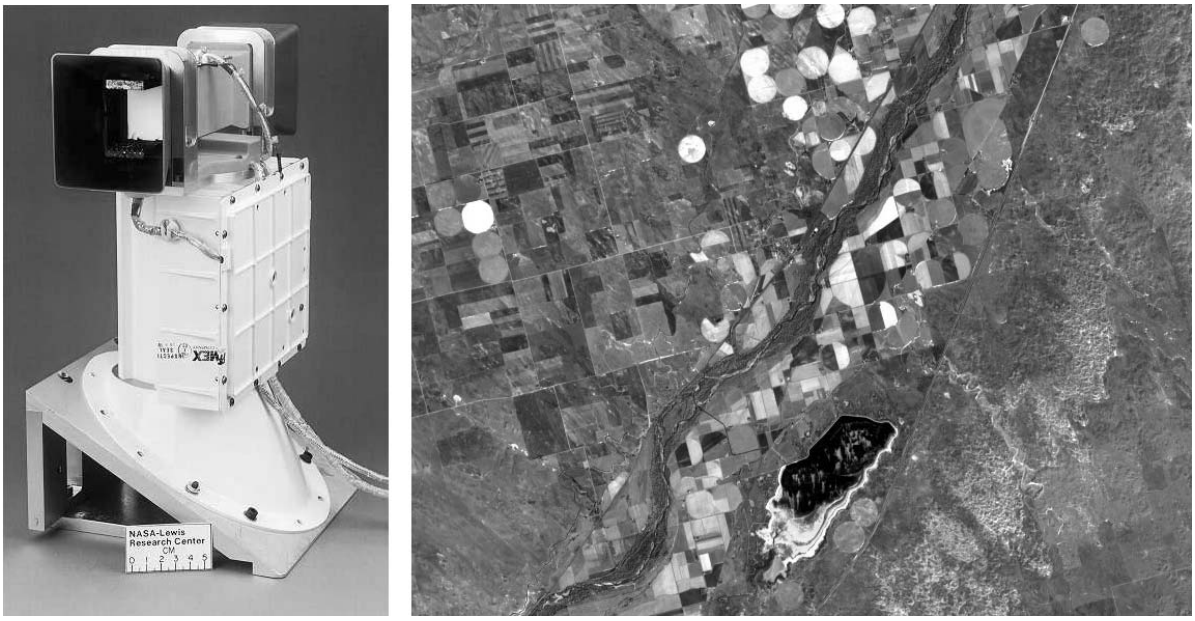

Left: Earth Observing-1 PPT. Right: Image from Advanced Landsat Imager taken under PPT control.

comparison to full momentum wheel control (see the photographs). In addition, other experiments have been performed to interrogate the effects of PPT operation on communication packages and light reflection from spacecraft surfaces. Future experiments will investigate the possibility of orbit-raising maneuvers, spacecraft roll, and concurrent operation with the Hyperion imager.

Future applications envisioned for pulsed plasma thrusters include longer life, higher precision, multiaxis thruster configurations for three-axis attitude control systems or high-precision, formation-flying systems. Advanced components, such as a "dry" mica-foil capacitor, a wear-resistant spark plug, and a multichannel power processing unit have been developed under contract with Unison Industries, General Dynamics, and C.U. Aerospace. Over the last year, evaluation tests have been conducted to determine power processing unit efficiency, atmospheric functionality, vacuum functionality, thruster performance evaluation, thermal performance, and component life.

Find out more information about this research:

Earth Observing-1 PPT experiment:
http://space-power.grc.nasa.gov/ppo/projects/eo1/

Earth Observing-1:
http://eo1.gsfc.nasa.gov

Glenn contact:
Eric J. Pencil, 216–977–7463,
Eric.J.Pencil@nasa.gov

Authors: Eric J. Pencil, Scott W. Benson, Lynn A. Arrington, John Frus, W. Andrew Hoskins, and Rodney Burton

Headquarters program office:
OAT, OSS

Programs/Projects: EO–1, ESE

New Technique of High-Performance Torque Control Developed for Induction Machines

Two forms of high-performance torque control for motor drives have been described in the literature: field orientation control and direct torque control. Field orientation control has been the method of choice for previous NASA electromechanical actuator research efforts with induction motors. Direct torque control has the potential to offer some advantages over field orientation, including ease of implementation and faster response. However, the most common form of direct torque control is not suitable for the high-speed, low-stator-flux linkage induction machines designed for electromechanical actuators with the presently available sample rates of digital control systems (higher sample rates are required). In addition, this form of direct torque control is not suitable for the addition of a high-frequency carrier signal necessary for the "self-sensing" (sensorless) position estimation technique. This technique enables low- and zero-speed position sensorless operation of the machine. Sensorless operation is desirable to reduce the number of necessary feedback signals and transducers, thus improving the reliability and reducing the mass and volume of the system.

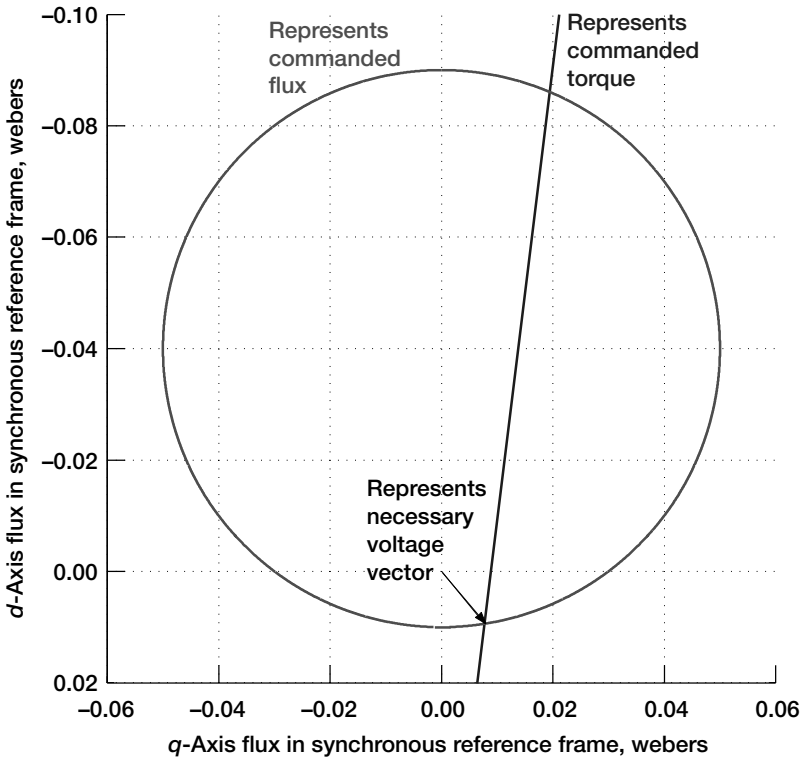

Voltage vector solution to a commanded torque and stator flux.

This research was directed at developing an alternative form of direct torque control known as a "deadbeat," or inverse model, solution. This form uses pulse-width modulation of the voltage applied to the machine, thus reducing the necessary sample and switching frequency for the high-speed

NASA motor. In addition, the structure of the deadbeat form allows the addition of the high-frequency carrier signal so that low- and zero-speed sensorless operation is possible.

The new deadbeat solution is based on using the stator and rotor flux as state variables. This choice of state variables leads to a simple graphical representation of the solution as the intersection of a constant torque line with a constant stator flux circle. Previous solutions have been expressed only in complex mathematical terms without a method to clearly visualize the solution. The graphical technique allows a more insightful understanding of the operation of the machine under various conditions.

The figure on the preceding page shows the graphical solution for a given operating condition and commanded torque and flux. The vector drawn from the origin to the intersection of the line and the circle represents the voltage vector to apply to the machine to achieve the commanded torque and flux. In the control algorithm, the required voltage vector is summed with the high-frequency carrier signal voltage and the total is synthesized by pulse-width modulation of a constant direct-current voltage. The result is a high-performance sensorless torque control suitable for a high-speed induction machine.

Bibliography
Kenny, Barbara H.; and Lorenz, Robert D.: Stator and Rotor Flux Based Deadbeat Direct Torque Control of Induction Machines. NASA/TM—2001-211100/REV1, 2002. http://gltrs.grc.nasa.gov/cgi-bin/GLTRS/browse.pl?2002/TM-2001-211100-REV1.html

Find out more about the research of Glenn's Power and On-Board Propulsion Technology Division:
http://powerweb.grc.nasa.gov/branches/5450.html

Glenn contact:
Dr. Barbara H. Kenny, 216–433–6289, Barbara.H.Kenny@nasa.gov

Author: Dr. Barbara H. Kenny

Headquarters program office: OAT

Programs/Projects: Energetics, RLV

New Active Optical Technique Developed for Measuring Low-Earth-Orbit Atomic Oxygen Erosion of Polymers

Polymers such as polyimide Kapton (DuPont) and Teflon FEP (DuPont, fluorinated ethylene propylene) are commonly used spacecraft materials because of desirable properties such as flexibility, low density, and in the case of FEP, a low solar absorptance and high thermal emittance. Polymers on the exterior of spacecraft in the low-Earth-orbit (LEO) environment are exposed to energetic atomic oxygen. Atomic oxygen reaction with polymers causes erosion, which is a threat to spacecraft performance and durability. It is, therefore, important to understand the atomic oxygen erosion yield *E* (the volume loss per incident oxygen atom) of polymers being considered in spacecraft design. The most common technique for determining *E* is a passive technique based on mass-loss measurements of samples exposed to LEO atomic oxygen during a spaceflight experiment. There are certain disadvantages to this technique. First, because it is passive, data are not obtained until after the flight is completed. Also, obtaining the preflight and postflight mass measurements is complicated by the fact that many polymers absorb water and, therefore, the mass change due to water absorption can affect the *E* data. This is particularly true for experiments that receive low atomic oxygen exposures or for samples that have a very low *E*. An active atomic oxygen erosion technique based on optical measurements has been developed that has certain advantages over the mass-

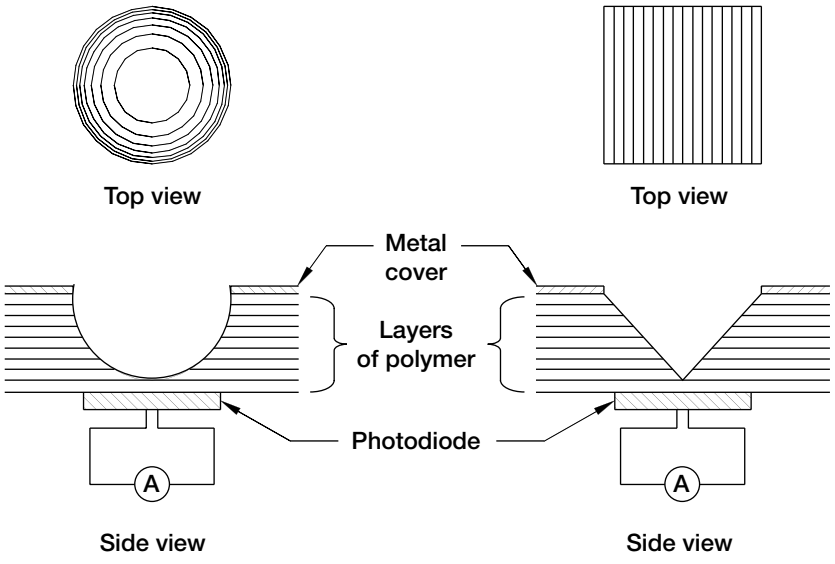

Optical atomic oxygen erosion measurement technique. Left: Circular-parabolic-shaped well polymer layer. Right: Rectangular V-shaped well polymer layer.

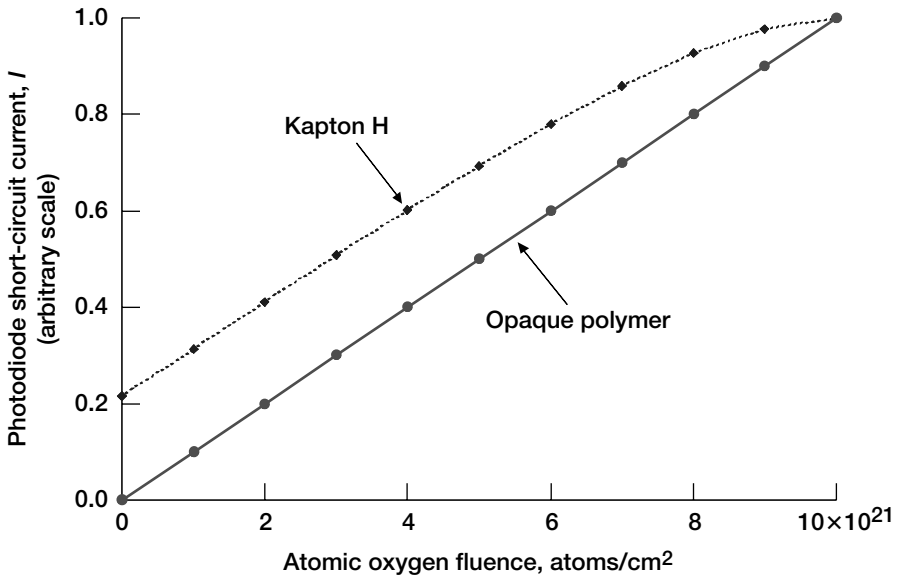

Short-circuit current as a function of atomic oxygen fluence for the optical atomic oxygen erosion measurement techniques shown in the preceding drawings.

loss technique. This in situ technique can simultaneously provide the erosion yield data on-orbit and the atomic oxygen exposure fluence, which is needed for erosion yield determination.

In the optical technique, either sunlight or artificial light can be used to measure the erosion of semitransparent or opaque polymers as a result of atomic oxygen attack. The technique is simple and adaptable to a rather wide range of polymers, providing that they have a sufficiently high optical absorption coefficient. If one covers a photodiode with a uniformly thick sheet of semitransparent polymer such as Kapton H polyimide, then as atomic oxygen erodes the polymer, the short-circuit current from the photodiode will increase in an exponential manner with fluence. This nonlinear response with fluence results in a lack of sensitivity for measuring low atomic oxygen fluences. However, if one uses a variable-thickness polymer or carbon sample, which is configured as shown in the drawing on the preceding page, then a linear response can be achieved for opaque materials using a parabolic well for a circular geometry detector (see the drawing on the left) or a V-shaped well for a rectangular-geometry detector (see the drawing on the right). Variable-thickness samples can be fabricated using many thin polymer layers. For semitransparent polymers such as Kapton H polyimide, there is an initial short-circuit current that is greater than zero. This current has a slightly nonlinear dependence on atomic oxygen fluence in comparison to opaque materials such as black Kapton, as shown in the graph. For this graph, the total thickness of Kapton H was assumed to be 0.03 cm. The photodiode short-circuit current shown in the graph was generated on the basis of preliminary measurements—a total reflectance ρ of 0.0424 and an optical absorption coefficient α of 146.5 cm^{-1}.

In addition to obtaining on-orbit data, the advantage of this active erosion and erosion yield measurement technique is its simplicity and reliance upon well-characterized fluence witness materials as well as a nearly linear photodiode short-circuit current dependence upon atomic oxygen fluence. The optical technique is useful for measuring either atomic oxygen fluence or erosion, depending on the information desired. To measure the atomic oxygen erosion yield of a test material, one would need to have two photodiode sensors, one for the test material and one that uses a known erosion yield material (such as Kapton) to measure the atomic oxygen fluence.

Find out more about this research:
http://www.grc.nasa.gov/WWW/epbranch/

Glenn contacts:
Bruce A. Banks, 216–433–2308, Bruce.A.Banks@nasa.gov; and
Kim K. de Groh, 216–433–2297, Kim.K.deGroh@nasa.gov

Authors: Bruce A. Banks, Kim K. de Groh, and Rikako Demko

Headquarters program office: OAT

Programs/Projects: ISS, EOS, DOD, Future LEO spacecraft

Thermal Contributions to the Degradation of Ground-Laboratory- and Space-Irradiated Teflon Investigated

The Hubble Space Telescope (HST) is covered with two primary types of thermal control materials, radiators and multilayer insulation blankets, which passively control temperatures during orbit. Both of these thermal control materials utilize back-surface metalized Teflon FEP (DuPont, fluorinated ethylene propylene) as the exterior (space-facing) layer because of its excellent optical properties (low solar absorptance and high thermal emittance). The aluminized-FEP (Al-FEP) outermost layer of the multilayer insulation blankets on the HST has become embrittled while in space, resulting in severe on-orbit cracking (see the photographs). During the second servicing mission, an extremely embrittled piece of Al-FEP was retrieved that had curled, exposing the back-surface aluminum to space (see the photograph on the right). Because the aluminum surface has a lower thermal emittance than the FEP, this curled piece reached 200 °C during orbit, 150 °C higher than the nominal temperature extreme. To better understand the effect of temperature on the rate of degradation, and on the mechanism of degradation, of this insulation material in the low-Earth-orbit environment, researchers at the NASA Glenn Research Center conducted experiments to determine the effect of heating on the degradation of FEP that has been irradiated in a ground laboratory facility or in space on the HST. For this study, Teflon FEP retrieved from the HST during the third servicing mission after 9.7 years of space exposure was provided to Glenn by the NASA Goddard Space Flight Center.

Samples of pristine FEP were irradiated with 15.3-kV copper x rays. The x-ray exposure was not intended to simulate the full extent of damage occurring on Hubble, but to cause limited irradiation-induced polymer damage such that the additional degradation due to heating would be measurable. Samples of pristine, x-ray irradiated, and HST-retrieved FEP were heat treated from 50 to 200 °C at 25 °C intervals in a high-vacuum facility and evaluated for changes in tensile properties and density. The results indicate that although heating does not degrade the tensile properties of nonirradiated Teflon, there is a significant dependence on the degradation of the percent elongation at failure, and hence embrittlement, of irradiated Teflon as a function of heating temperature, with dramatic degradation occurring at 100 °C and higher exposures (see the graph on the following page). The density of nonheated irradiated FEP (ground or space irradiated) was found to be essentially the same as that of pristine FEP, although these samples are significantly embrittled. This indicates that irradiation induces scission in the polymer chains, resulting in embrittlement, but the polymer chain packing is not affected. Gradual increases in the density occurred with heating from 23 to 75 °C for all samples, with significant increases occurring at 100 °C and higher exposures. Larger increases occurred for the irradiated samples than for the pristine FEP. These results, which show that irradiated FEP experiences greater increases in density than pristine FEP for the same heat treatment, provide insight into the mechanisms of damage of the FEP. They indicate that irradiation causes bonds to break, which allows for greater mobility and crystallization upon heating than that which occurs with nonirradiated FEP. The tensile results and heated density data support chain scission as the primary mechanism of degradation of FEP in the space environment. The results show the significance of the on-orbit service temperature of FEP with respect to its degradation in the low-Earth-orbit space environment, which is important to understand when designing future spacecraft thermal systems.

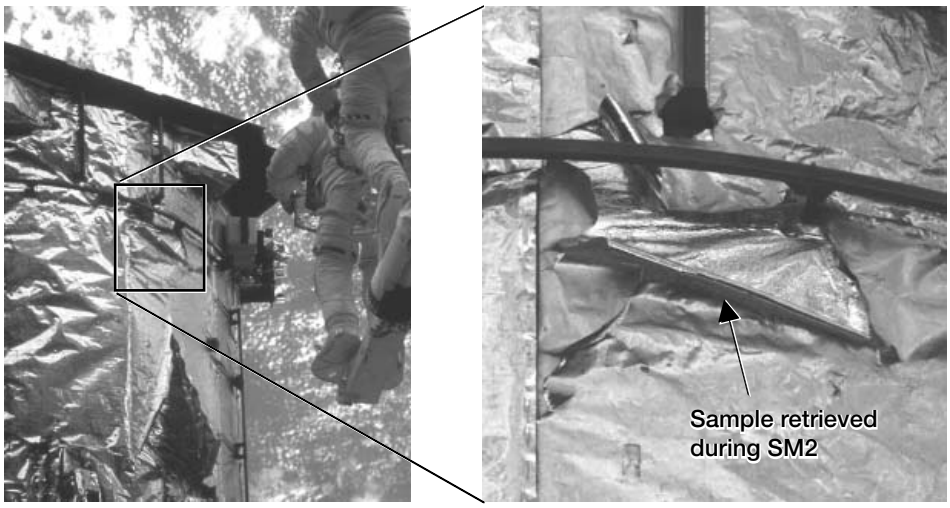

Multilayer insulation damage on the HST as witnessed during the second servicing mission. Left: Two cracked areas in the multilayer insulation outer layer, a large vertical crack and above it a tightly curled area. Right: Closeup of the tightly curled Al-FEP prior to retrieval.

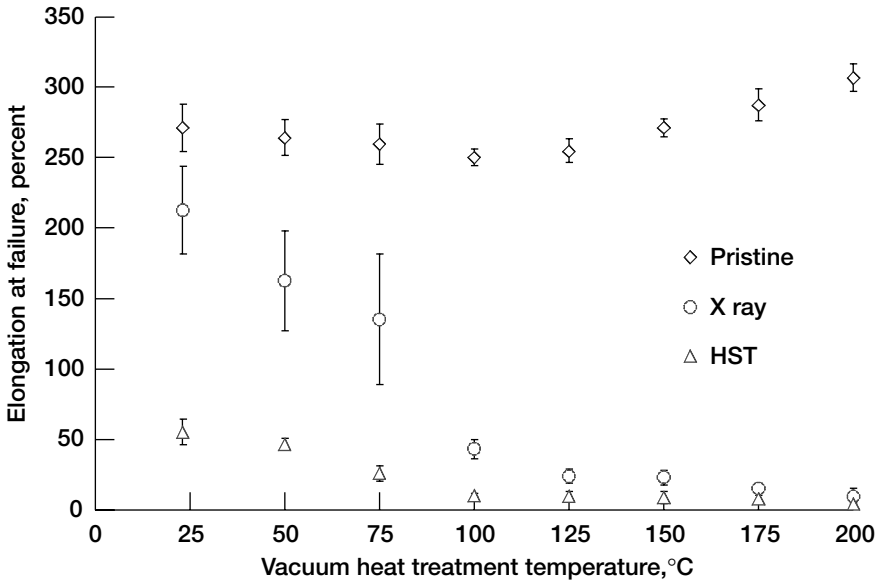

Percent elongation at failure of pristine, ground laboratory x-ray-exposed FEP, and FEP retrieved from the HST as a function of vacuum heat-treatment temperature.

Find out more about this research:
http://www.grc.nasa.gov/WWW/epbranch/

Glenn contact:
Kim K. de Groh, 216–433–2297, Kim.K.deGroh@nasa.gov

Authors:
Kim K. de Groh and Morgana Martin

Headquarters program office: OAT

Programs/Projects: ISS, EOS, DOD, Future LEO spacecraft

Greener Method Developed for Intercalating Graphite Fibers With Bromine

The electrical resistivity of graphite fibers can be lowered by as much as a factor of 10 by the process of intercalation: the insertion of guest atoms or molecules between the graphene planes. Composites fabricated from such resistivity-enhanced fibers are excellent candidates for the replacement of metallic components such as electromagnetic interference shields and grounding planes (ref. 1). The most promising intercalate for such applications is bromine because of the stability of the intercalation compounds in air, vacuum, humidity, and high temperature.

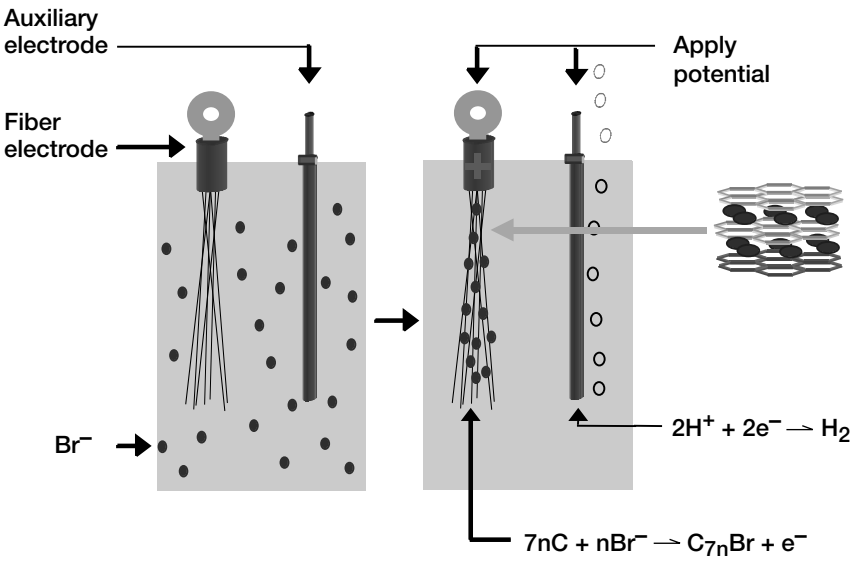

Method used to carry out the electrochemical intercalation of graphite fibers using Br^-.

These fibers have been fabricated primarily by exposing pitch-based or vapor-grown graphite fibers to bromine vapor. Bromine vapors are caustic and toxic. In addition, bromine gas has been implicated in the depletion of the Earth's protective one layer. If a synthesis route could be developed that used the relatively innocuous bromide ion (Br^-), the synthesis could be made less dangerous, and the possible effect on the ozone layer could be reduced.

Electrochemical methods have used Br^- to form bromine-intercalation compounds with graphite fibers and foils. However, the resulting compounds did not have resistivity values as low as those formed using the vapor diffusion method. Researchers

working in the Electro-Physics Branch of the NASA Glenn Research Center have found that, if the temperature is lowered to near the freezing point and the electrochemical current is kept very high, the same low-resistivity intercalation compound is formed as by the vapor diffusion method. The intercalation mechanism is thought to involve the formation of Br_2 at the surface of the fiber, which then intercalates the graphite by the same mechanism as the vapor diffusion method. Glenn's researchers also found that, in keeping with this mechanism, highly crystalline graphite can be intercalated by an aqueous Br_2 without the benefit of electrochemical current. This technique could greatly simplify and make much safer the industrial-scale synthesis of bromine-intercalated graphite fibers.

References

1. Gaier, J.R.: Intercalated Graphite Fiber Composites as EMI Shields in Aerospace Structures. IEEE Trans. Electromagn. Compat., vol. 34, issue 3, pt. 1, 1992, pp. 351–356.

Glenn contact:
Dr. James R. Gaier,
260–982–5075 (Feb-May, Sept-Dec),
216–433–6686 (Jan, Jun-Aug),
James.R.Gaier@nasa.gov

Author: Dr. James R. Gaier

Headquarters program office: OAT

Programs/Projects: High-conductivity, low-weight applications such as aerospace electronics enclosures, notebook computers, and cell phones

Solar Selective Coatings Prepared From Thin-Film Molecular Mixtures and Evaluated

Thin films composed of molecular mixtures of metal and dielectric are being considered for use as solar selective coatings for a variety of space power applications. By controlling molecular mixing during ion-beam sputter deposition, researchers can tailor the solar selective coatings to have the combined properties of high solar absorptance and low infrared emittance. On orbit, these combined properties simultaneously maximize the amount of solar energy captured by the coating and minimize the amount of thermal energy radiated. The solar selective coatings are envisioned for use on minisatellites, for applications where solar energy is used to power heat engines or to heat remote regions in the interior of the spacecraft. Such systems may be useful for various missions, particularly those to middle Earth orbit.

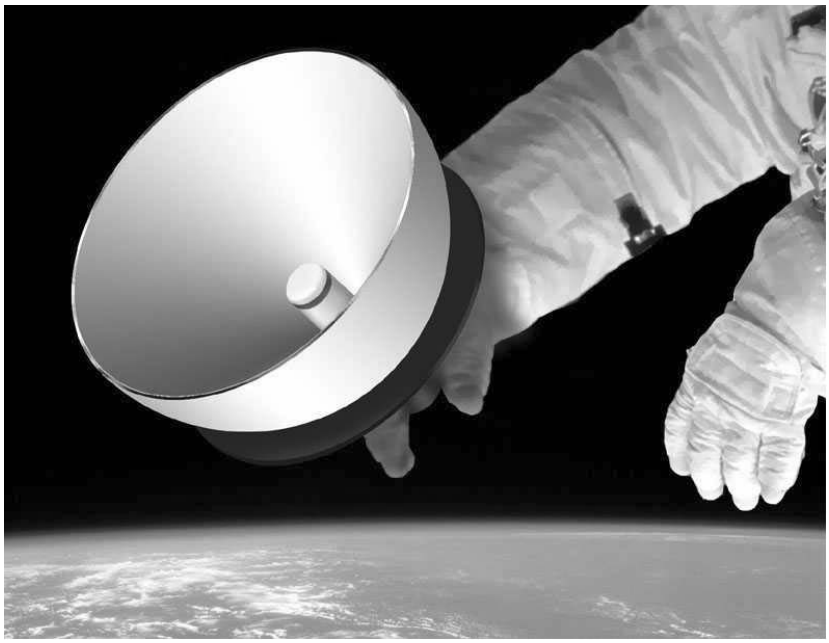

Artist's concept of a Stirling convertor employing a solar selective coating.

Sunlight must be concentrated by a factor of 100 or more to achieve the desired heat inlet operating temperature. At lower concentration factors, the temperature of the heat inlet surface of the heat engine is too low for efficient operation, and at high concentration factors, cavity type heat receivers become attractive. The illustration shows an artist's concept of a heat engine, with the annular heat absorbing surface near the focus of the concentrator coated with a solar selective coating. In this artist's concept, the heat-absorbing surface powers a small Stirling convertor. The astronaut's gloved hand is provided for scale.

Several thin-film molecular mixtures have been prepared and evaluated to date, including mixtures of aluminum and aluminum oxide, nickel and aluminum oxide, titanium and aluminum oxide, and platinum and aluminum oxide. For example, a 2400-Å-thick mixture of titanium and aluminum oxide was found to have a solar absorptance of 0.93 and an infrared emittance of 0.06. On the basis of tests

performed under flowing nitrogen at temperatures as high as 680 °C, the coating appeared to be durable at elevated temperatures. Additional durability testing is planned, including exposure to atomic oxygen, vacuum ultraviolet radiation, and high-energy electrons.

Find out more about this research: http://www.grc.nasa.gov/WWW/epbranch/ephome.htm

Glenn contact:
Dr. Don Jaworske, 216–433–2312, Donald.A.Jaworske@nasa.gov

Author: Dr. Don A. Jaworske

Headquarters program office: OAT

Programs/Projects: DDF, Power System Surfaces/Materials Technology

Power Electronics Being Developed for Deep Space Cryogenic Applications

Electronic circuits and systems designed for deep space missions need to operate reliably and efficiently in harsh environments that include very low temperatures. Spacecraft that operate in such cold environments carry a large number of heaters so that the ambient temperature for the onboard electronics remains near 20 °C. Electronics that can operate at cryogenic temperatures will simplify system design and reduce system size and weight by eliminating the heaters and their associated structures. As a result, system development and launch cost will be reduced.

At the NASA Glenn Research Center, an ongoing program is focusing on the development of power electronics geared for deep space low-temperature environments. The research and development efforts include electrical components design, circuit design and construction, and system integration and demonstration at cryogenic temperatures. Investigations are being carried out on circuits and systems that are targeted for use in NASA missions where low temperatures will be encountered: devices such as ceramic and tantalum capacitors, metal film resistors, semiconductor switches, magnetics, and integrated circuits including dc/dc converters, operational amplifiers, voltage references, and motor controllers. Test activities cover a wide range of device and circuit performance under simple as well as complex test conditions, such as multistress and thermal cycling. The figure shows the effect of low-temperature conditions on the switching characteristics of an advanced silicon-on-insulator field effect transistor. For gate voltages (V_{GS}) below 2.6 V, drain currents at –190 °C are lower than drain currents at room temperature (20 °C).

Researchers in the Low Temperature Electronics Program at Glenn collaborate with other NASA centers, various Government agencies, aerospace companies, and academia to develop technologies that will support NASA missions such as Next Generation Space Telescope and Mars 07, as well as commercial advanced satellites.

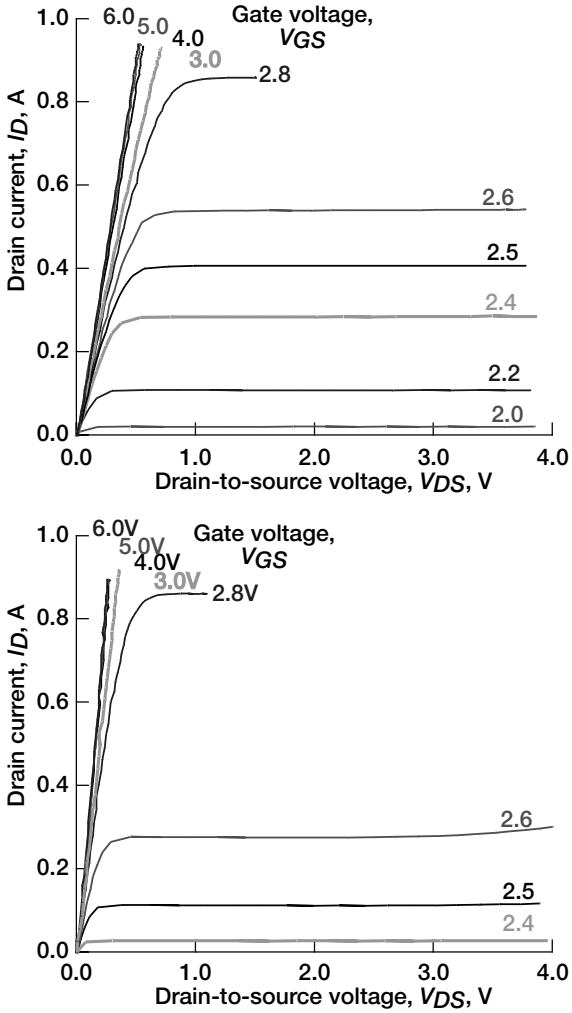

Switching characteristics of an advanced silicon-on-insulator field effect transistor. Top: At 20 °C. Bottom: At –190 °C.

Find out more about this research:
http://www.grc.nasa.gov/WWW/epbranch/ephome.htm

Glenn contact:
Richard L. Patterson, 216–433–8166, Richard.L.Patterson@nasa.gov

Authors: Richard L. Patterson and Ahmad Hammoud

Headquarters program office:
OA (Chief Engineer)

Programs/Projects: NEPP, NEPAG, NGST, Mars 07, Galex, CloudSat

Microelectromechanical System (MEMS) Device Being Developed for Active Cooling and Temperature Control

High-capacity cooling options remain limited for many small-scale applications such as microelectronic components, miniature sensors, and microsystems. A microelectromechanical system (MEMS) using a Stirling thermodynamic cycle to provide cooling or heating directly to a thermally loaded surface is being developed at the NASA Glenn Research Center to meet this need. The device can be used strictly in the cooling mode or can be switched between cooling and heating modes in milliseconds for precise temperature control. Fabrication and assembly employ techniques routinely used in the semiconductor processing industry. Benefits of the MEMS cooler include scalability to fractions of a millimeter, modularity for increased capacity and staging to low temperatures, simple interfaces, limited failure modes, and minimal induced vibration.

The MEMS cooler has potential applications across a broad range of industries such as the biomedical, computer, automotive, and aerospace industries. The basic capabilities it provides can be categorized into four key areas:

(1) Extended environmental temperature range in harsh environments

(2) Lower operating temperatures for electronics and other components

(3) Precision spatial and temporal thermal control for temperature-sensitive devices

(4) The enabling of microsystem devices that require active cooling and/or temperature control

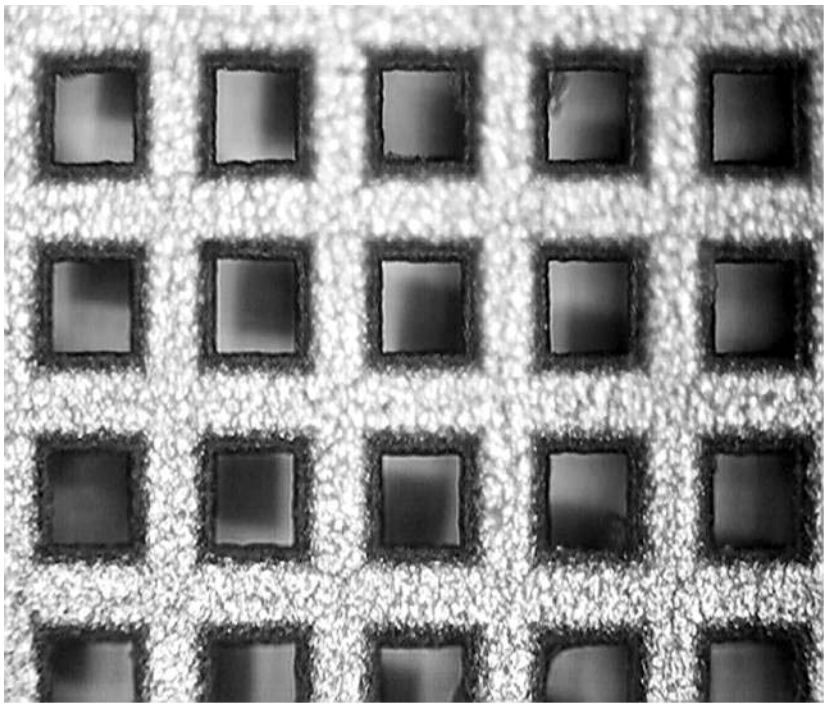

Regenerator microphotograph showing 100-μm openings.

The rapidly expanding capabilities of semiconductor processing in general, and microsystems packaging in particular, present a new opportunity to extend Stirling-cycle cooling to the MEMS domain. The comparatively high capacity and efficiency possible with a MEMS Stirling cooler provides a level of active cooling that is impossible at the microscale with current state-of-the-art techniques. The MEMS cooler technology builds on decades of research at Glenn on Stirling-cycle machines, and capitalizes on Glenn's emerging microsystems capabilities.

A working model of a MEMS cooler device is being assembled and tested at the Johns Hopkins University Applied Physics Laboratory under a Glenn grant. Initial testing will focus on MEMS regenerator performance. The 1- by 1-cm regenerator was fabricated for NASA by Polar Technologies. Commercial (non-MEMS) piezoelectric actuators will be used to drive the compression and expansion diaphragms, which are the only moving parts of the device. The diaphragms are deflected toward and away from the regenerator region in phase-shifted sinusoidal fashion to produce the Stirling cycle. Expansion of the working gas directly beneath the expansion diaphragm in each cycle creates a cold end for extracting heat, whereas compression at the other end creates a hot region for dissipating heat. Heat is transferred to and from the working gas as it is forced through the regenerator region by the moving diaphragms.

Following regenerator characterization tests, the piezoelectric actuators will be replaced with MEMS electrostatic comb-drive actuators fabricated at

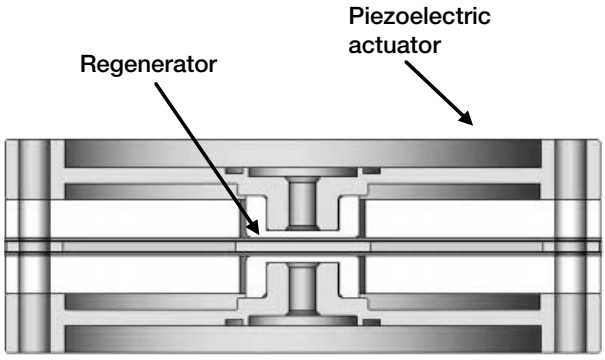

MEMS regenerator with piezoelectric actuators.

Johns Hopkins in preparation for performance tests of a full working model in 2003.

Analysis of the MEMS cooler has been completed and indicates a theoretical performance that is an order-of-magnitude improvement over existing state-of-the-art techniques for cooling small-scale components. Research on the MEMS cooler is a collaborative effort of Glenn and Johns Hopkins. A patent for this technology (Microscalable Thermal Control Device, U.S. Patent 6,385,973 B1) was granted in May 2002.

Find out more about the research of Glenn's Thermo-Mechanical Systems Branch:
http://www.grc.nasa.gov/WWW/tmsb/

Bibliography

Moran, Matthew E.: Multidisciplinary Analysis of a Microsystem Device for Thermal Control. Proceedings of the 11th Thermal and Fluids Analysis Workshop. NASA/CP—2002-211486, 2002, pp. 173–186.

Glenn contacts:
Duane E. Beach, 216–433–8324, Duane.E.Beach@nasa.gov; and Matthew E. Moran, 216–433–8324, Matthew.E.Moran@nasa.gov

Author: Duane E. Beach

Headquarters program office:
OAT (CTD)

Programs/Projects:
CTO, Space Power Technology

Special recognition: Best Paper in Session, 2001 International Symposium on Microelectronics, Micro-scale Avionics Thermal Management

Three-Dimensional Magnetic Analysis Technique Developed for Evaluating Stirling Convertor Linear Alternators

The Department of Energy, the Stirling Technology Company (STC), and the NASA Glenn Research Center are developing Stirling convertors for Stirling radioisotope generators to provide electrical power for future NASA deep space missions. STC is developing the 55-We technology demonstration convertor (TDC) under contract to the Department of Energy. The Department of Energy recently named Lockheed Martin as the system integration contractor for the Stirling radioisotope generator development project. Lockheed Martin will develop the Stirling radioisotope generator engineering unit and has contract options to develop the qualification unit and the first flight unit. Glenn's role includes an in-house project to provide convertor, component, and materials testing and evaluation in support of the overall power system development. As a part of this work, Glenn has established an in-house Stirling research laboratory for testing, analyzing, and evaluating Stirling machines. STC has built four 55-We convertors for NASA, and these are being tested at Glenn. A cross-sectional view of the 55-We TDC is shown in the figure. Of critical importance to the successful development

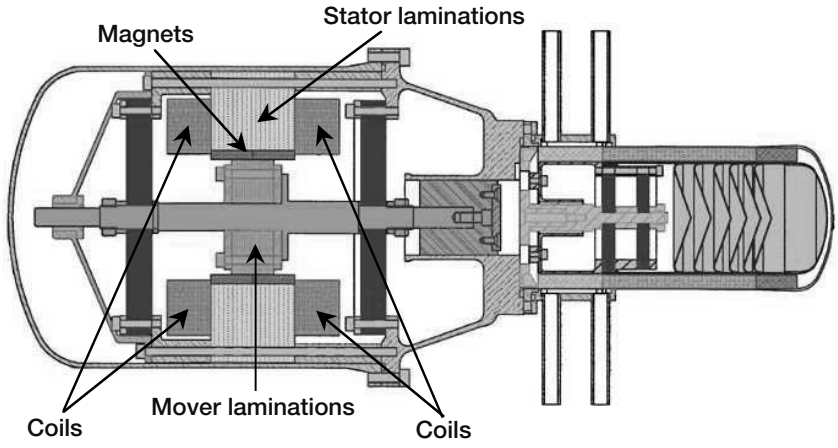

Cross section of STC's 55-We technology demonstration convertor (TDC).

of the Stirling convertor for space power applications is the development of a lightweight and highly efficient linear alternator. In support, Glenn has been developing finite element analysis and finite element method tools for performing various linear alternator thermal and electromagnetic analyses and evaluating design configurations.

A three-dimensional magnetostatic finite element model of STC's 55-We TDC linear alternator was developed to evaluate the demagnetization fields affecting the alternator magnets. Since the actual linear alternator hardware is symmetric to the quarter section about the axis of motion, only a quarter section of the alternator was modeled. The components modeled included the mover laminations, the neodymium-iron-boron magnets, the stator laminations, and the copper coils.

The three-dimensional magnetostatic model was then coupled with a circuit simulator model of the alternator load and convertor controller. The coupled model was then used to generate alternator terminal voltage and current predictions. The predicted voltage and current waveforms agreed well with the experimental data, which tended to validate the accuracy of the coupled model. The model was then used to generate predictions of the demagnetization fields acting on the alternator magnets for the alternator under load.

The preliminary model predictions indicate that the highest potential for demagnetization is along the inside surface of the uncovered magnets. The demagnetization field for the uncovered magnets when the mover is positioned at the end of a stroke is higher than it is when the mover is at the position of maximum induced voltage or maximum alternator current. Assuming normal load conditions, the model predicted that the onset of demagnetization is most likely to occur for magnet temperatures above 101 °C.

Find out more about the research of Glenn's Thermo-Mechanical Systems Branch:
http://www.grc.nasa.gov/WWW/tmsb

Glenn contact:
Steven M. Geng, 216–433–6145, Steven.M.Geng@nasa.gov

Author: Steven M. Geng

Headquarters program office: OSS

Programs/Projects: Advanced Radioisotope Power System, SRG

Brayton Power Conversion Unit Tested—Provides a Path to Future High-Power Electric Propulsion Missions

Closed-Brayton-cycle conversion technology has been identified as an excellent candidate for nuclear electric propulsion (NEP) power conversion systems. Advantages include high efficiency, long life, and high power density for power levels from about 10 kWe to 1 MWe, and beyond. An additional benefit for Brayton is the potential for the alternator to deliver very high voltage as required by the electric thrusters, minimizing the mass and power losses associated with the power management and distribution (PMAD).

To accelerate Brayton technology development for NEP, the NASA Glenn Research Center is developing a low-power NEP power systems test-bed that utilizes an existing 2-kWe

Brayton PCU installed at Vacuum Facility 6.

Brayton power conversion unit (PCU) from previous solar dynamic technology efforts. The PCU includes a turboalternator, a recuperator, and a gas cooler connected by gas ducts. The rotating assembly is supported by gas foil bearings and consists of a turbine, a compressor, a thrust rotor, and an alternator on a single shaft. The alternator produces alternating-current power that is rectified to 120-V direct-current power by the PMAD unit. The NEP power systems testbed will be utilized to conduct future investigations of operational control methods, high-voltage PMAD, electric thruster interactions, and advanced heat rejection techniques.

The PCU was tested in Glenn's Vacuum Facility 6. The Brayton PCU was modified from its original solar dynamic configuration by the removal of the heat receiver and retrofitting of the electrical resistance gas heater to simulate the thermal input of a steady-state nuclear source. Then, the Brayton PCU was installed in the 3-m test port of Vacuum Facility 6, as shown in the photograph. A series of tests were performed between June and August of 2002 that resulted in a total PCU operational time of about 24 hr. An initial test sequence on June 17 determined that the reconfigured unit was fully operational. Ensuing tests provided the operational data needed to characterize PCU performance over its full operating range.

The primary test variables used in operating the Brayton PCU were heater input power and rotor speed. Testing demonstrated a maximum steady-state alternating-current power output of 1835 W at a gas heater power of 9000 W and a rotor speed of 52 000 rpm. The corresponding measured turbine inlet gas temperature was 1076 K, and the compressor inlet gas temperature was 282 K. When insulation losses from the gas heater were neglected, the Brayton cycle efficiency for the maximum power point was calculated to be 24 percent. The net direct-current power output was 1750 W, indicating a PMAD efficiency of about 95 percent.

Find out more about this research:
http://www.grc.nasa.gov/WWW/tmsb/

Glenn contact:
Lee S. Mason, 216–977–7106,
Lee.S.Mason@nasa.gov

Author: Lee S. Mason

Headquarters program office: OSS

Programs/Projects:
In-Space Propulsion

Stirling Convertor Technologies Being Developed for a Stirling Radioisotope Generator

The Department of Energy, Lockheed Martin, Stirling Technology Company (STC), and the NASA Glenn Research Center are developing a high-efficiency Stirling Radioisotope Generator (SRG) for NASA space science missions. The SRG is being developed for multimission use, including providing electric power for unmanned Mars rovers and deep space missions. On Mars, rovers with SRGs would be used for missions that might not be able to

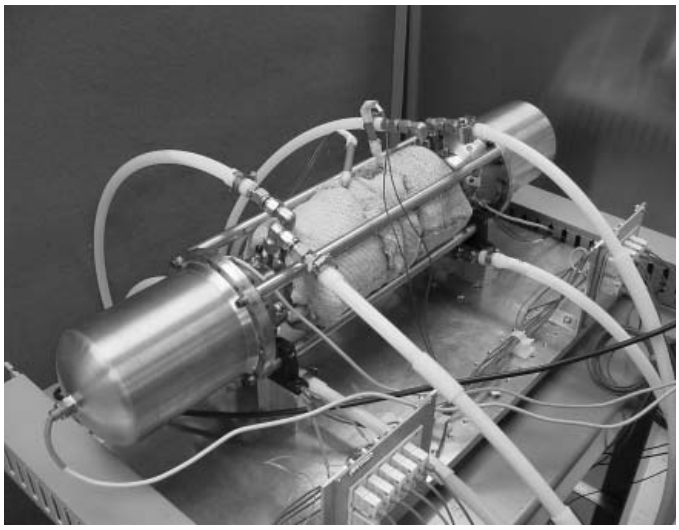

Stirling Technology Demonstration Convertors for a Stirling Radioisotope Generator being tested at Glenn.

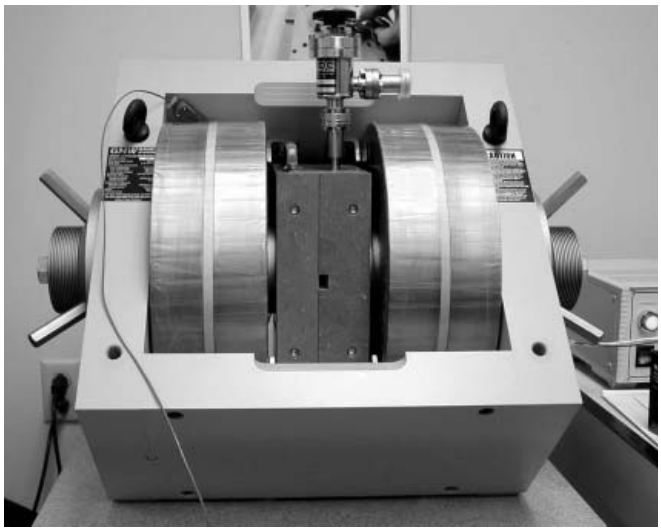

Aging tests of neodymium-iron-boron permanent magnets.

Inconel 718 creep testing.

use photovoltaic power systems, such as exploration at high Martian latitudes and missions of long duration. The projected SRG system efficiency of 23 percent will reduce the required amount of radioisotope by a factor of 4 or more in comparison to currently used Radioisotope Thermoelectric Generators.

The Department of Energy recently named Lockheed Martin as the system integration contractor. Lockheed Martin has begun to develop the SRG engineering unit under contract to the Department of Energy, and has contract options to develop the qualification unit and the first flight units. The developers expect the SRG to produce about 114 Wdc at the beginning of mission, using two opposed Stirling convertors and two General Purpose Heat Source modules. STC previously developed the Stirling convertor under contract to the Department of Energy and is now providing further development as a subcontractor to Lockheed Martin.

Glenn is conducting an in-house technology project to assist in developing the convertor for space qualification and mission implementation. A key milestone was recently reached with the accumulation of 12 000 hr of long-term aging on two types of neodymium-iron-boron permanent magnets. These tests are characterizing any possible aging in the strength or demagnetization resistance of the magnets used in the linear alternator. Preparations are underway for a thermal/vacuum system demonstration and unattended operation during endurance testing of the 55-We Technology Demonstration Convertors. In addition, Glenn is developing a charging system for the convertors to ensure clean fills of the helium working fluid and to monitor levels of any possible contaminants at different test intervals. Possible oxidation effects depend on the level of any oxygen contamination—regenerator materials and displacer radiation shields are now being evaluated for possible oxidation effects.

Heater head life assessment efforts are continuing, and a probabilistic durability assessment has been started. This will look at the effects of variations and uncertainties in the heater head geometry, convertor operating conditions, and Inconel 718 flight material creep data. Over 125 000 hr of creep testing at various stress levels have been completed on samples of the Inconel 718 heater head flight material. A test rig is nearing completion for structural benchmark testing of complete heater heads and heater head shells to factor in the effects of biaxial stresses and to calibrate and validate the heater head life model. The key magnet/lamination epoxy bond is being tested for performance and lifetime characteristics, and alternate methods of bonding and insulating lamination stacks for the linear alternator are being evaluated. Other efforts include independent verification testing of the Technology Demonstration Convertors, three-dimensional linear alternator magnetic analysis, launch environment characterization testing, electromagnetic interference and electromagnetic compatibility characterization and reduction, and reliability studies.

Glenn has also initiated efforts to develop advanced Stirling technologies. Cleveland State University is progressing toward a multidimensional Stirling computational fluid dynamics code capable of modeling complete convertors. A two-dimensional model is now operational. Validation efforts at both Cleveland State and the University of Minnesota are complementing the code development. This year, new efforts were started on the design for a lightweight convertor, advanced controllers, high-temperature materials, and an end-to-end system dynamics model. Performance and mass improvement goals have been established for second- and third-generation Stirling radioisotope power systems.

Find out more about the research of Glenn's Thermo-Mechanical Systems Branch: http://www.grc.nasa.gov/WWW/tmsb

References

1. Cockfield, Robert D.; and Chan, Tak S.: Stirling Radioisotope Generator for Mars Surface and Deep Space Missions. Proceedings of the Thirty-Seventh Intersociety Energy Conversion Engineering Conference. IECEC 2002 Paper No. 20188, 2002.
2. Thieme, Lanny G.; Schrieber, Jeffrey G.; and Mason, Lee S.: Stirling Technology Development at NASA GRC; Revised. NASA/TM—2001-211315/REV1, 2002. http://gltrs.grc.nasa.gov/cgi-bin/GLTRS/browse.pl?2002/TM-2001-211315-REV1.html
3. Thieme, Lanny G.; and Schreiber, Jeffrey G.: NASA GRC Stirling Technology Development Overview. Space Technology and Applications International Forum—STAIF 2003, Mohamed S. El-Genk, ed., AIP Conference Proceedings, vol. 654, 2003, pp. 613–620.

Glenn contacts:
Richard K. Shaltens, 216–433–6138, Richard.K.Shaltens@nasa.gov;
Jeffrey G. Schreiber, 216–433–6144, Jeffrey.G.Schreiber@nasa.gov; and
Lanny G. Thieme, 216–433–6119, Lanny.G.Thieme@nasa.gov

Author: Lanny G. Thieme

Headquarters program office: OSS

Programs/Projects:
SRG, Mars exploration, Mobile Science Laboratory, New Frontiers

Mercury Conditions for the MESSENGER Mission Simulated in High-Solar-Radiation Vacuum Tests

The MESSENGER (Mercury Surface, Space Environment, Geochemistry, and Ranging) spacecraft, planned for launch in March 2004, will perform two flybys of Mercury before entering a year-long orbit of the planet in September 2009. The mission will provide opportunities for detailed characterization of the surface, interior, atmosphere, and magnetosphere of the closest planet to the Sun. The NASA Glenn Research Center and the MESSENGER spacecraft integrator, the Johns Hopkins University Applied Physics Laboratory, have partnered under a Space Act Agreement to characterize a variety of critical components and materials under simulated conditions expected near Mercury. Glenn's Vacuum Facility 6, which is equipped with a solar simulator, can simulate the vacuum and high solar radiation anticipated in Mercury orbit.

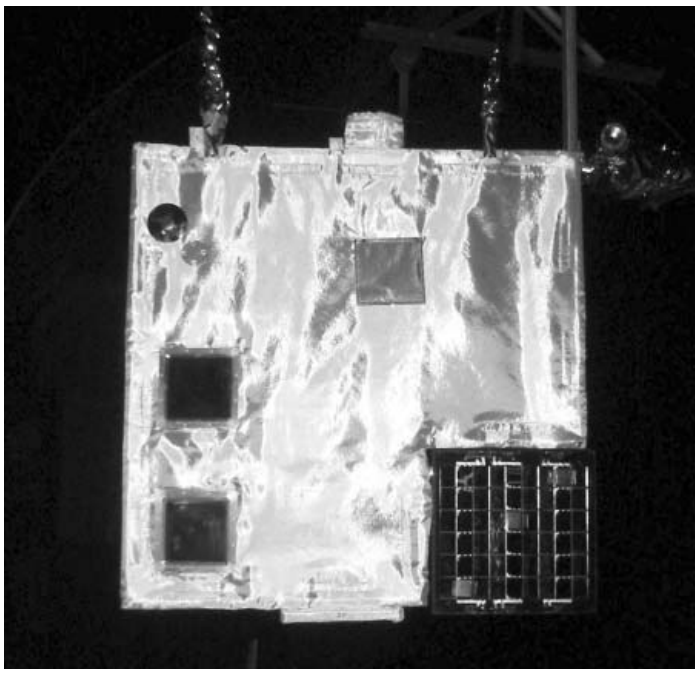

MESSENGER test hardware in the Tank 6 solar thermal vacuum facility.

In 2002, ten solar vacuum tests were conducted, including beginning of life, end of life, backside exposure, and solar panel thermal shock cycling tests. Components tested include candidate solar array panels, sensors, thermal shielding materials, and communication devices. As an example, for the solar panel thermal shock cycling test, two candidate solar array panels were suspended on a lift mechanism that lowered the panels into a liquid-nitrogen-cooled box. After reaching –140 °C, the panels were then lifted out of the box and exposed to the equivalent of 6 suns (8.1 kW/m^2). After five cold soak/heating cycles were completed successfully, there was no apparent degradation in panel performance. An anticipated 100-hr thermal shield life test is planned for autumn, followed by solar panel flight qualification tests in winter. Glenn's ongoing support to the MESSENGER program has been instrumental in identifying design solutions and validating thermal performance models under a very aggressive development schedule. The test data have assisted Johns Hopkins engineers in selecting a flight solar array vendor and a thermal shield design. MESSENGER is one in a series of missions in NASA's Discovery Program.

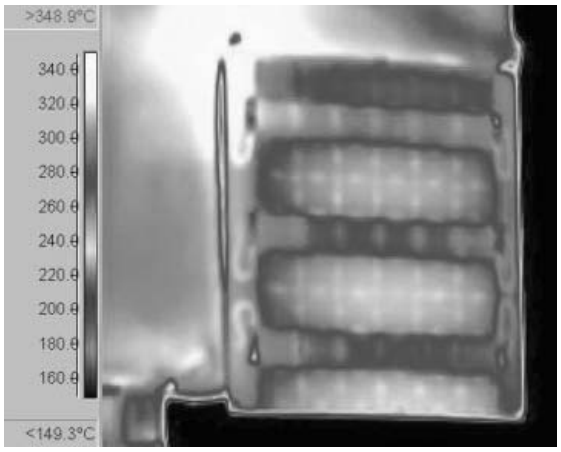

Infrared thermograph of a candidate MESSENGER solar array panel.

Find out more about MESSENGER:
http://messenger.jhuapl.edu

Glenn contact:
Wayne A. Wong, 216–433–6318,
Wayne.A.Wong@nasa.gov

Author: Wayne A. Wong

Headquarters program office: OSS

Programs/Projects:
Discovery, MESSENGER

Instrumentation and Controls

Advanced Packaging Technology Used in Fabricating a High-Temperature Silicon Carbide Pressure Sensor

The development of new aircraft engines requires the measurement of pressures in hot areas such as the combustor and the final stages of the compressor. The needs of the aircraft engine industry are not fully met by commercially available high-temperature pressure sensors, which are fabricated using silicon. Kulite Semiconductor Products and the NASA Glenn Research Center have been working together to develop silicon carbide (SiC) pressure sensors for use at high temperatures. At temperatures above 850 °F, silicon begins to lose its nearly ideal elastic properties, so the output of a silicon pressure sensor will drift. SiC, however, maintains its nearly ideal mechanical properties to extremely high temperatures. Given a suitable sensor material, a key to the development of a practical high-temperature pressure sensor is the package. A SiC pressure sensor capable of operating at 930 °F was fabricated using a newly developed package. The durability of this sensor was demonstrated in an on-engine test.

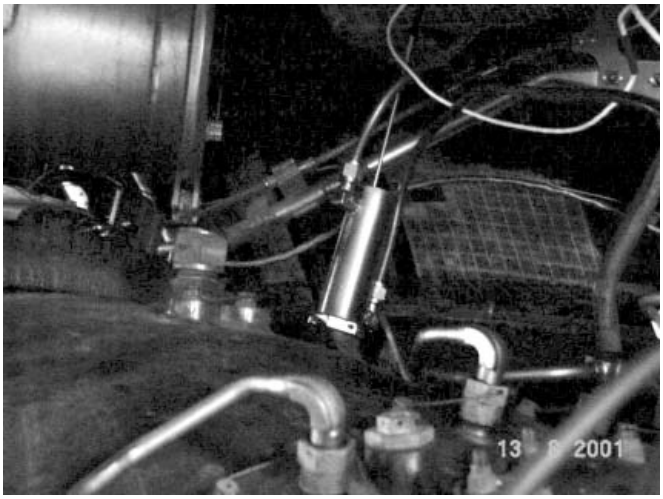

SiC pressure sensor installed in the combustor of an aircraft engine. The sensor is mounted in a water-cooled jacket.

The SiC pressure sensor uses a SiC diaphragm, which is fabricated using deep reactive ion etching. SiC strain gauges on the surface of the diaphragm sense the pressure difference across the diaphragm. Conventionally, the SiC chip is mounted to the package with the strain gauges outward, which exposes the sensitive metal contacts on the chip to the hostile measurement environment. In the new Kulite leadless package, the SiC chip is flipped over so that the metal contacts are protected from oxidation by a hermetic seal around the perimeter of the chip. In the leadless package, a conductive glass provides the electrical connection between the pins of the package and the chip, which eliminates the fragile gold wires used previously.

The durability of the leadless SiC pressure sensor was demonstrated when two 930 °F sensors were tested in the combustor of a Pratt & Whitney PW4000 series engine. Since the gas temperatures in these locations reach 1200 to 1300 °F, the sensors were installed in water-cooled jackets, as shown in the photograph. This was a

severe test because the pressure-sensing chips were exposed to the hot combustion gases. Prior to the installation of the SiC pressure sensors, two high-temperature silicon sensors, installed in the same locations, did not survive a single engine run. The durability of the leadless SiC pressure sensor was demonstrated when both SiC sensors operated properly throughout the two runs that were conducted.

Glenn contact:
Dr. Glenn M. Beheim, 216–433–3847, Glenn.M.Beheim@nasa.gov

Author: Dr. Glenn M. Beheim

Headquarters program office: OAT

Programs/Projects: HOTPC

Ceramic Packages Designed, Fabricated, and Assembled for SiC Microsystems

A series of ceramic substrates and thick-film metalization-based prototype microsystem packages designed for silicon carbide (SiC) high-temperature microsystems have been developed for operation in 500 °C harsh environments. These prototype packages were designed, fabricated, and assembled at the NASA Glenn Research Center. Both the electrical interconnection system and the die-attach scheme for this packaging system have been tested extensively at high temperatures. Printed circuit boards used to interconnect these chip-level packages and passive components also are being fabricated and tested.

NASA space and aeronautical missions need harsh-environment, especially high-temperature, operable microsystems for probing the inner solar planets and for in situ monitoring and control of next-generation aeronautical engines. Various SiC high-temperature-operable microelectromechanical system (MEMS) sensors, actuators, and electronics have been demonstrated at temperatures as high as 600 °C, but most of these devices were demonstrated only in the laboratory environment partially because systematic packaging technology for supporting these devices at temperatures of 500 °C and beyond was not available. Thus, the development of a systematic high-temperature packaging technology is essential for both in situ testing and the commercialization of high-temperature SiC MEMS.

Researchers at Glenn developed new prototype packages for high-temperature microsystems using ceramic substrates (aluminum nitride and 96- and 90-wt% aluminum oxides) and gold (Au) thick-film metalization. Packaging components, which include a thick-film metalization-based wirebond interconnection system and a low-electrical-resistance SiC die-attachment scheme, have been tested at temperatures up to 500 °C. The interconnection system composed of Au thick-film printed wire and 1-mil Au wire bond was tested in 500 °C oxidizing air with and without 50-mA direct current for over 5000 hr. The Au thick-film metalization-based

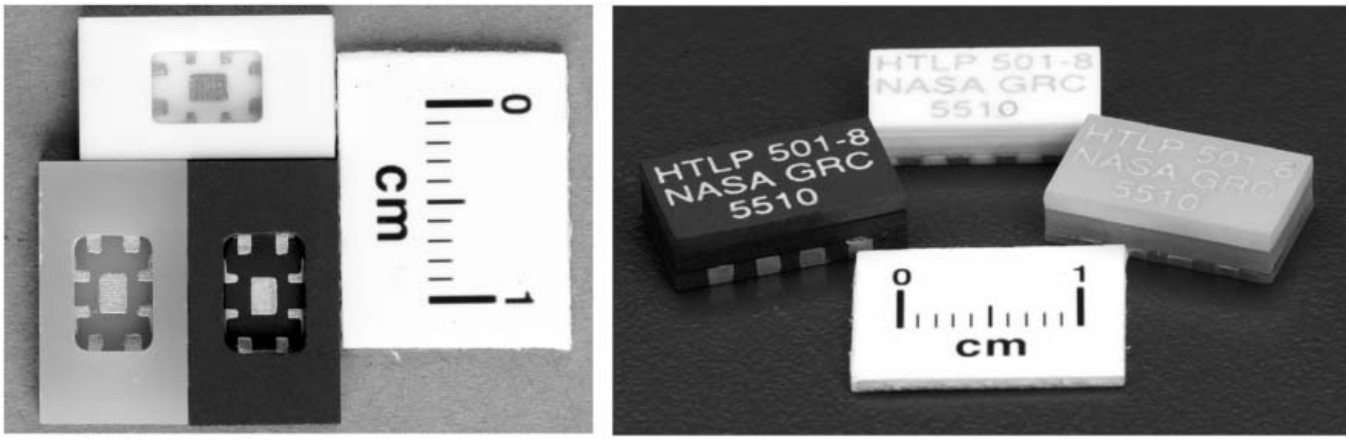

Prototype high-temperature microsystem packages composed of aluminum nitride and 96- and 90-wt% aluminum oxide substrates, and Au thick-film metalization being developed for SiC microsystems with sensors and electronic devices.

wirebond electrical interconnection system was also tested in an extremely dynamic thermal environment to assess thermal reliability. The I–V curve[1] of a SiC high-temperature diode was measured in oxidizing air at 500 °C for 1000 hr to electrically test the Au thick-film material-based die-attach assembly.

As required, the electrical resistance of a thick-film-based electrical interconnection system demonstrated low (2.5 times the room-temperature resistance of the Au conductor) and stable electrical resistance (decreased less than 5 percent during the 5000-hr continuous test). Also as required, the electrical isolation impedance between two neighboring printed wires (of the package shown in the photographs on the preceding page) that were not electrically joined by a wire bond remained high (>0.4 GΩ) at 500 °C in air. Gold ribbon-bond samples (1 by 2 mil) survived 500 thermal cycles between room temperature and 500 °C (with 50 mA direct current), at the rate of 53 °C/min, without electrical failure. An attached SiC diode demonstrated low (< 3.8 Ω-mm^2) and relatively consistent forward resistance from room temperature to 500 °C. These results indicate that the prototype package and the compatible die-attach scheme meet the initial design standards for low-power, long-term, and high-temperature operation. This technology will be further developed and evaluated for various MEMS devices and systems.

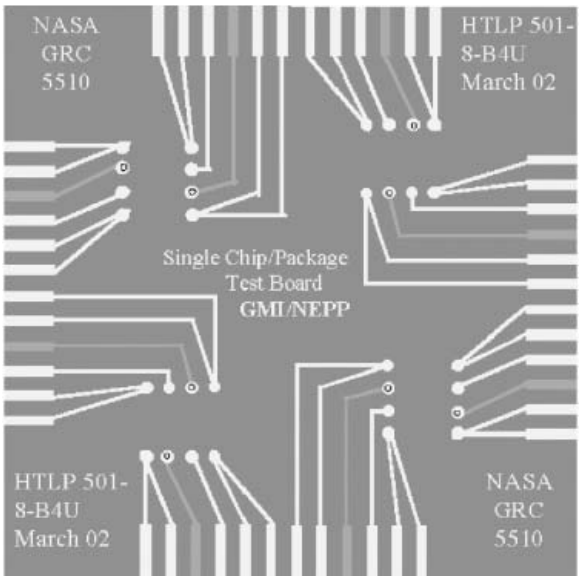

A prototype high-temperature printed circuit board designed for chip-level packages made of aluminum nitride or aluminum oxide substrates is being developed. The printed circuit board shown is designed for testing a single package or a packaged device or system at high temperatures.

Printed circuit boards to be used to interconnect these chip-level packages and passive components are being fabricated and tested. The figure shows the design of a printed circuit board to be used to characterize eight-pin low-power (packaged) devices or packages at temperatures up to 500 °C.

Find out more about this research: http://www.grc.nasa.gov/WWW/sensors/

Ohio Aerospace Institute (OAI) contact:
Dr. Liang-Yu Chen, 216–433–6458, Liangyu.Chen@grc.nasa.gov

Glenn contact:
Dr. Lawrence G. Matus, 216–433–3650, Lawrence.G.Matus@nasa.gov

U.S. Army, Vehicle Technology Directorate at Glenn contact:
Dr. Jih-Fen Lei, 216–433–6328, Jih-Fen.Lei@grc.nasa.gov

Author: Dr. Liang-Yu Chen

Headquarters program office:
OAT, OSS

Programs/Projects: GMI, NEPP, UEET

[1]Current-voltage curve.

Thin-Film Air-Mass-Flow Sensor of Improved Design Developed

Researchers at the NASA Glenn Research Center have developed a new air-mass-flow sensor to solve the problems of existing mass flow sensor designs. NASA's design consists of thin-film resistors in a Wheatstone bridge arrangement. The resistors are fabricated on a thin, constant-thickness airfoil to minimize disturbance to the airflow being measured. The photograph on the next page shows one of NASA's prototype sensors. In comparison to other air-mass-flow sensor designs, NASA's thin-film sensor is much more robust than hot wires, causes less airflow disturbance than pitot tubes, is more accurate than vane anemometers, and is much simpler to operate than thermocouple rakes.

NASA's thin-film air-mass-flow sensor works by converting the temperature difference seen at each leg of the thin-film Wheatstone bridge into a mass-flow rate. The figure at the bottom of the next page shows a schematic of this sensor with air flowing around it. The sensor operates as follows: current is applied to the bridge, which

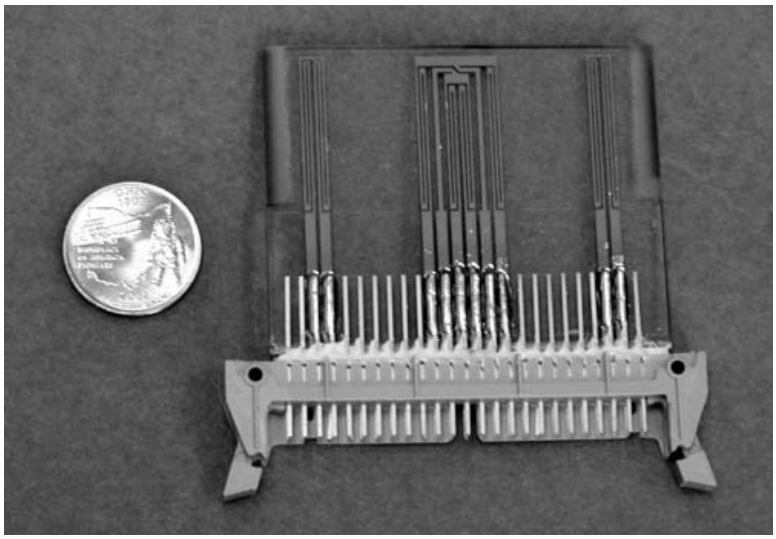

Thin-film air-mass-flow sensor of improved design.

increases its temperature. If there is no flow, all the arms are heated equally, the bridge remains in balance, and there is no signal. If there is flow, the air passing over the upstream legs of the bridge reduces the temperature of the upstream legs and that leads to reduced electrical resistance for those legs. After the air has picked up heat from the upstream legs, it continues and passes over the downstream legs of the bridge. The heated air raises the temperature of these legs, increasing their electrical resistance. The resistance difference between the upstream and downstream legs unbalances the bridge, causing a voltage difference that can be amplified and calibrated to the airflow rate. Separate sensors mounted on the airfoil measure the temperature of the airflow, which is used to complete the calculation for the mass of air passing by the sensor.

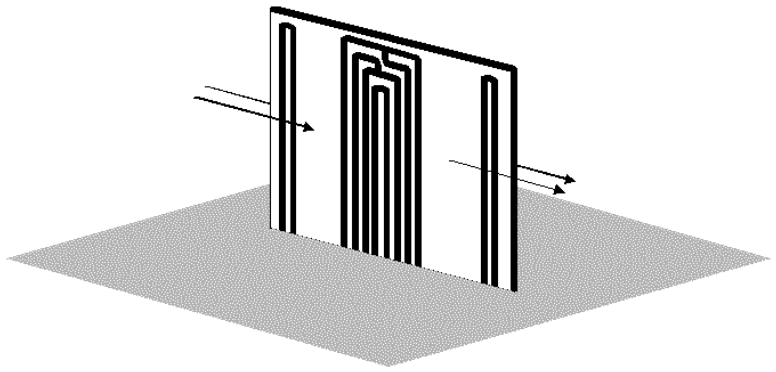

NASA's thin-film air-mass-flow sensor with air flowing around it.

A current application for air-mass-flow sensors is as part of the intake system for an internal combustion engine. A mass-flow sensor is used to provide accurate information about the amount of air entering the engine so that the amount of fuel can be adjusted to give the most efficient combustion. The ideal mass-flow sensor would be a rugged design that minimizes the disturbance to the flow stream and provides an accurate reading of both smooth and turbulent flows; NASA's design satisfies these requirements better than any existing design. Most of the mass-flow sensors used today are the hot wire variety. Hot wires can be fragile and cannot accurately measure a turbulent or reversing flow, which is often encountered in an intake manifold. Other types of mass-flow sensors include pitot tubes, vane anemometers, and thermocouple rakes—all of which suffer from some type of performance problem. Because it solves these performance problems while maintaining a simple design that lends itself to low-cost manufacturing techniques, NASA's thin-film resistance temperature detector air-mass-flow sensor should lead to more widespread use of mass-flow sensors.

Glenn contacts:
Gus Fralick, 216–433–3645, Gustave.C.Fralick@nasa.gov; and John Wrbanek, 216–433–2077, John.D.Wrbanek@nasa.gov

Authors: Gustave C. Fralick, John D. Wrbanek, and Dr. Danny P. Hwang

Headquarters program office: OAT

Programs/Projects: SRF

Microfabricated Gas Sensors Demonstrated in Fire and Emission Applications

A range of microfabricated chemical sensors are being developed to meet the needs of fire detection and emission monitoring in aerospace applications. These sensors have the advantages over traditional technology of minimal size, weight, and power consumption as well as the ability to be placed closer to where the measurements need to be made. Sensor arrays are being developed to address detection needs in environments where multiple species need to be measured. For example, the monitoring of chemical species such as carbon monoxide (CO), carbon dioxide (CO_2), hydrocarbons, and other species is important in the detection of fires on airplanes and spacecraft. In contrast, different sensors are necessary for characterizing some aircraft engine designs where the monitoring of nitrogen oxides (NO_x) and CO is of high interest. Demonstration of both fire and emission microsensor technology was achieved this year in a collaborative effort undertaken by the NASA Glenn Research Center, Case Western Reserve University, and Makel Engineering, Inc.

An array of candidate microfabricated fire detection sensors were tested in the Federal Aviation Administration's (FAA) Cargo Bay Test Facilities in a Boeing 707. Controlled fires are set in this cargo bay on a regular basis, and the behavior of the fire and fire detection equipment is monitored in this specially configured facility (see the figure below). Microfabricated sensors, including nanocrystalline tin oxide sensors and electrochemical oxygen/humidity sensors, monitored the cargo bay as fires were set. At the onset of several fires in the cargo bay, the sensors showed a very repeatable pattern and appropriate sensitivity and response characteristics. We concluded that the onset of fire can be detected with these sensors. Such chemical information is intended to complement existing fire detection technology and decrease the rate of false alarms.

Microfabricated emission sensors were tested in the exhaust stream of a JT–12 jet engine running diesel fuel (see the photographs on the next page) in collaboration with the Arnold Engineering Development Center. Samples were drawn through a rake of gas ports as the ports moved across the engine outlet, and comparative

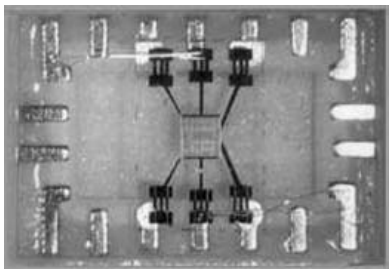

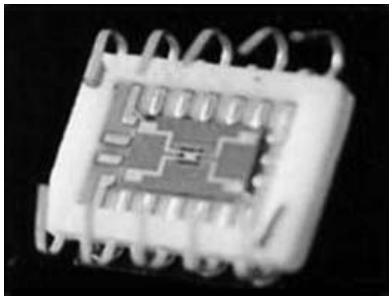

Fire detection testing and microfabricated sensors. Top left: Boeing 707 fuselage used for FAA fire detection testing. Top right: Fire detection sensors installed in an FAA fuselage in which a fire was set and the sensor response monitored. Bottom left: Tin oxide sensor tested. Bottom right: Oxygen-sensor tested.

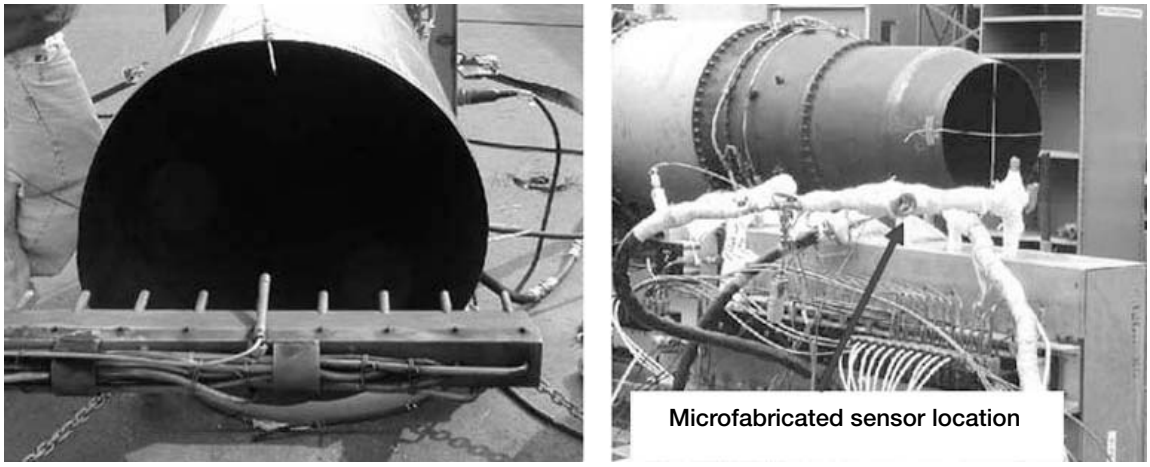

Microfabricated emissions sensors. Left: The rake sampling system at the outlet of the JT–12 jet engine. Right: Location of the sensors in the flow stream of the rake. The high-temperature operational capability of the sensors allow placement significantly closer to the engine outlet than traditional equipment.

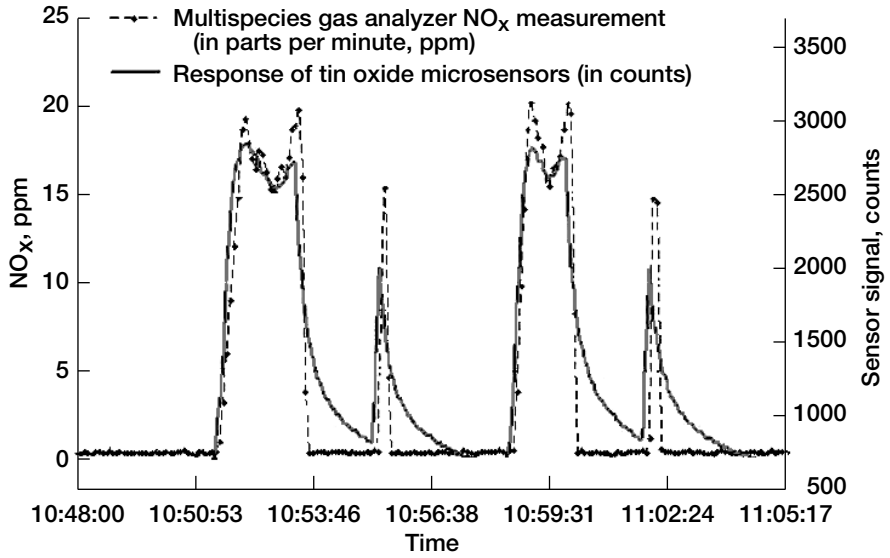

Comparison of the NO_x readings measured by the microfabricated sensors and multigas analyzers as the rake is moved across the engine exhaust outlet.

data were recorded for both the sensors and multigas analyzers associated with the facility. The sensor's response qualitatively paralleled the NO_x readings measured by the multigas analyzers as the rake was drawn across various points in the engine outlet (see the graph). Similar ability of the sensors to parallel the multigas analyzer results were seen in CO monitoring. The recovery time of the NO_x signal differs from that of the multigas analyzers perhaps because of the relative location of the sensors in the sampling stream. However, the advantage of the miniature sensor approach is its relative simplicity and the reduced response time associated with the sensors in the stream in comparison to the remotely located analyzers whose responses are delayed by the time necessary to transport the gas to the analyzers.

These tests demonstrate the use of microfabricated chemical sensor technology in a range of environments. Further work is necessary to correlate the sensor's quantitative responses with the species generated in both applications and to improve sensor packaging for the specific environment.

Find out more about this research:

Chemical species gas sensors:
http://www.grc.nasa.gov/WWW/chemsensors/

Glennan Microsystems:
http://www.glennan.org/

References

1. Hunter, Gary W., et al.: Microfabricated Chemical Sensors for Space Health Monitoring Applications. AIAA Paper 2001–4689, 2001.
2. Hunter, G.W., et al.: Development of Chemical Sensor Arrays for Harsh Environments. Sensors, 2002, Proceedings of IEEE, vol. 2, 2002, pp. 1126–1133.

Glenn contact:
Dr. Gary W. Hunter, 216–433–6459, Gary.W.Hunter@nasa.gov

Author: Dr. Gary W. Hunter

Headquarters program office: OAT

Programs/Projects: AvSP, STTR

Silicon Carbide Nanotube Synthesized

Carbon nanotubes (CNTs) have generated a great deal of scientific and commercial interest because of the countless envisioned applications that stem from their extraordinary materials properties. Included among these properties are high mechanical strength (tensile and modulus), high thermal conductivity, and electrical properties that make different forms of single-walled CNTs either conducting or semiconducting, and therefore, suitable for making ultraminiature, high-performance CNT-based electronics, sensors, and actuators. Among the limitations for CNTs is their inability to survive in high-temperature, harsh-environment applications. Silicon carbon nanotubes (SiCNTs) are being developed for their superior material properties under such conditions. For example, SiC is stable in regards to oxidation in air to temperatures exceeding 1000 °C, whereas carbon-based materials are limited to 600 °C. The high-temperature stability of SiCNTs is envisioned to enable high-temperature, harsh-environment nanofiber- and nanotube-reinforced ceramics. In addition, single-crystal SiC-based semiconductors are being developed for high-temperature, high-power electronics, and by analogy to CNTs with silicon semiconductors, SiCNTs with single-crystal SiC-based semiconductors may allow high-temperature harsh-environment nanoelectronics, nanosensors, and nanoactuators to be realized.

Another challenge in CNT development is the difficulty of chemically modifying the tube walls, which are composed of chemically stable graphene sheets. The chemical substitution of the CNTs' walls will be necessary for nanotube self-assembly and biological- and chemical-sensing applications. SiCNTs are expected to have a different multiple-bilayer wall structure, allowing the surface Si atoms to be functionalized readily with molecules that will allow SiCNTs to undergo self-assembly and be compatible with a variety of materials (for biotechnology applications and high-performance fiber-reinforced ceramics).

The NASA Glenn Research Center has been collaborating with Rensselaer Polytechnic Institute to realize the synthesis of SiC nanotubes. Several methodologies, including chemical conversion of CNTs to SiCNTs, direct SiCNT growth on catalyst, and template-derived SiCNTs (where the template acts as a nanomold) are being explored. In the template synthesis, polymer infiltration has resulted in polycrystalline/amorphous nanofibrils and nanobamboo, whereas chemical vapor deposition into these nanomolds has resulted in polycrystalline/amorphous hollow, uniform tubes.

Glenn contacts:
Dr. David J. Larkin, 216–433–8718, David.Larkin@nasa.gov; and
Dr. Michael A. Lienhard, 216–433–8932, Michael.A.Lienhard@nasa.gov

Authors: Dr. Michael A. Lienhard and Dr. David J. Larkin

Headquarters program office: OAT

Programs/Projects:
Propulsion and Power, UEET, CICT (NASA Ames Research Center)

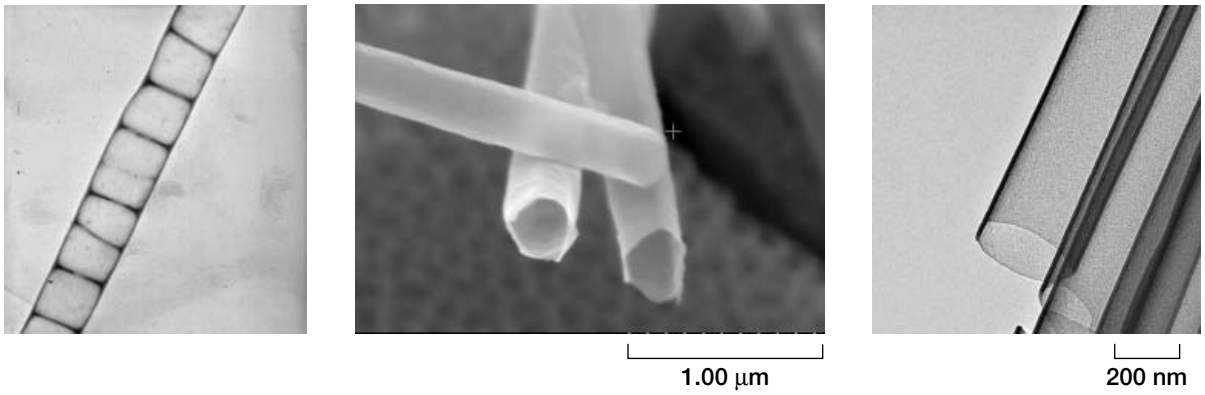

Left: Transmission electron microscope image of SiC nanobamboo, 200 nm in diameter. Center: Scanning electron microscope image of chemical-vapor-deposition-template SiCNTs, 200 nm in diameter. Right: Transmission electron microscope image of chemical-vapor-deposition-template SiCNTs, demonstrating thin, uniform walls.

Improved Silicon Carbide Crystals Grown From Atomically Flat Surfaces

The NASA Glenn Research Center is demonstrating that atomically flat (i.e., step-free) silicon carbide (SiC) surfaces are ideal for realizing greatly improved wide bandgap semiconductor films with lower crystal defect densities. Further development of these improved films could eventually enable harsh-environment electronics beneficial to jet engine and other aerospace and automotive applications, as well as much more efficient and compact power distribution and control. The technique demonstrated could also improve blue-light lasers and light-emitting-diode displays.

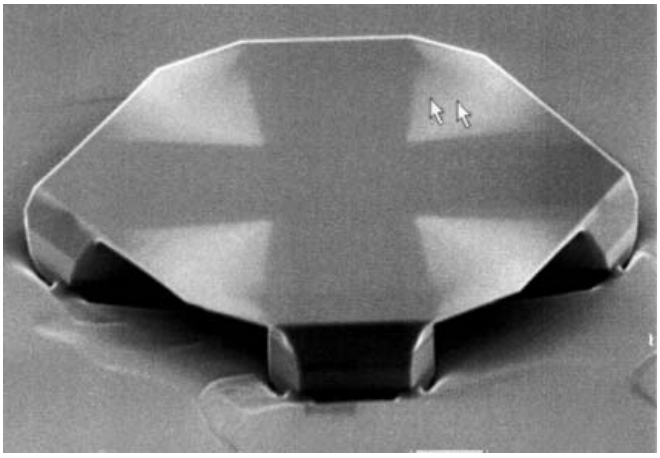

A flattened and enlarged SiC mesa. The lighter, V-shaped sections (see arrows) are the webbed material that was grown between the legs of the darker, plus-sign-shaped original mesa.

Step-free surfaces are produced on commercial on-axis 4H-SiC wafers by first dry etching trench patterns into the wafer surface to form an array of isolated growth mesas. Pure step-flow growth, which permits substrate polytype stacking to be maintained in the epilayer, is then used to grow all initial surface steps on top of each mesa over to the mesa edge, leaving behind an array of mesas with top surfaces entirely free of atomic steps. When a proper pregrowth mesa shape was chosen and new island nucleation was suppressed, thin cantilevered webs were grown that extended laterally from the top edges of step-free mesas. The photomicrograph above illustrates how thin lateral webbing produced an enlarged step-free hexagonal tabletop starting from a plus-shaped pregrowth mesa. Because the crystal structure of the webbing is established laterally from the top of the mesa sidewalls, successful overgrowth of crystal defects located in the substrate trenches below the webbing is accomplished.

The ideal step-free surfaces can then be used to carry out a step-free surface heteroepitaxy process that has produced the best-quality 3C-SiC films ever reported. Lowering the growth temperature after step-free surface formation induced island nucleation and growth of 3C-SiC on the step-free basal plane 4H-SiC surfaces. In this situation, the film crystal structure changed from a 4H structure to a 3C-SiC structure. In addition, we discovered that the initial 3C-SiC bilayers must be nucleated slowly to achieve 3C-SiC films free of stacking fault defects. The figure to the left compares 0.2- by 0.2-mm mesas, both topped with a nearly 2-μm-thick 3C-SiC film and thermally oxidized to reveal stacking fault defects, which were grown with a high initial island nucleation rate (left) and with a low initial island nucleation rate (right). The behavior observed in this figure is partly attributed to the difference in interatomic spacing between the 3C and 4H crystal structures of SiC. NASA scientists suggest that the single-island growth mode, whereby a single 3C island nucleates and expands laterally to cover the mesa before a second interfering 3C island nucleates, is required during the initial stages of growth to obtain high-quality 3C-SiC films. The experimental findings indicate that lattice mismatch was (at least partially) relieved without generating stacking faults that threaded

3C-SiC films on flattened mesas after thermal oxidation that reveals crystal defects. The defect-free film shown on the right was made using step-free surface heteroepitaxy.

to the surface of the film. Further growth and characterization experiments are being undertaken, including the fabrication of prototype 3C-SiC devices and attempting step-free surface heteroepitaxy of aluminum gallium nitride films on 4H- or 6H-SiC substrates.

Further information about the benefits of SiC electronics and research at Glenn is available online: http://www.grc.nasa.gov/WWW/SiC/SiC.html

PDF files of peer-reviewed scientific papers describing the work in detail also are available:
http://www.grc.nasa.gov/WWW/SiC/publications/ICSCRM2001Web.pdf
http://www.grc.nasa.gov/WWW/SiC/publications/ICSCRM2001-3Chepi.pdf

This technology is covered by U.S. Patents 6,461,994 B2 and 6,488,771 B1, which are available for licensing through the NASA Glenn Commercial Technology Office. **These patents can be accessed online at the U.S. Patent and Trademark Office:** http://www.uspto.gov

Glenn contacts:
Dr. Philip G. Neudeck, 216–433–8902, Philip.G.Neudeck@nasa.gov

Ohio Aerospace Institute (OAI) contact:
Andrew J. Trunek, 216–433–6736, Andrew.J.Trunek@grc.nasa.gov

Sest, Inc., contact:
J. Anthony Powell, 216–433–3652, J.A.Powell@grc.nasa.gov

Author: Dr. Philip G. Neudeck

Headquarters program office: OAT

Programs/Projects: CICT, ECT, UEET

Multiwavelength Pyrometer Developed for Use at Elevated Temperatures in Aerospace Applications

Researchers at the NASA Glenn Research Center have developed a unique multiwavelength pyrometer for aerospace applications. It has been shown to be a useful and versatile instrument for measuring the surface temperatures of ceramic zirconia thermal barrier coatings (TBCs) and alumina, even when their emissivity is unknown. The introduction of fiber optics into the pyrometer has greatly increased the ease of using this instrument. Direct comparison of measurements obtained using the pyrometer and thin-film thermocouples on a sample provided independent verification of pyrometry temperature measurement.

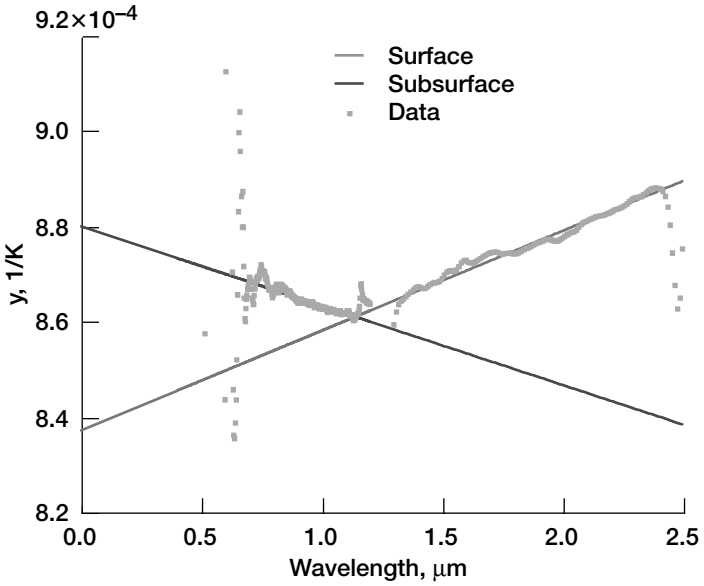

Surface and subsurface temperatures measured in a transparent glass. $y = 1/T - \lambda/c_2[\ln(\varepsilon\tau)]$, where T is the absolute temperature in kelvin, λ is the wavelength in meters, c_2 is the 2nd Plank radiation constant in meters times kelvin, ε is the material emissivity, and τ is the transmissivity of the intervening media. At $\lambda = 0$, the value of y is the inverse of the material's temperature.

Application of the pyrometer has also included simultaneous surface and bulk temperature measurement in a transparent material (shown in the graph), the measurement of combustion gas temperatures in the flames of an atmospheric burner, the measurement of the temperature distribution appearing on a large surface from the recording of just a single radiation spectrum emitted from this nonuniform temperature surface, and the measurement of some optical properties for special aeronautical materials—such as nanostructured layers.

The multiwavelength pyrometer temperature is obtained from a radiation spectrum recorded over a broad wavelength region by transforming it into a straight line segment(s) (as shown in the graph) in part or all of the spectral region. The intercept of the line segment(s) with the vertical axis at zero wavelength gives the

inverse of the temperature. In a two-color pyrometer, the two data points are also amenable to this analysis to determine the unknown temperature. Implicit in a two-color pyrometer is the assumption of wavelength-independent emissivity. Its two (and minimum) pieces of data are sufficient to determine this straight line. However, a multiwavelength pyrometer not only has improved accuracy but also confirms that the wavelength-independent emissivity assumption is valid when a multitude of data points are shown to lie on a simple straight line.

Glenn contact:
Gus Fralick, 216–433–3645,
Gustave.C.Fralick@nasa.gov

Author: Dr. Daniel L. Ng

Headquarters program office: OAT

Programs/Projects: HITEMP, HOTPC, Propulsion and Power

Bibliography

Ng, Daniel; and Fralick, Gustave: Use of a Multiwavelength Pyrometer in Several Elevated Temperature Aerospace Applications. Rev. Sci. Ins., vol. 72, issue 2, 2001, pp. 1522–1530.

Collaboration of the NASA Glenn Research Center and Rolls-Royce Developed Thin Film Multilayered Dielectrics for Harsh Environments

The use of thin films to electrically insulate thin film sensors on engine components minimizes the intrusiveness of the sensors and allows a more accurate measurement of the environment. A variety of insulating films were investigated for preventing electrical shorting caused by insulator failure between the sensor and the component. By alternating layers of sputtered high-temperature ceramics, a sequence of insulating layers was devised that (1) prevents pinholes from forming completely through the insulator and (2) maintains high electrical resistivity at high temperatures. The total thickness is only a fraction of that needed for conventional insulating techniques.

The Sensors and Electronics Technology Branch of the NASA Glenn Research Center has an in-house effort to develop thin film sensors for surface measurement in propulsion system research. Thin film sensors do not require special machining of the components on which they are mounted, and they are considerably thinner (less than 10 μm thick) than wire or foil sensors. The thin film sensors are thus much less disturbing to the operating environment and have a minimal impact on the physical characteristics of the supporting component.

To further this research, NASA Glenn and Rolls-Royce (Derby, UK), with assistance from the Ohio Aerospace Institute (OAI) and the Akima Corporation, pursued a joint investigation using multilayered thin film dielectrics as a reliable insulator in harsh environments. The use of a multilayered scheme is thought to be promising for the fabrication of electrically insulating thin films. A major cause of conduction in thin film dielectrics is the presence of defects, such as pinholes, that propagate through the film to the underlying substrate surface. By alternating the insulating material, each new growth pattern would deviate from the previous one, eliminating direct pathways for conduction to the substrate.

The film depositions and testing were conducted in the Instrument Research Laboratory at Glenn. The multilayered insulator test samples were made from alumina and stainless steel shims that were first covered with a sputtered underlayer of either yttria-stabilized zirconia or chromium carbide, and then overcoated with a sputtered top layer of alumina. An example of a test sample is shown in the photograph below. Each multilayered insulator sample was 5 μm thick, at least an order of magnitude thinner than conventional insulators. The insulating properties of the samples were tested in a high-temperature air oven to determine their suitability.

The multilayer insulators tested showed a stabilized film at temperatures in excess of 800 °C (1472 °F). The underlying materials in these multilayers allow thermal expansion stresses produced during the heating to be graded.

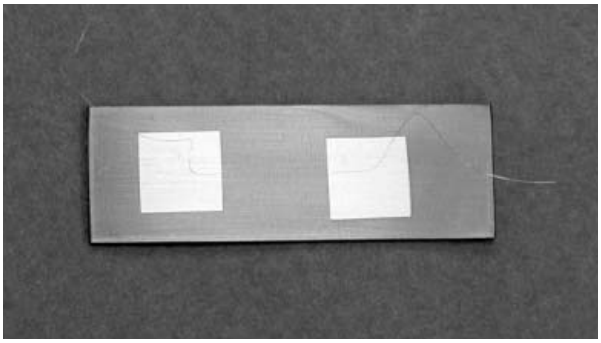

Zirconia-alumina multilayer on a metal substrate.

The chromium carbide-alumina multilayer had the best adhesion at high temperatures, presumably from the induced chemical bonding between the substrate and the chromium carbide underlayer. However, the zirconia-alumina multilayer proved to have slightly better insulating properties when adhering.

The application of the zirconia-alumina insulator has been demonstrated on a nickel-alloy fan blade, as shown in the photograph to the right. The insulators using thin film sensors still need to be tested in a relevant high-temperature combustion environment.

Glenn contacts: John Wrbanek, 216–433–2077, John.D.Wrbanek@nasa.gov; and Gus Fralick, 216–433–3645, Gustave.C.Fralick@nasa.gov

Authors: John D. Wrbanek, Gustave C. Fralick, A. Rachel Busfield, Valarie D. Thomas, and Charles A. Blaha

Headquarters program office: OAT

Programs/Projects: ASTP

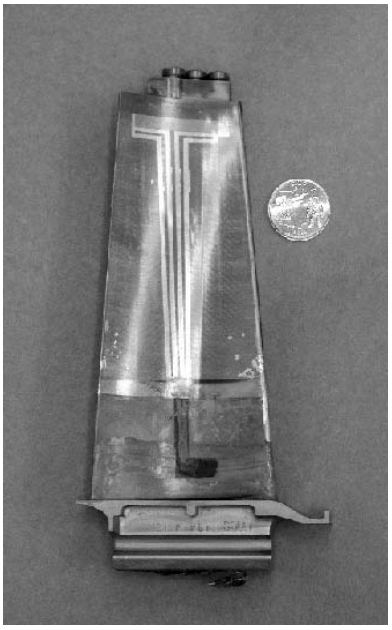

Zirconia-alumina multilayer insulating a resistance temperature detector on a nickel-alloy fan blade.

Fiber-Optic Bragg Gratings and Optical Holography Compared as Vibration Detectors

The NASA Glenn Research Center is interested in determining structural damage in engine components during flight to evaluate the health of aerospace propulsion systems. On the ground, we can use holography to detect structural damage by examining the characteristic mode shapes and frequencies of vibrating objects. We are studying the feasibility of using embedded fiber Bragg gratings (FBGs) to accomplish this goal in a flight-worthy system, by using the minimal intrusion and high sensitivity afforded by fiber optics. We have recently compared holographically imaged modes of vibrating plates with the corresponding dynamic strains detected by embedded FBGs.

We constructed an experimental setup for studying the responses of FBGs to dynamic excitations. One of the plates was made of a polymer matrix composite (PMC) with an FBG embedded in it, and the other one was made of copper with surface-mounted FBGs. The instrumented plates were mounted and vibrated, and time-averaged holography was used to measure their surface displacements. Simultaneously, the signals from the FBGs were detected and sent via fiber-optic cable to a quiet location about 20 m away for interrogation.

The top figure on the next page shows the test configuration used for the PMC plate. Experimental results are shown in the bottom figure. The FBG was embedded in the middle of the PMC plates, roughly within the center circular fringe in each of the interferograms shown in the bottom figure. Two resonant excitation frequencies were used: 706 and 3062 Hz. The plot in the figure shows a larger FBG signal at the higher frequency; this is because the plate bends more at higher order resonant modes, causing higher strain. This contrasts to the smaller displacements characteristic of higher frequencies, which are measured by holographic techniques.

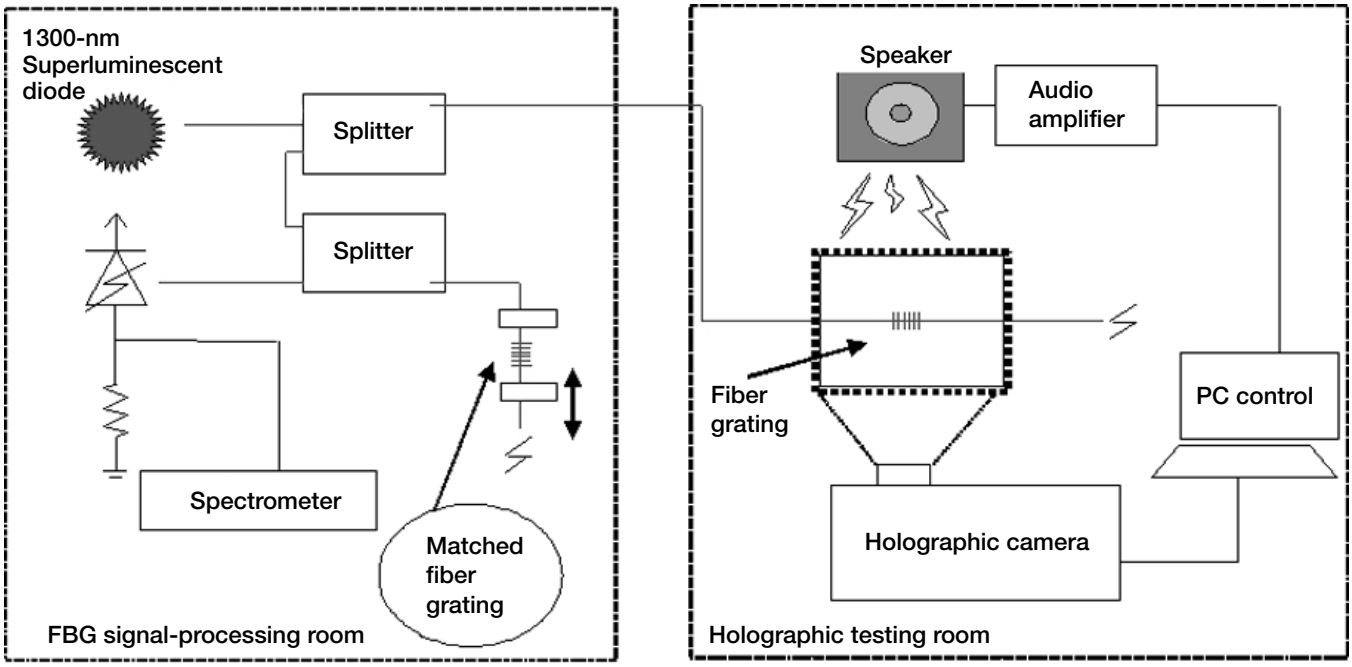

Test configuration showing FBG data processing and holographic testing equipment.

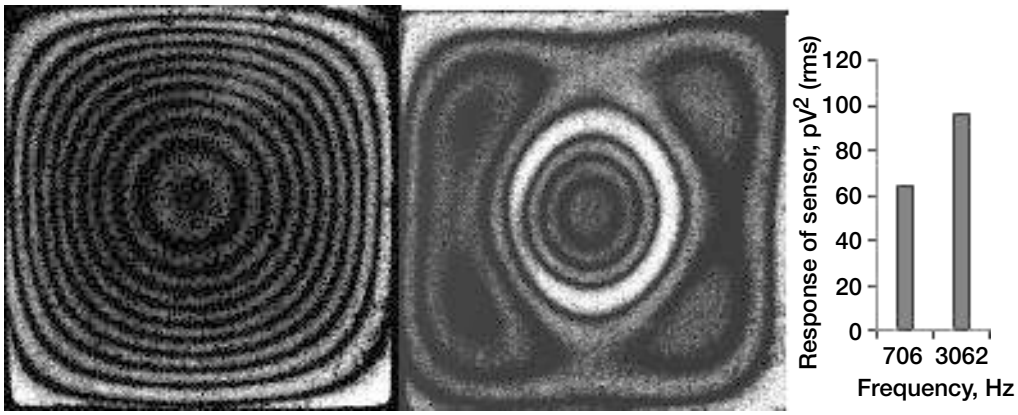

706 Hz 3062 Hz

Experimental results: Left: Holographic image of the 706-Hz resonant mode of the PMC plate. Center: Holographic image of the 3062 Hz resonant mode of the PMC plate. Right: Graph comparing the response of the embedded fiber sensor for two resonant frequencies.

References

1. Lekki, John, et al.: Evaluation of Mechanical Modal Characteristics Using Optical Techniques. NASA/TM—2002-211678, 2002. http://gltrs.grc.nasa.gov/cgi-bin/GLTRS/browse.pl?2002/TM-2002-211678.html

Glenn contacts:

Dr. Grigory Adamovsky, 216–433–3736, Grigory.Adamovsky-1@nasa.gov; and
John D. Lekki, 216–433–5650, John.D.Lekki@nasa.gov

Author: Dr. Grigory Adamovsky

Headquarters program office: OAT

Programs/Projects: Propulsion and Power, RAC

High-Temperature Sprayable Phosphor Coating Developed for Measuring Surface Temperatures

The use of phosphor thermography for noncontact temperature measurements in harsh environments has been proven over the last decade, but it has suffered from difficult application procedures such as vapor deposition or sputtering techniques. We have developed a high-temperature-sensitive paint that is easily applied with commercially available paint-spraying equipment and have successfully demonstrated it to temperatures up to 1500 °C. Selected phosphors have also shown measurable signals to 1700 °C, thus allowing a combination of phosphors to be used in high-temperature binders to make surface temperature measurements from ambient to over 1500 °C.

Phosphor thermography is an optical technique that measures the time response of fluorescence light, which is a function of the phosphor temperature. The phosphors are excited with short wavelength light (ultraviolet or blue), and they emit light at a longer wavelength. This technique has a benefit over other temperature measurements, such as thermocouples and infrared thermography, in difficult environments such as high blackbody backgrounds, vibration, flames, high electromagnetic noise, or where special windows may be needed. In addition, the sprayable phosphor paints easily cover large or complicated structures, providing full-surface information with a single measurement.

Oak Ridge National Laboratories developed and tested the high-temperature binders and phosphors under the direction of the NASA Glenn Research Center. Refractory materials doped with rare earth metals were selected for their performance at high temperature. Survivability, adhesion, and material compatibility tests were conducted at high temperatures in a small furnace while the fluorescent response from the phosphors was being measured. The photograph shows a painted sample in a furnace with a clearly visible fluorescing dot excited by a pulsed laser. Measuring the decay time of this fluorescence yields the surface temperature.

One new paint was recently tested in a rocket test stand at Glenn. The floor of a square duct nozzle was painted, and full-field lifetime decay measurements were acquired for multiple firings of the rocket. Good agreement with predicted results was obtained, matching temperature gradients along the length of the nozzle and clearly showing shock structures. These good results were very satisfactory given that the measurements were made looking through the combustion plume. Infrared pyrometry was incapable of making the surface measurements because of the interference from the rocket exhaust, which contaminated the infrared signature.

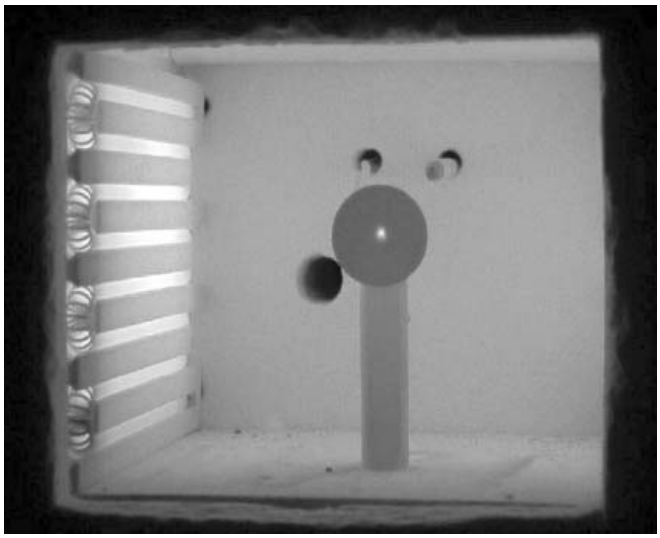

Furnace tests of binder/phosphor combinations showed detectable fluorescence above the background radiation on ceramic and metal substrates. This image was recorded at about 700 °C.

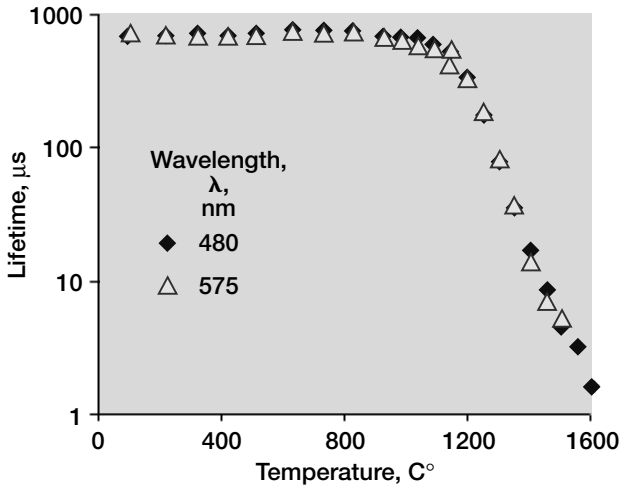

The fluorescence lifetime dependence of the phosphor YAG:Dy (0.28 percent) at high temperatures.

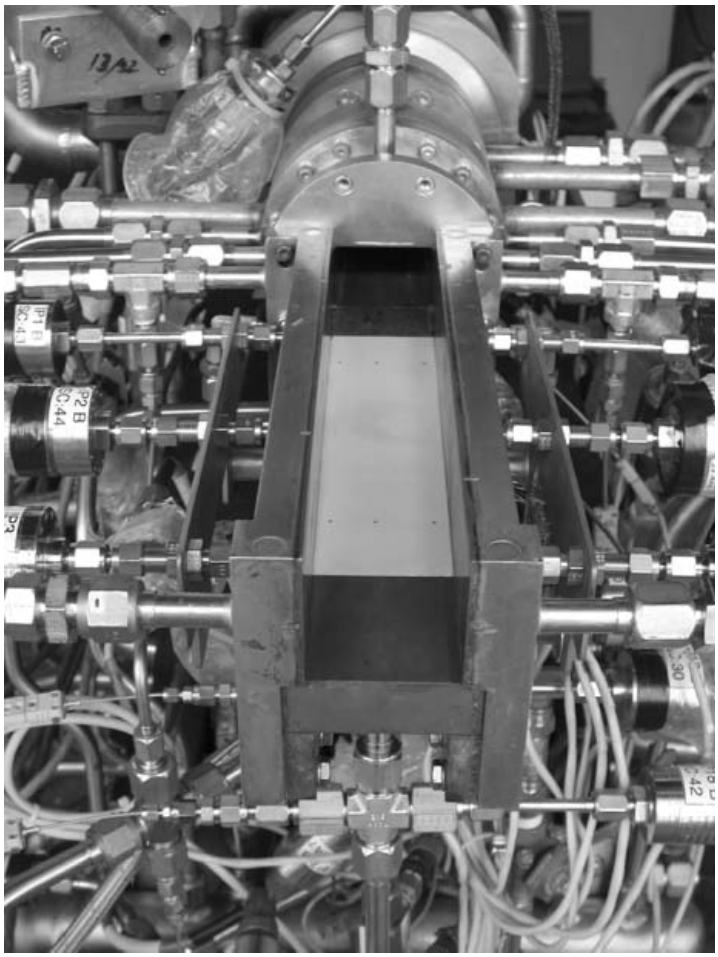

A water-cooled rocket nozzle painted in place with high-temperature phosphor paint. Flow is from back to front, and the excitation light source and camera are mounted above. The entire channel fills with flame when fired.

Find out more about this research:
http://www.grc.nasa.gov/WWW/OptInstr/

Glenn contact:
Timothy J. Bencic, 216–433–5690, Timothy.J.Bencic@nasa.gov

Author: Timothy J. Bencic

Headquarters program office: OAT

Programs/Projects: Hypersonics, STPO, Information Rich Test Instrumentation, Propulsion Systems R&T, RLV

Optical Tweezers Array and Nimble Tweezers Probe Generated by Spatial-Light Modulator

An optical tweezers is being developed at the NASA Glenn Research Center as a visible-light interface between ubiquitous laser technologies and the interrogation, visualization, manufacture, control, and energization of nanostructures such as silicon carbide (SiC) nanotubes. The tweezers uses one or more focused laser beams to hold micrometer-sized particles called tools (sometimes called tips in atomic-force-microscope terminology). A strongly focused laser beam has an associated light-pressure gradient that is strong enough to pull small particles to the focus, in spite of the oppositely directed scattering force; "optical tweezers" is the common term for this effect. The objective is to use the tools to create carefully shaped secondary traps to hold and assemble nanostructures that may contain from tens to hundreds of atoms. The interaction between a tool and the nanostructures is to be monitored optically as is done with scanning probe microscopes.

One of the initial efforts has been to create, shape, and control multiple tweezers beams. To this end, a programmable spatial-light modulator (SLM) has been used to modify the phase of a laser beam at up to 480 by 480 points. One program creates multiple, independently controllable tweezer beams whose shapes can be tailored by making the SLM an adaptive mirror in an interferometer (ref. 1). The beams leave the SLM at

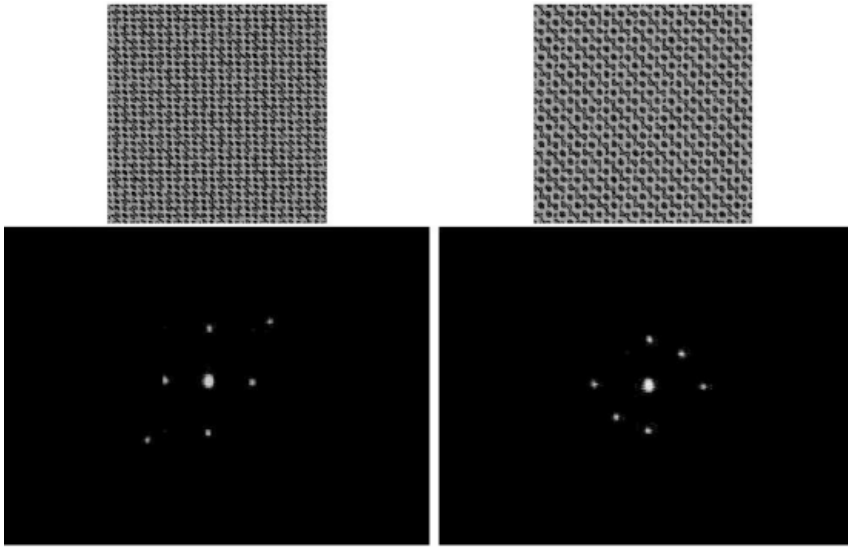

Pattern-programmed movement of tweezers beams using SLM. Top: Images show patterns displayed on SLM. Bottom: Patterns show resultant laser traps.

different angles, and an optical Fourier transform maps these beams to different positions in the focal plane of a microscope objective. The figure above shows two arrays of multiple beams created in this manner. The patterns displayed above the beam array control the intensity-to-phase transformation required in programming the SLM. Three of the seven beams displayed can be used as independently controllable beams.

The interferometer arrangement enables control of the intensity and phase profiles of the tweezers beams. Another device, called a nimble tweezers probe (ref. 2), was created at Glenn by adding a feature to the interferometer to render the polarizations of the two main interferometer beams orthogonal. The beams, then, do not interfere, but one beam is used to move particles individually to the multiple traps created by the other beam. The polarization is then rotated back to perform interferometric control of the filled traps. The figure to the right shows three different states of the tweezers traps. The traps are visible in the top frame but are unfilled. The center frame shows one trap containing a 9.6-μm sphere. The bottom frame shows four filled traps as well as a particle in a nimble tweezers trap to the right.

Work is in progress to calculate and measure forces and moments on generally shaped tools, to create an infrared version of the setup for biotechnology, to measure the second harmonic generated by the tool-nanostructure combinations for diagnostics, and to create a tweezers to operate under a vacuum.

References

1. Decker, Arthur J.: Interferometer Control of Optical Tweezers. NASA/TM—2002-211586, 2002. http://gltrs.grc.nasa.gov/cgi-bin/GLTRS/browse.pl?2002/TM-2002-211586.html
2. Jassemnejad, Baha: Nimble Optical Tweezer Beam for Tweezer-Array Manipulation and Interrogation. NASA Disclosure of Invention and New Technology, July 30, 2002.

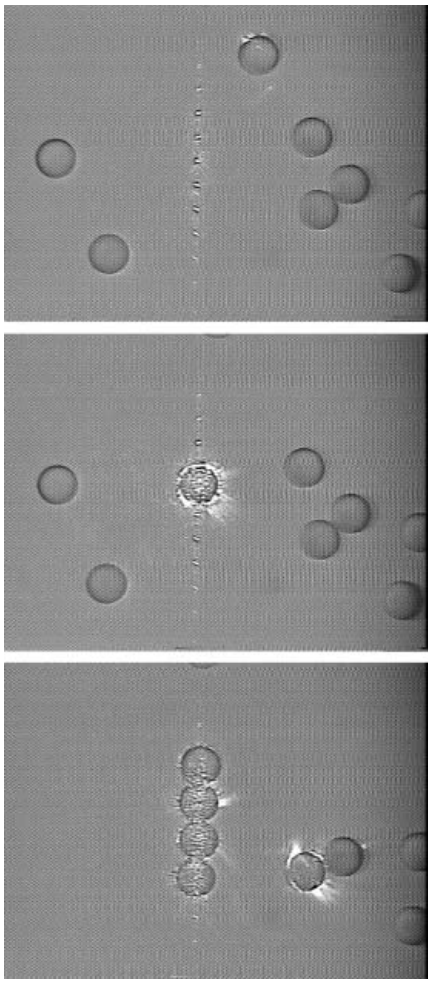

Generation of multiple traps and trapping of multiple particles. Top: Column of empty traps. Center: One particle trapped. Bottom: Four particles trapped (note guide particle in separate trap).

Glenn contact:
Dr. Arthur J. Decker, 216–433–3639, Arthur.J.Decker@nasa.gov

Authors: Dr. Arthur J. Decker, Baha Jassemnejad, Robin E. Seibel, and Kenneth E. Weiland

Headquarters program office: OAT

Programs/Projects: Propulsion Systems R&T, Microgravity Science

Mobile Sensor Technologies Being Developed

The NASA Glenn Research Center is developing small mobile platforms for sensor placement, as well as methods for communicating between roving platforms and a central command location.

The first part of this project is to use commercially available equipment to miniaturize an existing sensor platform. We developed a five-circuit-board suite, with an average board size of 1.5 by 3 cm. Shown in the photograph on the left, this suite provides all motor control, direction finding, and communications capabilities for a 27- by 21- by 40-mm prototype mobile platform (see the photograph on the right).

The second part of the project is to provide communications between mobile platforms, and also between multiple platforms and a central command location. This is accomplished with a low-power network labeled "SPAN," Sensor Platform Area Network, a local area network made up of proximity elements.

In practice, these proximity elements are composed of fixed- and mobile-sensor-laden science packages that communicate to each other via radiofrequency links. Data in the network will be shared by a central command location that will pass information into and out of the network through its access to a backbone element. The result will be a protocol portable to general purpose microcontrollers satisfying a host of sensor networking tasks. This network will enter the gap somewhere between television remotes and Bluetooth[1] but, unlike 802.15.4,[2] will not specify a physical layer, thus allowing for many data rates over optical, acoustical, radiofrequency, hardwire, or other media. Since the protocol will exist as portable C-code, developers may be able to embed it in a host of microcontrollers from commercial-to-space grade and, of course, to design it into ASICs.[3] Unlike in 802.15.4, the nodes will relate to each other as peers.

A demonstration of this protocol using the two test bed platforms was recently held. Two NASA modified, commercially available, mobile platforms (see the photograph on the next page) communicated and shared data with each other and a central command location. Web-based control and interrogation of similar mobile sensor platforms have also been demonstrated. Expected applications of this technology include robotic planetary exploration, astronaut-to-equipment communication, and remote aerospace engine inspections.

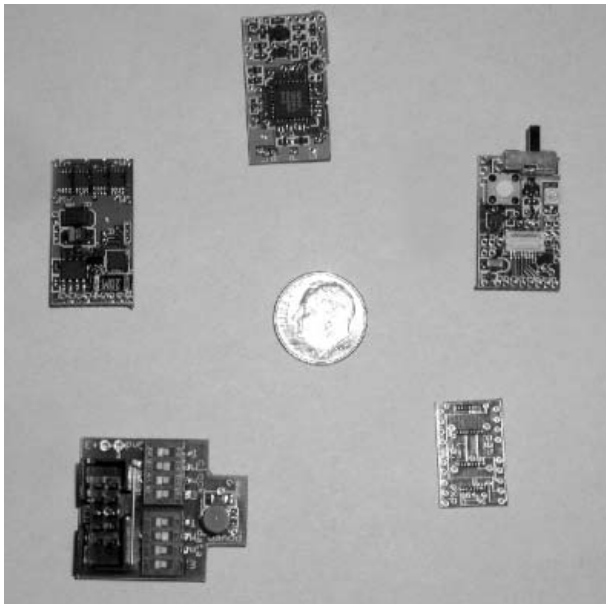

Sensor platform electronics suite.

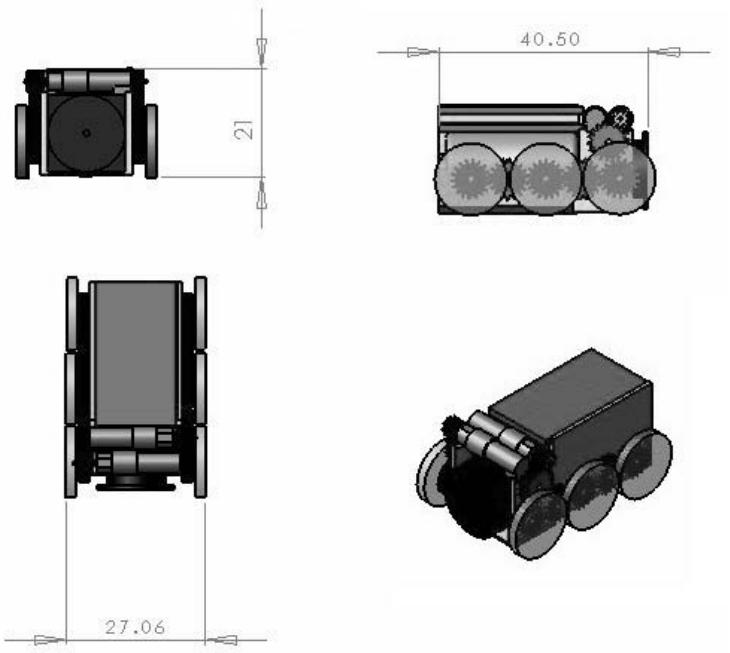

Mobile platform rendering. All dimensions given in millimeters.

[1]2.4-GHz ISM band, low-power network protocol for shortrange data and voice transfer.
[2]Proposed ISM band (band reserved for industrial, scientific, and medical purposes), low-power network protocol.
[3]Application specific integrated circuit—an integrated circuit fabricated to address a specific application.

Communications test bed (Koala experimental platform).

Glenn contacts:
Mike Krasowski, 216–433–3729, Michael.J.Krasowski@nasa.gov; and Larry Greer, 216–433–8770, Lawrence.C.Greer@nasa.gov

Authors:
Michael J. Krasowski, Lawrence C. Greer, and Lawrence G. Oberle

Headquarters program office: OAT

Programs/Projects:
Power and Propulsion, RAC, CICT, Space Communication Project

Rayleigh Scattering Diagnostic Used to Measure Velocity and Density Fluctuation Spectra

A new, molecular Rayleigh-scattering-based flow diagnostic developed at the NASA Glenn Research Center has been used for the first time to measure the power spectrum of both gas density and radial velocity components in the plumes of high-speed jets. The objective of the work is to develop an unseeded, nonintrusive dynamic measurement technique for studying turbulent flows in NASA test facilities. This technique provides aerothermodynamic data not previously obtainable. It is particularly important for supersonic flows, where hot wire and pitot probes are difficult to use and disturb the flow under study.

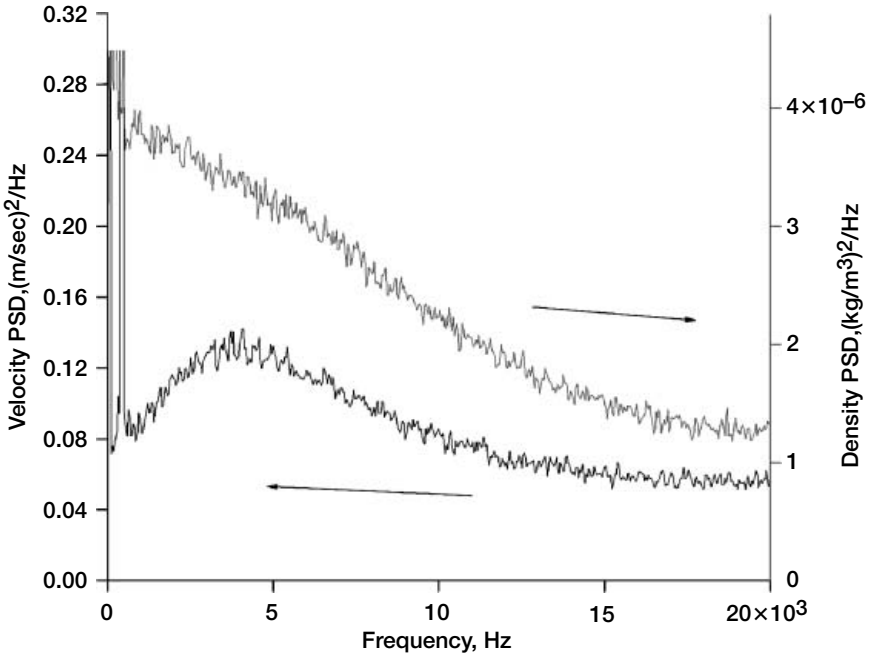

Power spectral densities (PSD) of velocity and density on the centerline of a Mach-1.8 supersonic free jet at a location 12 nozzle diameters downstream of the exit.

The effort is part of the nonintrusive instrumentation development program supporting propulsion research at the NASA Glenn Research Center. In particular, this work is measuring fluctuations in flow velocity, density, and temperature for jet noise studies. These data are valuable to researchers studying the correlation of flow fluctuations with far-field noise. One of the main objectives in jet noise research is to identify noise sources in the jet and to determine their contribution to noise generation.

The technique is based on analyzing light scattered from molecules within

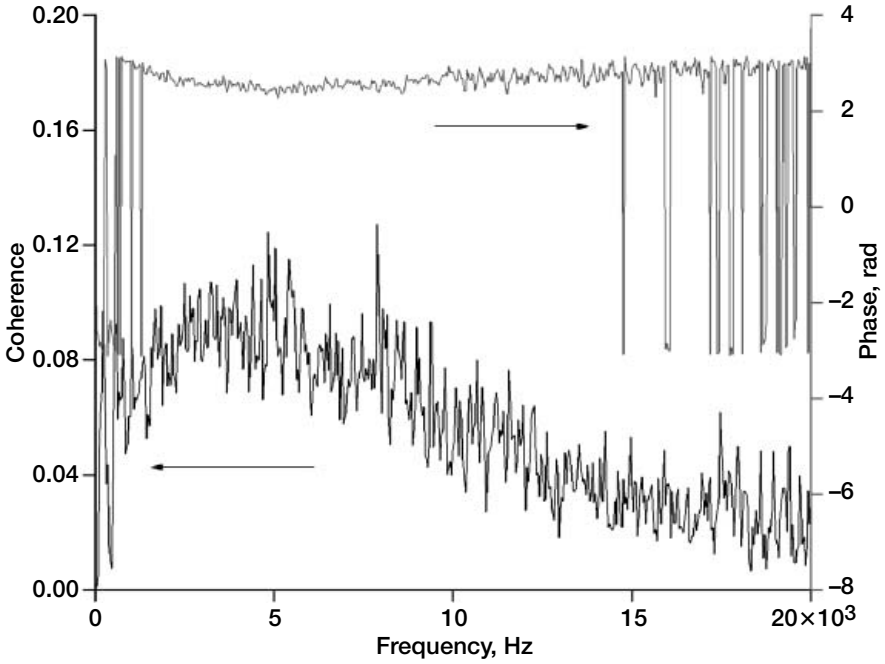

Cross spectra of velocity and density (coherence and phase) on the centerline of a Mach-1.8 supersonic free jet at a location 12 nozzle diameters downstream of the exit.

the jet using a Fabry-Perot interferometer operating in a static imaging mode. The PC-based data acquisition system can simultaneously sample velocity and density data at rates to about 100 kHz and can handle up to 10 million data records. We used this system to interrogate three different jet nozzle designs in a Glenn free-jet facility. Each nozzle had a 25.4-mm exit diameter. One was convergent, used for subsonic flow measurements and to produce a screeching underexpanded jet with a fully expanded Mach number of 1.42. The other nozzles (Mach 1.4 and 1.8) were convergent-divergent types. The radial component of velocity and gas density were simultaneously measured in this work.

A critical requirement in the use of molecular Rayleigh scattering for flow diagnostics is a clean, particle-free airflow. The primary air supply to the jet was filtered to remove particles. In addition, a 200-mm-diameter low-velocity filtered co-flow surrounded the jet. This co-flow was generated by an air-handling system that filtered the ambient air.

The graphs are examples of data taken along the centerline, 12 jet diameters downstream of the exit, in Mach 1.8 flow. As shown in the graph on the preceding page, the velocity spectrum has a peak at about 4000 Hz. On the other hand, the density spectrum does not exhibit a definite peak, with the spectral density increasing toward low frequencies. The graph to the left shows that the density and velocity have relatively strong coherence with a phase difference of about 2.5 radians.

This instrumentation development effort is continuing, with the goal of measuring two-point space-time correlations at sampling rates to 100 kHz. In addition, simultaneous far-field acoustic measurements will be taken to allow study of correlations between the flow physics and the emitted noise.

Find out more about the research of Glenn's Optical Instrumentation Technology Branch: http://www.grc.nasa.gov/WWW/OptInstr/

Reference

1. Seasholtz, Richard G.; Panda, Jayanta; and Elam, Kristie A.: Rayleigh Scattering Diagnostic for Measurement of Velocity and Density Fluctuation Spectra. AIAA–2002–0827, 2002.

Glenn contact:
Dr. Richard G. Seasholtz, 216–433–3754, Richard.G.Seasholtz@nasa.gov

Ohio Aerospace Institute (OAI) contact:
Dr. Jayanta Panda, 216–433–8891, Jayanta.Panda@grc.nasa.gov

Akima contact:
Kristie A. Elam, 216–433–3843, Kristie.A.Elam@grc.nasa.gov

Authors: Dr. Richard G. Seasholtz, Dr. Jayanta Panda, and Kristie A. Elam

Headquarters program office: OAT

Programs/Projects:
Propulsion Systems R&T, QAT

Microelectromechanical Systems (MEMS) Broadband Light Source Developed

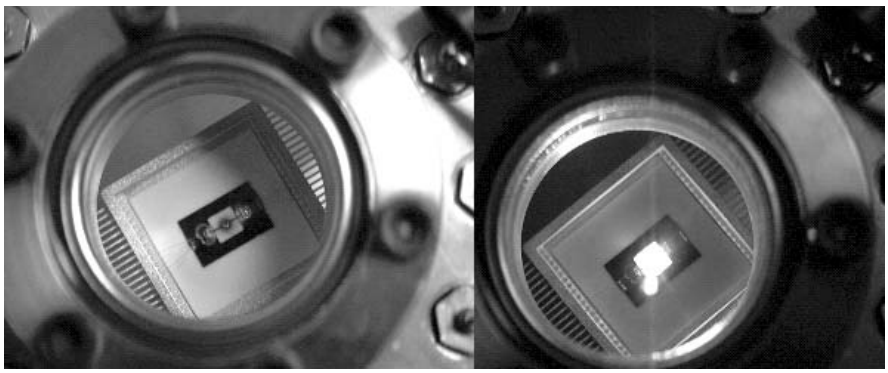

Prototype filament in vacuum chamber. Left: Device turned off. Right: Device turned on.

A miniature, low-power broadband light source has been developed for aerospace applications, including calibrating spectrometers and powering miniature optical sensors. The initial motivation for this research was based on flight tests of a Fabry-Perot fiber-optic temperature sensor system used to detect aircraft engine exhaust gas temperature. Although the feasibility of the sensor system was proven, the commercial light source optically powering the device was identified as a critical component requiring improvement. Problems with the light source included a long stabilization time (~1 hr), a large amount of heat generation, and a large input electrical power (6.5 W). Thus, we developed a new light source to enable the use of broadband optical sensors in aerospace applications.

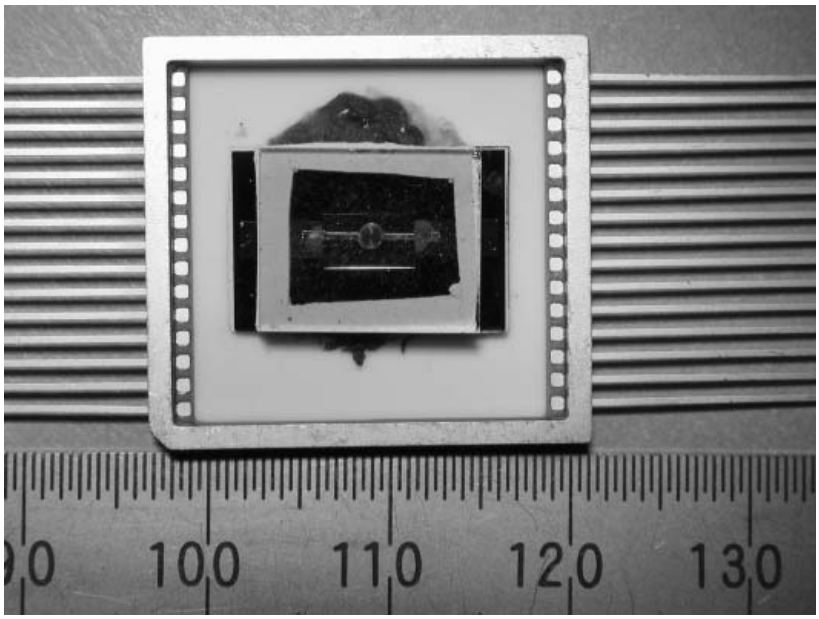

Prototype packaged device.

Semiconductor chip-based light sources, such as lasers and light-emitting diodes, have a relatively narrow range of emission wavelengths in comparison to incandescent sources. Incandescent light sources emit broadband radiation from visible to infrared wavelengths; the intensity at each wavelength is determined by the filament temperature and the materials chosen for the filament and the lamp window. However, present commercial incandescent light sources are large in size and inefficient, requiring several watts of electrical power to obtain the desired optical power, and they emit a large percentage of the input power as heat that must be dissipated.

The miniature light source, developed jointly by the NASA Glenn Research Center, the Jet Propulsion Laboratory, and the Lighting Innovations Institute, requires one-fifth the electrical input power of some commercial light sources, while providing similar output light power that is easily coupled to an optical fiber. Furthermore, it is small, rugged, and lightweight. Microfabrication technology was used to reduce the size, weight, power consumption, and potential cost—parameters critical to future aerospace applications. This chip-based light source has the potential for monolithic fabrication with on-chip drive electronics. Other uses for these light sources are in systems for vehicle navigation, remote sensing applications such as monitoring bridges for stress, calibration sources for spectrometers, light sources for space sensors, display lighting, addressable arrays, and industrial plant monitoring.

Two methods for filament fabrication are being developed: wet-chemical

etching and laser ablation. Both yield a 25-μm-thick tungsten spiral filament. The proof-of-concept filament shown in the top photographs on the preceding page was fabricated with the wet etch method. Then it was tested by heating it in a vacuum chamber using about 1.25 W of electrical power; it generated bright, blackbody radiation at approximately 2650 K (see the top photographs). The filament was packaged in Glenn's clean-room facilities (see the bottom photograph). This design uses three chips vacuum-sealed with glass tape. The bottom chip consists of a reflective film deposited on silicon, the middle chip contains a tungsten filament bonded to silicon, and the top layer is a transparent window. Lifetime testing on the package will begin shortly. The emitted optical power is expected to be approximately 1.0 W with the spectral peak at 1.1 μm.

Find out more about this research:
http: //www.grc.nasa.gov/WWW/OptInstr/tuma/MEMSwhite.html

Glenn contact:
Dr. Margaret Tuma, 216–433–8665, Margaret.L.Tuma-1@nasa.gov

Author: Dr. Margaret L. Tuma

Headquarters program office: OSS

Programs/Projects: NEPP

Digital Particle Image Velocimetry (DPIV) Used for Space-Time Correlations in Nozzle Flow

An optical measurement technique known as Digital Particle Image Velocimetry (DPIV) was used previously to characterize the first- and second-order statistical properties of both cold and hot jet flows from externally mixed nozzles in NASA Glenn Research Center's Nozzle Acoustic Test Rig. In this technique, an electronic camera records particles entrained in a flow as a laser light sheet is pulsed at two instances in time. Correlation processing of the recorded particle image pairs yields the two-component velocity field across the imaged plane of the flow. The information acquired using DPIV is being used to improve our understanding of the decay of turbulence in jet flows—a critical element for understanding the acoustic properties of the flow.

Dual DPIV system setup in the Small Hot Jet Acoustic Rig facility. The light sheets from each of the DPIV systems are visible in this photograph.

Recently, two independent DPIV systems were installed in Glenn's Small Hot Jet Acoustic Rig, enabling multiplane correlations in time and space. The data were collected over a range of different Mach numbers and temperature ratios. DPIV system 1 was fixed to a large traverse rig, and DPIV system 2 was mounted on a small traverse system mounted on the large traverse frame. The light sheets from the two DPIV systems were aligned to lie in the same axial plane, with DPIV system 2 being independently traversed downstream along the flow direction. For each measurement condition, the DPIV systems were started at a fully overlapping orientation. A polarization separation technique was used to avoid crosstalk between the two systems. Then, the DPIV systems fields were shifted axially apart, in successively increasing steps. The downstream DPIV system 2 was triggered at a short time delay after the upstream

DPIV system 1, where the time delay was proportional to the convective flow velocity in the shear layer of the jet flow and the axial separation of the two DPIV systems. The acquired data were processed to obtain the instantaneous velocity vector maps over a range of time delays and spatial separations. The velocity fields from the different DPIV systems were then cross-correlated to determine the degree of correlation remaining in the flow as the downstream convection distance was increased.

The new data provide Lagrangian measurements of the convective turbulent structures in the shear layer of an exhaust nozzle. These measurements, obtained in both cold and hot flows, will be used to validate and correct models for space-time velocity correlations—long a missing key to predicting jet noise.

Glenn contacts:
Dr. Mark Wernet, 216–433–3752, Mark.P.Wernet@nasa.gov; and
Dr. James Bridges, 216–433–2693, James.E.Bridges@nasa.gov

Authors: Dr. Mark P. Wernet and Dr. James E. Bridges

Headquarters program office: OAT

Programs/Projects: QAT

Compressor Performance Enhanced by Active Flow Control Over Stator Vanes

The application of active flow control technology to enhance turbomachinery system performance is being investigated at the NASA Glenn Research Center through experimental studies. Active flow control involves the use of sensors and actuators embedded within engine components to dynamically alter the internal flow path during off-nominal operation in order to optimize engine performance and maintain stable operation.

Modern compressors are already highly optimized components that must be designed to accommodate a broad range of operating conditions in a safe and efficient manner. Since overall engine performance is driven by compressor performance, advances in compressor technology that reduce weight and parts count, reduce fuel consumption, and lower maintenance costs will have a significant impact on the cost of aircraft ownership. Active flow control holds the promise of delivering such technology advances.

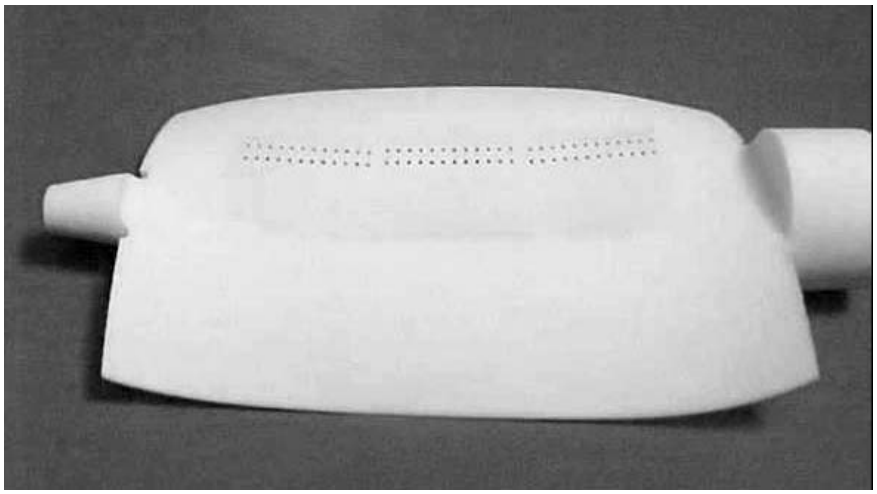

An example of a rapid prototype flow control vane using an array of angled holes to inject fluid ahead of separated flow on the suction surface.

In highly loaded modern compressors, the flow tends to separate from stator airfoils under conditions of low mass flow. These conditions are often encountered during critical periods such as takeoff and landing and, for military aircraft, the extreme maneuvers encountered during combat operations. Flow separation acts as a blockage in the flow path which limits pressure recovery and may trigger severe mechanical stress conditions such as stall or even surge. Flow control delays the onset of separation with the use of injected air ahead of the separation line. The low momentum fluid creating the blockage at the airfoil surface is energized by the

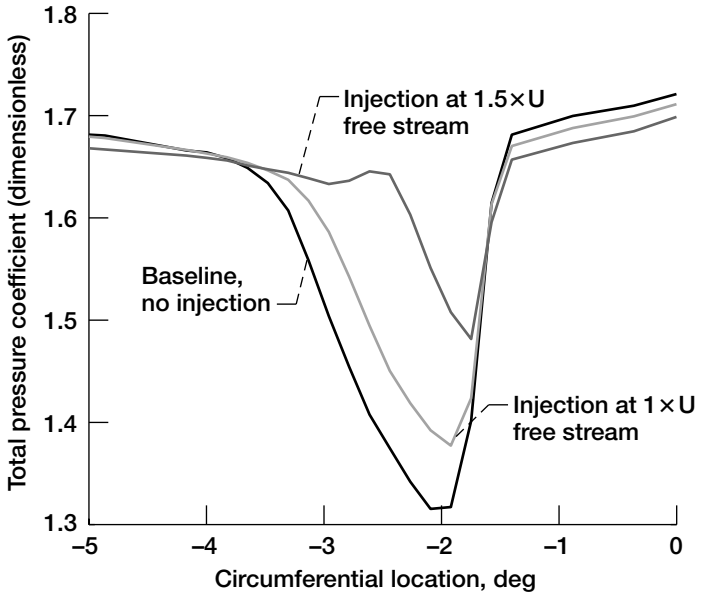

A plot of total pressure distribution in the blade wake at midspan with varying velocity levels of injected fluid. The air injected from the vane surface (for the two curves with injection) has a velocity of 1.5 times the free stream or power stream velocity through the machine.

injected air, and the blockage is eliminated, or at least minimized, to the point that it does not adversely affect engine performance. The photograph on the preceding page shows one example of a flow control vane using an array of holes on the vane surface.

Flow control is being applied at the surface of stator vanes in Glenn's Low-Speed Axial Compressor facility. This facility provides a flow field that accurately duplicates the aerodynamics of modern highly loaded compressors. Emphasis is being placed on the development of efficient actuators, effective injection schemes, robust sensors, and control methodologies for a practical system for a new generation of aircraft. The graph shows measurements of the circumferential total pressure distribution acquired at midspan downstream of a flow-controlled vane. The vane is operating beyond its design loading with a separated suction surface boundary layer. Injection through slots in the vane suction surface reduces the severity of separation, which is manifested as a reduction in the area of low total pressure downstream of the vane.

This work is partially funded by the Defense Advanced Research Program Agency (DARPA) and is being performed in collaboration with Honeywell and the Illinois Institute of Technology.

Glenn contacts:
Dennis Culley, 216–433–3797, Dennis.E.Culley@nasa.gov;
Dr. Michelle Bright, 216–433–2304, Michelle.M.Bright@nasa.gov; and
Dr. Anthony Strazisar, 216–433–5881, Anthony.J.Strazisar@nasa.gov

AP Solutions, Inc., contact:
Sue Prahst, 216–433–3746, Patricia.S.Prahst@grc.nasa.gov

Author: Dennis E. Culley

Headquarters program office: OAT

Programs/Projects:
Propulsion and Power, SEC

Active Control of High-Frequency Combustor Instability Demonstrated

To reduce the environmental impact of aerospace propulsion systems, extensive research is being done in the development of lean-burning (low fuel-to-air ratio) combustors that can reduce emissions throughout the mission cycle. However, these lean-burning combustors have an increased susceptibility to thermoacoustic instabilities—high-pressure oscillations much like sound waves that can cause severe high-frequency vibrations in the combustor. These pressure waves can fatigue the combustor components and even the downstream turbine blades. This can significantly decrease the combustor and turbine safe operating life. Thus, suppression of the thermoacoustic combustor instabilities is an enabling technology for lean, low-emissions combustors. Under the Propulsion and Power Program, the NASA Glenn Research Center in partnership with Pratt & Whitney, United Technologies Research Center, and Georgia Institute of Technology is developing technologies for the active control of combustion instabilities.

With active combustion control, fuel pulses are used to put pressure oscillations into the system. These oscillations, in turn, cancel out the pressure oscillations being produced by the instabilities. Thus, the engine can have lower pollutant emissions as well as long life.

The use of active combustion instability control to reduce thermoacoustic-driven combustor pressure oscillations was demonstrated for a high-frequency (530-Hz) instability on a single-nozzle combustor rig at United Technologies Research Center. This is the first known successful demonstration of high-frequency combustion instability suppression in a realistic aircraft engine environment. This rig, which emulates an actual engine instability experience, has many of the complexities of a real engine combustor (i.e., actual fuel nozzle and swirler, dilution cooling, etc.).

High-frequency fuel valve characterization rig.

A fuel-delivery system that is based on a high-frequency fuel valve from the Georgia Institute of Technology and that can pulse the fuel at the 530-Hz instability frequency was modeled, developed, and tested in a valve characterization rig assembled for this purpose (see the photograph). Because of the high frequency and low amplitude of the instability relative to the background combustor noise (see the graph on the next page), sophisticated control algorithms were developed that (1) identify the instability frequency from the noise and (2) apply fuel pulsations at the correct frequency and phase to reduce the instability. A model-based control method and an adaptive phase-shifting control method were both shown to reduce the pressure oscillations at the instability frequency (see the graph). Work is continuing to apply these advanced control methods to future low-emission combustor concepts.

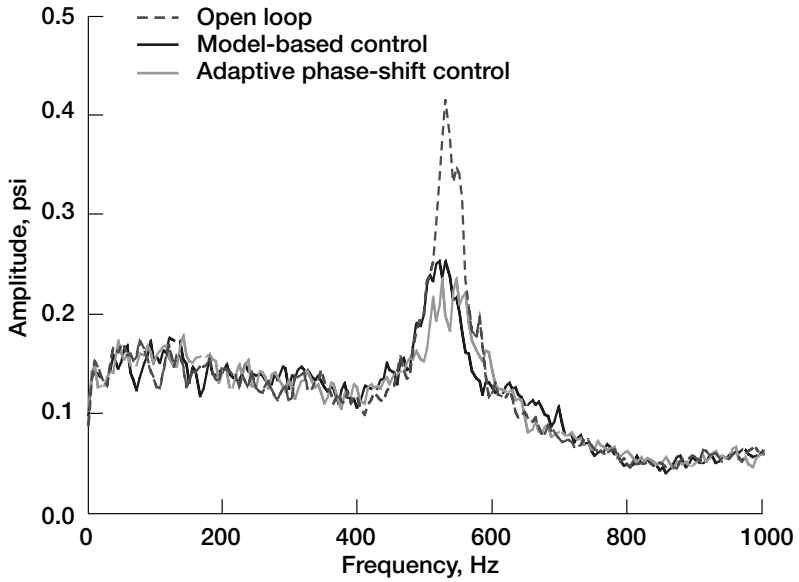

Amplitude spectra of the combustor pressure oscillations without instability control, with model-based instability control, and with adaptive phase-shifting instability control.

Find out more about this research:
Active combustion control:
http://www.grc.nasa.gov/WWW/cdtb/projects/combustor/

Glenn's Combustion Branch: http://www.grc.nasa.gov/WWW/combustion/

Glenn contacts:
John DeLaat, 216–433–3744, John.C.Delaat@nasa.gov; and
Dr. Clarence Chang, 216–433–8561, Clarence.T.Chang@nasa.gov

Authors: John C. DeLaat and Dr. Clarence T. Chang

Headquarters program office: OAT

Programs/Projects:
Propulsion and Power, SEC, UEET

Data-Mining Toolset Developed for Determining Turbine Engine Part Life Consumption

The current practice in aerospace turbine engine maintenance is to remove components defined as life-limited parts after a fixed time, on the basis of a predetermined number of flight cycles. Under this schedule-based maintenance practice, the worst-case usage scenario is used to determine the usable life of the component. As shown in the top graph, this practice often requires removing a part before its useful life is fully consumed, thus leading to higher maintenance cost. To address this issue, the NASA Glenn Research Center, in a collaborative effort with Pratt & Whitney, has developed a generic modular toolset that uses data-mining technology to parameterize life usage models for maintenance purposes.

The toolset enables a "condition-based" maintenance approach, where parts are removed on the basis of the cumulative history of the severity of operation they have experienced. The toolset uses data-mining technology to tune life-consumption models on the basis of operating and maintenance histories. The flight operating conditions, represented by measured variables within the engine, are correlated with repair records for the engines, generating a relationship between the operating condition of the part and its service life. As shown in the bottom graph, with the condition-based maintenance approach, the life-limited part is in service until its usable life is fully consumed. This approach will lower maintenance costs while maintaining the safety of the propulsion system.

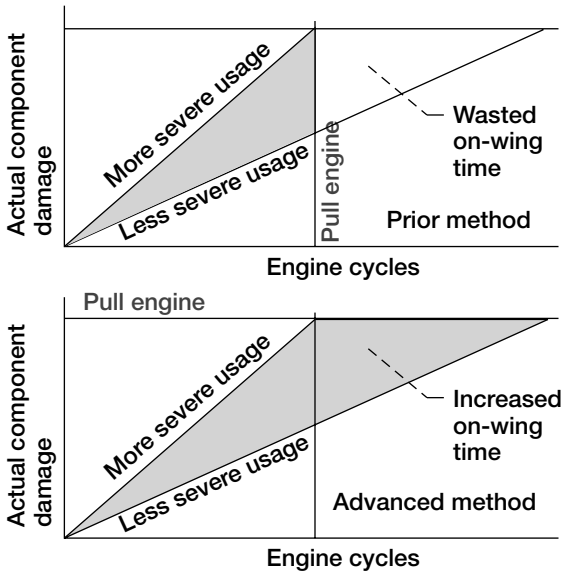

Top: Current schedule-based maintenance approach. Bottom: Condition-based maintenance approach enabled by data-mining toolset.

The toolset is a modular program that is easily customizable by users. First, appropriate parametric damage accumulation models, which will be functions of engine variables, must be defined. The tool then optimizes the models to match the historical data by computing an effective-cycle metric that reduces the unexplained variability in component life due to each damage mode by accounting for the variability in operational severity. The damage increment due to operating conditions experienced during each flight is used to compute the effective cycles and ultimately the replacement time. Utilities to handle data problems, such as gaps in the flight data records, are included in the toolset.

The tool was demonstrated using the first stage, high-pressure turbine blade of the PW4077 engine (Pratt & Whitney, East Hartford, CT). The damage modes considered were thermomechanical fatigue and oxidation/erosion. Each PW4077 engine contains 82 first-stage, high-pressure turbine blades, and data from a fleet of engines were used to tune the life-consumption models. The models took into account not only measured variables within the engine, but also unmeasured variables such as engine health parameters that are affected by degradation of the engine due to aging. The tool proved effective at predicting the average number of blades scrapped over time due to each damage mode, per engine, given the operating history of the engine. The customizable tools are available to interested parties within the aerospace community.

U.S. Army, Vehicle Technology Directorate at Glenn contact:
Jonathan Litt, 216–433–3748, Jonathan.S.Litt@grc.nasa.gov

Author: Jonathan S. Litt

Headquarters program office: OAT

Programs/Projects: AvSP

Performance Enhancement of Unsteady Ejectors Investigated Using a Pulsejet Driver

Unsteady ejectors are currently under investigation for use in some pulse detonation engine (PDE) propulsion systems. This is due primarily to their potential high performance in comparison to steady ejectors of similar dimensions relative to the source or driver jet. The performance metric of interest is the thrust augmentation ϕ defined as

$$\phi \equiv \frac{T^{\text{total}}}{T^{j}}$$

where T^{total} is the total thrust of the ejector and the driving jet combined and T^{j} is the thrust due to the driving jet alone.

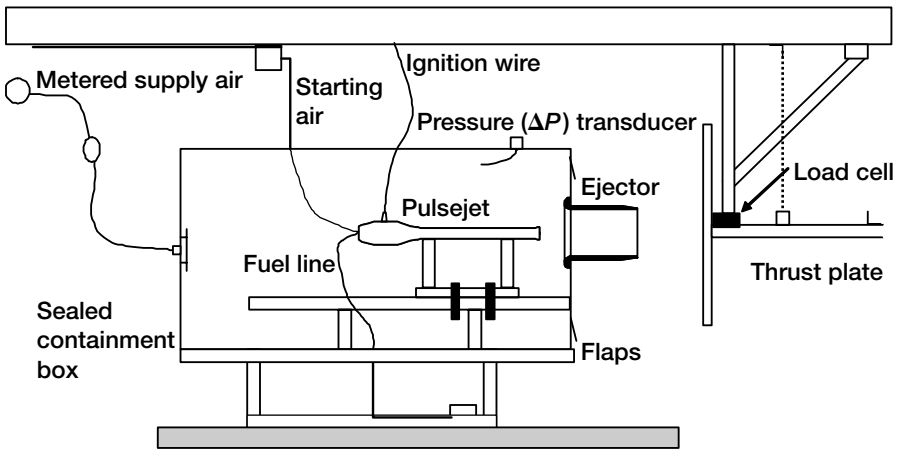

Experimental arrangement.

Although some experimental work has been done in the past to study thrust augmentation with unsteady ejectors, there is no proven theory by which optimal design parameters can be selected and an effective ejector constructed for a given pulsed flow. Therefore, an experimental facility was developed at the NASA Glenn Research Center to study the correlation between ejector design and performance, and to get a better understanding of the flow phenomena that result in thrust augmentation. A commercially available pulsejet was used for the unsteady driving jet. This was paired with a basic, yet flexible, ejector design that allowed parametric evaluation of the effects that length, diameter, and inlet radius have on performance.

The use of a pulsejet for such an experiment is advantageous for several reasons:

(1) Pulsejets are mechanically simple and inexpensive to build and operate, particularly when compared with the target ejector application, PDEs.

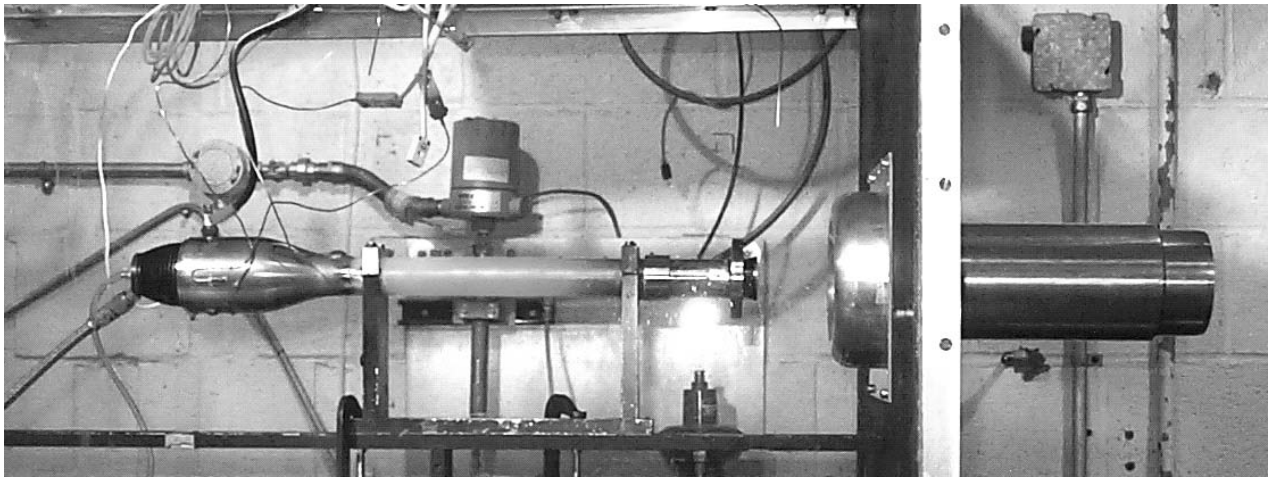

Operational pulsejet and ejector.

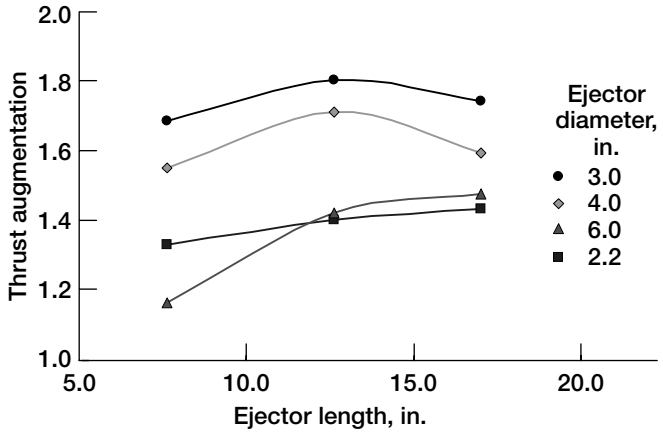

Measured thrust augmentation as a function of ejector length for different families of ejector diameter.

(2) Pulsejets resemble PDE's, having both high enthalpy exit flow, and very large fluctuations in exit velocity.

(3) Their 220-Hz operating frequency is similar to the target values of the PDEs being considered for flight.

The experimental setup is shown schematically in the drawing on the preceding page. The containment box shown allows measurement of flow entrainment along with thrust augmentation. The pulsejet and ejector system taken during operation are shown in the photograph.

Performance results from some of the ejector parameters investigated are shown in the graph. Here, thrust augmentation is plotted as a function of ejector length for several families of ejector diameter. It can be seen that large thrust augmentation values are obtained and that they are sensitive to both ejector length and diameter.

As detailed in reference 1, it was also found that ejector performance is sensitive to the spacing between the driver and ejector and to the radius of the ejector inlet. Furthermore, there appears to be a strong correlation between thrust augmentation and the formation number associated with the starting vortex emitted from the driver. The formation number is defined here as

$$F = \frac{\sqrt{\overline{u'^2}}}{2fd_j}$$

where f is the frequency of the primary source, $\sqrt{\overline{u'^2}}$ is root mean square of the source velocity fluctuation, and d_j is the source diameter. The presence and magnitude of a starting vortex has been determined using digital particle imaging velocimetry (DPIV) as described in reference 2. Future efforts will focus on validating the formation number correlation using other unsteady thrust sources, including an operational PDE, and on evaluating the effects of ram pressure (i.e., flight speed) on unsteady thrust augmentation.

References

1. Paxson, D.; Wilson, J.; and Dougherty, K.: Unsteady Ejector Performance: An Experimental Investigation Using a Pulsejet Driver. AIAA–2002–3915, 2002.
2. John, W., et al.: Conditionally Sampled Pulse Jet Driven Ejector Flow Field Using DPIV. AIAA Paper 2002–3231, 2002.

Glenn contact:
Dr. Daniel E. Paxson, 216–433–8334, Daniel.E.Paxson@nasa.gov

Author: Dr. Daniel E. Paxson

Headquarters program office: OAT

Programs/Projects:
Propulsion and Power, Pulse Detonation Engine Technology

Communications Technology

Aerospace Communications Security Technologies Demonstrated

In light of the events of September 11, 2001, NASA senior management requested an investigation of technologies and concepts to enhance aviation security. The investigation was to focus on near-term technologies that could be demonstrated within 90 days and implemented in less than 2 years.

In response to this request, an internal NASA Glenn Research Center Communications, Navigation, and Surveillance Aviation Security Tiger Team was assembled. The 2-year plan developed by the team included an investigation of multiple aviation security concepts, multiple aircraft platforms, and extensively leveraged datalink communications technologies. It incorporated industry partners from NASA's Graphical Weather-in-the-Cockpit research, which is within NASA's Aviation Safety Program.

Two concepts from the plan were selected for demonstration: remote "black box," and cockpit/cabin surveillance. The remote "black box" concept involves real-time downlinking of aircraft parameters for remote monitoring and archiving of aircraft data, which would assure access to the data following the loss or inaccessibility of an aircraft. The cockpit/cabin surveillance concept involves remote audio and/or visual surveillance of cockpit and cabin activity, which would allow immediate response to any security breach and would serve as a possible deterrent to such breaches.

The datalink selected for the demonstrations was VDL Mode 2 (VHF digital link), the first digital datalink for air-ground communications designed for aircraft use. VDL Mode 2 is beginning to be implemented through the deployment of ground stations and aircraft avionics installations, with the goal of being operational in 2 years.

The first demonstration was performed December 3, 2001, onboard the LearJet 25 at Glenn. NASA worked with Honeywell, Inc., for the broadcast VDL Mode 2 datalink capability and with actual Boeing 757 aircraft data. This demonstration used a cockpit-mounted camera for video surveillance and a coupling to the intercom system for audio surveillance. Audio, video, and "black box" data were simultaneously streamed to the ground, where they were displayed to a Glenn audience of senior management and aviation security team members.

The second demonstration was performed January 31, 2002, also onboard the LearJet 25. NASA worked with ARINC, Inc., for the bidirectional VDL Mode 2 datalink and with Teledyne, Inc., for aircraft data. This demonstration provided the same audio, video, and "black box" streaming data, and it showed the capability of controlling the operation from the ground. Also demonstrated were a self-contained, battery-powered global positioning system (GPS) receiver and an aircraft communication addressing reporting system (ACARS) transmitter, which could be triggered onboard or from the ground to transmit aircraft position reports. This transmitter could only be turned off by a command from the ground.

View from the cockpit camera.

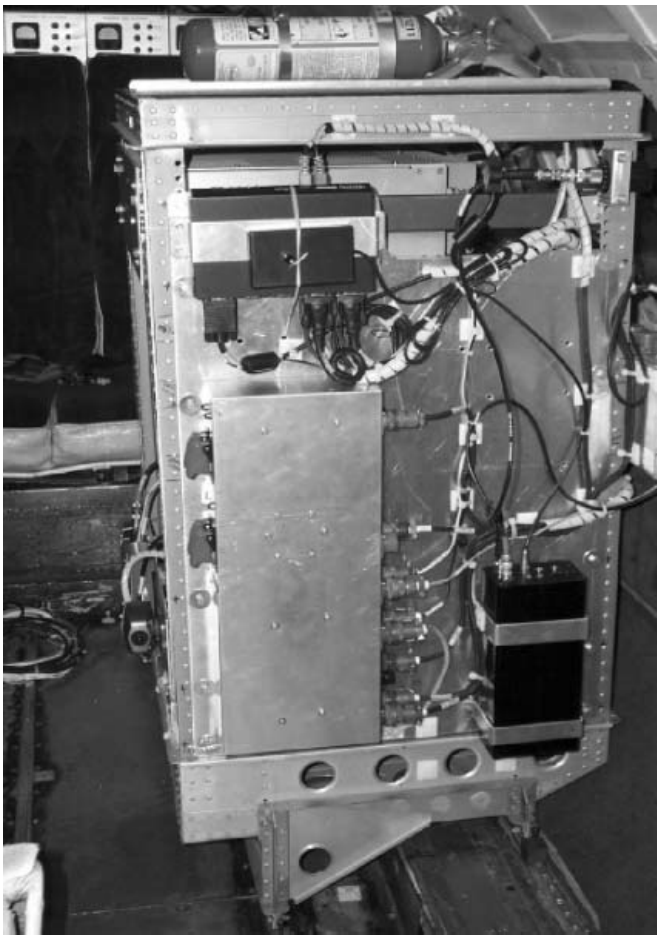

Aviation security equipment rack, installed in the LearJet.

The LearJet, used in the aviation security demonstrations.

These feasibility demonstrations showcased technologies that could be implemented within 2 years. However, much work still needs to take place for these and other technologies to be integrated into the near-term aviation communications infrastructure.

Glenn contacts:
James Griner, 216–433–5787, James.H.Griner@nasa.gov; and
Gus Martzaklis, 216–433–8966, Konstantinos.S.Martzaklis@nasa.gov

Authors: James H. Griner and Konstantinos S. Martzaklis

Headquarters program office: OAT

Programs/Projects: AvSP, AATT

Multibeam Phased-Array Antennas Developed and Characterized

Fixed-formation microsatellites have been proposed for future NASA missions to lower costs and improve data collection and reliability (ref. 1). Achieving seamless connectivity communications between these satellites requires the use of multibeam array antennas. As a result of NASA Glenn Research Center's collaborative efforts with the University of Colorado and Texas A&M University, two prototype multibeam array antennas have been developed and demonstrated at Ka-band frequencies. These arrays are designed to be dual-beam, dual-frequency arrays, with two fixed scan beams at around ±30°. They can be used in both ground and space systems for transmit and receive functions.

The first array, designed by the University of Colorado, is a space-fed lens (SFL) array that has significant advantages for multibeam applications. The spatial feed allows a multibeam configuration with only minor modification of the system design, avoiding the high complexity of the feed network required for conventional phased arrays. In addition, an SFL array generally has wider bandwidth, is lightweight, and can be fabricated at low cost. For large-array apertures, the SFL array has lower loss and can be easily optimized for a wide-angle scan (ref. 2). A photograph of the prototype SFL array is on the left.

The second array, designed by Texas A&M, is a piezoelectric-transducer-(PET) controlled phased array. The array achieves beam steering by using two piezoelectric sheets to actuate a dielectric perturber over the feed lines effecting a change in the phase velocity of the lines. For multibeam operation, a Rotman lens beam former was used with two input sources to create two independent beams. A photograph of the PET array is on the right.

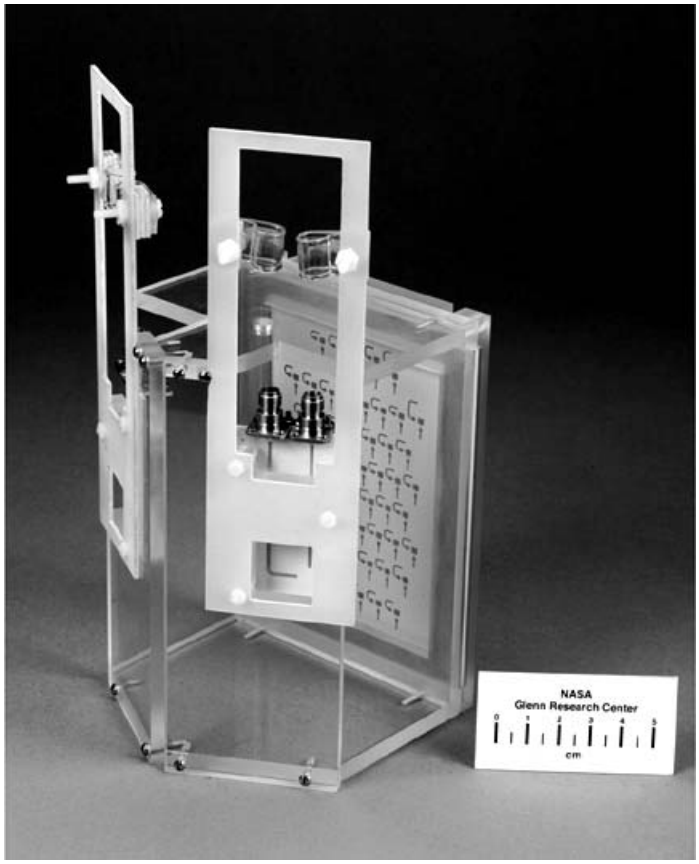

Rear view of the SFL array with dual feeds.

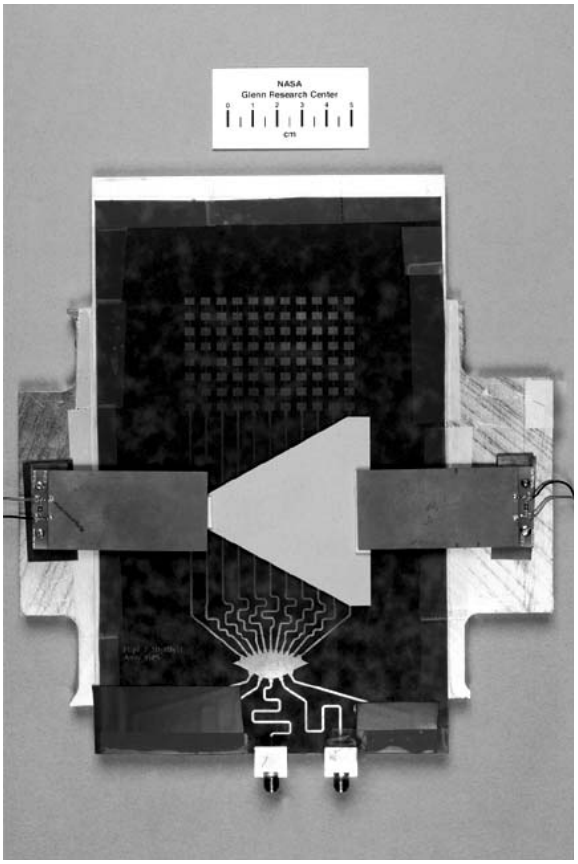

PET array of patch antenna elements.

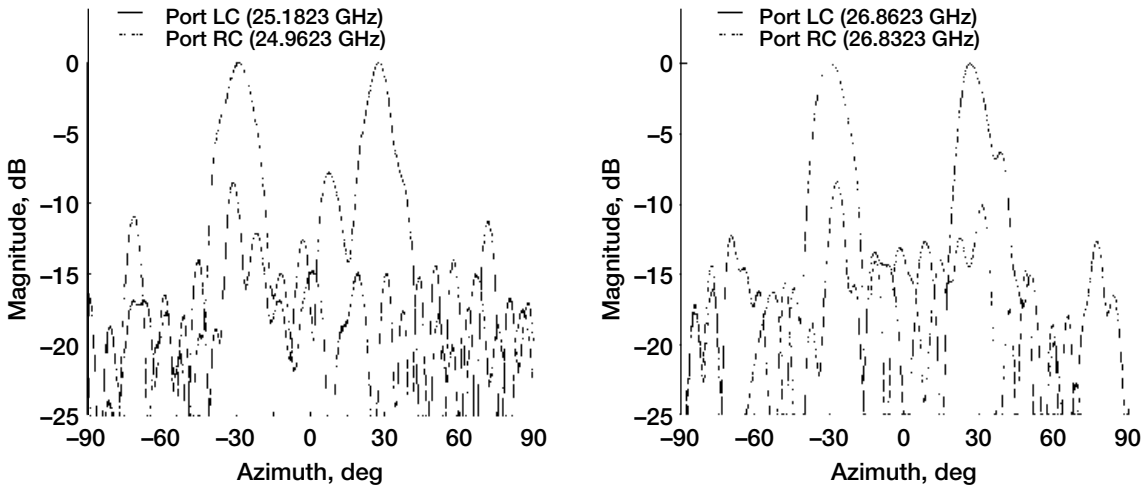

Radiation patterns for the SFL array. (Angular response of the Colorado lens.) Left: 24.7 GHz. Right: 26.7 GHz.

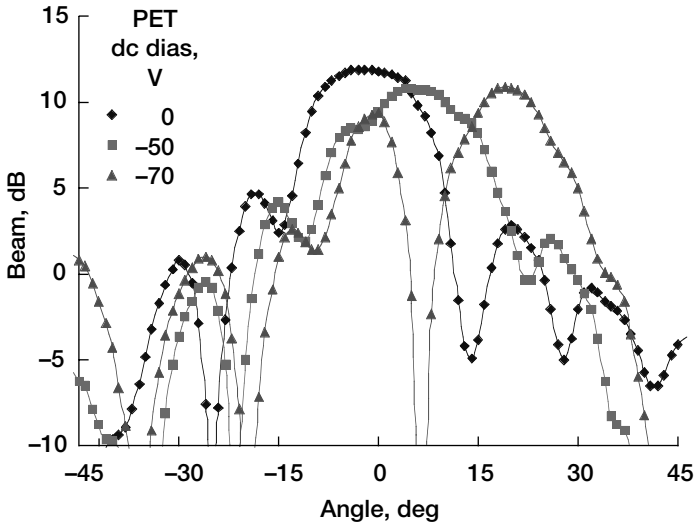

Radiation patterns for the PET array with different bias voltages at 31.1 GHz.

These two sets of graphs show the radiation patterns of the SFL and the PET arrays, respectively. Measured results exhibit excellent scan performance and close agreement with theory. Both arrays were also characterized in the compact range at Glenn; similar results were observed.

References

1. Spectrum Requirements and Allocation Survey Report and Recommendations. NASA Crosslink Spectrum Report, pt. 1, version 1.0, June 5, 2002.
2. Popovic, D.; and Popovic, Z.: Multibeam Antennas With Polarization and Angle Diversity. IEEE Trans. on Antenna and Propagation, vol. 50, May 2002, pp. 651–652.

Glenn contacts:
Dr. Richard Q. Lee, 216–433–3489, Richard.Q.Lee@nasa.gov; and
Dr. Félix. A. Miranda, 216–433–6589, Felix.A.Miranda@nasa.gov

Authors: Dr. Richard Q. Lee and Kevin M. Lambert

Headquarters program office: OAT

Programs/Projects: CICT

Fiber-Optic Network Architectures for Onboard Avionics Applications Investigated

This project is part of a study within the Advanced Air Transportation Technologies program undertaken at the NASA Glenn Research Center. The main focus of the program is the improvement of air transportation, with particular emphasis on air transportation safety. Current and future advances in digital data communications between an aircraft and the outside world will require high-bandwidth onboard communication networks. Radiofrequency (RF) systems, with their interconnection network based on coaxial cables and waveguides, increase the complexity of communication systems onboard modern civil and military aircraft with respect to weight, power consumption, and safety. In addition, safety and reliability concerns from electromagnetic interference between the RF components embedded in these communication systems exist.

A simple, reliable, and lightweight network that is free from the effects of electromagnetic interference and capable of supporting the broadband communications needs of future onboard digital avionics systems cannot be easily implemented using existing coaxial cable-based systems. Fiber-optical communication systems can meet all these challenges of modern avionics applications in an efficient, cost-effective manner.

The objective of this project is to present a number of optical network architectures for onboard RF signal distribution. Because of the emergence of a number of digital avionics devices requiring high-bandwidth connectivity, fiber-optic RF networks onboard modern aircraft will play a vital role in ensuring a low-noise, highly reliable RF communication system. Two approaches are being used for

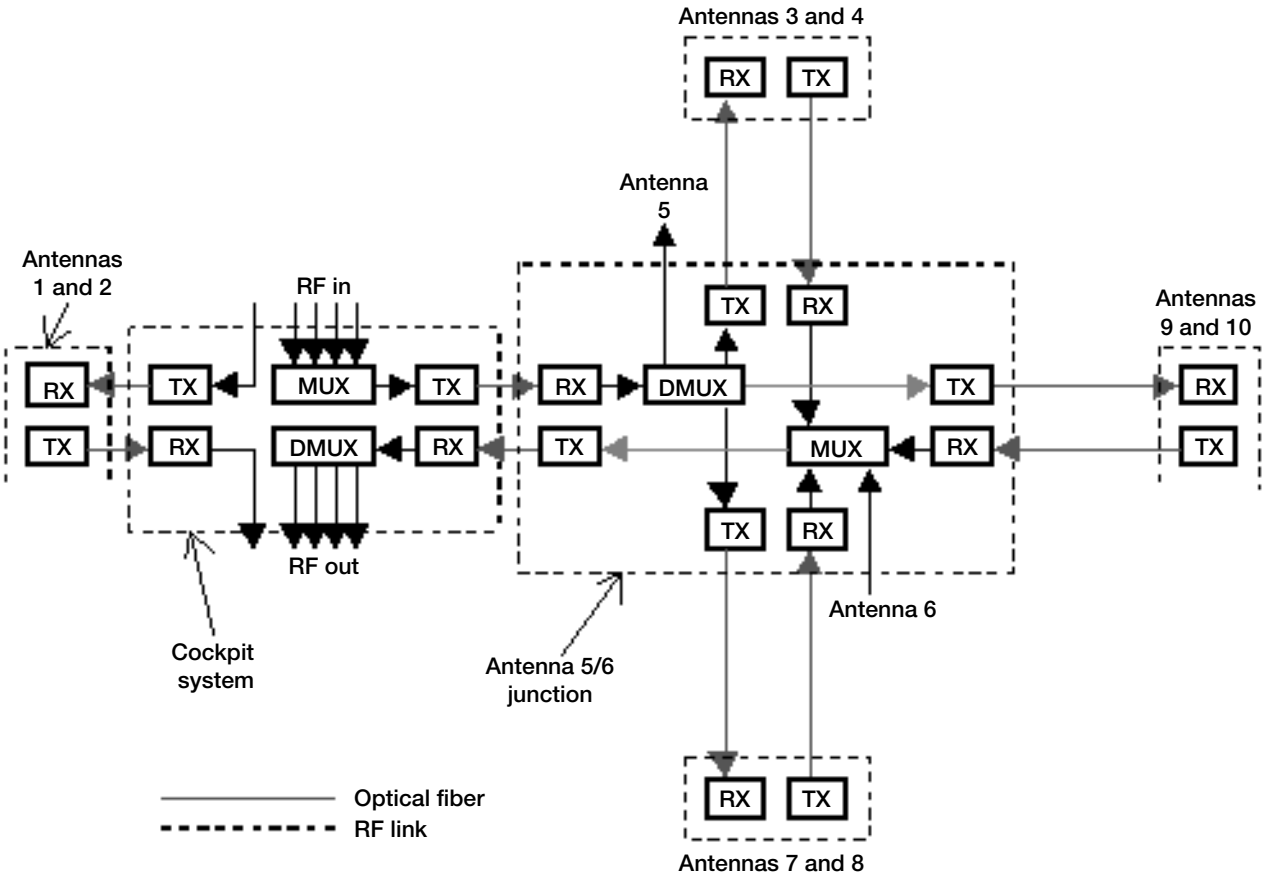

Hybrid RF-optical approach. MUX, RF power combiner (multiplexer); DMUX, RF demultiplexer; TX, optical transmitter; RX, optical receiver.

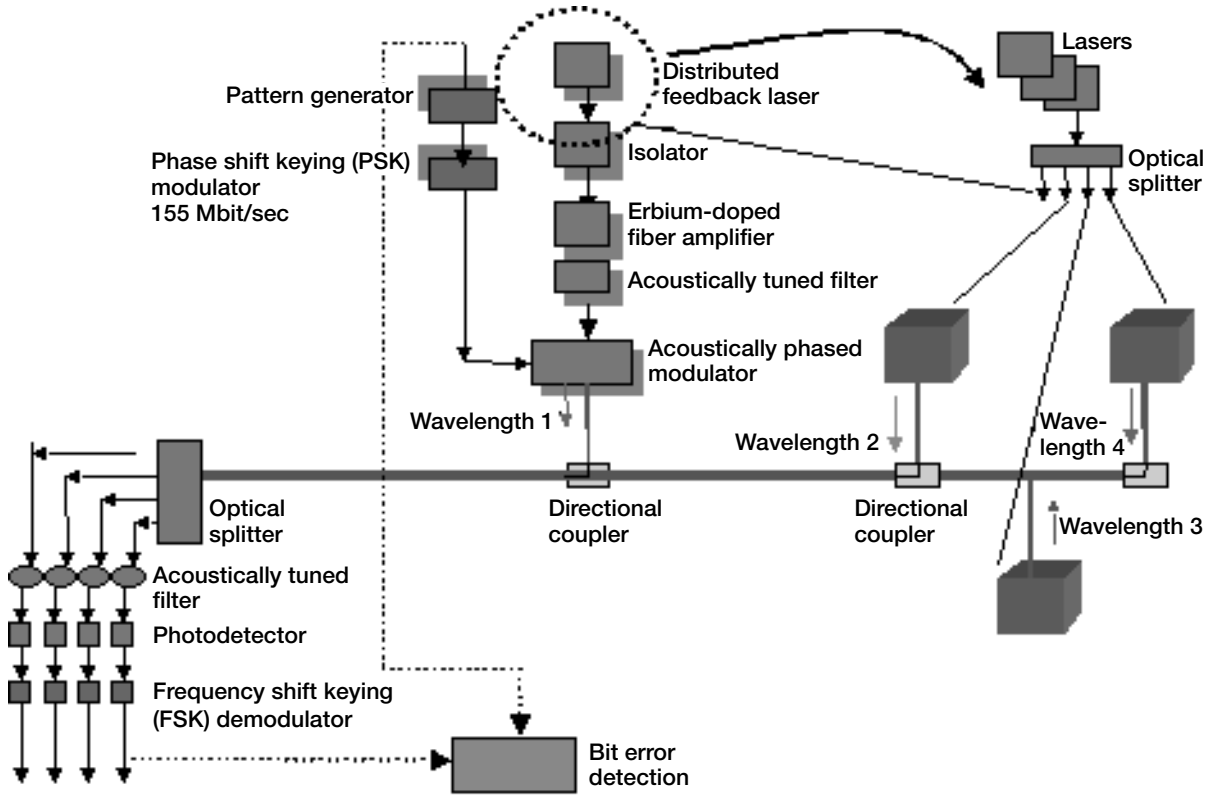

All optical solution using wavelength division multiplexing for implementation of multiple-source multiple-receiver network architecture.

network architectures for aircraft onboard fiber-optic distribution systems: a hybrid RF-optical network and an all-optical wavelength division multiplexing (WDM) network (ref. 1). For almost all cases, either a hybrid RF-optical approach or an all-optical approach can be taken, depending on the design specification requirements.

The hybrid RF-optical approach shown in the figure on the preceding page has the advantage of low signal loss due to repeated regeneration of the RF signal, and requires fewer fibers. The use of so many optical transmitters and receivers increases the weight and the cost of the hybrid system, however, and also increases electromagnetic interference. On the other hand, the all-optical WDM approach depicted in the figure on this page overcomes these difficulties by ensuring a continuous light-path from a fiber-optic transmitter to one or more fiber-optic receivers while sustaining a strong optical signal. Furthermore, an all-optical approach has the potential for replacing multiple-fiber cables by carrying a number of RF signals on different wavelengths on a single fiber simultaneously, thereby reducing the weight. In addition, all-optical solutions use a number of passive components like power combiners, power splitters, and wavelength demultiplexers, all of which require no power supply. Hence, an all-optical solution requires less power than the hybrid RF-optical solution.

Because of budget constraints, we only established the experimental platform for the all-optical WDM architecture described in the figure above. From this setup, the transmission of FM and AM signals[1] as well as frequency shift keying (FSK) digital modulation over fiber-optic links were investigated, and the overall systems performance was characterized by taking measurements of power loss, delay, signal-to-noise ratio, carrier-to-noise ratio, total harmonic distortion, and bit error rate. These experimental results have been described in detail in other publications (ref. 2). Among these measurements, signal-to-noise ratio and carrier-to-noise ratio are the most essential factors when evaluating the merits of a communication system.

The signal-to-noise ratios for AM and FM at 1310 and 1550 nm are approximately 55 and 40 dB, respectively. These measurements suggest good analog signal transmission over WDM fiber-optic links since they exceed the

[1]Frequency-modulated and amplitude-modulated signals.

30 dB standard for good AM and FM radio reception. In addition, the carrier-to-noise ratios for 1310 and 1550 nm are approximately 65 and 52 dB, respectively, which exceeds the standard quality level of 40 dB. With these results, the fiber-optic systems ensure good communication signal transmission between the antennas and the cockpit of an aircraft.

References

1. Alam, M.F., et al.: Fiber-Optic Network Architectures for On-Board Digital Avionics Signal Distribution. Int. J. Commun. Syst., vol. 15, nos. 2–3, 2002, pp. 175–190.
2. Slaveski, Filip, et al.: Transmission of RF Signals Over Optical Fiber for Avionics Applications. Presented at the 21st Digital Avionics System Conference, Technical section D, 3D2, IEEE, Oct. 2002.

Find out more about the research of Glenn's Applied RF Technology Branch:
http://ctd.grc.nasa.gov/5640/5640.html

Glenn contacts:
Dr. Hung Nguyen, 216–433–6590, Hung.D.Nguyen@nasa.gov;
Duc Ngo, 216–433–8651, Duc.H.Ngo@nasa.gov; and
Dr. Félix A. Miranda, 216–433–6589, Felix.A.Miranda@nasa.gov

Authors:
Dr. Hung D. Nguyen and Duc H. Ngo

Headquarters Program Office: OAT

Programs/Projects: AATT

Laser-Ablated $Ba_{0.50}Sr_{0.50}TiO_3/LaAlO_3$ Films Analyzed Statistically for Microwave Applications

Scanning phased-array antennas represent a highly desirable solution for futuristic near-Earth and deep space communication scenarios requiring vibration-free, rapid beam steering and enhanced reliability. The current state-of-practice in scanning phased arrays is represented by gallium arsenide (GaAs) monolithic microwave integrated circuit (MMIC) technology or ferrite phase shifters. Cost and weight are significant impediments to space applications. Moreover, conventional manifold-fed arrays suffer from beam-forming loss that places considerable burden on MMIC amplifiers. The inefficiency can result in severe thermal management problems.

The NASA Glenn Research Center is constructing an innovative type of scanning phased-array antenna, using thin-film ferroelectric barium-strontium-titanate-($Ba_xSr_{1-x}TiO_3$) based phase shifters, that promises to overcome these disadvantages. A critical milestone is the production of 616 identical 19-GHz phase shifters with an insertion loss of ≈4 dB, a phase shift of at least 337.5°, and a bandwidth of 3 percent. It is well known that ferroelectric film crystallinity and strain, affected by the substrate template, play an important role. $Ba_{0.50}Sr_{0.50}TiO_3$ films, nominally 400 nm thick, were deposited on forty-eight 0.25-mm-thick, 5-cm-diameter lanthanum-aluminate ($LaAlO_3$) wafers using pulsed laser deposition (PLD). The composition was selected as a compromise between tuning and loss for room-temperature operation (e.g., crystallinity progressively degrades for Ba concentrations in excess of 30 percent). As a prelude to fabricating the array, it was necessary to process, screen, and inventory a large number of samples. Variable angle ellipsometry was used to characterize the refractive index and film thickness across each wafer. Microstructural properties of the thin films were characterized using high-resolution x-ray diffractometry. Finally, prototype phase shifters and resonators were patterned on each wafer and radio-frequency-probed to measure tuning as a function of direct-current (dc) bias voltage as well as peak (0 field) permittivity and quality factor Q_o. This work presents the first statistically relevant study of film quality and microwave performance and represents a pivotal milestone toward spacecraft utilization of thin ferroelectric films for microwave applications.

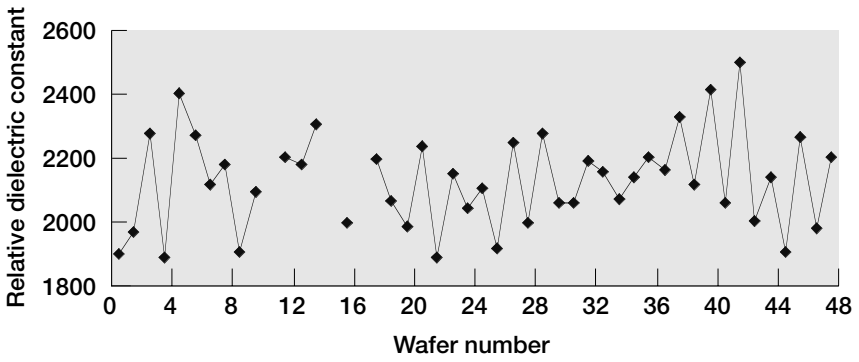

Peak (0 field) dielectric constant of the $Ba_{0.50}Sr_{0.50}TiO_3$ layer extracted from λ/2 and λ microstrip resonators.

For any phased-array antenna to be realized with ferroelectric materials, or any device technology for that matter, the phase shifters must be reproducible in terms of insertion loss and insertion phase shift. For example, random phase errors exceeding 45° can significantly degrade the main beam power. Very good reproducibility was obtained both across the 48 wafers and from wafer to wafer in terms of crystal quality. For wafers 1 to 24, the mean in-plane lattice parameter was 3.9816 Å (σ = 0.0021)[1] and the mean out-of-plane lattice parameter was 3.9637 Å (σ = 0.0012). For wafers 25 to 48, the mean in-plane lattice parameter was 3.9797Å (σ = 0.0016) and the mean out-of-plane lattice parameter was 3.9643 Å (σ = 0.0005). The full-width half-maximum (FWHM) of the (002) peak was generally better than 0.1° and significantly better than this for the second batch of 24 wafers.

On the basis of the ellipsometric analysis, the means and standard deviations (in parentheses) for the film thicknesses at the center, 12.7-mm off center, and 19.0-mm off center were 3767 Å (340 Å), 3677 Å (313 Å), and 3469 Å (273 Å), respectively. Film thickness plays a crucial role in microwave performance. Despite some variations in thickness and crystallinity, the microwave performance was very consistent. The mean Q_o was 14.1, with a standard deviation of 1.0. The mean insertion phase shift was 20.5°, with a standard deviation of 1.4°. The *Q* measurements suggest that the film quality, in terms of loss tangent, is very reproducible. The peak dielectric constant of the $Ba_{0.50}Sr_{0.50}TiO_3$ layer for each wafer is shown in the graph on the preceding page. The mean peak dielectric constant was 2129 with a standard deviation of 149.

In summary, the two batches totaling 48 PLD $Ba_{0.50}Sr_{0.50}TiO_3/LaAlO_3$ wafers are suitable, from a microwave point of view, for fabrication into phase shifters and incorporation into a state-of-the-art phased-array antenna. In the near future, the remaining 46 wafers will be patterned with approximately 30 phase shifters each. Then, the phase shifters will be sampled on-wafer (about 10 percent tested) and inventoried for use in the ferroelectric reflectarray antenna.

[1]Standard deviation.

Reference

1. Romanofsky, R., et al.: A Statistical Analysis of Laser Ablated $Ba_{0.50}Sr_{0.50}TiO_3/LaAlO_3$ Films for Microwave Applications. MRS Proceedings, vol. 720, 2002, pp. 111–122.

Glenn contacts:
Dr. Robert R. Romanofsky, 216–433–3507, Robert.R.Romanofsky@nasa.gov; and Sam Alterovitz, 216–433–3517, Samuel.A.Alterovitz@nasa.gov

Analex contact:
Carl Mueller, 216–433–8853, Carl.H.Mueller@grc.nasa.gov

Ohio Aerospace Institute (OAI) contact:
Fred Van Keuls, 216–433–3379, Frederick.W.Vankeuls@grc.nasa.gov

Author: Dr. Robert R. Romanofsky

Headquarters program office: OAT

Programs/Projects:
ESE, Space Science—any space platform requiring an agile but vibration-free communications system

Effects of a Scanning Reflectarray Antenna on Modulated Data Modeled

The ferroelectric reflectarray is a new type of scanning antenna under development for space and ground communications and radar applications at the NASA Glenn Research Center (see the illustration to the right). The reflectarray offers tremendous cost, gain, and efficiency advantages in comparison to the state-of-the-art phased arrays, but there is an inherent intersymbol interference (ISI) problem with digital communication data streams processed through the array because of the way the reflectarray is operated. This interference stems from the fact that the antenna beam is formed by the superposition of reflected waves from the array elements. The delays from the elements to the observation point of each wave differ. Ferroelectric phase shifters are designed to compensate for the modulo-2π phase differences so that the waves will constructively interfere at the sinusoidal carrier level; however, the delays of the integer-number multiple of the carrier period are not compensated

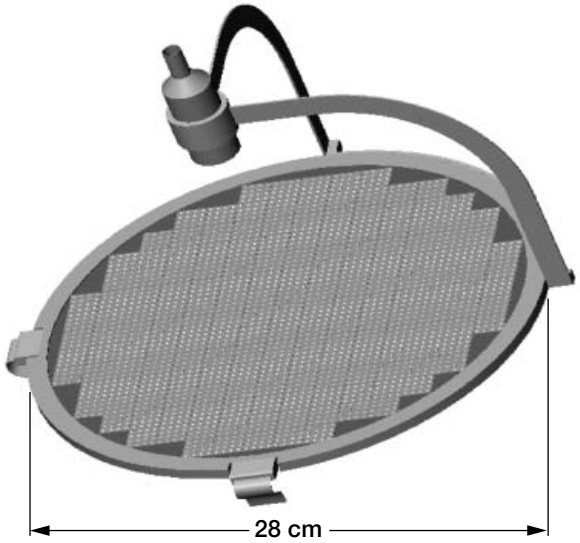

Ferroelectric reflectarray.

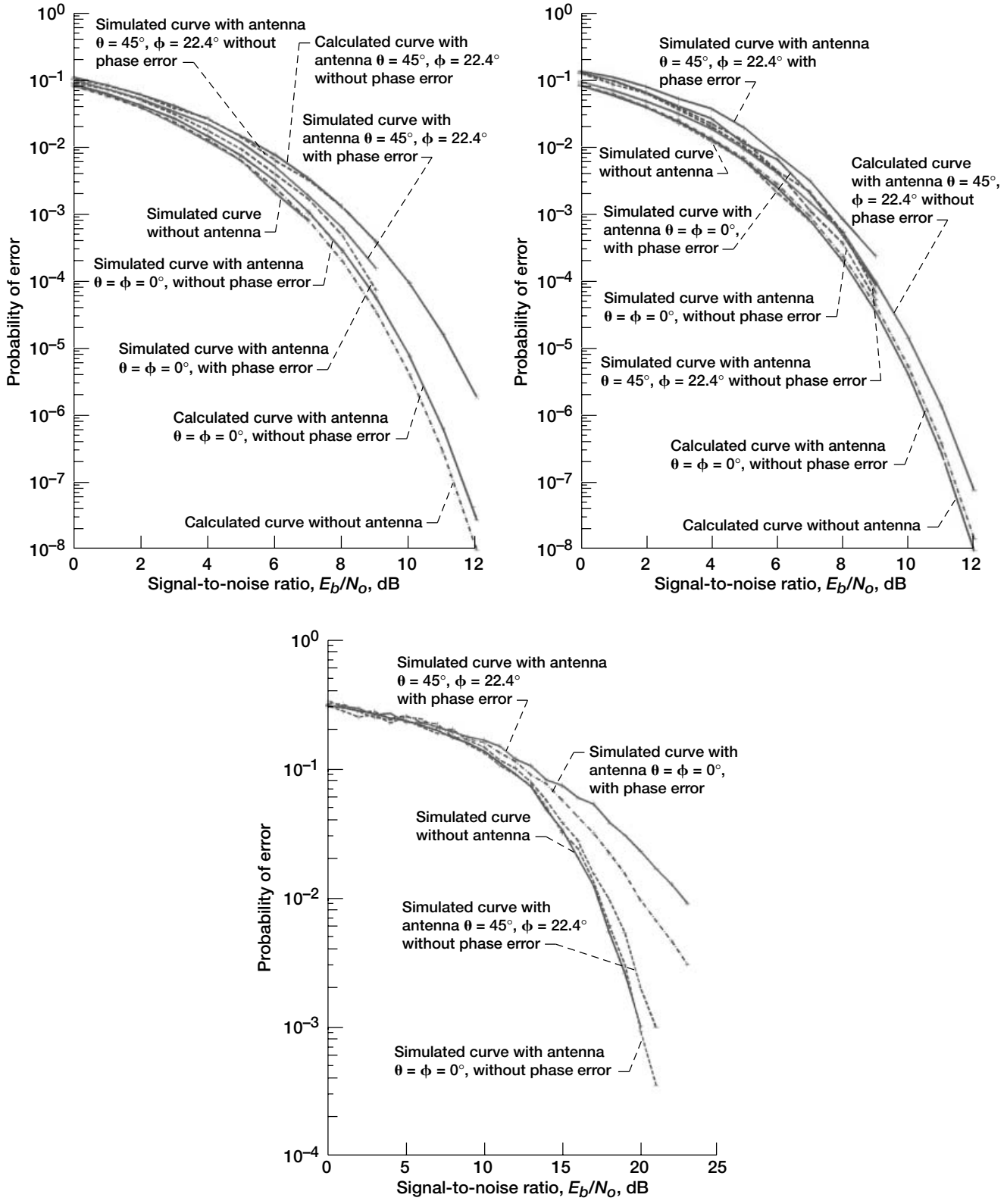

Top left: BER curves of BPSK: bit rate, Rb, 1.325 Gbps; symbol rate, Rs, 1.325 Gsps. Top right: BER curves of QPSK: Rb, 1.325 Gbps; Rs, 662.5 Msps. Bottom: BER curves of 256 QAM: Rb, 1.325 Gbps; Rs, 165.5 Msps.

for. This lack of compensation causes ISI in digital modulated signals. ISI has not been a problem with analog modulations and low-rate digital modulations since the distortion (or ISI) introduced is negligible. The problem becomes acute when the data rate gets higher, and the electrical size of the array gets bigger. Moreover, there are intrinsic transient effects associated with the phase shifters and the controller that executes the algorithm to direct the beam. That is, phase shifter updates to redirect the beam may be initiated simultaneously, but nonlinearity will cause different settling times.

The ISI problem and other effects ultimately limit the size (gain) and data rate of the reflectarray. An ISI analysis was required to prove or disprove the suitability of the reflectarray antenna for high-rate digitally modulated signals and to give guidance for determining antenna parameters. In this research, the nature of the ISI of the reflectarray has been mathematically modeled. ISI has been linked to the antenna geometry, the carrier frequency, the data rate, and the modulation scheme. A reflectarray with a diameter of 0.235 m, with 925 elements, and operating with a 26.5-GHz carrier was used for performance evaluation and simulation. The performance degradation due to ISI in terms of the bit error rate (BER) was numerically simulated and quantified for various antenna steering angles, various modulations, and data rates up to 1.325 Gbps. The effect of phase errors in the phase shifters was also analyzed and simulated. The results show that even though there is some loss in the signal-to-noise ratio (E_b/N_o), ranging from 1 to 2 dB, depending on the BER level, the conventional satellite communication modulation schemes, such as binary and quaternary phase shift keying (BPSK and QPSK), are still good schemes that can be used in systems with reflectarray antennas. Higher order PSK schemes and quadrature amplitude modulation (QAM) schemes are more susceptible to phase-shifter errors because of their more compact constellations. By similarity, these results are also applicable to direct radiating array antennas with minor modifications. This work will have a significant impact on the design of phased-array antennas, and the design of systems that use them.

The graphs on the preceding page show simulated and analytical curves of BER versus E_b/N_o for three different modulation schemes with and without phase errors uniformly distributed over $-\pi/8$ and $\pi/8$. Reflectarrays bring ISI to the transmitted signal and degrade the BER performance. In general, the phase shifter's phase errors induce further BER increases. The effect increases with the order of modulation. From the results, one can see that low-order modulations like BPSK, QPSK, 8PSK, and 16QAM are acceptable for the reflectarray antenna. Their total loss from ISI and phase errors is in the neighborhood of 1 dB at BER = 10^{-3}, which can be improved to 10^{-6} to 10^{-10} with typical error-control coding. QPSK is the best of these modulations since it doubles the data rate of BPSK within the same bandwidth while keeping the same BER performance in the additive white gaussian noise (AWGN) channel. In addition, it suffers less ISI loss with a reflectarray. This study shows that the reflectarray is suitable for data rates up to 1 Gbps but is sensitive to phase shifters' phase errors for high-order modulations. For the reflectarray to be used for high-order modulations, the phase errors must be kept very low.

Reference

1. Xiong, Fuqin; Yan Ma Pinchak, S.; and Romanofsky, R.R.: Modulation Study for Beam Steerable Reflectarray Anntennas. Presented at the IEEE 2002 Canadian Conference on Electrical and Computer Engineering, vol. 3, 2002, pp. 1265–1270.

Glenn contacts:

Dr. Robert R. Romanofsky, 216–433–3507, Robert.R.Romanofsky@nasa.gov

Authors:

Robert Romanofsky and Fuqin Xiong

Headquarters program office:

OSF (SCDS)

Programs/Projects:

ESE, Space Science—any space platform requiring a high data throughput phased-array antenna

Quantum Sensing and Communications Being Developed for Nanotechnology

An interdisciplinary quantum communications and sensing research effort has been underway at the NASA Glenn Research Center since the summer of 2000. Researchers in the Communications Technology, Instrumentation and Controls, and Propulsion and Turbomachinery Divisions have been working together to study and develop techniques that use the principle of quantum entanglement (QE). This work is supported principally by the Nanotechnology Base R&T program at Glenn. As applied to communications and sensing, QE is an emerging technology that holds promise as a new and innovative way to communicate faster and farther, and to sense, measure, and image environmental properties in ways that are not possible with existing technology.

Quantum entangled photons are "inseparable" as described by a wave function formalism. For two entangled photons, the term "inseparable" means that one cannot describe one photon without completely describing the other. This inseparability gives rise to what appears as "spooky," or nonintuitive, behavior because of the quantum nature of the process. For example, two entangled photons of lower energy can be created simultaneously from a single photon of higher energy in a process called spontaneous parametric down-conversion. Our research is focused on the use of polarization-entangled photons generated by passing a high-energy (blue) photon through a nonlinear beta barium borate crystal to generate two red photons that have orthogonal but entangled polarization states. Although the actual polarization state of any one photon is not known until it is measured, the act of measuring the polarization of one photon completely determines the polarization state of its twin because of entanglement. This unique relationship between the photons provides extra information about the system. For example, entanglement makes it easy to distinguish entangled photons from other photons impinging on a detector. For many other applications, ranging from quantum computation and information to quantum sensing, the entanglement property is critical.

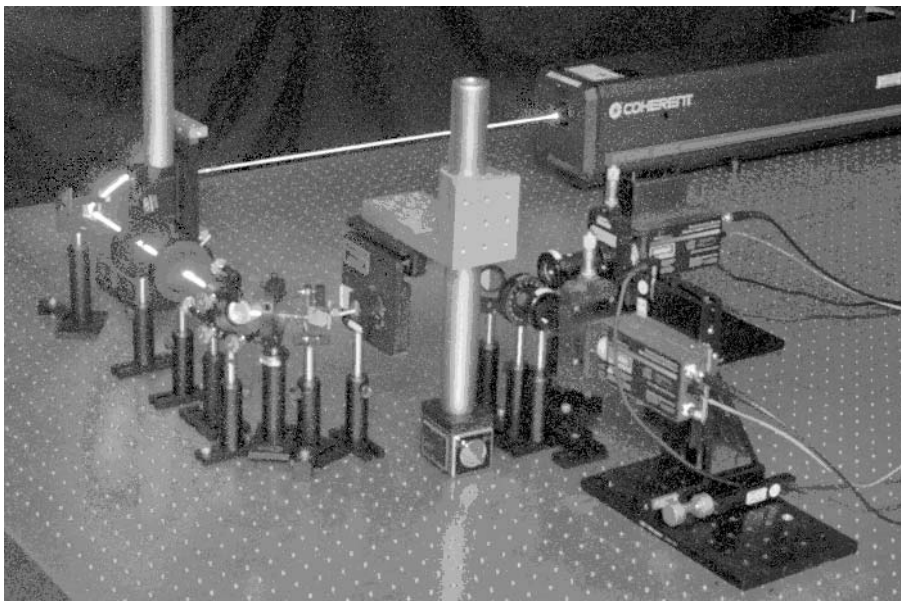

Quantum entanglement setup. Glenn personnel used this setup to verify the presence of entangled photons in the system.

After the Quantum Communications and Sensing laboratory was completed, our first goal was to verify the presence of entangled photons. The optical setup for this experiment is shown in the photograph. Once verification was complete, a technique known as the "quantum fax" was demonstrated. In this demonstration, an image of a double-slit pattern was "faxed" via a virtual quantum channel from one detector to another. In the demonstration, entangled red photon twins were sent down separate paths. One photon passed through a double slit, and the image of that slit was detected in the other photon (or "faxed") even though it never passed through a slit. Data from the quantum-faxed double-slit are shown in the graph on the next page.

Finally, a comprehensive model of a nanocommunications system using entangled photons was computationally simulated with support from an Undergraduate Student Research Program student. The results showed clearly the feasibility and utility of using quantum-entangled photons for ultra-low-power space communications. High-resolution images can be transmitted over 100 km in free space if entangled photon pairs are used to represent uncoded 8-bit data symbols with less than 27 nW of total photon flux.

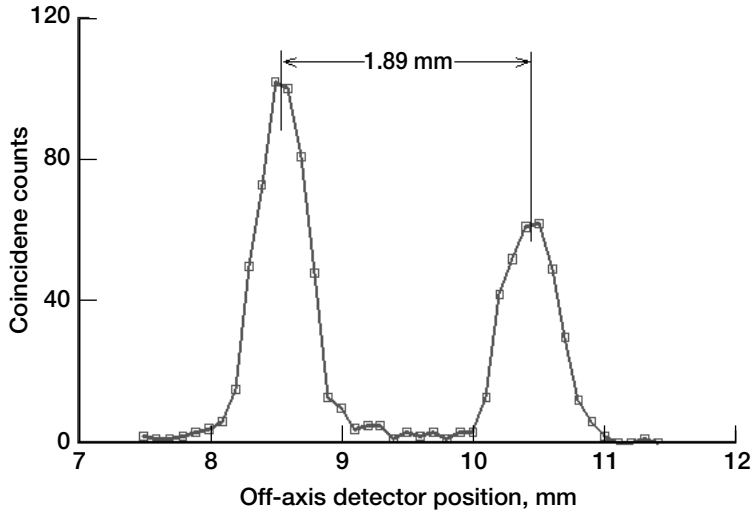

Results of the quantum fax experiment. This graph shows an image that was "quantum faxed" using polarization-entangled photons.

Glenn contacts:
Marc Seibert, 216–433–3535, Marc.A.Seibert@nasa.gov;
John Lekki, 216–433–5650, John.D.Lekki@nasa.gov;
Quang-Viet Nguyen, 216–433–3574, Quang-Viet.Nguyen-1@nasa.gov;
Terry Sanders, 216–433–5849, Terry.M.Sanders@nasa.gov; and
Kenneth Weiland, 216–433–3843, Kenneth.E.Weiland@nasa.gov

Authors: Dr. Quang-Viet Nguyen and Marc A. Seibert

Headquarters program office: OAT

Programs/Projects:
Space Communications, Propulsion and Power, Propulsion Systems R&T, Nanotechnology Base R&T

Space Networking Demonstrated for Distributed Human-Robotic Planetary Exploration

Communications and networking experts from the NASA Glenn Research Center designed and implemented an innovative communications infrastructure for a simulated human-robotic planetary mission. The mission, which was executed in the Arizona desert during the first 2 weeks of September 2002, involved a diverse team of researchers from several NASA centers and academic institutions.

NASA researchers are envisioning a human mission to the Moon or to Mars that will include both humans and robots. Humans generally ensure the overall quality of the mission, whereas robots ensure a level of accuracy in measurement that is difficult for suited explorers to attain. The interdisciplinary focus of this work is to study how robots and humans can best interact during exploration using spoken language and to obtain data for comparing human and robotic performance in gathering geological science data. Human subjects wearing an advanced ILC Mark III spacesuit worked alongside an extravehicular-activity robotic assistant rover to perform tasks representative of future exploration. Exploration tasks included geophone instrument deployment and field mapping.

Glenn provided local communications between the "astronaut," the robot, various scientific instruments, and the base camp, and also connected this remote location to mission control and the world outside the field site. The proximity network at the field site was required to handle video, voice, and data transmissions from a variety of sources using Internet protocol. In addition, an innovative suit audio system was developed to facilitate human-robot interaction. This system enabled the extra-vehicular-activity robotic assistant to understand speech commands with very high reliability from a human in a pressurized spacesuit.

The overall communications architecture is shown in the figure on the next page. As information was received at the base camp, it was transmitted to "Earth" via a Ku-band satellite link between the Arizona desert and Glenn. For the video and voice data, a temporal delay was applied at Glenn prior to receipt at mission

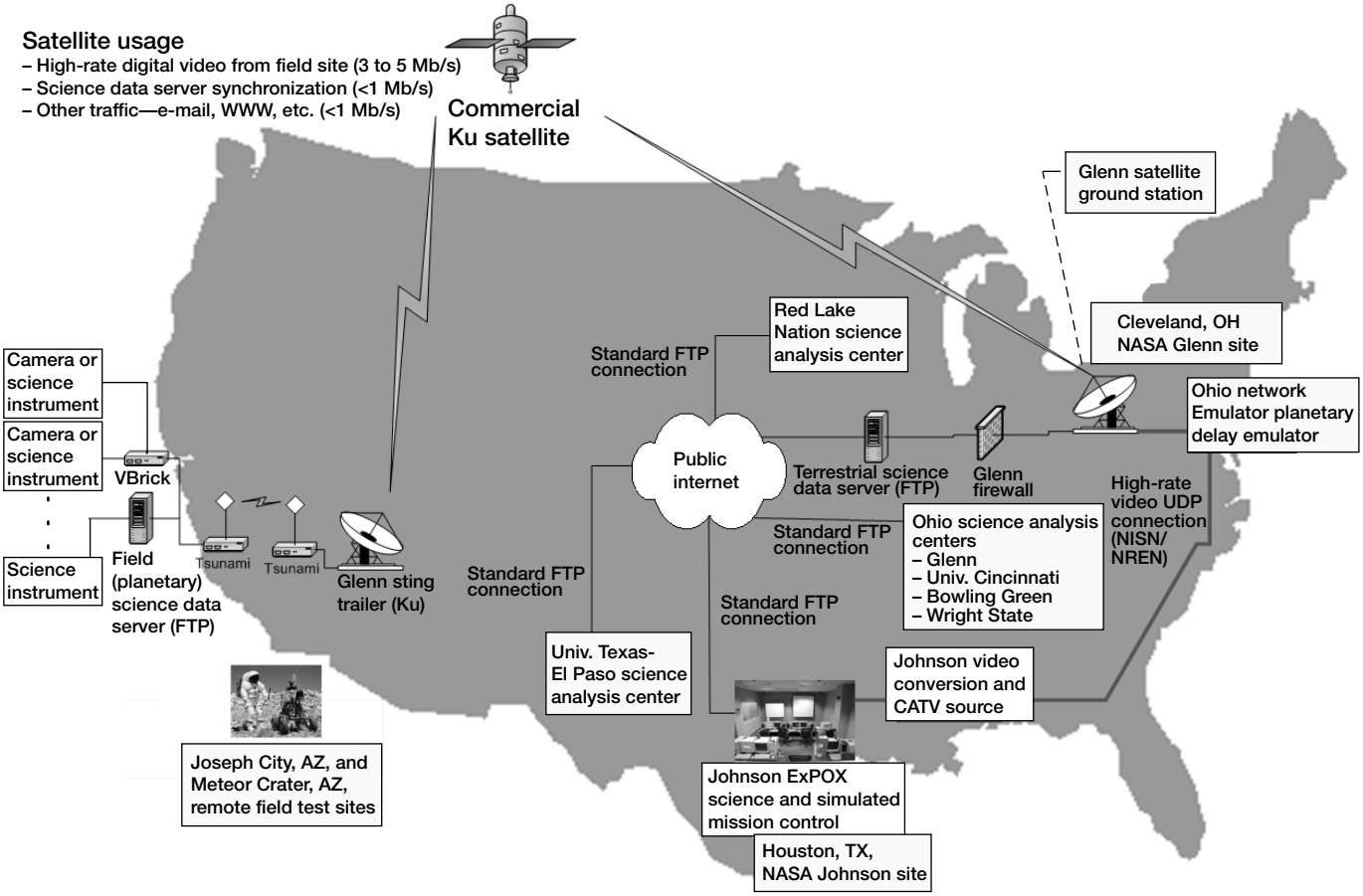

Overview of September 2002 space networking architecture test and demonstration. VBrick (VBrick Systems, Inc.), commercial video compression/decompression unit; ExPOC, Johnson's Exploration, Planning and Operations Center; CATV, Johnson's closed-circuit TV network; UDP, User Datagram Protocol, an Internet protocol; NISN, NASA Integrated Services Network; NREN, NASA Research and Education Network.

control in order to simulate the Mars communications delay of 5 to 20 min. The delay was emulated using the Planetary—Ohio Network Emulator (p-ONE), developed specifically for this program.

For the science data, a dual server replication architecture was implemented. In this architecture, science data were stored on a "planetary" (field science) server and synchronized with a mirroring server on "Earth." Scientists at Glenn, the NASA Johnson Space Center, and academic institutions were able to download field science data from the "Earth" server for analysis and provide immediate feedback to the field team. The innovative architecture minimized the use of the satellite link for file transmission and ensured that the science data were returned to "Earth" prior to sharing. In future experiments, synchronization will be delayed to simulate planetary communication delay.

The field demonstration this year simulated the most realistic interplanetary mission scenario to date, and results of the research will be incorporated into future field demonstrations and, eventually, space exploration missions. Glenn plans to build on this program in future field tests by incorporating more integrated proximity network communications and more realistic long-haul link emulations.

This successful demonstration was the culmination of research performed by several teams. The collaborators include communications experts from Glenn and the NASA Kennedy Space Center; spacesuit and control center experts from Johnson; robotics experts from Johnson and the NASA Ames Research Center; planetary exploration experts from Johnson, the Science Applications International

2002 Human-Robotic Exploration Field Team.

Corporation, the University of Houston, and Bowling Green State University; and geology experts from the University of Texas-El Paso, the University of Cincinnati, Bowling Green, Wright State University, Stanford University, Red Lake Nation tribal college, and the U.S. Geological Survey at Flagstaff. All teams are represented in the photograph.

Find out more about this research: http://ctd.grc.nasa.gov/5650/5650.html

Glenn contact:
Marc Seibert, 216–433–3535,
Marc.A.Seibert@nasa.gov

Authors: Thomas P. Bizon and Marc A. Seibert

Headquarters program office:
OHEDS (Advanced Programs), OAT

Programs/Projects: CICT

Turbomachinery and Propulsion Systems

Mechanisms of Rotating Instability in Axial Compressors Investigated

Rotating instability is a phenomenon that occurs in the tip flow region of axial compressor stages during stable operation. It can be observed in highly staggered rotors with significant tip clearance and is strongest at high-load operating points where the characteristic levels off. In this condition, the single-stage fan under investigation radiates an audible, whistling tone, and wall pressure spectra in the vicinity of the rotor disk exhibit nonrotational components. The following graph shows the spectrum of static pressure at a point on the endwall near the leading edge. A hump appears at roughly half of the blade passing frequency (BPF) and is characteristic of rotating instability.

A computational model was developed at the NASA Glenn Research Center to investigate the mechanism behind this phenomenon. A three-dimensional steady Navier-Stokes code that has been successfully tested for a wide range of turbomachinery flows was modified to execute a time-accurate simulation of the full annulus of the compressor. At the inlet of the computational domain, the total pressure, total temperature, and two velocity components are specified. Since no unsteady measurements of static pressure or other flow variables were available downstream of the rotor, circumferentially averaged static pressure was specified on the shroud at the outlet of the computational domain.

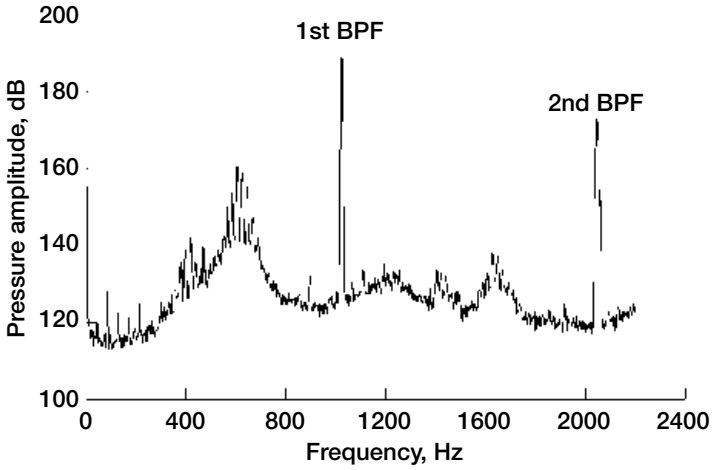

Wall pressure spectrum with rotating instability components; blade passing frequency, BPF, 1024 Hz.

A three-dimensional view of the vortex from the numerical model is shown in the following figure. Particle traces released near the leading edge tip have rolled up to illustrate the tip clearance vortex. Flow near the trailing edge is pushed forward by the axially reversed flow. It then interacts with the tip clearance flow and the incoming flow and results in the rotating instability vortex, the core of which is illustrated by total pressure shading on planes located successively downstream. The rotating instability vortex is formed periodically midway between the blades and moves toward the pressure side of the passage. The unsteady behavior of this vortex structure is the main mechanism of the rotating instability shown in the graph. The numerical model can be used to detect any possible occurrence of rotating instability when the tip clearance increases during engine service.

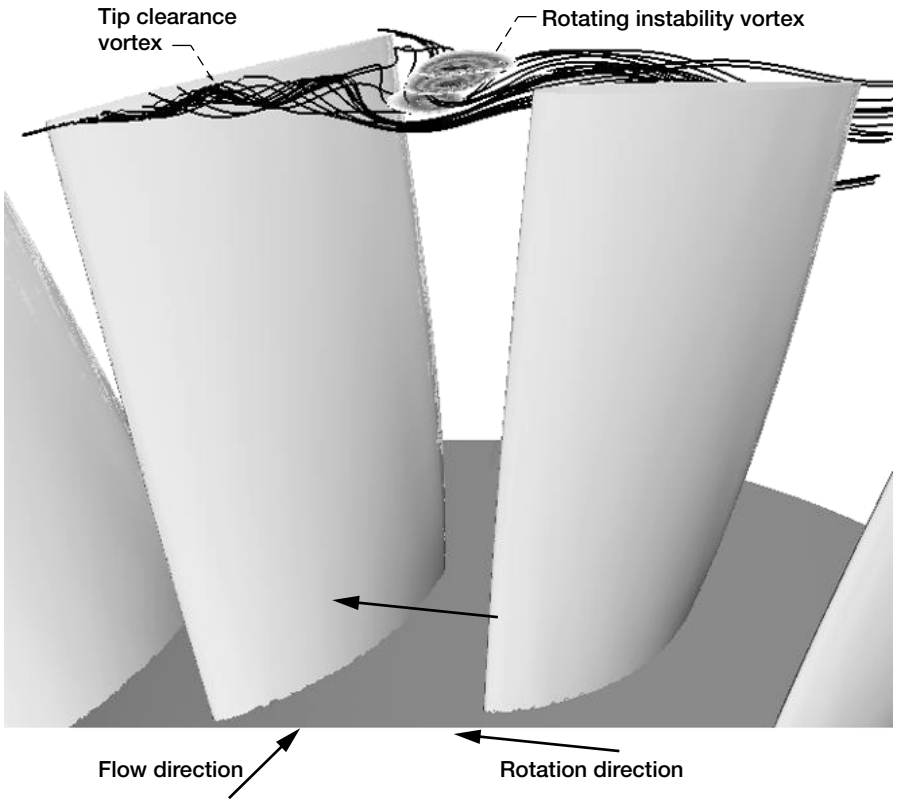

Structure of the instantaneous flow field including the tip clearance vortex and rotating instability vortex.

References

1. Hah, C.: A Navier-Stokes Analysis of Three-Dimensional Turbulent Flows Inside Turbine Blade Rows at Design and Off-Design Conditions. J. Eng. Gas Turbines Power, vol. 106, no. 3, 1984, pp. 421–429.
2. März, Joachim; Hah, Chunill; and Neise, Wolfgang: An Experimental and Numerical Investigation Into the Mechanisms of Rotating Instability. Trans. ASME J. Turbomachinery, vol. 124, no. 3, 2002, pp. 367–375.

Glenn contact:
Dr. Chunill Hah, 216–433–6377, Chunill.Hah-1@nasa.gov

Author: Dr. Chunill Hah

Headquarters program office: OAT

Programs/Projects:
Propulsion and Power, SEC

Two-Stage Axial Compressor Rig Designed To Develop and Validate Advanced Aerodynamic Technologies

Future aeropropulsion gas turbine engines must be affordable in addition to being energy efficient and environmentally benign. Progress in aerodynamic design capability is required not only to maximize the specific thrust of next-generation engines without sacrificing fuel consumption, but also to reduce parts count by increasing the aerodynamic loading of the compression system. To meet future compressor requirements, the NASA Glenn Research Center is investigating advanced aerodynamic design concepts that will lead to more compact, higher efficiency, and wider operability configurations than are currently in operation.

Preliminary aerodynamic design studies of highly loaded multistage axial compressors were conducted in-house to establish the level of technical advancements to be expected if rational enhancements are made to key aerodynamic technology elements of the current design systems. A four-stage research configuration with a compression ratio of 12:1 was conceived to evaluate how much efficiency could be improved at high loading levels by the use of turbomachinery computational fluid dynamics (CFD) and the latest aerodynamic design concepts. The objective was to configure a technology demonstrator compatible with anticipated future multistage core compressors for high-bypass-ratio turbofans. Although a specific application was not defined, the design was constrained by

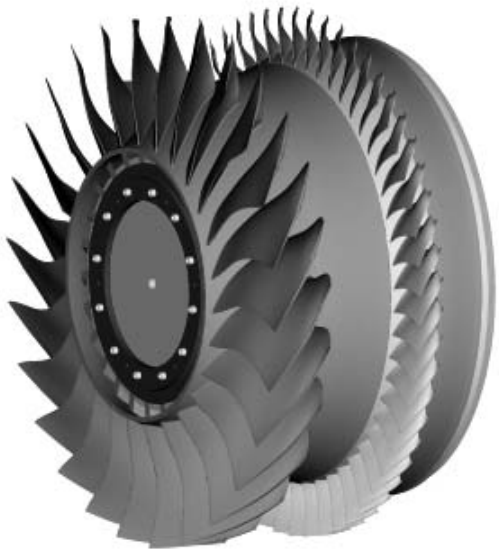

Solid model of rotor assembly for the two-stage axial compressor rig. The transonic rotor blades are swept forward to achieve a beneficial spanwise loading balance.

current aeromechanical and manufacturing practices. Three-dimensional blading and spanwise tailoring of vector diagrams guided by CFD were employed in an attempt to manage the aerodynamics of the high-loaded endwall regions. Multistage CFD simulations of the preliminary four-stage configuration indicated that efficiency was better than the state of the art. To advance the technology significantly beyond this preliminary design baseline, we identified performance-limiting fluid dynamic features, such as leakage-vortex-dominated endwall action and/or reaction and strong shock-boundary-layer interactions.

Further performance gains require design methods that effectively extend the custom-tailored blading philosophy into the endwall regions and allow adequate matching of blade rows in the multistage environment. The first two stages of the four-stage configuration were extracted to serve as a proof-of-concept vehicle. A blade inverse aerodynamic design method developed by Dang (ref. 1) was coupled to the multistage CFD code of Adamczyk (ref. 2) to refine the aerodynamics of the two-stage configuration. An efficiency potential significantly higher than the state of the art was projected on the basis of engineering analysis supported by CFD. Glenn's Engineering Design and Analysis Division has transformed the aerodynamic definition of the two-stage configuration into a mechanical design of a rig to be manufactured and assembled for research and development by the summer of 2003. This rig will serve three main purposes: (1) verification and calibration of design methods, (2) provision of a testbed for new aerodynamic design concepts, and (3) elucidation of the performance-limiting issues in this class of compressor.

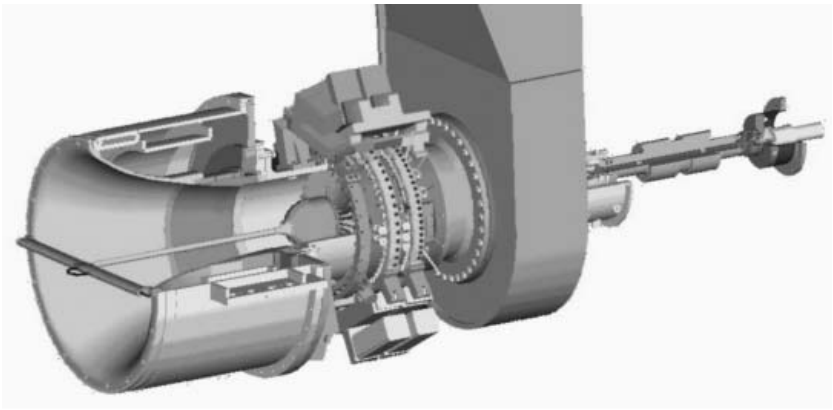

Computer-aided design (CAD) drawing of a two-stage rig planned to be manufactured and assembled by end of fiscal year 2003.

Find out more about this research:

Glenn's Compressor Branch: http://www.grc.nasa.gov/WWW/5810/

Ultra-Efficient Engine Technology Program:
http://www.ueet.nasa.gov/techareas/Turbomachinery.html

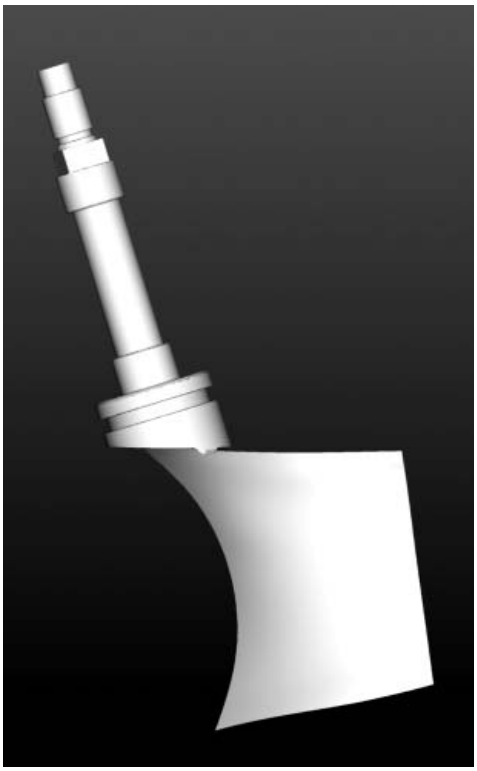

Side view of variable stagger stator. The variable stagger is employed to rematch the stages at off-design operation.

References

1. Dang, T.Q.: A Fully Three-Dimensional Inverse Method for Turbomachinery Blading in Transonic Flows. Trans. ASME J. Turbomachinery, vol. 115, no. 2, 1993, pp. 354–361.
2. Adamczyk, John J.: Aerodynamic Analysis of Multistage Turbomachinery Flows in Support of Aerodynamic Design. Trans. ASME J. Turbomachinery, vol. 122, no. 2, 2000, pp. 189–217.

U.S. Army, Vehicle Technology Center at Glenn contacts:
Dr. Michael D. Hathaway, 216–433–6250, Michael.D.Hathaway@grc.nasa.gov; and Dr. Louis M. Larosiliere, 216–433–3403, Louis.M.Larosiliere@grc.nasa.gov

Glenn contacts:
Loretta M. Shaw, 216–433–3806, Loretta.M.Shaw@nasa.gov; and Dr. Randall M. Chriss, 216–433–6516, Randall.M.Chriss@nasa.gov

Author: Dr. Louis M. Larosiliere

Headquarters program office: OAT

Programs/Projects: UEET

Centrifugal Compressor Surge Controlled

Compressor surge is a condition affecting both aerospace and industrial compression systems that employ turbomachinery. Surge is an unstable operating condition that can lead to the loss of an aircraft in aerospace applications and cause severe damage to industrial systems. Most compressors have a stability limit that is defined by a minimum flow rate on a pressure-rise-versus-flow-rate characteristic curve. Surge margin refers to a margin of safety between the normal operating point of the compressor and the stability limit. Events, both external and internal to the compression system, will occasionally move compressor operation to a point that is beyond its stability limit, causing a surge condition. Technology that increases the stable operating range of the compressor or provides a means to recover from surge will improve the safety and performance of turbomachinery-based compression systems.

Air injection has been demonstrated to improve centrifugal compressor stability at the NASA Glenn Research Center. In earlier work, air was injected through the hub surface of the vaned diffuser in a 4:1 pressure ratio centrifugal compressor to provide a 14-percent improvement in surge margin. Currently, the technology has been applied to the shroud surface of the diffuser and greater improvements have been achieved. The ability to recover from surge has also been demonstrated.

Air was injected into the diffuser through the shroud surface of the flow path between the impeller trailing edge and the leading edge of the diffuser vanes. Eight injector nozzles were positioned quasi-uniformly about the circumference of the diffuser. The nozzle flow path and discharge shape were designed to produce a jet that remained attached to the surface as it traveled into the diffuser passage. Several orientations of the injected airstream and variations in the number of active nozzles were tested. Range improvements were demonstrated both when an external source was used for the injected air and when an internal source was used that took injection air from the compressor flow path.

U.S. Army, Vehicle Technology Directorate at Glenn contact:
Gary J. Skoch, 216–433–3396, Gary.J.Skoch@grc.nasa.gov

Glenn contacts:
Loretta M. Shaw, 216–433–3931, Loretta.M.Shaw@nasa.gov; and
Dr. Anthony J. Strazisar, 216–433–5881, Anthony.J.Strazisar@nasa.gov

Author: Gary J. Skoch

Headquarters program office: OAT

Programs/Projects:
Propulsion and Power, SEC, UEET

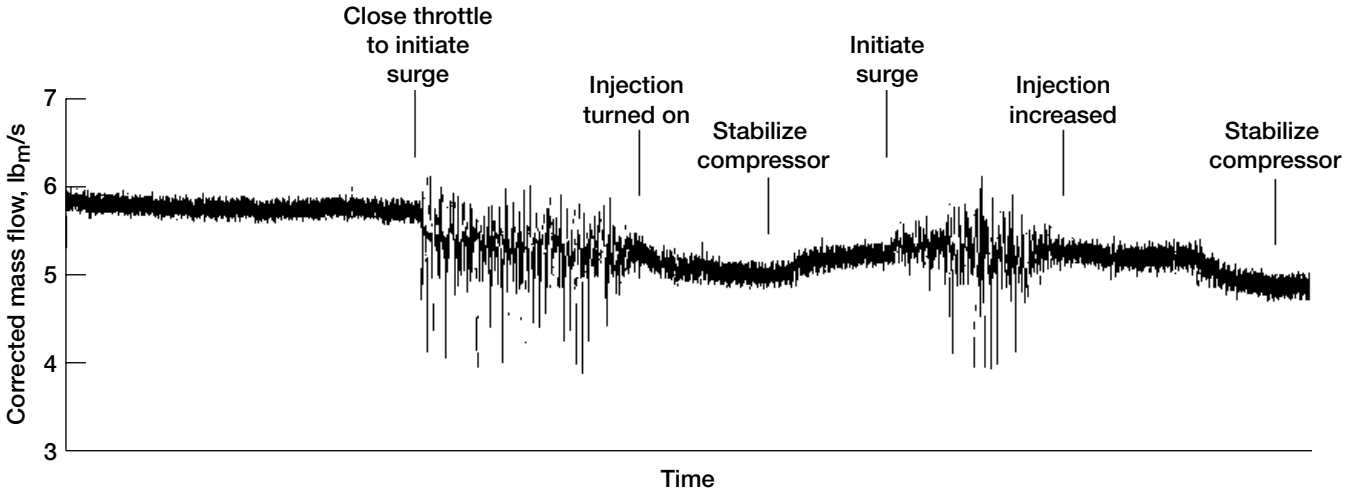

Controlling surge in a 4:1 pressure ratio centrifugal compressor operating at 80-percent of design speed.

Significance of Compressor Blade Row Interactions on Loss Production Investigated

The performance of compressors and the sophistication of analysis tools have reached a level such that less well understood flow mechanisms are gaining importance to designers. In current design systems, the effect on performance of many of these mechanisms, such as blade row interactions, is not typically addressed rigorously. A detailed set of Laser Doppler Velocimetry data was used to confirm the fidelity of an unsteady model of a transonic compressor stage (rotor-stator) simulated with the TURBO unsteady multistage turbomachinery solver. The kinematics of the velocity field were accurately simulated, and the unsteady simulation was then used to assess changes in loss production due to unsteady blade-row-interaction mechanisms. This work was done at the NASA Glenn Research Center in support of the Ultra-Efficient Engine Technology Program.

The interaction of the upstream rotor wakes with the downstream stator leading edge and boundary layers is an example of a blade row interaction loss. The figure shows a snapshot of the stator flow field from the unsteady simulation at one instant in time. The vectors show the magnitude and direction of the disturbance velocity (instantaneous velocity minus time mean velocity). The vectors are colored by entropy. The rotor wakes appear as regions of high entropy and large disturbance velocity. The vectors show the "negative jet" effect of the rotor wakes on the stator boundary layers. That is, the rotor wakes transport high-entropy stator suction surface boundary layer fluid out into the core flow, and the high-entropy rotor wake fluid accumulates on the stator pressure surface. Also, the large change in incidence angle onto the stator blade as the rotor wake is chopped can cause additional loss over what would be seen in a steady simulation.

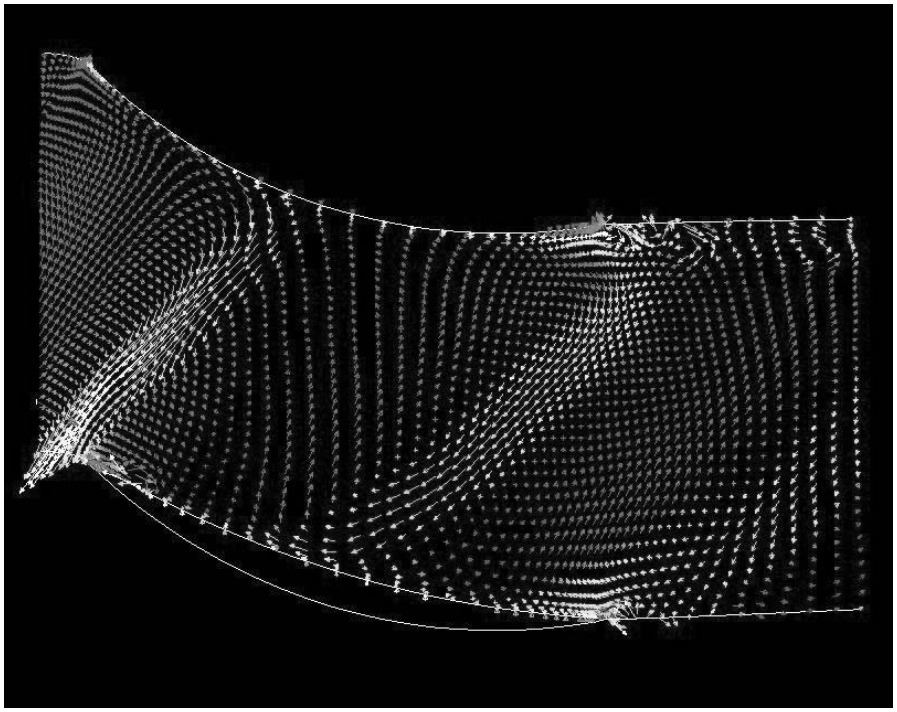

Disturbance velocity field of the stator at an instant in time. Velocity vectors are colored by entropy. This figure is shown in color in the online version of this article (http://www.grc.nasa.gov/WWW/RT2002/5000/5810vanzante.html).

The unsteady simulations were analyzed in detail for effects of the stator on the rotor loss production and the impact of the rotor wakes on stator loss production. The overall conclusions follow. Rotor loss production is not significantly affected by the back-pressure variations generated by the presence of the stator. However, it is not known if loss production in an embedded stator is affected by downstream static pressure variations. Time average stator loss is increased because of the rotor wake/stator leading edge interaction and the rotor wake/stator boundary layer interaction. The distribution of losses in the stator is changed significantly, with losses increasing in the pressure surface boundary layer and core flow.

Reference

1. Van Zante, Dale E.; To, Wai-Ming; and Chen, Jen-Ping: Blade Row Interaction Effects on the Performance of a Moderately Loaded NASA Transonic Compressor Stage. ASME Paper GT–2002–30575, 2002.

Glenn contact:
Dr. Dale Van Zante, 216–433–3640, Dale.E.VanZante@nasa.gov

AP Solutions, Inc.:
Dr. Wai Ming To, 216–433–5937, WaiMing.To@grc.nasa.gov

Author: Dr. Dale E. Van Zante

Headquarters program office: OAT

Programs/Projects:
Propulsion and Power, UEET

Glenn-HT Code Validated for Complex Turbine Blade Cooling Passage

This work is motivated by the need to accurately predict heat transfer in turbomachinery. For efficient gas turbine operation, flow temperatures in the hot gas path exceed acceptable metal temperatures in many regions of the engine. So that the integrity of the parts can be maintained for an acceptable engine life, the parts must be cooled. Efficient cooling schemes require accurate heat transfer prediction to minimize regions that are overcooled and, even more importantly, to ensure adequate cooling in high-heat-flux regions.

A numerical study validated the predictive capabilities of the Glenn-HT code in complex turbine blade cooling passages. Simulation results were compared with experimental data made available by the General Electric Global Research Center. The geometry consists of a two-pass serpentine passage that tapers toward the trailing edge, as well as from the hub to the tip (see the following sketch). The upflow channel has an average aspect ratio of roughly 14:1, whereas the exit passage aspect ratio is about 5:1. The upflow channel is split in an interrupted way and is smooth on the trailing edge side of the split and turbulated on the other side. A turning vane is placed near the tip of the upflow channel. Reynolds numbers ranging from 31 000 to 61 000, based on inlet conditions, were simulated numerically.

The simulation was performed at the NASA Glenn Research Center using the Glenn-HT code. The Glenn-HT code is a full three-dimensional Navier-Stokes solver using the Wilcox k-ω turbulence model. It has evolved over the years into a highly accurate, robust research tool with over 40 papers published relative to the code and its application. A structured multiblock grid is used with approximately 4.5 million cells. Pressure and heat transfer distributions compare well between the simulation and the experimental data. Although there are some regions with discrepancies, in general the agreement is very good for both pressure and heat transfer.

The figure on the next page compares the heat transfer predicted by Glenn-HT with the experimental results. Qualitatively, the comparison is very good. High heat transfer is observed between the turbulators, as expected. In addition, the low streak emanating from the tip of the split between passages 1A and 1B is closely matched. Very high values after the final rib in passage 1B, as well as the low region around the tip of the split between passages 1B and 2, are visible in both the experiment and simulation.

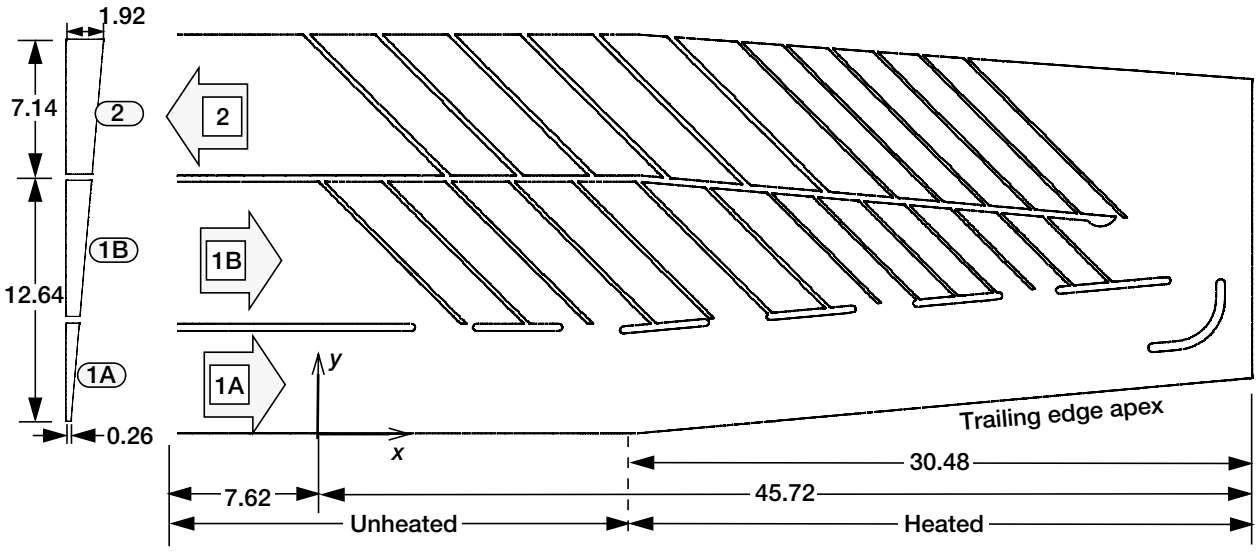

Schematic of geometry showing flat lower surface and inlet cross section. All dimensions are given in centimeters.

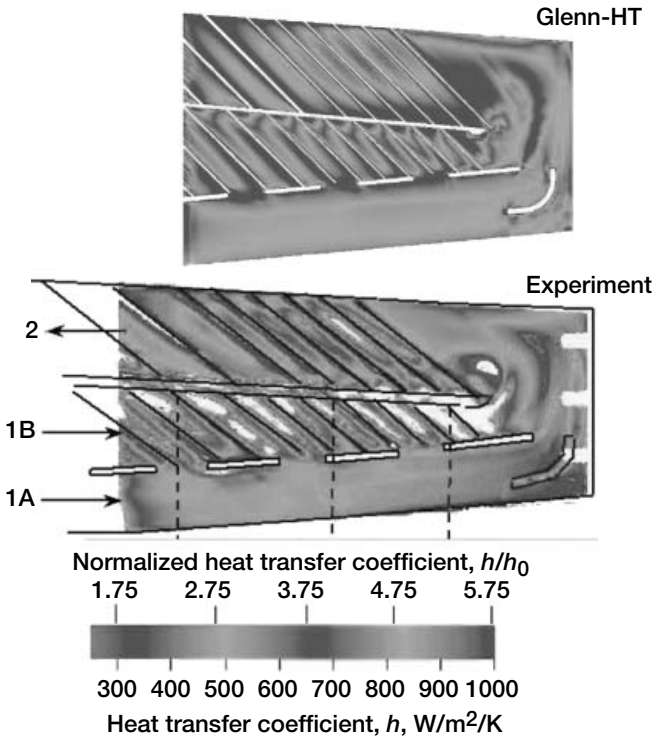

Heat transfer coefficient on flat lower surface; comparison between the Glenn-HT simulation and the experimental results. This figure is shown in color in the online version of this article (http://www.grc.nasa.gov/WWW/RT2002/5000/5820rigby.html).

Find out more about the research of Glenn's Turbine Branch:
http://www.grc.nasa.gov/WWW/TURBINE/Turbine.htm

References

1. Bunker, Ronald S., et al.: Heat Transfer in a Complex Trailing Edge Passage for a High Pressure Turbine Blade. ASME Paper GT–2002–30212–Pt–1, 2002.
2. Rigby, David L.; and Bunker, Ronald S.: Heat Transfer in a Complex Trailing Edge Passage for a High Pressure Turbine Blade. Part 2: Simulation Results, NASA/CR—2002-211701, 2002. http://gltrs.grc.nasa.gov/cgi-bin/GLTRS/browse.pl?2002/CR-2002-211701.html

QSS contact:
Dr. David L. Rigby, 216–433–5965, David.L.Rigby@grc.nasa.gov

Glenn contact:
Dr. Raymond E. Gaugler, 216–433–5882, Raymond.E.Gaugler@nasa.gov

Author: Dr. David L. Rigby

Headquarters program office: OAT

Programs/Projects:
Propulsion Systems R&T, UEET

National Combustion Code Validated Against Lean Direct Injection Flow-Field Data

Most combustion processes have, in some way or another, a recirculating flow field. This recirculation stabilizes the reaction zone, or flame, but an unnecessarily large recirculation zone can result in high nitrogen oxide (NO_x) values for combustion systems. The size of this recirculation zone is crucial to the performance of state-of-the-art, low-emissions hardware. If this is a large-scale combustion process, the flow field will probably be turbulent and, therefore, three-dimensional. This research dealt primarily with flow fields resulting from lean direct injection (LDI) concepts, as described in Research & Technology 2001 (ref. 1). LDI is a concept that depends heavily on the design of the swirler. The LDI concept has the potential to reduce NO_x values from 50 to 70 percent of current values, with good flame stability characteristics. It is cost effective and (hopefully) beneficial to do most of the design work for an LDI swirler using computer-aided design (CAD) and computer-aided engineering (CAE) tools. Computational fluid dynamics (CFD) codes are CAE tools that can calculate three-dimensional flows in complex geometries. However, CFD codes are only beginning to correctly calculate the flow fields for complex devices, and the related combustion models usually remove a large portion of the flow physics.

The National Combustion Code (NCC) is a state-of-the-art CFD program designed specifically for combustion processes. The features of NCC pertaining to this study are (1) the use of unstructured grids (ref. 2), (2) massively parallel computing—with almost perfectly linear scalability (ref. 3), (3) a dynamic wall function with the effect of an adverse pressure gradient (ref. 4), (4) low-Reynolds-number wall treatment (ref. 5), and (5) a cubic nonlinear k-ε turbulence model (refs. 6 and 7). The combination of these features is usually not available in other CFD codes and gives the NCC an advantage when computing recirculating turbulent flows.

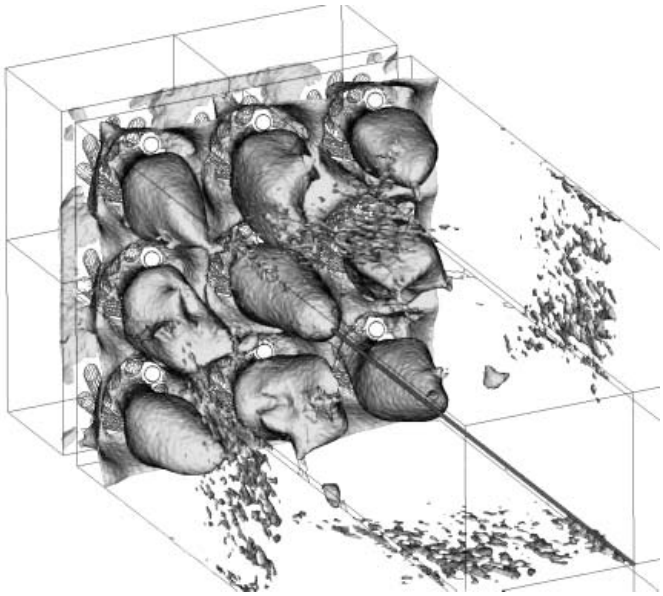

NCC computations of the 35° co-rotating swirler. Pressure drop, 4 percent; atmospheric pressure; cubic, nonlinear k-ε turbulence model; low-Reynolds-number wall treatment.

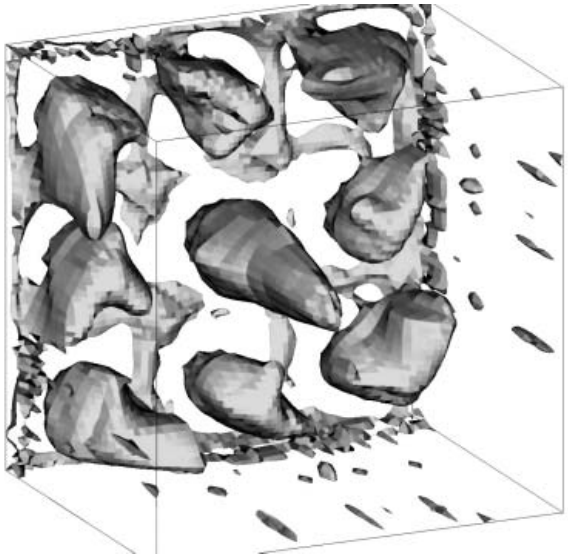

Laser Doppler velocimetry measurements of the 35° LDI swirler. Static pressure drop, 4 percent; atmospheric pressure.

These features need to be validated before the NCC is accepted as a design tool. The NCC was previously benchmarked for simple flows (ref. 8), and large-scale validations are being conducted (ref. 9).

The purpose of this study was to quantify how well the NCC calculates a turbulent, three-dimensional, recirculating flow field. The comparison was against three-dimensional laser Doppler velocimetry (LDV) measurements on a prototype LDI swirler (ref. 10). This configuration used nine groups of eight holes drilled at a 35° angle to induce swirl. These nine groups created swirl in the same direction, or a co-rotating pattern. The static pressure drop across the holes was fixed at approximately 4 percent. Computations were performed on one-quarter of the geometry, because the geometry is considered rotationally periodic every 90°. The final computational grid used was approximately 2.26 million tetrahedral cells, and a cubic nonlinear k-ε model was used to model turbulence. The NCC results were then compared with time-averaged LDV data. The LDV measurements were performed on the full geometry, but four-ninths of the geometry was measured. One-, two-, and three-dimensional representations of both flow fields are presented. The NCC computations compare both qualitatively and quantitatively well with the LDV data, but differences exist downstream. The comparison is encouraging and shows that NCC can be used for future injector design studies.

Find out more about the research of the Combustion Branch:
http://www.grc.nasa.gov/WWW/combustion/

References

1. Tacina, Robert R., et al.: Sector Tests of a Low-No_x, Lean, Direct-Injection, Multipoint Integrated Module Combustor Concept Conducted. Research & Technology 2001, NASA/TM—2002-211333, 2002, p. 116. http://www.grc.nasa.gov/WWW/RT2001/5000/5830tacina.html
2. Stubbs, Robert M.; and Liu, Nan-Suey: Preview of the National Combustion Code. AIAA Paper 97–3114, 1997.
3. Quealy, A., et al.: National Combustion Code: Parallel Implementation and Performance. NASA/TM—2000-209801 (AIAA Paper 2000–0336), 2000. http://gltrs.grc.nasa.gov/cgi-bin/GLTRS/browse.pl?2000/TM-2000-209801.html
4. Shih, Tsan-Hsing, et al.: Generalized Wall Function for Complex Turbulent Flows. NASA/TM—2000-209936, 2000. http://gltrs.grc.nasa.gov/cgi-bin/GLTRS/browse.pl?2000/TM-2000-209936.html

5. Chien, Kuei-Yuan: Predictions of Channel and Boundary-Layer Flows with a Low-Reynolds-Number Turbulence Model. AIAA J., vol. 20, no. 1, 1982, pp. 33–38.
6. Shih, Tsan-Hsing, et al.: Modeling of Turbulent Swirling Flows. NASA TM–113112, 1997.
7. Shih, Tsan-Hsing; Liu, Nan-Suey; and Chen, Kuo-Huey: A Non-Linear k-Epsilon Model for Turbulent Shear Flows. AIAA Paper 98–3983, 1998.
8. Chen, K.-H, et al.: Benchmark Test Cases for the National Combustion Code. AIAA 98–3855, 1998.
9. Iannetti, Anthony C.; and Chen, Kuo-Huey: Initial Comparison of National Combustion Code Simulations to Experimental Gas Turbine Combustor Data Using Various Chemistry Modules. AIAA–2000–0330, 2000.
10. Iannetti, Anthony C., et al.: Towards Accurate Prediction of Turbulent, Three-Dimensional, Recirculating Flows With the NCC. AIAA Paper 2001–0809, 2001.

Glenn contact:
Anthony C. Iannetti, 216–433–5586, Anthony.C.Iannetti@nasa.gov

Author: Anthony C. Iannetti

Headquarters program office: OAT

Programs/Projects: Propulsion and Power, SEC, UEET, HPCCP

Special recognition: This research was part of the 2001 Turning Goals Into Reality award (TGIR) for Emissions Reduction.

High-Pressure Gaseous Burner (HPGB) Facility Became Operational

A gas-fueled high-pressure combustion facility with optical access, developed over the last 3 years, is now collecting research data in a production mode. The High-Pressure Gaseous Burner (HPGB) rig at the NASA Glenn Research Center can operate at sustained pressures up to 60 atm with a variety of gaseous fuels and liquid jet fuel. The facility is unique because it is the only continuous-flow, hydrogen-capable 60-atm rig in the world with optical access. It will provide researchers with new insights into flame conditions that simulate the environment inside the ultra-high-pressure-ratio combustion chambers of tomorrow's advanced aircraft engines. The facility provides optical access to the flame zone through four fused-silica optical windows, enabling the calibration of nonintrusive optical diagnostics to measure chemical species and temperature. The data from the HPGB rig enable the validation of numerical codes that simulate gas turbine combustors.

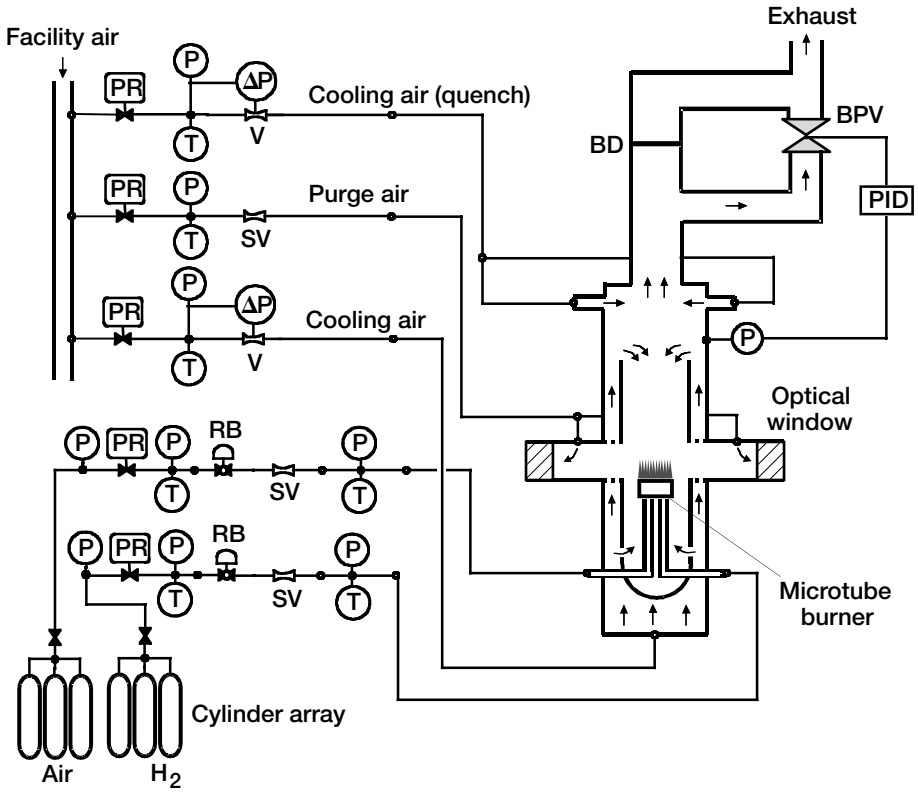

High-pressure gaseous burner rig and gas flow system. P, pressure transducer; T, thermocouple; PR, remotely operated regulator; RB, remotely operated ball valve; V, venturi; SV, sonic venturi; BPV, back-pressure valve; PID, process controller; BD, burst disk.

This schematic shows the high-pressure burner rig and gas flow system. For pressures up to 30 atm, ambient-temperature air from the facility 450-psi compressor provides the 30-atm cooling air. For pressures above 30 atm, the cooling air is provided by a compressed-air tank array mounted on a trailer. The cooling air is introduced at the bottom of the rig for liner cooling (0.25 lbm/s maximum) and is introduced at the upper side as "quenching" airflow (0.20 lbm/s maximum). These airflows are controlled by remotely operated regulators using calibrated venturi flowmeters.

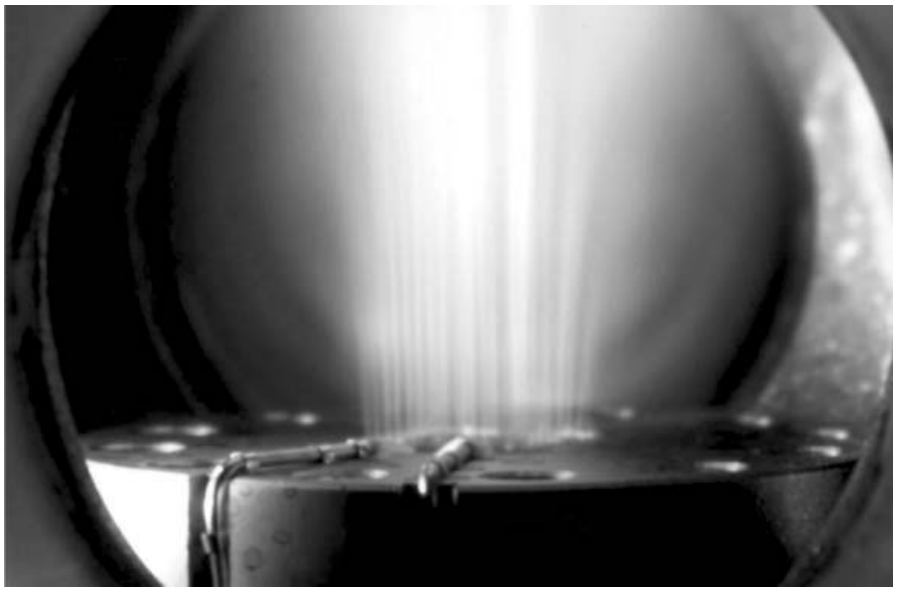

Photograph of a 20-atm hydrogen-air flame produced by the microtube burner in the HPGB facility operating at an equivalence ratio of 1.4. The diameter of the burner active region is approximately 0.75 in.

Approximately 10 percent or less of the total cooling flow rate of the facility air is used as purge flow for the optical windows during experiments to prevent water vapor condensation on the interior surfaces of the windows. The rig chamber pressure is regulated via a remotely controlled back-pressure valve mounted at the top of the chamber. A feedback-controlled process controller system stabilizes the chamber pressure to better than 1-percent accuracy for any given set point. For optical access, the burner rig has four ultraviolet-grade fused-silica windows with 44-mm-thick by 85-mm clear apertures located around the periphery of the flame zone. A burst disk (set at 935 psig) placed between the pressure chamber and facility exhaust pipe prevents overpressure conditions.

The specially designed microtube array burner is mounted inside the air-cooled high-temperature liner casing within the rig. The photograph shows the flame produced by the microtube burner at a pressure of 20 atm and an equivalence ratio of 1.4. The burner was designed to provide a uniform combustion product zone downstream of the flame for calibrating the laser Raman diagnostic system. The oxidizer air and the hydrogen fuel are provided by 12-pack cylinder arrays at a nominal pressure of 150 atm. The flow rates of the air and fuel can be precisely controlled with better than 0.5-percent accuracy using sonic venturi flowmeters in conjunction with computer-operated pressure regulators and valves. The flows can be adjusted to vary the flame's equivalence ratio ϕ from about 0.3 (very fuel-lean) to 4 (fuel-rich), providing a wide span of combustion products in the flame zone for optical diagnostics calibration. The maximum fuel flow rate is limited by the cooling capacity of the facility (400 000 Btu/hr). For the current series of experiments, only hydrogen-air mixtures are required; however, the facility is designed to accommodate different fuels and oxidizers including carbon monoxide, methane, oxygen-argon, and pure oxygen. All aspects of the facility operation, including startup, shutdown, and automatic safety shutdowns are controlled and monitored via an icon-based touch-screen software system and a programmable logic controller in conjunction with a cost-effective four-PC server cluster.

Glenn contacts:
Dr. Quang-Viet Nguyen, 216–433–3574, Quang-Viet.Nguyen-1@nasa.gov;
William K. Thompson, 216–433–2638, William.K.Thompson@nasa.gov,
Gary V. Lorenz, 216–433–5996, Gary.V.Lorenz@nasa.gov; and
Paulette E. Adams, 216–433–5237, Paulette.E.Adams@nasa.gov

National Research Council contact:
Dr. Jun Kojima, 440–962–3095, Jun.Kojima@grc.nasa.gov

QSS Group, Inc., contact:
Gregg Calhoun, 216–433–5782, Gregory.G.Calhoun@grc.nasa.gov

Akima Corp. contact:
Raymond C. Lotenero, 216–433–2849, Raymond.C.Lotenero@grc.nasa.gov

Author: Dr. Quang-Viet Nguyen

Headquarters program office: OAT

Programs/Projects: UEET, ZCET, SEC

Spontaneous Raman Scattering (SRS) System for Calibrating High-Pressure Flames Became Operational

A high-performance spontaneous Raman scattering (SRS) system for measuring quantitative species concentration and temperature in high-pressure flames is now operational. The system is located in Glenn's Engine Research Building. Raman scattering is perhaps the only optical diagnostic technique that permits the simultaneous (single-shot) measurement of all major species (N_2, O_2, CO_2, H_2O, CO, H_2, and CH_4) as well as temperature in combustion systems. The preliminary data acquired with this new system in a 20-atm hydrogen-air (H_2-air) flame show excellent spectral coverage, good resolution, and a signal-to-noise ratio high enough for the data to serve as a calibration standard. This new SRS diagnostic system is used in conjunction with the newly developed High-Pressure Gaseous Burner facility (ref. 1). The main purpose of this diagnostic system and the High-Pressure Gaseous Burner facility is to acquire and establish a comprehensive Raman-scattering spectral database calibration standard for the combustion diagnostic community. A secondary purpose of the system is to provide actual measurements in standardized flames to validate computational combustion models. The High-Pressure Gaseous Burner facility and its associated SRS system will provide researchers throughout the world with new insights into flame conditions that simulate the environment inside the ultra-high-pressure-ratio combustion chambers of tomorrow's advanced aircraft engines.

The schematic shows the SRS system, and the photograph on the next page shows the system in operation. The SRS system was designed in-house by Dr. Quang-Viet Nguyen of

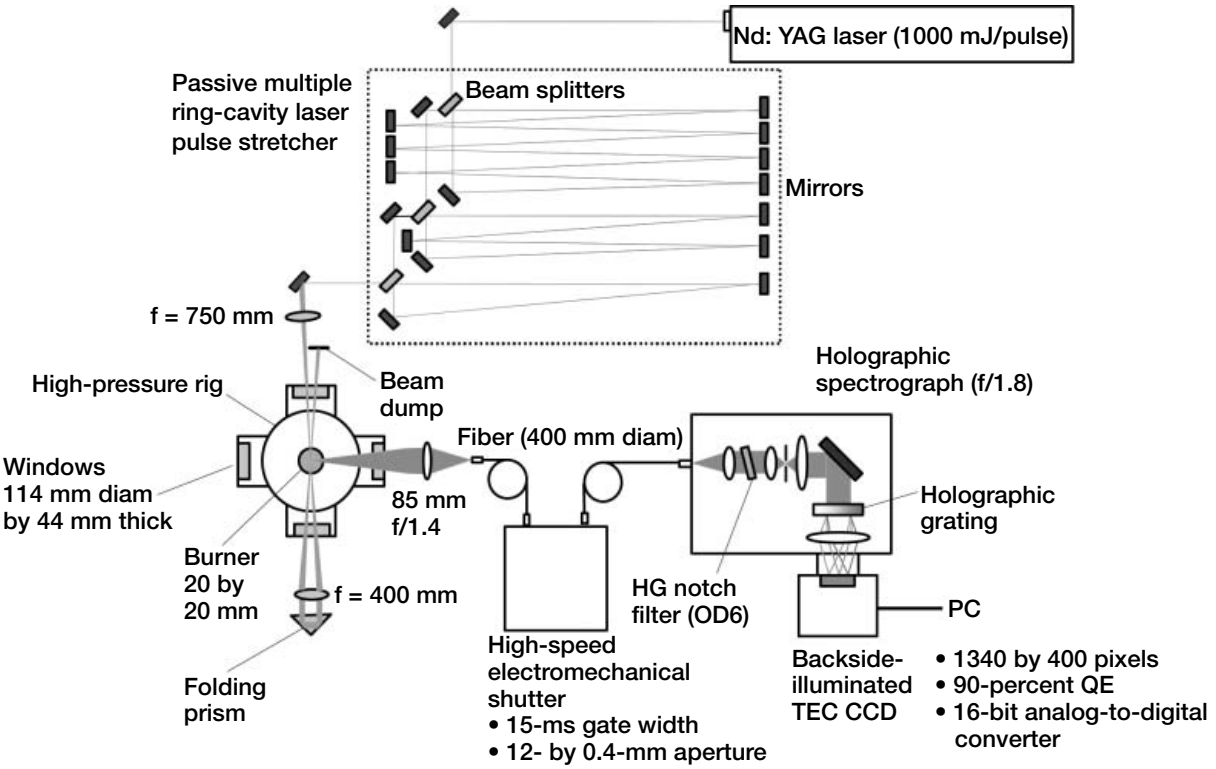

High-performance SRS system. The output of a frequency-doubled pulsed Nd:YAG (neodymium-doped yttrium aluminum garnet) laser (532 nm) is temporally stretched using a passive three-cavity optical delay line. The stretched laser output (1000 mJ over 80 ns) is then focused into the measurement zone inside the high-pressure rig. The Raman-scattered light (signal) is collected perpendicular to the excitation laser beam and fiber-optically coupled into a high-speed electromechanical shutter system to reject background luminosity. The output of the shutter system is fiber-optically coupled to a high-speed holographic spectrograph fitted with a thermoelectrically cooled backside-illuminated charge-couple device (CCD) camera. The CCD camera images are processed by computer to yield the Raman-scattering spectrum. The spatial resolution of the probe volume is approximately 1.4 by 0.5 mm. (HG, holographic grating; OD6, optical density 6 (provides a 6-order magnitude attenuation in optical intensity); TEC, thermoelectrically cooled; QE, quantum efficiency (efficiency of detecting a single photon).)

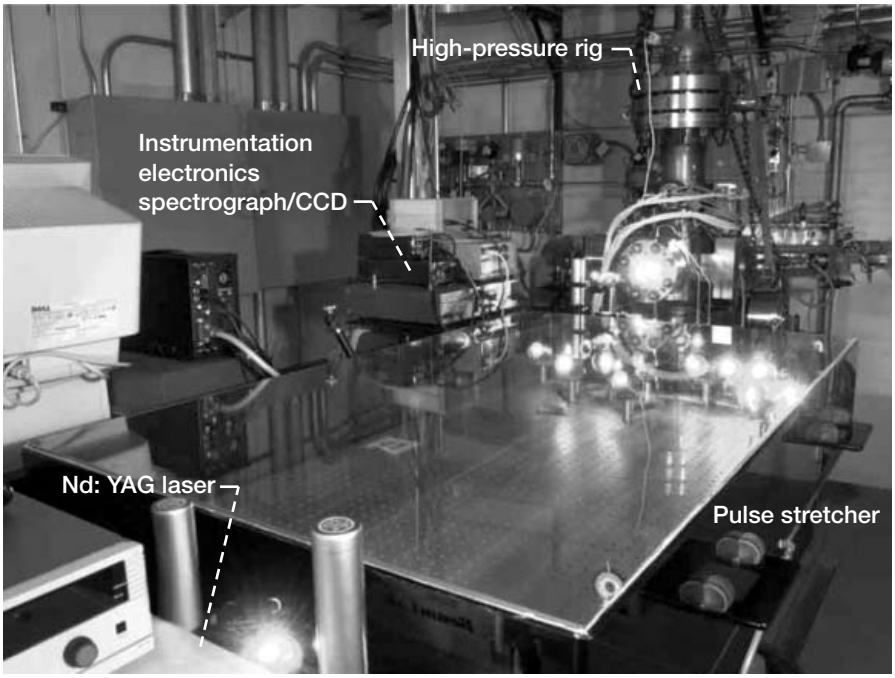

Photograph of the SRS diagnostic system in the High-Pressure Gaseous Burner facility. The bright green light scattered from the pulse stretcher mirrors is the 532-nm wavelength excitation laser light. This figure is shown in color in the online version of this article (http://www.grc.nasa.gov/WWW/RT2002/5000/5830nguyen2.html).

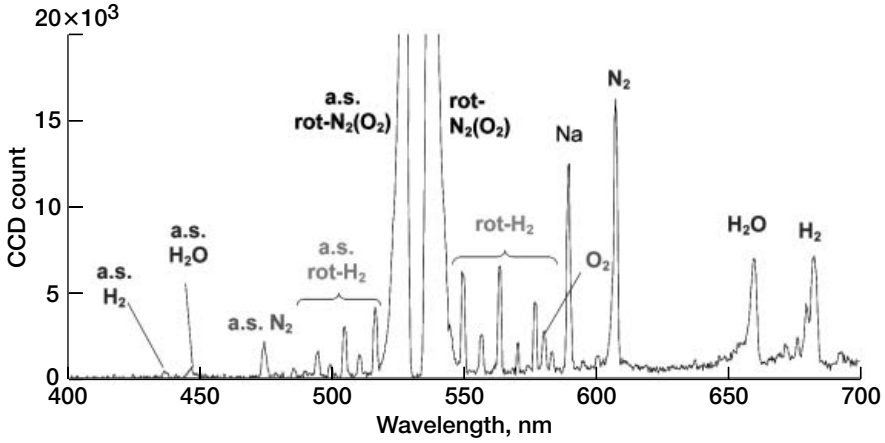

SRS spectrum of a H_2-air flame at a rig pressure of 20 atm and an equivalence ratio of 1.4. The spectrum was averaged over 250 laser shots and collected at a low spectral resolution of 40 cm^{-1}. The entire visible spectrum from 400 to 700 nm can be captured in a single spectrum, enabling the simultaneous quantitative determination of species temperature and concentration (a.s., anti-Stokes; rot, rotational).

Glenn's Combustion Branch and built with the help of Dr. Jun Kojima (National Research Council Research Associate) and Raymond Lotenero (Akima Corp.). Many strategies and techniques are employed to maximize the weak Raman signal, including a high-pulse-energy (1000-mJ/pulse) laser, a pulse stretcher to avoid damaging the optical windows, a laser beam that is folded back through the probe volume to double the energy, high-speed optics and spectrograph to maximize collection efficiencies, and a custom-designed electromechanical shutter and backside-illuminated charge-coupled device (CCD) camera to achieve 90-percent quantum efficiency.

The following graph shows the SRS spectrum of a H_2-air flame at a rig pressure of 20 atm and an equivalence ratio of 1.4. The two large features centered at 532 nm are the pure-rotational Raman features of nitrogen (N_2) and some oxygen (O_2). The spectral features to the left of the excitation wavelength (532 nm) are the anti-Stokes-shifted Raman-scattering signals, whereas the features to the right are the Stokes-shifted Raman-scattering signals. Both the shape of the spectral features and the ratio of Stokes to anti-Stokes signals permit temperature measurement with about 50-K accuracy. The amplitudes of the peaks enable major species concentration determination with about 2 mol% accuracy. Correlating the measured Raman signal response with chemical equilibrium predictions based on measured reactant flow rates allows one to map out a quantitative calibration of the SRS signals versus interferences. This process is repeated for many different flame conditions, different flame reactants, and different pressures.

We have also developed a comprehensive theoretical Raman-scattering model for all the major species in hydrocarbon-air. As an example, the figure on the next page shows a theoretically calculated vibration-rotation Raman spectrum of H_2 compared with experimental data. The data were obtained at a spectral resolution of 10 cm^{-1} in a 20-atm H_2-air flame at an equivalence ratio of 1.4. The fitted temperature of 1890 K derived from the spectral shape is consistent with the temperature derived from both the pure-rotational spectrum of H_2 and the vibration-rotation spectrum of N_2.

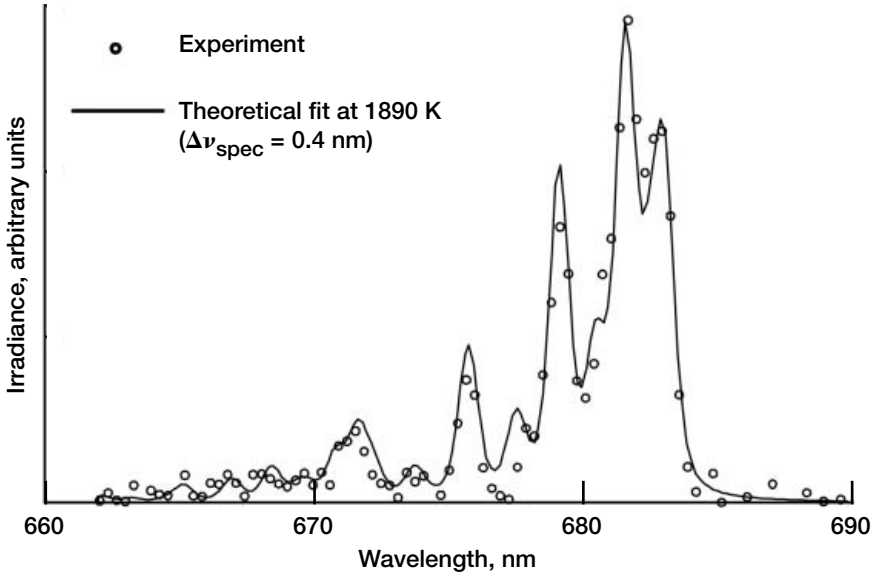

Comparison of a comprehensive theoretical model of Raman scattering that includes the effects of pressure broadening with the experimentally measured vibration-rotation Raman spectrum of H_2 at a pressure of 20 atm in a 20-atm H_2-air flame; $\Delta\nu_{spec}$, spectral resolution of the spectrograph.

Reference

1. Nguyen, Quang-Viet: High-Pressure Gaseous Burner (HPGB) Facility Became Operational. Research & Technology 2002, NASA/TM—2002-211990, 2003, pp. 116–117. http://www.grc.nasa.gov/WWW/RT2002/5000/5830nguyen1.html

Find out more about the research of Glenn's Combustion Branch:
http://www.grc.nasa.gov/WWW/combustion/

Glenn contact:
Dr. Quang-Viet Nguyen, 216–433–3574, Quang-Viet.Nguyen-1@nasa.gov

Author: Dr. Quang-Viet Nguyen

Headquarters program office: OAT

Programs/Projects: UEET, ZCET, SEC

Nanotechnology Investigated for Future Gelled and Metallized Gelled Fuels

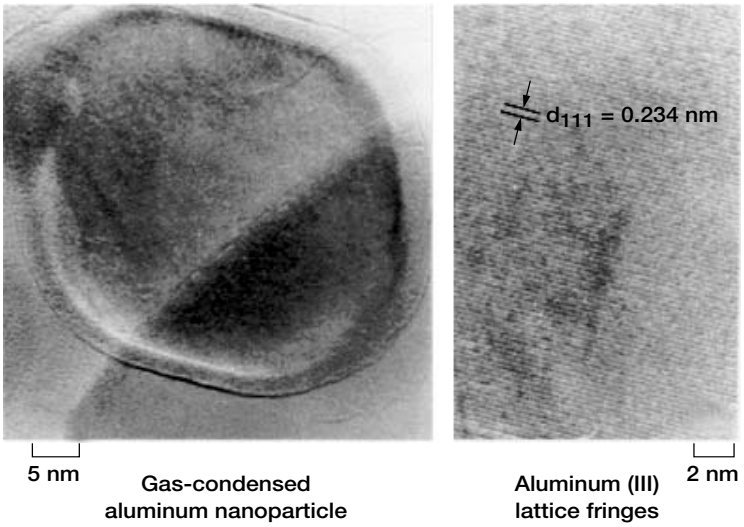

Typical aluminum nanoparticle created by Technanogy, Inc., with an aluminum vaporization process. The particles are from 20 to 100 nm in diameter. The interior aluminum is crystalline. No structural defects are apparent. There is a 2.5-nm-thick Al_2O_3 passivation layer. (Copyright Los Alamos National Laboratory; used with permission.)

The objective of this research is to create combustion data for gelled and metallized gelled fuels using unique nanometer-sized gellant particles and/or nanometer-sized aluminum particles. Researchers at the NASA Glenn Research Center are formulating the fuels for both gas turbine and pulsed detonation engines. We intend to demonstrate metallized gelled fuel ignition characteristics for pulse detonation engines with JP/aluminum fuel and for gas turbine engines with gelled JP, propane, and methane fuel.

The fuels to be created are revolutionary as they will deliver the highest theoretically maximum performance of gelled and metallized gelled fuels. Past combustion work has used micrometer-sized particles, which

Nanoparticle gellants produced by TRW. The gellant is similar to an aerogel, has a fluffy powder consistency, and has a surface area of 900 m^2/g. (Copyright TRW; used with permission.)

have limited the combustion performance of gelled and metallized gelled fuels. The new fuel used nanometer-sized aluminum oxide particles, which reduce the losses due to mismatch in the gas and solid phases in the exhaust. Gelled fuels provide higher density, added safety, reduced fuel slosh, reduced leakage, and increased exhaust velocity. Altogether, these benefits reduce the overall size and mass of the vehicle, increasing its flexibility.

Glenn obtained 75-lb of aluminum nanoparticles from Technanogy, Inc. (Irvine, CA) to create the new nanoengineered fuels. The photomicrograph on the preceding page shows a typical particle created in Technanogy's aluminum vaporization process. The particle is surrounded by a 2- to 3-nm-thick coating of aluminum oxide, which prevents it from immediately igniting in air. The particles have diameters ranging from 20 to 100 nm.

Nanoengineered gellants were created by TRW (Redondo, Beach, CA). These nanogellants are similar to aerogels, are created with a supercritical drying process, and have surface areas ranging from 800 to 1000 m^2/g. These ultra-high surface areas allow very little gellant to successfully gel the liquid fuel (less than 0.7 wt% for liquid hydrocarbons).

The most critical part of the fuel development is the proper selection of the amount of gellant and the weight percentage of the aluminum particles. Glenn will formulate the final fuel. Precise processing of the nanoengineered aluminum particles is a key to the project's success. Critical to the best formulation and processing of these new fuels is the development of a new cryogenic viscometer by Glenn and Sierra Lobo (Milan, OH). This viscometer will allow the intimate and complete mixing of the nanometer gellants, the nanoparticles of aluminum, and the liquid fuels. A NASA building is being converted for the safe processing of the nanogellants and aluminum nanoparticles and for the safe mixing of these components with the liquid fuels.

Find out more about Small Business Innovation Research of fuels and space propellants: http://sbir.grc.nasa.gov/launch/foctopsb.htm

References

1. Palaszewski, Bryan A.: Metallized Gelled Propellants: Historical and Future Developments. Invited Plenary Lecture, Presented at the 8th International Workshop on Combustion and Propulsion, Pozzuoli, Naples, Italy, sponsored by AIDAA, FiatAvio, Politecnico di Milano, and Unversita di Napoli "Federico II," June 16–21, 2002.
2. Palaszewski, B.: Hydrogen Power in Space Vehicles. Renewable Energy: Trends and Prospects, S.K. Majumdar, E.W. Miller, and A.I. Panah, eds., Pennsylvania Academy of Science, Easton, PA, July 2002, ISBN 0–945809–17–4.
3. Palaszewski, Bryan: Propellant Modification. 1999 McGraw-Hill Encyclopedia of Science and Technology, 8th Edition, Sybil P. Parker, ed., McGraw Hill, New York, NY, 1999. Abstract available online: http://www.accessscience.com/

Glenn contact:
Bryan Palaszewski, 216–977–7493,
Fax 216–433–5802,
Bryan.A.Palaszewski@nasa.gov

Author: Bryan A. Palaszewski

Headquarters program office: OAT

Programs/Projects: RAC

Solid Hydrogen Particles and Flow Rates Analyzed for Atomic Fuels

Researchers at the NASA Glenn Research Center improved their understanding of tiny particles of frozen hydrogen, an ice that exists at –452 °F (about 4 K, or 4 degrees above absolute zero). This research is directed toward improved very high specific impulse aerospace vehicles (refs. 1 to 4).

The experiments were conducted at Glenn's Small Multipurpose Research Facility (SMIRF, ref. 5). The experimental setup was placed in the facility's vacuum tank to prevent heat leaks and subsequent boiloff of the liquid helium. Supporting systems maintained the temperature and pressure of the liquid helium bath where the solid particles were created.

Solid hydrogen particle formation was tested from February 23 to April 2, 2001. Millimeter-sized solid-hydrogen particles were formed in a Dewar of liquid helium as a prelude to creating atomic fuels and propellants for aerospace vehicles. Atomic fuels or propellants are created when atomic boron, carbon, or hydrogen is stored in solid hydrogen particles. The current testing characterized the solid hydrogen particles without the atomic species, as a first step to creating a feed system for the atomic fuels and propellants. This testing did not create atomic species, but only sought to understand the solid hydrogen particle formation and behavior in the liquid helium.

In these tests, video images of the solid particle formation were recorded, and the total mass flow rate of the hydrogen was measured. The mass of hydrogen that went into the gaseous phase was also recorded using a commercially available residual gas analyzer. The temperatures, pressures, and flow rates of the liquids and gases in the test apparatus were recorded as well.

Testing conducted in 1999 recorded particles as small as 2 to 5 mm in diameter. The current testing extended the testing conditions to a very cold Dewar ullage gas of about 20 to 90 K above the 4 K liquid helium. With the very cold Dewar gas, the hydrogen freezing process took on new dimensions, in some cases creating particles so small that they seemed to be microscopic, appearing as infinitesimally small scintillations on the videotaped images.

With a warm ullage gas (170 to 250 K), the current testing also found that the efficiency of creating the solid hydrogen was about 66 to 69 percent. This means that up to 34 percent

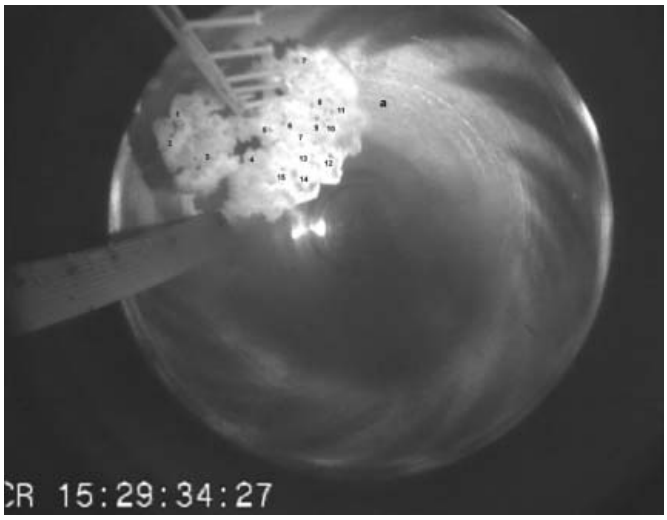

Photograph of solid hydrogen particles floating on the surface of a liquid helium bath. A large number of the frozen particles have clumped together.

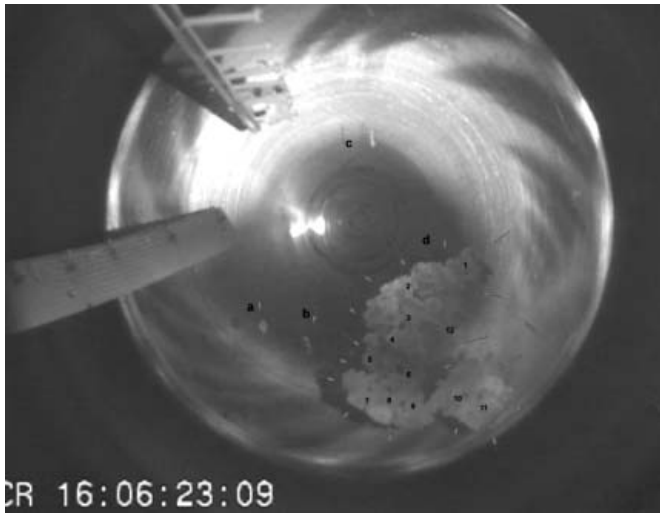

Photograph of the solid hydrogen particles with unique shapes for the clumped crystals. Some are shaped like long bars.

of the hydrogen entering the Dewar was lost, implying that although a large fraction of the hydrogen froze, about one-third was lost up the stack. This is based on analyses of 2 of the 11 days of data. The remaining experiments, conducted with a lower ullage gas temperature, may lead to higher efficiency solid-hydrogen production. Data from these remaining experiments are under continuing analysis.

Find out more about Small Business Innovation Research on fuels and space propellants: http://sbir.grc.nasa.gov/launch/foctopsb.htm

References

1. Palaszewski, B.: Solid Hydrogen Experiments for Atomic Propellants: Particle Formation Energy and Imaging Analyses. AIAA Paper 2002–4092, 2002.
2. Palaszewski, Bryan: Solid Hydrogen Experiments for Atomic Propellants—Image Analyses. AIAA Paper 2001–3233, 2001.
3. Palaszewski, Bryan: Solid Hydrogen Experiments for Atomic Propellants. AIAA–2000–3855, 2000.
4. Palaszewski, Bryan: Launch Vehicle Performance for Bipropellant Propulsion Using Atomic Propellants With Oxygen. AIAA Paper 99–2837, 1999.
5. Dempsey, P.J.; and Stochl, R.J.: Supplemental Multilayer Insulation Research Facility. NASA TM–106991, 1995.

Glenn contact:
Bryan Palaszewski, 216–977–7493,
Fax 216–433–5802,
Bryan.A.Palaszewski@nasa.gov

Author: Bryan A. Palaszewski

Headquarters program office: OAT

Programs/Projects:
ASTP, STR, supported by MSFC

Low NO_x, Lean Direct Wall Injection Combustor Concept Developed

The low-emissions combustor development at the NASA Glenn Research Center is directed toward advanced high-pressure aircraft gas turbine applications. The emphasis of this research is to reduce nitrogen oxides (NO_x) at high-power conditions and to maintain carbon monoxide and unburned hydrocarbons at their current low levels at low-power conditions. Low-NO_x combustors can be classified into rich burn and lean burn concepts. Lean burn combustors can be further classified into lean-premixed-prevaporized (LPP) and lean direct injection (LDI) combustors. In both concepts, all the combustor air, except for liner cooling flow, enters through the combustor dome so that the combustion occurs at the lowest possible flame temperature. The LPP concept has been shown to have the lowest NO_x emissions, but for advanced high-pressure-ratio engines, the possibly of autoignition or flashback precludes its use. LDI differs from LPP in that the fuel is injected directly into the flame zone and, thus, does not have the potential for autoignition or flashback and should have greater stability. However, since it is not premixed and prevaporized, the key is good atomization and mixing of the fuel quickly and uniformly so that flame temperatures are low and NO_x formation levels are comparable to those of LPP.

Ultra-low-NO_x combustor concept that injects fuel from the wall of a venturi section (LDWI), counter to the air swirl. The air swirl is generated upstream of the Venturi section. Shown is a module for flame-tube testing with an enclosed pilot burner.

In this LDI concept, the air is swirled upstream of a venturi section and the

fuel is injected radially inward into the airstream from the venturi throat section using six plain-orifice injectors. Important aspects of this technique are (1) a liquid jet should be used (not a thin-film, hollow-cone spray typical of a conventional pressure-swirl atomizer), and (2) the jet should be injected radially inward from the mixer wall toward the approaching swirling airflow at an inclined angle with respect to the radial direction. The advantage of the lean direct wall injection (LDWI) concept is its use of a swirling airflow both for atomizing the injected liquid jets and for mixing the atomized sprays in a short period of time. In the case of coaxially injected sprays, the strong centripetal forces of swirling airflow tend to sustain the liquid droplets (or fuel vapor) inside the core recirculating zones, resulting in a relatively slow mixing process. In the LDWI mode, however, the swirling airflow abruptly breaks the liquid jet into small droplets and the droplets are mixed quickly, within 25-mm downstream of the injection point.

Flame-tube tests were conducted with inlet temperatures up to 810 K, inlet pressures up to 2760 kPa, and flame temperatures up to 2100 K. A correlation was developed relating the NO_x emissions to the inlet temperature, inlet pressure, fuel-to-air ratio, and pressure drop. If 15 percent of the combustion air would be used for liner cooling and an advanced engine cycle was used, for the best configuration, we estimate that the NO_x emissions using the correlation would be less than 75 percent of the 1996 International Civil Aviation Organization (ICAO) standard for emissions.

Glenn contact:
Robert R. Tacina, 216–433–3588,
Robert.R.Tacina@nasa.gov

Authors: Robert R. Tacina,
Changlie Wey, and Kyung J. Choi

Headquarters program office: OAT

Programs/Projects: SEC, UEET

Large-Eddy Simulation Code Developed for Propulsion Applications

A large-eddy simulation (LES) code was developed at the NASA Glenn Research Center to provide more accurate and detailed computational analyses of propulsion flow fields. The accuracy of current computational fluid dynamics (CFD) methods is limited primarily by their inability to properly account for the turbulent motion present in virtually all propulsion flows. Because the efficiency and performance of a propulsion system are highly dependent on the details of this turbulent motion, it is critical for CFD to accurately model it. The LES code promises to give new CFD simulations an advantage over older methods by directly computing the large turbulent eddies, to correctly predict their effect on a propulsion system.

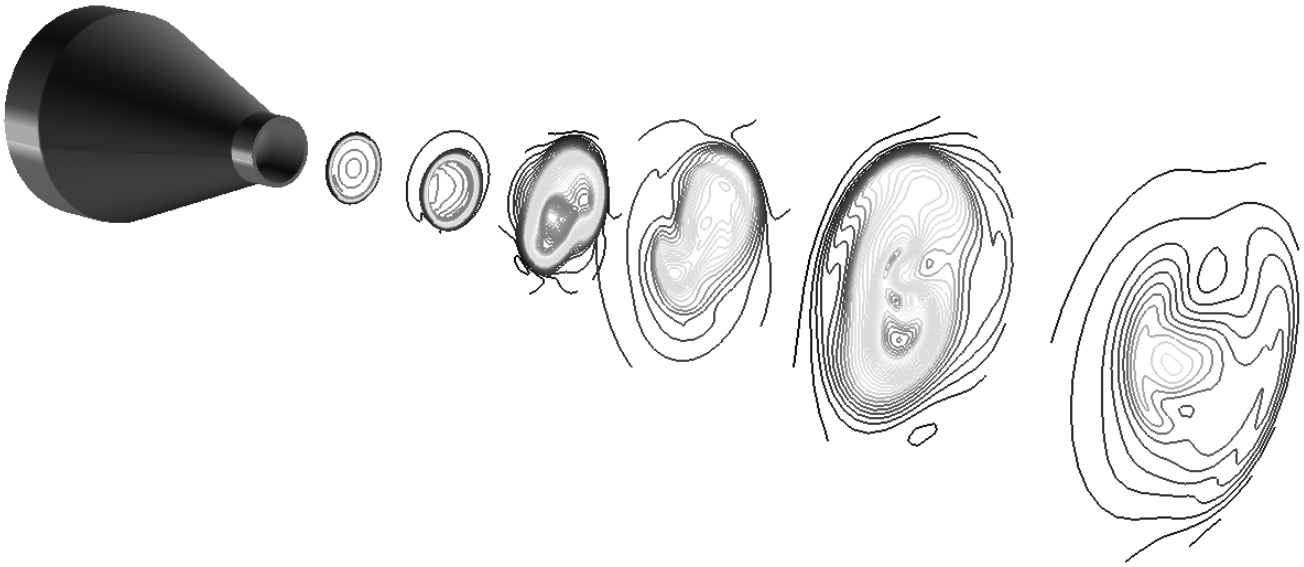

Cross-plane Mach number contours for a Mach 1.4 jet.

Turbulent motion is a random, unsteady process whose behavior is difficult to predict through computer simulations. Current methods are based on Reynolds-Averaged Navier-Stokes (RANS) analyses that rely on models to represent the effect of turbulence within a flow field. The quality of the results depends on the quality of the model and its applicability to the type of flow field being studied. LES promises to be more accurate because it drastically reduces the amount of modeling necessary. It is the logical step toward improving turbulent flow predictions. In LES, the large-scale dominant turbulent motion is computed directly, leaving only the less significant small turbulent scales to be modeled. As part of the prediction, the LES method generates detailed information on the turbulence itself, providing important information for other applications, such as aeroacoustics.

The LES code developed at Glenn for propulsion flow fields is being used to both analyze propulsion system components and test improved LES algorithms (subgrid-scale models, filters, and numerical schemes). The code solves the compressible Favre-filtered Navier-Stokes equations using an explicit fourth-order accurate numerical scheme, it incorporates a compressible form of Smagorinsky's model for the subgrid-scale turbulence, and it uses generalized curvilinear coordinates to allow analysis of a wide range of geometries. The code runs in parallel on shared memory multiprocessor computers and is written in Fortran 90 with dynamic memory allocation.

A sample result for a Mach-1.4 round jet is presented in the figure on the preceding page. Instantaneous Mach number contours in several cross-planes downstream of the nozzle exit are shown, illustrating how an LES captures the large unsteady three-dimensional turbulent structures present in the jet.

References

1. DeBonis, James R.; and Scott, James N.: Large-Eddy Simulation of a Turbulent Compressible Round Jet. AIAA J., vol. 40, no. 7, 2002, pp. 1346–1354.
2. DeBonis, James R.; and Scott, James N.: Study of the Error and Efficiency of Numerical Schemes for Computational Aeroacoustics. AIAA J., vol. 40, no. 2, 2002, pp. 227–234.
3. DeBonis, James R.: The Numerical Analysis of a Turbulent Compressible Jet. NASA/TM—2001-210716, 2001. http://gltrs.grc.nasa.gov/cgi-bin/GLTRS/browse.pl?2001/TM-2001-210716.html

Glenn contact:
Dr. James R. DeBonis, 216–433–6581, James.R.DeBonis@nasa.gov

Author: Dr. James R. DeBonis

Headquarters Program Office: OAT

Programs/Projects:
Vehicle Systems, Propulsion and Power

Sound Sources Identified in High-Speed Jets by Correlating Flow Density Fluctuations With Far-Field Noise

Noise sources in high-speed jets were identified by directly correlating flow density fluctuation (cause) to far-field sound pressure fluctuation (effect). The experimental study was performed in a nozzle facility at the NASA Glenn Research Center in support of NASA's initiative to reduce the noise emitted by commercial airplanes.

Previous efforts to use this correlation method have failed because the tools for measuring jet turbulence were intrusive. In the present experiment, a molecular Rayleigh-scattering technique was used that depended on laser light scattering by gas molecules in air. The technique allowed accurate measurement of air density fluctuations from different points in the plume. The study was conducted in shock-free, unheated jets of Mach numbers 0.95, 1.4, and 1.8. The turbulent motion, as evident from density fluctuation spectra was remarkably similar in all three jets, whereas the noise sources were significantly different. The correlation study was conducted by keeping a microphone at a fixed location (at the peak noise emission angle of 30° to the jet axis and 50 nozzle diameters away) while moving the laser probe volume from point to point in the flow. The following figure shows maps of the nondimensional coherence value measured at different Strouhal frequencies ([frequency + diameter]/jet speed) in the supersonic Mach 1.8 and subsonic Mach 0.95 jets. The higher the coherence, the stronger the source was.

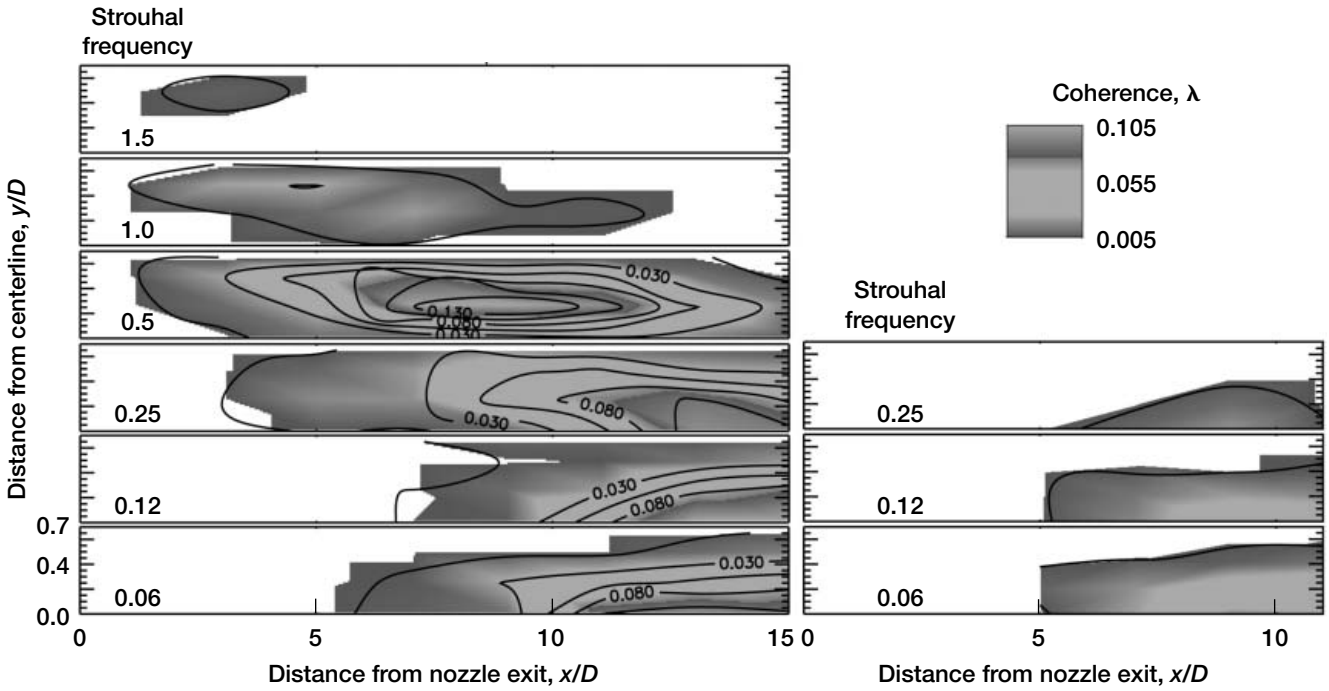

Source distribution for sound radiation at 30° to the jet axis and at the indicated Strouhal frequencies. The plotted variable is the coherence between the flow density fluctuations and the sound pressure fluctuations at the microphone location. Left: Mach 1.8 plume. Right: Mach 0.95 plume. This figure is shown in color in the online version of this article (http://www.grc.nasa.gov/WWW/RT2002/5000/5860panda.html).

The figure shows that density fluctuations from the end of the potential core (x/D = 7 and 10 for the Mach 0.95 and 1.8 jets, respectively) is the strongest source in both jets. The higher frequency noise is emitted close to the nozzle exit in the Mach 1.8 jet. This high-frequency source, however, cannot be detected in the subsonic Mach 0.95 jet. The differences in sound sources are due to the supersonic convective speed of turbulent eddies (compared with the ambient sound speed) in the Mach 1.8 jet and subsonic speed in the Mach 0.95 jet.

Reference

1. Panda, J.; and Seasholtz, R.G.: Experimental Investigation of Density Fluctuations in High-Speed Jets and Correlation With Generated Noise. J. Fluid Mech., vol. 450, 2002, pp. 97–130.

Ohio Aerospace Institute (OAI) contact:
Dr. Jayanta Panda, 216–433–8891, Jayanta.Panda@grc.nasa.gov

Glenn contact:
Dr. Richard G. Seasholtz, 216–433–3754, Richard.G.Seasholtz@nasa.gov

Authors: Dr. Jayanta Panda and Dr. Richard G. Seasholtz

Headquarters program office: OAT

Programs/Projects: QAT, SPT, SRF

Special recognition:
Best paper award, AIAA Northern Ohio Section, 2002.

Air-Breathing Launch Vehicle Technology Being Developed

Of the technical factors that would contribute to lowering the cost of space access, reusability has high potential. The primary objective of the GTX program (ref. 1) is to determine whether or not air-breathing propulsion can enable reusable single-stage-to-orbit (SSTO) operations. The approach is based on maturation of a reference vehicle design with focus on the integration and flight-weight construction of its air-breathing rocket-based combined-cycle (RBCC) propulsion system.

The following graph shows the effect of the equivalent, effective specific impulse I^*, a system-level efficiency parameter, on the dry weight fraction required for SSTO. Three classes of SSTO systems are shown. SSTO rockets such as the VentureStar (ref. 2) concept are limited to the lower I^* range and rely on advancements in structural and material technologies that were to be provided by NASA's recently terminated X–33 (ref. 3) program. Increasing I^* appears to make SSTO vehicles more practical by increasing the allowable dry weight fraction. However, the weight of the air-breathing propulsion system, the effects of atmospheric flight on the configuration, and any added complexity must be considered before a benefit can be claimed. An upper limit to I^* is represented by the "high-performance" air-breathers, of which the National Aerospace Plane (ref. 4) is a good example. High-specific-impulse low-speed systems and acceleration to high scramjet Mach numbers result in a dry weight budget of 30 wt%. These configurations are biased more toward aeropropulsion than structural efficiency, however, and they grow to an impractical scale at closure, especially if existing runways must be used. The optimum I^* for a reusable SSTO vehicle may be between these two extremes. The vertically launched GTX reference vehicle, shown in the figure on the next page, represents this "middle-class"

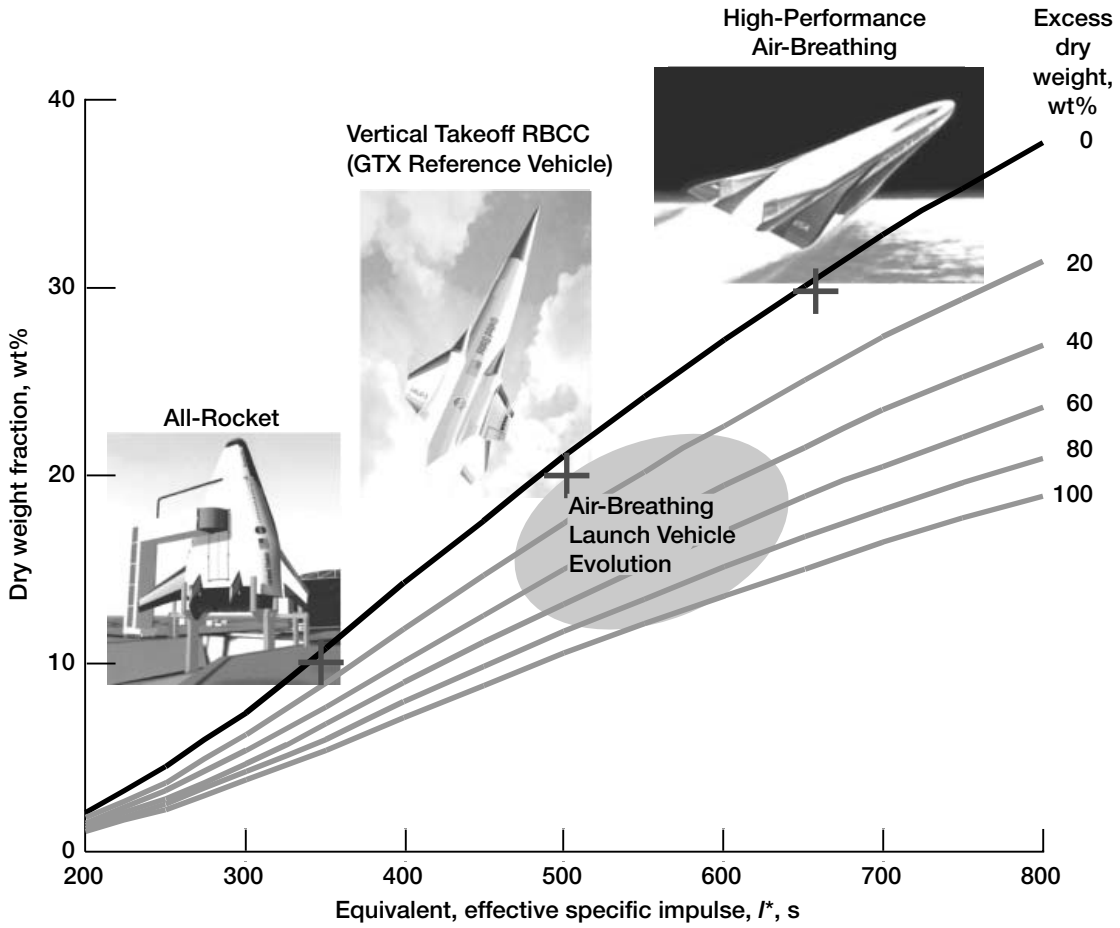

Effect of aeropropulsion efficiency on the SSTO dry weight fraction for a 220-nmi flight from a 28.5° easterly launch into a circular orbit (RBCC, rocket-based combined cycle).

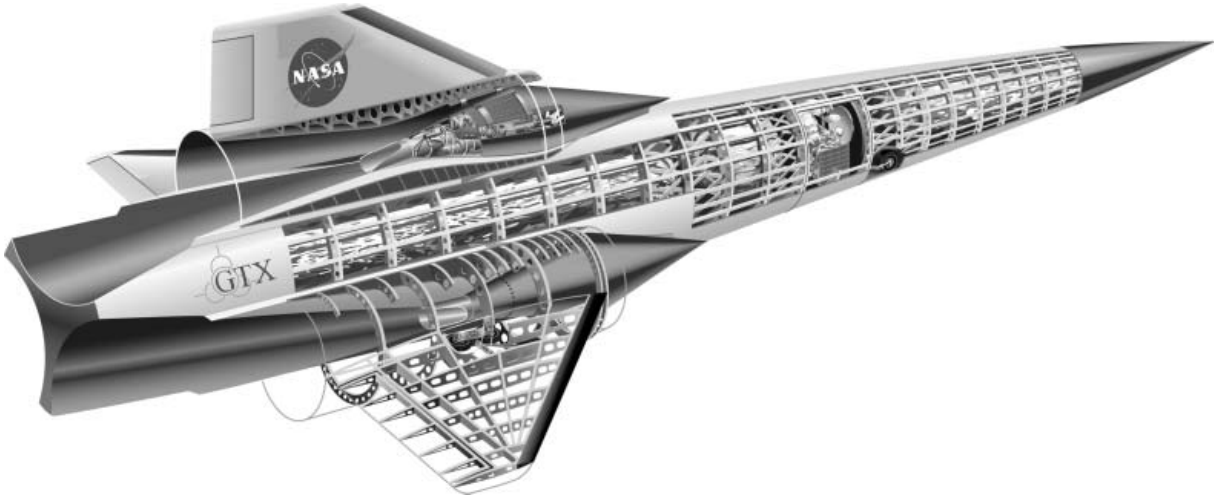

GTX reference vehicle.

*I** range, achievable with a relatively simple combined-cycle propulsion system with rocketlike performance at low speed, a moderate maximum air-breathing Mach number, and a structurally efficient configuration. The GTX program will determine whether or not this approach will result in a reusable SSTO vehicle at a practical scale. Increased excess dry weight resulting from future improvements could be used to increase payload, reduce vehicle size, and increase reliability.

Validation of system performance will ultimately require the construction and operation of a series of demonstration vehicles (ref. 5). To this end, researchers at the NASA Glenn Research Center have identified a comprehensive suite of propulsion component and system test rigs for developing and validating the design. Reference 1 provides an overview and the status of each test rig. Notable accomplishments in fiscal year 2002 include (1) the completion of inlet testing in Glenn's 1- by 1-Foot Supersonic Wind Tunnel and (2) the first phase of direct-connect flow path testing in Glenn's Engine Components Research Laboratory. In addition, finite-element modeling and optimization of the propulsion system and vehicle were also completed in fiscal year 2002 (ref. 6). Research on the lightweight, regeneratively cooled panels required for constructing the air-breathing flow path was initiated (ref. 7). Computational fluid dynamics (CFD) has been used extensively throughout the program for aerodynamic design, pretest prediction, and extrapolation of test results to reference vehicle scale and flight conditions. Recent work includes three-dimensional calculations of the various fuel injection and mixing processes resident in the multimode flow path (ref. 8).

References

1. Trefny, Charles J.; and Roche, Joseph M.: Performance Validation Approach for the GTX Air-Breathing Launch Vehicle. NASA/TM—2002-211495, 2002. http://gltrs.grc.nasa.gov/cgi-bin/GLTRS/browse.pl?2002/TM-2002-211495.html
2. Baumgartner, Robert I.: VentureStar Single Stage To Orbit Reusable Launch Vehicle Program Overview. Proceedings of the Space Technology and Applications International Forum and Second Conference on Next Generation Launch Systems, Albuquerque, NM, 1997.
3. Cook, Stephen A.: The Reusable Launch Vehicle Technology Program and the X–33 Advanced Technology Demonstrator. NASA TM–111868, 1995.
4. Sypniewski, Carl J.: The NASP Challenge—Technical Breakthrough. AIAA Paper 89–5017, 1989.
5. Krivanek, T.M., et al.: Affordable Flight Demonstration of the GTX Air-Breathing SSTO Vehicle Concept. Proceedings of the 26th JANNAF Airbreathing Propulsion Subcommittee Meeting, CPIA–PUB–713–VOL–1, 2002. Available from Chemical Propulsion Information Agency (CPIA).
6. Hunter, J.E.; McCurdy, D.R.; and Dunn, P.W.: GTX Reference Vehicle Structural Validation Methods and Weight Summary. Proceedings of the 26th JANNAF Airbreathing Propulsion Subcommittee Meeting, CPIA–PUB–713–VOL–1, 2002. Available from Chemical Propulsion Information Agency (CPIA).
7. Warburton, B.; and Jaskowiak, M.: GTX Heat-Exchanger Technology Verification. Proceedings of the 26th JANNAF Airbreathing Propulsion Subcommittee Meeting, CPIA–PUB–713–VOL–1, 2002. Available from Chemical Propulsion Information Agency (CPIA).
8. Steffen, C.J., Jr.; and Bond, R.B.; and Edwards, J.R.: Three Dimensional CFD Analysis of the GTX Combustor. NASA/TM—2002-211572, 2002. http://gltrs.grc.nasa.gov/cgi-bin/GLTRS/browse.pl?2002/TM-2002-211572.html

Glenn contact:
Dr. Charles J. Trefny, 216–433–2162, Charles.J.Trefny@nasa.gov

Author: Dr. Charles J. Trefny

Headquarters program office: OAT

Programs/Projects: Propulsion and Power, Propulsion Systems R&T, ASTP

Structures and Acoustics

High-Fidelity Micromechanics Model Enhanced for Multiphase Particulate Materials

This 3-year effort involves the development of a comprehensive micromechanics model and a related computer code, capable of accurately estimating both the average response and the local stress and strain fields in the individual phases, assuming both elastic and inelastic behavior. During the first year (fiscal year 2001) of the investigation, a version of the model called the High-Fidelity Generalized Method of Cells (HFGMC) was successfully completed for the thermoinelastic response of continuously reinforced multiphased materials with arbitrary periodic microstructures (refs. 1 and 2). The model's excellent predictive capability for both the macroscopic response and the microlevel stress and strain fields was demonstrated through comparison with exact analytical and finite-element solutions. This year, HFGMC was further extended in two technologically significant ways. The first enhancement entailed the incorporation of fiber/matrix debonding capability into the two-dimensional version of HFGMC for modeling the response of unidirectionally reinforced composites such as titanium matrix composites, which exhibit poor fiber/matrix bond. Comparison with experimental data validated the model's predictive capability. The second enhancement entailed further generalization of HFGMC to three dimensions to enable modeling the response of particulate-reinforced (discontinuous) composites in the elastic material behavior domain. Next year, the three-dimensional version will be generalized to encompass inelastic effects due to plasticity, viscoplasticity, and damage, as well as coupled electromagnetothermomechanical (including piezoelectric) effects.

The predictive capability of the elastic, three-dimensional version of HFGMC is illustrated in the graphs, where the average shear modulus of a dispersion of spherical particles embedded in a matrix is compared with the predictions of the original GMC model (ref. 3) and the three-phase model (ref. 4). Two extreme shear modulus ratios of spherical particles and surrounding matrix were chosen to provide a high contrast and, thus, a demanding test of the model's predictive capability. In the left graph, the effective shear modulus was determined as a function of the inclusion volume fraction for the case when the inclusion phase is 20 times stiffer than the matrix phase. The right graph shows a case that simulates a matrix with spherical pores whose shear stiffness is 0.005 that of the matrix. The superior predictive capability of HFGMC relative to GMC is a direct result of HFGMC's better local displacement field representation, which produces the so-called shear coupling effects indispensable in accurately capturing locally discontinuous phenomena such as damage, debonding, and material porosity.

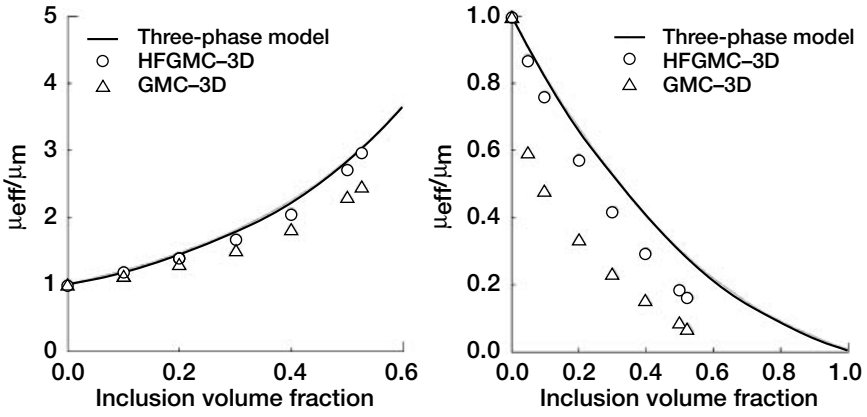

Effective shear moduli as a function of the inclusion volume fraction for a dispersion of spherical particles in a matrix. Left: μ_i/μ_m = 20/1. Right: μ_i/μ_m = 1/200. μ_{eff}, macroscopic effective shear modulus of the composite; μ_i, shear modulus of the inclusion; μ_m, shear modulus of the matrix.

References

1. Aboudi, J.; Pindera, M.-J.; Arnold, S.M.: Linear Thermoelastic Higher-Order Theory for Periodic Multiphase Materials. J. Appl. Mech. Trans. ASME, vol. 68, 2001, pp. 697–707.
2. Aboudi, J.; Pindera, M.-J., and Arnold, S.M.: Higher-Order Theory for Periodic Multiphase Materials With Inelastic Phases. Int. J. Plasticity (NASA/TM—2002-211469), 2002.
3. Arnold, S.M., et al.: Micromechanics Analysis Code With Generalized Method of Cells (MAC/GMC). User Guide: Version 3.0, NASA/TM—1999-209070, 1999. http:/gltrs.grc.nasa.gov/cgi-bin/GLTRS/browse.pl?1999/TM-1999-209070.html
4. Christensen, R.M.: Mechanics of Composite Materials. John Wiley & Sons, New York, NY, 1979.

Glenn contact:
Dr. Steven M. Arnold, 216–433–3334, Steven.M.Arnold@nasa.gov

Authors: Prof. Marek-Jerzy Pindera and Dr. Steven M. Arnold

Headquarters program office: OAT

Programs/Projects: RLV, RAC

Structural Anomalies Detected in Ceramic Matrix Composites Using Combined Nondestructive Evaluation and Finite Element Analysis (NDE and FEA)

Most reverse engineering approaches involve imaging or digitizing an object and then creating a computerized reconstruction that can be integrated, in three dimensions, into a particular design environment. The rapid prototyping technique builds high-quality physical prototypes directly from computer-aided design files. This fundamental technique for interpreting and interacting with large data sets is being used here via Velocity^2 (an integrated image-processing software, ref. 1) using computed tomography (CT) data to produce a prototype three-dimensional test specimen model for analyses.

A study at the NASA Glenn Research Center proposes to use these capabilities to conduct a combined nondestructive evaluation (NDE) and finite element analysis (FEA) to screen pretest and posttest structural anomalies in structural components. A tensile specimen made of silicon nitrite (Si_3N_4) ceramic matrix composite was considered to evaluate structural durability and deformity. Ceramic matrix composites are being sought as candidate materials to replace nickel-base superalloys for turbine engine applications. They have the unique characteristics of being able to withstand higher operating temperatures and harsh combustion environments. In addition, their low densities relative to metals help reduce component mass (ref. 2).

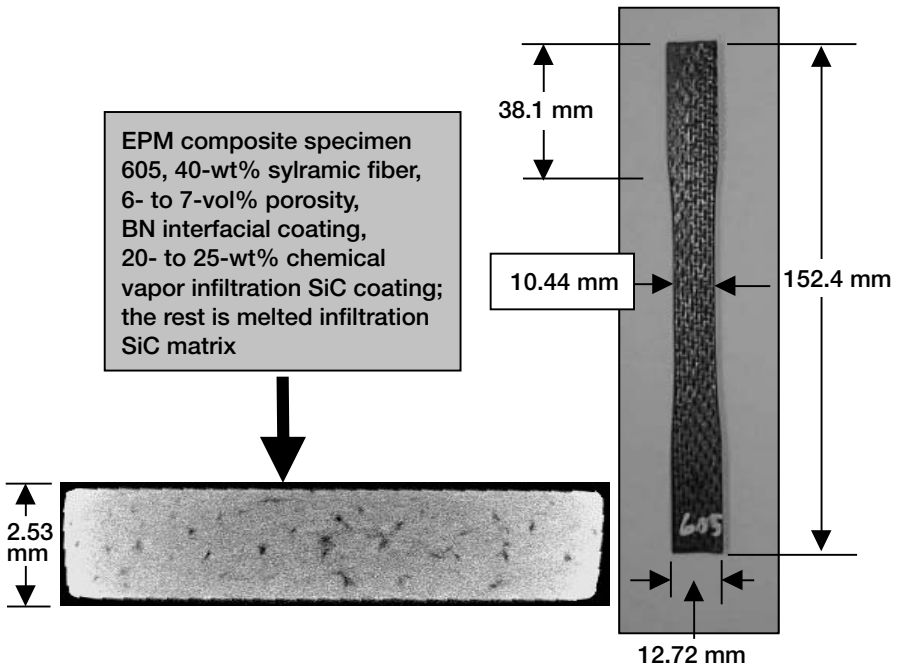

Ceramic matrix composite tensile specimen, showing dimensions, and a selected CT slice. Left: CT image. Right: Enabling propulsion material (EPM) specimen 605.

Detailed three-dimensional volume rendering of the tensile test specimen was successfully carried out with Velocity^2 (ref. 1) using two-dimensional images that were generated via computed tomography. Subsequent, three-dimensional finite element analyses were performed, and the results obtained were compared with those predicted by NDE-based calculations and experimental tests. It was shown that Velocity^2 software can be used to render a three-dimensional object from a series of CT scan images with a minimum level of complexity. The analytical results (ref. 3) show that the high-stress regions correlated well with the damage sites identified by the CT scans and the experimental data. Furthermore, modeling of the voids collected via NDE offered an analytical advantage that resulted in more accurate assessments of the material's structural strength. The figure to the left shows a CT scan image of the specimen test section illustrating various hidden structural entities in the material and an optical image of the test specimen considered in this study. The figure on the next page represents the stress response predicted from the finite element analyses (ref. 3) for a selected CT slice where it clearly illustrates the correspondence of the high stress risers due to voids in the material with those predicted by the NDE. This study is continuing, and efforts are concentrated on improving the modeling capabilities to imitate the structural anomalies as detected.

References

1. Velocity^2 Pro™. Processing and 3D reconstruction visualization software, version 2, Image3, LLC, Salt Lake City, UT, July 1998. (Also NASA/TM—2002-209952, 2002.)

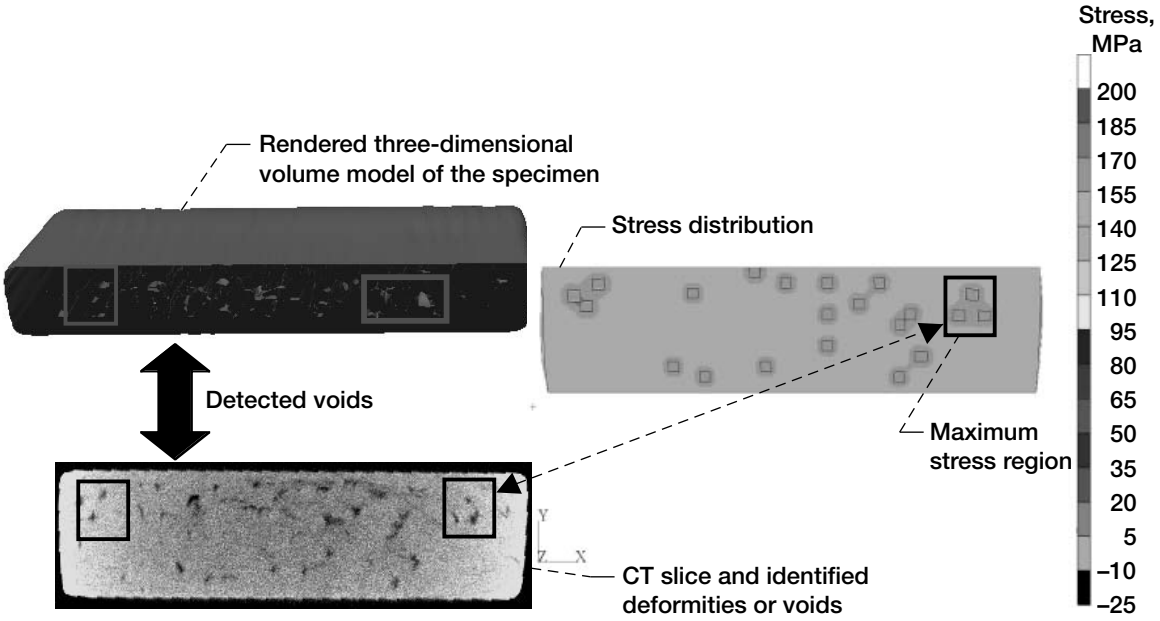

A matching section of a three-dimensional volume NDE-generated model and a CT image slice with a three-dimensional finite element result showing the stress state under tensile loading conditions. This figure is shown in color in the online version of this article (http://www.grc.nasa.gov/WWW/RT2002/5000/5920aziz1.html).

2. Abdul-Aziz, Ali; Baaklini, George Y.; and Bhatt, Ramakrishna T.: Design Evaluation Using Finite Element Analysis of Cooled Silicon Nitride Plates for a Turbine Blade Application. NASA/TM—2001-210819, 2001. http://gltrs.grc.nasa.gov/cgi-bin/GLTRS/browse.pl?2001/TM-2001-210819.html
3. ANSYS Finite Element Program, ANSYS Release 5.4, ANSYS, Inc., Canonsburg, PA, 2000. (Also NASA/TM—2002-211688, 2002.)

Cleveland State University contact:
Dr. Ali Abdul-Aziz, 216–433–6729, Fax 216–977–7150, Ali.Abdul-aziz@grc.nasa.gov

Glenn contact:
Dr. George Baaklini, 216–433–6016, Fax 216–977–7150, George.Y.Baaklini@nasa.gov

U.S. Army, Vehicle Technology Directorate at Glenn contact:
Dr. Ramakrishna Bhatt, 216–433–5513, Fax 216–977–7150, Ramakrishna.T.Bhatt@grc.nasa.gov

Authors: Dr. Ali Abdul-Aziz, Dr. George Y. Baaklini, Dr. Ramakrishna T. Bhatt

Headquarters program office: OAT

Programs/Projects: HOTPC

Thermal Response of Cooled Silicon Nitride Plate Due to Thermal Conductivity Effects Analyzed

Lightweight, strong, tough high-temperature materials are required to complement efficiency improvements for next-generation gas turbine engines that can operate with minimum cooling. Because of their low density, high-temperature strength, and high thermal conductivity, ceramics are being investigated as materials to replace the nickel-base superalloys that are currently used for engine hot-section components. Ceramic structures can withstand higher operating temperatures and a harsh combustion environment. In addition, their low densities relative to metals help reduce component mass (ref. 1). To complement the effectiveness of the ceramics and their applicability for turbine engine applications, a parametric study using the finite element method is being carried out.

The NASA Glenn Research Center remains very active in conducting and supporting a variety of research activities related to ceramic matrix composites through both experimental and analytical efforts (ref. 1). The objectives of this work are to develop manufacturing technology, develop a thermal and environmental barrier coating (TBC/EBC), develop an analytical modeling capability to predict

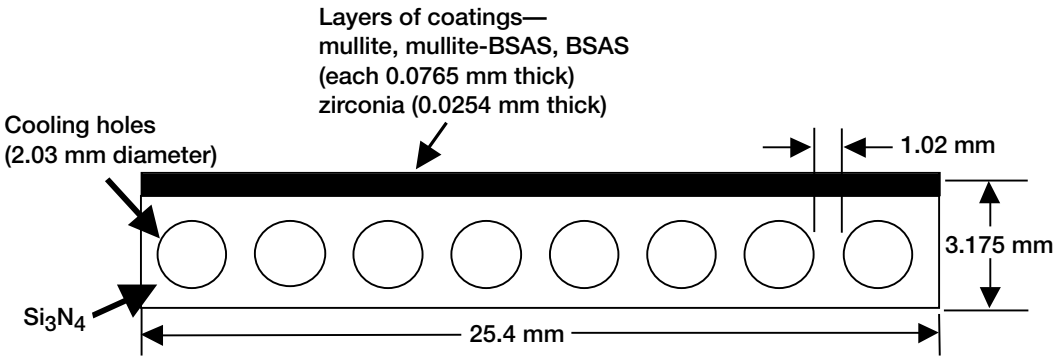

Monolithic Si_3N_4 cooling-panel cross section.

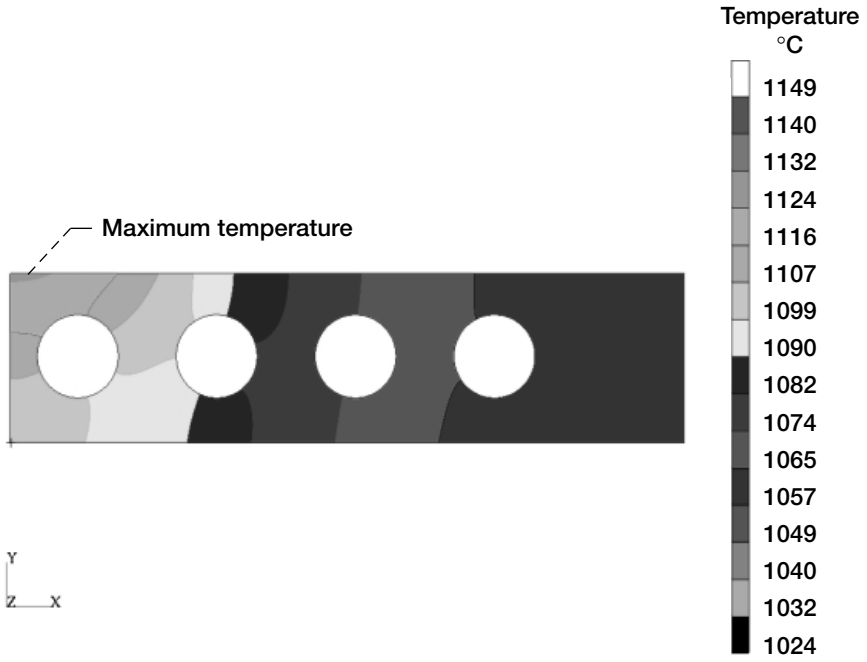

Temperature distribution at a thermal conductivity of 100 W/m-°C for circular cooling holes with cooling. This figure is shown in color in the online version of this article (http://www.grc.nasa.gov/WWW/RT2002/5000/5920aziz2.html).

thermomechanical stresses, and perform a minimal burner rig test on silicon nitride (Si_3N_4) and SiC/SiC turbine nozzle vanes under simulated engine conditions. Moreover, we intend to generate a detailed database of the material's property characteristics and their effects on structural response. We expect to offer a wide range of data since the modeling will account for other variables, such as cooling channel geometry and spacing. Comprehensive analyses have begun on a plate specimen with Si_3N_4 cooling holes.

Two-dimensional finite element analyses were performed in the form of a parametric study wherein heat transfer and stress analyses were conducted under steady-state conditions. The calculations were made under linear elastic conditions where the behavior of the material was defined by two material constants: Young's modulus and Poisson's ratio. The sketch at the top of this page shows the geometry of the silicon nitride plate with cooling holes. The test specimen consists of four layers of coating and the silicon nitride substrate arranged in the following order: a top layer of mullite, a second layer of combined mullite and 20 wt% BSAS (barium strontium aluminosilicate), a third layer of BSAS, and a fourth layer of zirconia.

The figure to the left shows a typical temperature distribution generated by the ANSYS finite-element-analysis code. Convective flame impingement was imposed over one-quarter of the top of the plate while convective cooling was imposed at the bottom of the plate and inside the cooling channels. The results indicate that the maximum temperature is at the middle section of the plate as anticipated. The graph on the next page represents the stress variations due to thermal conductivity changes and cooling channel size and configuration. This shows that the stress decreases as the thermal conductivity increases and that lower stresses are reported for the circular channel configurations. Furthermore, the material temperature can be reduced substantially depending on the cooling channel configuration and the boundary conditions applied. The analytical efforts performed here are expected to assist greatly in ongoing burner rig testing research and activities. Additional details regarding this work can be found in reference 3.

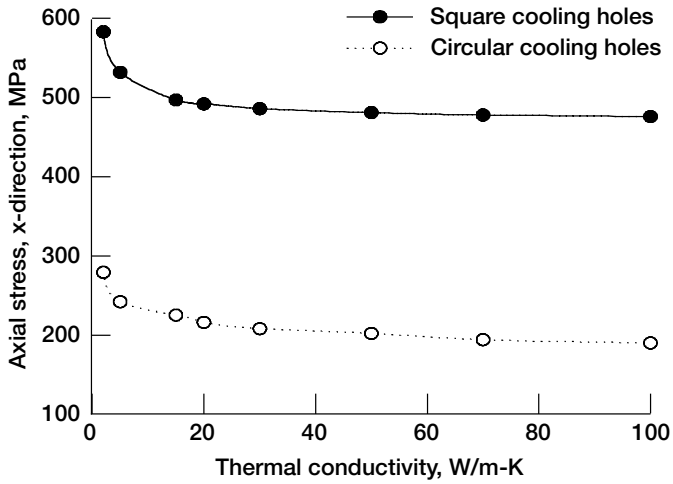

Axial stress for the silicon nitride cooling panel along the x-axis as a function of the thermal conductivity with cooling for two different cooling holes configurations.

References

1. Abdul-Aziz, Ali; Baaklini, George Y.; and Bhatt, Ramakrishna T.: Design Evaluation Using Finite Element Analysis of Cooled Silicon Nitride Plates for a Turbine Blade Application. NASA/TM—2001-210819, 2001. http://gltrs.grc.nasa.gov/cgi-bin/GLTRS/browse.pl?2001/TM-2001-210819.html
2. ANSYS Finite Element Program, ANSYS Release 5.7, ANSYS, Inc., Canonsburg, PA, 2000.
3. Abdul-Aziz, A.; and Bhatt, R.T.: Influence of Cooling Hole Geometry and Material Conductivity on the Thermal Response of Cooled Silicon Nitride Plate. Ceram. Eng. Sci. Proc., vol. 23, no. 3, 2002, pp. 125–132.

Cleveland State University contact:
Dr. Ali Abdul-Aziz, 216–433–6729,
Fax 216–977–7150,
Ali.Abdul-aziz@grc.nasa.gov

Glenn contact:
Dr. George Y. Baaklini, 216–433–6016,
Fax 216–977–7150,
George.Y.Baaklini@nasa.gov

U.S. Army, Vehicle Technology Directorate at Glenn contact:
Dr. Ramakrishna T. Bhatt, 216–433–5513,
Fax 216–977–7150,
Ramakrishna.T.Bhatt@grc.nasa.gov

Authors: Dr. Ali Abdul-Aziz,
Dr. Ramakrishna T. Bhatt, and
Dr. George Y. Baaklini

Headquarters program office: OAT

Programs/Projects: HOTPC

Methods Developed by the Tools for Engine Diagnostics Task to Monitor and Predict Rotor Damage in Real Time

Tools for Engine Diagnostics is a major task in the Propulsion System Health Management area of the Single Aircraft Accident Prevention project under NASA's Aviation Safety Program. The major goal of the Aviation Safety Program is to reduce fatal aircraft accidents by 80 percent within 10 years and by 90 percent within 25 years. The goal of the Propulsion System Health Management area is to eliminate propulsion system malfunctions as a primary or contributing factor to the cause of aircraft accidents. The purpose of Tools for Engine Diagnostics, a 2-yr-old task, is to establish and improve tools for engine diagnostics and prognostics that measure the deformation and damage of rotating engine components at the ground level and that perform intermittent or continuous monitoring on the engine wing.

In this work, nondestructive-evaluation- (NDE-) based technology is combined with model-dependent disk spin experimental simulation systems, like finite element modeling (FEM) and modal norms, to monitor and predict rotor damage in real time. Fracture mechanics time-dependent fatigue crack growth and damage-mechanics-based life estimation are being developed, and their potential use investigated. In addition, wireless eddy current and advanced acoustics are being developed for on-wing and just-in-time NDE engine inspection to provide deeper access and higher sensitivity to extend on-wing capabilities and improve inspection readiness. In the long run, these methods could establish a base for prognostic sensing while an engine is running, without any overt actions, like inspections. This damage-detection strategy includes experimentally acquired vibration-, eddy-current- and capacitance-based displacement measurements and analytically computed FEM-, modal norms-, and conventional rotordynamics-based models of well-defined damages and critical mass imbalances in rotating disks and rotors.

Reference 1 briefly describes the approach adapted at the NASA Glenn Research Center for monitoring the health of rotating subscale engine disks and blisks. Two spin facilities were built, a single high-temperature disk spin system and a

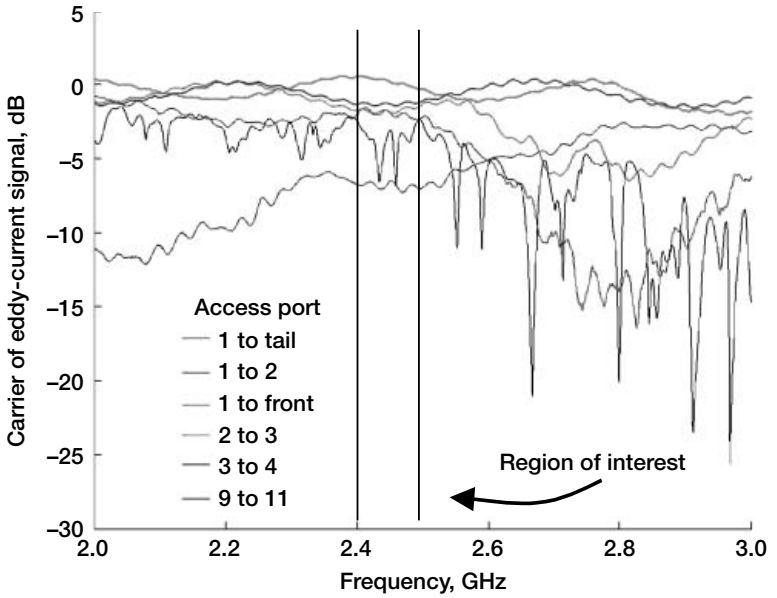

Eddy-current magnitude plot between engine access ports from 2 to 3 GHz.

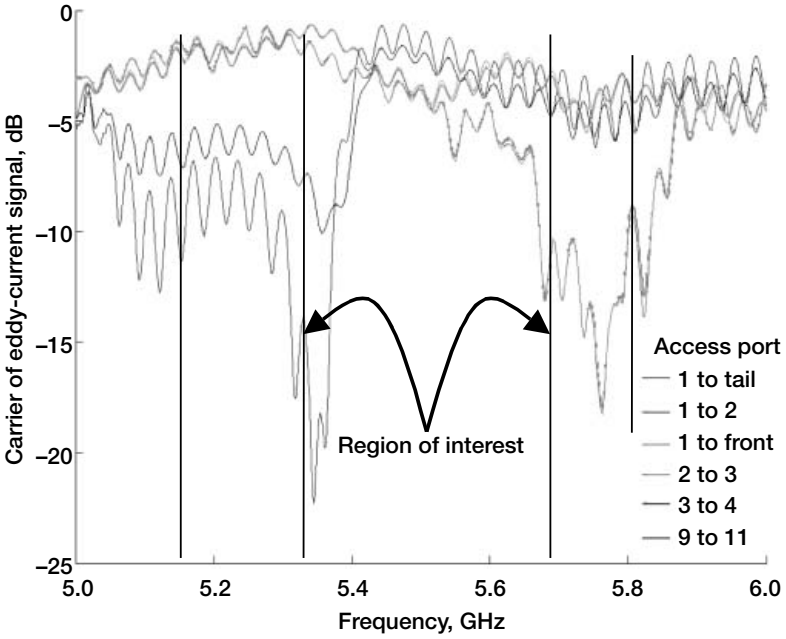

Eddy-current magnitude plot between engine access ports from 5 to 6 GHz.

room-temperature multidisk spin system, both equipped with advanced NDE sensors and rotordynamic software analysis based on center-of-mass and revolutions-per-minute changes. In addition, preliminary modeling of cracked disks with modal norms via reduction in modulus demonstrated that the method can locate damage and qualify its effect from changes in the natural modes of the damaged structure. These rotor and disk health-monitoring facilities can now be used to improve the understanding of field damage phenomena by experimentally simulating them with a whole suite of modeling approaches, like center-of-mass changes, conventional rotordynamics, and modal norms analysis. Time-dependent fatigue crack growth routines and defect-energy damage detection schemes, once fully developed, will give a more accurate estimation of safe life for engine components.

Preliminary NDE results from nonlinear surface acoustic waves demonstrated sensitivity to fatigue damage via higher harmonics. Also, thermal acoustics demonstrated that critical-size cracks can be detected in high- and low-cycle fatigue samples as well as in compressor blades. However, more work is in progress for the final selection of a just-in-time NDE technique for ground-based in-engine and on-wing inspection. Preliminary wireless eddy current was found to be feasible for remote communication and on-wing inspection deep in the engine. It was also demonstrated that communication data between ports can be acquired in frequency bands reserved for industrial, scientific, and medical purposes, called ISM bands. More work is planned for wireless eddy-current inspection sensitivity so that it becomes comparable to current wired inspection (see the graphs). These preliminary NDE results and damage detection strategy approaches, when fully developed by the end of the program, will improve prognostic sensing while the engine is running, assuring safety and reducing maintenance costs by eliminating overt actions, like teardown inspections.

Reference

1. Baaklini, G.Y., et al.: Tools for Engine Diagnostics Under the NASA Aviation Safety Program. Materials Evaluation, vol. 60, no. 7, July 2002, pp. 878–883.

Glenn contact:
Dr. George Baaklini, 216–433–6016, George.Y.Baaklini@nasa.gov

Authors: Dr. George Y. Baaklini, Kevin Smith, David Raulerson, Dr. Andrew L. Gyekenyesi, Dr. Jerzy T. Sawicki, and Lisa Brasche

Headquarters program office: OAT

Programs/Projects: AvSP

Hydrostatic Stress Effects Incorporated Into the Analysis of the High-Strain-Rate Deformation of Polymer Matrix Composites

Procedures for modeling the effect of high strain rate on composite materials are needed for designing reliable composite engine cases that are lighter than the metal cases in current use. The types of polymer matrix composites that are likely to be used in such an application have a deformation response that is nonlinear and that varies with strain rate. The nonlinearity and strain rate dependence of the composite response is primarily due to the matrix constituent. Therefore, in developing material models to be used in the design of impact-resistant composite engine cases, the deformation of the polymer matrix must be correctly analyzed. However, unlike in metals, the nonlinear response of polymers depends on the hydrostatic stresses, which must be accounted for within an analytical model. An experimental program has been carried out through a university grant with the Ohio State University to obtain tensile and shear deformation data for a representative polymer for strain rates ranging from quasi-static to high rates of several hundred per second. This information has been used at the NASA Glenn Research Center to develop, characterize, and correlate a material model in which the strain-rate dependence and nonlinearity (including hydrostatic stress effects) of the polymer are correctly analyzed.

To obtain the material data, Glenn's researchers designed and fabricated test specimens of a representative toughened epoxy resin. Quasi-static tests at low strain rates and split Hopkinson bar tests at high strain rates were then conducted at the Ohio State University. The experimental data confirmed the strong effects of strain rate on both the tensile and shear deformation of the polymer. For the analytical model, Glenn researchers modified state variable constitutive equations previously used for the viscoplastic analysis of metals to allow for the analysis of the nonlinear, strain-rate-dependent polymer deformation. Specifically, we accounted for the effects of hydrostatic stresses. An important discovery in the course of this work was that the hydrostatic stress effects varied during the loading process, which needed to be accounted for within the constitutive equations. The model is characterized primarily by shear data, with tensile data used to characterize the hydrostatic stress effects.

The graph on the left shows the experimental and computed shear-stress/shear-strain curves over a variety of strain rates for the toughened epoxy, and the graph on the right shows the experimental and computed tensile-stress/tensile-strain curves over a variety of strain rates for the same material. In both cases, the nonlinearity and the strain-rate dependence of the polymer deformation are correctly computed. Although not shown here, if the model was characterized using shear data only and the hydrostatic stress effects were not included, the computed tensile stresses would be significantly higher than their experimental values in the nonlinear portion of the stress-strain curve. The constitutive

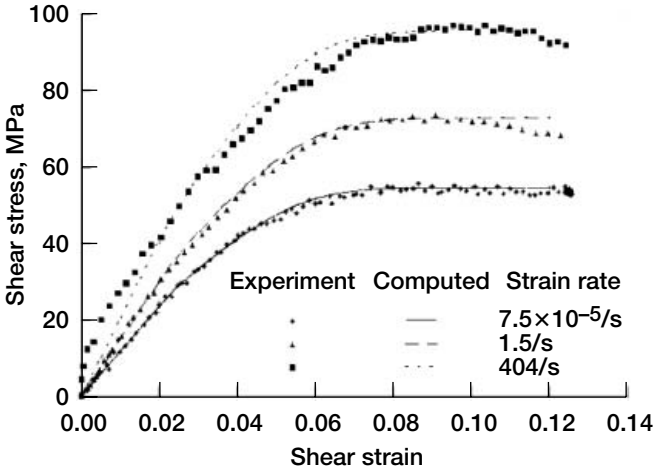

Experimental and computed shear-stress/shear-strain curves for representative toughened epoxy at strain rates of 7.5×10^{-5}/s, 1.5/s, and 404/s.

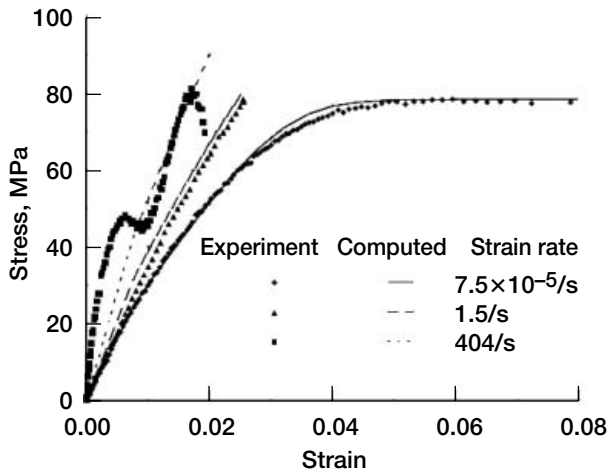

Experimental and computed tensile-stress/tensile-strain curves for representative toughened epoxy at strain rates of 5×10^{-5}/s, 1.4/s, and 470/s.

equations can be implemented into a micromechanics model to allow for the computation of the nonlinear, strain-rate-dependent deformation of polymer matrix composites.

Glenn contacts:
Dr. Robert K. Goldberg, 216–433–3330, Robert.K.Goldberg@nasa.gov; and
Dr. Gary D. Roberts, 216–433–3244, Gary.D.Roberts@nasa.gov

Authors: Dr. Robert K. Goldberg and Dr. Gary D. Roberts

Headquarters program office: OAT

Programs/Projects:
Propulsion Systems R&T, Ultra Safe

Delaminations Investigated With Ultrasonic Spectroscopy

A previous study suggested that the ultrasonic spectroscopy technique identified possible disbonds or delaminations in polymer matrix composite (PMC) rings sectioned from flywheel rotors (ref. 1). These results went unsubstantiated by other nondestructive evaluation (NDE) methods. To explain the results, PMC rings were further investigated with ultrasonic spectroscopy (ref. 2). The ultrasonic spectroscopy system utilizes a continuous-swept sine waveform as the input. After the swept sine wave traverses the material, the captured waveform is subjected to two fast Fourier transforms. The second fast Fourier transform along with equalization of the frequency spectrum, allows for evaluation of the fundamental resonant frequency. The full-thickness resonance, the resonance corresponding to the location of the intentional disbond, and the frequency spectrum were examined in an effort to characterize the sensitivity of the NDE method to various delamination conditions.

Ultrasonic spectroscopy responses were acquired as a delamination was initiated into a PMC ring section as shown in the photographs. A full circular ring was cut into four 90° sections. A groove was machined into the ring section near location 5. Next, a delamination was introduced by wedging a screwdriver into the groove. Transducers were clamped to the outer face of the composite ring section at location 3 while the delamination was initiated and propagated through the section, as illustrated in the photographs. C-clamps were used to hold the transducers in place and keep coupling conditions constant. The clamps were not overly compressive to allow the delamination to propagate through location 3. Ten stages of ultrasonic and optical data were collected with the screwdriver holding the delamination open. The first stage was prior to initiating a delamination. Successive readings were collected as the delamination propagated toward, then through, location 3, where the transducers were located. The final stage, stage 10, was defined as a full delamination through the ultrasonic path of the transducers at location 3. The optical measurements of the apparent delamination openings were taken from the outside surface of the composite ring.

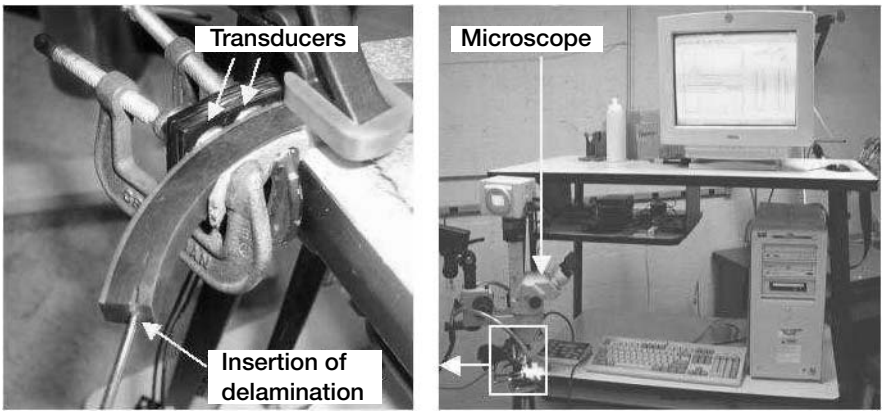

Experimental setup. Left: Transducers clamped to the outer face of a composite ring section while inserting a delamination. Right: Optical microscope and ultrasonic spectroscopy system utilized to collect data in 10 stages.

Only the full-thickness resonance was produced in a defect-free composite ring prior to initiating a delamination. Progression of a delamination into a monitored region of a composite ring section was detected as a change in the resonant frequencies. When a delamination with an apparent opening near 0.05 mm (0.002 in.) entered the ultrasonic path, it was detected as the appearance of a new resonance corresponding to the location of that delamination. The graphs on the next page show the ultrasonic spectroscopy response before and after the delamination enters the path of the transducers. A delamination with an apparent opening of approximately 0.07 mm (0.003 in.) through the whole ultrasonic path of the transducers resulted in a single resonance corresponding to its location without the presence of the full-thickness resonance. On the basis of these results, ultrasonic spectroscopy is a viable NDE tool in detecting and

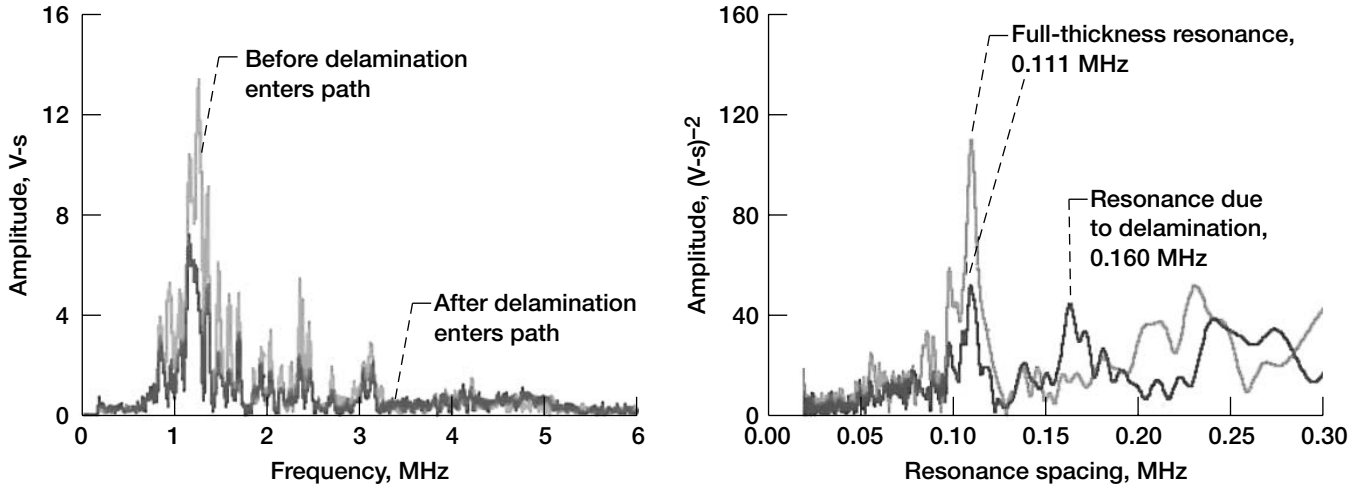

The spectrum (left) and the spectrum resonance spacing (right) immediately before and after the delamination enters the transducer path exhibiting a reduction in amplitude in the spectrum and the appearance of a resonance due to the delamination in the spectrum resonance spacing. The 0.05-mm-thick delamination was through less than a quarter of the ultrasonic wave path.

monitoring delaminations in composite rings to be used in flywheel rotors. These results can be extended to detecting delaminations in PMC materials.

References

1. Harmon, L.M.; and Baaklini, G.Y.: Ultrasonic Spectroscopy of Composite Rims for Flywheel Rotors. Review of Quantitative Nondestructive Evaluation, D.O. Thompson and D.E. Chimenti, eds., vol. 21, American Institute of Physics, CP615, 2002, pp. 1086–1093.
2. Harmon, Laura M., et al.: Investigations of Delaminations With Ultrasonic Spectroscopy. Nondestructive Evaluation and Health Monitoring of Aerospace Materials and Civil Infrastructures, Proceedings of SPIE, Andrew L. Gyekenyesi, et al., eds., vol. 4704, 2002.

Cleveland State University contact:
Laura M. Cosgriff, 216–433–3866, Laura.M.Cosgriff@grc.nasa.gov

Glenn contact:
Dr. George Y. Baaklini, 216–433–6016, George.Y.Baaklini@nasa.gov

Author: Laura M. Cosgriff

Headquarters program office: OAT

Programs/Projects: RSL

Fretting Fatigue of Gamma TiAl Studied

Gamma titanium-aluminum alloy (γ-TiAl) is an attractive new material for aerospace applications because of its low density and high specific strength in comparison to currently used titanium and nickel-base alloys. Potential applications for this material are compressor and low-pressure turbine blades. These blades are fitted into either the compressor or turbine disks via a dovetail connection. The dovetail region experiences a complex stress state due to the alternating centrifugal force and the natural high-frequency vibration of the blade. Because of the dovetail configuration and the complex stress state, fretting is often a problem in this area. Furthermore, the local stress state becomes more complex when the influence of the metal-metal contact and the edge of the contact is evaluated. Titanium and titanium-based alloys in the clean state exhibit strong adhesive bonds when in contact with themselves and other materials (refs. 1 and 2). This adhesion causes heavy surface damage and high friction in practical cases. Although the wear produced by fretting may be mild, the reduction in fatigue life can be substantial. Thus, there is the potential for fretting problems with these TiAl applications. Since TiAl is an emerging material, there has been limited information about its fretting behavior.

This study at the NASA Glenn Research Center provides preliminary information about the resistance of TiAl to fretting. The wear mechanisms in Ti-48Al-2Cr-2Nb were investigated in an earlier study (ref. 3). This investigation has been supplemented to include the influence of fretting on fatigue strength (ref. 4). Ti-48Al-2Cr-2Nb fatigue samples were fretted using wear pads of Inconel 718, a common disk material. One pad was rectangular with a flat wear surface. The second pad was wedgelike with a knife edge. The specimen was heated to various temperatures, and the contact pads were brought into

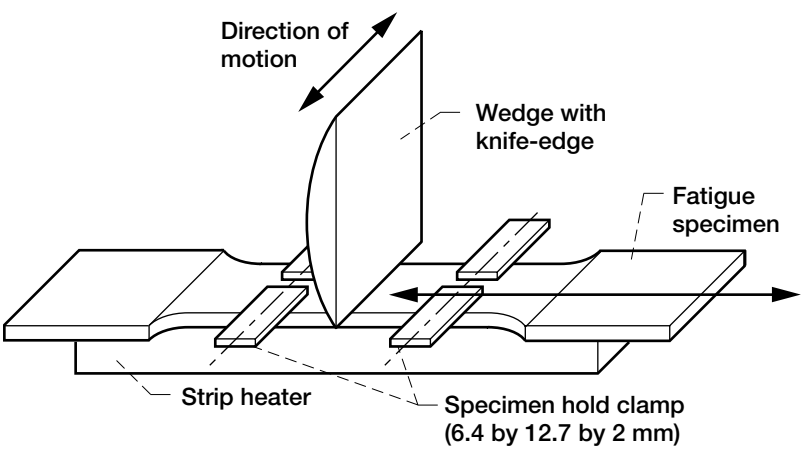

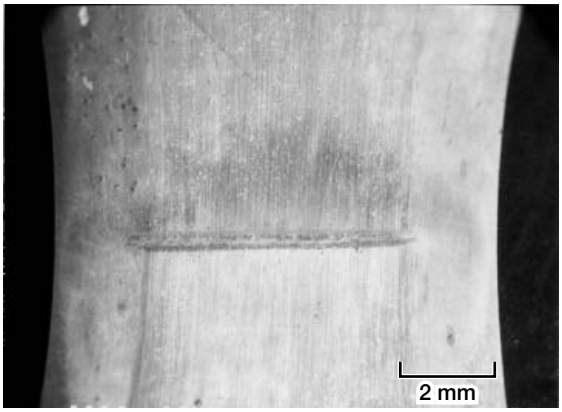

Left: Fretting setup. Right: Wear pattern on TiAl specimen gauge.

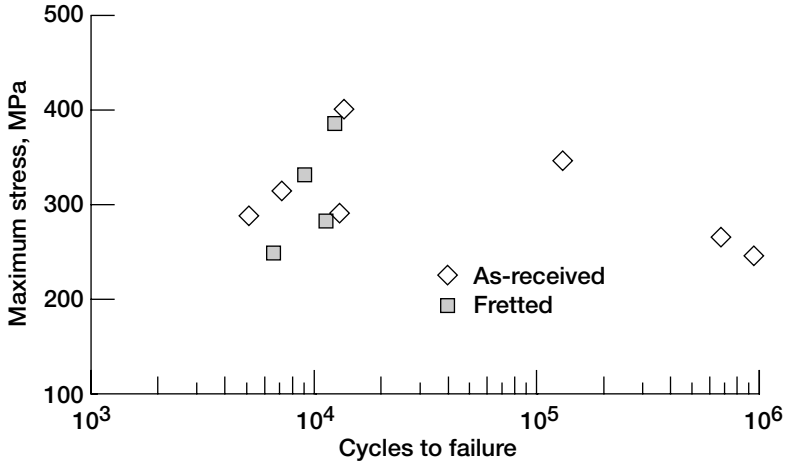

Fatigue test results of fretted and unfretted samples.

contact against the sample (see the sketch). The pads were oscillated against the samples with amplitudes of up to 90 μm and loads up to 450 N. Typical wear patterns are shown on the gauge of the fatigue sample in the photomicrograph. The samples were subsequently fatigue tested at a temperature of 650 °C, a frequency of 80 Hz, and a load ratio of 0.05. A step test method was employed using a block size of 10^6 cycles and a step size of 14 MPa.

The results were somewhat unexpected: the fretted samples had lives equivalent to those of the unfretted samples (see the graph). This is easily explained since none of the fretted samples failed at the fret, but elsewhere in the gauge. Metallographic cross sections revealed slight impressions approximately 3 μm deep in the gauge of the fatigue specimen from the fretting process. However, no subsurface cracking was observed. Thus, the damage from the fretting process was not very severe. These results suggest that TiAl has good fretting resistance. In fact, with reciprocating pin-on-flat[1] tests, TiAl had much better wear resistance than Ti-6Al-4V (ref. 3), which is a typical compressor blade material. Although only preliminary, the results suggest that TiAl has sufficient fretting resistance to withstand the wear in dovetail applications.

[1]In these tests, a pin is vibrated on a flat piece of material to induce wear of either the pin or the flat material.

References

1. Miyoshi, Kazuhisa: Aerospace Mechanisms and Tribology Technology Case Study. Tribology Int., vol. 32, no. 11, 1999, pp. 673–685.
2. Miyoshi, K., et al.: Sliding Wear and Fretting Wear of Diamondlike Carbon-Based, Functionally Graded Nanocomposite Coatings. Wear, vols. 225–229, pt. 1, 1999, pp. 65–73.
3. Miyoshi, Kazuhisa, et al.: Evaluation of Ti-48Al-2Cr-2Nb Under Fretting Conditions. NASA/TM—2001-211205, 2001. http://gltrs.grc.nasa.gov/cgi-bin/GLTRS/browse.pl?2001/TM-2001-211205.html
4. Miyoshi, Kazuhisa; Lerch, Bradley A.; and Draper, Susan L.: Preliminary Study on Fatigue Strengths of Fretted Ti-48Al-2Cr-2Nb. NASA/TM—2002-211718, 2002. http:/gltrs.grc.nasa.gov/cgi-bin/GLTRS/browse.pl?2002/TM-2002-211718.html

Glenn contacts:
Dr. Bradley A. Lerch, 216–433–5522, Bradley.A.Lerch@nasa.gov; and
Dr. Kazuhisa Miyoshi, 216–433–6078, Kazuhisa.Miyoshi-1@nasa.gov

Authors:
Dr. Kazuhisa Miyoshi, Dr. Bradley A. Lerch, and Susan L. Draper

Headquarters program office: OAT

Programs/Projects: Ultra Safe

Strength Differential Measured in Inconel 718: Effects of Hydrostatic Pressure Studied

Aeropropulsion components, such as disks, blades, and shafts, are commonly subjected to multiaxial stress states at elevated temperatures. Experimental results from loadings as complex as those experienced in service are needed to help guide the development of accurate viscoplastic, multiaxial deformation models that can be used to improve the design of these components. During a recent study on multiaxial deformation (ref. 1) on a common aerospace material, Inconel 718, it was shown that the material in the aged state exhibits a strength differential effect (SDE), whereby the uniaxial compressive yield and subsequent flow behavior are significantly higher than those in uniaxial tension. Thus, this material cannot be described by a standard von Mises yield formulation. There have been other formulations postulated (ref. 2) that involve other combinations of the stress invariants, including the effect of hydrostatic stress. The question remained as to which invariants are necessary in the flow model. To capture the physical mechanisms occurring during deformation and reflect them in the plasticity formulation, researchers examined the flow of Inconel 718 under various amounts of hydrostatic stress to determine whether or not hydrostatic stress is needed in the formulation.

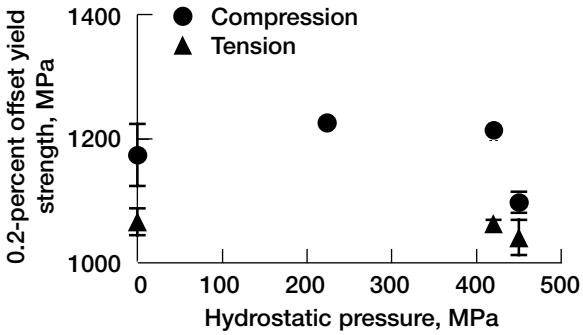

Tension (triangles) and compression (circles) yield strength as a function of hydrostatic pressure.

Under NASA Grant NCC3–464, monitored by the NASA Glenn Research Center, a series of tensile tests were conducted at Case Western Reserve University on aged (precipitation hardened) Inconel 718 at 650 °C and with superimposed hydrostatic pressure. Dogbone-shaped tensile specimens (3-mm-diameter gauge by 16-mm gauge length) and cylindrical compression specimens (3-mm-diameter gauge by 6-mm gauge length) were strain gauged and loaded in a high-pressure testing apparatus. Hydrostatic pressures were obtained with argon and ranged from 210 to 630 MPa. The aged Inconel 718 showed a pronounced difference in the tension and compression yield strength (i.e., an SDE), as previously observed. Also, there were no significant effects of hydrostatic pressure on either the tensile and compressive yield strength (see the graph) or on the magnitude of the SDE. This behavior is not consistent with the pressure-dependent theory of the SDE, which postulates that the SDE is associated with pressure-dependent and/or internal friction-dependent deformation associated with non-Schmid effects at the crystal level (refs. 3 and 4). Flow in Inconel 718 appears to be independent of hydrostatic pressure, suggesting that this invariant may be removed from the phenomenological constitutive model. As part of an ongoing effort to develop advanced constitutive models, Glenn's Life Prediction Branch coordinated this work with that of research on the multiaxial deformation behavior of Inconel 718 being conducted at Pennsylvania State University under NASA Grant NCC597.

References

1. Gil, C.M.; Lissenden, C.J.; Lerch, B.A.: Yield of Inconel 718 by Axial-Torsional Loading at Temperatures up to 649 °C. J. Test. Eval., vol. 27, no. 5, 1999, pp. 327–336.
2. Iyer, Saiganesh: Viscoplastic Model Development to Account for Strength Differential: Application to Aged Inconel 718 at Elevated Temperature. NASA/CR—2001-210715, 2001.
3. Brünig, Michael: Numerical Analysis and Large Strain Elastic-Viscoplastic Behavior of Hydrostatic Stress-Sensitive Metals. Int. J. Solids Struct., vol. 38, issue 4, 2001, pp. 635–656.
4. Kuroda, M.; and Kuwabara, T.: Shear-Band Development in Polycrystalline Metal With Strength-Differential Effect and Plastic Volume Expansion. Proc. Royal Soc. London Series A, vol. 458, 2002, pp. 2243–2259.

Glenn contact:
Dr. Bradley A. Lerch, 216–433–5522, Bradley.A.Lerch@nasa.gov

Authors:
Prof. John J. Lewandowski, Paul Wesseling, Nishad S. Prabhu, Joel Larose, Prof. Cliff J. Lissenden, and Dr. Bradley A. Lerch

Headquarters program office: OAT

Programs/Projects: HOTPC

Flaw Detection for Composite Materials Improved by Advanced Thermal Image Reconstruction Techniques

The development of advanced composite materials for use in space and propulsion components has seen considerable growth over the past few years. In addition to improvements that have been made in material properties and processing techniques, similar growth must be seen in the development of methods for the detection of flaws, either generated in service or during manufacturing. Thermal imaging techniques have proven to be successful for the nondestructive evaluation (NDE) of composite materials, but their detection capabilities decrease as flaw depth increases. The purpose of this research is to investigate advanced thermal imaging methods and thermal image processing technologies to increase the maximum depth below surface that a flaw can be detected and improve the contrast between flawed regions and sound regions.

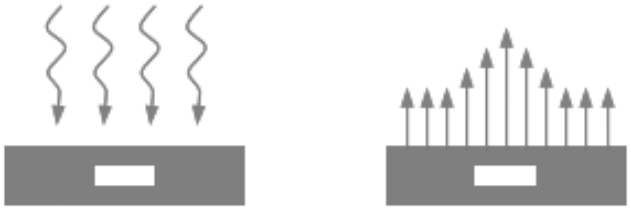

Flash thermography setup. Left: A specimen is heated with a pulse of thermal energy. Right: As the thermal front conducts through the material, defects such as delaminations prevent the flow of heat and result in a higher surface temperature directly above the specimen.

One of the more widely used methods for the thermographic inspection of materials and components is pulsed thermography. As the name implies, the technique imparts a pulse of thermal energy, usually provided by a photographic flash lamp, on the surface of a specimen. The thermal energy on the surface is conducted into the cooler interior of the sample. In turn, there is a reduction of the surface temperature over time. This surface cooling occurs in a uniform manner as long as the material properties are consistent throughout the specimen. Subsurface defects that possess different material properties (thermal conductivity, density, or heat capacity) affect the flow of heat in that particular region. This resistance in the conductive path causes a different cooling rate at the surface directly above the defect, when compared with the surrounding defect-free material. The change in the subsurface conduction is seen as a nonuniform surface temperature profile as a function of time (see the figures above). Unprocessed, as-received data are typically displayed sequentially on a computer monitor in a movie fashion. Images are then visually inspected for signs of a subsurface defect by locating areas with anomalous surface temperatures. Since the method depends on the interaction of the defect with the advancing thermal front, defects that are located at greater depths show up later in time. Because of lateral diffusion, deeper defects tend to have less contrast than flaws near the surface do.

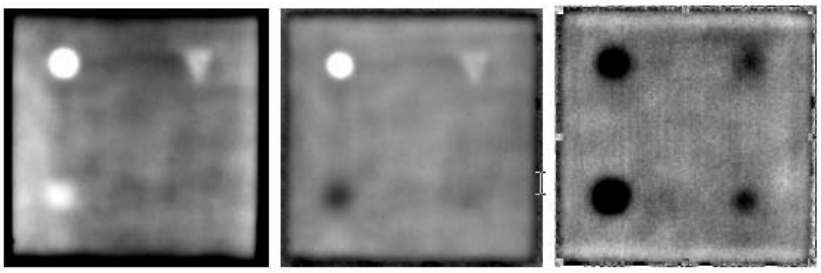

Pulsed thermography results for a C/SiC specimen with seeded flaws. Left: Raw thermal image data. Center and right: First and second derivative images generated from the reconstructed thermal data.

A new technique for the processing of thermal image data has been applied at the NASA Glenn Research Center to improve detection capabilities. This method involves the creation of a set of mathematical equations that represent the time response of each pixel in the raw data set. This "reconstruction" process exploits certain general features of the thermal response of materials to pulsed heating, and has been shown to significantly improve the detection of subsurface features without the use of a reference. The three images shown in the figure to the left illustrate this improvement. The image to the left represents an unprocessed thermal image of a C/SiC test specimen after the application of the flash input. The specimen contains four seeded defects, located at various depths below the surface. Using the raw thermal data, three of the four defects were identified, with the deepest defect undetected. The center and right images were created using the image-reconstruction algorithms and represent derivatives of the original thermal signal. The instantaneous slope information generated from the reconstructed data set was used successfully to locate the deepest defect. In addition, the contrast between defect locations and defect-free

areas was improved dramatically. We expect that these improvements will greatly enhance the inspection capabilities of composite materials used in the Ultra-Efficient Engine Technology (UEET) project, Reusable Launch Vehicle (RLV) program, and Higher Operating Temperature Propulsion Components (HOTPC) project.

Cleveland State University contact:
Richard Martin, 216–433–3684, Richard.E.Martin@grc.nasa.gov

Ohio Aerospace Institute (OAI) contact:
Dr. Andrew Gyekenyesi, 216–433–8155, Andrew.L.Gyekenyesi@grc.nasa.gov

Glenn contact:
Dr. George Y. Baaklini, 216–433–6016, George.Y.Baaklini@nasa.gov

Authors: Richard E. Martin and Dr. Andrew L. Gyekenyesi

Headquarters program office: OAT

Programs/Projects:
UEET, RLV, HOTPC

A Step Made Toward Designing Microelectromechanical System (MEMS) Structures With High Reliability

The mechanical design of microelectromechanical systems—particularly for micropower generation applications—requires the ability to predict the strength capacity of load-carrying components over the service life of the device. These microdevices, which typically are made of brittle materials such as polysilicon, show wide scatter (stochastic behavior) in strength as well as a different average strength for different sized structures (size effect). These behaviors necessitate either costly and time-consuming trial-and-error designs or, more efficiently, the development of a probabilistic design methodology for MEMS. Over the years, the NASA Glenn Research Center's Life Prediction Branch has developed the CARES/*Life* probabilistic design methodology to predict the reliability of advanced ceramic components. In this study, done in collaboration with Johns Hopkins University, the ability of the CARES/*Life* code to predict the reliability of polysilicon microsized structures with stress concentrations is successfully demonstrated.

The photograph on the left shows the microtensile specimen geometry used for the tests. Specimens were 3.5 μm thick with gross widths of either 20 or 50 μm. Fracture loads were measured for three shapes: a specimen with straight sides and a uniform cross section, a specimen with a central hole, and a specimen with symmetric double notches (see the photograph on the right). A total of 226 measurements were made to generate statistically significant information, with about 30 specimens fractured for each test geometry.

The graph on the next page shows the results of the experiments. Average strengths are shown along with the scatter bands for a standard deviation of ±1. The strengths shown correspond to the peak average stresses found in the specimens. For example, for the notched specimen, the peak stress occurs at the notch root. The graph also shows that the fracture stresses for the holed and notched specimens are significantly higher than those for the straight-sided, uniform cross-section specimens. For bulk brittle materials, such as advanced ceramics, this difference in strength is termed the "size-effect." Size effect means that when the volume of material under high stress increases there is a higher likelihood of a weaker flaw being present. Hence, a component with a

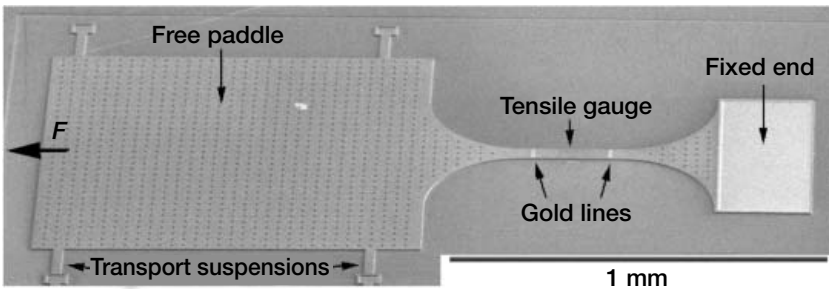

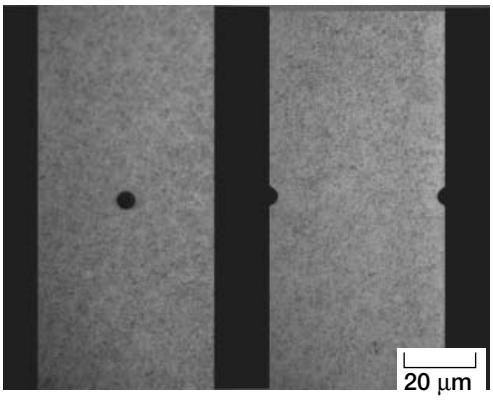

Left: Scanning electron microscope image of a test specimen. Right: Photograph of gauge sections of 50-μm-wide hole-and-notch specimens.

stress concentration would be expected to have a higher average strength than a component without a stress concentration because the amount of material under high stress is smaller with the specimen with the stress concentration. Although size effect is well known in bulk ceramics, its existence in MEMS is an active area of investigation. One can predict size effect by combining the Weibull distribution with integrating the stress state over the volume (or area) of the component. Showing the existence of size effect in MEMS and that it can be predicted using the Weibull distribution would establish the foundation for a MEMS structures probabilistic design methodology.

The fracture strengths of MEMS devices are known to be affected by surface defects and the resultant surface roughness from the manufacturing process. Such variability can directly affect the failure modes and, in turn, the reliability of the device. The following photomicrographs show the source of the defects responsible for the strength response. Typically, these flaws were located at or near the region of highest stress along the sidewalls of the specimen. Photographs (b) and (d) also show the considerable roughness of the sidewall in comparison to the upper and lower surfaces of the specimen.

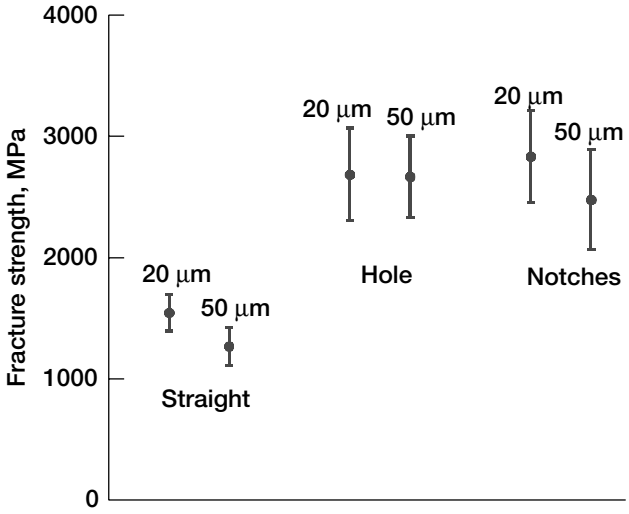

Measured local fracture strengths ±1 standard deviation.

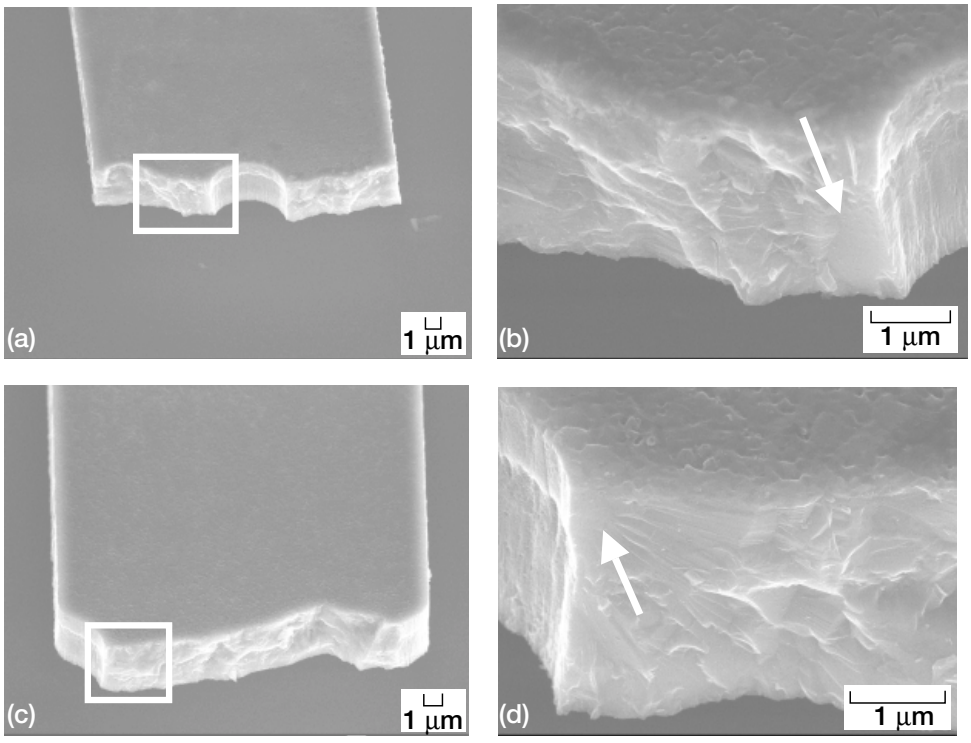

Overview of the fracture surfaces of a hole specimen (a) and a notch specimen (c). Both are 20 μm wide. Magnified views of the area within the white rectangles in (a) and (c) are shown on the right in (b) and (d), respectively. The white arrows point to the border between the mirror region and the mist-and-hackle region.

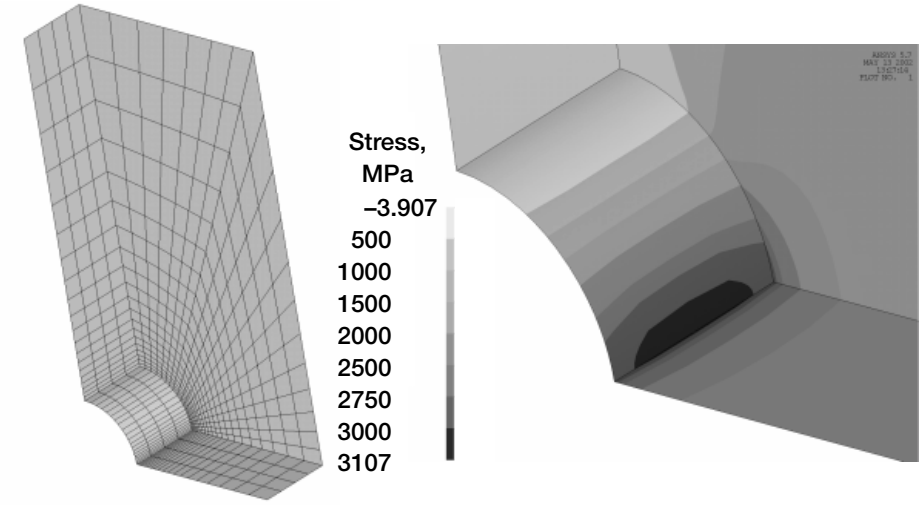

Left: Finite element mesh of a sample with an edge notch (quarter model). Specimen width, 20 μm; specimen thickness, 3.5 μm; notch radius, 2.5 μm. Right: Stress distribution at the root of the notch for a gross stress of 1000 MPa.

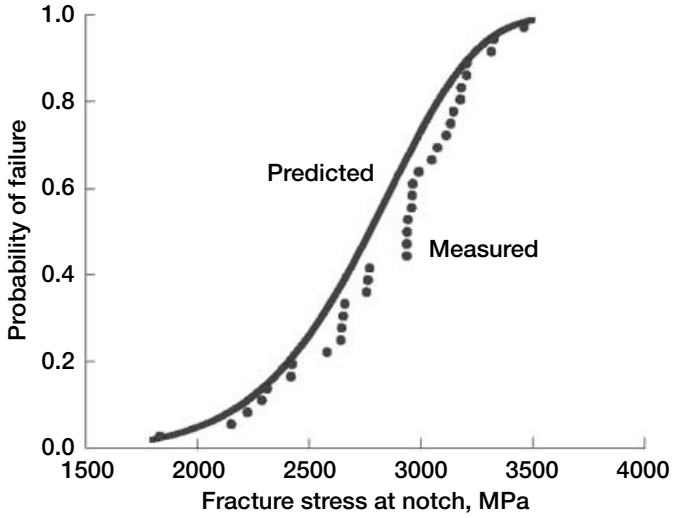

CARES/Life prediction of the sidewall failure probability versus the stress at the notch for the 20-μm-wide specimen.

Consequently, one would expect the strength response of the specimens to be controlled by the area and distribution of stresses along the sidewalls.

NASA's CARES/*Life* program was used to test if the baseline material properties from uniaxial (uniform cross section) tensile tests could predict the overall reliability response of the more complicated structures with the stress concentrators. CARES/*Life* requires results from finite element analysis in order to make component reliability predictions. The figures at the top of this page show the finite element mesh and stress analysis results for the notched specimen. Reliability analysis was performed as a function of (1) specimen volume, (2) specimen surface area, and (3) specimen sidewall surface area. The final graph shows the CARES/*Life* predictions for failure probability versus stress at the notch root for the 20-μm-wide specimen. These results were within 3 percent of the experimental values when the analysis was based on the sidewall area. When the reliability analyses were performed as a function of the total surface area and volume, results differed by 21 and 51 percent, respectively. Similar trends were observed with the other notched and holed specimen geometries. These results, coupled with the fractographic observations of the origin of strength-controlling flaws, added confidence to the correctness of basing the reliability analysis on the sidewall surface area.

Overall, Weibull statistics—on which CARES/*Life* is based—were quite successful in predicting the failure probability of MEMS components with stress concentrators. One can take baseline material properties from uniaxial tensile tests and use them in conjunction with finite element analysis to predict the overall strength of complicated components. This is commensurate with traditional mechanical design, but with the addition of Weibull statistics. This work is a confirmatory step toward the establishment of a comprehensive MEMS probabilistic design methodology.

Find out more about this research:
http://www.grc.nasa.gov/WWW/LPB/cares/

Glenn contact:
Noel Nemeth, 216–433–3215, Noel.N.Nemeth@nasa.gov

Author: Noel N. Nemeth

Headquarters program office: OAT

Programs/Projects: RAC, Gen 3, GMI

High-Performance Acousto-Ultrasonic Scan System Being Developed

Acousto-ultrasonic (AU) interrogation is a single-sided nondestructive evaluation (NDE) technique employing separated sending and receiving transducers. It is used for assessing the microstructural condition and distributed damage state of the material between the transducers. AU is complementary to more traditional NDE methods, such as ultrasonic c-scan, x-ray radiography, and thermographic inspection, which tend to be used primarily for discrete flaw detection. Throughout its history, AU has been used to inspect polymer matrix composites, metal matrix composites, ceramic matrix composites, and even monolithic metallic materials. The development of a high-performance automated AU scan system for characterizing within-sample microstructural and property homogeneity is currently in a prototype stage at NASA. This year, essential AU technology was reviewed. In addition, the basic hardware and software configuration for the scanner was developed, and preliminary results with the system were described.

Mechanical and environmental loads applied to composite materials can cause distributed damage (as well as discrete defects) that plays a significant role in the degradation of physical properties. Such damage includes fiber/matrix debonding (interface failure), matrix microcracking, and

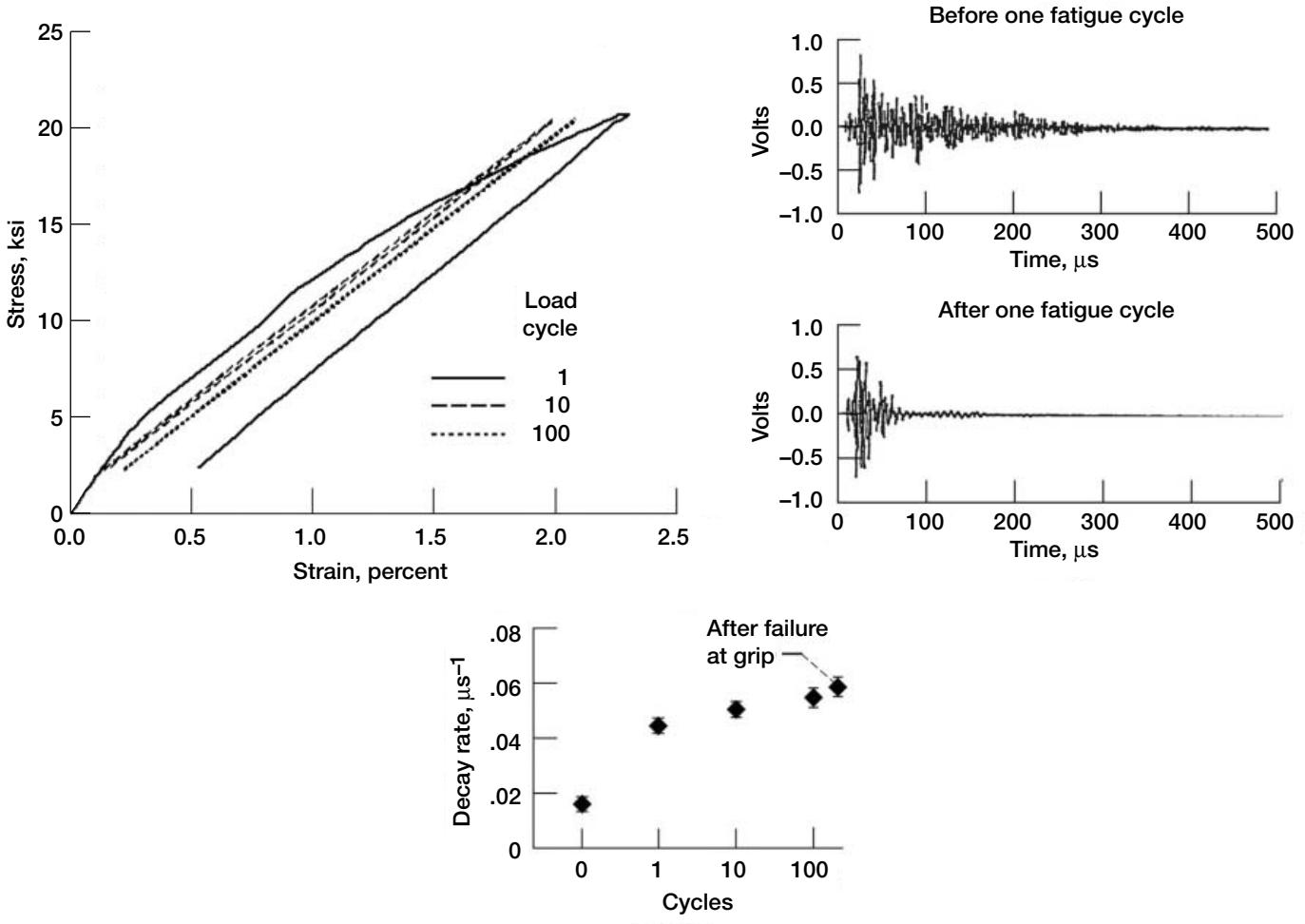

Top left: The stress-strain curves show the decrease in modulus (slope) with increase in strain upon application of the first cycle (note the curvature); subsequent fatigue cycle loading shows moduli similar to that after 1 cycle (note that the slopes of the different stress-strain curves are nearly parallel). Top right: Acousto-ultrasonic wavetrains before and after one fatigue cycle loading show a dramatic change correlating with the decrease in modulus. Bottom: Ultrasonic decay rate derived from waveforms in the top right graph shows a large increase after one fatigue cycle loading and only a moderate increase upon subsequent loading, in agreement with load curves in the top left graph.

fiber fracture and buckling. Investigations at the NASA Glenn Research Center have shown that traditional NDE scan inspection methods such as ultrasonic c-scan, x-ray imaging, and thermographic imaging tend to be more suited to discrete defect detection rather than the characterization of accumulated distributed microdamage in composites. Since AU is focused on assessing the distributed microdamage state of the material in between the sending and receiving transducers, it has proven to be quite suitable for assessing the relative composite material state.

One major success story at Glenn with AU measurements has been the correlation between the ultrasonic decay rate obtained during AU inspection and the mechanical modulus (stiffness) seen during fatigue experiments with silicon carbide/silicon carbide (SiC/SiC) ceramic matrix composite samples. As shown in the figure on the preceding page, ultrasonic decay increased as the modulus decreased for the ceramic matrix composite tensile fatigue samples. The likely microstructural reason for the decrease in modulus (and increase in ultrasonic decay) is the matrix microcracking that commonly occurs during fatigue testing of these materials. Ultrasonic decay has shown the capability to track the pattern of transverse cracking and fiber breakage in these composites.

The data in the figure were obtained over a small region of a specimen. Scanning capability would allow researchers and practitioners to focus in on exactly where damage is and is not occurring in samples and components that that have been mechanically and thermally loaded. The AU scan system is planned to have both automated scan and interactive point measurement capabilities within one system. All functions will be automated with software interfaces replacing hardware instrument interfaces where possible. The scan capability is close to completion with regards to the basic operations of motion control, load control, data acquisition, online presignal and postsignal processing, and waveform data and image recording and saving. Currently, images of 18 different parameters (including ultrasonic decay) of the AU signal are formed in real time. Detailed system specifications are available upon request. We plan to develop the system to scan curved as well as platelike components.

Glenn contact:
Don Roth, 216–433–6017,
Donald.J.Roth@nasa.gov

Authors: Don J. Roth, Richard E. Martin, Laura M. Cosgriff, Dr. Andrew L. Gyekenyesi, and Harold E. Kautz

Headquarters program office: OAT

Programs/Projects:
UEET, Propulsion Systems R&T, RLV

Methodology Improved for Estimating Life-Prediction Parameters for the Design of Industrial Components

One of the factors limiting structural ceramics in long-term applications is stress corrosion, or slow crack growth. For example, airborne water can cause degradation and failure of ceramic components subjected to static loads. Thus, the design of structural components from advanced ceramics requires the measurement of the life-prediction parameters for the particular ceramic material and environment of interest. Recently, the American Society for Testing and Materials standard C1368–97 (ref. 1) allowed life-prediction parameters to be measured with such fast stress rates and correspondingly short experimental failure times that significant errors in the life-prediction parameters occurred (ref. 2). As a result, components could not be accurately designed for a long time-to-failure.

One application where a long time-to-failure is expected is microwave windows that are used in the production of nuclear materials (ref. 3). Recent ultraslow and standard-rate testing of a window material for Los Alamos National Laboratory demonstrated the existence of multiple regions of the slow crack growth curve, in agreement with the theory shown in the left figure on the next page. The tests indicated that the short failure times allowed by the standard resulted in a factor of 3 error in the life parameter n, as shown in the right figure on the next page. In addition, we determined that by increasing the concentration of the corrosive media, the diffusion-related phenomenon that made the parameters inaccurate could be avoided, thereby allowing faster, time-saving rates to be employed in some situations.

The results have been used to revise the American Society for Testing and Materials standard C1368–01 (ref. 4) and thereby provide engineers with better data for designing industrial components with long failure times.

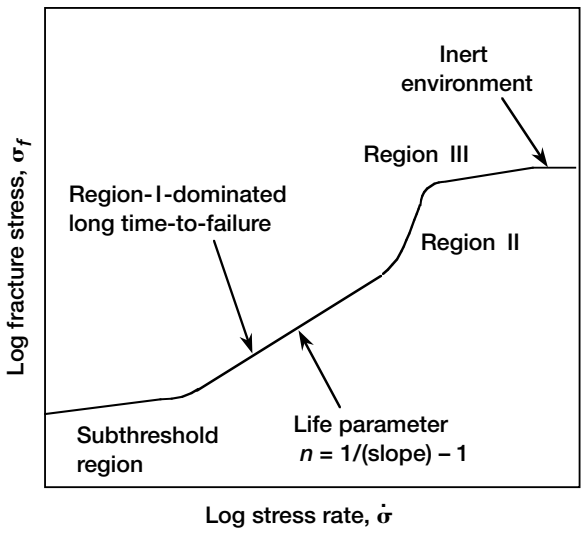

Generalized fracture strength as a function of stress rate for ceramics and glasses exhibiting environmentally induced slow crack growth. Crack growth theory indicates that the slope of the curve changes over the life of the component.

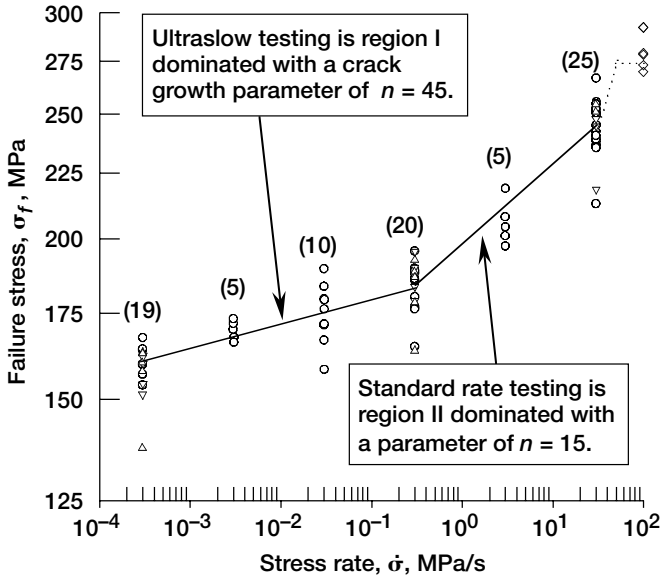

Fracture stress as a function of stress rate for alumina used in a microwave window. The data were generated in accordance with the American Society for Testing and Materials standard test method C1368–97, and at slower rates than required. The ultra-slow-rate data agree with the theory that the slope should change at short failure times. Measurements made with the fast rates recommended in the standard result in a factor of 3 error in the estimated life-prediction parameter n.

References

1. Standard Test Method for Determination of Slow Crack Growth Parameters of Advanced Ceramics by Constant Stress-Rate Flexural Testing at Ambient Temperature. Annual Book of ASTM Standards, ASTM C 1368–97, vol. 15.01, 1998, pp. 688–696.
2. Salem, J.A.; and Jenkins, M.G.: The Effect of Stress Rate on Slow Crack Growth Parameter Estimates. Fracture Testing of Monolithic/Composite Materials, J.A. Salem, G.D. Quinn, and Michael G. Jenkins, eds., ASTM STP–1409, 2002, pp. 213–227.
3. Daily, L.D., et al.: Simulation of High-Average Power Windows for Accelerator Production of Tritium. Proceedings of LINAC98, Chicago, IL, 1998.
4. Salem, J.A.: Standard Test Method for Determination of Slow Crack Growth Parameters of Advanced Ceramics by Constant Stress-Rate Flexural Testing at Ambient Temperature. 2001 Annual Book of ASTM Standards, ASTM C 1368–01, vol. 15.01, 2001, pp. 632–640.

Glenn contact:
Dr. Jonathan Salem, 216–433–3313, Jonathan.A.Salem@nasa.gov

Author: Dr. Jonathan A. Salem

Headquarters program office: OAT

Programs/Projects:
HOTPC, Space Act

Special recognition:
American Society for Testing and Materials Award of Merit

Life-Prediction Parameters of Sapphire Determined for the Design of a Space Station Combustion Facility Window

To characterize the stress corrosion parameters and predict the life of a sapphire window being considered for use in the International Space Station's Fluids and Combustion Facility, researchers at the NASA Glenn Research Center conducted stress corrosion tests, fracture toughness tests, and reliability analyses, as shown in the figures. Standardized test methods, developed and updated by the author under the auspices of American Society for Testing and Materials, were employed. One interesting finding is that sapphire exhibits a susceptibility to stress corrosion in water similar to that of glass. In addition to generating the stress corrosion parameters and fracture toughness data, closed-form expressions for the variances of the crack growth parameters were derived. The expressions allow confidence bands to be easily placed on life predictions of ceramic components.

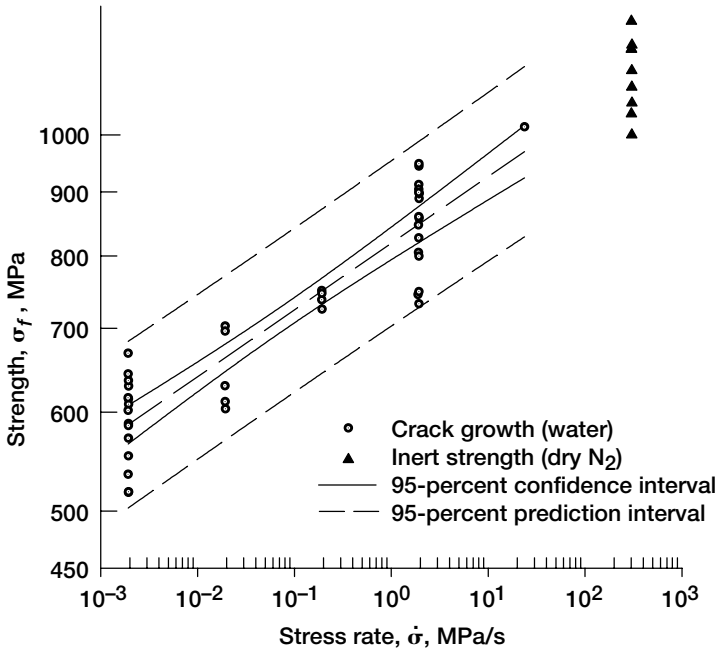

Fracture stress as a function of stress rate for sapphire tested in distilled water and dry nitrogen in accordance with the American Society for Testing and Materials standard test method C1368–01. The decreasing fracture strength with decreasing stress rate indicates time-dependent material degradation due to stress corrosion.

Brittle materials such as sapphire and quartz are required for windows in a variety of applications such as the Fluids and Combustion Facility. To minimize the launch weight of such facilities, researchers must design the windows to be as lightweight as possible. The safe use of lightweight, brittle windows in structural applications is limited by two factors: low fracture toughness and slow crack growth, or stress corrosion. Stress corrosion of these and other optical materials can occur in relatively common environments, such as humid air.

Access to the data has been requested by designers for use in the life prediction of a Northrop Grumman F16 instrument window and a Jet Propulsion Laboratory instrument window. One Space Act Agreement has been formed. Future work includes the measurement of the life of subscale windows.

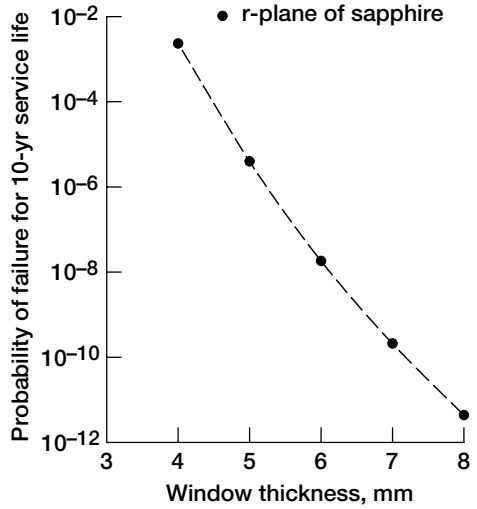

Probability of failure for a sapphire window as a function of the window thickness. The analysis was performed for a 10-yr service life.

Glenn contacts:
Dr. Jonathan Salem, 216–433–3313, Jonathan.A.Salem@nasa.gov; and
Dr. Anthony Calomino, 216–433–3311, Anthony.M.Calomino@nasa.gov

Author: Dr. Jonathan Salem

Headquarters program office: OBPR

Programs/Projects: Microgravity Science, ISS

Special recognition: ASTM Award of Appreciation

Time-Dependent Material Data Essential for the Durability Analysis of Composite Flywheels Provided by Compressive Experiments

Successful spaceflight operations require onboard power management systems that reliably achieve mission objectives for a minimal launch weight. Because of their high specific energies and potential for reduced maintenance and logistics, composite flywheels (see the figure below) are an attractive alternative to electrochemical batteries. The Rotor Durability Team, which comprises members from the Ohio Aerospace Institute (OAI) and the NASA Glenn Research Center, completed a program of elevated temperature testing at Glenn's Life Prediction Branch's Fatigue Laboratory. The experiments provided unique design data essential to the safety and durability of flywheel energy storage systems for the International Space Station and other manned spaceflight applications. Analysis of the experimental data (ref. 1) demonstrated that the compressive stress relaxation of composite flywheel rotor material is significantly greater than the commonly available tensile stress relaxation data. Durability analysis of compression preloaded flywheel rotors is required for accurate safe-life predictions for use in the International Space Station.

The high operational speeds and specific energies of composite flywheel rotors are attained by using the substantial load-carrying capacity of carbon fibers wound in the hoop direction. In contrast, the long-term durability of such rotors may actually be limited by the time- and temperature-dependent behavior of the polymer constituent of the composite: the epoxy matrix. The behavior of the epoxy dominates the uniaxial properties transverse to the fiber in the radial direction and the shear properties. This proposition was investigated for the prototypical rotor material, IM7/8552. Flat-filament wound panels were manufactured by the University of Texas Center for Electro Mechanics using the same process as for composite rotors. Coupon specimens, sectioned normal and parallel to the winding axis, were tested in compression and tension at room temperature, 95 °C, and 135 °C for strain rates from 5×10^{-6}/s to 5×10^{-3}/s. Creep and stress relaxation testing ran 72 hr, followed by a 72-hr recovery. Time-, temperature-, and load-sign-(compressive/tensile) dependent effects were significant transverse to the fiber. Under a fixed deformation of –0.5 percent strain for 72 hr, compressive stresses relaxed 16.4 percent at 135 °C and 13 percent at 95 °C. Tensile stresses relaxed only 7 percent in 72 hr at 135 °C for 0.5 percent strain. The graph on the next page shows the remarkable difference between the tensile and compressive stress relaxation response.

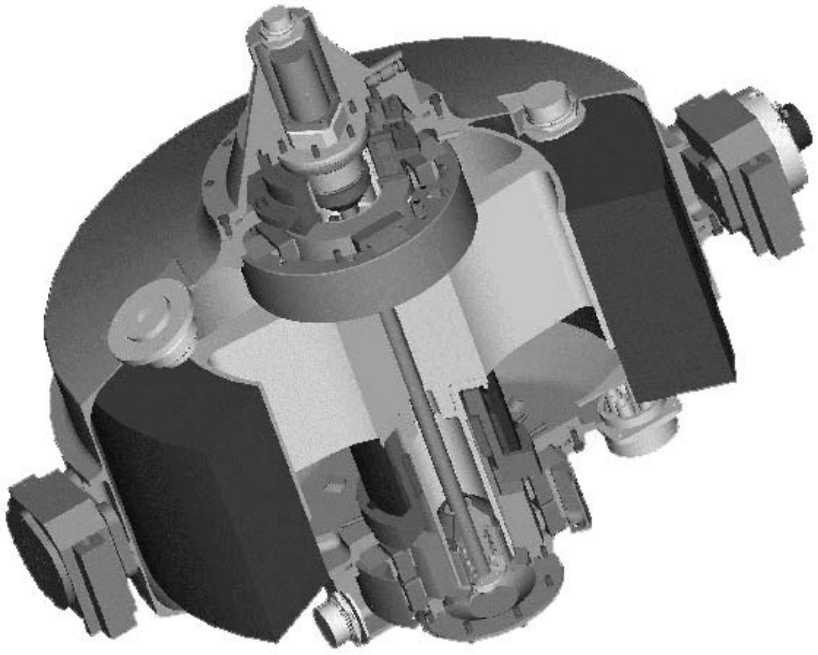

Filament-wound composite flywheel rotor for space applications.

In conclusion, the definition of a linear hereditary material response and the application of Boltzman's principle of superposition to describe the behavior observed here is problematic if not intractable. Undoubtedly, microstuctural analysis including the influence of residual stresses due to processing will be needed to resolve the observed paradoxes. Within the scope of these experiments, uniaxial compressive stress relaxation data may be used to bound the amount of relaxation with the time of radial preload stresses in flywheel rotors. These experimental results are now being used in simulations of the

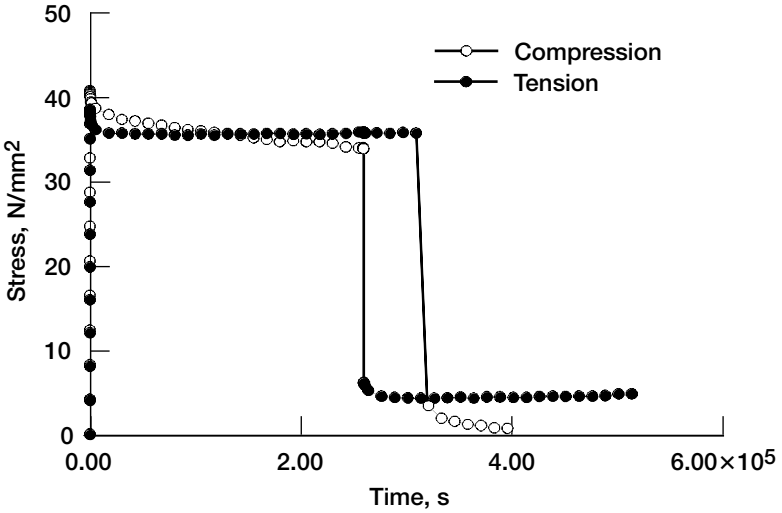

Comparison of the absolute compressive and tensile stress relaxation response at 135 °C at a constant applied strain of ±0.5 percent.

long-term performance of composite rotors (ref. 2), demonstrating the importance and implications of having the appropriate material representation when predicting the durability of current and future rotor designs.

References

1. Thesken, J.C., et al.: Time-Temperature Dependent Response of Filament Wound Composites for Flywheel Rotors. Composite Materials: Testing and Design Fourteenth Volume, ASTM STP–1436, C.E. Bakis, ed., ASTM International, West Conshohocken, PA, To be published in 2003.
2. Saleeb, A.F.; Arnold, S.M.; and Al-Zoubi, N.R.: A Study of Time Dependent and Anisotropic Effects on the Deformation Response of Two Flywheel Rotor Designs. Composite Materials: Testing and Design Fourteenth Volume, ASTM STP–1436, C.E. Bakis, ed., ASTM International, West Conshohocken, PA, To be published in 2003.

Ohio Aerospace Institute (OAI) contact:
Dr. John C. Thesken, 216–433–3012, John.C.Thesken@grc.nasa.gov

Glenn contacts:
Dr. Cheryl L. Bowman, 216–433–8462, Cheryl.L.Bowman@nasa.gov; and Dr. Steven M. Arnold, 216–433–3334, Steven.M.Arnold@nasa.gov

Authors:
Dr. John C. Thesken, Dr. Cheryl L. Bowman, and Dr. Steven M. Arnold

Headquarters program office: OAT

Programs/Projects:
Propulsion and Power, RSL, ISS

Special recognition:
2002 Space Flight Awareness Team Award given for outstanding support given to the Rotor Safe Life Program for developing a basic understanding of time-dependent behavior of preloaded composite flywheel rotors for the International Space Station.

Particulate Titanium Matrix Composites Tested—Show Promise for Space Propulsion Applications

New manufacturing technologies can now produce uniformly distributed particle-strengthened titanium matrix composites (TMCs) at lower cost than many types of continuous-fiber composites. The photomicrograph on the next page shows one such TMC. The innovative process results in near-final-shape components having a material stiffness up to 26-percent greater than that of components made with conventional titanium materials. This benefit is achieved with no significant increase in the weight of the component. The improved mechanical performance and low-cost manufacturing capability motivated a review of particulate-reinforced metal composite technology as a way to lower the cost and weight of space-access propulsion systems.

Focusing on the elevated-temperature properties of titanium alloy Ti-6Al-4V as the matrix material, researchers at the NASA Glenn Research Center conducted experiments to verify the improved performance of the alloy containing 10 wt% of ceramic titanium carbide (TiC) particles. The appropriate blend of metal and ceramic powder underwent a series of cold and hot isostatic pressing procedures to yield bar stock. A set of round dog-bone specimens was manufactured from a small sample of the bars. The TMC material proved to have good machinability at this particle concentration as there was no difficulty in producing high-quality specimens.

Tensile and low-cycle fatigue testing was done at 427 °C, a benchmark test temperature common to several previous titanium test programs. At

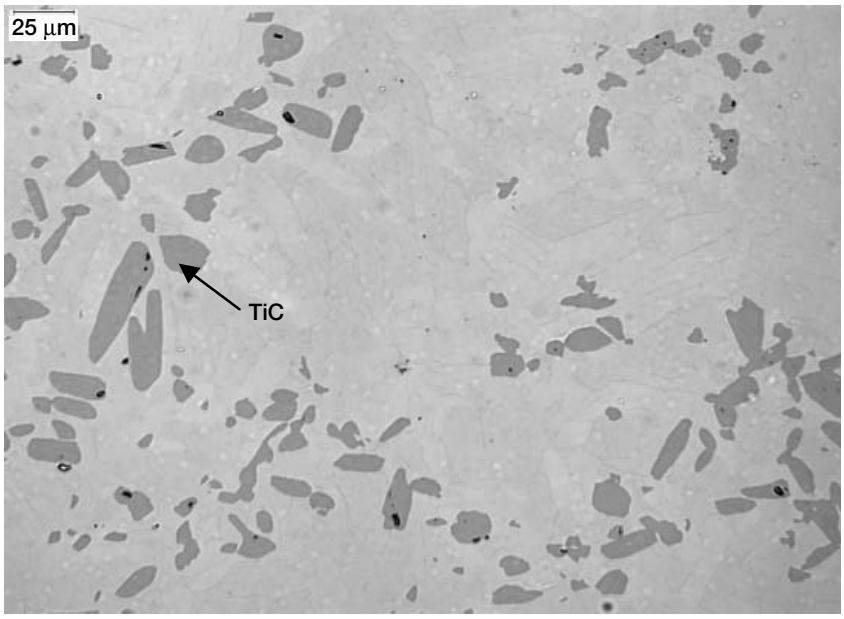

Photomicrograph showing the distribution of titanium carbide particles in a matrix of titanium alloy, Ti-6Al-4V.

the relatively low particle concentrations used in these tests, the material stiffness of the TMC was improved 19 percent over that of the plain Ti-6Al-4V alloy when tested at 427 °C. As the stress-strain curve in the graph shows, the yield strength and tensile strength of the composite are 23- and 14-percent greater than those of the plain alloy. However, the composite's greater strength is offset by a ductility reduced by one-fifth and a fatigue life reduced by one-third of the plain alloy's property. This is expected because the ceramic particles act as stress risers in the matrix material. Although operational life is reduced relative to the unreinforced material, it is noteworthy that low-cycle fatigue at 1-percent strain range does not degrade the composite's superior material stiffness. At these temperature levels and for stiffness-driven applications, particulate-reinforced TMC is an attractive alternative to other lightweight materials, such as aluminum matrix composites and carbon-fiber-reinforced polymers. The completion of the exploratory study resulted in the selection of 10 wt% titanium carbide composite CermeTi (Dynamet Technology, Inc., Burlington, MA) for more rigorous evaluation of its deformation, long-term fatigue, and durability.

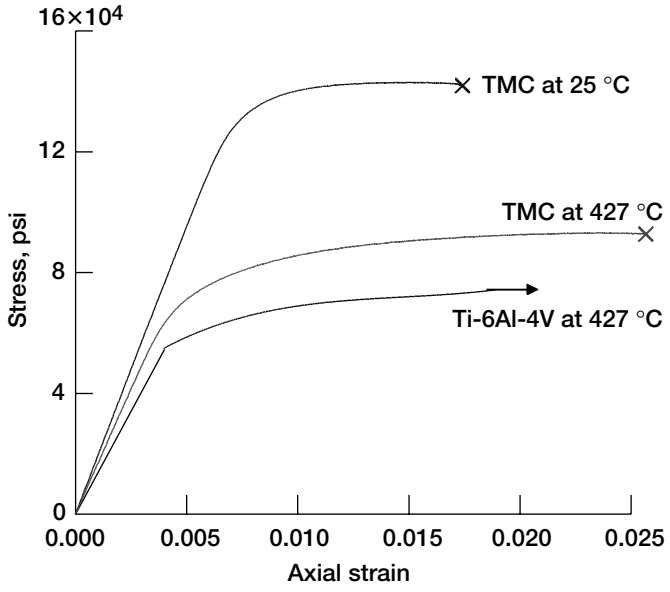

The stress-strain response of titanium matrix composite at room temperature and 427 °C in comparison to Ti-6Al-4V alloy at 427 °C. Strain rate, 0.001.

In this regard, an experimental program has been designed including tensile and compression static, creep and relaxation, and low- and high-cycle fatigue studies. The specimen geometries were selected to investigate the influence of lateral constraint and notch sensitivity. The literature indicates that metal matrix composites perform well in high-cycle fatigue and that reduced lateral constraint may also be beneficial. Verification of such characteristics would be useful to propulsion system designers seeking to employ this material in future applications. Finally, the resulting data will also support the development of a fundamental understanding of metal matrix composites operating at elevated temperatures and should lead to the development of a constitutive model for these materials.

Ohio Aerospace Institute (OAI) contact:
Dr. John C. Thesken, 216–433–3012
John.C.Thesken@grc.nasa.gov

Glenn contacts:
Dr. Bradley A. Lerch, 216–433–5522,
Bradley.A.Lerch@nasa.gov; and
Dr. Steven M. Arnold, 216–433–3334,
Steven.M.Arnold@nasa.gov

Authors:
Dr. John C. Thesken, Dr. Bradley A. Lerch, and Dr. Steven M. Arnold

Headquarters program office: OAT

Programs/Projects: HOTPC, Gen 3

Unsteady Flowfield in a High-Pressure Turbine Modeled by TURBO

Forced response, or resonant vibrations, in turbomachinery components can cause blades to crack or fail because of the large vibratory blade stresses and subsequent high-cycle fatigue. Forced-response vibrations occur when turbomachinery blades are subjected to periodic excitation at a frequency close to their natural frequency. Rotor blades in a turbine are constantly subjected to periodic excitations when they pass through the spatially nonuniform flowfield created by upstream vanes. Accurate numerical prediction of the unsteady aerodynamics phenomena that cause forced-response vibrations can lead to an improved understanding of the problem and offer potential approaches to reduce or eliminate specific forced-response problems.

The objective of the current work was to validate an unsteady aerodynamics code (named TURBO) for the modeling of the unsteady blade row interactions that can cause forced-response vibrations. The three-dimensional, unsteady, multi-blade-row, Reynolds-averaged Navier-Stokes turbomachinery code named TURBO was used to model a high-pressure turbine stage for which benchmark data were recently acquired under a NASA contract by researchers at the Ohio State University. The test article was an initial design for a high-pressure turbine stage that experienced forced-response vibrations which were eliminated by increasing the axial gap. The data, acquired in a short duration or shock tunnel test facility, included unsteady blade surface pressures and vibratory strains.

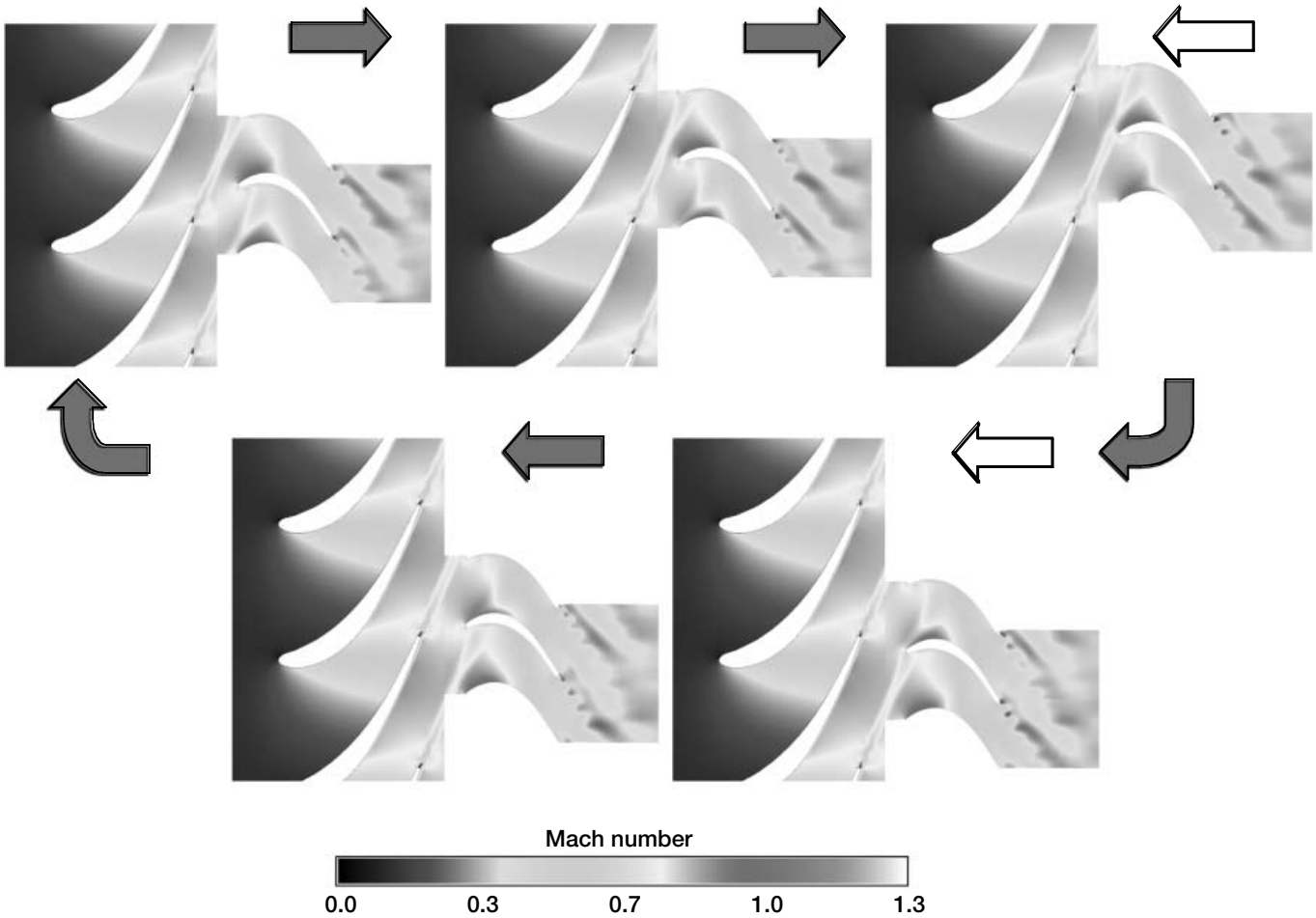

Unsteady flowfield in a high-pressure turbine stage shown as a sequence of five plots of instantaneous Mach number contours. This figure is shown in color in the online version of this article (http://www.grc.nasa.gov/WWW/RT2002/5000/5930bakhle.html).

The unsteady flowfield was computed using the TURBO code for two axial gaps at resonant crossings of modes 2, 3, and 4. Two grids were used to evaluate the effects of spatial discretization. Numerical studies were performed to ensure that the computational results were nearly independent of the choice of numerical input parameters. Unsteady blade surface pressures were compared with data at 50- and 85-percent span, which were the locations of the pressure transducers in the experiment. In addition, plots of the flowfield were prepared to understand how the upstream vane wakes interacted with the downstream rotor (see the figure on the preceding page).

The computational results agreed quite well with the experimental data at both spanwise locations and at the various operating conditions. The mean loading was seen to be higher near the tip than at the midspan location. The trend was reversed for unsteady loading, with the higher unsteady loads occurring at the midspan. A comparison of the surface pressure for small and large gaps showed that the main pressure peak near the leading edge was smaller for the larger axial gap. This work has provided further validation of the TURBO code for unsteady aerodynamic computations of turbomachinery blade rows. The unsteady aerodynamic calculations described here were performed under a grant by a University of Toledo researcher in collaboration with NASA Glenn Research Center and Honeywell researchers.

Reference

1. Bakhle, Milind A., et al.: Calculation and Correlation of the Unsteady Flowfield in a High Pressure Turbine. NASA/TM—2002-211475, 2002. http://gltrs.grc.nasa.gov/cgi-bin/GLTRS/browse.pl?2002/TM-2002-211475.html

University of Toledo contact:
Dr. Milind A. Bakhle, 216–433–6037, Milind.A.Bakhle@grc.nasa.gov

Authors:
Dr. Milind A. Bakhle and Oral Mehmed

Headquarters program office: OAT

Programs/Projects:
Propulsion Systems R&T

High-Frequency Testing of Composite Fan Vanes With Erosion-Resistant Coating Conducted

The mechanical integrity of hard, erosion-resistant coatings were tested using the Structural Dynamics Laboratory at the NASA Glenn Research Center. Under the guidance of Structural Mechanics and Dynamics Branch personnel, fixturing and test procedures were developed at Glenn to simulate engine vibratory conditions on coated polymer-matrix-composite bypass vanes using a slip table in the Structural Dynamics Laboratory. Results from the high-frequency mechanical bench testing, along with concurrent erosion testing of coupons and vanes, provided sufficient confidence to engine-endurance test similarly coated vane segments. The knowledge gained from this program will be applied to the development of oxidation- and erosion-resistant coatings for polymer matrix composite blades and vanes in future advanced turbine engines.

Fan bypass vanes from the AE3007 (Rolls Royce America, Indianapolis, IN) gas turbine engine were coated by Engelhard (Windsor, CT) with compliant bond coatings and hard ceramic coatings. The coatings were developed collaboratively by Glenn and Allison Advanced Development Corporation (AADC)/Rolls Royce America through research sponsored by the High-Temperature Engine Materials Technology Project (HITEMP) and the Higher Operating Temperature Propulsion Components (HOTPC) project. High-cycle fatigue was performed through high-frequency vibratory testing on a shaker table.

Vane resonant frequency modes were surveyed from 50 to 3000 Hz at input loads from 1g to 55g on both uncoated production vanes and vanes with the erosion-resistant coating. Vanes were instrumented with both lightweight accelerometers and strain gauges to establish resonance, mode shape, and strain amplitudes. Two high-frequency dwell conditions were chosen to excite two strain levels: one approaching the vane's maximum allowable design strain and another near the expected maximum strain during engine operation. Six specimens were tested per dwell condition. Pretest and posttest inspections were performed optically at up to ×60 magnification and using a fluorescent-dye penetrant.

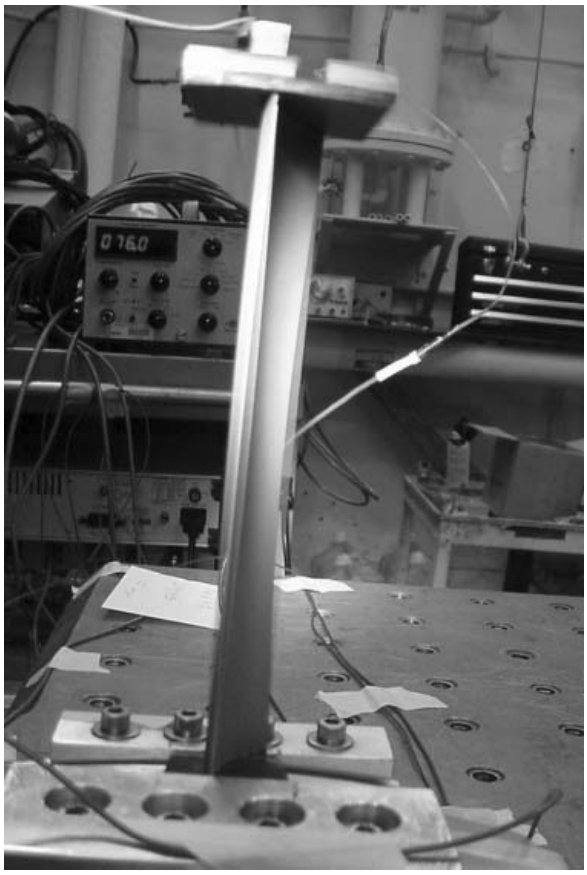

Coated vane undergoing vibratory testing with displacement amplitudes visible in photograph shadowing. Total vane height is approximately 15 cm (6 in.).

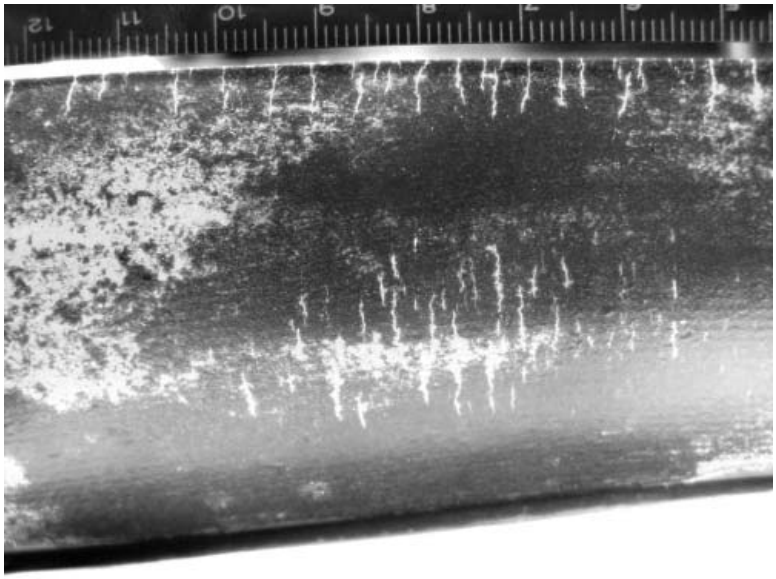

Trailing edge and convex midsection cracks visible with fluorescent dye after 10 million cycles at a strain amplitude of 1300 to 1400 με. The scale marker is in centimeters. Maximum crack length is about 0.7 cm on the edge and 1.8 cm in the midsection.

Accumulation of 10 million cycles at a strain amplitude of two to three times that expected in the engine (approximately 670 Hz and 20g) led to the development of multiple cracks in the coating that were only detectable using fluorescent-dye penetrant inspection. Cracks were prevalent on the trailing edge and on the convex side of the midsection. No cracking or spalling was evident using standard optical inspection at up to ×60 magnification. Further inspection may reveal whether these fine cracks penetrated the coating or were strictly on the surface.

The dwell condition that simulated actual engine conditions produced no obvious surface flaws even after up to 80 million cycles had been accumulated at strain amplitudes produced at approximately 1500 Hz and 45g.

Find out more about this research:

Structural Mechanics & Dynamics Branch:
http://structures.grc.nasa.gov/5930/

Polymers Branch:
http://www.grc.nasa.gov/WWW/MDWeb/5150/Polymers.html

Structural Dynamics Laboratory:
http://www.grc.nasa.gov/WWW/Facilities/int/sdl/

Glenn contacts:
Dr. Cheryl Bowman, 216–433–8462, Cheryl.L.Bowman@nasa.gov;
Dr. James K. Sutter, 216–433–3226, James.K.Sutter@nasa.gov; and
Gail Perusek, 216–433–8729, Gail.P.Perusek@nasa.gov

Authors: Dr. Cheryl L. Bowman, Dr. James K. Sutter, Dr. Subhash Naik, Kim D. Otten, and Gail P. Perusek

Headquarters program office: OAT

Programs/Projects:
Propulsion and Power, HOTPC, HITEMP

Optimal Controller Tested for a Magnetically Suspended Five-Axis Dynamic Spin Rig

NASA Glenn Research Center's Structural Mechanics and Dynamics Branch has developed a fully suspended magnetic bearing system for their Dynamic Spin Rig, which performs vibration tests of turbomachinery blades and components under spinning conditions in a vacuum. Two heteropolar radial magnetic bearings and a thrust magnetic bearing and the associated control system were integrated into the Dynamic Spin Rig to provide magnetic excitation as well as noncontact magnetic suspension of the 35-lb vertical rotor with blades to induce turbomachinery blade vibration (ref. 1).

The new system can provide longer run times at higher speeds and larger vibration amplitudes for rotating blades. Also, it was proven that bearing mechanical life was substantially extended and flexibility was increased in the excitation orientation (direction and phasing).

The first controller we tested for the rotor magnetic suspension was a decentralized proportional-integral-derivative (PID) controller because it was easy to implement. A simple PID controller was sufficient to suppress the vibration amplitude at critical modes. The PID controller had a relatively large control current with high-frequency noise that frequently caused power amplifier and coil burnouts.

Looking for more vibration amplitude suppression and stable rotor orbits at

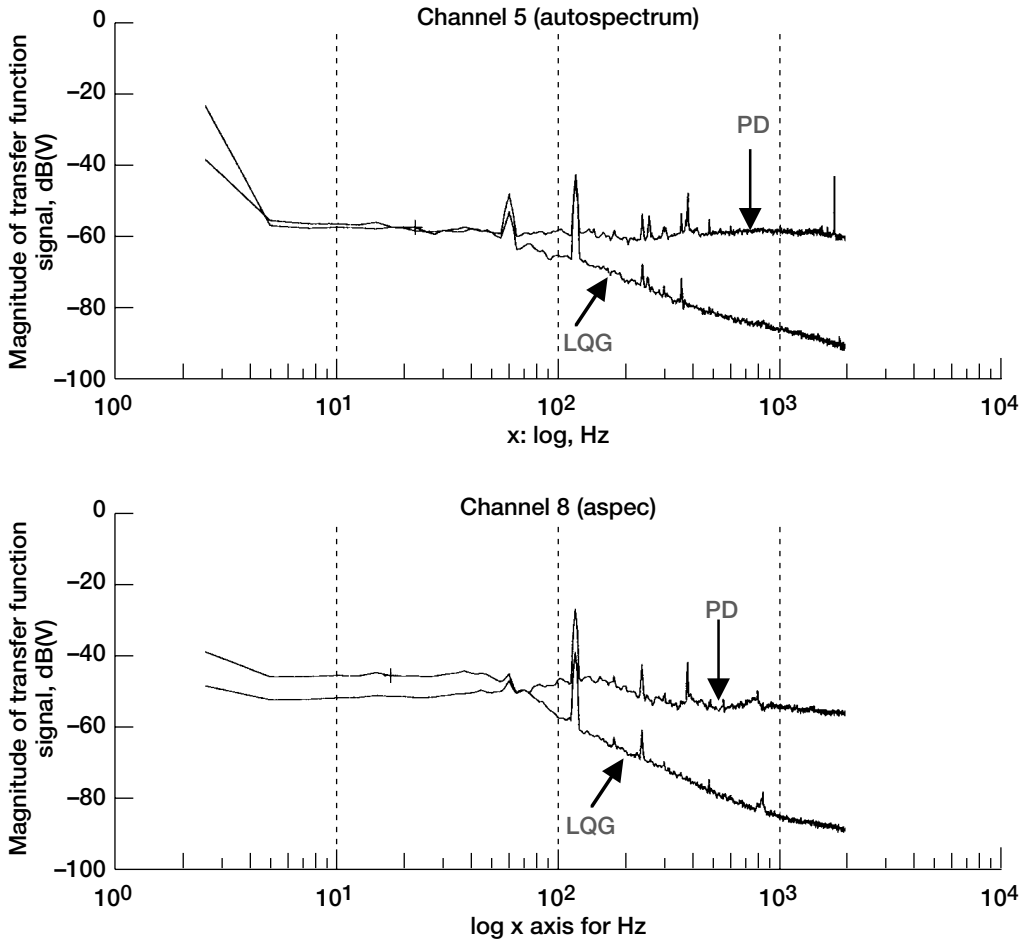

Power spectrum of the upper and lower control currents with the PD controller and LQG regulator, respectively.

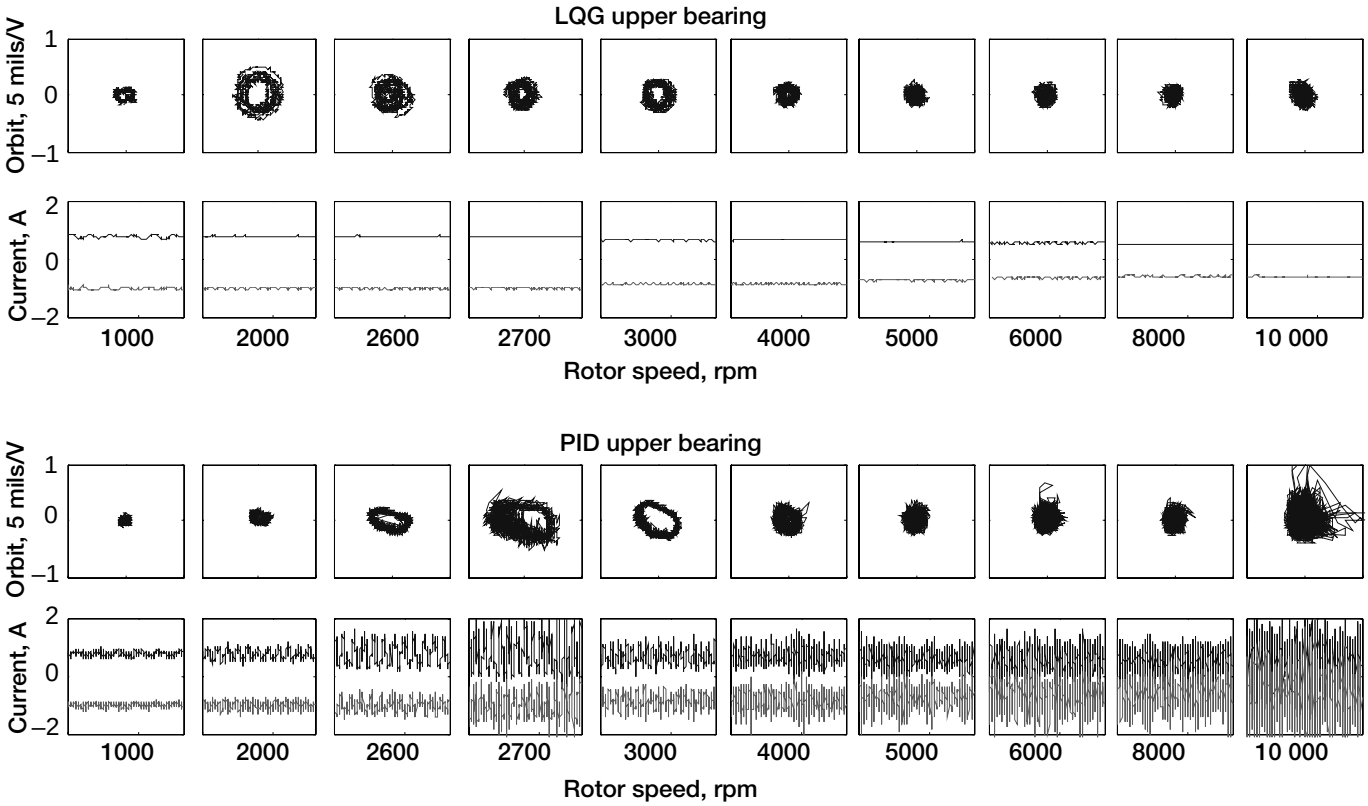

The upper rotor orbits and control currents with the PD controller and LQG regulator.

critical modes, we tested a centralized modal controller, which can inherently control critical modes, including bouncing and tilting modes. The rotor orbit over the operating range was reduced by approximately 20 percent, but control current and noise level remained almost the same as for the proportional-derivative (PD) controller.

Next, we tested a control force integral feedback, where the control force was integrated over time slowly and added to the feedback force output until the time-averaged control force became zero (ref. 2). The test results showed better rotor orbit and control current, but the high-frequency noise level that is crucial to good experimental damping test results still remained.

All the controllers worked well in terms of the rotor orbit (position control) and control current level throughout the operating range up to 10 000 rpm. However, we needed to reduce the high-frequency magnetic bearing control noise, which may couple into the blade vibration measuring circuits and provide poor experimental damping test results. Consequently, we tested a linear quadratic gaussian (LQG) regulator that was developed on the basis of a simple second-order experimental plant model that approximates the rotor and magnetic bearing system. The test results showed that in comparison to the PID controller, the LQG controller reduced rotor orbit by about 50 percent. In addition, it significantly reduced the high-frequency control noise level throughout the operating range (see the graphs on the preceding page). Finally, clean rotor orbits and lower control current were achieved over the operating range (see the figures on this page). Thus, the LQG controller was the best controller to use for damping tests on the new magnetically suspended five-axis Dynamic Spin Rig.

References

1. Choi, Benjamin, et al.: A Comparison Study of Magnetic Bearing Controllers for a Fully Suspended Dynamic Spin Rig. ISMB–8–Paper–0160, 2002.
2. Brown, Gerald V.: DC Control Effort Minimized for Magnetic-Bearing-Supported Shaft. Research and Technology 2000, NASA/TM—2001-210605, 2001, p. 125. http://gltrs.grc.nasa.gov/cgi-bin/GLTRS/browse.pl?2001/TM-2001-210605.html

Glenn contacts:

Dr. Benjamin Choi, 216–433–6040, Benjamin.B.Choi@nasa.gov;
Dr. Dexter Johnson, 216–433–6046, Dexter.Johnson-1@nasa.gov; and
Carlos Morrison, 216–433–8447, Carlos.R.Morrison@nasa.gov

Author: Dr. Benjamin B. Choi

Headquarters program office: OAT

Program/Projects: SEC

Ultra-High-Power-Density Motor Being Developed for Future Aircraft

To support the Revolutionary Aeropropulsion Concept Program, NASA Glenn Research Center's Structural Mechanics and Dynamics Branch is developing a compact, nonpolluting, bearingless electric machine with electric power supplied by fuel cells for future more-electric aircraft. The use of such electric drives for propulsive fans or propellers depends on the successful development of ultra-high-power-density machines that can generate power densities of 50 hp/lb or more, whereas conventional electric machines generate usually 0.2 hp/lb.

One possible candidate for such ultra-high-power-density machines, a round-rotor synchronous machine with an engineering current density as high as 20 000 A/cm^2 was selected to investigate how much torque and power can be produced. A simple synchronous machine model that consists of rotor and stator windings and back-irons was considered first. The model had a sinusoidally distributed winding that produces a sinusoidal distribution of flux *P* poles. Excitation of the rotor winding produced *P* poles of rotor flux, which interacted with the *P* stator poles to produce torque.

This year we made significant contributions to this research:

(1) We conducted a constant tip-speed scaling study for synchronous round-rotor machines. To obtain the specified design and geometry of this high-power-density motor, we had to optimize the design. We analytically verified that Long's contention, "Specific power is mainly a function of rotor surface speed," is approximately correct. At first, we kept the rotor surface speed constant for the scaled-up motors. Then, we increased the gap diameter by integer multiples of its initial value. It was proven that if surface speed, pole pitch, and electrical frequency are held constant, motors with different sizes develop the same power density.

(2) We developed the Electromagnetic Analysis of Synchronous Machines code. This analytical tool and finite element model code uses AnSoft to analyze and optimize the performance of high-power-density synchronous machines (see the figures). This software gives us the basic tools to provide detailed quantitative results and the ability to determine optimal designs for synchronous round-rotor machines. This work showed the feasibility of using this technology for a future more-electric engine, making advances on the Ultra-High Power Density Motor project.

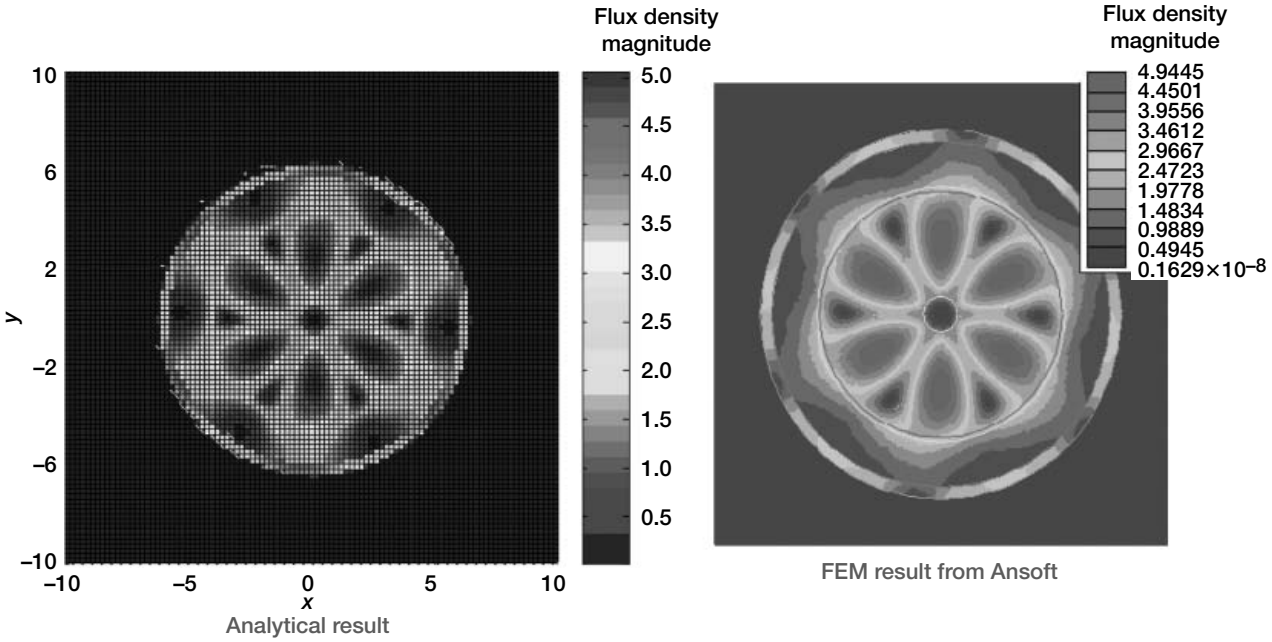

Flux density magnitude of a six-pole analytical model with a 1-cm-thick back-iron[1] (90° phase angle). This figure is shown in color in the online version of this article (http://www.grc.nasa.gov/WWW/RT2002/5000/5930choi2.html).

[1]Stack of thin iron layers to hold coil winding.

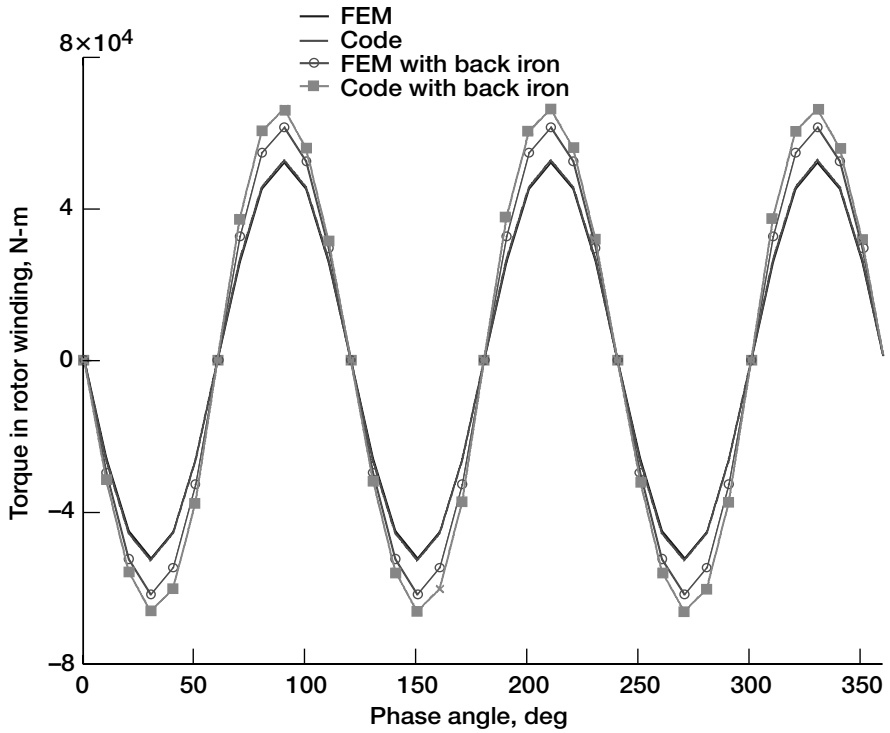

Torque in the six-pole synchronous motor with and without 1-cm-thick stator back-iron (10° increment).

Glen contacts:
Dr. Benjamin Choi, 216–433–6040, Benjamin.B. Choi@nasa.gov; and Gerald V. Brown, 216–433–6047, Gerald.V.Brown@nasa.gov

Author: Dr. Benjamin B. Choi

Headquarters program office: OAT

Program/Projects:
RAC, Ultra-High Power Density Motor

Spin Testing for Durability Began on a Self-Tuning Impact Damper for Turbomachinery Blades

NASA has a program to develop passive damping technology for turbomachinery blade airfoils to reduce blade vibration. Spin tests in flat plates and turbine blades have shown that a self-tuning impact damper being developed is effective. Spin testing completed this year in NASA Glenn Research Center's Dynamic Spin Rig showed as much as a 50-percent reduction in the resonant response of a damper in a Pratt & Whitney turbine blade. We plan to investigate its durability and effectiveness in upcoming spin tests.

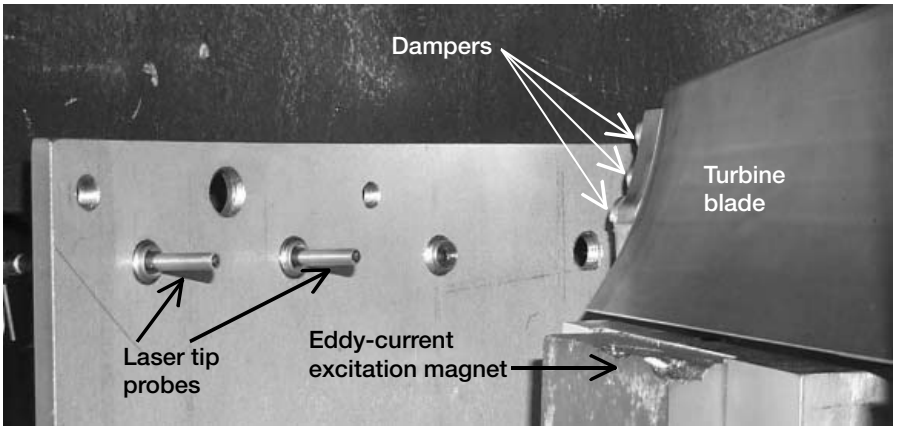

Glenn's Dynamic Spin Facility—Pratt & Whitney turbine blade with self-tuning impact dampers installed at the blade tip.

NASA and Pratt & Whitney will collaborate under a Space Act Agreement to perform spin testing of the impact damper to verify damping effectiveness and damper durability. Pratt & Whitney will provide the turbine blade and damper hardware for the tests. NASA will provide the facility and perform the tests. Effectiveness and durability will be investigated during and after sustained sweeps of rotor speed through resonance. Tests of a platform wedge damper are also planned to compare its effectiveness

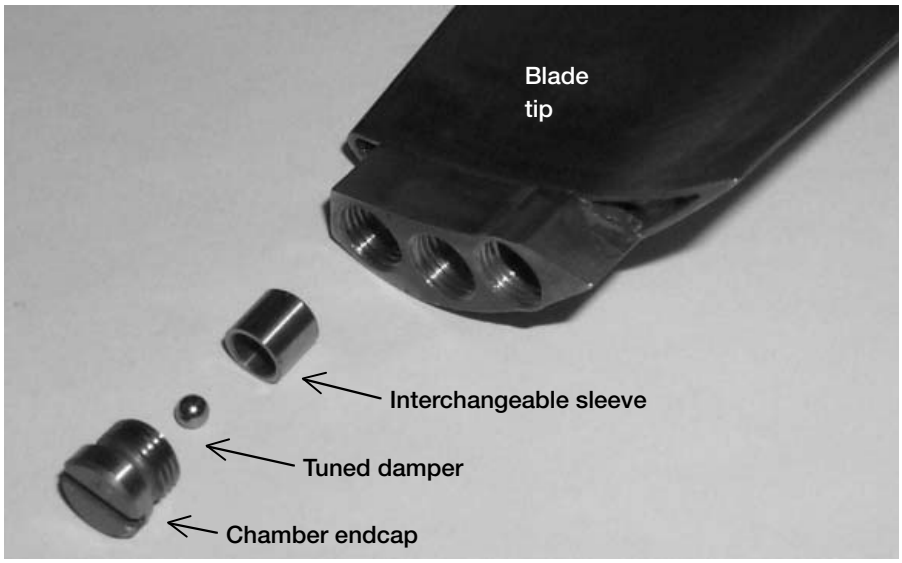

Turbine blade with exploded view of the self-tuning impact damper.

with that of the impact damper. Results from baseline tests without dampers will be used to measure damping effectiveness.

The self-tuning impact damper combines two damping methods—the tuned mass damper and the impact damper. It consists of a ball located within a cavity in the blade. This ball rolls back and forth on a spherical trough under centrifugal load (tuned mass damper) and can strike the walls of the cavity (impact damper). The ball's rolling natural frequency is proportional to the rotor speed and can be designed to follow an engine-order line (integer multiple of rotor speed). Aerodynamic forcing frequencies typically follow these engine-order lines, and a damper tuned to the engine order will most effectively reduce blade vibrations when the resonant frequency equals the engine-order forcing frequency.

This damper has been tested in flat plates and turbine blades in the Dynamic Spin Facility. During testing, a pair of plates or blades rotates in vacuum. Excitation is provided by one of three methods—eddy-current engine-order excitation (ECE), electromechanical shakers, and magnetic bearing excitation. The eddy-current system consists of magnets located circumferentially around the rotor. As a blade passes a magnet, a force is imparted on the blade. The number of magnets used can be varied to change the desired engine order of the excitation. The magnets are remotely raised or lowered to change the magnitude of the force on the blades. The other two methods apply force to the rotating shaft itself at frequencies independent of the rotor speed. During testing, blade vibration is monitored with strain gauges and laser displacement probes.

Bibliography

Duffy, Kirsten P.; Bagley, Ronald L.; and Mehmed, Oral: On a Self-Tuning Impact Vibration Damper for Rotating Turbomachinery. NASA/TM—2000-210215 (AIAA Paper 2000–3100), 2000. http://gltrs.grc.nasa.gov/cgi-bin/GLTRS/browse.pl?2000/TM-2000-210215.html

Duffy, Kirsten P.; Mehmed, Oral; and Johnson, Dexter: Self-Tuning Impact Dampers for Fan and Turbine Blades. Proceedings of the 6th National Turbine Engine High Cycle Fatigue (HCF) Conference. Session 10A: Passive Damping 1. Wright-Patterson AFB, OH, 2001.

University of Toledo contact:
Dr. Kirsten Duffy, 216–433–3880, Kirsten.P.Duffy@grc.nasa.gov

Authors:
Dr. Kirsten P. Duffy and Oral Mehmed

Headquarters program office: OAT

Programs/Projects: SEC

Flywheels Upgraded for Systems Research

With the advent of high-strength composite materials and microelectronics, flywheels are becoming attractive as a means of storing electrical energy. In addition to the high energy density that flywheels provide, other advantages over conventional electrochemical batteries include long life, high reliability, high efficiency, greater operational flexibility, and higher depths of discharge. High pulse energy is another capability that flywheels can provide. These attributes are favorable for satellites as well as terrestrial energy storage applications. In addition to energy storage for satellites, the several flywheels operating concurrently can provide attitude control, thus combine two functions into one system. This translates into significant weight savings.

The NASA Glenn Research Center is involved in the development of this technology for space and terrestrial applications. Glenn is well suited for this research because of its world-class expertise in power electronics design, rotor dynamics, composite material research, magnetic bearings, and motor design and control. Several Glenn organizations are working together on this program. The Structural Mechanics and Dynamics Branch is providing magnetic bearing, controls, and mechanical engineering skills. It is working with the Electrical Systems Development Branch, which has expertise in motors and generators, controls, and avionics systems. Facility support is being provided by the Space Electronic Test Engineering Branch, and the program is being managed by the Space Flight Project Branch.

NASA is funding an Aerospace Flywheel Technology Development Program to design, fabricate, and test the Attitude Control/Energy Storage Experiment (ACESE). Two flywheels will be integrated onto a single power bus and run simultaneously to demonstrate a combined energy storage and 1-degree-of-freedom momentum control system. An algorithm that independently regulates direct-current bus voltage and net torque output will be experimentally demonstrated.

The major tasks completed this year were upgrades of the two flywheel modules to be used for the ACESE demonstration and assembly of the High Energy Flywheel Facility where the testing will be conducted. Both flywheel modules received upgraded avionics, position sensors, and control systems. One module was redesigned to incorporate a higher energy, longer life rotor. These upgrades will enable the system-level test program. The two technology demonstrator flywheel modules will be integrated at Glenn's High Energy Flywheel Facility. This facility consists of an airtable where the modules are mounted and surrounded by a water-containment safety system. This photograph of the setup shows thermal, vacuum, and instrumentation support hardware on the upper platform.

Two-flywheel system on airtable.

The current experiment will be a hardware demonstration of a flywheel system that provides both power bus regulation and single-axis torque and attitude control. The long-term objective is to extend this work to a bus regulation and 3-degree-of-freedom attitude control system representative of a satellite platform.

References

1. Jansen, Ralph H., et al.: Redesign of Glenn Research Center D1 Flywheel Module. NASA/TM—2002-211788, 2002. http://gltrs.grc.nasa.gov/cgi-bin/GLTRS/browse.pl?2002/TM-2002-211788.html
2. Kascak, Peter E., et al.: Single Axis Attitude Control and DC Bus Regulation With Two Flywheels. NASA/TM—2002-211812, 2002. http://gltrs.grc.nasa.gov/cgi-bin/GLTRS/browse.pl?2002/TM-2002-211812.html
3. Dever, Timothy P.; Brown, Gerald V.; and Jansen, Ralph H.: Estimator Based Controller for High Speed Flywheel Magnetic Bearing System. NASA/TM—2002-211795, 2002. http://gltrs.grc.nasa.gov/cgi-bin/GLTRS/browse.pl?2002/TM-2002-211795.html
4. Trase, Larry M.: The Evaluation and Implementation of a Water Containment System to Support Aerospace Flywheel Testing. NASA/TM—2002-211722, 2002. http://gltrs.grc.nasa.gov/cgi-bin/GLTRS/browse.pl?2002/TM-2002-211722.html
5. Kenny, Barbara H.; and Kascak, Peter E.: Sensorless Control of Permanent Magnet Machine for NASA Flywheel Technology Development. NASA/TM—2002-211726, 2002. http://gltrs.grc.nasa.gov/cgi-bin/GLTRS/browse.pl?2002/TM-2002-211726.html
6. Dever, Timothy P., et al.: Evaluation and Improvement of Eddy Current Position Sensors in Magnetically Suspended Flywheel Systems. NASA/CR—2001-211137, 2001. http://gltrs.grc.nasa.gov/cgi-bin/GLTRS/browse.pl?2001/CR-2001-211137.html
7. Kenny, Barbara H., et al.: Advanced Motor Control Test Facility for NASA GRC Flywheel Energy Storage System Technology Development Unit. NASA/TM—2001-210986, 2001. http://gltrs.grc.nasa.gov/cgi-bin/GLTRS/browse.pl?2001/TM-2001-210986.html
8. Kascak, Peter E., et al.: International Space Station Bus Regulation With NASA Glenn Research Center Flywheel Energy Storage System Development Unit. NASA/TM—2001-211138, 2001. http://gltrs.grc.nasa.gov/cgi-bin/GLTRS/browse.pl?2001/TM-2001-211138.html
9. McLallin, Kerry L., et al.: Aerospace Flywheel Technology Development for IPACS Applications. NASA/TM—2001-211093, 2001. http://gltrs.grc.nasa.gov/cgi-bin/GLTRS/browse.pl?2001/TM-2001-211093.html

University of Toledo contact:
Ralph Jansen, 216–433–6038,
Ralph.H.Jansen@grc.nasa.gov

Glenn contact:
Ray Beach, 216–433–5320,
Raymond.F.Beach@nasa.gov

Author: Ralph H. Jansen

Headquarters program office: OAT

Programs/Projects: Energetics, ACESE

Active Blade Vibration Control Being Developed and Tested

Gas turbine engines are currently being designed to have increased performance, lower weight and manufacturing costs, and higher reliability. Consequently, turbomachinery components, such as turbine and compressor blades, have designs that are susceptible to new vibration problems and eventual in-service failure due to high-cycle fatigue. To address this problem, researchers at the NASA Glenn Research Center are developing and testing innovative active blade vibration control concepts. Preliminary results of using an active blade vibration control system, involving a rotor supported by an active magnetic bearing in Glenn's Dynamic Spin Rig, indicate promising results (see the photograph on the next page). Active blade vibration control was achieved using feedback of blade strain gauge signals within the magnetic bearing control loop. The vibration amplitude was reduced substantially (see the graphs). Also, vibration amplitude amplification was demonstrated; this could be used to enhance structural mode identification, if desired. These results were for a nonrotating two-bladed disk. Tests for rotating blades are planned.

Current and future active blade vibration control research is planned to use a fully magnetically suspended rotor and smart materials. For the fully magnetically suspended rotor work, three magnetic bearings (two radial and one axial) will be used as actuators instead of one magnetic bearing. This will allow additional degrees of freedom to be used for control. For the smart materials work, control effectors located on and off the blade will be considered. Piezoelectric materials will be considered for on-the-blade actuation, and actuator

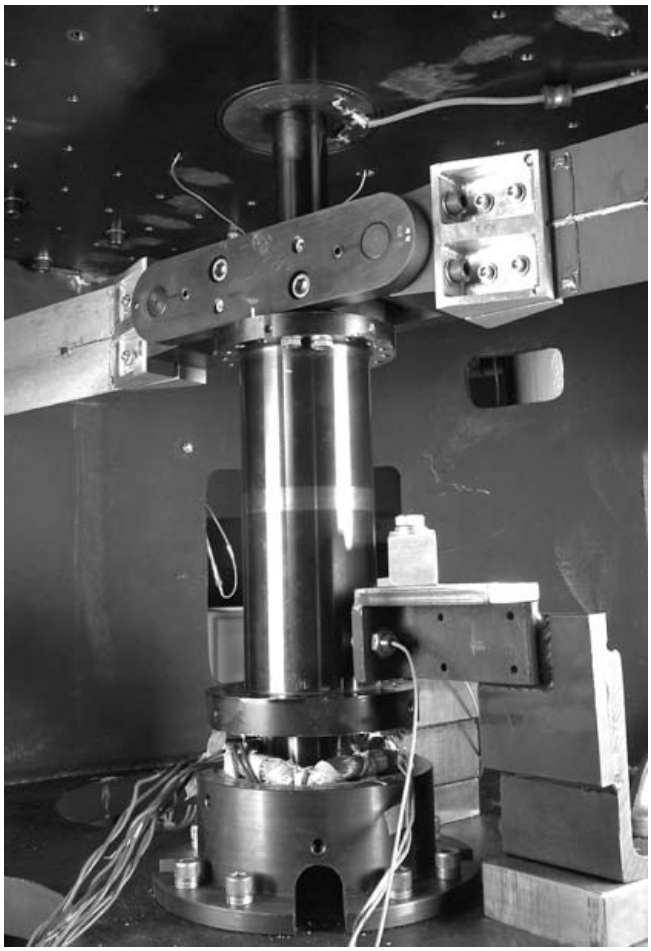

A two-bladed rotor, oriented vertically, which is supported by a radial active magnetic bearing used for active blade vibration control in the NASA Glenn Dynamic Spin Rig facility.

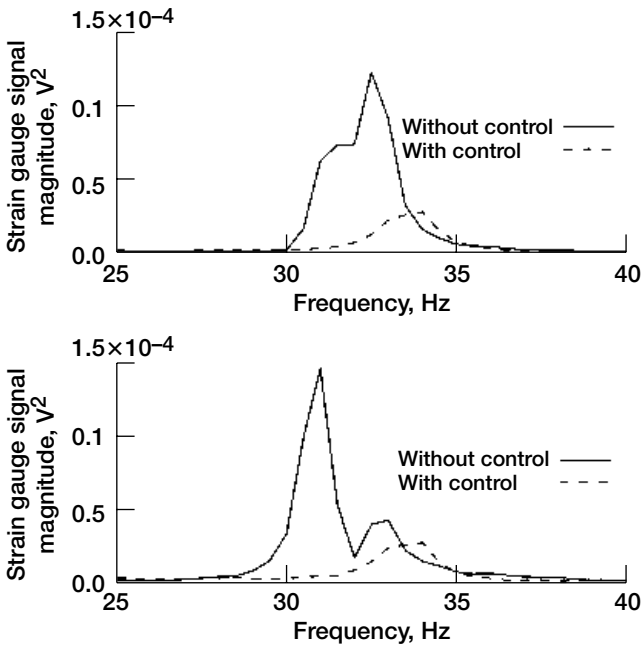

Power spectral density of strain gauge signals for flat plates using the active blade vibration control system with and without strain gauge feedback to the magnetic bearing, for a nonrotating shaft. Top: Blade B. Bottom: Blade A.

placement on a stator vane, or other nearby structure, will be investigated for off-the-blade actuation. Initial work will focus on determining the feasibility of these methods by performing basic analysis and simple experiments involving feedback control. Further development will include a detailed design of the system along with an extensive test and evaluation plan.

Reference

1. Johnson, Dexter; Brown, Gerald V.; and Mehmed, Oral: A Magnetic Suspension and Excitation System for Spin Vibration Testing of Turbomachinery Blades. AIAA Paper 98–1851, 1998.

Find out more about this research:
http://structures.grc.nasa.gov/5930/

Glenn contact:
Dr. Dexter Johnson, 216–433–6046, Dexter.Johnson-1@nasa.gov

Author: Dr. Dexter Johnson

Headquarters program office: OAT

Programs/Projects: SEC

Noninterference Systems Developed for Measuring and Monitoring Rotor Blade Vibrations

In the noninterference measurement of blade vibrations, a laser light beam is transmitted to the rotor blade tips through a single optical fiber, and the reflected light from the blade tips is collected by a receiving fiber-optic bundle and conducted to a photodetector. Transmitting and receiving fibers are integrated in an optical probe that is enclosed in a metal tube which also houses a miniature lens that focuses light on the blade tips. Vibratory blade amplitudes can be deduced from the measurement of the instantaneous time of arrival of the blades and the knowledge of the rotor speed.

The in-house noninterference blade-vibration measurement system was developed in response to requirements to monitor blade vibrations in several tests where conventional strain gauges could not be installed or where there was a need to back up strain gauges should critical gauges fail during the test. These types of measurements are also performed in the aircraft engine industry using proprietary in-house technology.

Two methods of measurement were developed for vibrations that are synchronous with a rotor shaft. One method requires only one sensor; however, it is necessary to continuously record the data while the rotor is being swept through the resonance. In the other method, typically four sensors are employed and the vibratory amplitude is deduced from the data by performing a least square fit to a harmonic function. This method does not require continuous recording of data through the resonance and, therefore, is better suited for monitoring. The single-probe method was tested in the Carl facility at the Wright-Patterson Air Force Base, and the multiple-probe method was tested in NASA Glenn Research Center's Spin Rig facility, which uses permanent magnets to excite synchronous vibrations. Representative results from this test are illustrated in the bar chart.

Nonsynchronous vibrations were measured online during testing of the Quiet High Speed Fan in Glenn's 9- by 15-Foot Low-Speed Wind Tunnel. Three sensors were employed, enabling a reconstruction of the vibratory patterns at the leading and trailing edges at the tip span, as well as a determination of vibratory amplitudes for every blade.

Glenn contact:
Dr. Anatole Kurkov, 216–433–5695, Anatole.P.Kurkov@nasa.gov

Author: Dr. Anatole P. Kurkov

Headquarters program office: OAT

Programs/Projects: UEET, QAT

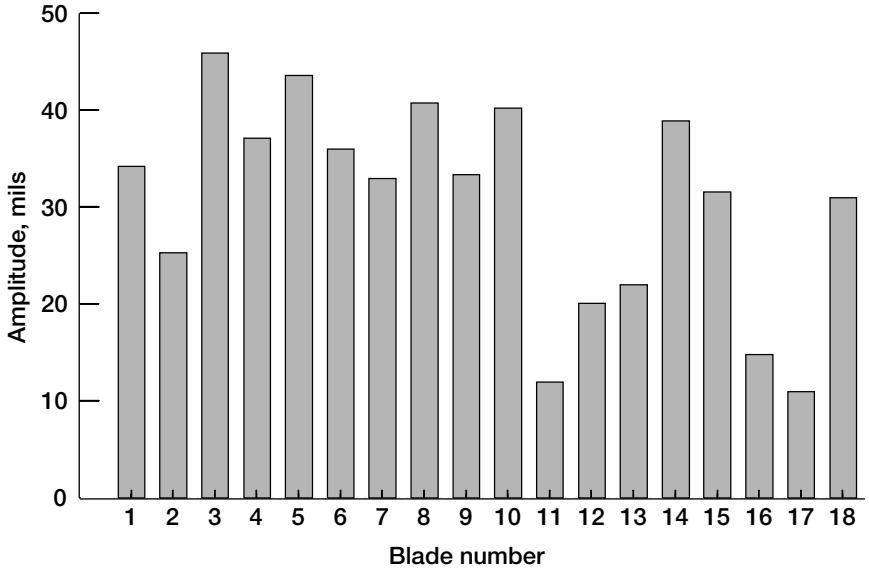

Blade-to-blade resonant amplitude variation for a fan rotor subject to a 5-engine-order excitation.

New Tools Being Developed for Engine-Airframe Blade-Out Structural Simulations

One of the primary concerns of aircraft structure designers is the accurate simulation of the blade-out event. This is required for the aircraft to pass Federal Aviation Administration (FAA) certification and to ensure that the aircraft is safe for operation. Typically, the most severe blade-out occurs when a first-stage fan blade in a high-bypass gas turbine engine is released. Structural loading results from both the impact of the blade onto the containment ring and the subsequent instantaneous unbalance of the rotating components. Reliable simulations of blade-out are required to ensure structural integrity during flight as well as to guarantee successful blade-out certification testing. The loads generated by these analyses are critical to the design teams for several components of the airplane structures including the engine, nacelle, strut, and wing, as well as the aircraft fuselage.

Currently, a collection of simulation tools is used for aircraft structural design. Detailed high-fidelity simulation tools are used to capture the structural loads resulting from blade loss, and then these loads are used as input into an overall system model that includes complete structural models of both the engines and the airframe. The detailed simulation (shown in the figure) includes the time-dependent trajectory of the lost blade and its interactions with the containment structure, and the system simulation includes the lost blade loadings and the interactions between the rotating turbomachinery and the remaining aircraft structural components. General-purpose finite element structural analysis codes are typically used and special provisions are made to include transient effects from the blade loss and rotational effects resulting from the engine's turbomachinery. To develop and validate these new tools with test data, the NASA Glenn Research Center has teamed with GE Aircraft Engines, Pratt & Whitney, Boeing Commercial Aircraft, Rolls-Royce, and MSC.Software.

Detailed blade-fan case interaction model.

Progress to date on this project includes expanding the general-purpose finite element code, NASTRAN, to perform rotordynamic analysis of complete engine-airframe systems. Capabilities that have been implemented into the code are frequency response (windmilling), complex modes (damped critical and whirl speeds), and static analysis (maneuver loads). Future plans include a nonlinear enhancement for blade-out simulation and construction of a test rig to determine blade-case interaction characteristics.

Glenn contacts:
Dr. Charles Lawrence, 216–433–6048, Charles.Lawrence-1@nasa.gov; and Kelly S. Carney, 216–433–2386, Kelly.S.Carney@nasa.gov

Author: Dr. Charles Lawrence

Headquarters Program Office: OAT

Programs/Projects:
Propulsion Systems R&T, Ultra Safe

Experimental and Analytical Studies of Smart Morphing Structures Being Conducted

The development of morphing aeropropulsion structural components offers the potential to significantly improve the performance of existing aircraft engines through the introduction of new inherent capabilities for shape control, vibration damping, noise reduction, health monitoring, and flow manipulation. One of the key factors in the successful development of morphing structures is the maturation of smart materials technologies.

In NASA Glenn Research Center's Structural Mechanics and Dynamics Branch, analytical efforts are ongoing to develop comprehensive finite element models for smart materials to facilitate the experimental characterization of these materials. Finite element studies have been conducted to investigate the impact of stacking and curvature on the force and displacement response of piezoelectric actuators (ref. 1). Experimental studies are also being conducted to characterize a variety of different smart materials in the Smart Materials and Structures Laboratory at the University of Akron under a cooperative agreement. Shape memory alloy actuators have been used to achieve precision position control while reducing energy consumption (ref. 2). Several prototype magnetorheological fluid devices have been developed to investigate the capability to instantaneously damp out motion and to statically hold a position under applied loads. Also, piezoelectric actuators have been successfully used to compensate for thermal distortions generated by film heaters in a composite beam (ref. 3).

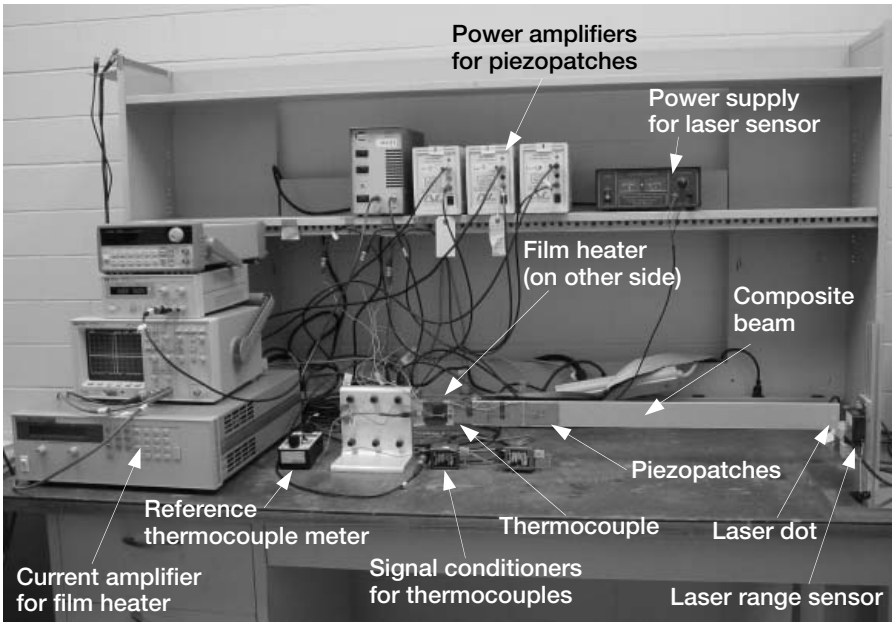

Experimental setup for composite beam with attached piezoelectric actuators subjected to thermal loading.

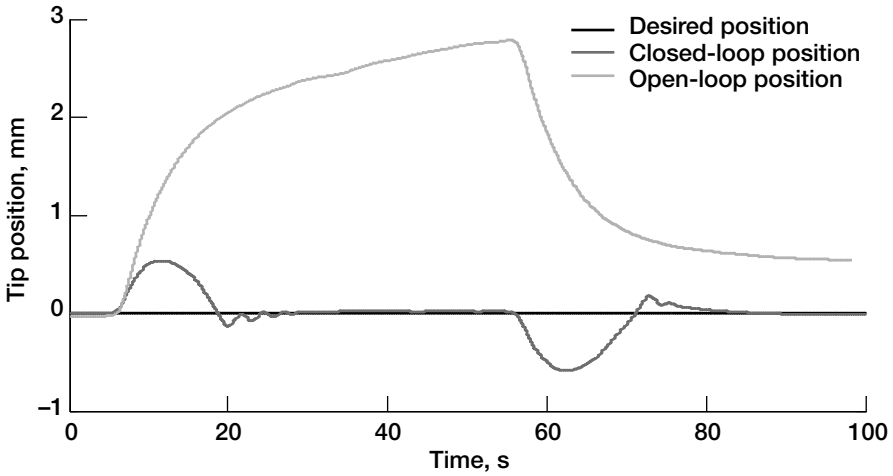

Comparison of the initial thermal deformation at the free end of the beam with the controlled deflection.

The photograph shows the experimental setup for the cantilevered composite beam with attached piezoceramic patches subjected to thermal loadings, along with the instrumentation required to control and acquire data. The graph depicts the corresponding deflection with time near the free end of the beam. The open-loop position indicates the initial thermally induced deformation of the beam, whereas the closed-loop position shows the compensated deformation achieved by activating the piezoceramic actuators. By returning the beam to the original desired position, this research demonstrates the potential use of smart materials for shape control to achieve morphing structures.

References

1. Lee, Ho-Jun: Modeling the Quasi-Static Force-Displacement Response of Curved and Straight Piezoelectric Actuators. AIAA Paper 2002–1549, 2002.
2. Ma, N.; and Song, G.: Control of a Shape Memory Alloy Actuator Using Pulse Width (PW) Modulation. 2002 SPIE International Symposium on Smart Structures and Materials, San Diego, CA, 2002, pp. 348–359.
3. Zhou, X.; Song, G.; and Binienda, W.: Thermal Deformation Compensation of a Composite Beam Using Piezoelectric Actuators. 2002 SPIE International Symposium on Smart Structures and Materials, San Diego, CA, 2002, pp. 334–344.

Glenn contact:
Dr. Ho-Jun Lee, 216–433–3316, Ho-Jun.Lee-1@nasa.gov

Authors: Dr. Ho-Jun Lee and Prof. Gangbing Song

Headquarters program office: OAT

Programs/Projects: RAC

Explicit Finite Element Techniques Used to Characterize Splashdown of the Space Shuttle Solid Rocket Booster Aft Skirt

NASA Glenn Research Center's Structural Mechanics Branch has years of expertise in using explicit finite element methods to predict the outcome of ballistic impact events. Shuttle engineers from the NASA Marshall Space Flight Center and NASA Kennedy Space Flight Center required assistance in assessing the structural loads that a newly proposed thrust vector control system for the space shuttle solid rocket booster (SRB) aft skirt would expect to see during its recovery splashdown.

The new design was to replace existing hydrazine propellant tanks with helium propellant tanks. The intent of this was to eliminate hydrazine, a toxic and hazardous substance, from the system, making it safer from a propellant standpoint. The proposed

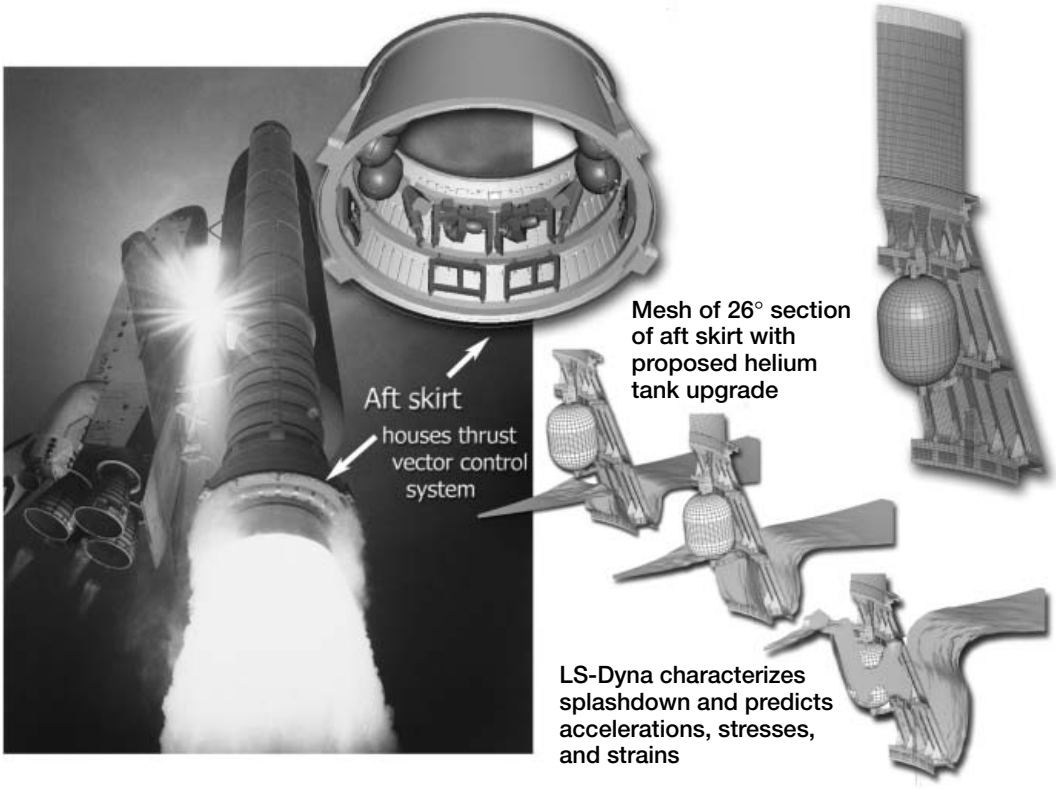

Thrust vector control system located in the aft skirt of the space shuttle SRB, finite element model of proposed helium tank/aft skirt used to analyze water impact, and three representative images of a predicted splashdown event of this model.

helium tanks, however, required nearly six times the volume of hydrazine tanks, resulting in significantly more tank area exposed to water impact during SRB splashdown. It would be crucial to understand what the new impact loads would be as a result of a design change to the thrust vector control before any such change could be implemented to a flight system.

LS-Dyna (Livermore-Software Technology Corp. (LST), Livermore, CA) was employed to perform the analysis, using its multimaterial arbitrary Lagrangian-Eulerian (ALE) methodology to represent water-structure interaction during impact. Impact loads were predicted for the proposed tank upgrades on a 26° section of a full-scale aft skirt, providing insight to the water impact event.

The efforts of this work contribute to the improvement of flight safety for the space shuttles, which is paramount to NASA's strategic mission.

Find out more about this research:
ballistics.grc.nasa.gov

Glenn contact:
Matt Melis, 216–433–3322,
Matthew.E.Melis@nasa.gov

Author: Matthew E. Melis

Headquarters program office: OSMA

Programs/Projects: RLV, AvSP

Analytical Failure Prediction Method Developed for Woven and Braided Composites

Historically, advances in aerospace engine performance and durability have been linked to improvements in materials. Recent developments in ceramic matrix composites (CMCs) have led to increased interest in CMCs to achieve revolutionary gains in engine performance. The use of CMCs promises many advantages for advanced turbomachinery engine development and may be especially beneficial for aerospace engines. The most beneficial aspects of CMC material, may be its ability to maintain strength to over 2500 °F, its internal material damping, and its relatively low density. Ceramic matrix composites reinforced with two-dimensional woven and braided fabric preforms are being considered for NASA's next-generation reusable rocket turbomachinery applications (for example, see the top figure on the next page). However, the architecture of a textile composite is complex, and therefore, the parameters controlling its strength properties are numerous. This necessitates the development of engineering approaches that combine analytical methods with limited testing to provide effective, validated design analyses for the textile composite structures development.

A micromechanics textile composite analysis code has been developed at the NASA Glenn Research Center to predict progressive damage for textile composite structures, especially for brittle material composite systems. The repeating unit cell (RUC) of a textile composite is usually used to represent it (ref. 1). The thermal and mechanical properties of the RUC are considered to be the same as those of the composite. In this study, the micromechanics, the shear lag, and the continuum fracture mechanics models were integrated with a statistical model in the RUC to predict the progressive damage failures of textile composite structures. Textile composite failure is defined as the loss of the loading capability of the RUC, which depends on the stiffness reduction due to material slice (matrix slice and yarn slice) failures and nonlinear material properties. To account for these phenomena in a more accurate manner, we developed a new analysis code to demonstrate the proposed methodologies with comparisons to material test data obtained with carbon-fiber-reinforced silicon carbide matrix plain-weave composites as well as various polymer matrix composites (PMCs) available in the literature for a code validation, and some of the results are presented in reference 2. Good comparisons with a full range of the test data have established the feasibility of the proposed analysis techniques and their ability to model the progressive failure analysis for the textile composite structures, as shown in the graphs on the next page.

References

1. Naik, Rajiv A.; Ifju, Peter G.; and Masters, John E.: Effect of Fiber Architecture Parameters on Deformation Fields and Elastic Moduli of 2-D Braided Composites. J. Comp. Mater., vol. 28, no. 7, 1994, pp. 656–681.
2. Min, J.B.; Shi, Y.; and Card, M.F.: Progressive Failure Analysis Modeling Techniques for Ceramic Matrix Textile Composites. AIAA Paper 2002–1400, 2002.

Glenn contact:
Dr. James B. Min, 216–433–2587,
James.B.Min@nasa.gov

Author: Dr. James B. Min

Headquarters program office: OAT

Programs/Projects:
RLV, UEET, TBCC, RBCC, ASTP

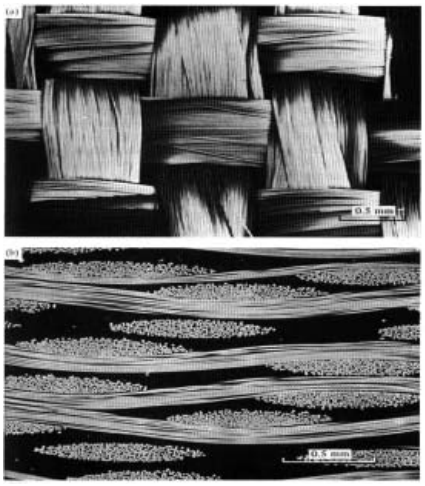

Woven structure

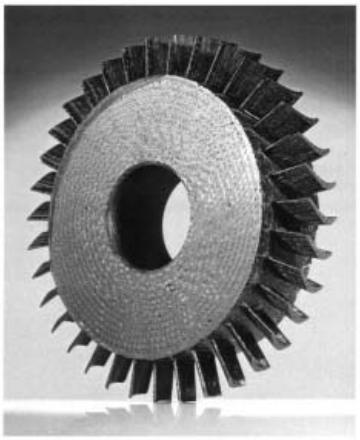

Integrally braided turbine blisk

Rocket exit cone

Integrally braided stator

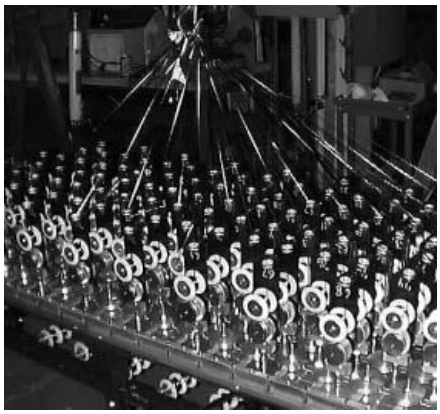

Two- and three-dimensional woven/braiding equipment

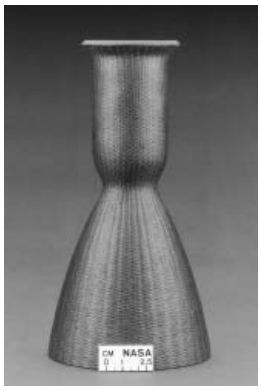

Combustion components

Examples of textile composite components.

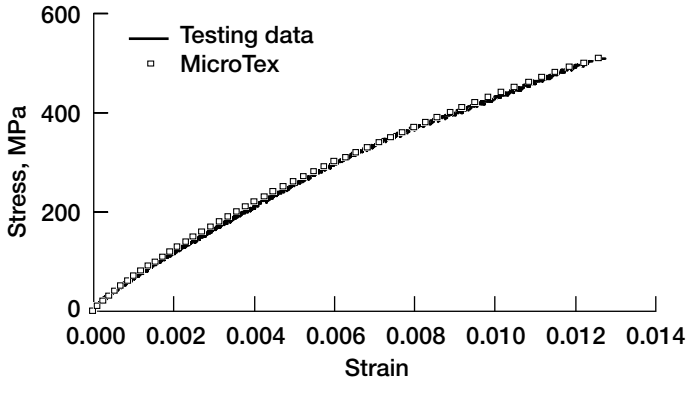

Stress-strain for [0°/90°] C/SiC plain-weave composite.

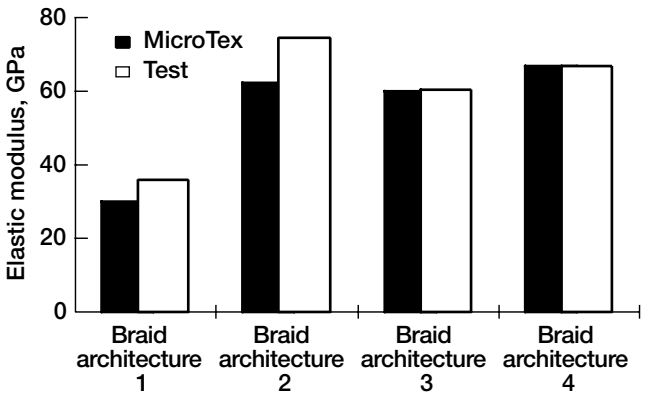

Comparison of elastic modulus for four different braided architectures.

Dynamic Spin Rig Upgraded With a Five-Axis-Controlled Three-Magnetic-Bearing Support System With Forward Excitation

The NASA Glenn Research Center Dynamic Spin Rig is used for experimental evaluation of vibration analysis methods and dynamic characteristics for rotating systems (ref. 1). Measurements are made while rotors are spun and vibrated in a vacuum chamber. The rig has been upgraded with a new active magnetic bearing rotor support and excitation system. This design is expected to provide operational improvements over the existing rig. The rig will be able to be operated in either the old or new configuration.

In the old configuration, two ball bearings support the vertical shaft of the rig, with the test article located between the bearings. Because the bearings operate in a vacuum, lubrication is limited to grease. This limits bearing life and speed. In addition, the old configuration employs two voice-coil electromagnetic shakers to apply oscillatory axial forces or transverse moments to the rotor shaft through a thrust bearing. The excitation amplitudes that can be imparted to the test article with this system are not adequate for components that are highly damped. It is expected that the new design will overcome these limitations.

A preliminary upgrade of the Dynamic Spin Rig (ref. 2) incorporated a single heteropolar radial active magnetic bearing, which allows for both magnetic excitation and suspension of the rotor. The magnetic bearing replaced the lower mechanical ball bearing and gave improved operations. Results from that upgrade have been used in building a total magnetically suspended rotor (see the engineering drawing of the rig on the next page). The new design, called the Five-Axis Three Magnetic Bearing Dynamic Spin Rig, has five independent axes of controlled motion. There is an *x*-axis and a *y*-axis translation at each upper and lower magnetic radial bearing, as well as a *z*-axis translation at the magnetic thrust bearing. Both radial bearings are heteropolar. Simultaneously energizing the bearings (refs. 3 and 4) fully levitates the rotor. This rig design allows for higher excitation amplitudes (by virtue of full rotor suspension, which permits larger rotor translation and tilt displacements) than are achievable with the older rig configuration. At the time of this writing, the rig was operated up to 10 000 rpm with an unbladed rotor. For a detailed description of the rig, see reference 5.

References

1. Brown, G.V., et al.: Lewis Research Center Spin Rig and Its Use in Vibration Analysis of Rotating Systems. NASA TP–2304, 1984.
2. Johnson, Dexter; Brown, Gerald V.; and Mehmed, Oral: A Magnetic Suspension and Excitation System for Spin Vibration Testing of Turbomachinery Blades. NASA/TM—1998-206976, 1998.
3. Morrison, Carlos R.: A Comprehensive C++ Controller for a Magnetically Supported Vertical Rotor, 1.0. NASA/TM—2001-210701, 2001. http://gltrs.grc.nasa.gov/cgi-bin/GLTRS/browse.pl?2001/TM-2001-210701.html
4. Choi, Benjamin, et al.: A Comparison Study of Magnetic Bearing Controllers for a Fully Suspended Dynamic Spin Rig. ISMB–8–Paper 0160, Proceedings of the 8th International Symposium on Magnetic Bearings, Mito, Japan, 2002, pp. 387–392.
5. Morrison, Carlos R., et al: A Fully Suspended Five-Axis Three-Magnetic-Bearing Dynamic Spin Rig. To be published as a NASA TP, 2003.

Glenn contacts:
Carlos R. Morrison, 216–433–8447, Carlos.R.Morrison@nasa.gov;
Dr. Dexter Johnson, 216–433–6046, Dexter.Johnson-1@nasa.gov;
Andrew Provenza, 216–433–6025, Andrew.J.Provenza@nasa.gov; and
Dr. Benjamin Choi, 216–433–6040, Benjamin.B.Choi@nasa.gov

QSS contact:
Timothy Czaruk, 216–433–3296, Timothy.M.Czaruk@nasa.gov

University of Toledo contact:
Ralph Jansen, 216–433–2191, Ralph.H.Jansen@grc.nasa.gov

U.S. Army, Vehicle Technology Directorate at Glenn contact:
Gerald Montague, 216–433–6252, Gerald.T.Montague@grc.nasa.gov

Authors:
Carlos R. Morrison and Oral Mehmed

Headquarters program office: OAT

Programs/Projects: SEC

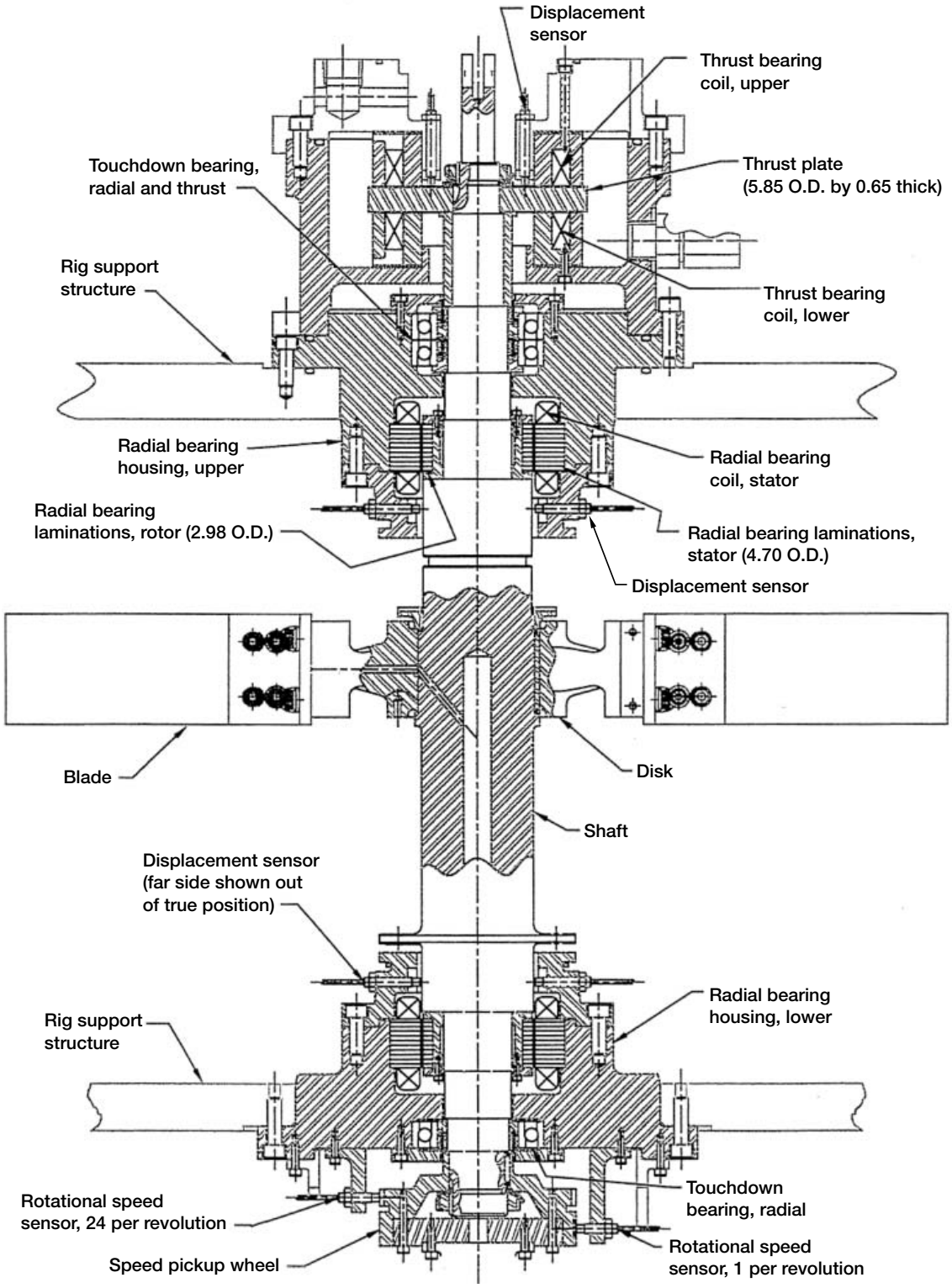

Glenn's upgraded Five-Axis Three Magnetic Bearing Dynamic Spin Rig. All dimensions are given in inches. O.D., outer diameter.

Neural Network and Regression Methods Demonstrated in the Design Optimization of a Subsonic Aircraft

The neural network and regression methods of NASA Glenn Research Center's COMETBOARDS design optimization testbed were used to generate approximate analysis and design models for a subsonic aircraft operating at Mach 0.85 cruise speed. The analytical model is defined by nine design variables: wing aspect ratio, engine thrust, wing area, sweep angle, chord-thickness ratio, turbine temperature, pressure ratio, bypass ratio, fan pressure; and eight response parameters: weight, landing velocity, takeoff and landing field lengths, approach thrust, overall efficiency, and compressor pressure and temperature. The variables were adjusted to optimally balance the engines to the airframe. The solution strategy included a sensitivity model and the soft analysis model. Researchers generated the sensitivity model by training the approximators to predict an optimum design. The trained neural network predicted all response variables, within 5-percent error. This was reduced to 1 percent by the regression method.

The soft analysis model was developed to replace aircraft analysis as the reanalyzer in design optimization. Soft models have been generated for a neural network method, a regression method, and a hybrid method obtained by combining the approximators. The performance of the models is graphed for aircraft weight versus thrust as well as for wing area and turbine temperature. The regression method followed the analytical solution with little error. The neural network exhibited 5-percent maximum error over all parameters. Performance of the hybrid method was intermediate in comparison to the individual approximators. Error in the response variable is smaller than that shown in the figure because of a distortion scale factor. The overall performance of the approximators was considered to be satisfactory because aircraft analysis with NASA Langley Research Center's FLOPS (Flight Optimization System) code is a synthesis of diverse disciplines: weight estimation, aerodynamic analysis, engine cycle analysis, propulsion data interpolation, mission performance, airfield length for landing and takeoff, noise footprint, and others.

Glenn contact:
Dale A. Hopkins, 216–433–3260, Dale.A.Hopkins@nasa.gov

Ohio Aerospace Institute (OAI) contact:
Dr. Surya N. Patnaik, 216–433–5916, Surya.N.Patnaik@grc.nasa.gov

Authors: Dale A. Hopkins, Thomas M. Lavelle, and Dr. Surya N. Patnaik

Headquarter program office: OAT

Program/Projects:
Propulsion Systems R&T

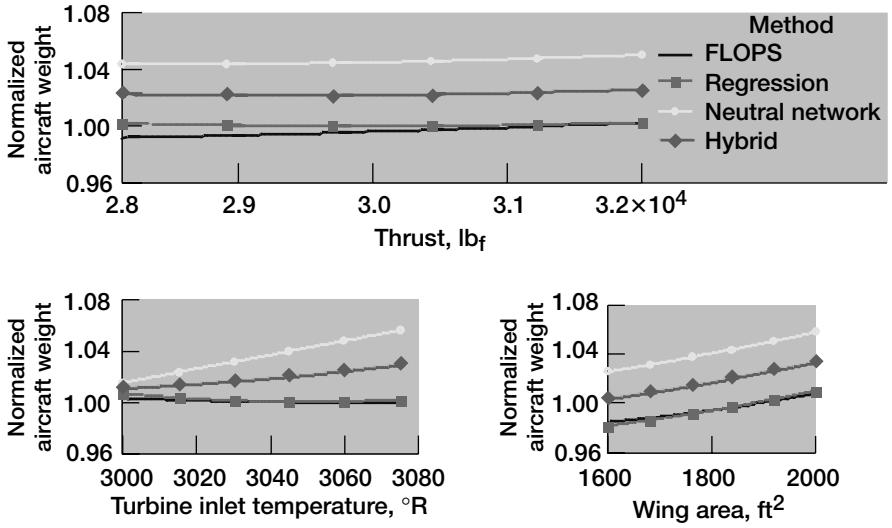

Performance of neural network and regression methods for a subsonic aircraft. Top: Normalized aircraft weight versus thrust. Bottom left: Weight versus turbine inlet temperature. Bottom right: Weight versus wing area.

Magnetic Suspension Being Developed for Future Lube-Free Turbomachinery Application

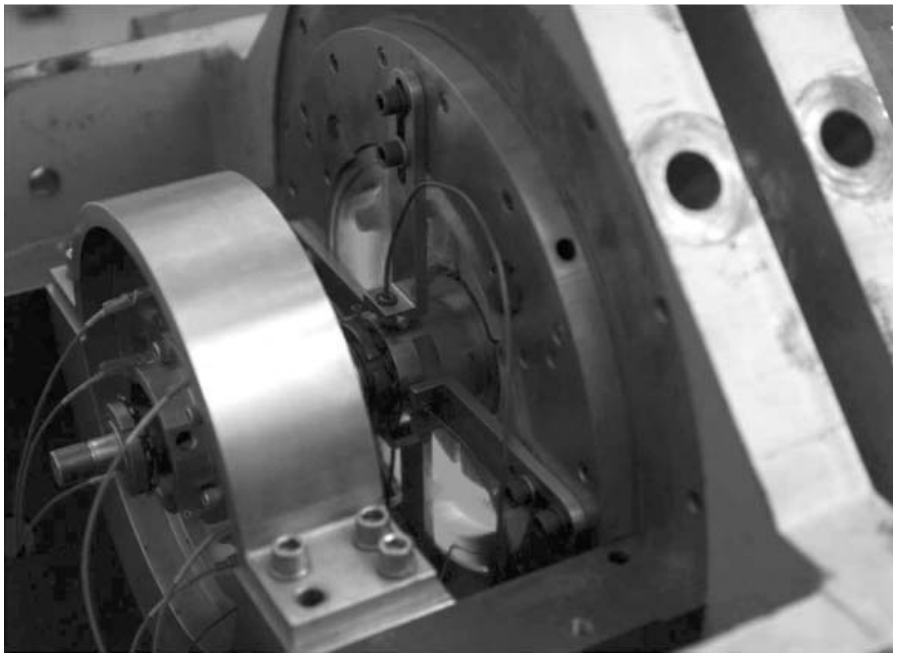

Glenn's third-generation radial magnetic bearing at 1000 °F.

The NASA Glenn Research Center, the U.S. Army, Texas A&M University, and other industrial partners are continuing to work together to develop magnetic suspension technology to withstand the harsh environmental conditions inside current and future turbomachinery. In fiscal year 2002, our third-generation radial magnetic bearing successfully controlled rotor motion while at 1000 °F (540 °C) and 20 000 rpm. The ability to command the rotor's position while spinning at this speed was also demonstrated. Future work is planned to include radial bearing tests to 1100 °F (593 °C) and 30 000 rpm. In fiscal year 2003, we plan to test a high-temperature thrust bearing.

This third-generation radial magnetic bearing was designed specifically to operate at 1000 °F with high force production. The stator design includes six individual C-cores that slide into a common back-iron. The modular nature of the stator allows for improved winding of the poles with specially insulated silver wire.

High-temperature eddy-current probes are used to measure rotor position. Centrifugal and thermal growth are compensated for by summing probes on opposite sides of the rotor on each axis. Currently, only two independent axes are used in the control; however, this bearing can be controlled along three axes to provide redundancy. A proportional-integral-derivative (PID) controller, rolled off at 400 Hz, was used to provide levitation and control. This controller was written in Simulink and compiled to run on a power-PC-based digital-signal-processing system. The control loop time was 25 μs. Tri-state pulse width modulators were used to provide alternating-current power to the stator coils.

Open-loop experimental force and power measurements were also recorded at temperatures up to 1000 °F and rotor speeds up to 15 000 rpm. The experimentally measured force produced by a single C-core using 22 A was 600 lb (2.67 kN) at room temperature and 380 lb (1.69 kN) at 1000 °F. Results of testing under rotating conditions showed that rotor speed has a negligible effect on the bearing's load capacity. A single C-core required approximately 340 W of power to generate 190 lb (8.45 kN) of magnetic force at 1000 °F. However, lower force and higher power at elevated temperatures were due primarily to a larger air gap caused by different component heating rates—they were not due to magnetic material property degradation. Analytical thermal calculations showed that the air gap could have been at least 28-percent larger at 1000 °F.

References

1. Provenza, A., et al.: High Temperature Characterization of a Magnetic Bearing for Turbomachinery. ASME Paper GT2003–38870, Proceedings of ASME/IGTI Turbo Expo 2003, Power for Land, Sea & Air, Atlanta, GA, June 16–19, 2003.
2. Minihan, Thomas, et al.: Fail Safe, High Temperature Magnetic Bearings. ASME GT–2002–30595, 2002.

U.S. Army, Vehicle Technology Directorate at Glenn contact:
Gerald T. Montague, 216–433–6252, Gerald.T.Montague@grc.nasa.gov

Glenn contact:
Andrew J. Provenza, 216–433–6025, Andrew.J.Provenza@nasa.gov

Author: Andrew J. Provenza

Headquarters program office: OAT

Programs/Projects:
SEC, TBCC, IHPTET, VAATE

Probabilistic Aeroelastic Analysis Developed for Turbomachinery Components

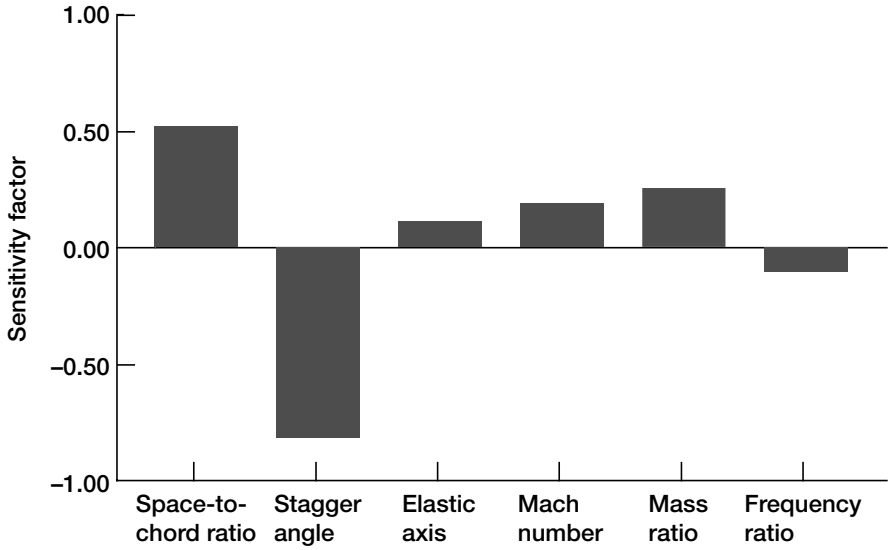

Sensitivity factors of damping (probability level 0.978).

Aeroelastic analyses for advanced turbomachines are being developed for use at the NASA Glenn Research Center and industry. However, these analyses at present are used for turbomachinery design with uncertainties accounted for by using safety factors. This approach may lead to overly conservative designs, thereby reducing the potential of designing higher efficiency engines. An integration of the deterministic aeroelastic analysis methods with probabilistic analysis methods offers the potential to design efficient engines with fewer aeroelastic problems and to make a quantum leap toward designing safe reliable engines.

In this research, probabilistic analysis is integrated with aeroelastic analysis: (1) to determine the parameters that most affect the aeroelastic characteristics (forced response and stability) of a turbomachine component such as a fan, compressor, or turbine and (2) to give the acceptable standard deviation on the design parameters for an aeroelastically stable system. The approach taken is to combine the aeroelastic analysis of the MISER (MIStuned Engine Response) code with the FPI (fast probability integration) code. The role of MISER is to provide the functional relationships that tie the structural and aerodynamic parameters (the primitive variables) to the forced response amplitudes and stability eigenvalues (the response properties). The role of FPI is to perform probabilistic analyses by utilizing the response properties generated by MISER. The results are a probability density function for the response properties. The probabilistic sensitivities of the response variables to uncertainty in primitive variables are obtained as a byproduct of the FPI technique.

The combined analysis of aeroelastic and probabilistic analysis is applied to a 12-bladed cascade vibrating in bending and torsion. Out of the total 11 design parameters, 6 are considered as having probabilistic variation. The six parameters are space-to-chord ratio (SBYC), stagger angle (GAMA), elastic axis (ELAXS), Mach number (MACH), mass ratio (MASSR), and frequency ratio (WHWB). The cascade is considered to be in subsonic flow with Mach 0.7. The results of the probabilistic aeroelastic analysis are the probability density function of predicted aerodynamic damping and frequency for flutter and the response amplitudes for forced response.

The bar chart to the left shows the design variables that affect the aerodynamic damping. It can be seen from the figure that the space-to-chord ratio and the stagger angle affect the aerodynamic damping most.

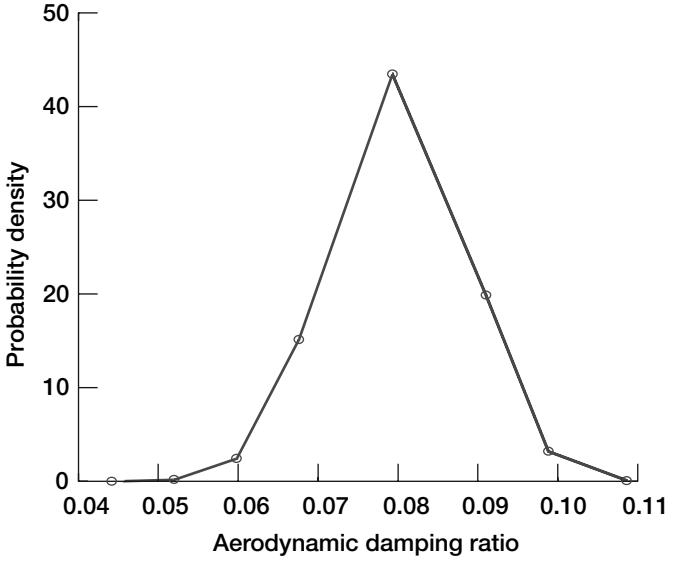

Probability density function of damping, torsion mode; mean, 0.0787; standard deviation, 0.0078.

The graph on the preceding page shows the probability density function of aerodynamic damping for the torsion mode. It shows that the aerodynamic damping has a mean value of about 0.08 and a range of 0.05 to 0.11. The results of the bar chart reveal that reducing the scatter of the space-to-chord ratio and the stagger angle give the highest payoff in reducing the scatter range (standard deviation) of aerodynamic damping. The probabilistic aeroelastic calculations described here were performed under a NASA grant by University of Toledo researchers in collaboration with Glenn researchers.

University of Toledo contacts:
Dr. T.S.R. Reddy, 216–433–6083, Tondapu.S.Reddy@grc.nasa.gov; and
Dr. Subodh K. Mital, 216–433–3261, Subodh.K.Mital@grc.nasa.gov

Glenn contacts:
Dr. Shantaram S. Pai , 216–433–3255, Shantaram.S.Pai@nasa.gov; and
George L. Stefko, 216–433–3920, George.L.Stefko@nasa.gov

Authors: Dr. T.S.R. Reddy, Dr. Subodh K. Mital, George L. Stefko, and Dr. Shantaram S. Pai

Headquarters program office: OAT

Programs/Projects:
Propulsion Systems R&T

Fast-Running Aeroelastic Code Based on Unsteady Linearized Aerodynamic Solver Developed

The NASA Glenn Research Center has been developing aeroelastic analyses for turbomachines for use by NASA and industry. An aeroelastic analysis consists of a structural dynamic model, an unsteady aerodynamic model, and a procedure to couple the two models. The structural models are well developed. Hence, most of the development for the aeroelastic analysis of turbomachines has involved adapting and using unsteady aerodynamic models.

Two methods are used in developing unsteady aerodynamic analysis procedures for the flutter and forced response of turbomachines: (1) the time domain method and (2) the frequency domain method. Codes based on time domain methods require considerable computational time and, hence, cannot be used during the design process. Frequency domain methods eliminate the time dependence by assuming harmonic motion and, hence, require less computational time. Early frequency domain analyses methods neglected the important physics of steady loading on the analyses for simplicity. A fast-running unsteady aerodynamic code, LINFLUX, which includes steady loading and is based on the frequency domain method, has been modified for flutter and response calculations.

LINFLUX solves unsteady linearized Euler equations for calculating the unsteady aerodynamic forces on the blades, starting from a steady nonlinear aerodynamic solution. First, we obtained a steady aerodynamic solution for a given flow condition using the nonlinear unsteady aerodynamic code TURBO. A blade vibration analysis was done to determine the frequencies and mode shapes of the vibrating blades, and an interface code was used to convert the steady aerodynamic solution to a form required by LINFLUX. A preprocessor was used to interpolate the mode shapes from the structural dynamic mesh onto the computational dynamics mesh. Then, we used LINFLUX to calculate the unsteady aerodynamic forces for a given mode, frequency, and phase angle. A post-processor read these unsteady pressures and calculated the generalized aerodynamic forces, eigenvalues, and response amplitudes. The eigenvalues determine the flutter frequency and damping.

As a test case, the flutter of a helical fan was calculated with LINFLUX and compared with calculations from TURBO–AE, a nonlinear time domain code, and from ASTROP2, a code based on linear unsteady aerodynamics.

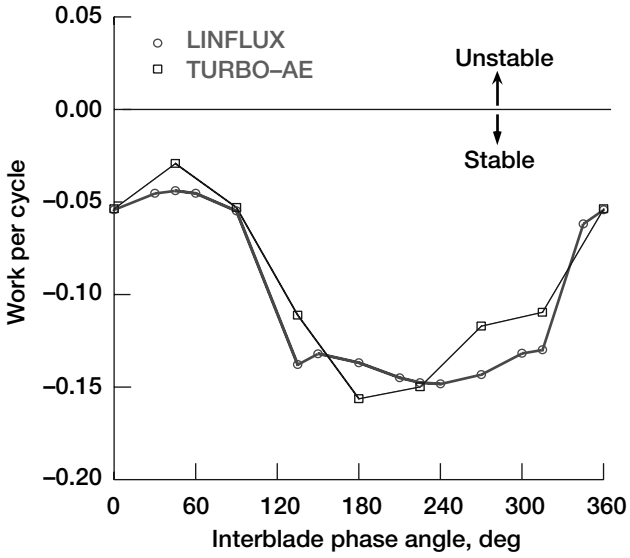

Work per cycle versus interblade phase angle for the pitching motion of a helical fan.

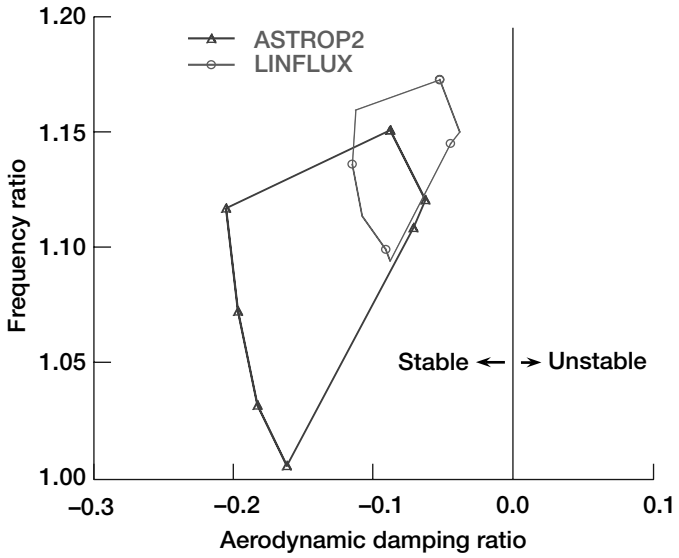

Root locus plot showing frequency versus aerodynamic damping for the second mode of a helical fan.

The graph on the left shows the work done per cycle for the pitching mode calculated by LINFLUX and TURBO–AE. The LINFLUX calculations show a very good comparison with TURBO–AE calculations.

The graph on the right shows the eigenvalues calculated for a helical fan. The calculations were plotted as frequency versus damping for the second mode. As seen from the figure, the predictions made with LINFLUX agree well with those made with ASTROP2.

The LINFLUX code was 6 to 7 times faster than the nonlinear time-domain code and can be used in the initial design phase. The aeroelastic development calculations described here were performed under a NASA grant by University of Toledo researchers in collaboration with Glenn researchers.

University of Toledo contacts:
Dr. T.S.R. Reddy, 216–433–6083, Tondapu.S.Reddy@grc.nasa.gov; and Dr. Milind A. Bakhle, 216–433–6037, Milind.A.Bakhle@grc.nasa.gov

Authors:
Dr. T.S.R. Reddy, Dr. Milind A. Bakhle, Oral Mehmed, and Prof. T. Keith, Jr.

Headquarters program office: OAT

Programs/Projects:
Propulsion Systems R&T

Forward-Swept Fan Flutter Calculated Using the TURBO Code

Flutter, a self-excited dynamic instability arising because of fluid structure interaction, can be a significant design problem for rotor blades in gas turbines. Blade shapes influenced by noise-reduction requirements increase the likelihood of flutter in modern blade designs. Validated numerical methods provide designers an invaluable tool to calculate and avoid the flutter instability during the design phase. Toward this objective, a flutter analysis code, TURBO, was developed and validated by researchers from the NASA Glenn Research Center and other researchers working under grants and contracts with Glenn. The TURBO code, which is based on unsteady three-dimensional Reynolds-averaged Navier-Stokes equations was used to calculate the observed flutter of a forward-swept fan. The forward-swept experimental fan, designed to reduce noise, showed flutter at part-speed conditions during wind tunnel tests. The forward-swept experimental fan shown in the photograph on the next page consisted of 22 forward-swept inserted blades. The steady performance of the fan was mapped first at three different speed lines. Then, we calculated flutter by calculating the work done by the fluid on the rotor blades for the three speed lines. The blades were prescribed a harmonic motion at the natural frequency, mode shape, and

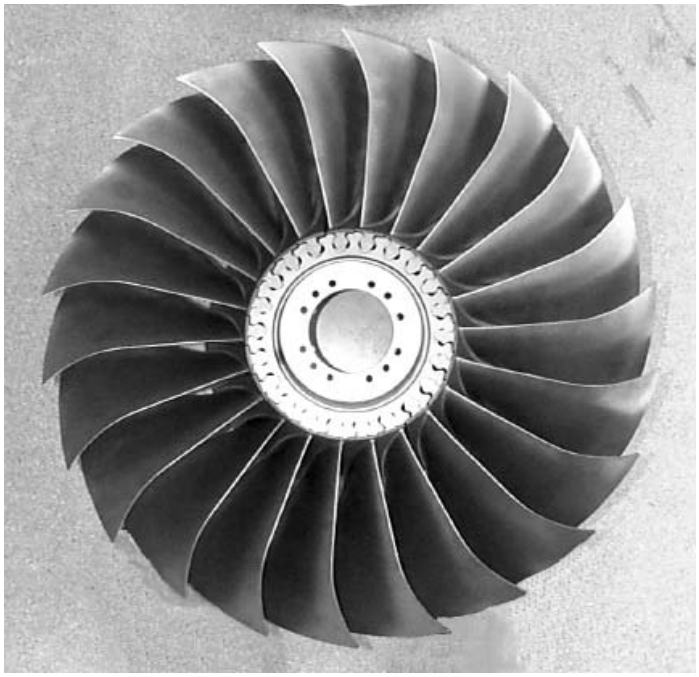

Forward-swept fan.

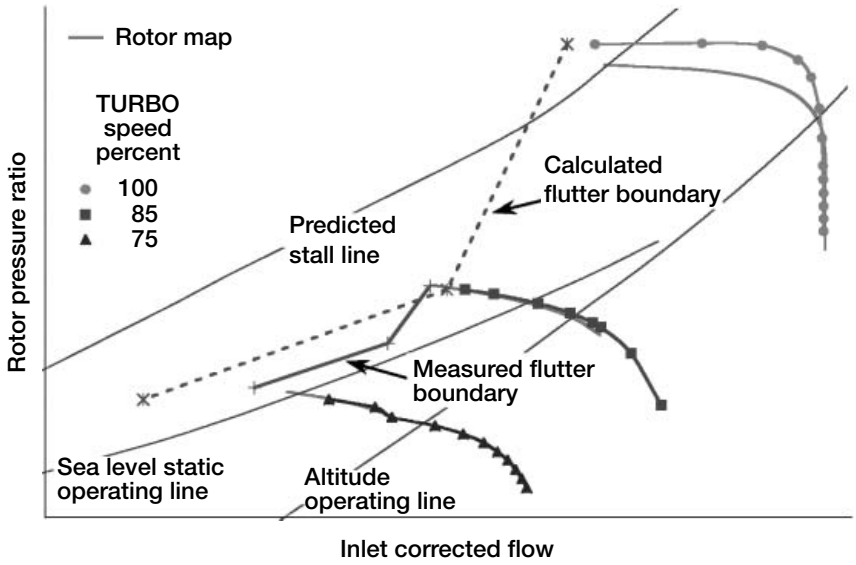

Comparison of calculated flutter boundary and performance for the forward-swept fan with experimental data.

nodal diameter of interest. The work done on the blade by the fluid over one cycle of vibration was converted to a more meaningful damping value referred to as aerodynamic damping. A negative aerodynamic damping implies a dynamically unstable blade, or blade with flutter. The aerodynamic damping was calculated at a minimum of two operating points on a given speed line. The flutter point was then calculated as the mass flow point where the aerodynamic damping value went to zero.

The results obtained for three different speed lines are shown in the graph. The steady performance and the calculated and observed flutter points are also shown in this figure. The flutter was observed for a two-nodal diameter forward traveling wave in the first natural mode. The calculated flutter point also corresponds to the first natural mode and the two-nodal-diameter pattern. Very good correlation was found between the analysis and measurements. The code correctly identified the observed flutter and the characteristics of the flutter. Several parametric studies were also carried out to better understand the flutter behavior. During the study, we found that the effect of variations in inflow and exit boundary conditions, tip gap, and vibration amplitude was limited and did not strongly affect the calculated flutter point. We also found that for operating conditions where flutter was dictated by presence of a shock wave, an inviscid analysis gave results qualitatively similar to viscous analysis. Thus, the inviscid analysis could be used successfully in a design environment for screening the designs. A more rigorous viscous analysis could then be calculated at critical points identified by the inviscid analysis. Both the viscous and the inviscid analyses with the TURBO code are currently being used to redesign the forward-swept fan to be flutter free.

University of Toledo contacts:
Dr. Rakesh Srivastava, 216–433–6045, Rakesh.Srivastava@grc.nasa.gov, and Dr. Milind A. Bakhle, 216–433–6037, Milind.A.Bakhle@grc.nasa.gov

Glenn contact:
George L. Stefko, 216–433–3920, George.L.Stefko@nasa.gov

Authors:
Dr. Rakesh Srivastava, Dr. Milind A. Bakhle, and George L. Stefko

Headquarters program office: OAT

Programs/Projects: QAT

Influence of Shock Wave on the Flutter Behavior of Fan Blades Investigated

Modern fan designs have blades with forward sweep; a lean, thin cross section; and a wide chord to improve performance and reduce noise. These geometric features coupled with the presence of a shock wave can lead to flutter instability. Flutter is a self-excited dynamic instability arising because of fluid-structure interaction, which causes the energy from the surrounding fluid to be extracted by the vibrating structure. An in-flight occurrence of flutter could be catastrophic and is a significant design issue for rotor blades in gas turbines. Understanding the flutter behavior and the influence of flow features on flutter will lead to a better and safer design. An aeroelastic analysis code, TURBO, has been developed and validated for flutter calculations at the NASA Glenn Research Center. The code has been used to understand the occurrence of flutter in a forward-swept fan design. The forward-swept fan, which consists of 22 inserted blades, encountered flutter during wind tunnel tests at part speed conditions.

The TURBO code solves the Reynolds-averaged three-dimensional Navier-Stokes equations to calculate the work done on a vibrating blade by the surrounding fluid. The work is calculated for a prescribed harmonic motion in the mode and nodal diameter pattern of interest. The work done over one cycle of blade vibration can be converted to a more meaningful damping value referred to as aerodynamic damping. The flutter point can then be calculated by extrapolating the performance characteristics at which the aerodynamic damping goes to zero. The TURBO code calculated the observed flutter of the forward swept fan, correctly identifying the mode and nodal diameter of the observed flutter. The study indicated that the shock wave location and strength have a strong influence on blade stability. The following graph shows the distribution of work on the blade surface at 95 percent of the span. Also shown on this figure is the steady pressure coefficient identifying the shock wave and its location. It is clearly seen that the work done by the fluid is centered around the shock wave. It was found that as the operating conditions changed and the shock wave location moved on the blade surface, the area of work associated with the shock wave also moved. The work calculated was found to be strongly dependent on the shock wave strength as well.

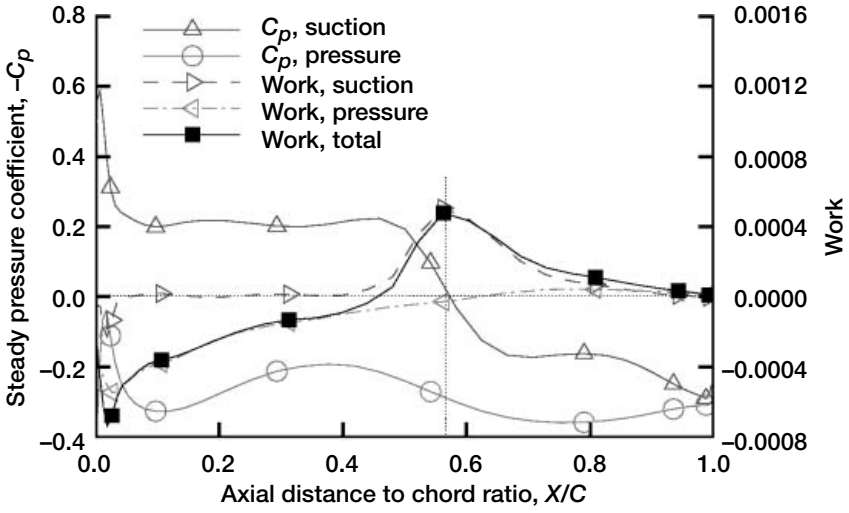

Pressure coefficient and work distribution at 95-percent span for the forward-swept fan blade operating near stall.

The figure on the next page shows the distribution of total work on the blade surface for different mass flow conditions. Both stabilizing and destabilizing areas of work were found to be associated with shock waves present on the blade surfaces. For the fan geometry analyzed, we found the suction surface shock wave to be destabilizing, whereas the pressure surface shock wave had a stabilizing effect. We also found that accurate blade shape, accounting for deformations due to operating aerodynamic and centrifugal loading, is important for the accurate prediction of the flutter boundary.

University of Toledo contacts:
Dr. Rakesh Srivastava, 216–433–6045, Rakesh.Srivastava@grc.nasa.gov, and Dr. Milind A. Bakhle, 216–433–6037, Milind.A.Bakhle@grc.nasa.gov

Glenn contact:
George L. Stefko, 216–433–3920, George.L.Stefko@nasa.gov

Authors:
Dr. Rakesh Srivastava, Dr. Milind A. Bakhle, and George L. Stefko

Headquarters program office: OAT

Programs/Projects: QAT

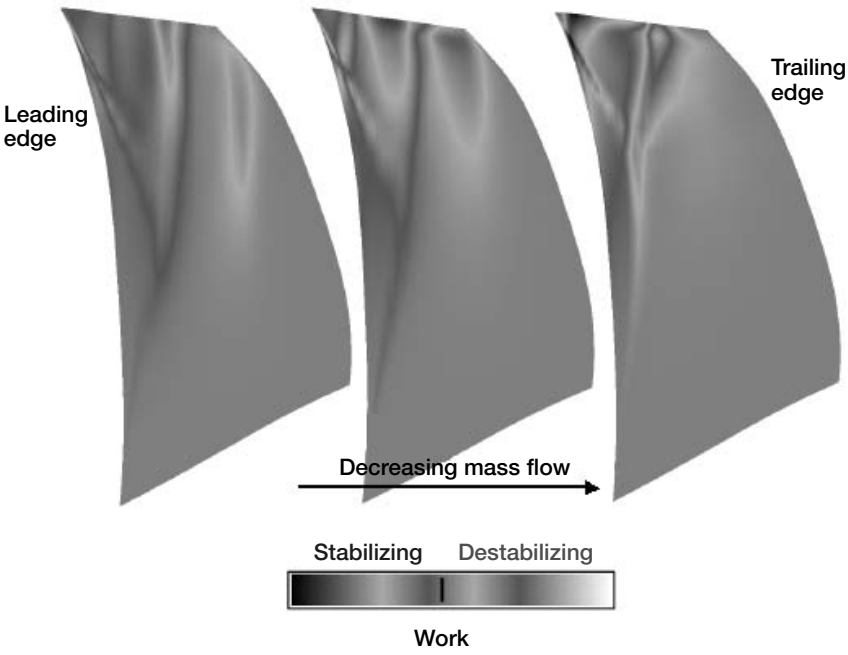

Work distribution on the blade surface for various mass flows operating at a part speed operating condition.This figure is shown in color in the online version of this article (http://www.grc.nasa.gov/WWW/RT2002/5000/5930srivastava2.html).

Fan Noise Source Diagnostic Test Completed and Documented

In June of 2002, a comprehensive aeroacoustic research project called the Fan Noise Source Diagnostic Test (SDT) culminated in a dedicated session in the 8th AIAA/CEAS Aeroacoustics Conference in Breckenridge, Colorado.

The specially organized session offered an international forum to disseminate the results (see refs. 1 to 6) from a yearlong test that was conducted in 1999 in NASA Glenn Research Center's 9- by 15-Foot Low-Speed Wind Tunnel on a 22-in. scale-model turbofan bypass stage, which was designed to be representative of current aircraft engine technology. The test was a cooperative effort involving Glenn, the NASA Langley Research Center, GE Aircraft Engines, and the Boeing Company. The principal objective of the project was to study the source mechanisms of noise in a modern high-bypass-ratio turbofan engine through detailed aerodynamic and acoustic measurements.

The 22-in. rig used for the Fan Noise Source Diagnostic Test shown in Glenn's 9- by 15-Foot Low-Speed Wind Tunnel.

Partially assembled fan stages showing the three outlet guide vanes (OGV) tested. From left to right, the baseline 54-vane radial OGV, the 26-vane radial OGV, and the 26-vane swept OGV.

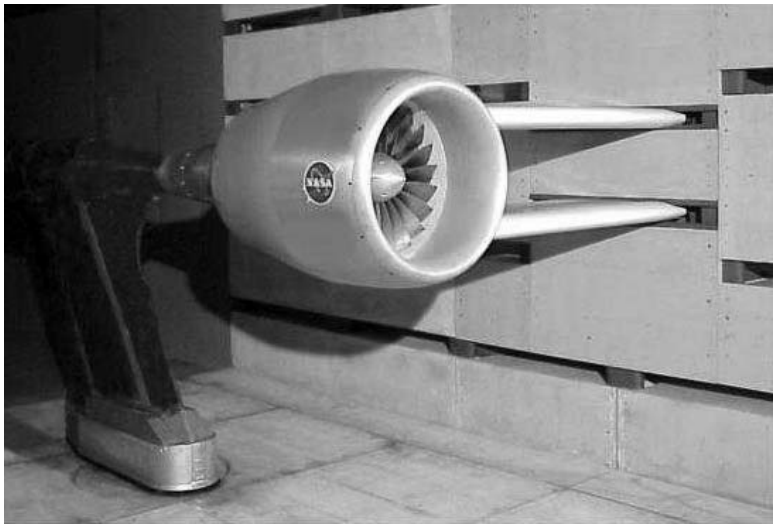

The SDT rig in its rotor-alone configuration. The centerbody and the fan nacelle are independently supported, and the position of the nacelle relative to the centerbody is controlled in real time using an active centering system.

The test involved assessing the noise characteristics of three outlet guide vane designs, identifying and characterizing specific broadband noise sources within the model bypass stage, and investigating the characteristics of the fan steady (mean) and unsteady (perturbation) flow fields using advanced diagnostic test methods. The database of the acquired data includes detailed hot-wire and laser Doppler velocimetry (LDV) diagnostics of the fan tip and wake flows, outlet guide vane unsteady surface pressure measurements, in-duct and far-field noise measurements, and fan and stage performance characteristics. A special feature of the SDT fan rig is its ability to be run in a rotor-alone mode: that is, without stators. Using a unique active centering system for which the design team received the 2000 Steve V. Szabo Engineering Excellence Award, the independently supported rig centerbody and fan nacelle can be positioned, in real time, to within specified tolerances, thus enabling meaningful rotor-alone measurements of the fan flow and noise characteristics. For years to come, the resulting aggregate of aero and acoustic databases obtained in the SDT test will be used by NASA and the U.S. aerospace industry to validate theoretical aerodynamic and aeroacoustic codes and guide the direction of future modeling efforts.

References

1. Hughes, C.E.; Jeracki, R.J.; and Miller, C.J.: Fan Noise Source Diagnostic Test—Rotor-Alone Nacelle Aerodynamic Performance Results. AIAA Paper 2002–2426, June 2002.
2. Podboy, G.G.; and Helland, S.M.: Fan Noise Source Diagnostic Test—Two-Point Hot-Wire Results. AIAA Paper 2002–2431, June 2002.
3. Premo, J.W.: Fan Noise Source Diagnostic Test—Circumferential Mode Measurements. AIAA Paper 2002–2429, June 2002.
4. Heidelberg, L.J.: Fan Noise Source Diagnostic Test—Tone Modal Structure Results. AIAA Paper 2002–2428, June 2002.
5. Woodward, R.P., et al.: Fan Noise Source Diagnostic Test—Farfield Acoustic Results. AIAA Paper 2002–2427, June 2002.
6. Envia, E.: Fan Noise Source Diagnostic Test—Vane Unsteady Pressure Results. AIAA Paper 2002–2430, June 2002.

Find out more about this research:
http://www.grc.nasa.gov/WWW/5900/5940/

Glenn contacts:

Dr. Ed Envia, 216–433–8956, Edmane.Envia-1@nasa.gov;
Christopher E. Hughes, 216–433–3924, Christopher.E.Hughes@nasa.gov;
Gary G. Podboy, 216–433–3916, Gary.G.Podboy@nasa.gov; and
Richard P. Woodward, 216–433–3923, Richard.P.Woodward@nasa.gov

Author: Dr. Edmane Envia

Headquarters program office: OAT

Programs/Projects: ASTP, QAT

Special recognition: 2000 Steve V. Szabo Engineering Excellence Award

Helicopter transmission integrity is critical to helicopter safety because helicopters depend on the power train for propulsion, lift, and flight maneuvering. To detect impending transmission failures, the ideal diagnostic tools used in the health-monitoring system would provide real-time health monitoring of the transmission, demonstrate a high level of reliable detection to minimize false alarms, and provide end users with clear information on the health of the sys-

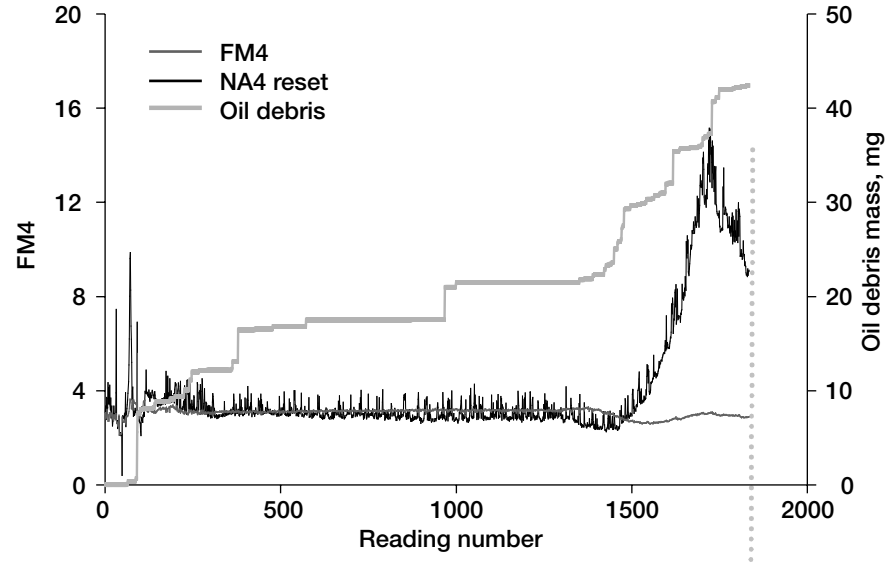

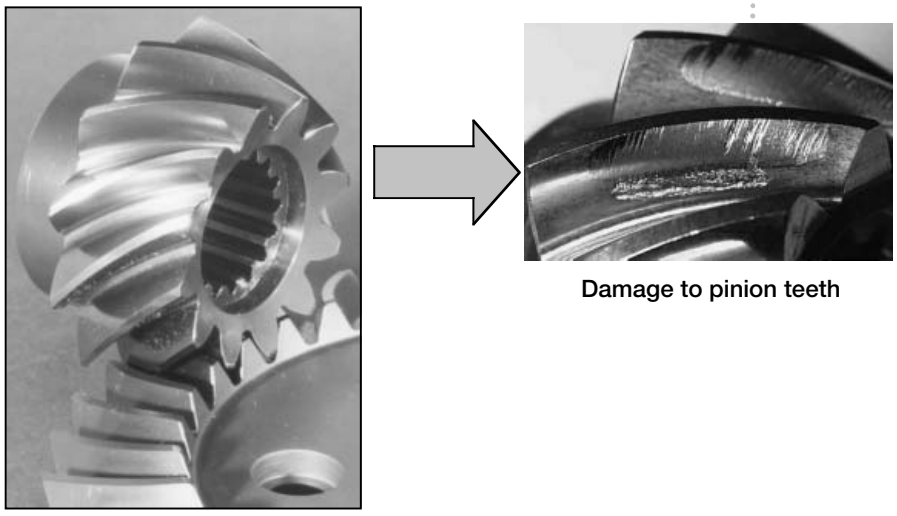

Damage to pinion teeth

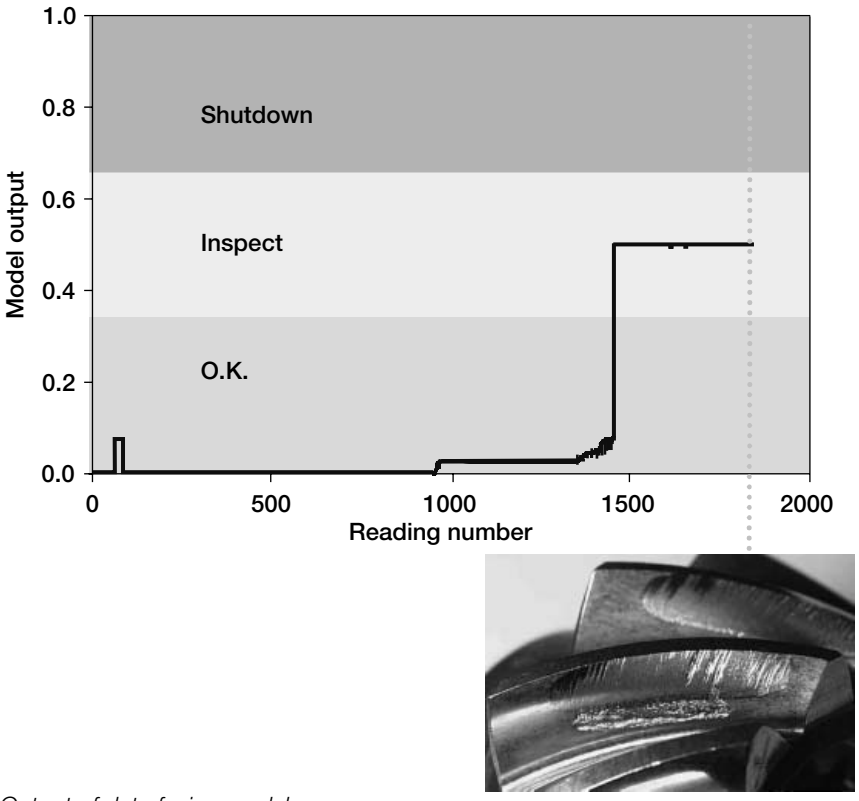

Output of data fusion model.

Analysis of the data collected during these experiments demonstrated the advantage of fusing the features of different measurement technologies. The output gives clear, reliable information to end users making decisions about the health of the geared system. Results indicate that combining the two technologies greatly improves the detection of damage on spiral bevel gears.

The following two plots show the data collected from one experiment with pitting damage. The figure on the preceding page shows the vibration algorithms FM4 and NA4 and the amount of debris measured by the oil debris sensor.

The figure on this page is the output of the data fusion model used to integrate the oil and vibration data.

Bibliography

Dempsey, Paula J.: Gear Damage Detection Using Oil Debris Analysis. NASA/TM—2001-210936, 2001. http://gltrs.grc.nasa.gov/cgi-bin/GLTRS/browse.pl?2001/TM-2001-210936.html

Dempsey, Paula J.: Integrating Oil Debris and Vibration Measurements for Intelligent Machine Health Monitoring. Ph.D. Thesis, Univ. of Toledo, 2002.

Dempsey, Paula J.; Handschuh, Robert F.; and Afjeh, Abdollah A.: Spiral Bevel Gear Damage Detection Using Decision Fusion Analysis. NASA/TM—2002-211814, 2002. http://gltrs.grc.nasa.gov/cgi-bin/GLTRS/browse.pl?2002/TM-2002-211814.html

Glenn contact:
Dr. Paula J. Dempsey, 216–433–3398, Paula.J.Dempsey@nasa.gov

U.S. Army, Vehicle Technology Directorate at Glenn contact:
Dr. Robert F. Handschuh, 216–433–3969, Robert.F.Handschuh@grc.nasa.gov

Authors: Dr. Paula J. Dempsey and Dr. Robert F. Handschuh

Headquarters program office: OAT

Programs/Projects:
CICT, ITSR, Intelligent Controls and Diagnostics Task, Intelligent Health and Safety Monitoring Element

Control Surface Seals Investigated for Re-Entry Vehicles

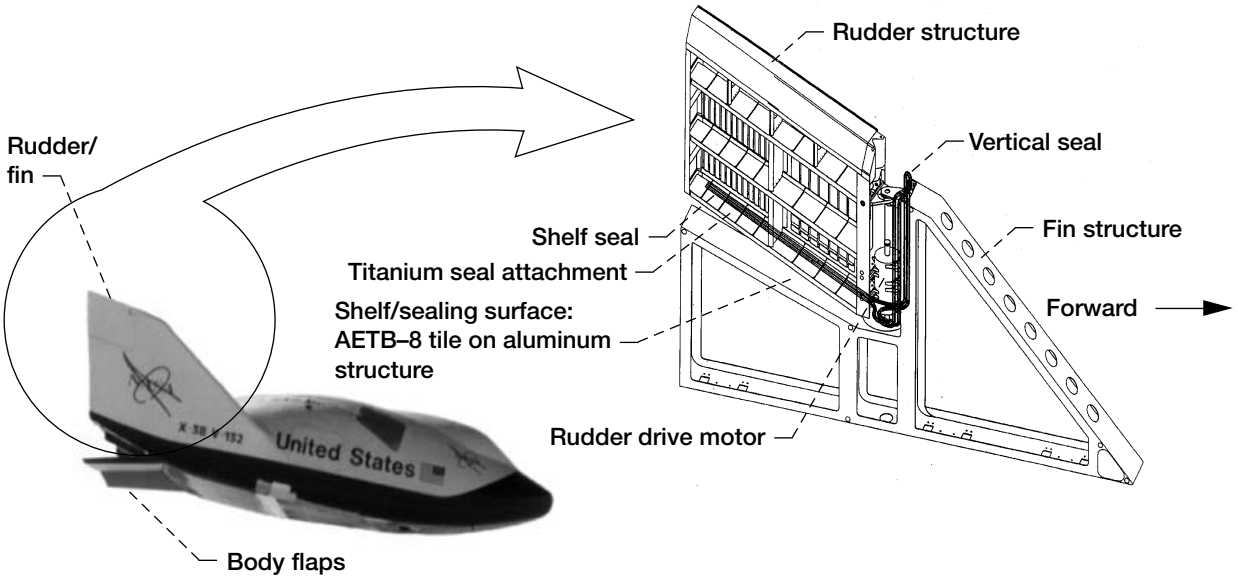

X–38 rudder/fin seal assembly with rudder/fin structure and seal locations. (AETB–8 is the shuttle tile material.)

Re-entry vehicles generally use control surfaces (e.g., rudders, body flaps, and elevons) to steer or guide them as they pass into and through the Earth's atmosphere. High-temperature seals are required around control surfaces both along hinge lines and in areas where control surface edges seal against the vehicle body to limit hot gas ingestion and the transfer of heat to underlying low-temperature structures. Working with the NASA Johnson Space Center, the Seals Team at the NASA Glenn Research Center completed a series of tests on the baseline seal design for the rudder/fin control surface interfaces of the X–38 vehicle. This seal application was chosen as a case study to evaluate a currently available control surface seal design for applications in future re-entry vehicles. The structures of the rudder/fin assembly and its associated seals are shown in the illustration above.

Tests performed at Glenn indicated that exposure of the seals in a compressed state at simulated seal re-entry temperatures (1900 °F) resulted in a large permanent set and loss of seal resiliency (see the photograph). This could be of concern because the seals are required to maintain contact with the sealing surfaces while the vehicle goes through the maximum re-entry heating cycle to prevent hot gases from leaking past the seals and damaging interior low-temperature structures. Because these seals experienced a large permanent set and lost resiliency upon temperature exposure, designers were forced to redesign the X–38 rudder/fin vertical rub surface to ensure that the seals remain in contact with the sealing surface during re-entry (as shown in the schematic on the next page).

Glenn researchers performed room-temperature compression tests to determine seal loading characteristics. Compression test results showed that seal unit loads and contact pressures were below the limits that Johnson had set as goals for the seals. In the rudder/fin seal location on the vehicle, the seals are in contact with shuttle thermal tiles along the horizontal rub surface and are moved across the tiles as the rudder is rotated during re-entry. Low seal unit loads and contact pressures are required to limit the loads on these tiles and minimize any damage that the seals could cause.

In fiscal year 2002, Glenn researchers performed a series of room-temperature seal flow tests under a variety of test conditions. Seals were tested in an as-received condition and after being scrubbed over shuttle thermal tiles for 1000 cycles. Flow tests were performed on two segments of the scrub-tested seal, the section with the most damage and the section with the least damage.

Seals before (left) and after (right) 1900 °F temperature exposure.

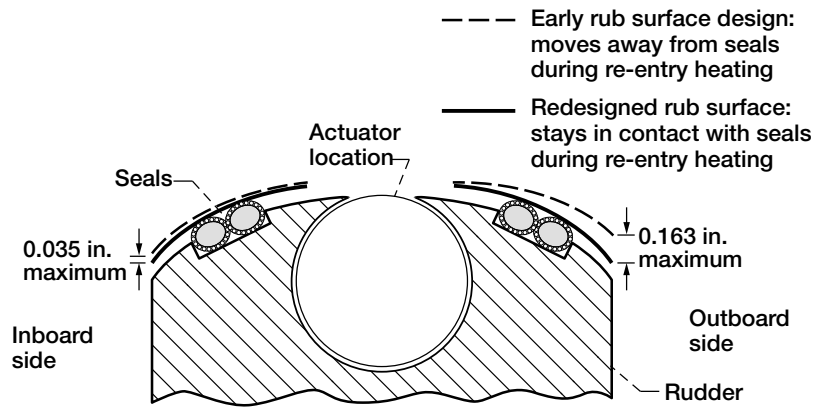

X–38 rudder/fin cross section showing vertical Inconel rub surface redesigned to accommodate lack of seal resiliency. (Note: not drawn to scale.)

Tests were also performed using either a flat plate in contact with the seals or a plate with a groove in it to simulate a gap between two thermal tiles that the seals might be in contact with. The results of these flow tests are presented in the following graph.

The tests performed at Glenn verified that the baseline seal design is satisfactory for the X–38 application. However, requirements for higher temperature limits and 100- to 1000-cycle reusability in future reusable launch vehicles necessitate the development of high-temperature seal designs that remain resilient for multiple missions while still exhibiting low flow rates and good wear resistance.

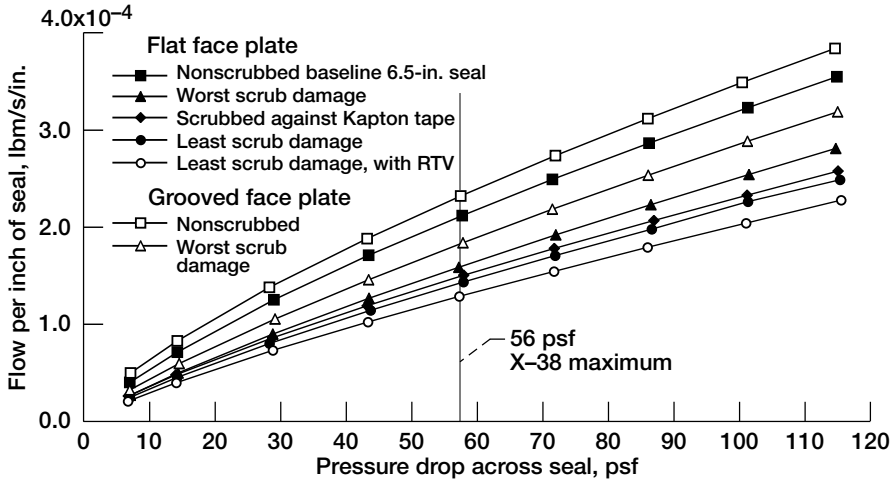

Flow versus pressure data for 6.5-in. double seals at 20-percent compression under different test conditions with a gap of 0.25 in. RTV, room-temperature, vulcanized rubber material.

Find out more about this research:

Structural seals and thermal barriers: http://www.grc.nasa.gov/WWW/structuralseal/

High-temperature, flexible, fiber preform seal: http://www.grc.nasa.gov/WWW/structuralseal/InventYr/1996Inv_Yr.htm

Glenn's Mechanical Components Branch: http://www.grc.nasa.gov/WWW/5900/5950/

Bibliography

Dunlap, Patrick H., Jr., et al.: Investigations of Control Surface Seals for Re-Entry Vehicles, NASA/TM—2002-211708 (AIAA Paper 2002–3941), 2002. http://www.grc.nasa.gov/WWW/structuralseal/papers/TM-2002-211708.pdf and http://gltrs.grc.nasa.gov/GLTRS/

Dunlap, Patrick H., Jr., and Steinetz, Bruce M.: Rudder/Fin Seals Investigated for the X–38 Re-Entry Vehicle. Research & Technology 2001, NASA/TM—2002-211333, 2002, pp. 160–162. http://www.grc.nasa.gov/WWW/RT2001/5000/5950dunlap.html

Glenn contacts:

Patrick H. Dunlap, Jr., 216–433–3017, Patrick.H.Dunlap@nasa.gov; and
Dr. Bruce M. Steinetz, 216–433–3302, Bruce.M.Steinetz@nasa.gov

Authors: Patrick H. Dunlap, Jr., and Dr. Bruce M. Steinetz

Headquarters program office: OAT

Programs/Projects:
X–38, ASTP, 3rd Generation RLV, Advanced Control Surface Seals, Advanced Propulsion System Seals

Thermal Behavior of High-Speed Helical Gear Trains Investigated

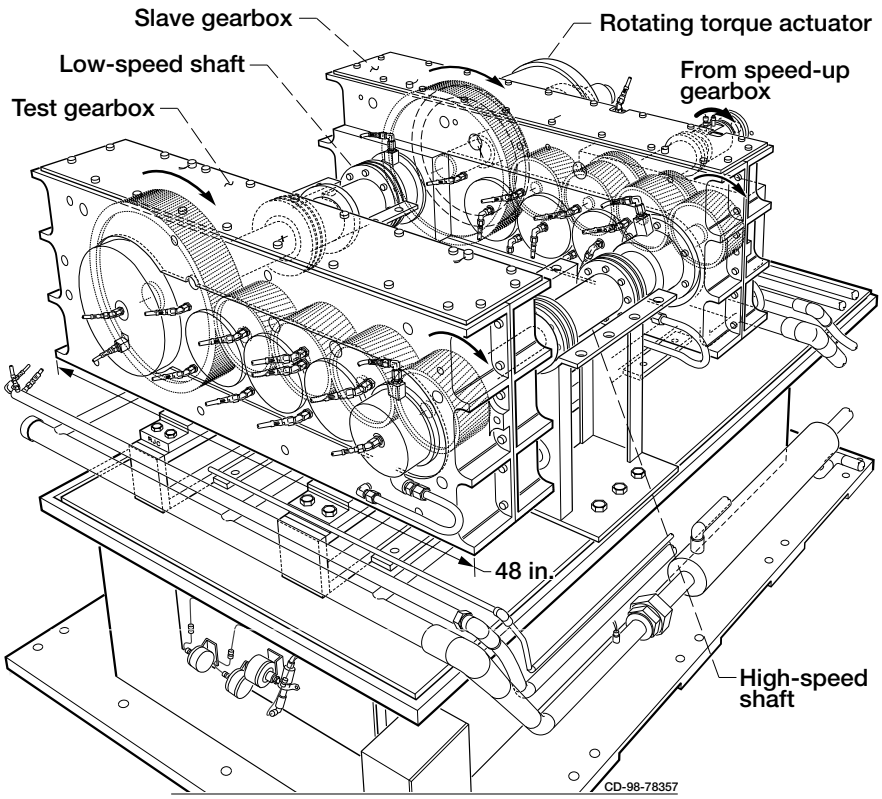

Top: NASA Glenn Research Center's High-Speed Helical Gear Train Test Facility. Bottom: Photograph of the high-speed helical gear train hardware.

High-speed and heavily loaded gearing are commonplace in the rotorcraft systems employed in helicopter and tiltrotor transmissions. The components are expected to deliver high power from the gas turbine engines to the high-torque, low-speed rotor, reducing the shaft rotational speed in the range of 25:1 to 100:1. These components are designed for high power-to-weight ratios, thus the components are fabricated as light as possible with the best materials and processing to transmit the required torque and carry the resultant loads without compromising the reliability of the drive system. This is a difficult task that is meticulously analyzed and thoroughly tested experimentally prior to being applied on a new or redesigned aircraft.

In some areas of gear design, no data are available internal to the manufacturer or through the open literature to improve the operational behavior of a component or system prior to prototype development. Gear-tooth bending and contact stress are usually the first considerations in designing a new transmission system. A variety of established methods exist for calculating these gear stresses, such as AGMA (American Gear Manufacturers Association) equations and finite element analysis. Conversely, the thermal behavior or thermal operational characteristics of a geared system are not well understood and are not well represented in the open literature. A design that would be successful from a bending and contact stress viewpoint can end up being a failure because of the system's thermal operational characteristics (high operational temperatures, gear tooth scoring, and high drive system losses due to high pitch line velocities).

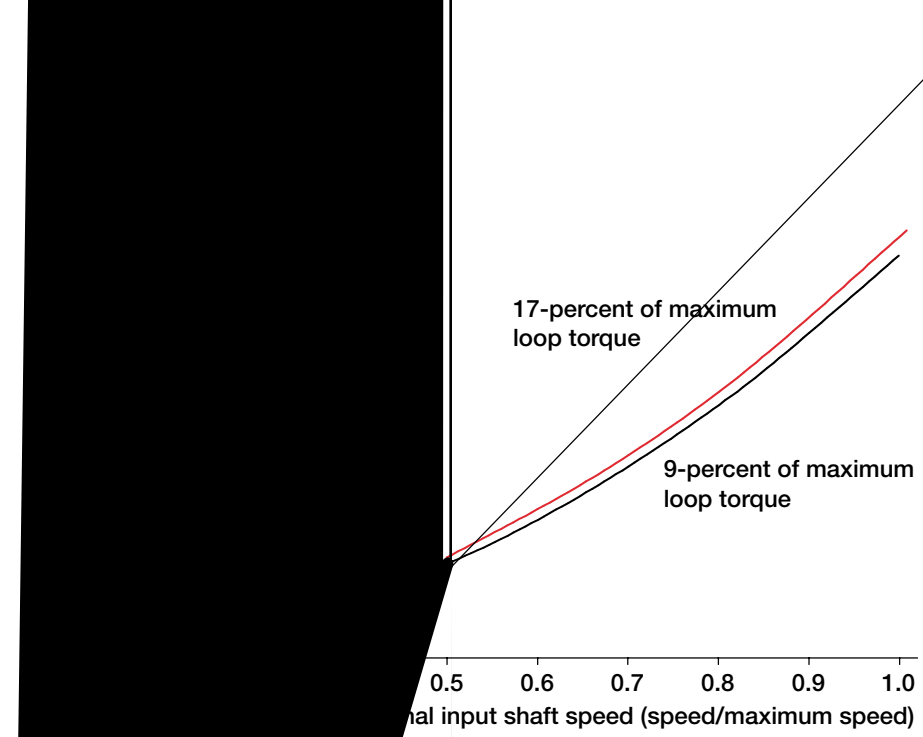
17-percent of maximum
loop torque
9-percent of maximum
loop torque
0.5
0.6
0.7
0.8
0.9
1.0
al input shaft speed (speed/maximum speed)

0.4 0.6 0.8 1.0

High-Speed, High-Temperature Finger Seal Test Evaluated

A finger seal, designed and fabricated by Honeywell Engines, Systems and Services, was tested at the NASA Glenn Research Center at surface speeds up to 1200 ft/s, air temperatures up to 1200 °F, and pressures across the seal of 75 psid. These are the first test results obtained with NASA's new High-Temperature, High-Speed Turbine Seal Test Rig (see the photograph). The finger seal is an innovative design recently patented (ref. 1) by AlliedSignal Engines, which has demonstrated considerably lower leakage than commonly used labyrinth seals and is considerably cheaper than brush seals. The cost to produce finger seals is estimated to be about half of the cost to produce brush seals. Replacing labyrinth seals with finger seals at locations that have high-pressure drops in gas turbine engines, typically main engine and thrust seals, can reduce air leakage at each location by 50 percent or more. This directly results in a 0.7- to 1.4-percent reduction in specific fuel consumption and a 0.35- to 0.7-percent reduction in direct operating costs (ref. 2). Because the finger seal is a contacting seal, this testing was conducted to address concerns about its heat generation and life capability at the higher speeds and temperatures required for advanced engines. The test results showed that the seal leakage and wear performance are acceptable for advanced engines (ref. 3).

The finger seal (see the figure on the next page) is made of a stack of sheet stock elements shaped like washers. The center elements are machined to create a series of slender curved beams or fingers around the inner diameter. These finger elements are oriented so that the fingers of one element cover the spaces between the fingers of the adjacent element. Spacers and cover plates are placed on either side of the stack of finger elements, and the whole assembly is riveted together near the outer diameter of the stack. The fingers act like cantilever beams and flex away from the rotor to accommodate centrifugal and thermal growth and

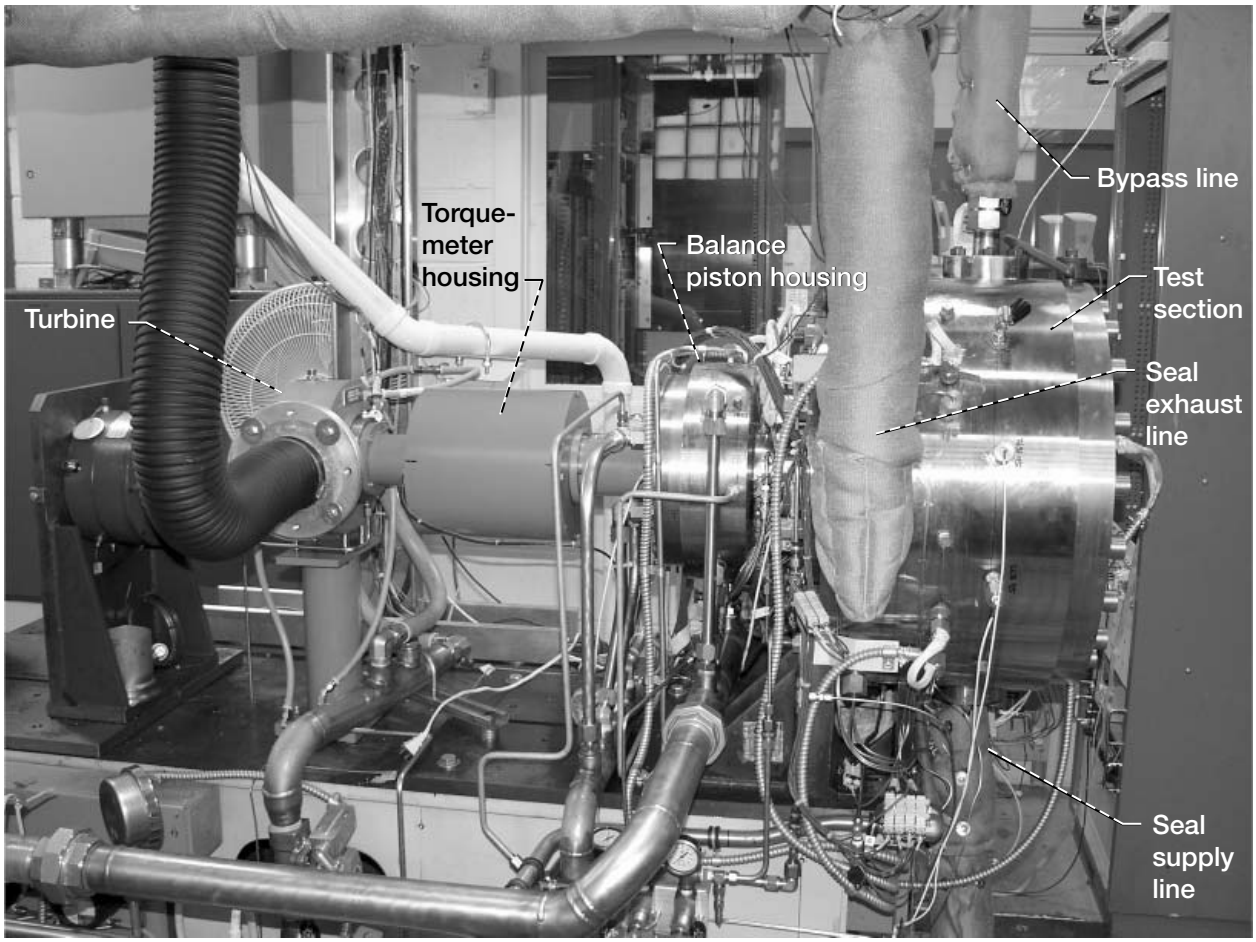

High-temperature, high-speed turbine seal rig.

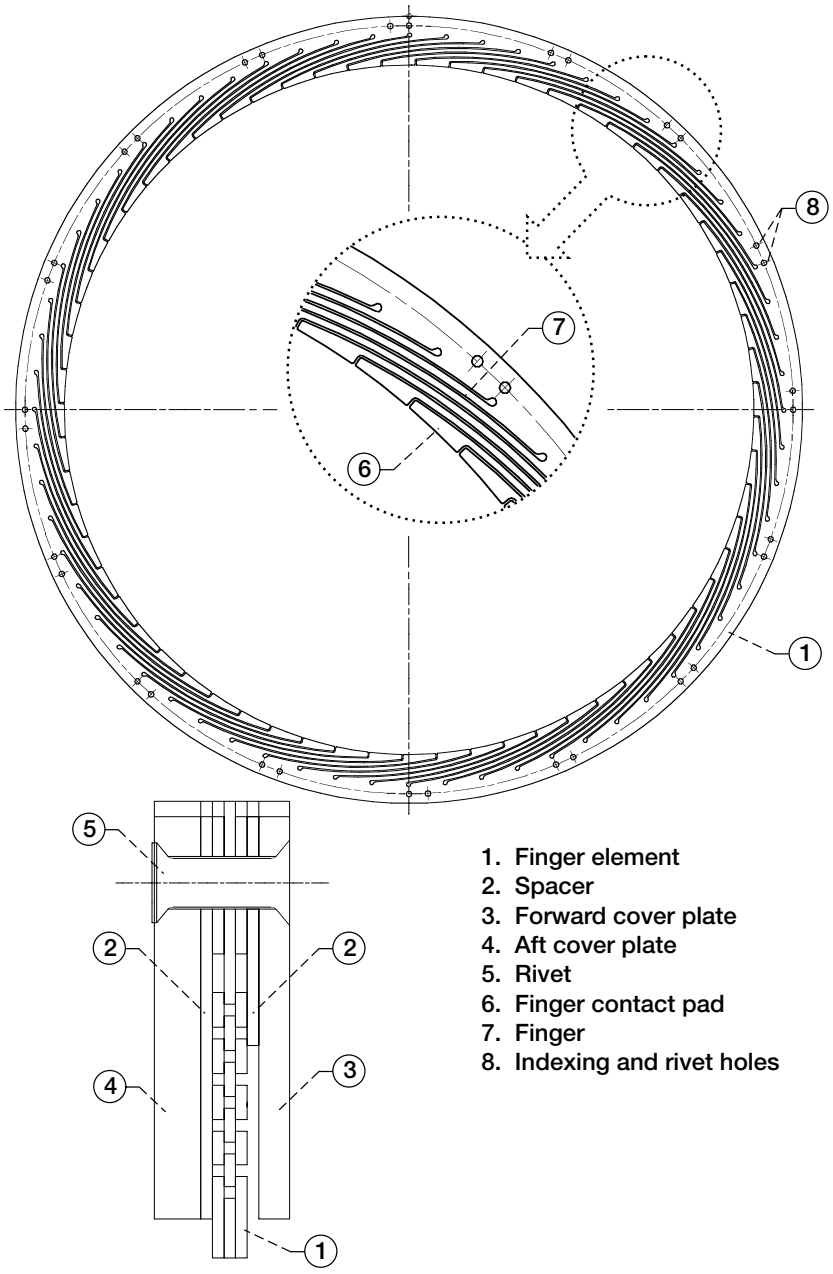

1. Finger element
2. Spacer
3. Forward cover plate
4. Aft cover plate
5. Rivet
6. Finger contact pad
7. Finger
8. Indexing and rivet holes

Finger seal design.

rotordynamic motions of the rotor. The cobalt-base alloy AMS5537, which combines good formability and excellent high-temperature properties, was used to make the finger seal. The 8.5-in.-diameter test rotor was made of MAR–M–247 and was coated with chrome carbide using high-velocity oxygen fuel thermal spraying.

The flow factor, which is an indicator of seal leakage performance, met or exceeded performance goals during endurance testing that simulated expected advanced-engine-rated power conditions. Most of the seal wear occurred in the initial performance test. The chrome carbide coating performed well, with a wear track depth less than 0.00025 in. The maximum finger seal power loss, which occurred at 1200 ft/s and 75 psid across the seal, was 14 hp. Further design improvements can be made to reduce the finger seal power loss. Also, the finger seal power loss is comparable to the brush seal power loss as shown in the graph on the next page.

Find out more about turbine seal work at Glenn:

Glenn's Mechanical Components Branch: http://www.grc.nasa.gov/WWW/5900/5950/

Turbine Seals:
http://www.grc.nasa.gov/WWW/TurbineSeal/TurbineSeal.html

References

1. Arora, Gulshan K.; and Glick, Donald L.: Pressure Balanced Finger Seal. U.S. Patent 6,196,550, March 6, 2001.
2. Steinetz, Bruce M.; Hendricks, Robert C.; and Munson, John: Advanced Seal Technology Role in Meeting Next Generation Turbine Engine Goals. NASA/TM—1998-206961, 1998. http://gltrs.grc.nasa.gov/cgi-bin/GLTRS/browse.pl?1998/TM-1998-206961.html

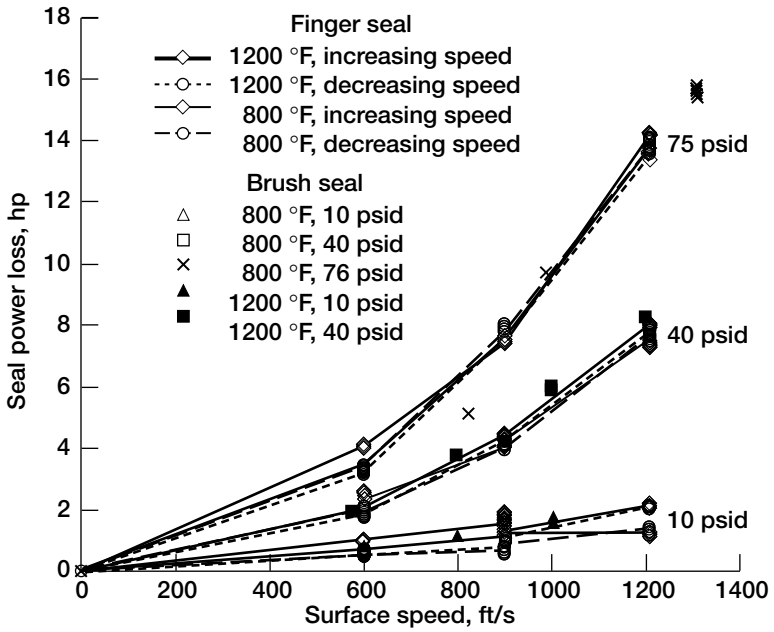

Finger seal and brush seal power loss versus speed at average seal inlet air temperatures of 800 and 1200 °F and pressure drops across the seal of 10-, 40-, and 75-psid.

3. Proctor, Margaret P.; Kumar, Arun; and Delgado, Irebert R.: High-Speed, High-Temperature Finger Seal Test Results. NASA/TM—2002-211589, 2002. http://gltrs.grc.nasa.gov/cgi-bin/GLTRS/browse.pl?2002/TM-2002-211589.html

Glenn contact:
Margaret P. Proctor, 216–977–7526, Margaret.P.Proctor@nasa.gov

U.S. Army Research Laboratory at Glenn contact:
Irebert R. Delgado, 216–433–3935, Irebert.R.Delgado@grc.nasa.gov

Author: Margaret P. Proctor

Headquarters program office: OAT

Programs/Projects:
IHPTET, SEC, ASTP

Oil-Free Turbomachinery Research Enhanced by Thrust Bearing Test Capability

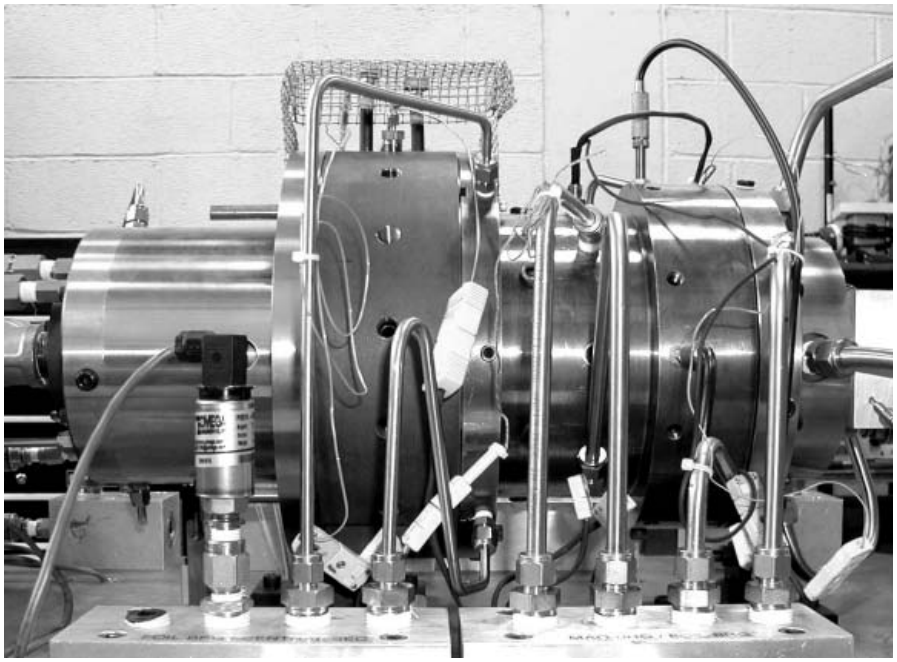

Thrust foil air bearing test rig.

NASA Glenn Research Center's Oil-Free Turbomachinery research team is developing aircraft turbine engines that will not require an oil lubrication system. Oil systems are required today to lubricate rolling-element bearings used by the turbine and fan shafts. For the Oil-Free Turbomachinery concept, researchers combined the most advanced foil (air) bearings from industry with NASA-developed high-temperature solid lubricant technology. In 1999, the world's first Oil-Free turbocharger was demonstrated using these technologies. Now we are working with industry to demonstrate Oil-Free turbomachinery technology in a small business jet engine, the EJ–22 produced by Williams International and developed during Glenn's recently concluded General Aviation Propulsion (GAP) program. Eliminating

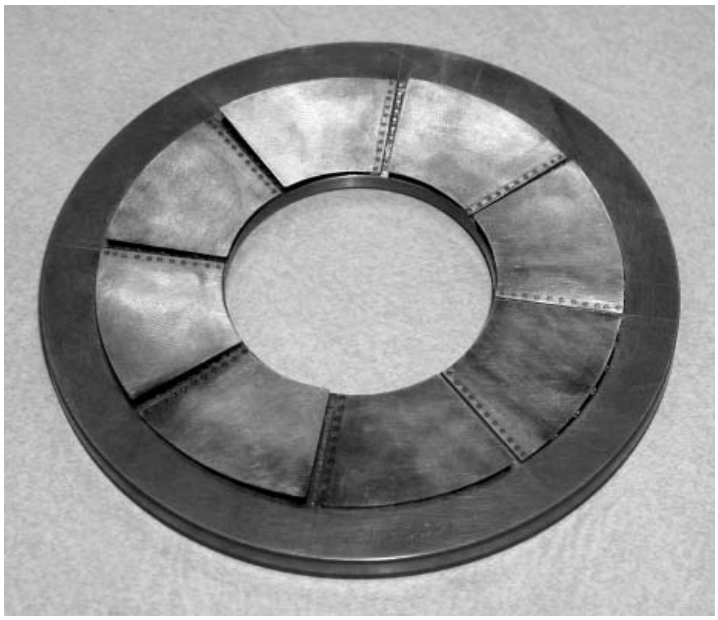

Thrust foil air bearing.

the oil system in this engine will make it simpler, lighter (approximately 15 percent), more reliable, and less costly to purchase and maintain.

Propulsion gas turbines will place high demands on foil air bearings, especially the thrust bearings. Up until now, the Oil-Free Turbomachinery research team only had the capability to test radial, journal bearings. This research has resulted in major improvements in the bearings' performance, but journal bearings are cylindrical, and can only support radial shaft loads. To counteract axial thrust loads, thrust foil bearings, which are disk shaped, are required. Since relatively little research has been conducted on thrust foil air bearings, their performance lags behind that of journal bearings.

To remedy this situation, the state-of-the-art Thrust Bearing Test Rig was added to our laboratory. This unique test facility was designed and manufactured by Mohawk Innovative Technology of Albany, New York, under a Small Business Innovation Research (SBIR) Phase III contract. The test rig can test thrust foil bearings to 80 000 rpm under loads as high as 3500 N (700 lb) and at temperatures to 650 °C (1200 °F). The test bearing and runner are heated by electric resistance heating, both by a coil around the test articles and by heating air that is blasted at the spinning bearing runner. Together, these heat sources simulate the hot environment that is expected inside the turbofan engine. A hydrostatic (externally pressurized) bearing is used to support the test thrust bearing and allow torque, which translates into bearing friction, to be accurately measured while still allowing heavy loads to be applied to the test bearing. The turbine-driven rotating runner side of the rig employs foil journal bearings to control the radial motion of the shaft, making the rig itself a secondary test bed for Oil-Free bearing technologies. An active magnetic thrust bearing counteracts the thrust loads from the test thrust foil bearing.

Tests using the facility are underway, and data are being fed back to industry to modify and improve bearing design and manufacturing. This rig will also allow NASA scientists and engineers to develop and test solid lubricants that are applied to the bearing foils or runner and can enhance bearing performance and life.

Find out more about this research:
http://www.grc.nasa.gov/WWW/Oilfree

Glenn contacts:
Steve Bauman, 216–433–3826,
Steven.W.Bauman@nasa.gov; and
Dr. Christopher DellaCorte,
216–433–6056,
Christopher.DeLlacorte-1@nasa.gov

Author: Steven W. Bauman

Headquarter program office: OAT

Programs/Projects:
Propulsion and Power, Propulsion Systems R&T, SBIR, UEET

Alloy Interface Interdiffusion Modeled

With renewed interest in developing nuclear-powered deep space probes, attention will return to improving the metallurgical processing of potential nuclear fuels so that they remain dimensionally stable over the years required for a successful mission. Previous work on fuel alloys at the NASA Glenn Research Center was primarily empirical, with virtually no continuing research. Even when empirical studies are exacting, they often fail to provide enough insight to guide future research efforts. In addition, from a fundamental theoretical standpoint, the actinide metals (which include materials used for nuclear fuels) pose a severe challenge to modern electronic-structure theory. Recent advances in quantum approximate atomistic modeling, coupled with first-principles derivation of needed input parameters, can help researchers develop new alloys for nuclear propulsion.

Of particular relevance in these programs is the study of surfaces and interfaces, where engineered systems typically fail. Since the invention of scanning tunneling microscopy (STM) and the subsequent development of various scanning-probe-based techniques, unprecedented spatial resolution has been achieved using various surface probe methods, from near-field optical to scanning capacitance, even discrete I–V curves as a function of nanoposition. These surface analytic techniques have been fueled by and in turn fuel nanotechnology. In the study of surfaces, these relatively recent additions to a surface scientist's options join proven techniques for surface study such as small-spot auger electron spectrometry (AES), x-ray photoelectron spectroscopy (XPS), secondary ion mass spectrometry (SIMS), low energy electron diffraction (LEED) and others for the investigation of metallurgical problem areas. Interfacial analysis, even with the latest experimental tools, is a more challenging task because of the

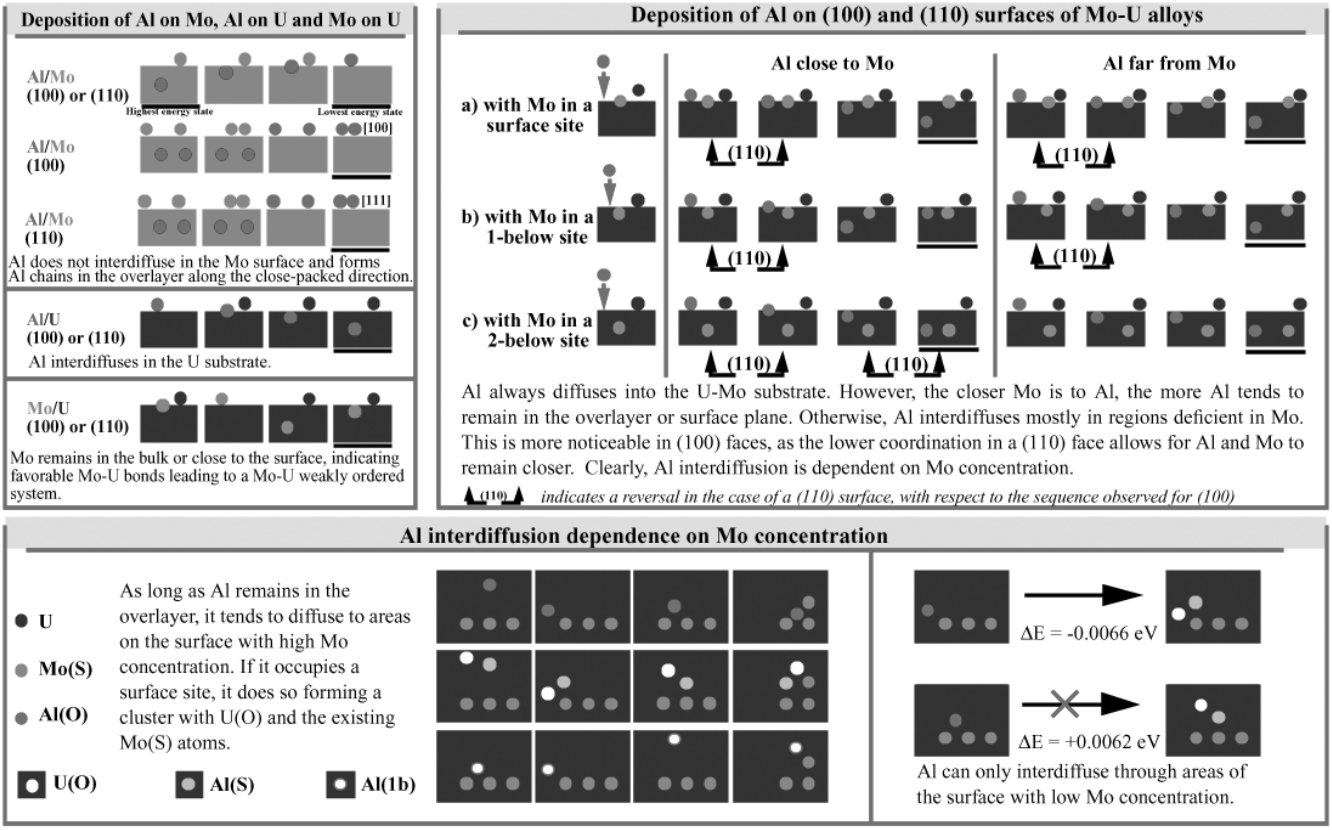

Modeling results for the interdiffusion of Al in U-Mo alloys. The panel in the top left corner shows the binary cases, where one element (Al or Mo) is deposited on a single-element substrate (Mo or U) as a function of the crystal face ((100) or (110)). The panel in the top right corner displays the behavior of a deposited Al atom in a U-Mo alloy as a function of the surface orientation of the alloy and the closeness to Mo atoms in solution (representing regions of high or low Mo concentration in the alloy). The lower panel indicates that the interdiffusion of Al in the U-Mo substrate is the result of a series of energetically allowed transitions. In all cases, X(L) indicates an atom of species X (Al, U, or Mo) located in a surface site (S) or in the layer immediately above (O) or below (1b).

additional problem of extracting either the interface or information from a buried interface for analysis. The shortcomings of the experimental techniques available are most apparent in issues related to nuclear materials, where research is further limited by the focus on very specific applications, thus reducing the body of available data for these systems.

In recent years, the development of low-enrichment uranium fuel has been the main focus for many researchers. The development of high-density uranium (U) alloys with an increased concentration of U is one of the key prerequisites for developing high-neutron-flux research reactors with low enrichment uranium fuel (ref. 1). The uranium-molybdenum (U-Mo) alloy system is one of the prospective candidates because a solid solution of Mo in γ-U has acceptable irradiation properties for reactor fuels. The prospect of using a U-Mo alloy as a reactor fuel is closely connected with the possibility of retaining a metastable gamma-phase state in alloys at temperatures below 560 °C during fuel element fabrication and irradiation. The reactor fuel consists of atomized U-Mo particles in an aluminum matrix. An interdiffusion or interfacial reaction, which affects the performance of nuclear fuel materials, is observed in the U-Mo/aluminum (Al) composites for low Mo composition. The experimental results indicate a large volume change, 26 vol%, for U-2 wt% Mo/Al, mainly due to the formation of voids and cracks resulting from nearly complete interdiffusion or an interfacial reaction, with uranium aluminide formation. However, no significant dimensional changes are observed in the U-10 wt% Mo/Al system. It is supposed that Mo atoms supersaturated in the grain boundary inhibit the diffusion of Al atoms (ref. 2). With such limited information, it is imperative to extend the scope of the tools used for the study of these issues, by including modeling techniques. In this article, we summarize results of an atomistic modeling description developed at the NASA Glenn Research Center of the main features observed experimentally in the diffusion of Al in the U-Mo solid solution. In what amounts to the first application of quantum approximate methods to nuclear materials, the ADW–SMP modeling package, which is based on the BFS (Bozzolo-Ferrante-Smith) method for alloys, was applied to the study of Al interdiffusion in U-Mo alloys.

The schematic on the preceding page displays a graphical description of the process of Al interdiffusion in U-Mo alloys. Several processes need to be included—the deposition of Al on Mo, Al on U, and Mo on U—to fully describe the contrasting behaviors that should be taken into account when interpreting the results of the ternary case. The right panel in the schematic describes the intricate mechanism leading to the interdiffusion of Al in the U-Mo alloy, and the lower panel identifies allowed and prohibited processes that result in the observed behavior. In all panels, processes are depicted from left to right in terms of decreasing energy (i.e., increasing likelihood of occurrence). This level of understanding, for the first time available for this type of system, is fundamental when determining the steps necessary for modifying the system.

Find out more about this research:

International Materials Science Consortium: http://www.icmsc.org

Glenn's Tribology & Surface Science Branch: http://www.grc.nasa.gov/WWW/SurfSci/

Ohio Aerospace Institute (OAI) contact:
Dr. Guillermo H. Bozzolo, 440–962–3103, Guillermo.H.Bozzolo@grc.nasa.gov

Glenn contact:
Dr. Phillip B. Abel, 216–433–6063, Phillip.B.Abel@nasa.gov

Authors:
Dr. Guillermo H. Bozzolo, Dr. Jorge E. Garces, and Dr. Phillip B. Abel

Headquarters program office: OAT

Programs/Projects: HOTPC

Industry Needs Fulfilled by Patented NASA PS300 Solid Lubricant Technology

In 1999, the NASA Glenn Research Center was awarded a patent (#5866518) for a new high-temperature solid lubricant coating material, PS300. A combination of wear-resistant metals and ceramics with solid lubricant additives, PS300 reduces friction and wear in sliding contacts from below ambient to over 650 °C. This lubricant is an outgrowth of over three decades of high-temperature tribological research and was specifically developed as a shaft lubricant to protect foil air bearings used in Oil-Free turbomachinery, like gas turbines. Foil bearings are lubricated by air at high speeds but experience sliding and wear during initial startup and shut down when a lubricating film of air has not yet developed. PS300 shaft coatings have successfully lubricated foil bearings for over 100 000 cycles without wearing out.

Several intrinsic characteristics of PS300, namely its good high-temperature friction and wear behavior, low material cost, ease of manufacturing, and thermal stability make it an ideal candidate technology to spin off from aerospace to industry. Two recent spinoff successes include using PS300 coatings to lubricate high-temperature, high-pressure steam turbine control valves used in advanced power plants and using PM300, a solid form made via powder metallurgy techniques, for bushings to lubricate high-temperature conveyor components in an industrial drying furnace.

Newly developed steam-turbine-based power plants achieve high efficiencies by operating at high steam pressures and temperatures sometimes exceeding 540 °C. In this environment, one steam turbine manufacturer experienced severe wear and sticking of their steam turbine control valves. To solve this problem, the NASA PS304 coating was plasma spray deposited onto the large (2-m-long) valve stems and was ground to the desired thickness and surface finish. These valves were put into service and, upon inspection at 1- and 2-yr intervals (during planned plant shutdowns), have shown no signs of wear or degradation. Numerous previous attempts to solve this problem with other materials (e.g., graphite and Teflon) were unsuccessful. Future power plant applications are planned.

PS300 powder used as starting material for both plasma-sprayed PS300 coatings and powder-metallurgy-formed PM300 bushings.

The second spinoff is in the welding rod industry. A major manufacturer of welding rods and equipment was experiencing wear and seizure of conveyor bushings in their welding rod drying furnaces, which had been in service for 50 years. The furnaces, which use bronze bushings to lubricate the conveyor system, originally had operated at a few hundred degrees centigrade. The modern process exposes the conveyor components to temperatures over 500 °C, which quickly degrades the best bronze bushings in a matter of days or weeks. This degradation results in lost time, product, and revenue. Attempts to use replacement bushings made from ceramics, graphite, and other advanced polymers failed. The environment was too severe. To respond to this technical need, Advanced Materials (ADMA), a NASA patent licensee working in conjunction with Glenn staff, fabricated free-standing bushings of PS300 material using powder metallurgy techniques. These powder metallurgy bushings are called PM300. The first of 12 furnaces were retrofitted with over 2000 bushings made of the PM300 material. These bushings have experienced no measurable wear after a successful year of service. In the upgraded furnace, product losses due to seized bushings no longer occur.

PM300 bushings used in industrial drying furnace conveyor system.

These two success stories, one for the PS300 coating and one for the new powder metallurgy form, PM300, clearly demonstrate the commercial value of this NASA patented technology. To date, three commercial, nonexclusive licenses have been granted and more are being sought.

Find out more about this research:
http://www.grc.nasa.gov/www/Oilfree

Glenn contacts:
Dr. Christopher DellaCorte, 216–433–6056, Christopher.DeLlaCorte-1@nasa.gov;
Brian. J. Edmonds, 216–433–8963, Brian.J.Edmonds@nasa.gov; and
Kathleen K. Needham, 216–433–2802, Kathleen.K.Needham@nasa.gov

Author: Dr. Christopher DellaCorte

Headquarters Program Office:
OAT, CTO

Programs/Projects: Propulsion and Power, CTO, Technology Transfer

Transition of PS300 Solid Lubricant Coating Technology to Field Aided by Demonstration on Key Substrate Alloys

PS300 is a high-temperature solid lubricant coating originally developed to lubricate nickel-based superalloy shafts operating against foil air bearings in Oil-Free turbomachinery applications. PS300 is a plasma-spray-deposited coating developed at the NASA Glenn Research Center. It is available for nonexclusive licensing and has found applications in aerospace and industry. PS300 reduces friction and wear from below room temperature to over 650 °C in both oxidizing and reducing environments. Early development centered on coating nickel-based shafts for use in turbomachinery. Potential industrial and aerospace customers, however, expressed interest in using the coating on a wide variety of substrates including steels, stainless steels, and nonferrous alloys like aluminum and titanium. To support this interest, a research program was carried out at Glenn in which nine different substrate candidate materials were evaluated for suitability with the PS300 coating. The materials were first coated with PS300 and then tested for coating strength and adhesion both before and after exposure to high-temperature air.

The results clearly showed that PS300 is a suitable coating for superalloys, steels, and stainless steels over a wide temperature range to at least 650 °C. When applied to aluminum and titanium, care must be taken. Exposure to temperatures above 500 °C on these alloys (which are not considered high-temperature materials) resulted in coating delamination. For all other substrates, PS300 properties are not affected by the type of substrate. This suggests that in many applications, lower cost substrates with PS300 coatings can be substituted for high-performance alloys without sacrificing tribological properties.

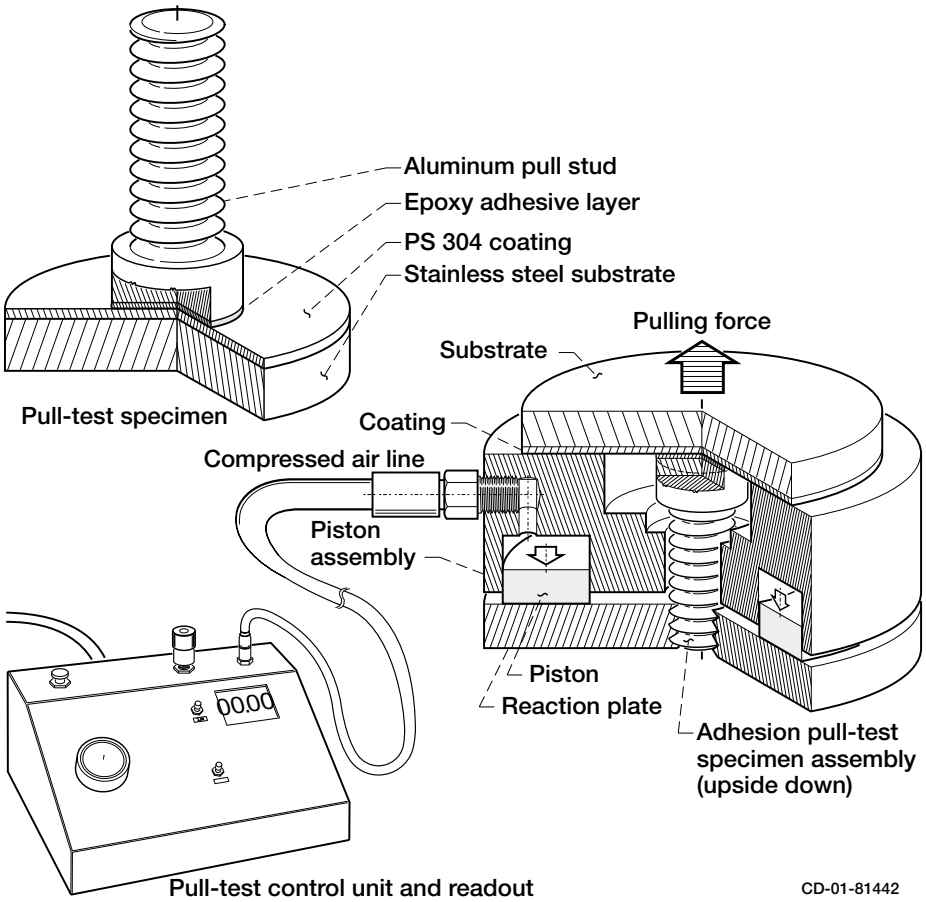

PS300 coating test specimens glued to pull stud for testing.

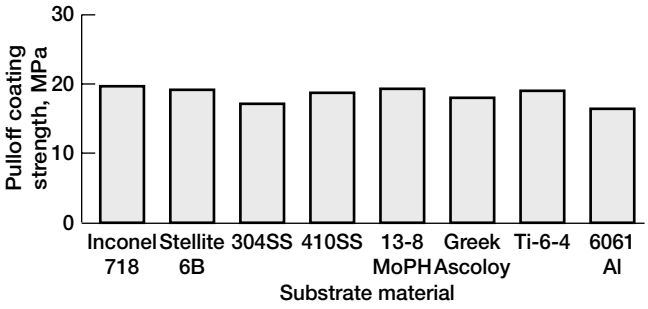

PS300 coating pulloff strength on various substrates in the as-deposited condition.

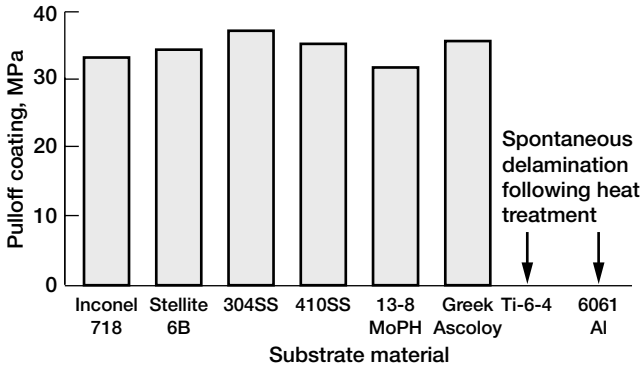

PS300 coating pulloff strength after air heat treatment at 650 °C for 100 hr. Strength nearly doubles.

Bibliography

DellaCorte, Christopher: The Effects of Substrate Material and Thermal Processing Atmosphere on the Strength of PS304: A High Temperature Solid Lubricant Coating. NASA/TM—2002-211483, 2002. http://gltrs.grc.nasa.gov/cgi-bin/GLTRS/browse.pl?2002/TM-2002-211483.html

Find out more about this research: www.grc.nasa.gov/WWW/Oilfree

Glenn contact:
Dr. Christopher DellaCorte, 216–433–6056, Christopher.DeLlaCorte-1@nasa.gov

Author: Dr. Christopher DellaCorte

Headquarters Program Office: OAT

Programs/Projects:
Propulsion and Power

White Light Used to Enable Enhanced Surface Topography, Geometry, and Wear Characterization of Oil-Free Bearings

A new optically based measuring capability that characterizes surface topography, geometry, and wear has been employed by NASA Glenn Research Center's Tribology and Surface Science Branch. To characterize complex parts in more detail, we are using a three-dimensional, surface structure analyzer—the NewView5000 manufactured by Zygo Corporation (Middlefield, CT). This system provides graphical images and high-resolution numerical analyses to accurately characterize surfaces. Because of the inherent complexity of the various analyzed assemblies, the machine has been pushed to its limits. For example, special hardware fixtures and measuring techniques were developed to characterize Oil-Free thrust bearings specifically. We performed a more detailed wear analysis using scanning white light interferometry to image and measure the bearing structure and topography, enabling a further understanding of bearing failure causes.

The system consists of two parts—a microscope and a high-end computer. Light directed through the microscope is split within the interferometric objective (lens). One portion is reflected off a highly polished internal reference surface in the objective and the other is reflected off the part to be measured. Both reflections are then captured by a solid-state camera that "sees" an interference between the two light wavefronts that results in dark and light bands called fringes. These fringes are analyzed and quantified into the surface topography of the part. Depths up to 100 μm (3937 μin.), with 0.1 nm (0.0039 μin.) vertical resolution and 0.4 nm (0.157 μin.) root mean square repeatability, are imaged independently of objective magnification. Lateral resolution, which depends on the pixel size from the field of view of the objective in use, ranges from 0.45 μm (17.7 μin.) at ×100 to 11.8 μm (464.5 μin.) at ×1. The data, which are collected without contacting the specimen, represent a wide dynamic range without affecting or damaging the surface of interest. Before and after test run images of a bare Inconel thrust bearing (see the figure) show the enhanced range of this system to determine more clearly the failure mechanisms involved.

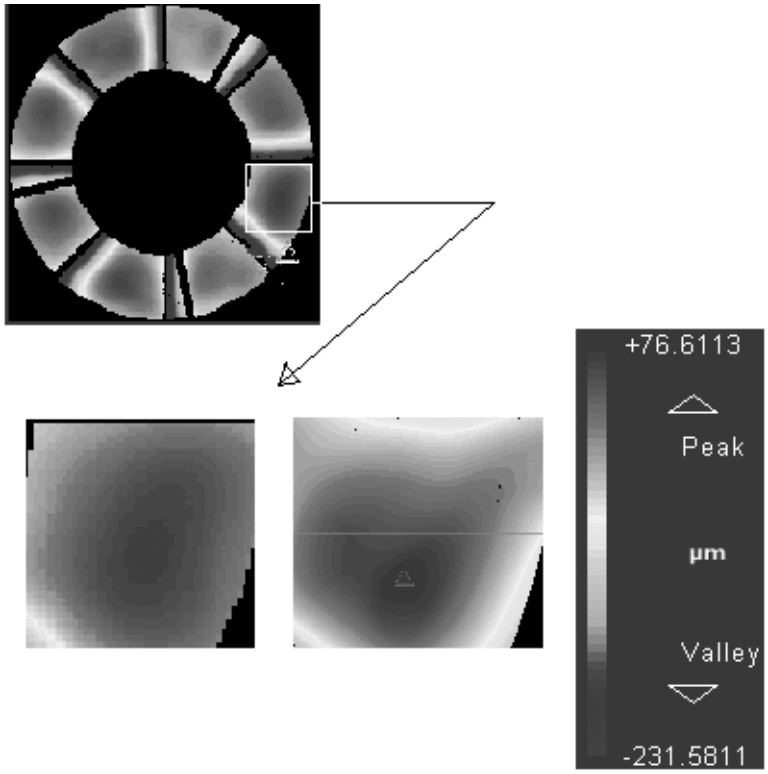

Surface topography of one of eight foil air thrust bearing pads. Left: Before test run. Right: After 100 start/stop cycles.This figure is shown in color in the online version of this article (http://www.grc.nasa.gov/WWW/RT2002/5000/5960lucero.html).

With this system, noncontacting three-dimensional surface topography and geometric measurements of up to 5 in. in diameter have been done by stitching together the numerous microscope scans required to image the whole part. This capability is far better than using a diamond stylus in one dimension, which is very limited in size and can affect the surface and/or measurement because of its necessary contact with the part. Using this optical method, one can determine a correlation between geometry, surface topography, and running/life performance from one bearing to another and investigate manufacturing quality control effects.

Find out more about this research:
http://www.grc.nasa.gov/WWW/Oilfree

Glenn contact:
John M. Lucero, 216–433–2684,
John.M.Lucero@nasa.gov

Author: John M. Lucero

Headquarters program office: OAT

Programs/Projects:
Propulsion and Power, UEET

In Situ, On-Demand Lubrication System Developed for Space Mechanisms

Many moving mechanical assemblies (MMA) for space mechanisms rely on liquid lubricants to provide reliable, long-term performance. The proper performance of the MMA is critical in assuring a successful mission. Historically, mission lifetimes were short and MMA duty cycles were minimal. As mission lifetimes were extended, other components, such as batteries and computers, failed before lubricated systems. However, improvements in these ancillary systems over the last decade have left the tribological systems of the MMAs as the limiting factor in determining spacecraft reliability.

Typically, MMAs are initially lubricated with a very small charge that is supposed to last the entire mission lifetime, often well in excess of 5 years. In many cases, the premature failure of a lubricated component can result in mission failure (refs. 1 to 3).

MMAs fail tribologically when the lubricant degrades or evaporates and, therefore, loses its ability to lubricate rubbing surfaces—bearing balls contacting raceways for example. Since the MMA is still mechanically intact when the lubricant degrades, if lubricant could be resupplied to the contact, the life of the MMA could be extended. Lubricant reservoirs have been used to resupply lubricant, but they are bulky, add complexity, and cannot be activated when needed (ref. 4). Rather, they continuously supply lubricant to the contact, often leading to an excess of lubricant.

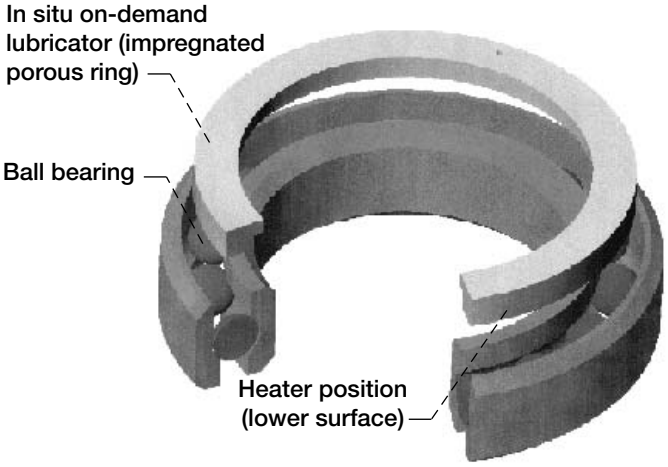

Drawing of the in situ, on-demand lubricator (porosity ≈ 25 vol% of oil that can be stored ≈ 94 mm^3) attached to the inner ring of a full complement ball bearing. Bore diameter, 19.05 mm (0.75 in.); outer diameter, 29.97 mm (1.18 in.); 24 balls with diameters of 3.175 mm (1/8 in.).

The lubricator reported here provides fresh lubricant to the ball-race contact in situ and on demand. The lubricant is stored in a porous cartridge attached to the inner or outer ring of a ball bearing. It is released by heating the cartridge to eject oil, taking advantage of the greater thermal expansion of the oil in comparison to the porous network. Heating can be activated by torque increases that signal the depletion of oil in the contact. The low surface tension of the oil in comparison to that of the ball bearing material is used, and the close proximity of the cartridge to the moving balls allows the lubricant to reach the ball-race contacts. This oil resupply system was successfully used to avoid a mechanism failure and reduce the torque to an acceptable level in a ball bearing initially operating without lubricant. The lifetime was extended in comparison to that of a similar ball bearing operating in the same conditions but without the lubricator attached to it. In addition, the in situ, on-demand lubricator consumes less than 1 W of power. This work was done in cooperation with the NASA Glenn Research Center's Tribology and Surface Sciences Branch.

References

1. Shapiro, Wilbur, et al.: Space Mechanisms Lessons Learned Study Volume I—Summary. NASA TM–107046, 1995. http://gltrs.grc.nasa.gov/cgi-bin/GLTRS/browse.pl?1995/TM-107046.html
2. Shapiro, Wilbur, et al.: Space Mechanisms Lessons Learned Study Volume II—Literature Review. NASA TM–107047, 1995. http://gltrs.grc.nasa.gov/cgi-bin/GLTRS/browse.pl?1995/TM-107047.html

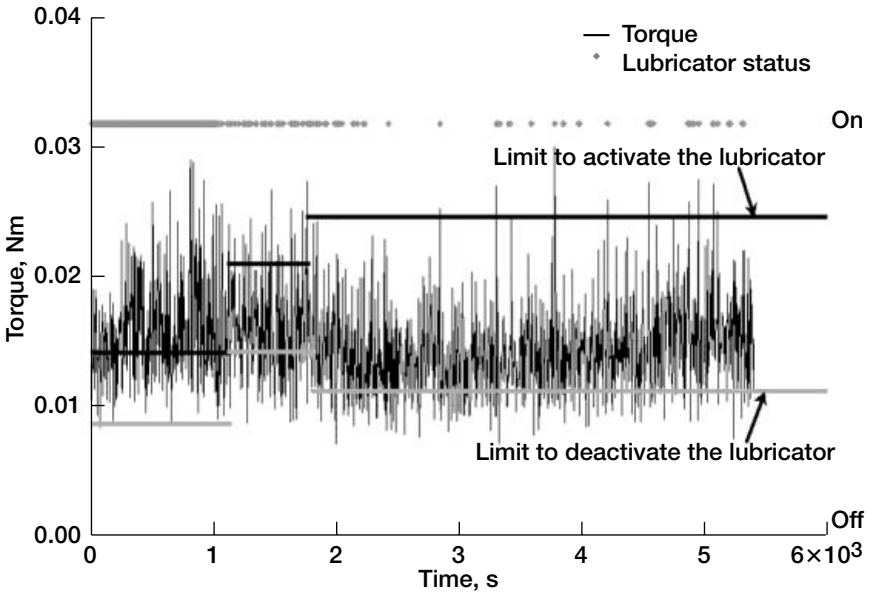

Stabilization of the torque trace of a ball bearing (load, 89 N (20 lb); speed, 200 rpm), initially unlubricated, with an in situ, on-demand lubricator impregnated with a synthetic oil.

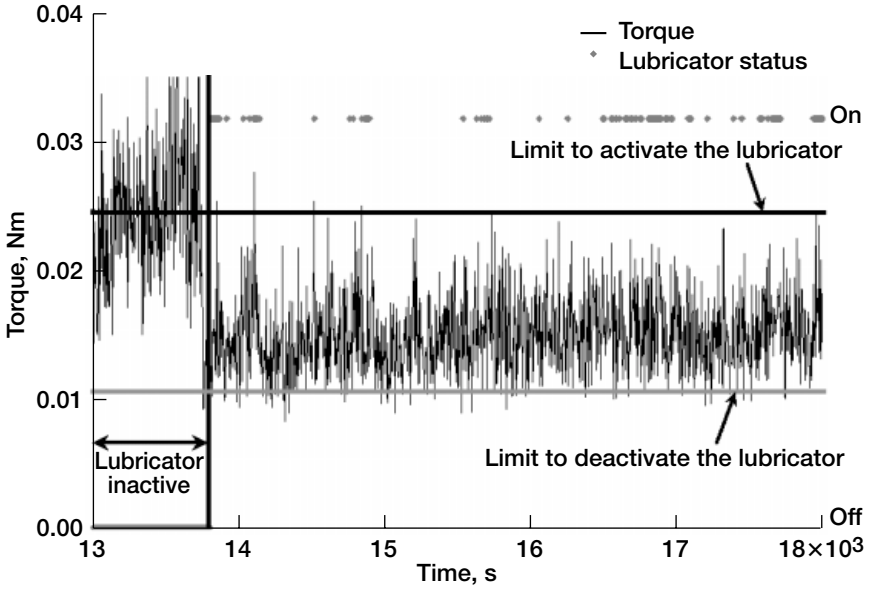

Decrease in the torque of a ball bearing (load, 89 N (20 lb); speed, 200 rpm), initially unlubricated, after reactivation of an in situ, on-demand lubricator impregnated with a synthetic oil.

3. Jones, William R., Jr.; and Jansen, Mark J.: Space Tribology. Modern Tribology Handbook, Vol. Two, CRC Press, Boca Raton, FL, 2001, pp. 1159–1186.
4. Zaretsky, E.V.: Liquid Lubrication in Space. Tribol. Int., vol. 23, no. 2, 1990, pp. 75–93.

National Research Council at Glenn contact:
Mario Marchetti, 216–433–5843, Mario.Marchetti@grc.nasa.gov

Glenn contact:
Dr. Stephen V. Pepper, 216–433–6061, Stephen.V.Pepper@nasa.gov

Sest, Inc., contacts:
William R. Jones, Jr., 216–433–6051, William.R.Jones@grc.nasa.gov; and Mark J. Jansen, 216–433–6054, Mark.J.Jansen@grc.nasa.gov

Authors: Mario Marchetti, William R. Jones, Jr., Dr. Stephen V. Pepper, Mark J. Jansen, and Roamer E. Predmore

Headquarters program office: OAT

Programs/Projects: GOES

Special recognition: This work was performed while the main author held a National Research Council Research Associateship Award in Glenn's Tribology and Surface Science Branch.

Radial Clearance Found To Play a Key Role in the Performance of Compliant Foil Air Bearings

Compliant foil air bearings are at the forefront of the Oil-Free turbomachinery revolution, which supports gas turbine engines with hydrodynamic bearings that use air instead of oil as the working fluid. These types of bearings have been around for almost 50 years and have found a home in several commercial applications, such as in air cycle machines, turbocompressors, and microturbines, but are now being aggressively pursued for use in small and midrange aircraft gas turbine engines. Benefits include higher operating speeds and temperatures, lower maintenance costs, and greater reliability. The Oil-Free Turbomachinery team at the NASA Glenn Research Center is working to foster the transition of Oil-Free technology into gas turbine engines by performing in-house experiments on foil air bearings in order to gain a greater insight into their complex operating principles.

A research program recently undertaken at Glenn focused on the concept of radial clearance and its influence on bearing performance. The tests were conducted on foil bearings with different radial clearances. As defined for a foil bearing, radial clearance is a measure of the small amount of shaft radial motion that is present from "play" that exists in the elastic support structure, such as between the top and bump foils and the bump foils and bearing shell (see the drawing). With an insufficient amount of radial clearance, the bearing imparts a high preload on the shaft, which when excessive, can reduce the load-carrying capability of the bearing. On the other hand, systems using foil bearings with excessive radial clearance may experience rotordynamic instabilities because of low bearing preload. Therefore, without a more thorough understanding of radial clearance, it is difficult to accurately predict the performance of a given bearing design.

The test program demonstrated that there is a direct correlation between radial clearance and the performance of foil air bearings. As shown in the graph, an optimum radial clearance exists that will maximize the amount of load that the bearing is capable of supporting. With respect to this optimum, two different performance regimes were observed that are a function of the amount of radial clearance. Tests showed that bearings with radial clearances below the optimum in regime I were susceptible to sudden seizure, a failure mode indicative of thermal runaway caused by high preload. The high preload is in response to an insufficient amount of radial clearance available to accommodate the thermal growth of the bearing and shaft. However, radial clearances greater than the optimum in regime II resulted in low bearing preloads that did not cause any heat-related

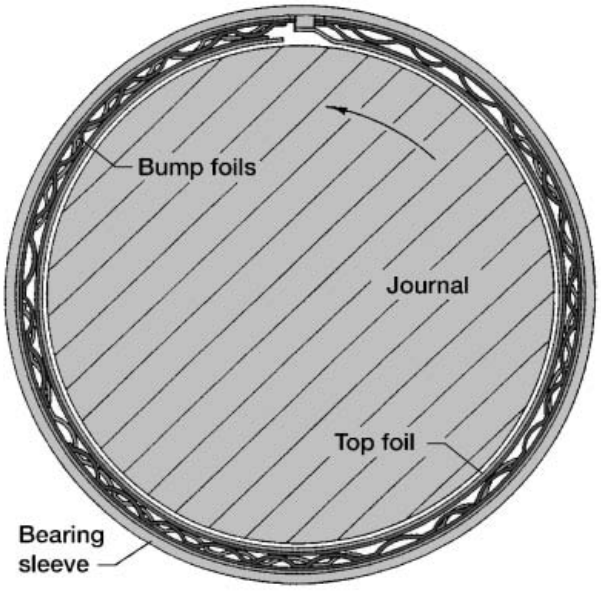

Foil bearing cross section.

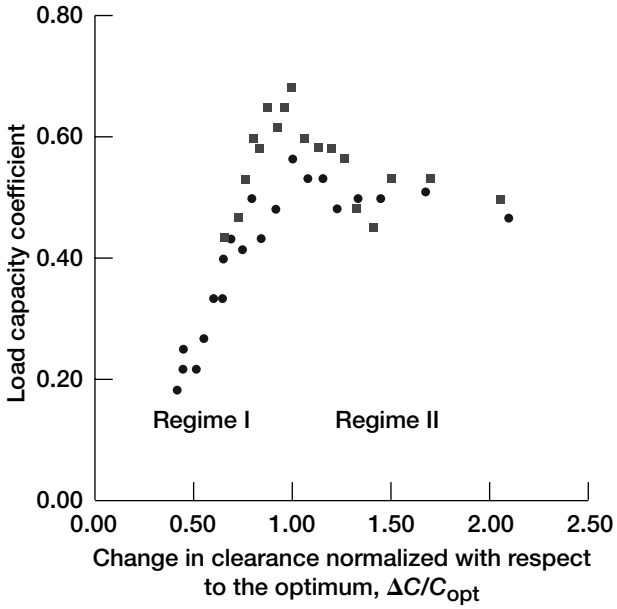

Bearing load capacity coefficient versus clearance.

problems, and the failure mode was due to fluid-film breakdown. In fact, bearings operating with radial clearances twice as much as the optimum suffered a decrease in the maximum load capacity of only about 20 percent.

Therefore, special attention has to be given to the range of operating conditions expected in the bearing/shaft system since changes in temperature, centrifugal, and hydrodynamic effects can all affect radial clearance. This enhanced understanding of foil air bearing behavior will greatly aid our efforts to transition Oil-Free technology to future aircraft engines.

Bibliography

Radil; Kevin; Howard, Samuel; and Dykas, Brian: The Role of Radial Clearance on the Performance of Foil Air Bearings. NASA/TM—2002-211705, 2002. http://gltrs.grc.nasa.gov/cgi-bin/GLTRS/browse.pl?2002/TM-2002-211705.html

Find out more about this research:
http://www.grc.nasa.gov/WWW/Oilfree/

U.S. Army, Vehicle Technology Directorate at Glenn contact:
Kevin C. Radil, 216–433–5047, Kevin.C.Radil@grc.nasa.gov

Glenn contact:
Dr. S. Adam Howard, 216–433–6076, Samuel.A.Howard@nasa.gov

Author: Kevin C. Radil

Headquarters program office: OAT

Programs/Projects: Propulsion and Power, Propulsion Systems R&T

Commercialization of NASA PS304 Solid Lubricant Coating Enhanced by Fundamental Powder Flow Research

The NASA Glenn Research Center has developed a patented high-temperature solid lubricant coating, designated PS304, for reducing friction and wear in bearing systems. The material used to produce the coating is initially a blend of metallic and ceramic powders that are deposited on the bearing surface by the plasma spray process. PS304 was developed to lubricate foil air bearings in Oil-Free turbomachinery, where the moving surfaces are coated with a hydrodynamic air film except at the beginning and end of an operation cycle when the air film is not present. The coating has been successful in several applications including turbochargers, land-based turbines, and industrial drying furnace conveyor components, with current development activities directed at implementation in Oil-Free aeropropulsion engines.

For the PS304 coating to be transferred to industrial use, the deposition process must be predictable and the coating material cost should be low. Since the early development of PS304, problems have sporadically surfaced where the powder blend would clog in the deposition equipment (powder hoppers, feed lines, and spray gun nozzles). The reasons for this behavior were unclear and appeared to be unrepeatable from powder batch to batch.

Anecdotal evidence suggested that high humidity and feedstock particles that were too small interfered with deposition reproducibility, so Glenn researchers conducted a series of controlled experiments to investigate the problem. In typical laboratory conditions, Glenn researchers found that the shape and the size of the feedstock particles were more important than humidity for effective control of the deposition process. An additional benefit of this study was the development of a novel powder fabrication process for one of the components of PS304.

The ceramic material that provides high-temperature solid lubrication in the coating, BaF_2-CaF_2, is traditionally made in a manner that generates many small, angularly shaped particles (top photomicrograph on the next page), which impede powder flow and affect the deposition process. In the new process, this constituent was made by melt atomization such that the resultant powder particles were smooth with far fewer fine particles (center and bottom photomicrographs). Feedstock prepared with these powders exhibit improved flowability, lower variance in flow rate, and reduced susceptibility to humidity. As shown in the graph, the angular powder degrades feedstock flow, whereas the spherical powder does not. Recently completed testing shows that the rounded powder follows the line predicted by the rule of mixtures (see the graph). Because the number of steps required to produce the powder by atomization is significantly reduced, the material cost is much lower, enhancing commercial transfer. Licensing agreements are under development for powder production.

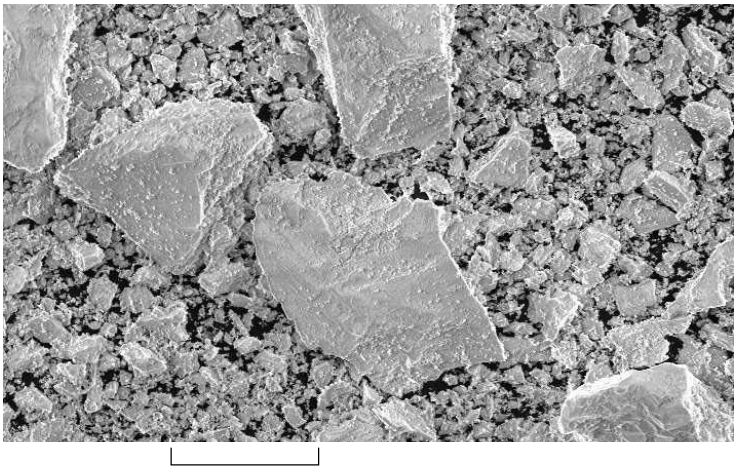

Ceramic solid lubricant particles in PS304. Using rounded or spherical particles, respectively, gives increasingly better flow properties to the feedstock powder blend. Top: Angular morphology. Center: Rounded morphology. Bottom: Spherical morphology.

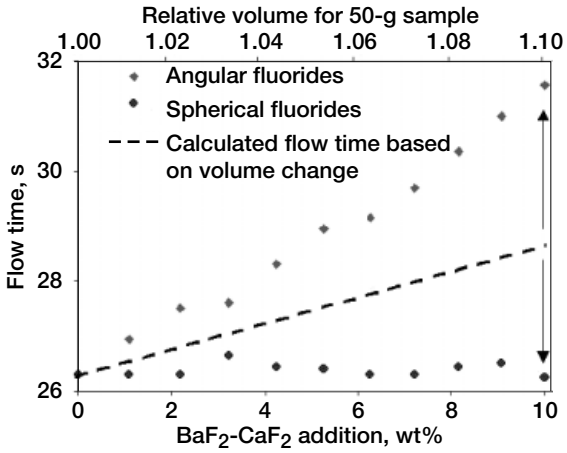

Influence of BaF_2-CaF_2 powder addition on the flow rate of PS304 feedstock.

Bibliography

Stanford, Malcolm K.; and DellaCorte, Christopher: Effects of Humidity on the Flow Characteristics of PS304 Plasma Spray Feedstock Powder Blend. NASA/TM—2002-211549, 2002. http://gltrs.grc.nasa.gov/cgi-bin/GLTRS/browse.pl?2002/TM-2002-211549.html

Stanford, Malcolm K.; DellaCorte, Christopher; and Eylon, Daniel: Particle Morphology Effects on Flow Characteristics of PS304 Plasma Spray Coating Feedstock Powder Blend. NASA/TM—2002-211206, 2002. http://gltrs.grc.nasa.gov/cgi-bin/GLTRS/browse.pl?2002/TM-2002-211206.html

Stanford, Malcolm K.; DellaCorte, Christopher; and Eylon, Daniel: Particle Size Effects on Flow Properties of PS304 Plasma Spray Feedstock Powder Blend. NASA/TM—2002-211550, 2002. http://gltrs.grc.nasa.gov/cgi-bin/GLTRS/browse.pl?2002/TM-2002-211550.html

Find out more about this research:
http://www.grc.nasa.gov/WWW/Oilfree/

Glenn contact:
Dr. Malcolm K. Stanford, 216–433–3387, Malcolm.K.Stanford@nasa.gov

Author: Dr. Malcolm K. Stanford

Headquarters Program Office: OAT

Programs/Projects:
Propulsion and Power

NASA PS304 Lubricant Tested in World's First Commercial Oil-Free Gas Turbine

In a marriage of research and commercial technology, a 30-kW Oil-Free Capstone microturbine electrical generator unit has been installed and is serving as a test bed for long-term life-cycle testing of NASA-developed PS304 shaft coatings. The coatings are used to reduce friction and wear of the turbine engine's foil air bearings during startup and shut down when sliding occurs, prior to the formation of a lubricating air film. This testing supports NASA Glenn Research Center's effort to develop Oil-Free gas turbine aircraft propulsion systems, which will employ advanced foil air bearings and NASA's PS304 high-temperature solid lubricant to replace the ball bearings and lubricating oil found in conventional engines. Glenn's Oil-Free Turbomachinery team's current project is the demonstration of an Oil-Free business jet engine. In anticipation of future flight certification of Oil-Free aircraft engines, long-term endurance and durability tests are being conducted in a relevant gas turbine environment using the Capstone microturbine engine. By operating the engine now, valuable performance data for PS304 shaft coatings and for industry's foil air bearings are being accumulated.

Capstone microturbine installed in lab.

The Capstone microturbine is a gas-turbine-driven electrical generator unit manufactured by the Capstone Turbine Corporation (Chatsworth, CA) and is an ideal test bed for the NASA coating technology because it uses foil air bearings and operates at high shaft speeds (up to 96 000 rpm) and temperatures. These conditions are very similar to those expected in future Oil-Free aeropropulsion engine applications. The Capstone microturbine is the world's first commercially available gas turbine engine to use this Oil-Free bearing technology.

In addition to applying PS304 coatings to the engine shafting, other modifications to the system were made that allow the electrical power output to be captured. While the facility is testing PS304 shaft coatings, the 30-kW of electrical power generated is being phase and frequency matched and put back onto the local utility grid instead of wasted via dissipative heating. The microturbine test rig was activated in May 2002 and has logged over 1200 hr of testing near peak operating conditions to date. At regular intervals, the engine will be dismantled for inspection then reassembled for more testing. Aircraft gas turbines are designed to run for up to 20 000 hr, and it is anticipated that the Capstone microturbine will provide nearly double that valuable technology test time over the next several years.

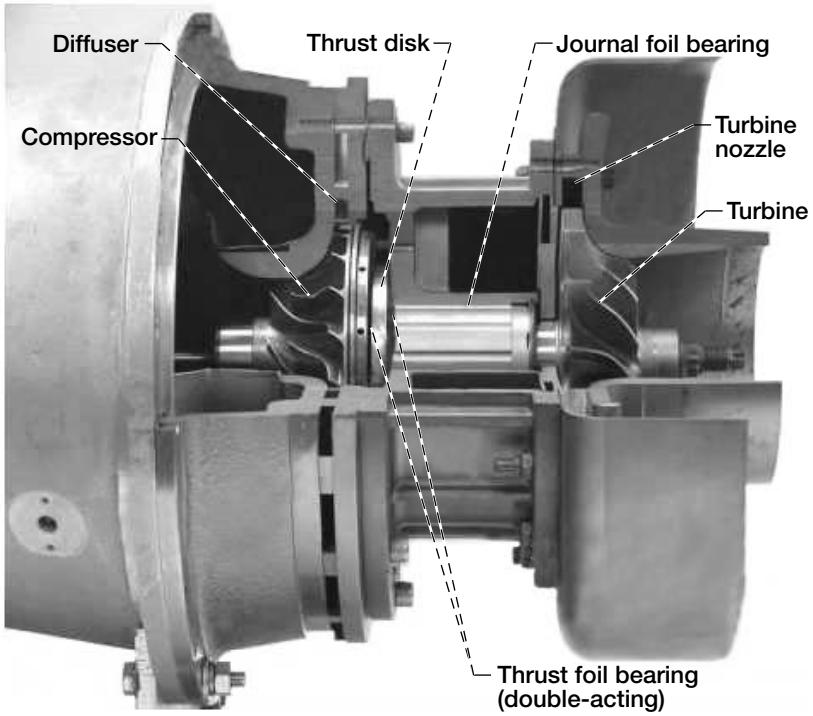

Cross-section cutaway photographic view of Oil-Free turbine engine.

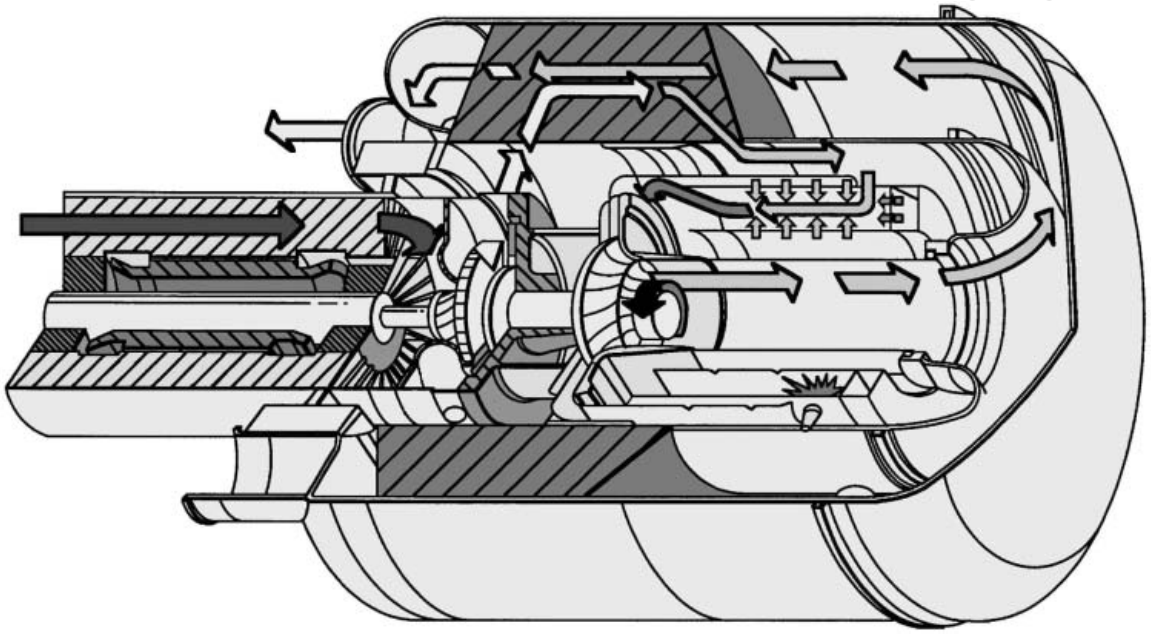

Cross-section cutaway illustration of generator and engine.

Find out more about this research: http://www.grc.nasa.gov/WWW/Oilfree/

Glenn contacts:
Harold F. Weaver, 216–433–8869, Harold.F.Weaver@nasa.gov; and
Dr. Christopher DellaCorte, 216–433–6056 Christopher.DeLlaCorte-1@nasa.gov

Author: Harold F. Weaver

Headquarters program office: OAT

Programs/Projects: Propulsion and Power, Propulsion Systems R&T

R&T 2002

Space

Space Communications

Phased-Array System Characterized

In future satellite communication systems, demands for faster access and more information are expected to increase because of the continuous growth of the Internet and direct-to-user satellite requirements. Meeting these requirements will require multibeam satellite systems having an onboard active phased-array antenna system. Phased-array-antenna-based communications links are anticipated to deliver high data rates without the risk of the single-point failure of the gimbaled motors and transmitters used in reflector-based systems. Phased-array antennas contain a multitude of radiating elements, typically arranged in a rectangular or triangular tessellation. Beams are formed by electrically adjusting the relative phase of the radiating elements using ferrite or semiconductor devices. Phased-array antennas have been developed mainly for radar applications but are being used more now for space-based communications applications because of their advantages in scanning, reconfigurability, weight, and power.

Operation of high-rate, high-frequency phased-array systems has been shown theoretically to degrade performance on the order of 3 to 4 dB at large scan angles (see the graphs). Determining the extent of these degrading system effects requires system-level characterization techniques, which are a battery of specialized tests that include modulation and antenna correlations under dynamic operating conditions. Once these degradation effects are fully characterized, mitigation techniques will be proposed and tested. The specialized tests are being performed experimentally in NASA Glenn Research Center's Far-Field Anechoic Chamber. In addition, Glenn engineers are using Matlab/Simulink to perform theoretical computations.

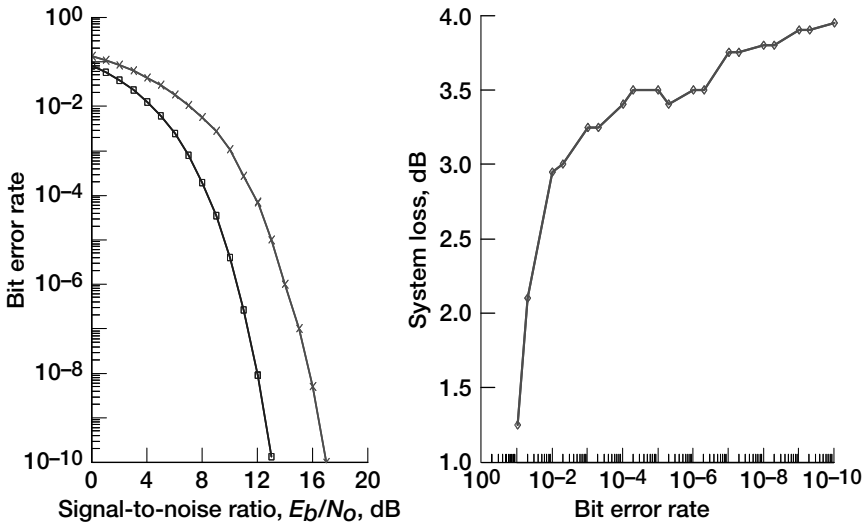

Theoretical model of phased-array-antenna intersymbol interference. Left: quadrature phase-shift keying/binary phase-shift keying (QPSK/BPSK) worst-case bit error rate performance. Right: System loss—QPSK and BPSK.

In the past year, static characterization tests have been initiated using a 91-element receive array. The tests performed so far include the effects of beam-steering transients and wide-angle scanning. Wide-angle scanning degradation is caused by the introduction of intersymbol interference into the link. The intersymbol interference is due to the timing error between signals radiating from the array elements caused by a physical 360° limitation in the phase shifters. The results of the wide-angle scanning characterization performed to date indicate <1-dB performance savings for medium data rates of 220 Mbps, but they validate the model and expectation of 2- to 3-dB savings for higher data rates as envisioned by NASA's major enterprises.

Transient effects in the radiofrequency (RF) communications channel are observed when the beam of a phased-array antenna is switched from one pointing direction to another. Such effects can be attributed to electrical ringing of the antennas' phase shifters or to system implementation effects such as the nonsimultaneous switching of the phase shifters. In particular, testing has revealed implementation-specific transient effects in the RF channel that are associated with digital clocking pulses that occur with transfers of data from the beam-steering controller to the digital electronics of the phased-array antenna being tested. Effects of the digital clocking pulses are observed prior to the beam switch, and they have a significant effect on the RF path of the system. Observed changes to the RF channel clearly increase the average bit error rate in the individual symbols during beam-switch transient events, however, a

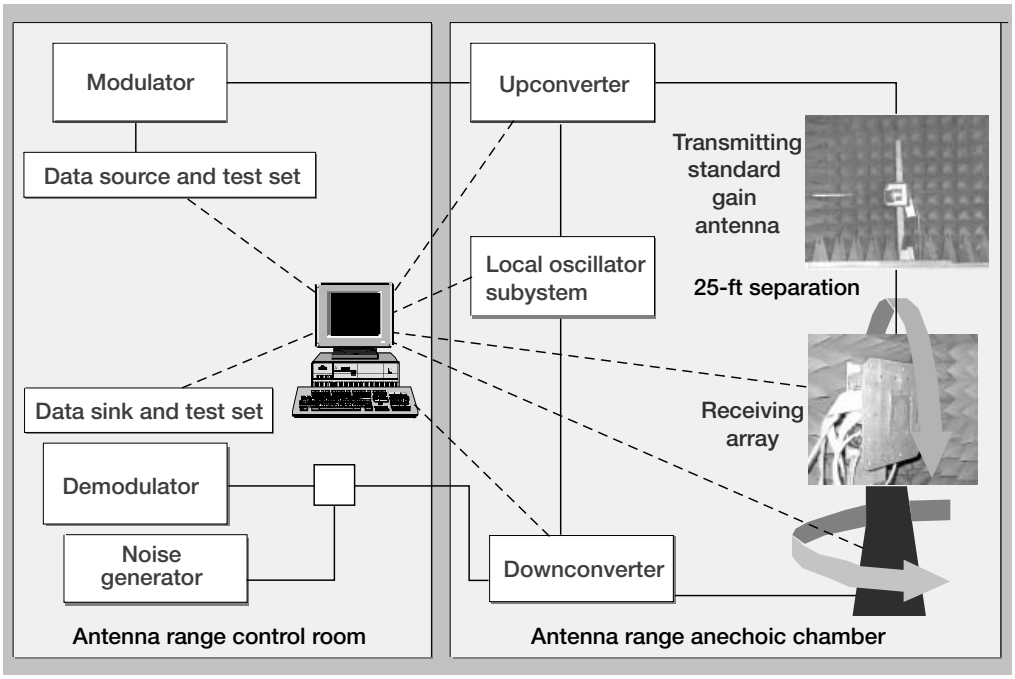

Dynamic system emulation.

potentially more serious effect is the loss of receiver synchronization with the communications signal brought by the transients.

Phased-array antennas are highly advantageous in a low-Earth orbiting satellite system where high data rates direct to users on the ground are required. Experiments are being conducted at Glenn to characterize high-data-rate phased-array links in a simulated low-Earth-orbit environment. These experiments characterize phased-array antennas interacting with various modulation techniques at high data rates and other variables to provide a more complete understanding of the operational characteristics that are experienced in a low-Earth-orbit environment. In these experiments, the low-Earth-orbit environment is simulated by dynamically scanning the array while simultaneously rotating the range pedestal in the complementary direction. The optimal beam switch pattern for when the satellite passes over a user can be verified. The block diagram above shows this dynamic system emulation capability.

A savings of 2 to 3 dB in array-based system performance could reduce the number of antenna elements by 25 to 30 percent, saving cost and prime power. Once system losses have been identified and mitigated, system designers no longer need to design added link margin to cover these losses. Thus, addressing these losses in advance reduces the antenna size, yielding cost, power, and mass savings. Glenn's facilities provide an enviroment to operate the beam-steering control of array antennas in a manner expected for flightlike, aerospace, or surface mobile scenarios. Dynamic array scanning with synchronized pedestal control allows system engineers to simulate typical array operation and gather firsthand experience in array behavior and expected system performance under realistic conditions.

Find out more about this research:
http://spacecom.grc.nasa.gov

Glenn contacts:
Sandra Johnson, 216–433–8016, Sandra.K.Johnson@nasa.gov;
Richard Reinhart, 216–433–6588, Richard.C.Reinhart@nasa.gov;
Dr. Obed S. Sands, 216–433–2607, Obed.S.Sands@nasa.gov; and
Dr. Roberto Acosta, 216–433–6640, Roberto.J.Acosta@nasa.gov

Authors: Sandra K. Johnson, Richard C. Reinhart, Dr. Obed S. Sands, and Dr. Roberto J. Acosta

Headquarters program office:
OSF, Space Communication and Data Systems

Programs/Projects: Earth and space science missions in near Earth orbit, constellation and ad hoc networks, space communications

Microgravity Science

Field Effects of Buoyancy on a Premixed Turbulent Flame Studied by Particle Image Velocimetry

Typical laboratory flames for the scientific investigation of flame/turbulence interactions are prone to buoyancy effects. Buoyancy acts on these open flame systems and provides upstream feedbacks that control the global flame properties as well as local turbulence/flame interactions. Consequently the flame structures, stabilization limits, and turbulent reaction rates are directly or indirectly coupled with buoyancy. The objective of this study is to characterize the differences between premixed turbulent flames pointing upwards (1g), pointing downwards (–1g), and in microgravity (μg). The configuration is an inverted conical flame stabilized by a small cone-shaped bluff body that we call CLEAN Flames (Cone-Stabilized Lean Flames). We use two laser diagnostics to capture the velocity and scalar fields. Particle image velocimetry (PIV) measures the mean and root mean square velocities and planar imaging by the flame fronts method outlines the flame wrinkle topology. The results were obtained under typical conditions of small domestic heating systems such as water heaters, ovens, and furnaces. Significant differences between the 1g and –1g flames point to the need for including buoyancy contributions in theoretical and numerical calculations. In Earth gravity, there is a complex coupling of buoyancy with the turbulent flow and heat release in the flame. An investigation of buoyancy-free flames in microgravity will provide the key to discern gravity contributions. Data obtained in microgravity flames will provide the benchmark for interpreting and analyzing 1g and –1g flame results.

This study is being conducted by the Lawrence Berkeley National Laboratory, with project management and assistance in hardware development, engineering feasibility, and other efforts provided by the NASA Glenn Research Center. The study is focusing on lean premixed combustion, which is a proven method to reduce the formation of pollutants such as nitrogen oxides (NO_x). However, its adaptation to many industrial heating systems is prone to buoyancy influences that affect heat distribution, system reliability, and even safety provisions. At present, only rudimentary knowledge is available to guide combustion engineers to avoid or overcome buoyancy problems. In addition, turbulent combustion is considered to be the most important unsolved problem in combustion science, and current theoretical and numerical combustion models cannot handle buoyancy effects yet. Our research will benefit both combustion science and technology. Experimentalists will gain new insights for identifying and interpreting buoyancy contributions to laboratory flames.

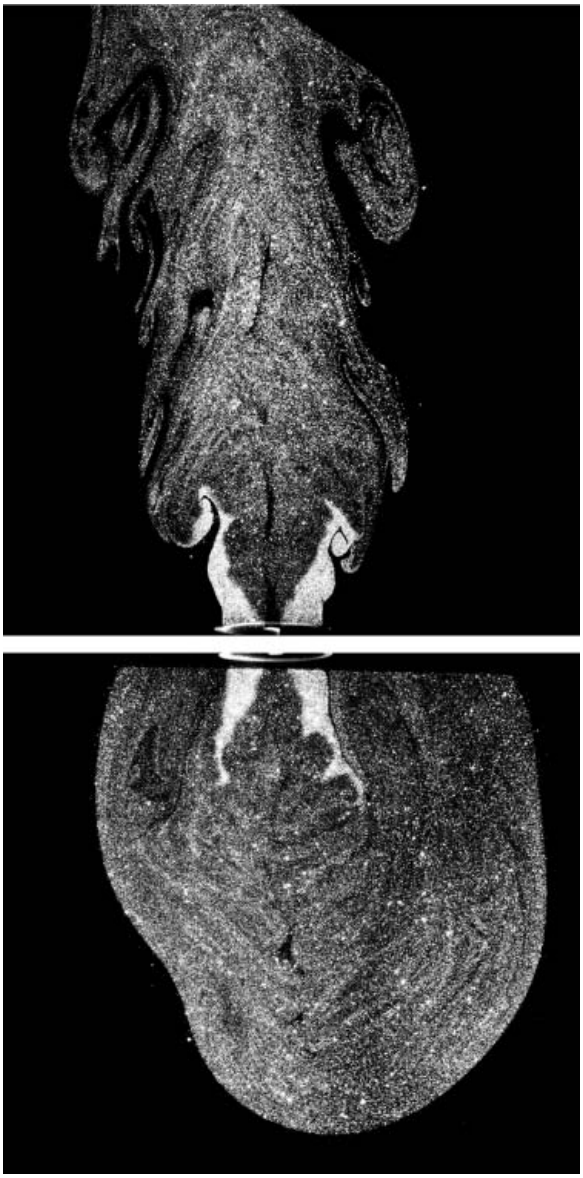

Flow-field images. Top: 1g. Buoyancy forces aligned with the flow direction augment instabilities in the products plume. Bottom: –1g. The importance of buoyancy is clear as reversing the flow direction suppresses instabilities and dramatically alters the flow field.

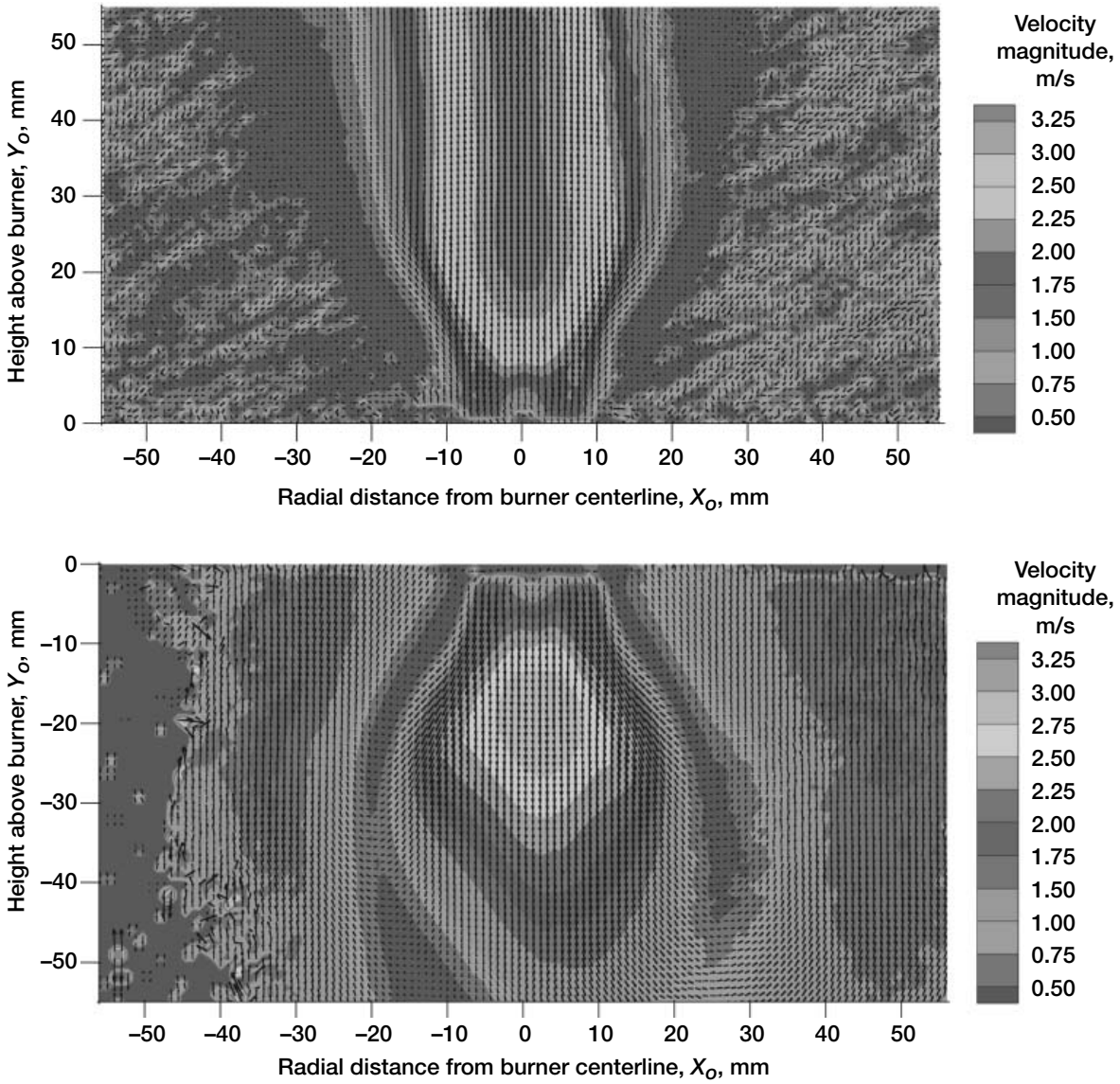

Preliminary PIV results. Top: 1g. Bottom: –1g. This figure is shown in color in the online version of this article (http://www.grc.nasa.gov/WWW/RT2002/6000/6711cheng.html).

Theoretical and numerical researchers will have a set of reference data to improve the fidelity of turbulent combustion models and to develop methods to address the problems of flame/chamber coupling. Combustion engineers will gain scientifically based scaling information to handle buoyancy influences on practical systems.

Glenn contact:
Paul Greenberg, 216–433–3621, Paul.S.Greenberg@nasa.gov

Lawrence Berkeley National Laboratory contact:
Robert K. Cheng, 510–486–5438, RKCheng@lbl.gov

Author: Robert K. Cheng

Headquarters program office: OBPR

Programs/Projects: Microgravity Science

Fan Beam Emission Tomography Demonstrated Successfully in the Reduced-Gravity Environment of Drop Towers

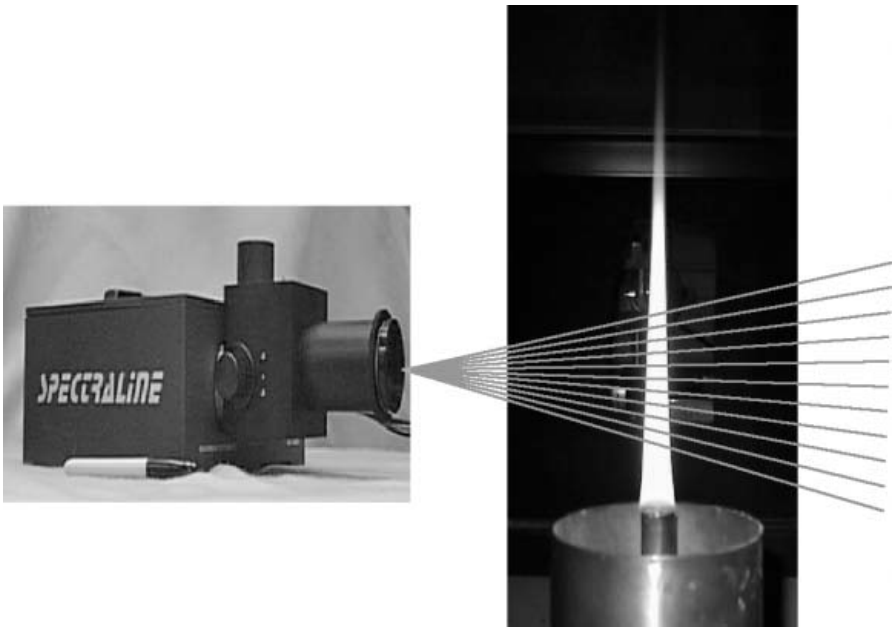

Scanning spectrometer with an ethylene laminar flame with air coflow.

Fires onboard manned spacecraft and launch vehicles are a particularly feared hazard because one cannot jump ship while in orbit 240 nmi above the Earth at 17 000 mph! Understanding the physical properties of fires in free fall and on orbit is, therefore, a very important endeavor for NASA's Human Exploration and Development of Space (HEDS) enterprise. However, detailed information concerning the structure of microgravity fires remained elusive until recently since robustness, limited power, limited volume, and limited mass place severe constraints on diagnostic equipment for use in space and in NASA Glenn Research Center's reduced-gravity facilities. Under NASA Research Associate funding since 2001, En'Urga, Inc. (Dr. Sivathanu, principal investigator, and Dr. Lim, coinvestigator) in collaboration with Glenn (Dr. Feikema, coinvestigator) have successfully demonstrated a new technology for use in microgravity combustion. A midinfrared scanning spectrometer has been developed by En'Urga and tested at Glenn to measure 30 spectra per second at different spatial locations in a flame from 1.8 to 4.8 μm. The spectra clearly show water vapor, soot, and carbon dioxide emissions from the flame. A deconvolution program is being developed to transform the spectra into spatial profiles of soot volume fraction, gas temperature, water vapor concentration, and carbon dioxide concentration. This is a particularly important technological achievement since, for the first time in weightlessness, one instrument can measure simultaneously and nonintrusively many parameters that previously required multiple instruments. This instrument will enable combustion researchers in the microgravity program to obtain detailed information concerning flame and fire phenomenon in reduced gravity. This information will help improve the models and safety of manned spacecraft. Spinoff technologies may be used in areas such as biological diagnostics, food processing industries, automotive industries, and aircraft manufacturing. Jet engine manufacturers also may benefit from the development of flight-weight diagnostic capabilities.

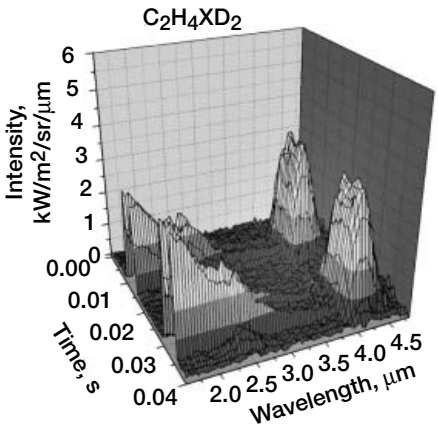

Sample transient microgravity flame spectra collected in Glenn's 2.2-Second Drop Tower. Water vapor peaks near 2.0 μm and carbon dioxide peaks near 4.0 μm.

Glenn contact:
Dr. Douglas Feikema, 216–433–5707, Douglas.A.Feikema@nasa.gov

En'Urga, Inc. contact:
Yudaya Sivathanu, 765–497–3269, sivathan@enurga.com

Author: Dr. Douglas A. Feikema

Headquarters program office: OBPR

Programs/Projects: Microgravity Combustion Science, HEDS

Radiative Enhancement Effects on Flame Spread (REEFS) Project Studied "Green House" Effects on Fire Spread

The Radiative Enhancement Effects on Flame Spread (REEFS) project, slated for flight aboard the International Space Station, reached a major milestone by holding its Science Concept Review this year. REEFS is led by principal investigator Paul Ronney from the University of Southern California in conjunction with a project team from the NASA Glenn Research Center. The study is focusing on flame spread over flat solid fuel beds to improve our understanding of more complex fires, such as those found in manned spacecraft and terrestrial buildings. The investigation has direct implications for fire safety, both for space and Earth applications, and extends previous work with emphasis on the atmospheres and flow environments likely to be present in fires that might occur in microgravity. These atmospheres will contain radiatively active gases such as carbon dioxide (CO_2) from combustion products, and likely gaseous fuels such as carbon monoxide (CO) from incomplete combustion of solid fuel, as well as flows induced by ventilation currents.

During tests in the 2.2-Second Drop Tower and KC–135 aircraft at Glenn, the principal investigator introduced the use of foam fuels for flame spread experiments over thermally thick fuels to obtain large spread rates in comparison to those of dense fuels such as PMMA. This enables meaningful results to be obtained even in the 2.2 s available in drop tower experiments.

Thick-fuel flame spread experiments using foam fuels gave indications that, in contrast to conventional understanding, steady spread can occur over thick fuels even in quiescent microgravity environments, especially when a radiatively active diluent gas such as CO_2 is employed, as the principal investigator had hypothesized. As with thin fuels, the spread rates at microgravity can even exceed those at Earth gravity when a radiatively active diluent gas is used. Measurements of radiative emission from O_2/CO_2 atmosphere tests in microgravity revealed that there is substantial emission, absorption, and reemission. Hence, it was shown that the faster flame spread rates are due to radiative transfer from the flame to the unburned fuel surface (the "green house" effect) and that this heat transfer enhancement can lead to steady spread even when conductive heat transfer from the flame to the fuel bed is negligible.

These findings are particularly noteworthy considering that the International Space Station employs CO_2 fire extinguishers; the results suggest that helium may be a better fire suppressant/extinguishing agent on both mass and mole bases in microgravity even though CO_2 is much better on a mole basis in Earth gravity.

REEFS plans to use the FEANICS (Flow Enclosure Accommodating Novel Investigations in Combustion of Solids) insert that will go into the Combustion Integrated Rack facility on the International Space Station. FEANICS is a generically designed flow tunnel for solid fuel and spacecraft fire safety combustion experiments conducted by several investigators.

Glenn contact:
Dr. Suleyman Gokoglu, 216–433–5499, Suleyman.A.Gokoglu@nasa.gov

Authors: Dr. Suleyman A. Gokoglu and Prof. Paul Ronney

Headquarters program office: OBPR

Programs/Projects:
Microgravity Science, REEFS

Front-view image of flame spread over a thick, 10-cm-wide solid fuel bed. Flame spreads toward the bottom of the image. The bright band in the lower part of the images is the flame front; the upper bright band is from the ignition source. Top: Microgravity. Bottom: Earth gravity.

Interaction Between Flames and Electric Fields Studied

The interaction between flames and electric fields has long been an interesting research subject that has theoretical importance as well as practical significance. Many of the reactions in a flame follow an ionic pathway: that is, positive and negative ions are formed during the intermediate steps of the reaction. When an external electric field is applied, the ions move according to the electric force (the Coulomb force) exerted on them. The motion of the ions modifies the chemistry because the reacting species are altered, it changes the velocity field of the flame, and it alters the electric field distribution. As a result, the flame will change its shape and location to meet all thermal, chemical, and electrical constraints. In normal gravity, the strong buoyant effect often makes the flame multidimensional and, thus, hinders the detailed study of the problem.

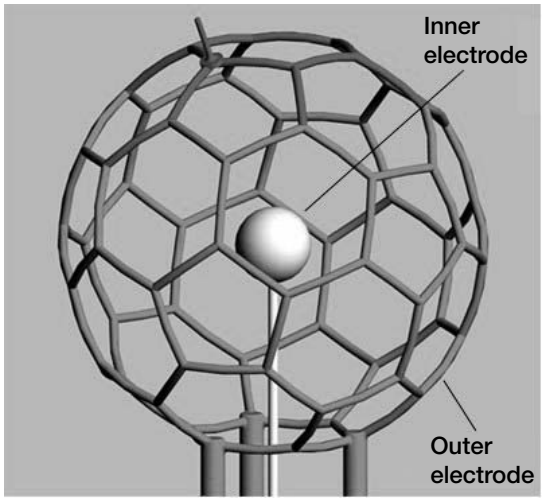

Spherical electrodes between which spherical flames will be established and studied in microgravity.

This project utilizes the microgravity environment provided by the 2.2-Second Drop Tower at the NASA Glenn Research Center to create a one-dimensional, spherically symmetric flame and electric field. In the experiments, the fuel gas (methane, propane, or ethylene) is issued from a spherical porous brass burner that also acts as an inner electrode. The burner is surrounded by a concentric spherical Faraday cage serving as an outer electrode (see the figure to the right), and an adjustable, dc, high-voltage source feeds the desired voltage to the two electrodes. The established electric field has spherical equipotential surfaces between the two electrodes, except in the local area where a thin stainless steel tube is connected to the burner to provide the fuel passage and electrical connection. In microgravity, flames with large spherical portions can be established between the two electrodes.

Results from these studies are clarifying the effects of electric field strength and polarity and the effects of fuel type on (1) flame shape and size, (2) flame sooting propensity, (3) flame unsteadiness, and (4) flame extinction behavior. For a given type of fuel with a fixed-mass flow rate, the flame radius of the spherical portion and the flame shape of the nonspherical portion strongly depend on the electric field strength and polarity. For example, for ethylene flames, when the outer electrode is positively charged with respect to the inner electrode, the flame radius is affected little, whereas for the reversed polarity, the flame radius shrinks significantly and the nonspherical portions of the flame sometimes undergo unsteady pulsations. At high field intensities, local flame extinction is also observed. The figure to the left shows images of ethylene flames burning in air at atmospheric pressure at a fuel flow rate of 2.3 mg/s under various applied voltages, 1.8 s after the drop commenced.

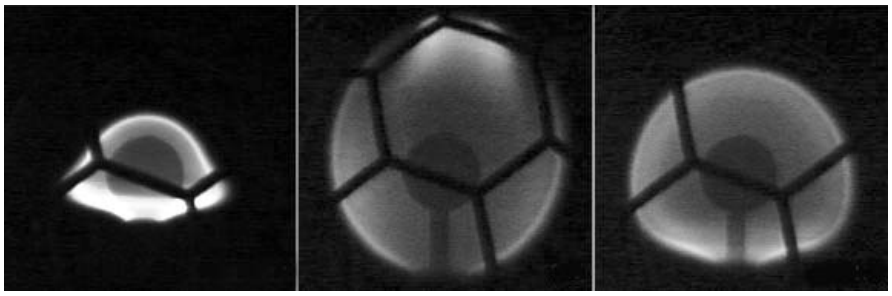

Images of ethylene flames burning in 1 atm pressure in microgravity subject to different dc voltages between the two electrodes (voltage of the outer electrode with respect to the inner electrode). The dark lines in the images are the out-of-focus member of the outer electrode. Left: –1.8 kV. Center: 0 V. Right: 1.8 kV.

National Center for Microgravity Research contacts:
Dr. Zeng-Guang Yuan, 216–433–2838, Zengguang.Yuan@grc.nasa.gov; and Dr. Uday Hegde, 216–433–8744, Uday.Hegde@grc.nasa.gov

Authors: Dr. Zeng-Guang Yuan and Dr. Uday Hegde

Headquarters program office: OBPR

Programs/Projects:
Microgravity Science

Ocular Blood Flow Measured Noninvasively in Zero Gravity

In spaceflight or a reduced-gravity environment, bodily fluids shift to the upper extremities of the body. The pressure inside the eye, or intraocular pressure, changes significantly. A significant number of astronauts report changes in visual acuity during orbital flight. To date this remains of unknown etiology. Could choroidal engorgement be the primary mechanism and a change in the curvature or shape of the cornea or lens be the secondary mechanism for this change in visual acuity? Perfused blood flow in the dense meshwork of capillaries of the choroidal tissue (see the folllowing illustration) provides necessary nutrients to the outer layers of the retina (photoreceptors) to keep it healthy and maintain good vision. Unlike the vascular system, the choroid has no baroreceptors to autoregulate fluid shifts, so it can remain engorged, pushing the macula forward and causing a hyperopic (farsighted) shift of the eye. Experiments by researchers at the NASA Glenn Research Center could help answer this question and facilitate planning for long-duration missions.

We are investigating the effects of zero gravity on the choroidal blood flow of volunteer subjects. This pilot project plans to determine if choroidal blood flow is autoregulated in a reduced-gravity environment. It will help ascertain in future experiments if there is a relationship between changing intraocular pressure and a systemic blood pressure with the choroidal flow. These experiments are being conducted onboard a wide-body aircraft (KC–135) during parabolic flight trajectories (which produce environments varying from low to high gravity). A low-power (~100 μW) continuous-wave (CW) solid-state laser operating at a wavelength of ~780 nm is being used to measure frequency shift in a head-mounted miniature laser Doppler flowmeter. The Doppler shift results from red blood cells flowing through the choroids. This yields parametric measurements of blood volume, speed, and flow. Each measurement takes approximately 15 s to complete.

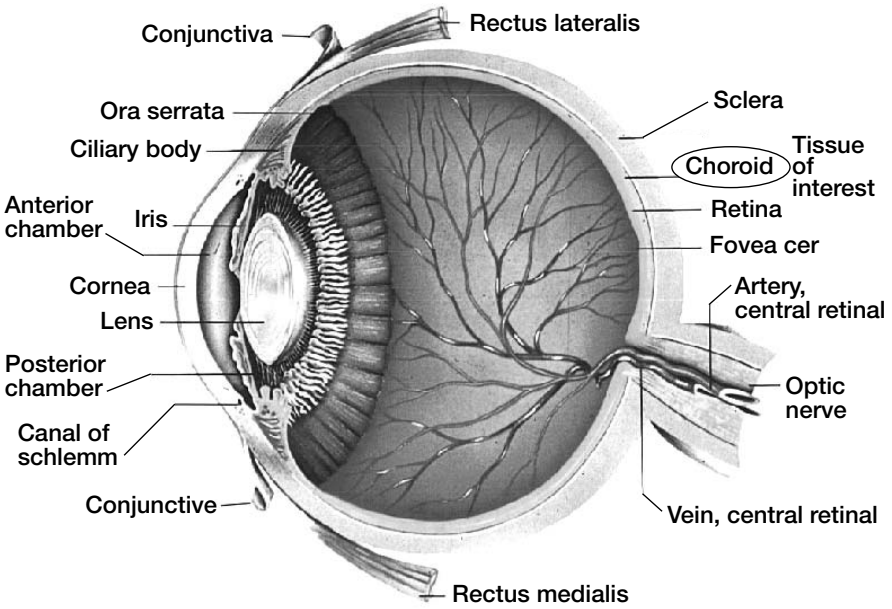

Blood flow is measured in the dense meshwork of capillaries in the back of the retina in a tissue layer called the choroid (see circled region).

In these experiments, the incident laser light shifts in frequency after it interacts with the red blood cells flowing in the choroidal tissue. This frequency shift is proportional to the speed of the moving red blood cells: $\Delta f = 1/2\pi(K_s - K_i)V_{RBC}$, where K_s and K_i are the wave vectors of the scattered and incident light, respectively, with magnitude $2\pi n/\lambda$, where n is the refractive index of the medium, λ is the wave length of light in vacuum, and V_{RBC} is the velocity of the red blood cells. The experimental scheme uses heterodyne detection, in which the light scattered from red blood cells is mixed with light reflected from the nonmoving tissue at an avalanche photodiode (APD) photodetector. After the electronic processing of these signals, a power spectrum is obtained and parameters such as blood volume, speed, and red blood cell flux are calculated.

The optical system (see the schematic diagram on the next page) for the illumination and detection of ocular tissue consists of 18 parts. First the source, a laser diode controlled by an electronic driver, is imaged and magnified by two lenses (lenses 1 and 2) on a pinhole (for pseudoconfocal arrangement on the detection path). A neutral-density filter located between the lenses and the pinhole attenuates the power. Two other lenses (lenses 3 and 4) image the pinhole on an intermediate image plane. A pupil determines the beam size, and a polarized beam splitter redirects the light collected from the eye on the detection path. Both the pupil and the polarized beam splitter

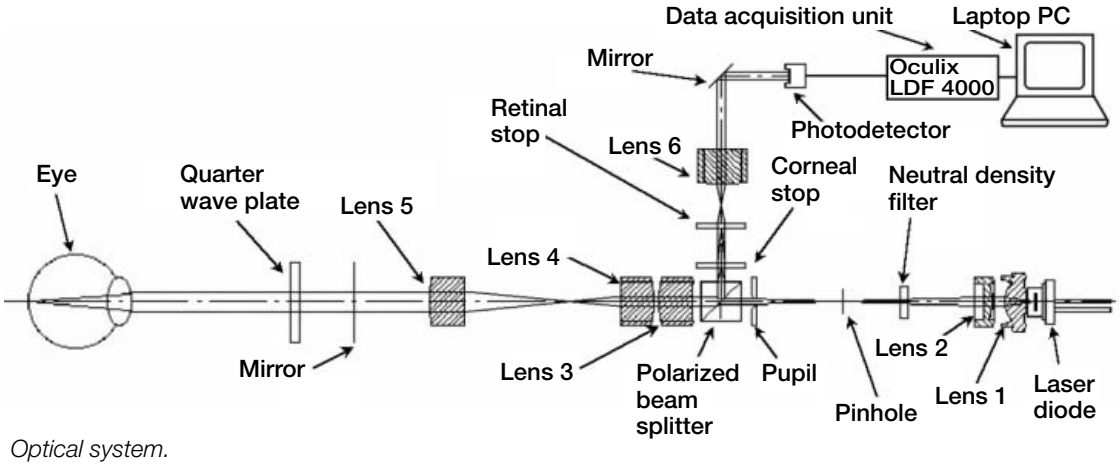

Optical system.

are located between the pinhole and lens 3. Lens 5 collimates the beam, and the eye lens refocuses it on the probed tissue. This lens is placed on a translational stage to allow image adjustment at the retina for myopic or hyperopic (near-sighted or far-sighted) eyes. A mirror deflects the path for 90° redirection in the eye axis, and a quarter waveplate modifies the polarization state of the beam. The power at the exit pupil of the laser Doppler flowmeter instrument or the power falling on the subject's cornea is 100 μW. The light is then reflected back along the same path to the beam splitter, where it is redirected along the detection path. Light reflected from the cornea is focused on the corneal stop, where it is prevented from continuing along the detection path. Likewise, light reflected from the retina is focused on the retinal stop. The remaining light of interest from the probed tissue is then collimated by lens 6 and redirected by a mirror onto the photodetector. The data are then sent to the data acquisition unit (Oculix LDF 4000), where the information is analyzed and sent to a laptop PC for display and storage. During the experiment, the arterial blood pressure (BP) is monitored continuously from heart beat to heart beat (Colin model 7000).

These two photographs show the instrument rack onboard the KC–135 and the head-mounted LDV on a volunteer subject (Dr. Rafat Ansari). Preliminary data on ocular blood velocity and arterial BP are presented in the graphs on the next page. Both the velocity of the red blood cells flowing in the choroid and the arterial BP changed as gravity levels were varied during the parabolic flight of the KC–135. The red blood cell velocity increased consistently in reduced gravity and decreased in high gravity. The BP (both systolic and dystolic) decreased in low gravity and increased in high gravity. More experiments are being done at the time of this writing to understand this phenomenon.

Support for this research was provided by an Interagency Agreement between NASA and the National Eye Institute of the National Institutes of Health, by the John Glenn Biomedical Engineering Consortium, and by a Collaborative Research Agreement between the National Center for Microgravity Research at Glenn and the Institut de Recherche en Ophthalmologie in Switzerland.

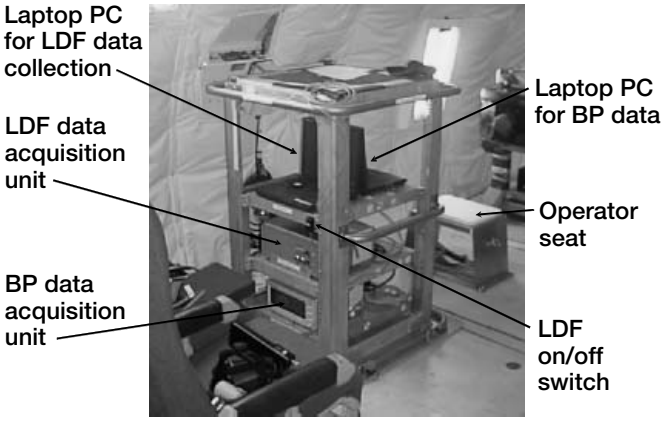

Instrument rack for ocular blood flow experiments onboard the KC–135 aircraft.

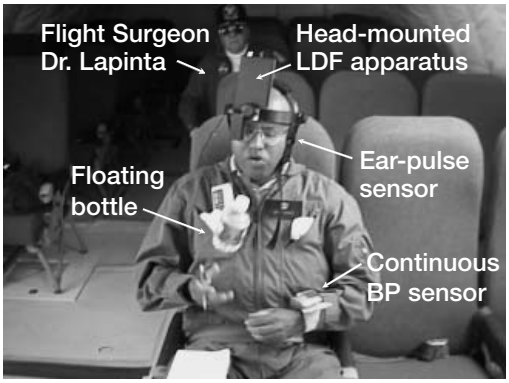

Head-mounted LDF instrument on a volunteer subject monitors ocular blood flow in 0g onboard the KC–135 aircraft.

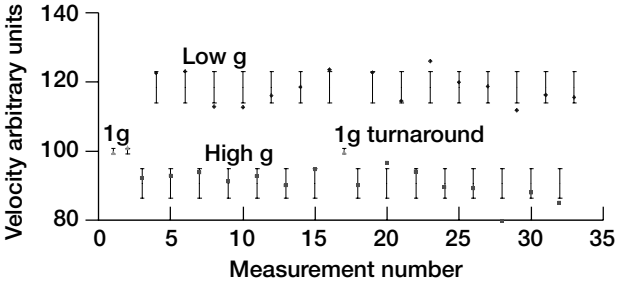

Blood velocity data with ± standard deviation error bars from two consecutive parabolic flight sets.

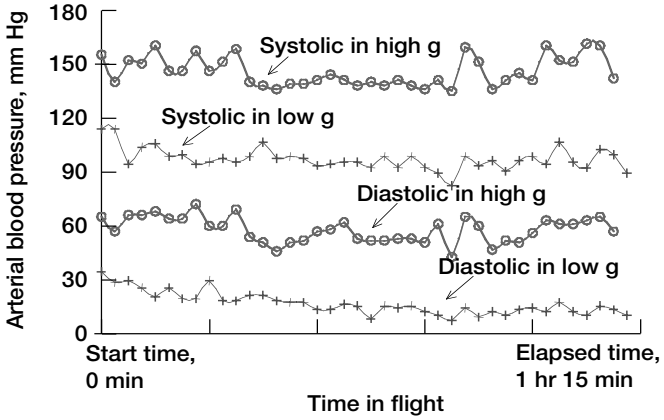

Arterial blood pressure data measured in parabolic flight.

Glenn contact:
Dr. Rafat R. Ansari, 216–433–5008, Fax 216–977–7138, Rafat.R.Ansari@nasa.gov

Authors: Dr. Rafat R. Ansari, Dr. Francis K. Manuel, Martial Geiser, Fabrice Moret, Russell K. Messer, James F. King, and Dr. Kwang I. Suh

Headquarters program office: OBPR

Programs/Projects: Microgravity Science

Contact Angle of Drops Measured on Nontransparent Surfaces and Capillary Flow Visualized

The spreading of a liquid on a solid surface is important for various practical processes, and contact-angle measurements provide an elegant method to characterize the interfacial properties of the liquid with the solid substrates. The complex physical processes occurring when a liquid contacts a solid play an important role in determining the performance of chemical processes and materials. Applications for these processes are in printing, coating, gluing, textile dyeing, and adhesives and in the pharmaceutical industry, biomedical research, adhesives, flat panel display manufacturing, surfactant chemistry, and thermal engineering.

A very simple, accurate, and unique hybrid optical technique for simultaneously measuring the dynamic contact angle and the spreading rate of a liquid drop (with flow visualization in the drop) on a nontransparent metal substrate has been demonstrated at the NASA Glenn Research Center to obtain comprehensive information about contact angles along the periphery of the drop. This process is a new method for measuring contact angles of drops and extends our ability to understand the spreading process of drops by providing information on capillary convection within drops and the effects of evaporation on contact angles over the entire circumference of the drop. These effects are critical to understanding the spreading process but are beyond the range of standard testing procedures. Contact angles anywhere on the circumference can be determined simultaneously. The direct benefits of this technology will be a better understanding of how liquids interact with surfaces, leading to improved and cheaper products as well as improved process control.

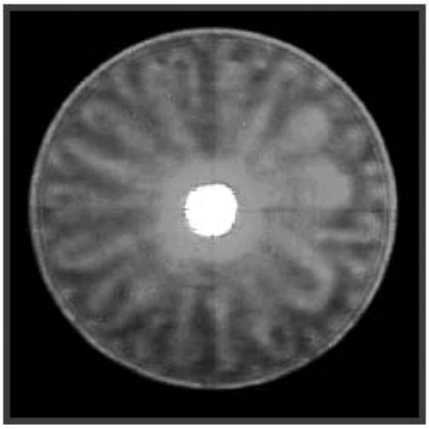

Instant reflection-refracted shadowgraph of Freon-113.

The apparatus (see the diagram on the next page) consists of an optical system composed of top-down photography and reflection-refracted shadowgraphy. Together, white light and helium-neon laser light are collimated and passed through a droplet

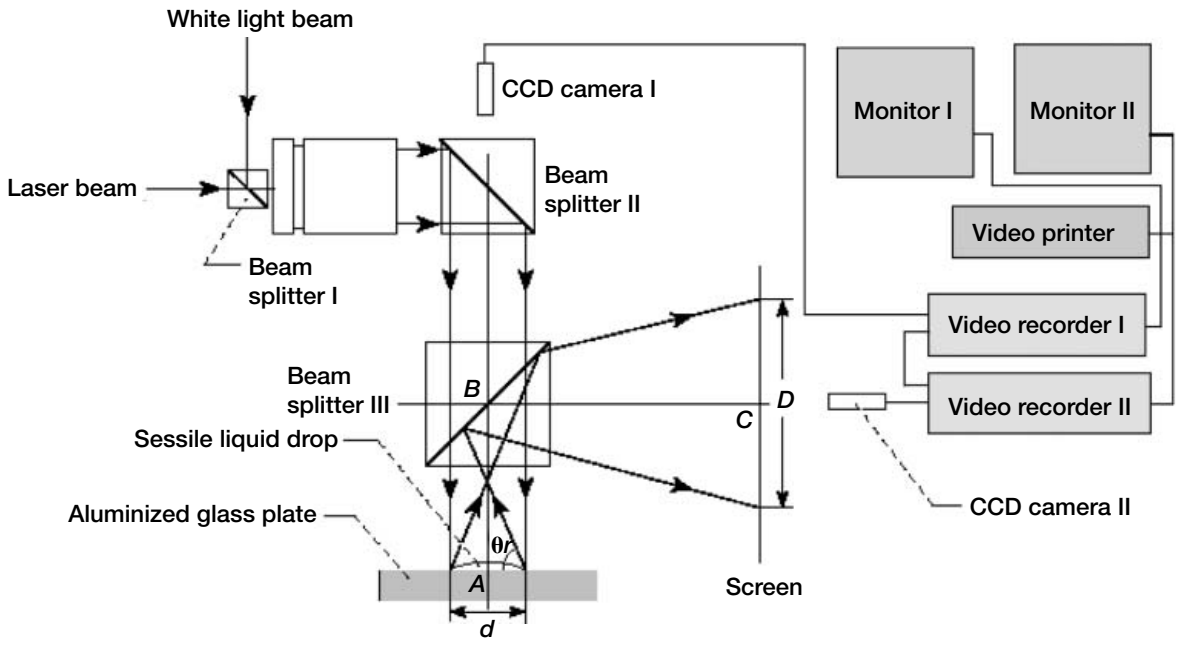

Hybrid optical system consisting of laser reflection-refracted shadowgraphy and direct photography.

placed on a smooth opaque surface (for example, aluminized glass plate). The light beams are reflected by the plate surface and refracted out of the droplet. A beam splitter reorients the reflection-refracted beams horizontally to a vertical screen from which data are recorded. A video recording system synchronously records time-dependent thermocapillary convection and the profile of an experimental droplet on two recorders. Data have shown that evaporation can play a role in inducing thermocapillary convection, depending on both the liquid and the environmental conditions. This patent-pending technology is currently available at the Fluid Physics Branch of Glenn's Microgravity Science Division.

References

1. Zhang, N.; and Chao, D.F.: Flow Visualization in Evaporating Liquid Drops and Measurement of Dynamic Contact Angles and Spreading Rate. J. Flow Visual. Image Proc., vol. 8, no. 2–3, 2001, pp. 303–312.
2. Zhang, Nengli; and Chao, David F.: A New Laser Shadowgraphy Method for Measurements of Dynamic Contact Angle and Simultaneous Flow Visualization in a Sessile Drop. Opt. Laser Technol., vol. 34, no. 3, 2002, pp. 243–248.

Glenn contact:
Dr. David F. Chao, 216–433–8320, David.F.Chao@nasa.gov

Authors: Dr. David F. Chao and Dr. Nengli Zhang

Headquarters program office: OBPR

Programs/Projects:
Microgravity Science

Two-Fluid Interface Instability Being Studied

The interface between two fluids of different density can experience instability when gravity acts normal to the surface. The relatively well known Rayleigh-Taylor (RT) instability results when the gravity is constant with a heavy fluid over a light fluid. An impulsive acceleration applied to the fluids results in the Richtmyer-Meshkov (RM) instability. The RM instability occurs regardless of the relative orientation of the heavy and light fluids. In many systems, the passing of a shock wave through the interface provides the impulsive acceleration. Both the RT and RM instabilities result in mixing at the interface. These instabilities arise in a diverse array of circumstances, including supernovas, oceans, supersonic combustion, and inertial confinement fusion (ICF). The area with the greatest current interest in RT and RM instabilities is ICF, which is an attempt to produce fusion energy for nuclear reactors from BB-sized pellets of deuterium and tritium. In the ICF experiments conducted so far, RM and RT instabilities have prevented the generation of net-positive energy. The $4 billion National Ignition Facility at Lawrence Livermore National Laboratory is being constructed to study these instabilities and to attempt to achieve net-positive yield in an ICF experiment.

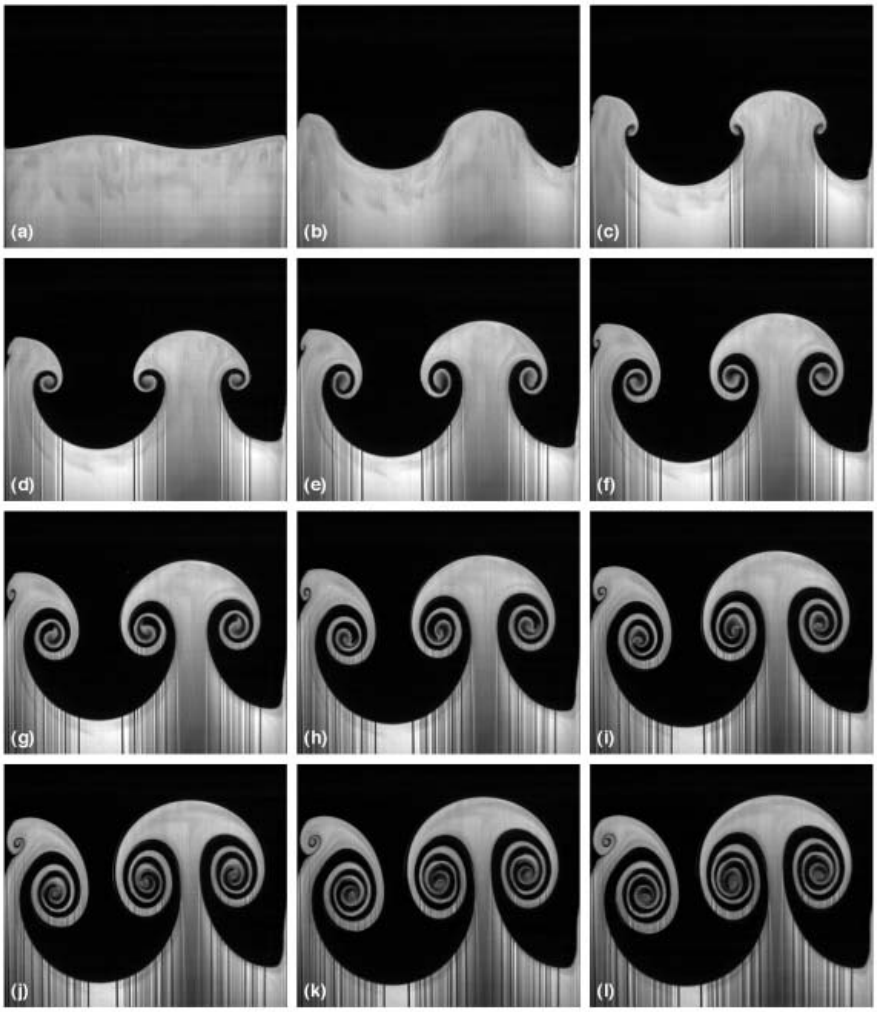

Sequence of images from an experiment with 1 1/2 waves and ka_i = 0.23. Times are relative to the midpoint of spring impact. (a) –14 ms. (b) 102 ms. (c) 186 ms. (d) 269 ms. (e) 353 ms. (f) 436 ms. (g) 529 ms. (h) 603 ms. (i) 686 ms. (j) 770 ms. (k) 853 ms. (l) 903 ms.

The NASA Glenn Research Center, in collaboration with Dr. Jeff Jacobs at the University of Arizona, has been studying RM instability with novel incompressible liquid-liquid experiments. Whereas ICF RM experiments are only a millimeter in size or smaller with time scales of nanoseconds and shock-tube RM experiments are centimeters in size with time scales of milliseconds, these liquid-liquid RM experiments occurred across a container width of 12 cm and a time of nearly 1 s. These experiments have allowed for much better visualization of the instability and have provided needed insight into the initial stages of the instability and its transition to turbulence. The experiments were conducted in a 3-m drop tower at the University of Arizona, with the impulsive acceleration provided by bouncing the fluid-filled container off of a retractable spring. The subsequent free fall as the experiment traveled in the drop tower allowed the instability to evolve in effective absence of the Earth's gravity.

The figure to the left is a sequence of planar, laser-induced fluorescence (PLIF) images showing the evolution of the RM instability. The instability is generated from a small-amplitude sinusoidal perturbation with an initial nondimensional amplitude ka_i of 0.23 and 1 1/2 waves inside the experiment tank. The direction of the acceleration in this case causes the perturbation to invert before growing, eventually forming a row of vortices of alternating sign. The peak amplitude is compared with various analytical models in the graph on the

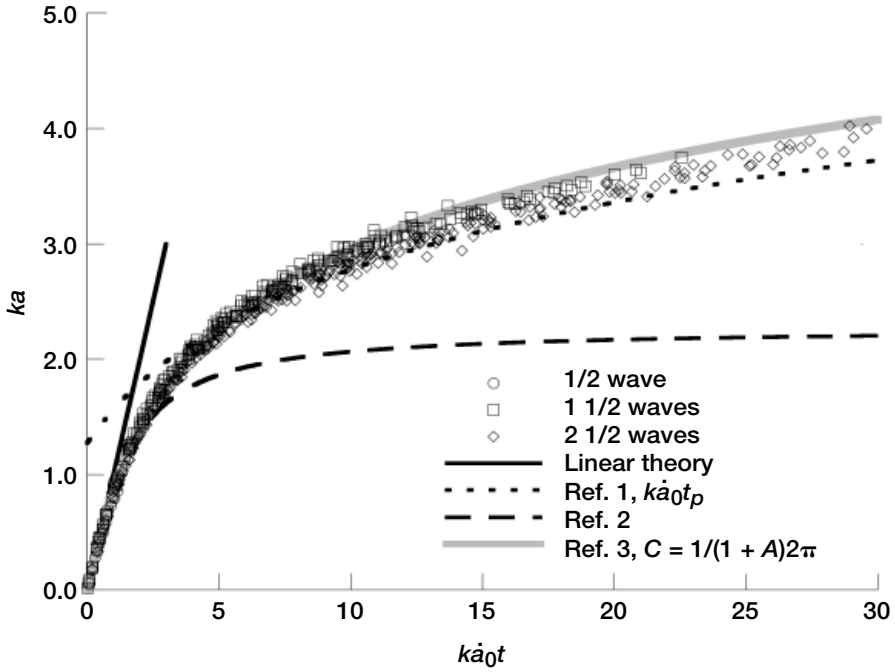

Plot of nondimensional amplitude ka versus nondimensional time $k\dot{a}_0t$ data along with curves from several theories.

next page. The experiments are in excellent agreement with linear stability theory at small amplitudes and with a vortex model developed in reference 1 after the vortices have fully developed. The amplitude was nearly independent of the Reynolds number *Re* on the basis of the (calculated) circulation of a vortex. However, the vortex evolution was a function of *Re*. A secondary instability of the vortex cores has also been observed, with the time to instability appearance proportional to $Re^{-1/2}$. A new apparatus is under construction that will operate in Glenn's 2.2-Second Drop Tower, more than doubling the observation time of the instability, in an effort to study the transition to a turbulent flow.

References

1. Jacobs, J.W.; and Sheeley, J.M.: Experimental Study of Incompressible Richtmyer-Meshkov Instability. Physics of Fluids, vol. 8, 1996, pp. 405–415.
2. Zhang, Q.; and Sohn, S.: Nonlinear Theory of Unstable Fluid Mixing Driven by Shock Wave. Physics of Fluids, vol. 9, 1997, pp. 1106–1124.
3. Sadot, O., et al.: Study of Nonlinear Evolution of Single-Mode and Two-Bubble Interaction Under Richtmyer-Meshkov Instability. Physical Review Letters, vol. 80, 1998, pp. 1654–1657.
4. Jones, M.A.; and Jacobs, J.W.: A Membraneless Experiment for the Study of Richtmyer-Meshkov Instability of a Shock-Accelerated Gas Interface. Physics of Fluids, vol. 9, 1997, pp. 3078–3085.
5. Waddell, J.T.; Niederhaus, C.E.; and Jacobs, J.W.: Experimental Study of Rayleigh-Taylor Instability: Low Atwood Number Liquid Systems With Single-Mode Initial Perturbations. Physics of Fluids, vol. 13, 2001, pp. 1263–1273.

Glenn contact:
Dr. Charles Niederhaus, 216–433–5461, Charles.E.Niederhaus@nasa.gov

Author: Dr. Charles E. Niederhaus

Headquarters program office: OBPR

Programs/Projects:
Microgravity Science

Growth and Remodeling of Blood Vessels Studied In Vivo With Fractal Analysis

Every cell in the human body must reside in close proximity to a blood vessel (within approximately 200 μm) because blood vessels provide the oxygen, metabolite, and fluid exchanges required for cellular existence. The growth and remodeling of blood vessels are required to support the normal physiology of embryonic development, reproductive biology, wound healing and adaptive remodeling to exercise, as well as abnormal tissue change in diseases such as cancer, diabetes, and coronary heart disease. Cardiovascular and hemodynamic (blood flow dynamics) alterations experienced by astronauts during long-term spaceflight, including orthostatic intolerance, fluid shifts

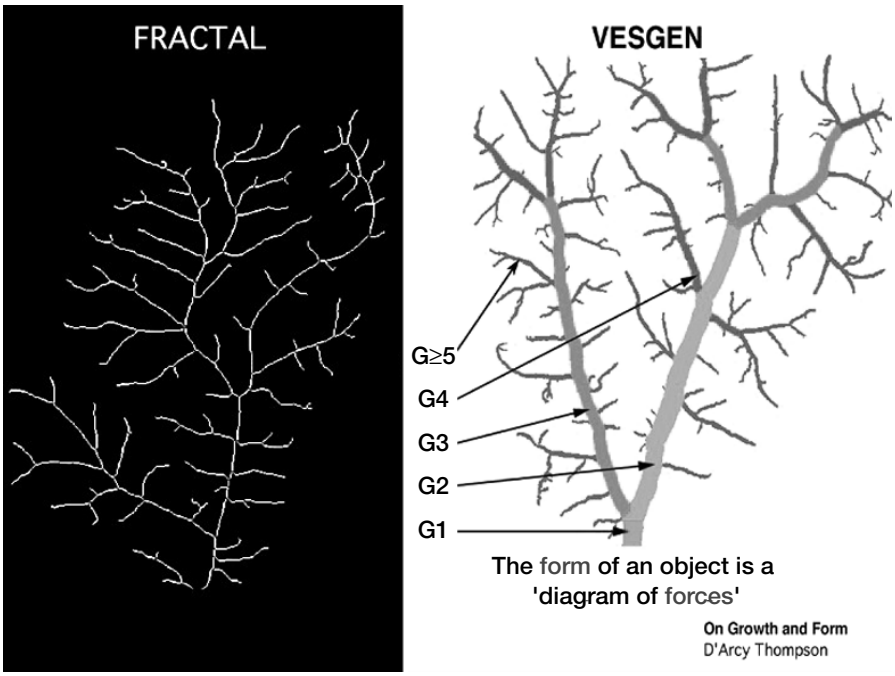

Growth and remodeling of blood vessels are measured with a fractal-based analysis of parameterized images, including skeletonized images (left), that also incorporates the branching generation of blood vessels (right) via the computer code VESGEN.

Compared with untreated blood vessels (left) in fertilized quail eggs, blood vessels were stimulated to grow (center) and inhibited from growing (right) by molecular regulators. Quail eggs are being flown as space biology experiments on the International Space Station and were originally flown on Mir.

in the body, and reduced numbers of red (erythrocyte) and white (immune) blood cells, are identified as risk factors of very high priority in the NASA task force report on risk reduction for human spaceflight, the "Critical Path Roadmap."

Blood vessels are difficult to study in the human body because the vasculature is a complex, highly branched, treelike structure embedded within three-dimensional opaque tissue. At the NASA Glenn Research Center, Patricia Parsons is using a novel in vivo model to study vessel growth in the chorioallantoic membrane (CAM) of quail eggs (see the figures on this page and the photographs on the next page), because the vascular tree of the CAM is two-dimensional and embedded within thin, transparent tissue (refs. 1 to 3). Modern fractal mathematics is used to measure and model the morphological stimulation and inhibition of blood vessel growth by molecular regulators of angiogenesis (the growth of new blood vessels). In collaboration with ophthalmologists at the invitation of Carl Kupfer, M.D., former Director of the National Eye Institute at the National Institutes of Health, the fractal-based methodology for measuring blood vessel growth and remodeling was extended successfully from the quail CAM to clinical photographs of human eyes for measurement of early-stage diabetic retinopathy (see the bottom figure on the next page and ref. 4). Late-stage diabetic retinopathy results in blindness; eye researchers are currently searching for early-stage therapeutic and diagnostic interventions to avoid the relatively unsuccessful intervention of late-stage laser surgery. In collaboration with researchers at Glenn, the Institute for Computational Mechanics in Propulsion (ICOMP)/Ohio Aerospace Institute (OAI), the Cleveland Clinic Foundation, and elsewhere, we are currently extending these techniques to the gene-targeted expression of specific molecular regulators of vascular growth and form, and the intravital study of hemodynamics as a critical component of vascular growth and remodeling.

References

1. Parsons-Wingerter, P., et al.: Fibroblast Growth Factor-2 Selectively Stimulates Angiogenesis of Small Vessels in Arterial Tree. Arterioscler. Thromb. Vasc. Biol., vol. 20, no. 5, 2000, pp. 1250–1256.

Mike Bronczek is imaging blood vessels in quail eggs intravitally prior to fractal-based quantification of vessel growth after culturing the eggs (shown on the white tray) in the new Vertebrate Cell Culture Facility at Glenn.

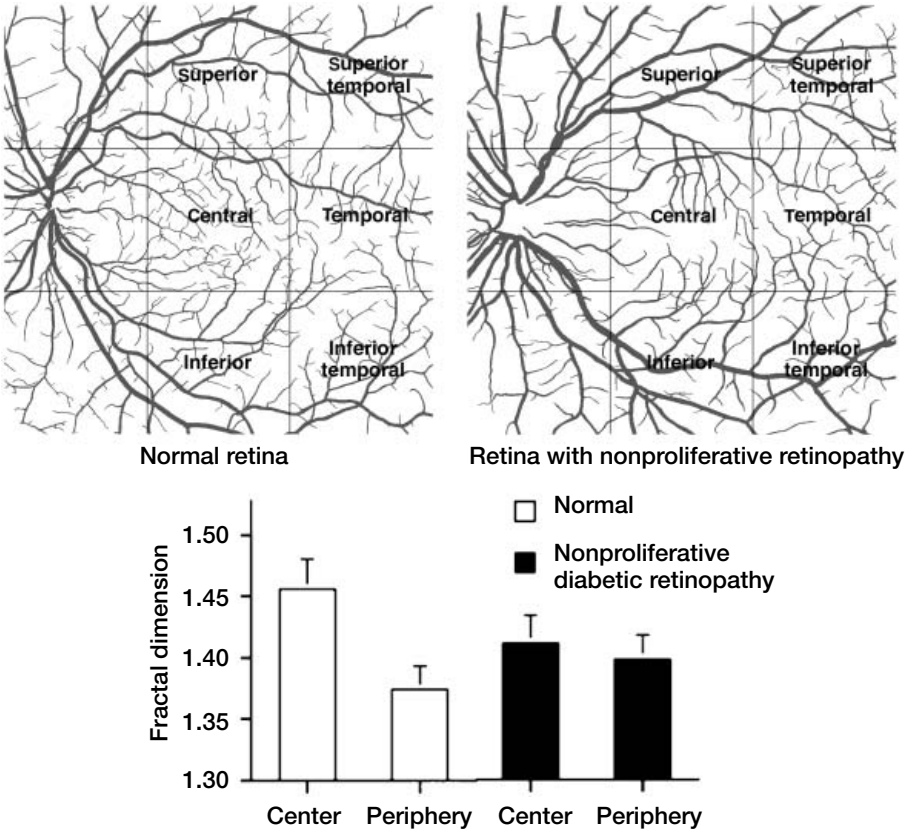

In clinical photographs of the human eye, fractal analysis measured the decrease of blood vessels in early-stage (nonproliferative) diabetic retinopathy (top right) compared with healthy blood vessels in the normal retina (top left).

2. Parsons-Wingerter P., et al.: Generational Analysis Reveals that TGF–β1 Inhibits the Rate of Angiogenesis In Vivo by Selective Decrease in the Number of New Vessels. Microvasc. Res., vol. 59, no. 2, 2000, pp. 221–232.
3. Parsons-Wingerter P., et al.: A Novel Assay of Angiogenesis in the Quail Chorioallantoic Membrane: Stimulation by bFGF and Inhibition by Angiostatin According to Fractal Dimension and Grid Intersection. Microvasc. Res., vol. 55, no. 3, 1998, pp. 201–214.
4. Avakian, Arpenik, et al.: Fractal Analysis of Region-Based Vascular Change in the Normal and Non-Proliferative Diabetic Retina. Curr. Eye Res., vol. 24, no. 4, 2002, pp. 274–280.

Glenn contact:
Dr. Patricia Parsons, 216–433–8796,
Patricia.A.Parsons-wingerter@nasa.gov

Author: Dr. Patricia A. Parsons

Headquarters program office: OBPR

Programs/Projects:
Microgravity Science

Special recognition: Under P. Parsons' mentorship, NASA LERCIP undergraduate scholars Samille Jackson and Jalaine Johnson won the Best Student Team award for their research on a novel molecular regulator of angiogenesis in the quail CAM in July 2002. Ophthalmology Resident Fellow, Arpenik Avakian, M.D., Ph.D., received a Leslie W. Nesmith Lectureship Award for "Quantification of the Change in Vascular Pattern in Nonproliferative Diabetic Retinopathy," by A. Avakian, R.E. Kalina, and P. Parsons-Wingerter, at The Schepens International Society Meeting, Jackson Hole, Wyoming, June 6–9, 1999.

Diffusivity Measured as a Function of Concentration

Optical diagnostic techniques have become an integral part of many measurements in industrial and research laboratories. Many types of interferometers and their phase-shifted versions have been used to measure optical wave fronts for lens testing and combustion and fluid flow diagnostics. One such instrument is the point diffraction interferometer (PDI), which is considered to be robust because it has a common-path design. However, the PDI is difficult to align and has limited measurement range for liquid phase applications. Interferometry and schlieren techniques have been widely used for many years for gas flow visualization.

For the first time, researchers at the NASA Glenn Research Center have been able to use a compact common path interferometer (CPI) to measure the concentration-dependent diffusion coefficient of two miscible liquids that diffuse into each other. The CPI is an optical technique that can be used to measure changes in the gradient of the refractive index of transparent materials. It is a shearing interferometer that shares the same optical path from a laser light source to the final imaging plane. It uses a Wollaston prism polarizer in combination with an analyzer (crystalline quartz retardation plate) instead of a PDI unit. The advantage of using the CPI over other optical techniques is that it can make quantitative measurements in liquids with large index of refraction variations, as often is the case in interface dynamics studies. This can be accomplished simply by using different polarizers for each particular experimental condition.

In previous work, we showed (refs. 1 to 3) that the instrument can easily measure the diffusion coefficient of miscible liquid pairs. Miscible fluid flows are important in enhanced oil recovery, fixed bed regeneration, hydrology, and filtration. The dynamics of miscible interfaces is an active area of research that has been identified to benefit from experimentation in reduced gravity, and the diffusivity is an important physical property in such experiments. Its measurement is required to determine the ranges for experimental parameters, such as the displacement speed, so that the effects of convection and diffusion are in optimal balance.

The molecular diffusion coefficient of liquids can be determined using physical relations between changes in the optical path length and liquid phase properties. Data obtained through the use of the CPI and compared with similar results from other techniques have demonstrated that the instrument is far superior for measuring the diffusivity of miscible liquids while keeping the system very compact and robust (ref. 4). Because of its compactness and ease of use, the CPI has been adopted for use in studies of interface dynamics as well as other diffusion-controlled process applications (ref. 4). This progress will permit the optimal design of experiments in microgravity that can quantitatively answer basic science questions about mass and thermal diffusion and their effects in transport processes. This instrument is a

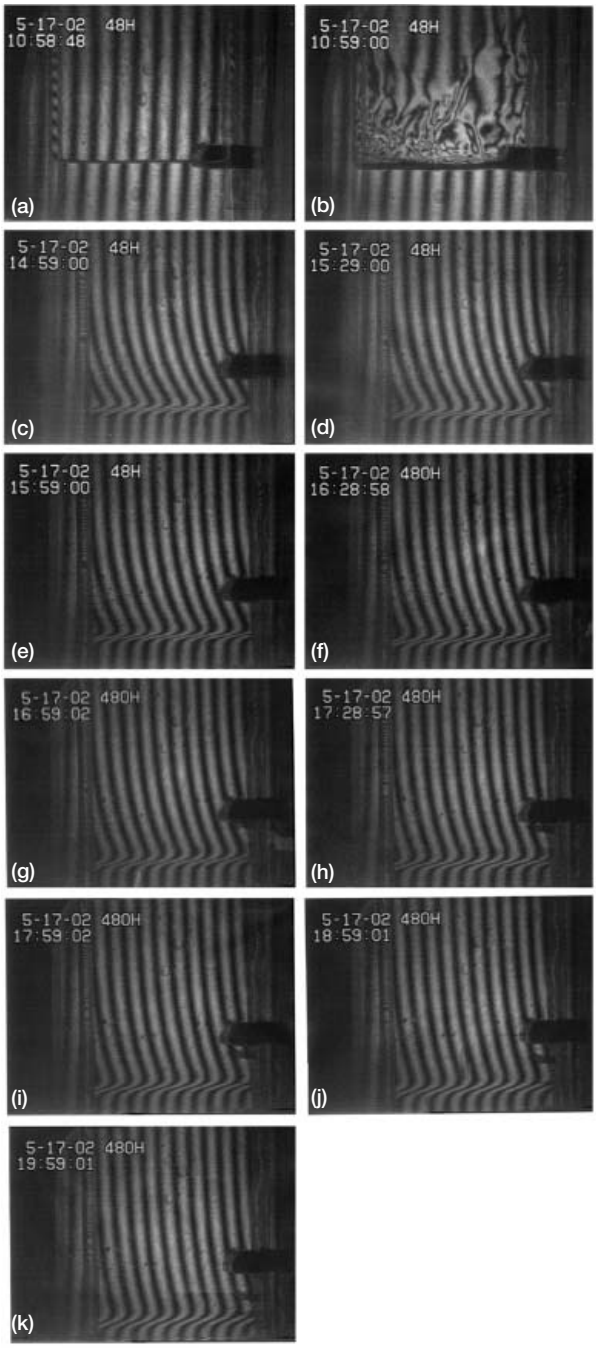

Interferograms representing the evolution of the concentration gradient at a water-glycerin interface. (a) Glycerin is present before water is added to the top. The horizontal dark fat line in all the panels is a fixed reference mark on the cell. The remaining panels show the evolution of the fringes at various times. (b) 0 min. (c) 240 min. (d) 270 min. (e) 300 min. (f) 330 min. (g) 360 min. (h) 420 min. (i) 480 min. (j) 540 min. (k) 600 min.

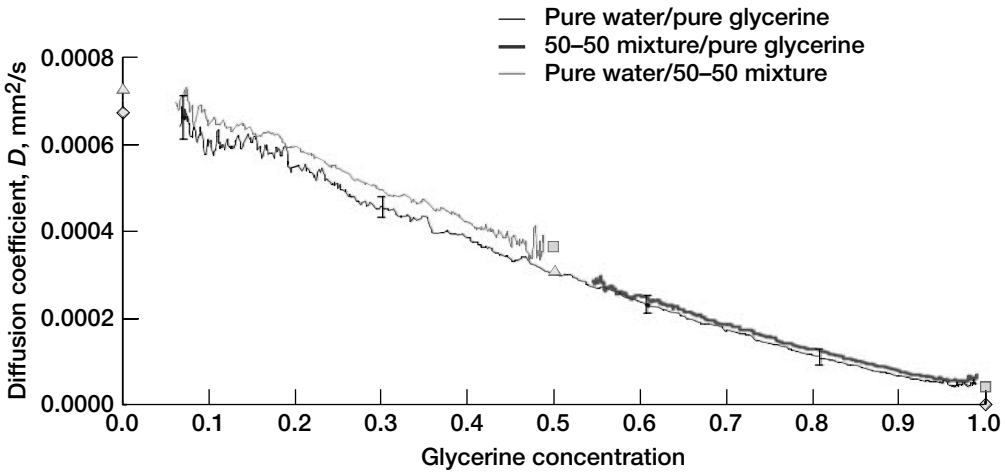

Diffusivity of water-glycerin system that represents the diffusion coefficient as a function of glycerin concentration. This figure also shows the diffusion coefficients obtained for the diffusion of pure water placed on top of a 50–50 mixture of water and glycerin and for the diffusion of a 50–50 mixture of water and glycerin placed on top of pure glycerin. The agreement of the measured diffusion coefficients for the three experiments is very good, indicating the robustness of the measurement technique. The filled symbols represent diffusivity at the endpoints where the concentration gradient contribution to the diffusivity is very small.

spinoff of a diagnostic development for microgravity fluid physics experiments at Glenn that used existing optics and electronics in the Fluid Physics laboratory for feasibility studies. Several scientists have expressed their interest in using this instrument for their research.

In the course of our use of this instrument, we realized that not all the fluids have a constant diffusion coefficient. The diffusivity of some liquid pairs change with concentration and time. This prompted us to search for a general method to process the raw data obtained using the CPI to measure the diffusion coefficient as a function of the local concentration. A general method was subsequently developed and reported (ref. 5).

The new data processing approach was applied to measure the concentration-dependent diffusivity of a pair of miscible fluids. The mathematical model of the new approach in using the CPI is discussed in references 3 and 5, and sample results are shown in the figures. The diffusivity results are in excellent agreement with available data. The physical properties measured are in support of a space experiment which is planned (ref. 4) to be conducted in the International Space Station in 2005.

References

1. Rashidnia, Nasser: Novel Diffusivity Measurement Optical Technique. Proceedings of the 9th International Symposium on Flow Visualization. Edinburgh, U.K., G.M. Carlomango and I. Grant, eds., paper 451, 2000, pp. 451.1–451.8.
2. Rashidnia, N., et al.: Measurement of the Diffusion Coefficient of Miscible Fluids Using Both Interferometry and Wiener's Method. Int. J. Therm., vol. 22, no. 2, 2001, pp. 547–555.
3. Rashidnia, Nasser; and Balasubramaniam, R.: Development of an Interferometer for Measurement of the Diffusion Coefficient of Miscible Liquids. Appl. Optics, vol. 41, no. 7, 2002, pp. 1337–1342.
4. Maxworthy, T., et al.: The Dynamics of Miscible Fluids: A Space Flight Experiment (MIDAS). AIAA 2001–5061, 2001.
5. Rashidnia, N.; Balasubramaniam, R.; and Boggess, M.: Concentration Dependent Diffusivity of Miscible Liquids Measured With Interferometry. Paper presented at the 10th International Symposium on Flow Visualization, paper no. F0040, Kyoto, Japan, 2002.

National Center for Microgravity Research contacts:
Dr. Nasser Rashidnia, 216–433–3622, Nasser.Rashidnia@grc.nasa.gov;
Ramaswamy Balasubramaniam, 216–433–2878, Ramaswamy.Balasubramaniam@grc.nasa.gov

Authors: Dr. Nasser Rashidnia and Ramaswamy Balasubramaniam

Headquarters program office: OBPR

Programs/Projects:
Microgravity Science

Design Study Conducted of a Stirred and Perfused Specimen Chamber for Culturing Suspended Cells on the International Space Station

A tightly knit numerical/experimental collaboration among the NASA Ames Research Center, NASA Glenn Research Center, and Payload Systems, Inc., was formed to analyze cell culturing systems for the International Space Station. The Cell Culture Unit is a facility scheduled for deployment on the space station by the Cell Culture Unit team at Ames. The facility houses multiple cell specimen chambers (CSCs), all of which have inlets and outlets to allow for replenishment of nutrients and for waste removal. For improved uniformity of nutrient and waste concentrations, each chamber has a pair of counterrotating stir bars as well. Although the CSC can be used to grow a wide variety of organic cells, the current study uses yeast as a model cell. Previous work identified ground-based protocols for perfusion and stirring to achieve yeast growth within the CSC that is comparable to that for yeast cultures grown in a shaken Ehrlenmeyer flask.

Three CSC designs were assessed from the standpoint of providing uniform concentration fields while minimizing fluid-induced shear stress. All three designs share the same footprint but vary in flow path, membrane design, and inlet/exit geometry. All were examined with the same net flow throughput, with and without stirring. For the Mark I, option 1 design (left figure), two inlet ports exhaust directly into the bottom and center of the chamber. Fluid must pass through a membrane situated above the inlets around the periphery of the chamber in order to reach the two exit ports at the left and right sides of the chamber. The Mark I, option 9 design (center figure) has one inlet at the left and one outlet at the right. Fluid must pass through a filter both exiting and leaving the chamber. In the Mark II, option 2 design (right figure), inlet and outlet ports are attached to a plenum to reduce flow velocities in the chamber. Membranes are located between the plena and the interior of the chamber. Since the ports are located on the same side of the CSC, the fluid path forms an inverted U, as seen in the figure on the right.

Using the ground-based protocols developed for yeast, flow visualization and dye concentration measurements were performed by Payload Systems, Inc., and numerical simulations were developed by Glenn. The numerical and experimental results were found to be in close agreement.

The isoconcentration contours in the figures show the resulting concentration field for all three chambers at a net flow rate of 0.9 ml/min and no stirring. These qualitatively match the fronts seen in the flow visualization as dye is introduced. For the Mark I, option 1 design, hemispherical contours around the inlets are apparent since the flow is not smoothed out by filter membranes, but rather exhausts directly into the chamber. If the inlets and outlets were on opposite sides of the chamber, the concentration contours would more closely resemble horizontal lines across the chamber. Although there are significant concentration gradients at the inlet of the Mark I, option 9 design, the contours show basically vertical profiles, indicating essentially unidirectional flow across the chamber. This is responsible for the high-quality flushing efficiency of this chamber observed in the flow visualization studies. There are substantial concentration gradients and nonuniformities in the Mark II, option 2 design because of the curved flow path from the inlet to the exit. Numerical analysis of velocity fields created by rotating stir bars (not shown) indicated that the most efficient mixing occurs in the Mark I, option 9 design.

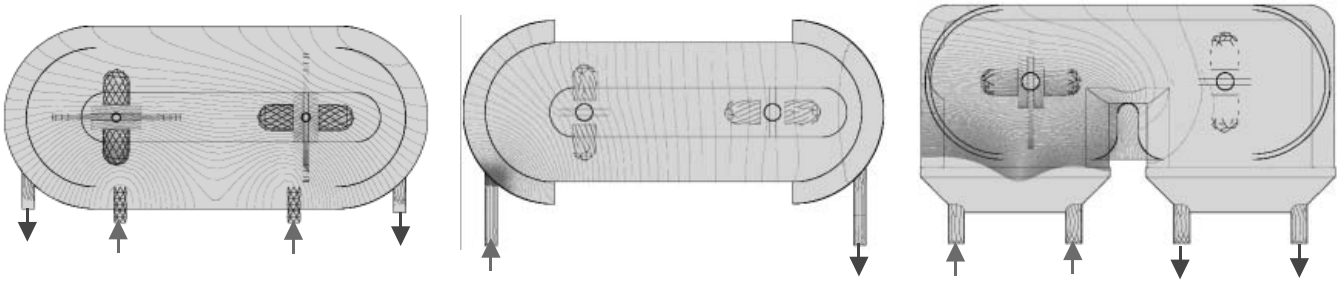

Mark I, option 1 **Mark I, option 9** **Mark II, option 2**

Isoconcentration contours generated by perfusion at 0.9 ml/min and no stirring.

As a result of this collaboration, the Mark I, option 9 design was chosen as the basis for the CSC. Current work involves improving the inlet design to enhance uniformity in the chamber as well as optimizing the stirring and perfusion protocols for spaceflight.

Find out more about research in Glenn's Computational Microgravity Laboratory: cml.grc.nasa.gov

Glenn contact:
Dr. Emily S. Nelson, 216–433–3268, Emily.S.Nelson@nasa.gov

National Center for Microgravity Research contact:
Dr. John P. Kizito, 216–433–2275, John.P.Kizito@grc.nasa.gov

Authors: Dr. Emily S. Nelson and Dr. John P. Kizito

Headquarters program office: OBPR

Programs/Projects:
Microgravity Science, Life Science

Advanced Microgravity Acceleration Measurement Systems (AMAMS) Being Developed

The Advanced Microgravity Acceleration Measurement Systems (AMAMS) project is part of NASA's Instrument Technology Development program to develop advanced sensor systems. The primary focus of the AMAMS project is to develop microelectromechanical systems (MEMS) for acceleration sensor systems to replace existing electromechanical sensor systems presently used to assess relative gravity levels aboard spacecraft. These systems are used to characterize both vehicle and payload responses to low-gravity vibroacoustic environments. The collection of microgravity acceleration data is useful to the microgravity life sciences, microgravity physical sciences, and structural dynamics communities. The inherent advantages of semiconductor-based systems are reduced size, mass, and power consumption, with enhanced long-term calibration stability.

The AMAMS represents the fifth generation of triaxial sensor heads developed at the NASA Glenn Research Center for collecting microgravity acceleration data. Since 1991, the Space Acceleration Measurement System (SAMS) program has supported over 25 shuttle missions and the space station Mir, and has ongoing operations on the International Space Station (ISS). The first

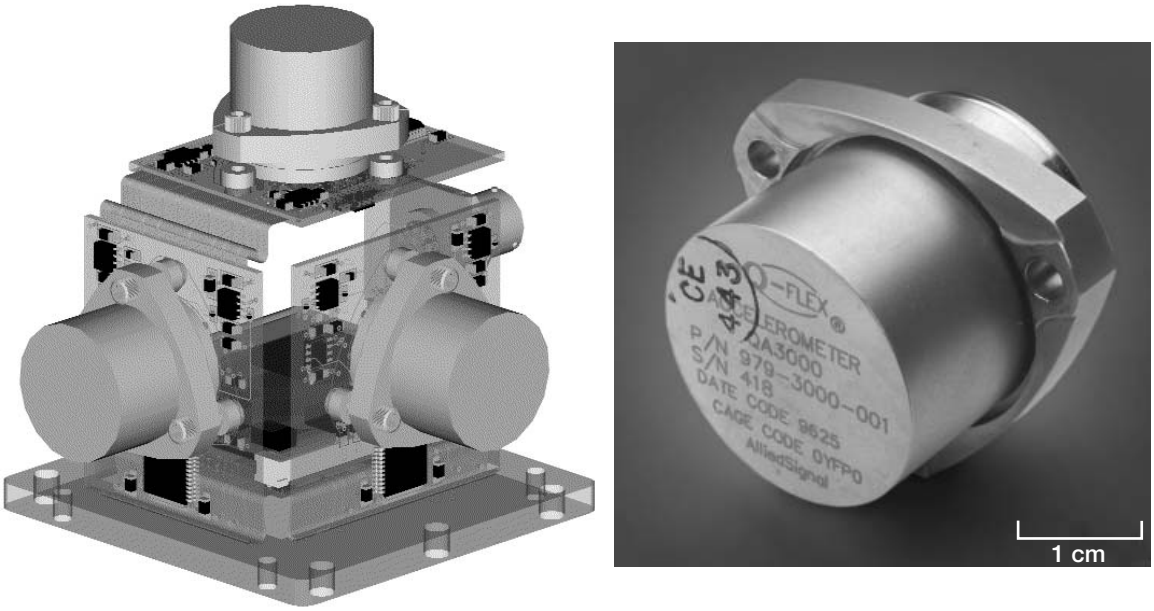

Left: SAMS TSH–ES showing mounting of the AlliedSignal QA–3000 and the electronic interface card. Right: One AlliedSignal QA–3000 accelerometer.

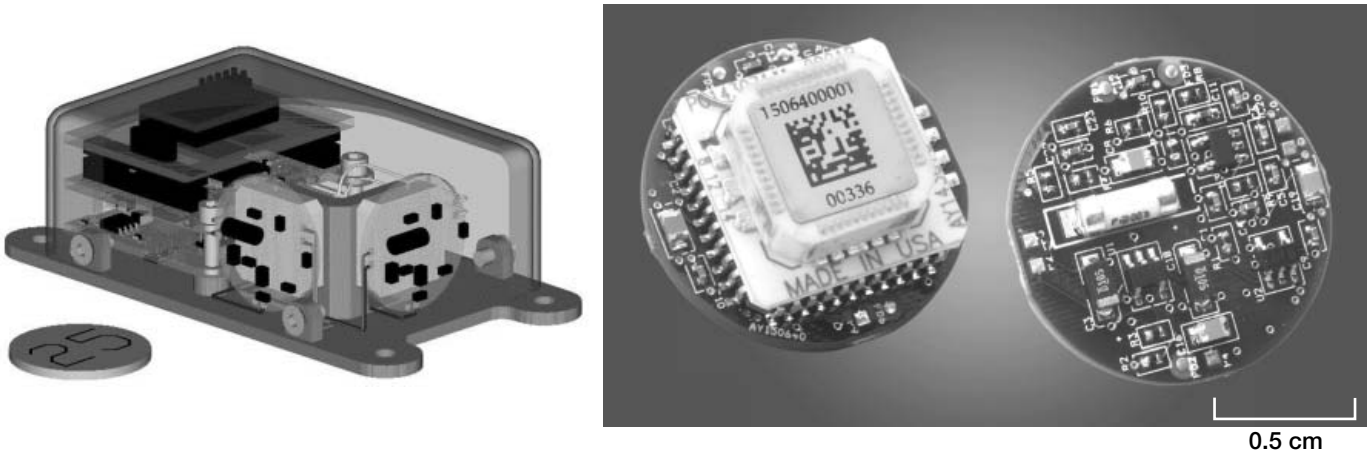

Top: AMAMS design using Applied MEMS accelerometer and electronic interface card. Note that the small size allows the accelerometers to face inward. Bottom: Top and bottom of one MEMS accelerometer.

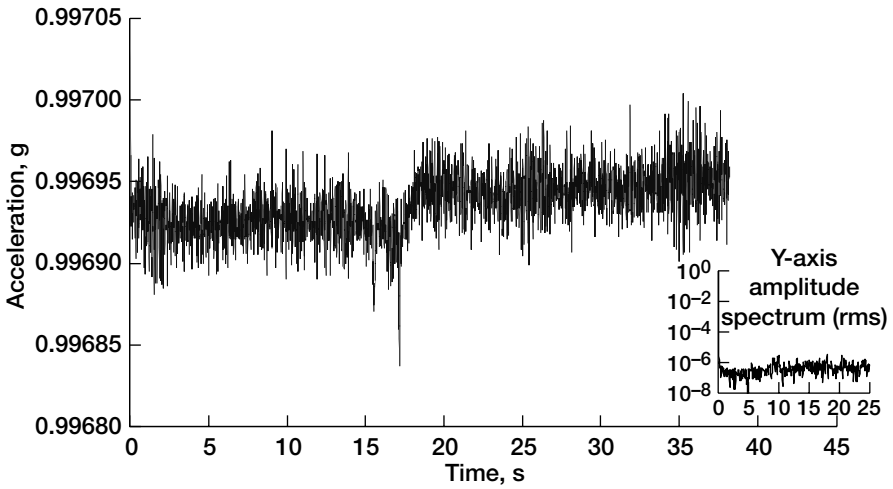

Applied MEMS sensor in triaxial sensor head breadboard on bench at 50-Hz sample rate.

four generations—SAMS (original design, 1991 to 1998), SAMS–FF (1999 to 2003), SAMS–II (for the ISS, 2001 to the present), and SAMS TSH–ES (Ethernet, 2002 to present)—used AlliedSignal Q-flex accelerometers (see the figure on the preceding page). AMAMS represents a new design approach using MEMS accelerometers (see the figure at the top of this page) and state-of-the-art analog-to-digital converters. In addition to saving a significant amount of on-orbit resources, we theorize that AMAMS would be more accurate than current sensors for long-duration (longer than 2 years) interplanetary missions since they use sensors without magnetics. The long-term accuracy and stability will be demonstrated with ground testing and operational experience.

A market survey assessed three different MEMS accelerometers from Honeywell, AlliedSignal, and Applied MEMS that could produce microgravity (10^{-6}g, or 1 μg) resolution. A test program was conducted, and it was determined that the Applied MEMS sensor had the best combination of characteristics for a microgravity triaxial sensor head. These MEMS sensors were developed for the seismic and geological exploration communities, where the reduced size and weight offer inherent advantages over conventional mechanical devices. Testing was conducted with the Applied MEMS sensor at the Space Power Facility at Glenn's Plum Brook Facility to determine the noise floor. The results (see the graph to the left) were very encouraging, yielding data that demonstrated that the Applied MEMS accelerometer combined with the prototype electronics can produce microgravity resolution in the general purpose 0.1- to 25-Hz range. The testing also verified the available 1500-Hz bandwidth of the Applied MEMS accelerometer.

A design has been completed for the prototype triaxial sensor head and has met the goals of the Instrument Technology Development program proposal. High-resolution, 24-bit delta-sigma analog-to-digital conversion circuitry is employed to utilize the large dynamic range of the accelerometers. This sensor head design is controlled with a commercial processor board and has an RS–422 serial interface for external control and data storage. The resulting sensor head meets the goals of sensitivity less than 1 μg, with a resulting packaging size under 8 $in.^3$, weight under 0.25 lb, power consumption less than 1 W, and component cost under $2500. This represents a 33-percent reduction in volume, an 87-percent reduction in cost, and a 50-percent reduction

in power consumption from previous designs. The prototype of this sensor is scheduled for completion in August 2003, and integrated testing is scheduled with the completed package.

In addition, a design study was conducted to investigate further miniaturization of the sensor package. This would be accomplished through the development of a custom hybrid package or application-specific integrated circuit (ASIC) for the signal conditioning and processor electronics circuitry. Several different designs were developed for progressively reducing the size as more sophisticated packaging techniques were employed. It is feasible to develop a triaxial sensor package that would be less than 5 $in.^3$ and would utilize an Ethernet interface so that it could be implemented in the International Space Station Ethernet local area network. The smaller size requires less volume and allows the sensors to be located closer to the measurement location.

This work is part of a multiyear (2001 to 2003) effort funded by NASA's Office of Biological and Physical Research and based on a competitive proposal coauthored by Thomas J. Kacpura and Ronald J. Sicker. The work will be performed primarily at Zin Technologies with NASA management oversight.

Find out more about this research:
http://microgravity.grc.nasa.gov/

Glenn contact:
Ronald J. Sicker, 216–433–6498,
Ronald.J.Sicker@nasa.gov

Zin Technologies contact:
Thomas J. Kacpura, 216–977–0420,
Thomas.J.Kacpura@grc.nasa.gov

Authors:
Ronald J. Sicker and Thomas J. Kacpura

Headquarters program office: OBPR

Programs/Projects:
Microgravity Science

Physics of Colloids in Space (PCS): Microgravity Experiment Completed Operations on the International Space Station

The Physics of Colloids in Space (PCS) experiment was accommodated within the International Space Station (ISS) Expedite the Processing of Experiments to Space Station (EXPRESS) Rack 2 and was remotely operated from early June 2001 until February 2002 from NASA Glenn Research Center's Telescience Support Center in Cleveland, Ohio, and from a remote site at Harvard University in Cambridge, Massachusetts. Remote operations enabled a significant number of hours of run time for this experiment with just a small number of ISS crew hours expended. PCS is an experiment conceived by principal investigator Professor David A. Weitz of Harvard University and coinvestigator Peter N. Pusey of the University of Edinburgh. It focused on the behavior of three different classes of colloidal suspensions (binary colloidal crystal alloys, colloid-polymer mixtures, and fractal gels). A colloidal suspension consists of fine particles (micrometer to submicrometer) suspended in a fluid, examples being paint, milk,

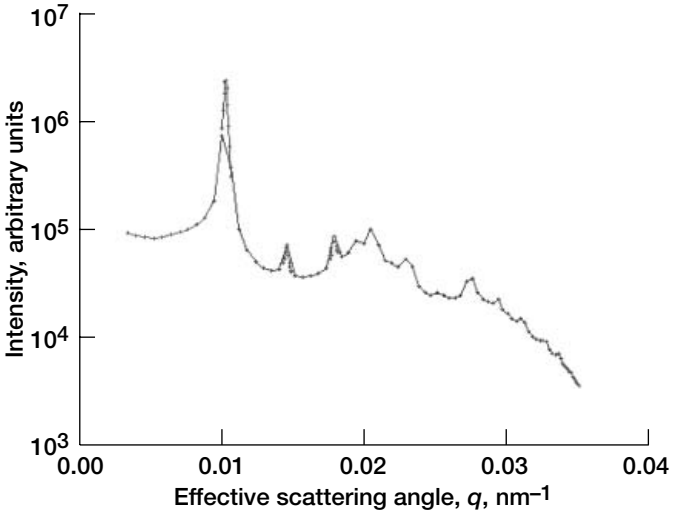

Diffraction pattern from the AB6 binary colloidal crystal alloy; 11 days, 4 hr after melting, q, effective scattering angle.

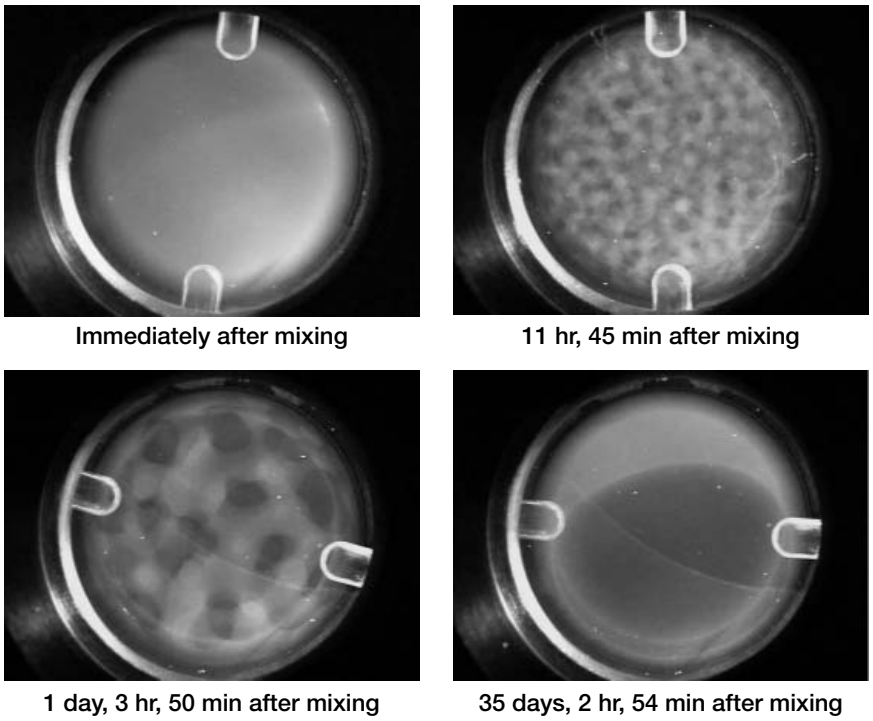

Phase separation of the colloid-polymer critical point sample.

salad dressings, and aerosols. The potential payoffs of PCS are improvements in the properties of paints, coatings, ceramics, and food- and drug-delivery products; improved manufacturing of products requiring either colloidal suspensions for processing or as precursors; and important first steps in the research and development of an entirely new class of materials that passively affect the properties of light passing through them. The sophisticated light-scattering instrumentation comprising PCS is capable of color imaging, dynamic and static light scattering from 11° to 169°, Bragg scattering from 10° to 60°, and laser light scattering at low angles from 0.3° to 6.0°. The PCS instrumentation performed remarkably well on orbit, demonstrating a flexibility that enabled experiments to be performed that had not been envisioned prior to launch.

While on-orbit on the ISS, PCS completed 2400 hours of science operations, and the principal investigator declared it to be a resounding success. Each of the eight sample cells worked well and produced interesting and important results. Crystal nucleation and growth and the resulting structures of two binary colloidal crystal alloys were studied, with the long-duration microgravity environment of the ISS facilitating extended studies on the growth and coarsening characteristics of the crystals. In another experiment run, the demixing of the colloid-polymer critical point sample was studied as it phase-separated into two phases, one that resembled a gas and one that resembled a liquid. This process was studied over four decades of length scale (from 1 μm to 1 cm) to observe behavior that could not be seen in this sample on Earth because sedimentation would cause the colloids to fall to the bottom of the cell faster than the demixing process could occur. To acquire this data, the PCS science and operations teams codesigned and coexecuted a unique diagnostic sequence that captured and condensed the first 16 hr of this sample's demixing into a 7-s time-lapse movie. In addition, the study of the gelation and aging of another colloid-polymer sample, the colloid-polymer

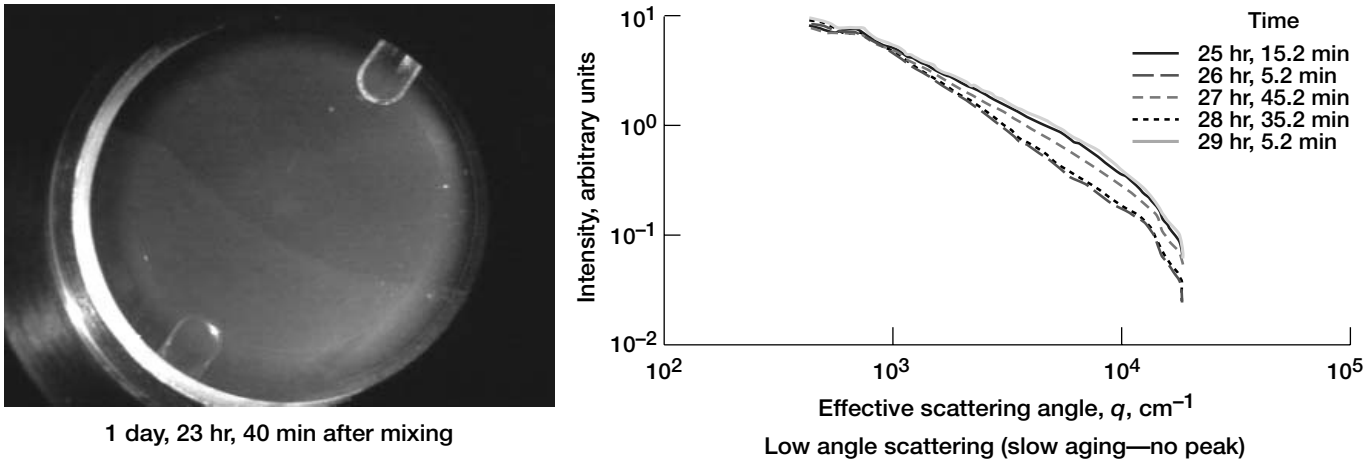

Gelation and aging of colloid-polymer gel sample.

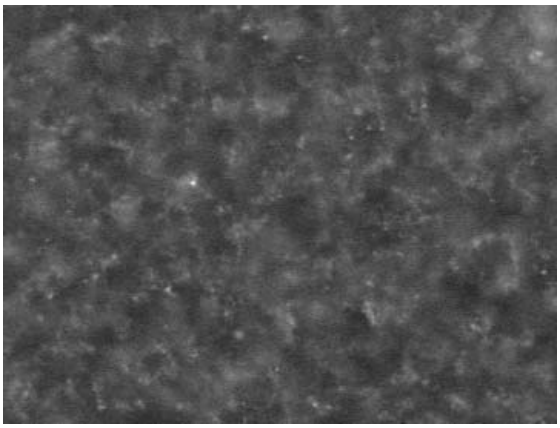

Polystyrene gel

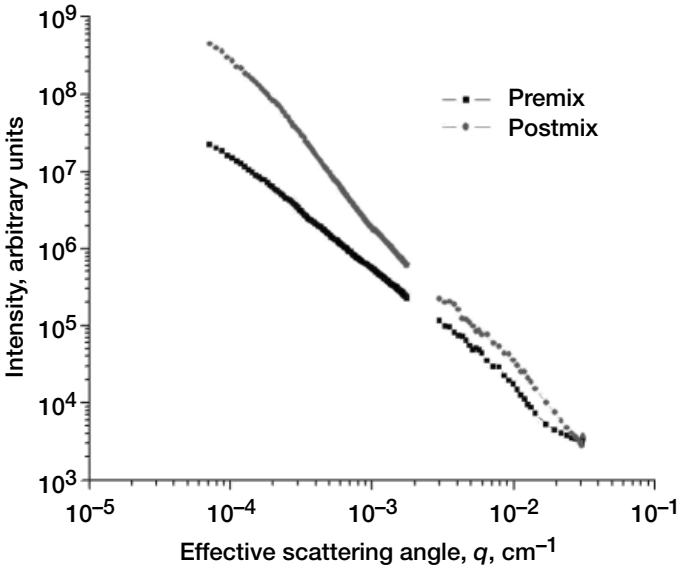

Aggregation behavior of polystyrene fractal gel sample. Left: Polystyrene gel—high-magnification image taken 10 days after constituent combination, showing aggregation occurring. Right: Polystyrene gel—static light scattering performed both before and after constituent combination; a tremendous increase in scattered light occurs.

gel, provided valuable information on gelation mechanisms, as did investigations on the extremely low concentration silica and polystyrene fractal gel samples. In virtually all cases, we enhanced our understanding of the science being investigated.

The PCS experiment was developed, launched, and operated by Zin Technologies under NASA contract NAS3–99154. PCS was deorbited in June 2002. The hardware will be replenished with another set of eight colloidal samples and is planned for relaunch in 2003.

Find out more about this research:

Glenn's PCS research (includes data on a sample-by-sample basis—being updated): http://microgravity.grc.nasa.gov/6712/pcs.htm

David Weitz at Harvard (introduces the principal investigator):
http://www.physics.harvard.edu/fac_staff/weitz.html

Principal investigator's group at Harvard (scientific focus areas of interest):
http://www.deas.harvard.edu/projects/weitzlab/

Glenn's microgravity research: http://microgravity.grc.nasa.gov/

Glenn's fluid physics research:
http://microgravity.grc.nasa.gov/MSD/MSD_htmls/fluids.html

Glenn contact:
Michael P. Doherty, 216–433–6641, Michael.P.Doherty@nasa.gov

National Center for Microgravity Research contact:
Dr. Subramanian Sankaran, 216–433–9335, Subramanian.Sankaran@grc.nasa.gov

Authors: Michael P. Doherty and Dr. Subramanian Sankaran

Headquarters program office: OBPR

Programs/Projects:
Microgravity Science

Coarsening Experiment Prepared for Flight

The Coarsening in Solid-Liquid Mixtures-2 (CSLM–2) experiment is a materials science spaceflight experiment whose purpose is to investigate the kinetics of competitive particle growth within a liquid matrix. During coarsening, small particles shrink by losing atoms to larger particles, causing the larger particles to grow. In this experiment, solid particles of tin will grow (coarsen) within a liquid lead-tin eutectic matrix. The following figures show the coarsening of tin particles in a lead-tin (Pb-Sn) eutectic as a function of time. By conducting this experiment in a microgravity environment, we can study a greater range of solid volume fractions, and the effects of sedimentation present in terrestrial experiments will be negligible. The CSLM–2 experiment flew November 2002 on space shuttle flight STS–113 for operation on the International Space Station, but it could not be run because of problems with the Microgravity Science Glovebox in the U.S. Laboratory module. Additional samples will be sent to ISS on subsequent shuttle flights.

The coarsening of particles within a matrix is a phenomenon that occurs in many metallic and other systems. For example, the second-phase particles in high-temperature turbine blade materials undergo coarsening at the operating temperature of the turbine. The coarsening process degrades the strength of the blade because turbine alloys containing a few large particles are weaker than those containing many small ones. Coarsening occurs in liquid-phase sintered materials such as tungsten carbide-cobalt, iron-copper, dental amalgam for fillings, and porcelain. The growth of liquid droplets in a vapor phase that occurs inside rain clouds (particularly near the equator, where the vapor pressure of water is high) is a commonplace example of the coarsening phenomenon. The CSLM–2 study will help define the mechanisms and rates of coarsening that govern all these systems.

In fiscal year 2002, the CSLM–2 project completed the fabrication, assembly, and testing of the flight hardware. The flight hardware consists of two main pieces of equipment, the sample processing unit (SPU) and the electronics control unit (ECU), as shown in the photographs on the next page. The SPU incorporates a small electric sample heater with a water quench system. The heater consists of a circular sample holder plate sandwiched by two thin-film kapton heaters with a circular ring heater around the perimeter. The holder plate has four cylindrical sample holes with four platinum resistance temperature devices for temperature monitoring and control.

The ECU contains the power supply, electrical control, and data storage components. There are three toggle switches on the front of the ECU that allow a crew member to power up the unit, activate the experiment run, and manually abort the run if necessary. There are also three indicator lights and a liquid crystal display (LCD) that show the status of the experiment and the temperatures of the resistance temperature devices in the sample holder. The temperature-time data from the experiment run are stored on a hard disk located in the ECU and telemetered to the NASA Telescience Support Center after experiment completion.

The CSLM–2 experiment runs do not need to be attended by an astronaut after activation. There is no need for real-time orbit-to-ground telemetry directly from the experimental apparatus. Non-real-time data will be downlinked via the Microgravity Science Glovebox laptop connected to the CSLM–2 hardware by an RS–422 data downlink.

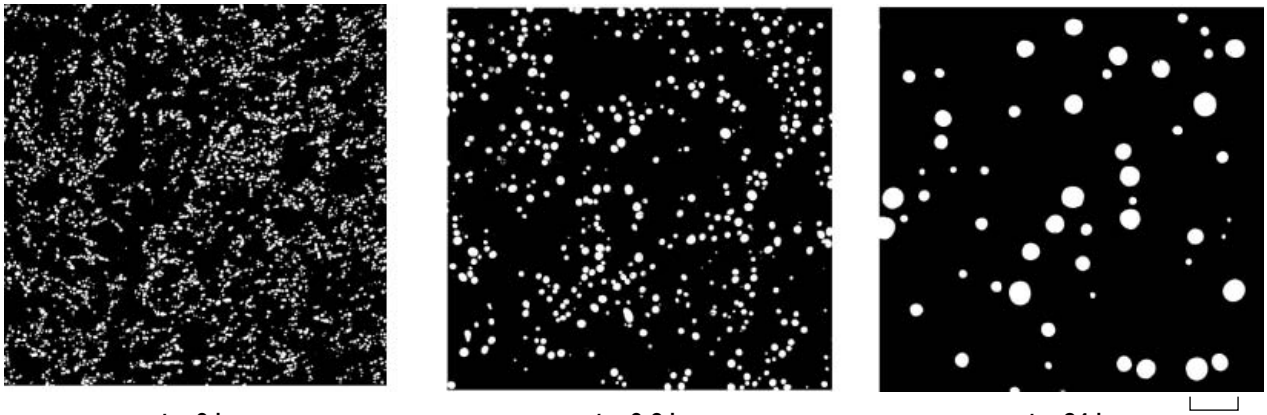

Solid Sn particles in a liquid Pb-Sn alloy. The size of the particles increases with coarsening time t. In many materials, such as Ni-based superalloys used in jet turbine blades, this increase in size has a dramatic effect on the properties of the alloy.

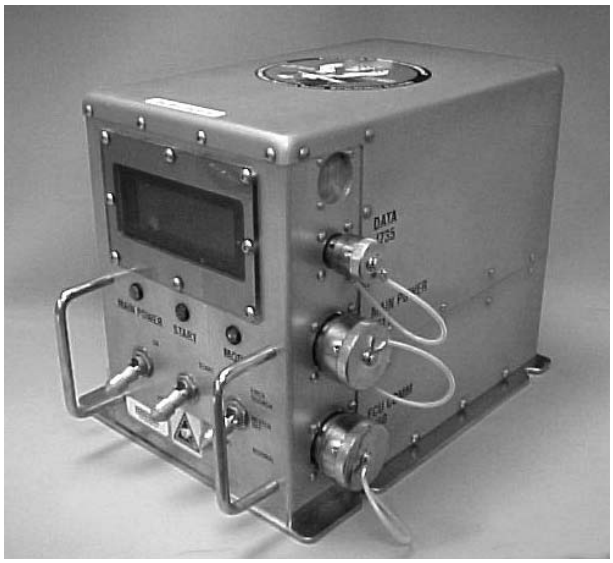

CSLM–2 sample processing unit.

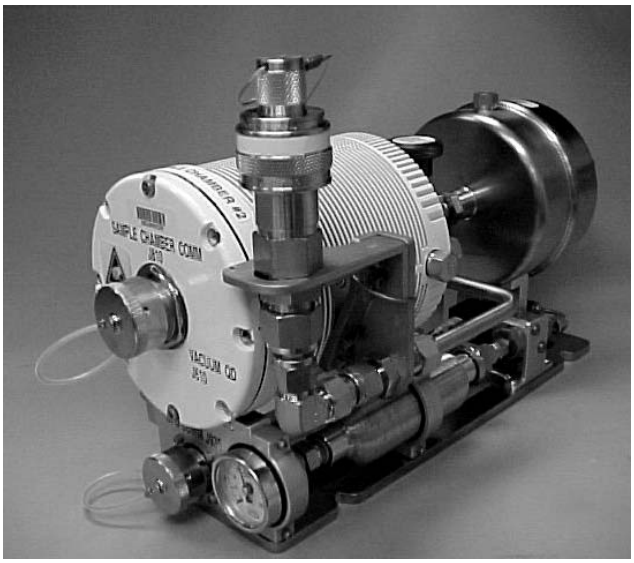

CSLM–2 electronics control unit.

References

1. Alkemper, J., et al.: Dynamics of Late-Stage Phase Separation: A Test of Theory. Phys. Rev. Lett., vol. 82, no. 13, 1999, pp. 2725–2728.
2. Calderon, H.A., et al.: Ostwald Ripening in Concentrated Alloys. Acta. Metall. Mater., vol. 42, no. 3, 1994, pp. 991–1000.
3. Snyder, V.A., et al.: The Influence of Temperature Gradients on Ostwald Ripening. Metall. Mater. Trans., vol. 30A, no. 9, 1999, pp. 2341–2348.
4. Snyder, V.A.; Alkemper, J.; and Voorhees, P.W.: The Development of Spatial Correlations During Ostwald Ripening: A Test of Theory. Acta Mater., vol. 48, no. 10, 2000, pp. 2689–2701.
5. Snyder, V.A.; Alkemper, J.; and Voorhees, P.W.: Transient Ostwald Ripening and the Disagreement Between Steady-State Coarsening Theory and Experiment. Acta Mater., vol. 49, 2001, p. 699.
6. Alkemper, J.; and Voorhees, P.W.: Quantitiative Serial Sectioning Analysis. J. Microscopy, vol. 201, 2000, p. 1.

Glenn contacts:
Dr. Walter Duval, 216–433–5023, Walter.M.Duval@nasa.gov; and
J. Mark Hickman, 216–977–7105, John.M.Hickman@nasa.gov

Author: J. Mark Hickman

Headquarters program office: OBPR

Programs/Projects:
Microgravity Science

New Technologies Being Developed for the Thermophoretic Sampling of Smoke Particulates in Microgravity

The Characterization of Smoke Particulate for Spacecraft Fire Detection, or Smoke, microgravity experiment is planned to be performed in the Microgravity Science Glovebox Facility on the International Space Station (ISS). This investigation, which is being developed by the NASA Glenn Research Center, ZIN Technologies, and the National Institute of Standards and Technologies (NIST), is based on the results and experience gained from the successful Comparative Soot Diagnostics experiment, which was flown as part of the USMP–3 (United States Microgravity Payload 3) mission on space shuttle flight STS–75. The Smoke experiment is designed to determine the particle size distributions of the smokes generated from a variety of overheated spacecraft materials and from microgravity fires. The objective is to provide the data that spacecraft designers need to properly design and implement fire detection in spacecraft. This investigation will also evaluate the performance of the smoke detectors currently in use aboard the space shuttle and ISS for the test materials in a microgravity environment.

As part of the suite of diagnostics required for the Smoke experiment,

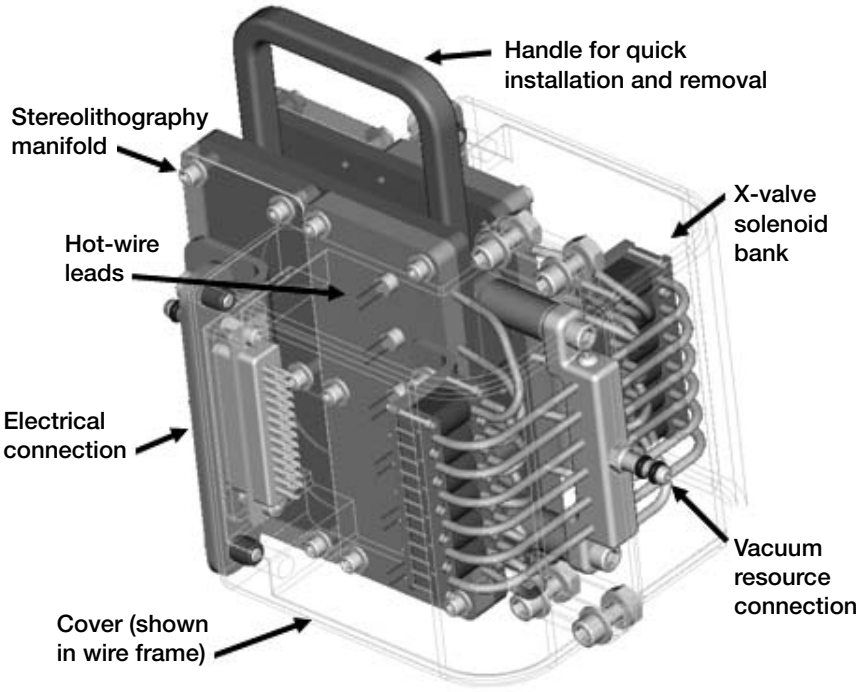

Smoke experiment—thermal precipitator.

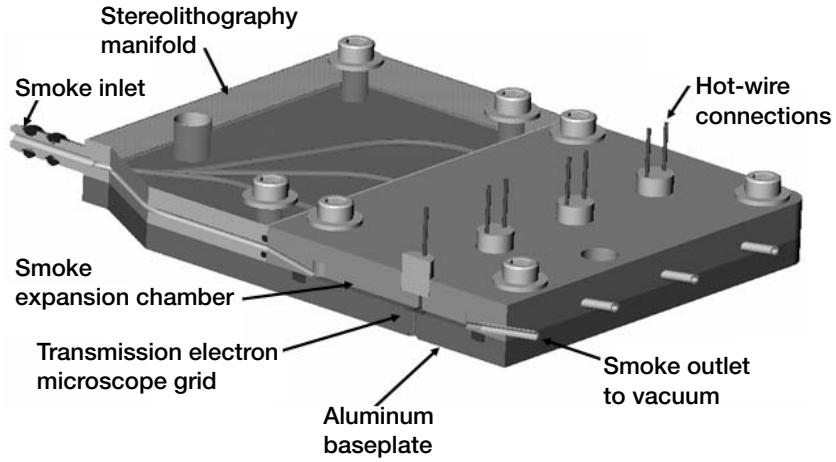

Smoke experiment—cut through view of thermal precipitator.

thermophoretic samplers, also called thermal precipitators, will be used to acquire representative samples of the smoke particulates generated when various materials (Teflon, silicon rubber, cellulose, and a liquid standard) are heated. These devices use a heated wire to drive the smoke onto a small collection grid (~1/8 in. in diameter) as it flows past. For each test point examined, a sample will be taken of the smoke within seconds of its generation, as well as another sample after a defined aging period, during which the sizes and geometries of the smoke particulates will have changed. These sample grids will be returned to Earth from the ISS after the completion of the experiment and examined under a transmission electron microscope.

Approximately 24 test points will be conducted for the Smoke investigation, with two samples required for each test. As conceptualized, each integrated thermal precipitator module will accommodate 12 thermophoretic samples. The experiment is being designed to require a minimum of ISS crew time for assembly and operation, and the current concept constitutes a significant improvement on the single sample design utilized for the Comparative Soot Diagnostics experiment.

To accommodate the large number of samples required for each thermal precipitator module, while minimizing the potential for cross-contamination of the samples, we incorporated separate flow paths for each sample grid into the design. These paths were sized (as small as 0.40 in. in diameter) to maintain a suitable flow velocity of 1 cm/s over the sample grids; and obstructions, which could impede particle flow, and potential leakage paths were minimized. This was accomplished through a manifold design within the unit that utilizes a unique fabrication technology called stereolithography. This technique, which takes a three-dimensional model and creates a part by solidifying a liquid polymer layer by layer, allows for a device to be formed without the restrictions imposed by more conventional molding or machining methods. Also, the semitransparent nature of the material allows for visual inspection of the internal flow paths as part of the verification process.

Another technology that makes this thermal precipitator design possible is the development of commercially available miniature valves that meet the flow control requirements of the Smoke experiment. Twelve such valves will be required for each thermal precipitator module. Finally, the individual transmission electron

microscope grids will be installed in the sample modules by "sandwiching" them between two plates without the use of adhesives, which minimizes the potential of damage from handling and facilitates their removal from the unit upon return to Earth. The design of the thermal precipitator unit and the utilization of available technologies will result in a device that minimizes the use of valuable crew time aboard the ISS while maximizing science return.

Glenn contacts:
Dr. David L. Urban, 216–433–2835, David.L.Urban@nasa.gov;
Dr. Gary Ruff, 216–433–5697, Gary.A.Ruff@nasa.gov; and
William A. Sheredy, 216–433–3685, William.A.Sheredy@nasa.gov

Author: William A. Sheredy

Headquarters program office: OBPR

Programs/Projects:
Microgravity Science

Power and Propulsion

Multifunctional Inflatable Structure Being Developed for the PowerSphere Concept

The continuing development of microsatellites and nanosatellites for low Earth orbits requires the collection of sufficient power for instruments onboard a low-weight, low-volume spacecraft. Because the overall surface area of a microsatellite or nanosatellite is small, body-mounted solar cells cannot provide enough power. The deployment of traditional, rigid, solar arrays necessitates larger satellite volumes and weights, and also requires extra apparatus for pointing. One solution to this power choke problem is the deployment of a spherical, inflatable power system. This power system, termed the "PowerSphere," has several advantages, including a high collection area, low weight and stowage volume, and the elimination of solar array pointing mechanisms.

NASA has funded a collaborative team of the Aerospace Corporation, ILC Dover, Lockheed Martin, and the NASA Glenn Research Center to develop the Multifunctional Inflatable Structure (MIS) for the PowerSphere concept through a NASA Research Announcement (NRA). Glenn is providing overall project and technical management of the effort as well as substantial technical contributions in simulated space environment testing, protective coatings development, and thin-film solar cell technology expertise. As the principle investigator for this development effort, the Aerospace Corporation is leading the technical development effort and is the originator of the PowerSphere concept. ILC Dover is developing the deployable, rigidizable MIS structure that will functionally join the thin-film solar cell panels, flexible power circuitry, and other systems to the central spacecraft payload interface. Lockheed Martin is developing the flexible circuitry elements for the MIS and is also contributing spacecraft integration expertise. The current 3-yr effort will culminate with the fabrication and testing of a fully functional engineering development unit. The PowerSphere MIS component technologies and system-level concept matured sufficiently in fiscal year 2002 to begin proof-of-concept fabrication and testing of MIS systems

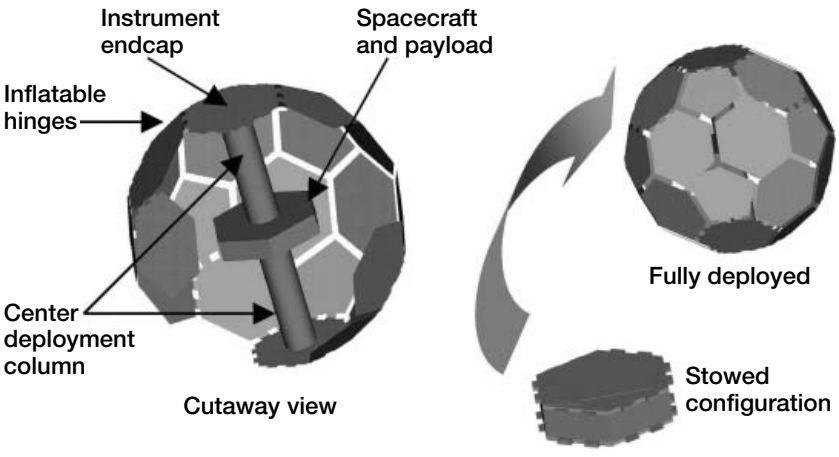

PowerSphere system concept.

in fiscal year 2003. Follow-on efforts are also being proposed to further advance the PowerSphere technology to flight readiness for potential spaceflight demonstrations incorporating a number of key power systems technologies.

The baseline design of the PowerSphere spherical solar array consists of two semispherical domes connected together to a central spacecraft. Each semispherical dome consists of hexagonal and pentagonal solar cell panels that together form a geodetic sphere (see the figure on the preceding page). Inflatable, ultraviolet rigidizable tubular hinges between solar cell panels and ultraviolet rigidizable isogrid center columns with imbedded flex circuitry form the MIS. In a stowed configuration, the solar cell panels are folded sequentially to the outside of the instrument decks. The center column will be z-folded between the instrument decks and the spacecraft housing for packaging. The instrument panel will secure the z-folded stack with launch ties. After launch, once the release tie is triggered, the center column and hinge tubes will inflate and ultraviolet radiation will cure each tube and center column into a rigid supporting column.

The reference configuration for the PowerSphere effort is a 0.6-m-diameter (fully deployed) spacecraft with a total mass of 4 kg (1 kg for the PowerSphere, 3 kg for the spacecraft) capable of producing 29 W of electricity with 10-percent-efficient thin-film solar cells. Potential NASA applications for the PowerSphere include surveys of Earth's Magnetotail, Solar Flotilla missions, planetary protection, sample return missions, multiplatform planet surface science, and formation flying interferometric astronomy science missions. This work is being funded by NASA under contract NAS3–01115.

Bibliography

Prater, Alonzo, et al.: Power Management and Distribution Concept for Microsatellites and Nanosatellites. IECEC SAE Paper 1999–01–2442, 1999.

Gilmore, D., et al.: Thermal Design Aspects of the Powersphere Concept. Paper presented at the 2nd International Conference on Integrated Micronanotechnology for Space Applications, Pasadena, CA, vol. 1, 1999, pp. 451–458.

Simburger, Edward J., et al.: Multifunctional Structures for the PowerSphere Concept. AIAA 2001–1343, 2001.

Glenn contacts:
Todd Peterson, 216–433–5350, Todd.T.Peterson@nasa.gov;
Tom Kerslake, 216–433–5373, Thomas.W.Kerslake@nasa.gov; and
Henry Curtis, 216–433–2231, Henry.B.Curtis@nasa.gov

Author: Todd T. Peterson

Headquarters program office: OAT

Programs/Projects:
Space Power Systems R&T

International Space Station Solar Array Bifacial Electrical Performance Model Developed

The first U.S. photovoltaic array (PVA) was activated on the International Space Station (ISS) in December 2000. Though normally Sun-tracking, U.S. ISS arrays are held stationary to minimize plume impingement from the space shuttle during docking and undocking, as well as during ISS assembly operations. Because of these operational constraints, it is not always possible to point the front side of the arrays at the Sun. In these cases, sunlight directly illuminates the backside of the PVA as well as albedo illumination on either the front or the back. Since the solar cells are mounted on a thin, solar transparent substrate, appreciable backside power (about one-third of the front-side power) is produced. To provide a more detailed assessment of the ISS power production capability, researchers at the NASA Glenn Research Center developed a PVA electrical performance model applicable to generalized bifacial illumination conditions. The model validation was done using on-orbit PVA performance.

For generalized PVA illumination, there is a direct solar component from the front or the back, and albedo components on the PVA front and/or back. The solar cell bifacial current-voltage, *IV*, values were calculated by superposing currents and scaling voltages with currents. Once the bifacial solar cell *IV* curve was obtained, the solar cell string *IV* curve was calculated by summing the voltage contribution of the individual series-connected cells and subtracting the

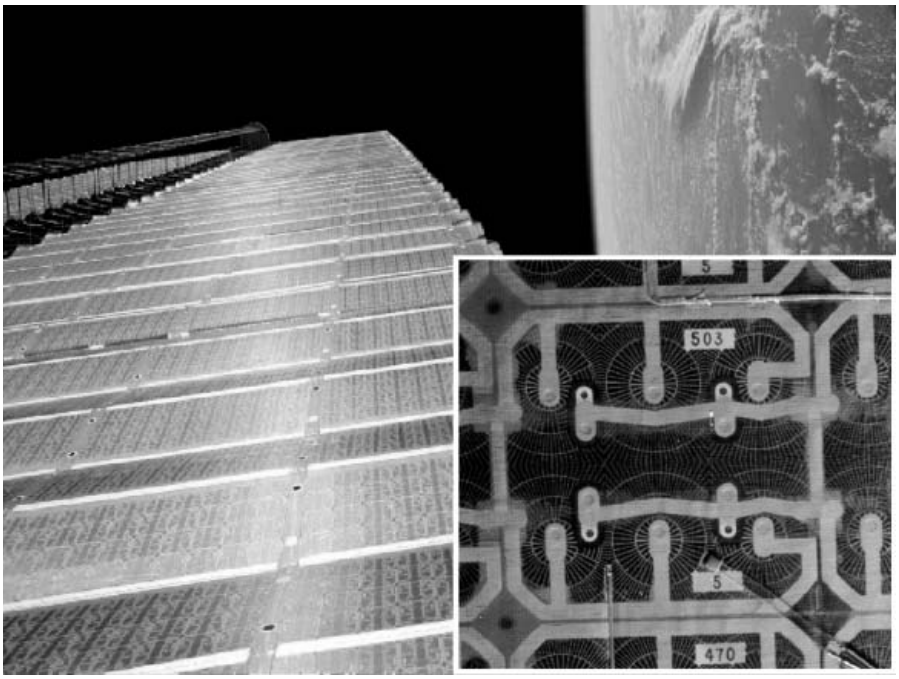

Backside of U.S. PVA showing series-connected, 8- by 8-cm crystalline silicon solar cells with gridded back contacts and copper flat printed circuit.

voltage drop in the cell interconnects, harness and cabling, blocking diode, and sequential shunt unit. String current was iteratively determined such that the cell voltage generation minus the line voltage loss satisfied the sequential shunt unit output voltage set point. In the presence of string shadowing, separate *IV* curves were calculated for shadowed and unshadowed string sections. Total PVA current capability was obtained by summing the current contribution of the individual strings. On the basis of the uncertainties in the analysis methods, data input, Earth albedo, and infrared emission, the estimated total root-sum-square uncertainty in the predicted current is ±6 percent for a Sun-tracking PVA.

This graph compares predicted and measured PVA current for a sample orbit selected on December 10, 2001. The qualitative comparison between measured and calculated PVA currents through the orbit Sun period is excellent. Quantitatively, the root-mean-square difference between measured and calculated values was 3.0 A on the back and 4.4 A on the front. This is equivalent to approximately 2 percent of PVA front-side current capability or 4 percent of PVA backside current capability. Front-illuminated current data are smooth and in good agreement with calculated values.

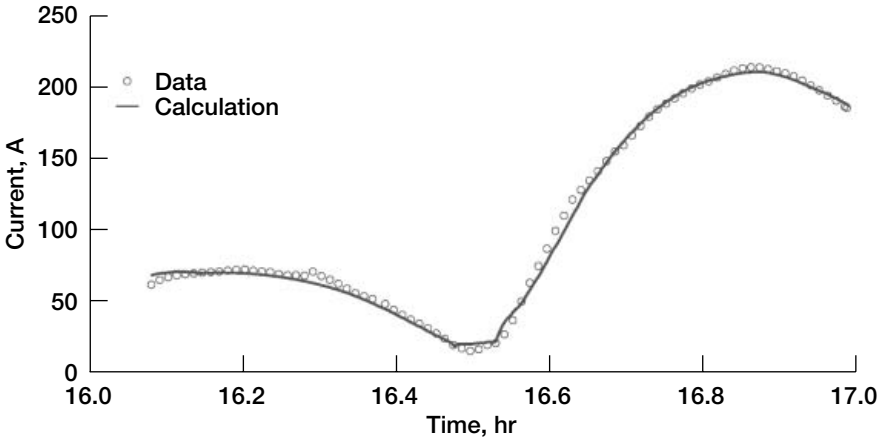

Comparison of predicted and measured PVA current for a sample orbit selected on December 10, 2001. (Extravehicular activity to install BGA thermal blankets.)

This bifacial PVA performance model developed by Glenn has further improved the correlation between predictions and on-orbit data. With this more accurate modeling capability, improved power predictions that support on-orbit operations, certification for flight readiness, and mission planning can be made. The code has been incorporated into the SPACE (System Power Analysis for Capability) power systems software and into software used by the NASA Johnson Space Center Mission Operations Directorate for day-to-day on-orbit ISS operations planning. Recently, the Space Station Program Office began relying on the power produced from the PVA backside for on-orbit operations and planning.

Glenn contacts:
Ann M. Delleur, 216–433–5519, Ann.Delleur@nasa.gov; and
Tom Kerslake, 216–433–5373, Thomas.W.Kerslake@nasa.gov

Authors:
Ann M. Delleur and Thomas W. Kerslake

Headquarters Program Office: OSF

Programs/Projects: ISS, Electrical Performance Modeling

International Space Station Power System Telemetry Compared With Analytically Derived Data for Shadowed Cases

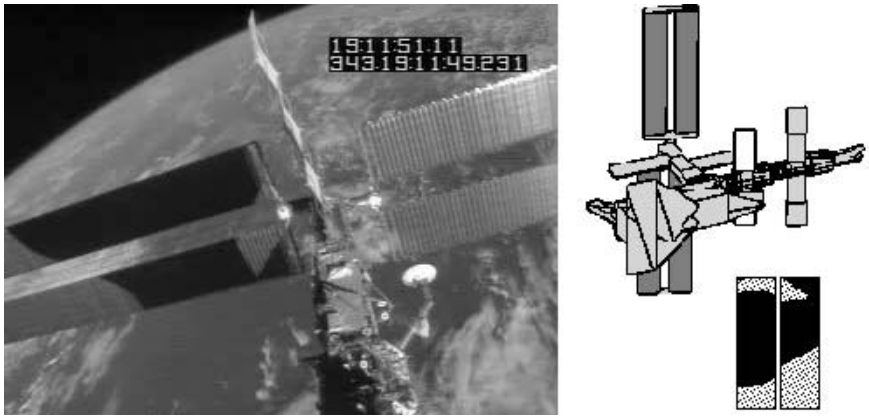

Video frame and SPACE-generated geometry and shadow patterns.

This article highlights fiscal year 2002 work performed by NASA Glenn Research Center personnel to validate algorithms and data developed in-house to predict shadowing effects on the International Space Station (ISS) solar arrays' power generation. The validation effort utilized video footage and on-orbit telemetry for cases spanning a 1-yr period. Validation was required because of the uncertainty of various aspects involved in shadowing analysis. Results show that a good comparison exists between actual and predicted shadowed power system performance for solar array front and backside shadowing.

In December 2000, the first ISS U.S. solar arrays were deployed. Since then, some of the largest shadow patterns ever observed on orbital solar arrays (~170 m^2) have occurred. Shadow patterns with significant durations and varied shapes have appeared. Power demands and shadowing events will increase in frequency and magnitude in a complex fashion that can only be predicted by a computer program such as the Glenn-developed power system tool called SPACE (System Power Analysis for Capability Evaluation). SPACE models the power hardware and integrates all analysis components (e.g., shadowing analysis) to determine the time-varying effect of load demand on the power system.

The development of the SPACE shadowing algorithms and geometry data required key assumptions: (1) that relatively low fidelity geometry models were acceptable (instead of highly detailed, but computationally prohibitive models), (2) that the Sun could be modeled as a point light source, and (3) that reflected energy from adjacent hardware was minimal.

Each year, the ISS travels through over 5500 orbits, with various flight attitudes, solar array pointing, and space shuttle docking locations. Since most orbits have some shadowing and analyzing every orbit is time prohibitive, only portions of orbits with adequate video documentary footage and recorded telemetry and that showed a significant effect of the shadow on the power were examined.

Acquiring telemetry data and correlating it with predictions is complicated because of data dropouts, sensor calibration, data conversion, and unsensored data. Also, because reflected sunlight from the Earth's surface affects the comparison (the exact amount is unknown), a range of values representing likely short term values were examined.

The figure shows a selected video frame and SPACE graphical output (a cartoon of the array from the Sun's viewpoint and the projected shadow pattern of one set of solar arrays) for one of the five analyzed cases. During this period, the ISS drifted 180° about one axis, causing the back of the locked solar array to face the Sun and be shadowed by the space shuttle. This case had a maximum of 62-percent shadowing of one wing (~170 m^2). It shows a good comparison using a high albedo assumption (justified by cloud cover shown in weather satellite images).

The shadowing algorithms and geometry models predicted shadowing effects at acceptable difference levels from telemetry (within 6 percent of solar array wing ampere-hour capability during a shadowing event). Differences are likely due to a combination of geometric model fidelity and the modeling of the Sun as a point light source (reflection effects were not apparent in the data).

Find out more about the research of Glenn's Power & Propulsion Office:
ppoweb.grc.nasa.gov

Glenn contact:
James Fincannon, 216–433–5405,
Homer.J.Fincannon@nasa.gov

Author: H. James Fincannon

Headquarters program office: OSF

Programs/Projects: ISS

R&T 2002

Engineering and Technical Services

Facilities and Test Engineering

Microsystems Fabrication Laboratory—New Class 100 Cleanroom Completed and Certified

A new Microsystems Fabrication Laboratory (MFL), a Class 100 cleanroom fabrication facility, was completed and certified in 2002 at the NASA Glenn Research Center. This facility, to be used by Glenn's Instrumentation and Controls Division, was designed and built as part of the NASA Construction of Facilities Program. The design, construction, and certification phases were managed by personnel from Glenn's Facilities and Test Engineering Division. Because of time constraints and the need for specialized cleanroom expertise, this 1000 ft^2 laboratory was completed using a design-build procurement. Facility Planning & Resources (Pittsburgh, PA) was selected as the prime contractor and provided the architectural design and project management. A major subcontractor, AdvanceTEC, LLC (Richmond, VA), provided the mechanical and electrical design and performed the construction services. Throughout this fast-track project, Facilities and Test Engineering Division personnel provided overall project management and worked closely with the contractors to ensure that the customers' needs were addressed and that the impact of the project implementation was minimized.

The new Microsystems Fabrication Laboratory is vital in expanding and improving the fabrication facilities and capabilities of Glenn's Instrumentation and Controls Division, which conducts research and development in sensing concepts, sensor technology, high-temperature electronics, and related areas such as electronic materials, electronic materials processing, and nanotechnology. Emphasis is on developing advanced capabilities for measuring and controlling aerospace propulsion systems, particularly in harsh environments and for safety applications. The new facility provides improved environmental conditions (cleanliness, temperature, and humidity) in comparison to the existing fabrication facilities. The layout features a new photolithography area, a thin-film deposition area, a thermal oxidation area, and support areas. The Microsystems Fabrication Laboratory will be used in fabricating thin-film sensors, growing electronic-grade oxides, and supporting the expected future growth in high-temperature and harsh-environment microelectromechanical systems (MEMS) research.

Glenn's new Microsystems Fabrication Laboratory.

Find out more about this research:

Instrumentation and Controls Division:
http://www.grc.nasa.gov/WWW/ictd

Sensors and Electronics Technology Branch:
http://www.grc.nasa.gov/WWW/sensors

Glenn contact:
Dr. Lawrence Matus, 216–433–3650, Lawrence.G.Matus@nasa.gov

Author: Frances M. Borato

Headquarters program office:
OMSF (FED), OAT

Programs/Projects: Propulsion and Power, GMI, ASTP, AvSP, UEET, NEPP

Static Frequency Converter System Installed and Tested

A new Static Frequency Converter (SFC) system has been installed and tested at the NASA Glenn Research Center's Central Air Equipment Building to provide consistent, reduced motor start times and improved reliability for the building's 14 large exhausters and compressors. The operational start times have been consistent around 2 min, 20 s per machine. This is at least a 3-min improvement (per machine) over the old variable-frequency motor generator sets. The SFC was designed and built by Asea Brown Boveri (ABB) and installed by Encompass Design Group (EDG) as part of a Construction of Facilities project managed by Glenn (Robert Scheidegger, project manager). The authors designed the Central Process Distributed Control Systems interface and control between the programmable logic controller, solid-state exciter, and switchgear, which was constructed by Gilcrest Electric.

Static Frequency Converter.

The new SFC is rated at 6500 kW and consists of a 12-pulse load-commutated rectifier, a direct-current (dc) link reactor, and a load-commutated inverter. The load-commutated rectifier converts the 60-cycle input voltage and current to a dc voltage and current. The dc reactor smoothes the rectified dc current and limits the fault current capability of the SFC. The load-commutated inverter then changes the dc voltage and current into an alternating current (ac) and voltage at a frequency between 2 and 60 Hz, depending on the requested speed setpoint given to the drive by the Central Process Distributed Control Systems. In addition, the SFC attempts to accelerate the motor at a constant torque level by maintaining a constant volts-per-hertz ratio. It accomplishes this by controlling the excitation current of the synchronous motor being started.

The start sequence begins with the SFC commanding the motor exciter to output a field current pulse. This allows the SFC to determine if the rotor is stationary prior to the start and to determine the rotor position. The SFC provides pulsating power to the motor stator winding until the rotor reaches a speed of 2 Hz. Then, it switches to the load-commutative mode. After this, the SFC accelerates the motor to a speed of 59 Hz in a constant-torque mode and activates the synchronizer that will transfer the motor to the utility when the voltage, frequency, and phase angle are matched to the utility bus.

The new SFC requires only cooling fans and has no moving parts, which can require large amounts of preventative maintenance to be reliable. All 14 machines can be started in about 35 min in contrast to the approximately 1 hr, 10 min needed with variable-frequency motor generator sets. A second SFC is being installed that will allow all 14 machines to be started reliably in 15 min.

Find out more about this research:
www.grc.nasa.gov/WWW/FTED/

Glenn contacts:
Donald P. Brown, 216–433–3934, Donald.P.Brown@nasa.gov; and Debashis Sadhukhan, 216–433–6567, Debashis.Sadhukhan-1@nasa.gov

Authors: Donald P. Brown and Debashis Sadhukhan

Headquarters program office:
Funded by CoF at Glenn

Programs/Projects: Glenn's Propulsion Systems Laboratories, users of Glenn's Central Air Equipment Building

6-ft High-Power Electric Propulsion Test Port, EPL Tank 5 Installed

High-power electric propulsion is a critical component of NASA's proposed missions to the outer planets. Mission studies have shown that high-power, high-specific-impulse propulsion systems can deliver 2000 kg of scientific payload to Pluto with trip times on the order of 10 years. Of greater significance is the ability of these propulsion systems to place this science payload in orbit around the planet, rather than making the fast fly-bys associated with traditional chemical propulsion systems. Significant ground test programs are required to develop the new technologies needed for thrusters operating at power levels exceeding 20 kW, an order of magnitude above the state of the art.

High-power electric propulsion research capability has been a hallmark of the NASA Glenn Research Center's Vacuum Facility 5 (VF5) facility for many years. VF5 has adequate pumping speed, power, and diagnostic systems to conduct thruster tests at power levels in excess of 100 kW. These tests were traditionally conducted in the main body of the tank, so the vacuum systems had to be cycled when test hardware needed to be modified or changed out.

This year, a 6-ft bell-jar port was added to consolidate the existing high-power electric propulsion test capabilities of VF5, allowing the test article to be installed in an isolated chamber. This operational change will significantly improve test efficiency and reduce costs by allowing changes in the test configuration without cycling the main body of the tank to atmospheric pressure. The port features a molecular turbopump that can pump down the tank independent of the test facility, and a rail system for installing the thruster and thrust stand. The auxiliary power, data, video, and thrust measurement systems are consolidated in permanent racks on the platform extension. A successful 50-kW Hall thruster test has been completed in the port with nominal facility performance.

Glenn contacts:
Stanley Grisnik, 216–977–7441, Stanley.P.Grisnik@nasa.gov;
Elmer Theman, 216–977–7442, Elmer.R.Theman@nasa.gov;
Henry Speier, 216–977–7420, Henry.J.Speier@nasa.gov; and
Robert Jankovsky, 216–977–7515, Robert.S.Jankovsky@nasa.gov

QSS contact:
Michael Swiatek, 216–433–3178, Michael.W.Swiatek@grc.nasa.gov

Authors: Stanley P. Grisnik, Elmer R. Theman, Michael W. Swiatek, Henry J. Speier, and Robert S. Jankovsky

Headquarters program office: OAT

Programs/Projects: Electric propulsion research, missions to the outer planets

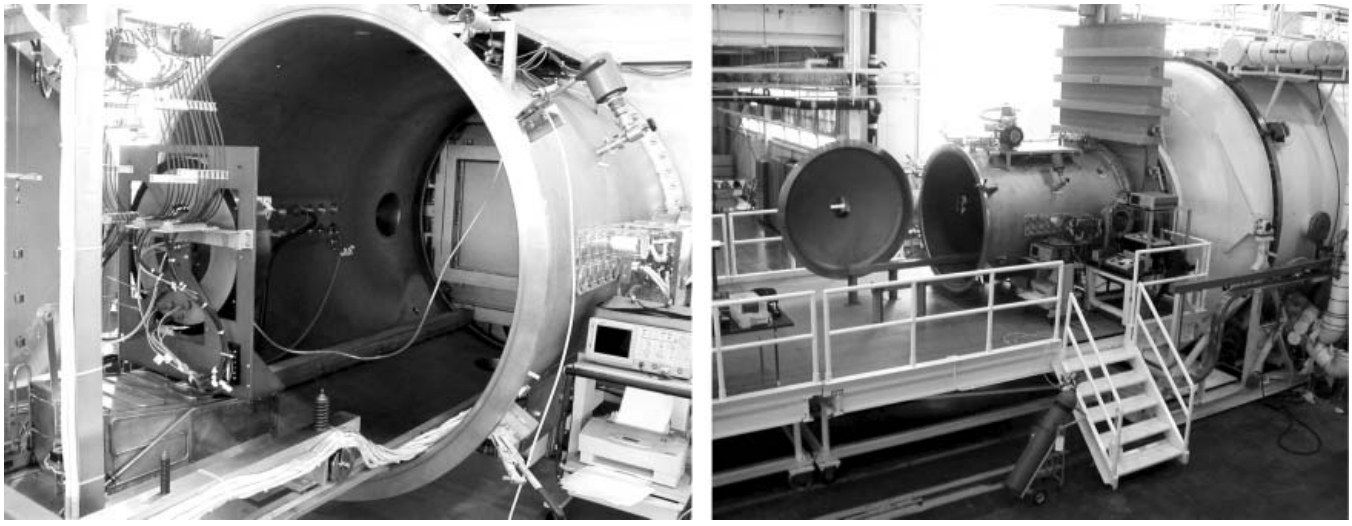

Left: 50-kW Hall thruster and thrust stand on rail system. Right: 6-ft test section and platform.

Research Combustion Lab Facility Capabilities and Throughput Enhanced by New Test Stands

A second test stand has been added to each of two test cells in the Research Combustion Laboratory at the NASA Glenn Research Center. This increased capacity will allow for faster buildup and transition between test programs supporting propulsion research, combustion studies, and advanced materials and structures evaluation. Cell 21 now has two stands capable of supplying gaseous or liquid oxygen, gaseous hydrogen, and gaseous or liquid hydrocarbon propellants (see the following photograph). It provides smaller flow rates to support ignition system testing and subscale propulsion research. Cell 22 has two larger stands providing gaseous hydrogen and oxygen propellants, and also can supply high-pressure cooling water (see the photograph on the next page). It is used primarily to support research testing of high-temperature composite materials and structures at typical rocket engine operating conditions.

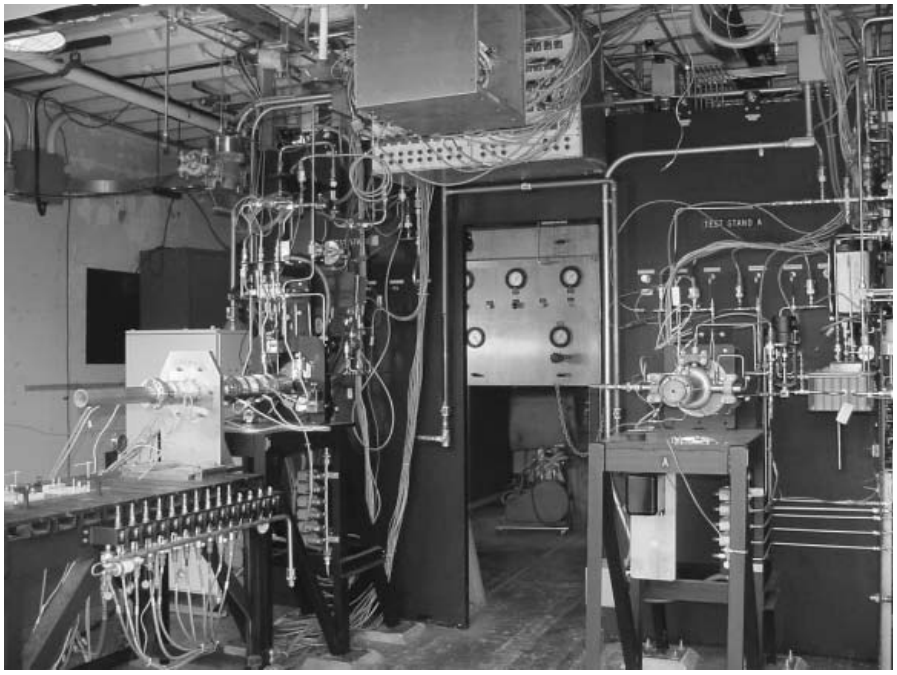

Test Cell 21: The original stand position is on the right. The new second stand is on the left, ready for pulse detonation engine testing.

In each cell, common controls operate the majority of the valves feeding the two stands. Feed line switching is done downstream of the main control valves by changing the connecting lines from the valve to the test article. Cell 21 also has auxiliary valve actuation on each stand to allow for close coupling at the test article. Each cell has a single data system that uses a central patch board to switch between the two test stands' instrumentation configurations. Switching between stands can be done rapidly, in some cases on a daily basis depending on the complexity of the individual test.

The two cells share gaseous oxygen and hydrogen supply trailers, and are typically run on alternating days or sometimes weeks. With the addition of the second stands, each cell can now accomplish more test preparation activity while the other cell is running. The new stands allow for greater flexibility in scheduling tests and provide for more efficient means of utilizing "unplanned" downtime. If a particular test program is delayed because of test hardware delivery or operability problems, another program can be ready and waiting to take advantage of the available time.

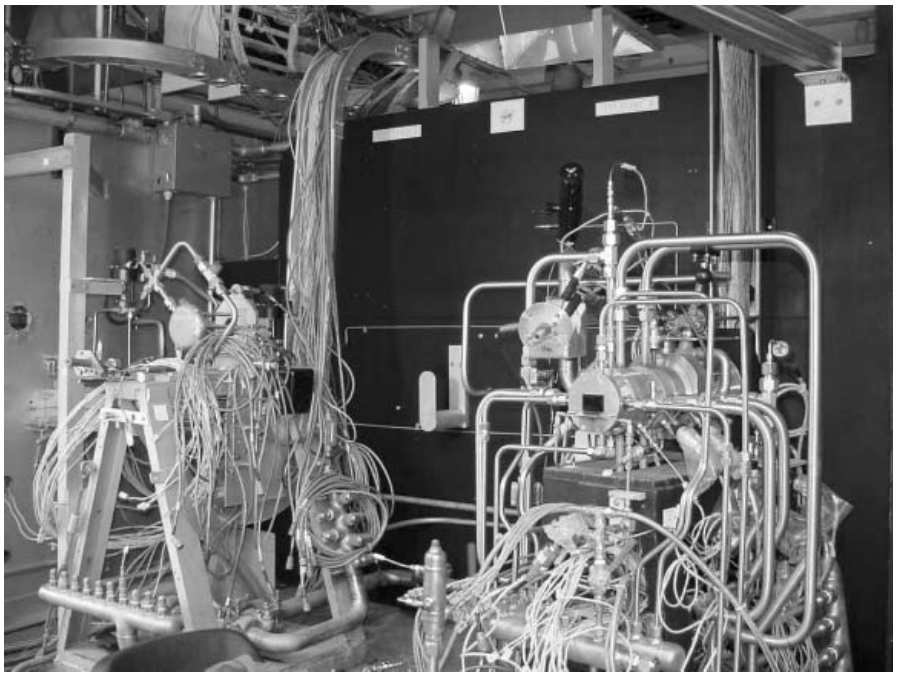

Test Cell 22: Left: Original stand. Right: New stand being prepared for an advanced materials nozzle extension test.

Find out more about this research:
http://www.grc.nasa.gov/WWW/CRL/

Glenn contacts:
Joseph Zoeckler, 216–977–7411, Joseph.G.Zoeckler@nasa.gov; and Wayne M. Bartlett, 216–433–5745, Wayne.M.Bartlett@nasa.gov

Author: Joseph G. Zoeckler

Headquarters program office: OAT

Programs/Projects: Propulsion Systems R&T, STPO, RLV, DDF

Short Takeoff and Vertical Landing Capability Upgraded in NASA Glenn's 9- by 15-Foot Low-Speed Wind Tunnel

The NASA Glenn Research Center supports short takeoff and vertical landing (STOVL) tests in its 9- by 15-Foot Low Speed Wind Tunnel (9×15 LSWT). As part of a facility capability upgrade, a dynamic actuation system (DAS) was fabricated to enhance the STOVL testing capabilities. The DAS serves as the mechanical interface between the 9×15 LSWT test section structure and the STOVL model to be tested. It provides vertical and horizontal translation of the model in the test section and maintains the model attitude (pitch, yaw, and roll) during translation. It also integrates a piping system to supply the model with exhaust and hot air to simulate the inlet suction and nozzle exhausts, respectively. Hot gas ingestion studies have been performed with the facility ground plane installed.

The DAS provides vertical (ascent and descent) translation speeds of up to 48 in./s and horizontal translation speeds of up to 12 in./s. Model pitch variations of ±7°, roll variations of ±5°, and yaw variations of 0° to 180° can be accommodated and are maintained within 0.25° throughout the translation profile. The hot air supply, generated by the facility heaters and regulated by control valves, provides three separate temperature zones to the model for STOVL and hot gas ingestion testing. Channels along the supertube provide instrumentation paths from the model to the facility data system for data collection purposes.

The DAS is supported by the 9×15 LSWT test section ceiling structure. A carriage that rides on two linear rails provides for horizontal translation of the system along the test section longitudinal axis. A vertical translation assembly, consisting of a cage and supertube, is secured to the carriage. The supertube traverses vertically through the cage on a set of linear rails. Both translation axes are hydraulically actuated and

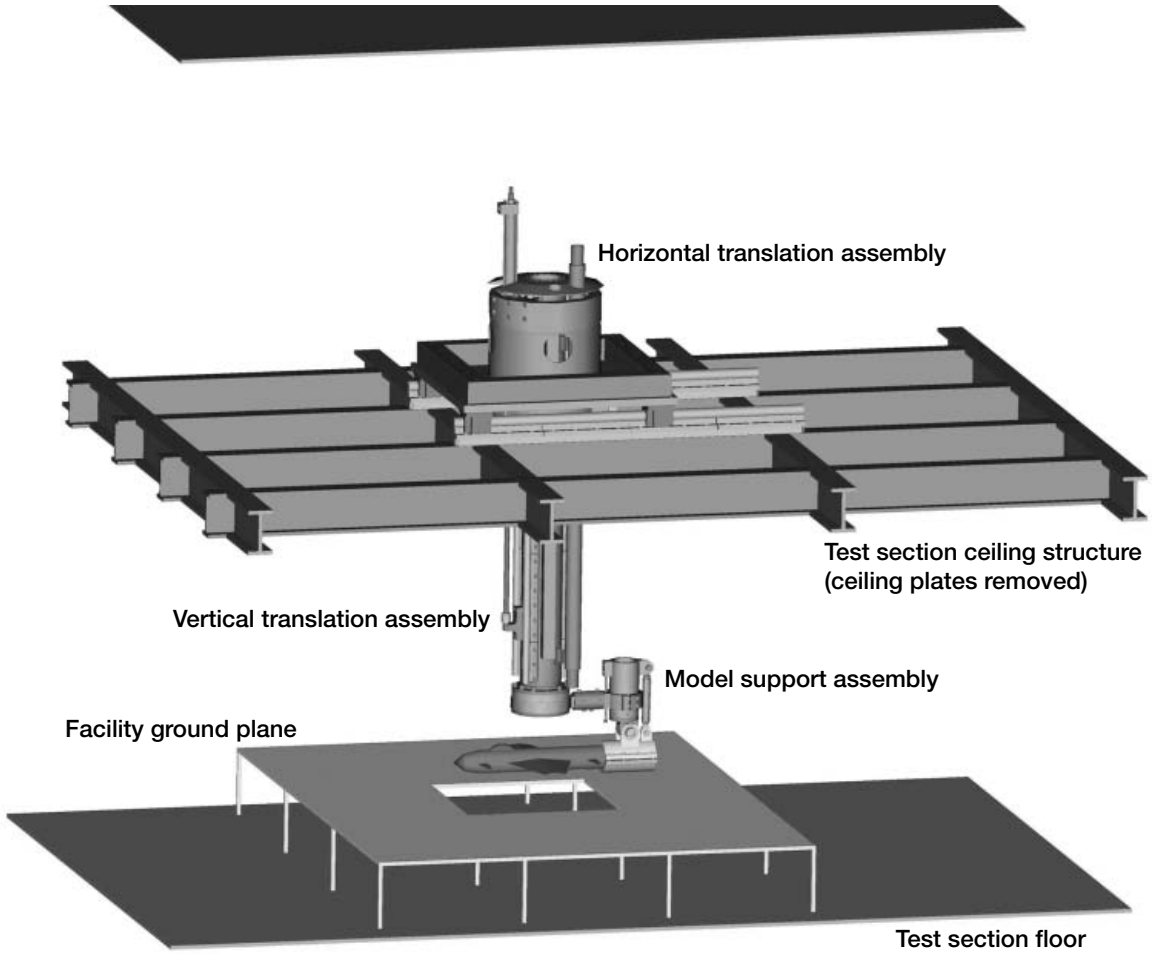

Dynamic actuation system in the 9x15 LSWT test section with the facility ground plane installed.

provide position and velocity profile control. The lower flange on the supertube serves as the model interface to the DAS. The supertube also serves as the exhaust path to the model and supports the hot air piping on its external surfaces.

The DAS is currently being assembled at the 9×15 LSWT facility. Following assembly and installation, a series of checkouts will be performed to confirm the operation of the system.

Find out more about this research:

Glenn's Facilities and Test Engineering Division:
http://www.grc.nasa.gov/WWW/RTD/

Glenn's Facilities Portal: http://facilities.grc.nasa.gov/

Glenn contact:
David E. Stark, 216–433–2922,
David.E.Stark@nasa.gov

U.S. Army, Vehicle Technology Directorate at Glenn contact:
Gary A. Klann, 216–433–5715,
Gary.A.Klann@grc.nasa.gov

Author: David E. Stark

Headquarters program office: OAT

Programs/Projects:
Power and Propulsion

Engineering Design and Analysis

Liquid Propellant Manipulated Acoustically

Fluids are difficult to manage in the space environment. Without gravity, the liquid and gas do not always remain separated as they do in the 1g environment of Earth. Instead the liquid and gas volumes mix and migrate under the influence of surface tension, thermodynamic forces, and external disturbances. As a result, liquid propellants may not be in a useable location or may even form a chaotic mix of liquid and gas bubbles.

In the past, mechanical pumps, baffles, and a variety of specialized passive devices have been used to control the liquid and gas volumes. These methods need to be carefully tuned to a specific configuration to be effective. With increasing emphasis on long-term human activity in space there is a trend toward liquid systems that are more flexible and provide greater control. We are exploring new methods of manipulating liquids by using the nonlinear acoustic effects achieved by using beams of highly directed high-intensity acoustic waves.

One effect is acoustic radiation pressure, which will be used to manipulate gas bubbles and liquid gas interfaces. It can be used to propel and control the position of gas bubbles and could force separate bubbles to coalesce. It may also be used to suppress free-surface sloshing.

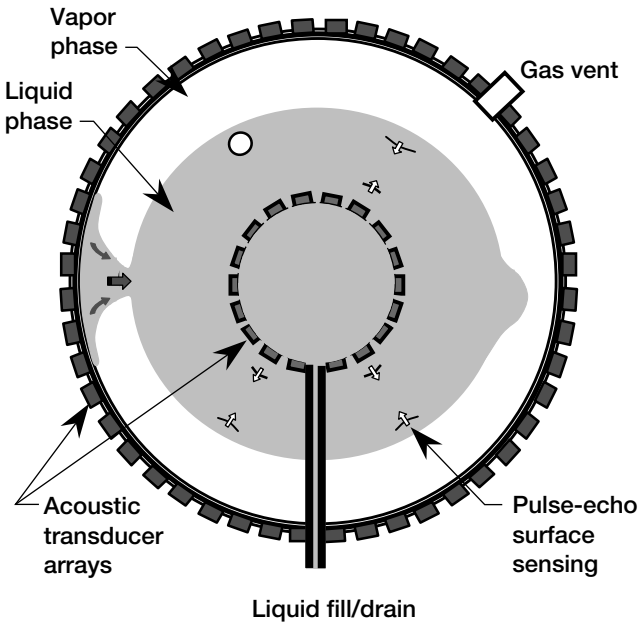

Acoustic "smart tank."

Another effect is acoustic streaming, which has been proven to create liquid currents without nozzles or mechanical propellers. Acoustic streaming can be used in a variety of ways, including in agitation liquids to suspend solid particles or to annihilate thermal gradients to suppress propellant boiloff. Acoustic radiation pressure and acoustic streaming can be combined to create liquid fountains that can transfer liquids over long distances. The system will employ acoustic phased arrays to steer and focus the acoustic beams electronically, making it possible to operate on multiple targets as needed.

Acoustic manipulation will be enhanced by the addition of acoustic imaging. This technique is akin to medical ultrasound and sonar. Acoustic imaging will be coupled with the manipulation techniques that will allow the system to both "see" as well as "act" on selected targets. This acoustic "smart tank" will be able to both map the contents of the propellant tank and control its behavior. This approach lends itself to automated control or control by remote operators.

In the first year of this research, the NASA Glenn Research Center has been working with Dr. Adin Mann of Iowa State University to develop a nonlinear acoustic model. This analytical model will aid us in the design of the acoustic devices and arrays, and it will predict radiation pressure and acoustic streaming. This information will then be used create fluid dynamic and thermodynamic models using existing computational fluid dynamic codes.

Glenn has also been designing a general purpose 64-channel acoustic liquid manipulation (ALM) acoustic phased-array system. This system is computer controlled and can be programmed to by a simple laptop to synthesize a variety of acoustic beam configurations and power levels. This system will be tested in laboratory tanks and with microgravity aircraft test models.

Glenn contacts:
Richard C. Oeftering, 216–433–2285, Richard.C.Oeftering@nasa.gov; and David J. Chato, 216–977–7488 David.J.Chato@nasa.gov

Authors: Richard C. Oeftering, David J. Chato, and Dr. Adin Mann III

Headquarters program office: Funded by SRF at Glenn

Programs/Projects: SRF

Midinfrared Temperature Measurement Technique Developed

Infrared thermography is the measuring of the temperature of an object by examining the spectral quantities of light emission. The microgravity combustion experiment Solid Inflammability Boundary at Low-Speeds (SIBAL) calls for full-field temperature measurements of a thin sheet of cellulosic fuel as a flame front moves across the fuel, and infrared thermography is the only technique that can accomplish this task. The thermography is accomplished by imaging the fuel with a midinfrared camera that is sensitive in the 3.0- to 5.0-μm wavelength region in conjunction with a 3.7- to 4.1-μm bandpass filter to eliminate unwanted infrared radiation from components other than the fuel. Problems have been encountered with the process of obtaining accurate temperature measurements from the fuel. The first of which is the wide temperature range that requires measurement. SIBAL calls for a temperature range of 420 to 1070 K corresponding to an in-band radiance ratio of 245:1—far too large a span for an infrared camera to cover in one "snapshot" since the entire range of temperatures will be in the field. Another problem encountered is that of the varying emissivity of the fuel as it burns. In typical cases, the emissivity remains constant over the temperature range of interest, allowing for a one-time calibration of the infrared imaging system. Unfortunately, standard calibration will not work for SIBAL thermography, because of the wide variance of emissivity.

A unique, multifaceted approach has been developed at the NASA Glenn Research Center for dealing with all the issues faced and to achieve the ultimate goal of accurate, full-field temperature measurements. First is the issue of the wide temperature span to be measured. This is accomplished by cycling through a series of integration times, each optimized to a specific range of temperatures and radiances. Each integration time must be calibrated beforehand to make sure that the combination of all integration times seamlessly cover the entire temperature range of interest.

Next is the issue of the varying emissivity. This is addressed by instrumenting the fuel surface with a small thermocouple for an in situ point temperature measurement. By comparing the point temperature measurement with the radiance measurement of a corresponding pixel group, temperature can be correlated to radiance, thus the system will be constantly calibrated. While emissivity will not be used in this scheme, it can be calculated from measurements at a later time.

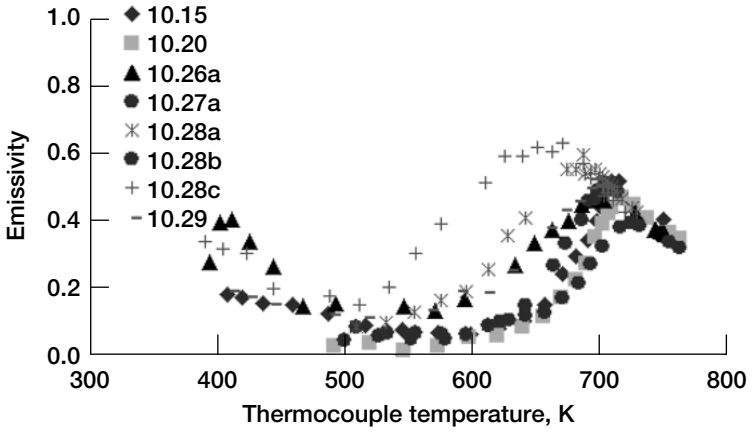

Preliminary test results showing wide range of emissivity variance and basic trends. Test used ashless filter paper at 4.0 psia with 21 vol% O_2 and upward burning.

These techniques will be pulled together and applied in image postprocessing. A software package is under development to parse images. This software will extract the optimized data out of an integration time that is within the calibrated range, while retaining the position of the images in the scene. The software will also correlate the temperature data with the measured radiance values and apply the correlation across the scene. Finally, it will bring all relevant and processed data into one composite image of accurate temperature data.

Preliminary testing has been completed and trends are evident in emissivity variance. An experiment rig is being completed to test the technique with higher fidelity instruments.

Find out more about this research:

Glenn's Engineering Development Division:
http://www.grc.nasa.gov/WWW/EDD/

Glenn's Diagnostic & Data Systems Branch:
http://www.grc.nasa.gov/WWW/7715/

Glenn contacts:
George R. Santosuosso, 216–433–9625, George.R.Santosuosso@nasa.gov;
Michael J. Lichter, 216–433–8588, Michael.J.Lichter@nasa.gov

National Center for Microgravity Research contact:
Richard D. Pettegrew, 216–433–8321, Richard.Pettegrew@grc.nasa.gov

Author: George R. Santosuosso

Headquarters program office: OBPR

Programs/Projects:
FEANICS, Microgravity Science

Hybrid Power Management (HPM) Program Resulted in Several New Applications

Hybrid Power Management (HPM) is the innovative integration of diverse, state-of-the-art power devices in an optimal configuration for space and terrestrial applications. The appropriate application and control of the various power devices significantly improves overall system performance and efficiency. The advanced power devices include ultracapacitors, fuel cells, and photovoltaics. HPM has extremely wide potential with applications from nanowatts to megawatts. Applications include power generation, transportation systems, biotechnology systems, and space power systems. HPM has the potential to significantly alleviate global energy concerns, improve the environment, and stimulate the economy.

The continuation of HPM through NASA Glenn Research Center's Commercial Technology Office resulted in several new successful applications of this pioneering technology for fiscal year 2002. A typical commercial alternating-current- (ac-) powered smoke detector is powered by an ac power system and has a battery for backup power in the event of a power outage. The battery must be replaced at least once a year. In contrast, the HPM smoke detector, which also is powered from an ac power system, has ultracapacitors for backup power in the event of a power outage. The ultracapacitors can provide 7 days of backup power, and they never need to be replaced; thus, they provide a safer, environmentally friendly, longer life solution.

A typical electric toothbrush is powered by batteries. The batteries provide reduced performance over time, and eventually need to be replaced and disposed of. The HPM toothbrush can be charged in 10 seconds and provides 2 minutes of operation, as typically required for tooth brushing. The ultracapacitors can be charged quickly, and never need replacement.

An electric bicycle also was tested. It has lead acid batteries that provide a range up to 20 miles, but the batteries require 4 hours to recharge. The range degrades over time, and the batteries must be replaced after about 300 charging cycles. The low-temperature performance of the batteries is greatly reduced. This year, the bicycle was tested with ultracapacitors. It charged in 5 minutes and provided 1 hour of operation at 10 mph for a 10-mi range. The ultracapacitors have unlimited life and can be charged quickly. The low-temperature performance of the ultracapacitors is excellent.

An electric utility vehicle also is being tested. It is equipped with lead acid batteries that must be watered weekly and replaced annually under normal use. The recharge time is 8 hours. The vehicle is being equipped with ultracapacitors that require no maintenance, have unlimited life, and can be charged in minutes rather than hours.

In addition, HPM is being considered for providing reliable, long-life energy storage systems, essential for space missions, such as the exploration of Mars, and deep space missions, such as the exploration of Europa. The technology is also being considered for various aeronautical electrical system applications.

Bibliography

Eichenberg, Dennis J.: Baseline Testing of the EV Global E-Bike With Asymmetric Ultracapacitors. NASA/TM—2002-211792, 2002. http://gltrs.grc.nasa.gov/cgi-bin/GLTRS/browse.pl?2002/TM-2002-211792.html

Glenn contact:
Dennis J. Eichenberg, 216–433–8360, Dennis.J.Eichenberg@nasa.gov

Author: Dennis J. Eichenberg

Headquarters program office: CTD

Programs/Projects: CTO, power generation, transportation, biotechnology, space power

Hybrid Power Management Program—Power for a Brighter Tomorrow. Left: Electric toothbrushes powered by ultracapacitors. Center: Utility vehicle powered by ultracapacitors. Right: Smoke detectors with ultracapacitor backup power.

Modular Avionics Concept Developed for Microgravity Space Experiments—FEANICS

The Flow Enclosure Accommodating Novel Investigations in Combustion of Solids (FEANICS) is a facility being developed at the NASA Glenn Research Center that will be integrated into the Combustion Integrated Rack onboard the International Space Station. FEANICS will support various experimental studies of solid combustion in a microgravity environment. The experiments will vary, and the FEANICS facility hardware combined with the Combustion Integrated Rack hardware is designed to meet the science requirements of the individual experiments.

The principal investigator (PI) avionics box contains the electrical hardware that would run the various experiments and connectors that will interface to the Combustion Integrated Rack. This box is being designed to accommodate all the common-fuel experiments. In the case of the thick fuel experiments: Flow Ignition and Spread Test (FIST), Analysis of Thermal and Hydrodynamic Instabilities in Near-limit Atmospheres (ATHINA), and Radiative Enhancement Effects on Flame Spread (REEFS), the PI avionics box would have all the necessary control and instrumentation electronics to handle each particular experiment in turn and would use a one-harness-fits-all wiring approach.

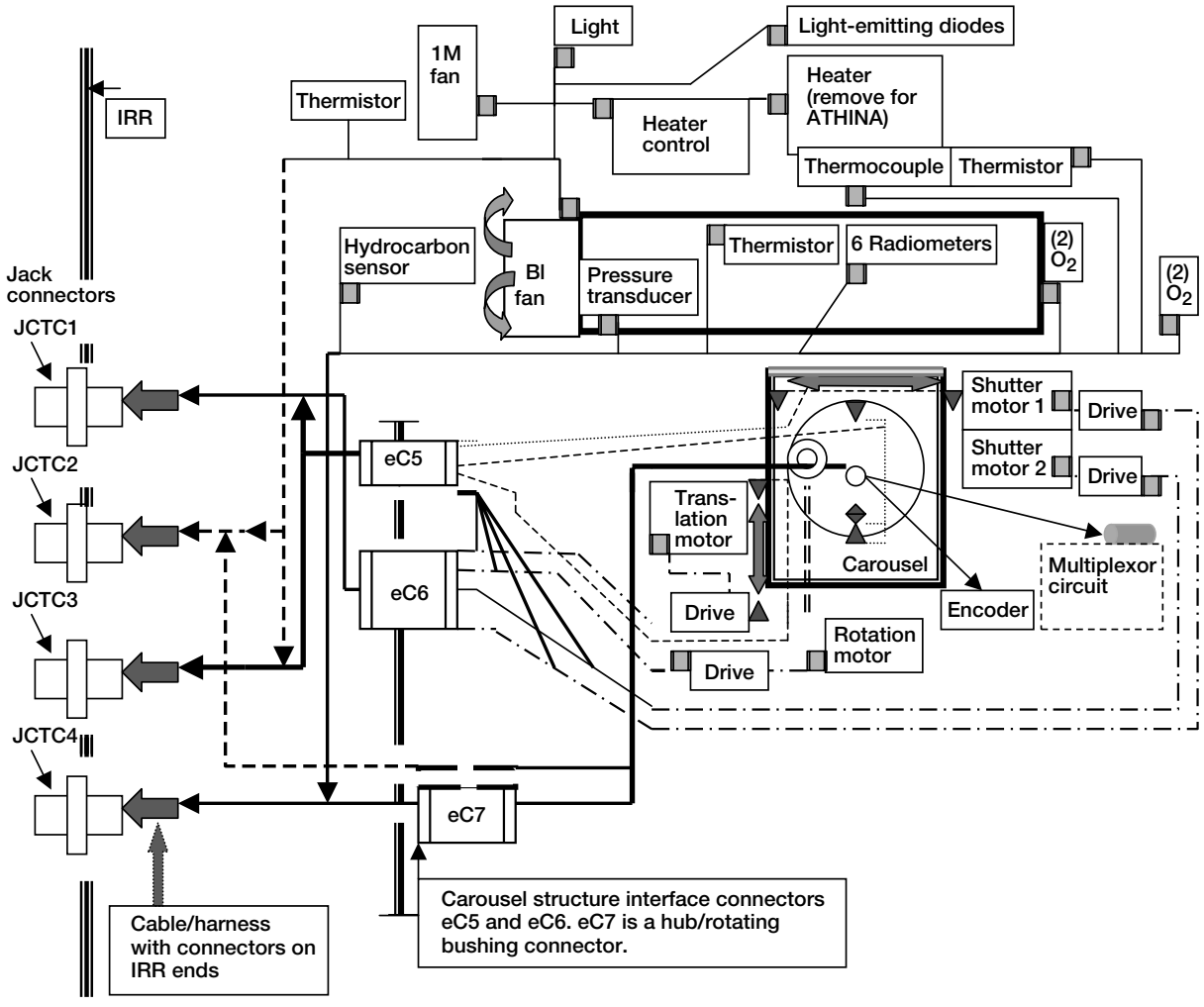

FIST, ATHINA, and REEFS (thick fuel) insert wiring and connectivity in FEANICS. JCTC1 to JCTC4, connectors carrying signals out of the IRR interface; 1M fan, air-mixing fan; B1 fan, blower fan for airflow control through the FEANICS insert tunnel; (2) O_2, two oxygen sensors.

The circuits unique to a particular experiment would be active under that particular experiment's software control. Unused circuits would be dormant, although powered up. When the next type of experiment was run, its unique circuitry would be made active while the previous experiment's circuitry would be made dormant, and so on. Thus, when any of the common fuel experiment's chamber electrical devices of structure were changed out, the PI avionics box electrical components would not have to be modified, just the experimental software would be changed via downloading.

The control signal and data connections between the PI avionics box and the combustion chamber's interface resource ring (IRR) would also not have to change with the various experimental runs. The common tunnel insert will contain all the electrical instrumentation and control devices for each experiment. The insert's cabling would be connected to dedicated connectors on the IRR. These would not be changed from experiment to experiment (FIST to ATHINA to REEFS), but the active pins in each connector would. This would depend on what PI avionics circuitry was active as mentioned earlier. Even though all the pins would be connected, only those pins associated with a particular experiment would carry signals. Similarly, the fuel carousel magazine would be changed from experiment to experiment, but its cable harness would connect to other dedicated IRR connectors handling thermocouple and radiometer data and motor/position switch plus igniter control signals. The number of thermocouple and radiometer data signals would change, but the motor/position switches would not. The PI avionics IRR-side connector pins handling the data signals would be wired to accommodate the worst-case number of signals. The corresponding carousel connector pins would be wired to handle only the necessary quantity of data signals for a particular experiment. Any unused signal/data pins would be terminated properly within the carousel's IRR-side cable harness (adding termination resistors or grounding unused pins depending on the PI avionics input/output circuitry used).

The benefits of this "plug-n-play" accomplishment include the following:

(1) Only one "master" harness and cable/connector set would be needed. This would lessen the mass needed to be transported to the space station and the onboard storage requirement. (A special harness would not be needed for each experiment.)

(2) Because the PI avionics box would not have to be modified for each new experiment, it would require less astronaut hands-on time. This also would lesson onboard storage requirements (only spares for the existing PI avionics box would have to be stored, not the original components for each experiment).

Find out more about FEANICS:
http://microgravity.grc.nasa.gov/feanics/feanics.html

Glenn contact:
Clifford Hausmann, 216–433–3809, Clifford.R.Hausmann@nasa.gov

Author: Clifford R. Hausmann

Headquarters program office: OBPR

Programs/Projects:
FEANICS, Microgravity Science

Hydrogen Fuel Capability Added to Combustor Flametube Rig

Facility capabilities have been expanded at Test Cell 23, Research Combustor Lab (RCL23) at the NASA Glenn Research Center, with a new gaseous hydrogen fuel system. The purpose of this facility is to test a variety of fuel nozzle and flameholder hardware configurations for use in aircraft combustors. Previously, this facility only had jet fuel available to perform these various combustor flametube tests. The new hydrogen fuel system will support the testing and development of aircraft combustors with zero carbon dioxide (CO_2) emissions. Research information generated from this test rig includes combustor emissions and performance data via gas sampling probes and emissions measuring equipment.

The new gaseous hydrogen system is being supplied from a 70 000-standard-ft^3 tube trailer at flow rates up to 0.05 lb/s (maximum). The hydrogen supply pressure is regulated, and the flow is controlled with a 1/2-in. remotely operated globe valve. Both a calibrated subsonic venturi and a coriolis mass flowmeter are

used to measure flow. Safety concerns required the placement of all hydrogen connections within purge boxes, each of which contains a small nitrogen flow that is vented past a hydrogen detector. If any hydrogen leaks occur, the hydrogen detectors alert the operators and automatically safe the facility.

Facility upgrades and modifications were also performed on other fluids systems, including the nitrogen gas, cooling water, and air systems. RCL23 can provide nonvitiated heated air to the research combustor, up to 350 psig at 1200 °F and 3.0 lb/s. Significant modernization of the facility control systems and the data acquisition systems was completed. A flexible control architecture was installed that allows quick changes of research configurations. The labor-intensive hardware interface has been removed and changed to a software-based system. In addition, the operation of this facility has been greatly enhanced with new software programming and graphic operator interface stations. Glenn's RCL23 facility systems were successfully checked out in the spring of 2002, and hydrogen combustor research testing began in the summer of 2002.

Glenn contact:
Bruce J. Frankenfield, 216–433–6456, Bruce.J.Frankenfield@nasa.gov

Author: Bruce J. Frankenfield

Headquarters program office: OAT

Programs/Projects:
Propulsion Systems R&T

Light Microscopy Module Fan Disturbance Characterized Through Microgravity Emissions Laboratory Testing

A Light Microscopy Module (LMM) is being engineered, designed, and developed at the NASA Glenn Research Center. The LMM is planned as a remotely controllable on-orbit microscope subrack facility, allowing flexible scheduling and control of physical science and biological science experiments within Glenn's Fluids Integrated Rack on the International Space Station. The LMM concept is a modified commercial research imaging light microscope with powerful laser-diagnostic hardware and interfaces, creating a one-of-a-kind, state-of-the-art microscopic research facility. The microscope will house several different objectives, corresponding to magnifications of ×10, ×40, ×50, ×63, and ×100. Features of the LMM include high-resolution color video microscopy, brightfield, darkfield, phase contrast, differential interference contrast, spectrophotometry, and confocal microscopy combined in a single configuration. Also, laser tweezers are integrated with the diagnostics as a sample manipulation technique. As part of the development phase of the LMM, it was necessary to quantify the microgravity disturbances generated by the control box fan. Isolating the fan was deemed necessary to reduce the fan speed harmonic amplitudes and to eliminate any broadband disturbances across the 60- to 70-Hz and 160- to 170-Hz frequency ranges.

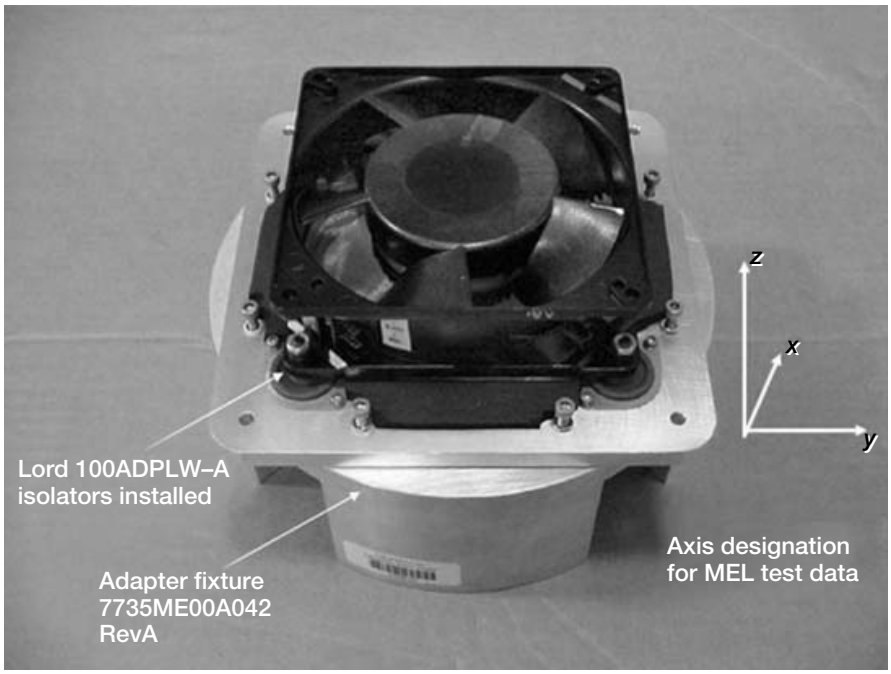

Light Microscopy Module control box fan.

The accelerations generated by a control box fan component of the LMM were measured in the Microgravity Emissions Laboratory (MEL). The MEL is a low-frequency measurement system developed to simulate and verify the on-orbit International Space Station (ISS) microgravity environment. The accelerations generated by various operating components of the ISS, if too large, could hinder the science performed onboard by disturbing the microgravity environment. The MEL facility gives customers a test-

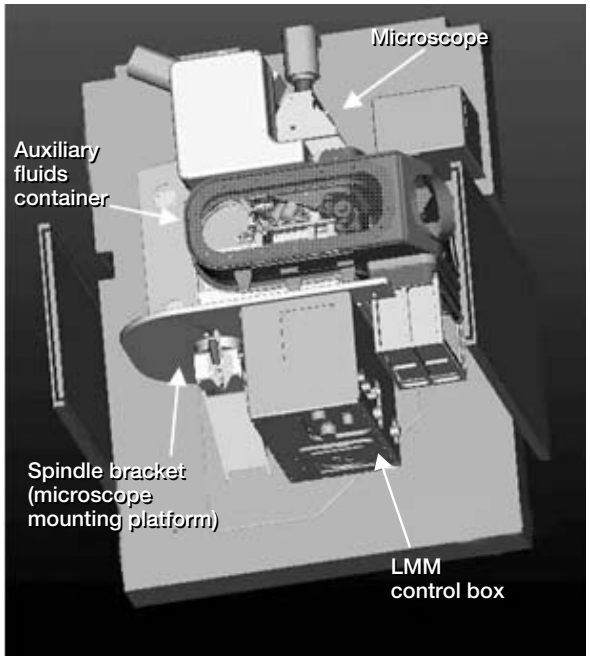

Light Microscopy Module.

verified way of measuring their compliance with ISS limitations on vibratory disturbance levels. The facility is unique in that inertial forces in 6 degrees of freedom can be characterized simultaneously for an operating test article. Vibratory disturbance levels are measured for engineering or flight-level hardware following development from component to subassembly through the rack-level configuration. The MEL can measure accelerations as small as 10^{-7}g, the accuracy needed to confirm compliance with ISS requirements.

Prior to MEL testing, LMM personnel reviewed the LMM assembly finite element analysis models to locate the natural frequencies in structural areas surrounding the location where the sample cells will reside. First natural frequencies of the X–Y stage and the microscope of the LMM were noted to be in the 60- to 70-Hz and 160- to 170-Hz ranges. The control box fan isolation would need to reduce any fan speed harmonics and broadband disturbances in these frequency ranges to maintain the functionality of the LMM.

As the inertial forces for the operating control box fan were characterized through MEL testing, results showed that the isolator initially selected did not reduce fan speed harmonics and broadband disturbances in the 60- to 70-Hz frequency range. MEL test personnel concluded that softer isolation would be needed. Trial tests of five Lord Corporation (Mechanical Products Division, Erie, PA) isolators with varying stiffness were completed. MEL test results indicated that the broadband disturbances and fan speed harmonic amplitudes were reduced for force and moment data sets in all 6 degrees of freedom when an isolator with a stiffness of 3 lb/in. was used. On the basis of the MEL results, LMM personnel implemented a design change for the control box fan. In conclusion, the MEL was used not only to characterize MEL inertial forces to assess compliance with ISS requirements for LMM but also to optimize the isolator selection and improve the design of the control box fan interface.

Find out more about this research:

LMM:
http://www.cleveland.feddata.com/lmm/
http://microgravity.grc.nasa.gov/6712/lmm.html

MEL:
http://www.grc.nasa.gov/WWW/MEL/

Glenn's Structural Systems Dynamics Branch:
http://www.grc.nasa.gov/WWW/SSDB/

Glenn contacts:
Susan M. Motil, 216–433–8589,
Susan.M.Motil@nasa.gov; and
Anne M. McNelis, 216–433–8880,
Anne.M.McNelis@nasa.gov

Northrup-Grumman Information Technology contact:
Tony Haecker, 216–925–1094,
Anthony.H.Haecker@grc.nasa.gov

ZIN Technologies, Inc., contact:
Sergey Samorezov, 216–433–5294,
Sergey.Samorezov@grc.nasa.gov

Authors:
Anne M. McNelis and Susan M. Motil

Headquarters program office:
OBPR, OLMSA

Programs/Projects:
Microgravity Science, LMM, FCF

Integrated Propulsion/Vehicle System Structurally Optimized

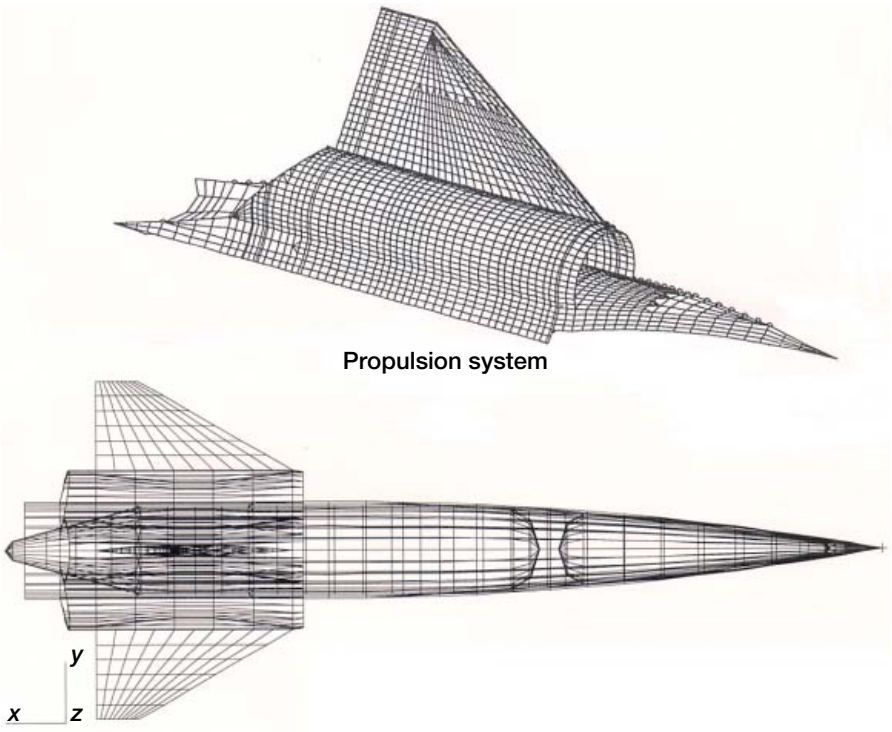

Finite element models for GTX assessment.

Ongoing research and testing are essential in the development of air-breathing hypersonic propulsion technology, and this year some positive advancement was made at the NASA Glenn Research Center. Recent work performed for GTX, a rocket-based combined-cycle, single-stage-to-orbit concept, included structural assessments of both the engine and flight vehicle. In the development of air-breathing engine technology, it is impractical to design and optimize components apart from the fully integrated system because tradeoffs must be made between performance and structural capability. Efforts were made to control the flight trajectory, for example, to minimize the aerodynamic heating effects. Structural optimization was applied to evaluate concept feasibility and was instrumental in the determination of the gross liftoff weight of the integrated system. Achieving low Earth orbit with even a small payload requires an aggressive approach to weight minimization through the use of lightweight, oxidation-resistant composite materials. Assessing the integrated system involved investigating the flight trajectory to determine where the critical load events occur in flight and then generating the corresponding environment at each of these events.

Structural evaluation requires the mapping of the critical flight loads to finite element models, including the combined effects of aerodynamic, inertial, combustion, and other loads. NASA's APAS code was used to generate aerodynamic pressure and temperature profiles at each critical event. The radiation equilibrium surface temperatures from APAS were used to predict temperatures through the thickness. Heat transfer solutions using NASA's MINIVER code and the SINDA code (Cullimore & Ring Technologies, Littleton, CO) were calculated at selective points external to the integrated vehicle system and then extrapolated over the entire exposed surface. FORTRAN codes were written to expedite the finite element mapping of the aerodynamic heating effects for the internal structure.

A detailed finite element model of the propulsion system was generated to establish a flight weight for one engine. A second finite element model, more coarsely meshed, of the full integrated system was generated for the overall assessment, mapping of loads, and system optimization. Loads were applied in a case-consistent fashion using MSC–NASTRAN (MSC.Software Corporation, Santa Ana, CA) for static analysis. NASTRAN has an inertia relief capability to simulate the vehicle in flight so that loads can be balanced. At each critical case in flight, the fuel depletion was taken into account to determine the net result of combined loads acting on the integrated system. The weight of the structure was optimized using HyperSizer (Collier Research Corporation, Hampton, VA). This code allows users to optimize a component structure according to the critical case for each component. This process was completed for each of the primary structures, leading to an overall optimization of the integrated flight system.

The methods used in this assessment were effective in defining and evaluating an integrated propulsion/vehicle structure. Results of the analyses were used to improve scaling laws and increase the accuracy in the GTX sizing tool.

Find out more about this research: http://www.grc.nasa.gov/WWW/pfablv/

Bibliography

Roche, Joseph M.: Preliminary Sizing Completed for Single-Stage-To-Orbit Launch Vehicles Powered by Rocket-Based Combined Cycle Technology. Research & Technology 2001. NASA/TM—2002-211333, 2002, p. 221. http://www.grc.nasa.gov/WWW/RT2001/7000/7740roche.html

Hunter, J.E.; McCurdy, D.R.; and Dunn, P.W.: GTX Reference Vehicle Structural Verification Methods and Weight Summary. NASA/TM—2002-211884, 2002. http://gltrs.grc.nasa.gov/cgi-bin/GLRS/browse.pl?2002/TM-2002-211884.html

Glenn contacts:
James E. Hunter, 216–433–2418, James.E.Hunter@nasa.gov; and
Patrick W. Dunn, 216–433–8726, Patrick.W.Dunn@nasa.gov

QSS Group, Inc., contact:
David R. McCurdy, 216–977–1022, David.R.Mccurdy@grc.nasa.gov

Authors: James E. Hunter and David R. McCurdy

Headquarters program office: OAT

Programs/Projects: Propulsion and Power

R&T 2002

Commercial Technology

Space Act Agreement Maker (SAAM) With Electronic Routing System (E-Router) Developed

Members of the Commercial Technology Office at the NASA Glenn Research Center have developed an exciting new tool that greatly reduces the lead time in creating and routing Space Act Agreements. The Space Act Agreement Maker (SAAM) is an e-government Web-based system that automates the initial drafting of Space Act Agreements by technical and program personnel. SAAM also is used for editing and will be used later for maintaining electronic copies of all Space Act Agreements. During the initial drafting, the software prompts NASA personnel proposing an agreement to answer questions regarding the agreement. On the basis of the answers, the software selects from a matrix of NASA "standard" clauses to produce a first draft of the agreement. The draft agreement and information submitted by the NASA personnel are electronically routed to Glenn's Commercial Technology Office for review and, where necessary, editing. The final version of the agreement, along with any supporting documentation, is then routed for electronic concurrence/approval to the necessary internal review participants using the electronic routing system (e-router). SAAM was developed cooperatively by Glenn's Commercial Technology Office and Glenn's Office of Chief Counsel. Currently, SAAM is being evaluated by the NASA Headquarters General Counsel Office for use at all NASA centers.

This system allows for the effective processing of Space Act Agreements for NASA's internal and external customers. Document control is maintained by a database. With SAAM's electronic routing, review times can be reduced significantly, allowing Glenn to more rapidly establish partnerships with industry.

Prior to the creation of SAAM, it took several hours to draft a Space Act Agreement. With SAAM in place, the document can be written in about 30 min. Using the e-router also saves time in determining where the agreement is in the routing process. The document can be tracked easily, and delays can be avoided. Important research with industry partners can commence quickly after preliminary discussions have been held.

The development of these products is in line with the expanding e-government initiative that is part of the Presidential Management Agenda. By using this product, NASA researchers can secure greater support from industry and academia partners.

The Space Act Agreement Maker has been very well received at NASA Headquarters and at some of the other NASA centers as well. We anticipate that the NASA Ames Research Center will have the system in place very soon, and that some of the other centers will use SAAM in the near future. The General Counsel's office at NASA Headquarters has encouraged the Glenn team to develop a similar system for processing patent licenses.

Find out more about this research:
http://technology.grc.nasa.gov

InDyne, Inc., contact:
Jason Crusan, 216–433–5564,
Jason.C.Crusan@grc.nasa.gov

Glenn contact:
Steven Fedor, 216–433–2144,
Steven.L.Fedor@nasa.gov

Author: Laurel J. Stauber

Headquarters program office: OAT

Programs/Projects: Program offices using Space Act Agreements

Definitions of NASA Headquarters Program Offices

OA Office of the Administrator

OAT Office of Aerospace Technology

- **CTD** Commercial Technology Division

OBPR Office of Biological and Physical Research

OHEDS Office of Human Exploration and Development of Space

OLMSA Office of Life & Microgravity Sciences & Applications

OMSF Office of Management Systems & Facilities

- **FED** Facilities Engineering Division

OSF Office of Space Flight

- **SCDS** Space Communications and Data Systems

OSMA Office of Safety and Mission Assurance

OSS Office of Space Science

Definitions of Programs and Projects

AATT	Advanced Air Transportation Technologies
ACESE	Attitude Control/Energy Storage Experiment
ASTP	Advanced Space Transportation Program
AvSP	Aviation Safety Program
CICT	Computing Information and Communications Technology Program
CloudSat	Cloud Cover Statistical Analysis Program
CoF	Construction of Facilities
CTO	Glenn's Commercial Technology Office
DDF	Director's Discretionary Fund (NASA Glenn)
DOD	Department of Defense
ECT	Enabling Concepts and Technology Program
EO–1	Earth Observing-1
EOS	Earth-Observing Systems
ESE	Earth Science Enterprise
FCF	Fluids and Combustion Facility
FEANICS	Flow Enclosure Accommodating Novel Investigations in Combustion of Solids
Galex	Galaxy Evolution Explorer
Gen 3	Third Generation Space Launch Vehicles
GMI	Glennan Microsystems Initiative
GOES	Geostationary Operational Environmental Satellite
HEDS	Human Exploration and Development of Space
HiPEP	High Power Electric Propulsion
HITEMP	Advanced High Temperature Engine Materials Technology Program
HOTPC	High Operating Temperature Propulsion Components
HPCCP	High-Performance Computing and Communications Program
IHPTET	Integrated High Performance Turbine Engine Technology
ISS	International Space Station
ITSR	Information Technology Strategic Research Project
LEO	Low Earth orbit
LMM	Light Microscopy Module
MESSENGER	Mercury Surface, Space Environment, Geochemistry, and Ranging spacecraft
MSFC	NASA Marshall Space Flight Center
NEPAG	NASA Electronic Parts Assurance Group

NEPP	NASA Electronic Parts and Packaging
NEXT	NASA's Evolutionary Xenon Thruster
NGST	Next Generation Space Telescope
NSTAR	NASA Solar Electric Propulsion Technology Application Readiness
PERS	Polymer Rechargeable System
QAT	Quiet Aircraft Technology
RAC	Revolutionary Aeropropulsion Concepts
RBCC	Rocket-Based Combined-Cycle
REEFS	Radiative Enhancement Effects on Flame Spread
RLV	Reusable Launch Vehicles
RSL	Rotor Safe Life
SBIR	Small Business Innovation Research
SEC	Smart Efficient Components
SEP	Solar Electric Propulsion
SILNT	Selected Integrated Low-Noise Transmissions for Rotorcraft
SLI	Strategic Launch Initiative
SPT	Supersonic Propulsion Technology
SRF	Glenn's Strategic Research Fund
SRG	Stirling Radioisotope Generator
SSP	Space Solar Power
STPO	Space Transportation Project Office
STR	Space Transportation Research
STTR	Small Business Technology Transfer
TBCC	Turbine-Based Combined Cycle
UEET	Ultra-Efficient Engine Technology
Ultra Safe	Ultra Safe Propulsion
VAATE	Versatile, Affordable, Advanced Technology Engine
VF5	Vacuum Facility 5
ZCET	Zero CO_2 Emission Technology

Index of Authors and Contacts

Both authors and contacts are listed in this index. Articles start on the page numbers following the names.

A

Abdul-Aziz, Dr. Ali *130, 131*
Abel, Dr. Phillip B. *10, 17, 189*
Acosta, Dr. Roberto J. *204*
Adamovsky, Dr. Grigory *78*
Adams, Paulette E. *116*
Alterovitz, Samuel A. *100*
Ansari, Dr. Rafat R. *211*
Arnold, Dr. Steven M. *129, 148, 149*
Arrington, Lynn A. *54*

B

Baaklini, Dr. George Y. *130, 131, 133, 136, 140*
Bakhle, Dr. Milind A. *151, 173, 174, 176*
Balasubramaniam, Ramaswamy *219*
Banks, Bruce A. *56*
Bansal, Dr. Narottam P. *36*
Barrett, Charles A. *15, 43*
Bartlett, Wayne M. *239*
Bauman, Steven W. *187*
Beach, Duane E. *62*
Beach, Raymond F. *159*
Beheim, Dr. Glenn M. *68*
Bencic, Timothy J. *80*
Benson, Scott W. *54*
Bhatt, Dr. Ramakrishna T. *130, 131*
Bizon, Thomas P. *105*
Blaha, Charles A. *77*
Borato, Frances M. *236*
Bowman, Dr. Cheryl L. *148, 152*
Bozzolo, Dr. Guillermo H. *10, 17, 189*
Brasche, Lisa *133*
Bridges, Dr. James E. *87*
Bright, Dr. Michelle M. *88*
Brown, Donald P. *237*
Brown, Gerald V. *156*
Burton, Rodney *54*
Busfield, A. Rachel *77*

C

Calhoun, Gregory G. *116*
Calomino, Dr. Anthony M. *45, 147*
Campbell, Sandi G. *28*
Carney, Kelly S. *163*
Cawley, Dr. James D. *23*
Chang, Dr. Clarence T. *90*
Chao, Dr. David F. *213*
Chato, David J. *242*
Chen, Dr. Liang-Yu *69*
Cheng, Robert K. *206*
Choi, Dr. Benjamin B. *154, 156, 168*
Choi, Kyung J. *123*
Chriss, Dr. Randall M. *109*
Copland, Evan *32*
Cosgriff, Laura M. *136, 144*
Crusan, Jason C. *252*
Culley, Dennis E. *88*
Cupp, Randall *40*
Curtis, Henry B. *230*
Czaruk, Timothy M. *168*

D

Daugherty, Elaine S. *10*
DeBonis, Dr. James R. *124*
Decker, Dr. Arthur J. *81*
de Groh, Kim K. *56, 58*
DeLaat, John C. *90*
Delgado, Irebert R. *185*
DellaCorte, Dr. Christopher *187, 191, 192, 200*
Delleur, Ann M. *231*
Demko, Rikako *56*
Dempsey, Dr. Paula J. *179*
Doherty, Michael P. *224*
Draper, Susan L. *12, 137*
Duffy, Dr. Kirsten P. *157*
Dunlap, Patrick H., Jr. *181*
Dunn, Patrick W. *249*
Duval, Dr. Walter M. *227*
Dynys, Dr. Frederick W. *21*

E

Eckel, Dr. Andrew J. *23*
Edmonds, Brian J. *191*
Eichenberg, Dennis J. *244*
Elam, Kristie A. *84*
Eldridge, Dr. Jeffrey I. *36*
Envia, Dr. Edmane *177*

F

Farmer, Dr. Serene C. *22, 39*
Fedor, Steven L. *252*
Feikema, Dr. Douglas A. *208*
Ferguson, Dr. Dale C. *48*
Fincannon, H. James *233*
Fink, Jeffery *31*
Fox, Dennis S. *36*
Fralick, Gustave C. *70, 76, 77*
Frankenfield, Bruce J. *246*
Frus, John *54*

G

Gabb, Dr. Timothy P. *13*
Gaier, Dr. James R. *59*
Galofaro, Joel T. *48*
Garces, Dr. Jorge E. *189*
Gaugler, Dr. Raymond E. *113*

Gayda, Dr. John *13, 14*
Geiser, Martial *211*
Geng, Steven M. *63*
Ghosn, Dr. Louis J. *43*
Gokoglu, Dr. Suleyman A. *209*
Goldberg, Dr. Robert K. *135*
Good, Dr. Brian S. *10*
Greenberg, Paul S. *206*
Greer, Lawrence C. *83*
Griner, James H. *94*
Grisnik, Stanley P. *238*
Gyekenyesi, Dr. Andrew L. *133, 140, 144*

H
Haecker, Anthony H. *247*
Hah, Dr. Chunill *108*
Halbig, Michael C. *23, 27*
Hammoud, Ahmad *61*
Handschuh, Dr. Robert F. *179, 183*
Hathaway, Dr. Michael D. *109*
Hausmann, Clifford R. *245*
Hebsur, Dr. Mohan G. *15, 16, 19*
Hegde, Dr. Uday *210*
Hickman, J. Mark *227*
Hofer, Richard R. *52*
Hopkins, Dale A. *170*
Horan, Dick *40*
Horowitz, Dr. Jay G. *49*
Hoskins, W. Andrew *54*
Howard, Dr. S. Adam *197*
Hughes, Christopher E. *177*
Hunter, Dr. Gary W. *72*
Hunter, James E. *249*
Hwang, Dr. Danny P. *70*

I
Iannetti, Anthony C. *114*

J
Jacobson, David T. *52*
Jacobson, Dr. Nathan S. *32, 34*
Jankovsky, Robert S. *52, 238*
Jansen, Mark J. *195*
Jansen, Ralph H. *159, 168*
Jaskowiak, Martha H. *25*
Jassemnejad, Baha *81*
Jaworske, Dr. Don A. *60*
Johnson, Dr. Dexter *154, 160, 168*
Johnson, Sandra K. *204*
Jones, William R., Jr. *195*

K
Kacpura, Thomas J. *222*
Kantzos, Dr. Pete T. *13, 14*
Kautz, Harold E. *144*
Keith, Prof. T., Jr. *173*
Kenny, Dr. Barbara H. *55*
Kerslake, Thomas W. *230, 231*
King, James F. *211*
Kiser, James D. *27*
Kizito, Dr. John P. *221*
Klann, Gary A. *240*
Kohout, Lisa L. *49*
Kojima, Dr. Jun *116*
Krasowski, Michael J. *83*
Krause, David L. *19*
Kurkov, Dr. Anatole P. *162*

L
Lambert, Kevin M. *96*
Lang, Dr. Jerry *26*
Larkin, Dr. David J. *74*
Larose, Joel *139*
Larosiliere, Dr. Louis M. *109*
Lavelle, Thomas M. *170*
Lawrence, Dr. Charles *163*
Lebron, Marisabel *29*
Lee, Dr. Ho-Jun *164*
Lee, Dr. Kang N. *36*
Lee, Dr. Richard Q. *96*
Lei, Dr. Jih-Fen *69*
Lekki, John D. *78, 104*
Lerch, Dr. Bradley A. *137, 139, 149*
Levine, Dr. Stanley R. *27*
Lewandowski, Prof. John J. *139*
Lichter, Michael J. *243*
Lienhard, Dr. Michael A. *74*
Lissenden, Prof. Cliff J. *139*
Litt, Jonathan S. *91*
Lorenz, Gary V. *116*
Lotenero, Raymond C. *116*
Lucero, John M. *194*

M
Ma, Kong *40*
Mann, Dr. Adin, III *242*
Manthey, Lori A. *2*
Manuel, Dr. Francis K. *211*
Manzella, David H. *52*
Manzo, Michelle A. *50*
Marchetti, Mario *195*
Martin, Morgana *58*
Martin, Richard E. *140, 144*
Martinez-Fernandez, Dr. Julian *22*
Martzaklis, Konstantinos S. *94*
Mason, Lee S. *64*
Matus, Dr. Lawrence G. *69, 236*
McCurdy, David R. *249*
McNelis, Anne M. *247*
Meador, Dr. Michael A. *29*
Mehmed, Oral *151, 157, 168, 173*
Melis, Matthew E. *165*
Messer, Russell K. *211*
Miller, Jason D. *13*
Miller, Dr. Robert A. *36, 37*
Min, Dr. James B. *166*
Miranda, Dr. Félix A. *96, 98*
Mital, Dr. Subodh K. *172*
Miyoshi, Dr. Kazuhisa *39, 40, 137*
Mondry, Richard *40*
Montague, Gerald T. *168, 171*
Moran, Matthew E. *62*
Moret, Fabrice *211*
Morrison, Carlos R. *154, 168*
Motil, Susan M. *247*
Mueller, Carl H. *100*

N
Naik, Dr. Subhash *40, 152*
Nathal, Dr. Michael V. *12, 15*
Needham, Kathleen K. *191*
Nelson, Dr. Emily S. *221*
Nemeth, Noel N. *141*
Nesbitt, Dr. James A. *15*
Neudeck, Dr. Philip G. *75*
Ng, Dr. Daniel L. *76*
Ngo, Duc H. *98*
Nguyen, Dr. Hung D. *98*
Nguyen, Dr. Quang-Viet *104, 116, 118*
Niederhaus, Dr. Charles E. *215*
Noebe, Dr. Ronald D. *10, 16, 17*

O
Oberle, Lawrence G. *83*
Oeftering, Richard C. *242*
Opila, Dr. Elizabeth J. *27, 42*
Otten, Kim D. *152*

P
Pai, Dr. Shantaram S. *172*
Palaszewski, Bryan A. *120, 122*
Palou, Jaime J. *34*
Panda, Dr. Jayanta *84, 125*
Parsons, Dr. Patricia A. *216*
Patnaik, Dr. Surya N. *170*
Patterson, Michael J. *53*
Patterson, Richard L. *61*
Paxson, Dr. Daniel E. *92*
Pencil, Eric. J *54*
Pepper, Dr. Stephen V. *195*
Perusek, Gail P. *152*
Peterson, Todd T. *230*
Pettegrew, Richard D. *243*
Pindera, Prof. Marek-Jerzy *129*
Podboy, Gary G. *177*
Powell, J. Anthony *75*
Prabhu, Nishad S. *139*
Prahst, P. Sue *88*
Predmore, Roamer E. *195*
Proctor, Margaret P. *185*
Provenza, Andrew J. *168, 171*

R
Radil, Kevin C. *197*
Raj, Dr. Sai V. *43*
Rashidnia, Dr. Nasser *219*
Raulerson, David *133*
Rawlin, Vincent K. *53*
Reddy, Dr. T.S.R. *172, 173*
Reinhart, Richard C. *204*
Reveley, Mary S. *3*
Revilock, Duane M. *16*
Rigby, Dr. David L. *113*
Roberts, Dr. Gary D. *135*
Robinson, R. Craig *45*
Romanofsky, Dr. Robert R. *100, 101*
Ronney, Prof. Paul *209*
Roth, Don J. *144*
Ruff, Dr. Gary A. *228*

S
Sadhukhan, Debashis *237*
Salem, Dr. Jonathan A. *27, 145, 147*
Samorezov, Sergey *247*
Sanders, Terry M. *104*
Sands, Dr. Obed S. *204*
Sankaran, Dr. Subramanian *224*
Santosuosso, George R. *243*
Sawicki, Dr. Jerzy T. *133*
Sayir, Dr. Ali *22, 39*
Schreiber, Jeffrey G. *65*
Seasholtz, Dr. Richard G. *84, 125*
Seibel, Robin E. *81*
Seibert, Marc A. *104, 105*
Shaltens, Richard K. *65*
Shaw, Loretta M. *109, 111*
Shaw, Dr. Robert J. *2*
Sheredy, William A. *228*
Shin, E. Eugene *31*
Sicker, Ronald J. *222*
Singh, Dr. Mrityunjay *27*
Sivathanu, Yudaya *208*
Skoch, Gary J. *111*
Smialek, Dr. James L. *8*
Smith, Kevin *133*
Song, Prof. Gangbing *164*
Sovey, James S. *53*
Speier, Henry J. *238*
Srivastava, Dr. Rakesh *174, 176*
Stanford, Dr. Malcolm K. *198*
Stark, David E. *240*
Stauber, Laurel J. *252*
Stefko, George L. *172, 174, 176*
Steinetz, Dr. Bruce M. *181*
Strazisar, Dr. Anthony J. *88, 111*
Suh, Dr. Kwang I. *211*
Sutter, Dr. James K. *31, 40, 152*
Swiatek, Michael W. *238*

T
Tacina, Robert R. *123*
Telesman, Dr. Jack *13*
Theman, Elmer R. *238*
Thesken, Dr. John C. *31, 148, 149*
Thieme, Lanny G. *65*
Thomas, Valarie D. *77*
Thompson, William K. *116*
To, Dr. Wai Ming *112*
Tong, Michael T. *4*
Trefny, Dr. Charles J. *127*
Trunek, Andrew J. *75*
Tuma, Dr. Margaret L. *86*

U
Urban, Dr. David L. *228*

V
Van Keuls, Frederick W. *100*
Van Zante, Dr. Dale E. *112*
Vayner, Boris V. *48*
Verrilli, Michael J. *42, 45*

W
Weaver, Harold F. *200*
Weiland, Kenneth E. *81, 104*
Wernet, Dr. Mark P. *87*
Wesseling, Paul *139*
Wey, Changlie *123*
Whittenberger, Dr. J. Daniel *19*
Wong, Wayne A. *67*
Woodward, Richard P. *177*
Wrbanek, John D. *70, 77*

X
Xiong, Fuqin *101*

Y
Yuan, Dr. Zeng-Guang *210*

Z
Zhang, Dr. Nengli *213*
Zhu, Dr. Dongming *36, 37*
Zoeckler, Joseph G. *239*

REPORT DOCUMENTATION PAGE

Form Approved
OMB No. 0704-0188

1. AGENCY USE ONLY (*Leave blank*)	2. REPORT DATE	3. REPORT TYPE AND DATES COVERED
	March 2003	Technical Memorandum

4. TITLE AND SUBTITLE

Research & Technology 2002

5. FUNDING NUMBERS

None

6. AUTHOR(S)

7. PERFORMING ORGANIZATION NAME(S) AND ADDRESS(ES)

National Aeronautics and Space Administration
John H. Glenn Research Center at Lewis Field
Cleveland, Ohio 44135–3191

8. PERFORMING ORGANIZATION REPORT NUMBER

E–13658

9. SPONSORING/MONITORING AGENCY NAME(S) AND ADDRESS(ES)

National Aeronautics and Space Administration
Washington, DC 20546–0001

10. SPONSORING/MONITORING AGENCY REPORT NUMBER

NASA TM—2003-211990

11. SUPPLEMENTARY NOTES

Responsible person, Walter S. Kim, organization code 9400, 216–433–3742.

12a. DISTRIBUTION/AVAILABILITY STATEMENT

Unclassified - Unlimited
Subject Categories: 01 and 31 Distribution: Nonstandard

Available electronically at http://gltrs.grc.nasa.gov/GLTRS
This publication is available from the NASA Center for AeroSpace Information, 301–621–0390.

12b. DISTRIBUTION CODE

13. ABSTRACT ***(Maximum 200 words)***

This report selectively summarizes NASA Glenn Research Center's research and technology accomplishments for fiscal year 2002. It comprises 166 short articles submitted by the staff scientists and engineers. The report is organized into five major sections: Aeronautics, Research and Technology, Space, Engineering and Technical Services, and Commercial Technology. A table of contents and author index have been developed to assist readers in finding articles of special interest. This report is not intended to be a comprehensive summary of all the research and technology work done over the past fiscal year. Most of the work is reported in Glenn-published technical reports, journal articles, and presentations prepared by Glenn staff and contractors. In addition, university grants have enabled faculty members and graduate students to engage in sponsored research that is reported at technical meetings or in journal articles. For each article in this report, a Glenn contact person has been identified, and where possible, a reference document is listed so that additional information can be easily obtained. The diversity of topics attests to the breadth of research and technology being pursued and to the skill mix of the staff that makes it possible. For more information about research at Glenn, visit us on the World Wide Web (http://www.grc.nasa.gov). This document is available online (http://www.grc.nasa.gov/WWW/RT). For publicly available reports, visit the Glenn Technical Report Server (http://gltrs.grc.nasa.gov/GLTRS/).

14. SUBJECT TERMS

Aeronautics; Aerospace engineering; Space flight; Space power; Materials; Structures; Electronics; Space experiments; Technology transfer

15. NUMBER OF PAGES

270

16. PRICE CODE

17. SECURITY CLASSIFICATION OF REPORT	18. SECURITY CLASSIFICATION OF THIS PAGE	19. SECURITY CLASSIFICATION OF ABSTRACT	20. LIMITATION OF ABSTRACT
Unclassified	Unclassified	Unclassified	